EXTREME MEDICINE

SCIENTIFIC AND PRACTICAL REVIEWED JOURNAL OF FMBA OF RUSSIA

SUBMISSION editor@fmba.press
CORRESPONDENCE editor@fmba.press
COLLABORATION manager@fmba.press
ADDRESS Volokolamskoe shosse, 30, str. 1, Moscow, 123182, Russia

Indexed in Scopus in 2022

Indexed in RSCI. IF 2018: 0,570

Listed in HAC 31.01.2020 (№ 1292)

Open access to archive

Issue DOI: 10.47183/mes.2023-03
The mass media registration certificate № 25124 issued on July 27, 2006
Founder and publisher: Federal medical-biological agency fmba.gov.ru

Approved for print 30.09.2023
Circulation: 500 copies. Printed by Print.Formula
www.print-formula.ru

МЕДИЦИНА ЭКСТРЕМАЛЬНЫХ СИТУАЦИЙ

НАУЧНО-ПРАКТИЧЕСКИЙ РЕЦЕНЗИРУЕМЫЙ ЖУРНАЛ ФМБА РОССИИ

ПОДАЧА РУКОПИСЕЙ editor@fmba.press
ПЕРЕПИСКА С РЕДАКЦИЕЙ editor@fmba.press
СОТРУДНИЧЕСТВО manager@fmba.press
АДРЕС РЕДАКЦИИ Волоколамское шоссе, д. 30, стр. 1, г. Москва, 123182, Россия

Журнал включен в Scopus в 2022 г.

Журнал включен в РИНЦ. IF 2018: 0,570

Журнал включен в Перечень 31.01.2020 (№ 1292)

Здесь находится открытый архив журнала

DOI выпуска: 10.47183/mes.2023-03
Свидетельство о регистрации средства массовой информации № ФС77-25124 от 27 июля 2006 года
Учредитель и издатель: Федеральное медико-биологическое агентство fmba.gov.ru

Подписано в печать 30.09.2023
Тираж 500 экз. Отпечатано в типографии Print.Formula
www.print-formula.ru

Contents
Содержание

THE EFFECT OF MODERATE AND LOW DOSES OF IONIZING RADIATION ON HIGHER NERVOUS ACTIVITY OF HUMANS AND ANIMALS

Atamanyuk NI ✉

Urals Research Center for Radiation Medicine of Federal Medical and Biological Agency, Chelyabinsk, Russia

According to the available data, the effect of high doses of ionizing radiation on the human central nervous system (CNS) takes form of cognitive dysfunction and increased risk of development of malignant neoplasms. At the same time, there is a growing concern about the possible effects of low, moderate doses of ionizing radiation and chronic irradiation, on cognitive functions, as well as their potential long-term consequences manifesting as neurodegenerative diseases. There is both epidemiological and experimental evidence confirming that low and moderate doses of ionizing radiation affect cognitive abilities. The underlying mechanisms include disruption of normal neurogenesis in the hippocampus, development of long-term sustained neuroinflammation, disorders of synaptic plasticity, energy metabolism, and oxidative status. On the part of CNS, the body is most sensitive to radiation during the period of active formation of the brain. Irradiated at that time, people may suffer consequences thereof for several months and years, or have them manifesting only much later, in old age. Improvement of radiation safety and development of means and ways of prevention and treatment of radiation-induced CNS disorders require further research efforts aimed at establishing causal relationships between chronic exposure to radiation and low-dose irradiation and their adverse effects on the part of CNS in the long term post-exposure.

Keywords: higher nervous activity, central nervous system, cognitive functions, neurogenesis, neuroinflammation, ionizing radiation, low doses, chronic radiation exposure

✉ **Correspondence should be addressed:** Natalia I. Atamanyuk
Vorovskogo, 68A, Chelyabinsk, 454141, Russia; vita_pulhra@mail.ru

Received: 24.06.2023 **Accepted:** 07.08.2023 **Published online:** 25.09.2023

DOI: 10.47183/mes.2023.029

ВЛИЯНИЕ СРЕДНИХ И МАЛЫХ ДОЗ ИОНИЗИРУЮЩЕГО ИЗЛУЧЕНИЯ НА ВЫСШУЮ НЕРВНУЮ ДЕЯТЕЛЬНОСТЬ ЧЕЛОВЕКА И ЖИВОТНЫХ

Н. И. Атаманюк ✉

Уральский научно-практический центр радиационной медицины Федерального медико-биологического агентства, Челябинск, Россия

Данные о влиянии высоких доз ионизирующего излучения на центральную нервную систему человека указывают на развитие когнитивной дисфункции и повышение риска развития злокачественных новообразований. При этом нарастает обеспокоенность по поводу возможного воздействия низких и умеренных доз ионизирующего излучения, действия хронического облучения на когнитивные функции и отдаленные эффекты в виде развития нейродегенеративных заболеваний. Имеются как эпидемиологические, так и экспериментальные свидетельства когнитивных эффектов низких и средних доз ионизирующего излучения. Механизмы, лежащие в их основе, касаются нарушения нормального нейрогенеза в области гиппокампа, развития длительно поддерживающегося нейровоспаления, нарушения синаптической пластичности, энергетического обмена и оксидативного статуса. Наибольшую чувствительность к радиационным эффектам со стороны центральной нервной системы организм проявляет в период активного формирования мозга. Последствия облучения в наиболее чувствительном периоде могут сохраняться в течение нескольких месяцев и лет или же проявиться только со временем, в пожилом возрасте. В целях повышения радиационной безопасности, для разработки средств профилактики и лечения радиационно-индуцированных нарушений со стороны ЦНС дальнейшие исследования должны быть направлены на установление причинно-следственных связей между хроническим радиационным воздействием и облучением в малых дозах и неблагоприятными эффектами со стороны ЦНС в течение длительного периода времени после облучения.

Ключевые слова: высшая нервная деятельность, центральная нервная система, когнитивные функции, нейрогенез, нейровоспаление, ионизирующее излучение, малые дозы, хроническое радиационное воздействие

✉ **Для корреспонденции:** Наталья Игоревна Атаманюк
ул. Воровского, д. 68 А, г. Челябинск, 454141, Россия; vita_pulhra@mail.ru

Статья получена: 24.06.2023 **Статья принята к печати:** 07.08.2023 **Опубликована онлайн:** 25.09.2023

DOI: 10.47183/mes.2023.029

The factors currently shaping the problem of radiation protection of people are the increasingly widespread introduction of nuclear technologies, planning of interplanetary flight programs, sharply increased risk of use of nuclear weapons and "dirty" bombs, need to protect healthy organs and tissues of patients during radiation therapy, and improving availability of nuclear medicine.

Traditionally, brain has been considered a fairly radioresistant organ. However, several animal and human studies [1-3] have presented accumulated data that demonstrates molecular genetic, morphofunctional, physiological changes in the brain, changes in higher nervous activity (mainly cognitive dysfunction, anxiety and depressive disorders) caused by moderate and low doses of radiation [1–3]. The 2012 UNSCEAR report defines doses below 0.1 Gy as low, doses from 0.1 to 1 Gy — moderate, if radiation is sparsely ionizing, and doses above 1 Gy — high [4].

The reports of both ICRP and UNSCEAR [5, 6] analyze reaction of the central nervous system to radiation exposure in the context of medical procedures, radiation accidents or work with ionizing radiation sources, with the considered consequences being higher risk of brain tumors and cognitive dysfunctions. The 2019 Report by the National Council on Radiation Protection & Measurements [7] contains the most complete summary of information about the effect of ionizing radiation on the central nervous system. The primary purpose of this report was to look into all possible aspects of the effect of cosmic radiation on brains and higher nervous activity of astronauts.

Understanding how low doses of ionizing radiation received by the brain affect cognitive and behavioral capabilities and patterns is essential for ensuring human radiation safety in cases of medical exposure, occupational exposure, including that associated with space missions outside the Earth's magnetic

field, as well as radioactive pollution of the environment. The epidemiological and experimental data describing the effect of low doses, the possible chronic exposure threshold value after which radiation begins to compromise functions of the central nervous system, remain quite limited and contradictory. Thus, it is possible to formulate a research problem about the cause-and-effect links between radiation exposure and development of early and long-term adverse effects on the part of the central nervous system (disorders of mental functions, neurodegenerative diseases, brain neoplasms). This review summarizes the currently available scientific data on this problem.

Epidemiological data

Overall, large doses of ionizing radiation received by the brain are an established risk factor promoting development of neoplasms and cognitive impairments. The latter, as a rule, has ties with deficiencies in hippocampus-dependent processes: verbal-semantic and spatial memory, learning, spatial information processing; such impairments develop in the long term after irradiation [8]. The causes of these long-lasting disorders are impairment of neurogenesis and oligodendrogenesis in the subependimal and hippocampal regions; blood-brain barrier deficiency; ablation of capillaries and damage to the microvascular endothelium [9], sustained activation of immunocompetent microglial cells and increased level of proinflammatory cytokines [10].

According to the 118 ICRP report [5], the threshold dose values for development of cognitive disorders in adults are 1–2 Gy, and for children exposed at the age under 18 months it is 0.1 Gy. The effect of low doses of ionizing radiation on young children in terms of subsequent decline of their cognitive capabilities was first shown on a Swedish cohort that received 100–250 mGy in the context of treatment of cutaneous haemangioma [11]; the researchers have proven the dose-dependent learning and logical thinking disorders suffered by the people from that cohort in adult age. Examination of people exposed to radiation at the prenatal stage as a result of contamination of the Techa river has shown that the respective group includes more subjects with non-psychotic mental impairments than the control group, the difference statistically significant. The prevailing disorders were of organic nature, i.e., cognitive and asthenic. The mean red bone marrow dose registered in the exposed group was 0.09 Gy, as calculated for the red bone marrow of a fetus [12]. However, authors of a systematic review [13] that included epidemiological studies published before 2018 have claimed insufficiency of the data to allow a reasoned conclusion about any effect on development of the central nervous system that low and moderate doses of ionizing radiation may have if received during prenatal life, childhood or adolescence, although they acknowledged the limited evidence of relationship between low and moderate doses and decline of the general cognitive and language capabilities.

The question of how ionizing radiation affects the risk of dementia and neurodegenerative disorders remains ambiguous. Examination of a cohort of employees working at the nuclear production cycle of Mayak Production Association (town of Ozersk, Chelyabinsk Region) has uncovered a linear relationship between the incidence of Parkinson's disease and the cumulative dose of gamma radiation, the findings confirmed after adjustment for gender and age [14]. Examination of a cohort of French nuclear power industry workers has shown a statistically significant link between the risk of dementia and Alzheimer's disease and the received dose of ionizing radiation, but authors of the report urge caution in interpretation of these results [15]. In a Japanese cohort of survivors of the Hiroshima and Nagasaki bombings comprised of those who received doses of radiation in childhood (0 to 4 Gy), the decline of neurocognitive functions correlated with age, without an identifiable link to the dose [16]. Another study of the same cohort did not reveal any increase in dementia incidence associated with the exposure to radiation [17]. A 2022 meta-analysis has shown a dose-dependent increase of risk of cerebrovascular diseases and Parkinson's diseases, as well as death therefrom, associated with low and moderate doses received in adulthood [18].

In a study involving Chernobyl nuclear accident liquidators, Loganovsky et al. note high incidence of cerebrovascular diseases, organic psychic and depressive disorders, cognitive impairments and dementia, the numbers climbing up with the dose received; some effects were found to manifest at the dose of 50 mSv and above [19]. Any analysis of data on the effects of radiation on population exposed thereto in the context of a nuclear accident should factor in the stress associated with the very fact of the exposure, which, regardless of the actual excessive background radiation or lack thereof, may up the frequency of psychic disorders [20]. Also, there are some difficulties in establishing causal relationships between radiation and psychoneurological effects in the context of analysis of epidemiological data: firstly, it is important to have a comparable control group (living standard, frequency and quality of medical care) when processing the data describing exposed population; secondly, investigations involving professionals should factor in conditions of health screenings preceding their admittance to work with sources of ionizing radiation; and thirdly, disease diagnosing and symptom interpretation activities should follow uniform standardized approaches.

As for the capability of low and moderate doses of ionizing radiation to increase the risk of neoplasms, a meta-analysis of studies published before 2022 revealed no links between such doses and the risk of CNS tumors in adults [21]. However, a 2022 paper summarizing assessment of risk of cancer and benign CNS tumors after exposure to X and Y rays (regardless of the source) during prenatal period or childhood, the doses being low and moderate, has shown an excessive risk of neoplasms associated with doses below 0.1 Gy, with the threshold value decreasing to 0.02 Gy for those exposed to background radiation from radioactive precipitation or medical equipment while in the mother's womb [22].

Experimental data

The data from experimental animal studies are much more abundant. Such work aims to establish the causal relationships and molecular and cell mechanisms behind the effects of radiation on the CNS. Mice are considered a representative model for investigation of radiation-induced effects on brain and violations of its development when the received dose is clinically significant, although animals cannot be said to allow a full reproduction of the cognitive alterations registered in human beings [23].

In animals, a one-time exposure to ionizing X rays, Y rays, or stream of protons or heavy ions that simulates cosmic radiation, compromises cognitive functions of learning, spatial memory, exploratory activity, and ups the anxiety level [2, 3, 24, 25]. There is a wide range of behavioral tests designed to examine these parameters.

There is a generally accepted concept that puts death of neural stem cells and impaired neurogenesis [26–29],

coupled with microglia's pro-inflammatory activation [26, 30], behind radiation-induced violations of mental functions. The process involves release of pro-inflammatory IL1β, TNFα and IL6 cytokines, increased expression of the genes of CCL2 (macrophage chemoattractant) and growing numbers of $CD68^+$ macrophages [31]. The weakening of the inflammatory response caused by the CCR2 receptor gene mutation supports preservation of the background number of neuronal $BrdU^+$ progenitor cells [31].

Under normal conditions, neurogenesis occurs in three regions of an adult brain: dentate gyrus, subventricular region and cortex cerebelli. It is the response of neuronal progenitor cells to radiation and altered neurogenesis in the hippocampus region that at least contributes to, if not causes, radiation-induced memory disorders and cognitive impairments that persist for some time after exposure. Various animal models were used to study radiation-induced changes in neurogenesis depending on the dose, fractionation regime, time after exposure and age at the time of exposure [27]. A targeted irradiation of the dentate gyrus of newborn mice at the dose of 1 Gy, as opposed to a full-body irradiation at the same dose, leads to alterations in cell differentiation 3 months after exposure (the shares of $BrdU^+/NeuN^+$ cells go down, share of $BrdU^+/GFAP^+$ goes up), and some deterioration of the animals' spatial memory [28].

The most pronounced effects are seen following irradiation during embryonic development or neonatal periods. There are periods of brain development that are critical for its normal maturation. In many mammalian species, this is the time of perinatal development, but in case of mice and rats, such critical period extends to the first 3–4 weeks of life. Mice, in particular, are particularly vulnerable to radiation on days 3 through 10 after birth [29, 32].

One-time moderate dose during embryonic development or neonatal period changed mice's spontaneous behavior in the new environment in their adulthood; these persistent changes indicated compromised ability of mice to integrate sensory information into motor production [26, 32], impaired spatial memory and ability to learn, increased anxiety level [33, 34], altered social behavior [34], modified ability to explore and adjust to a new environment [26, 35]; motor activity and coordination were also disrupted [34]. In different papers, the age of manifestation of such behavioral changes ranged from 4 to 15 months.

Hippocampal neurogenesis defects persist and accompany changes in the cognitive functions that appear in the long term period after exposure [26]. The ratio of pools of maturing neurons changes: in the early stages, the proportion of radial glial-like $GFAP^+$ cells increases and the share of proliferating $PCNA^+$ progenitor cells decreases, followed by a compensatory growth of the $PCNA^+$ cells and progenitor neurogenic type-2 cells $Sox2^+$, which further leads to a drop in the density of mature granule neurons $NeuN^+$ and proliferating $PCNA^+$ cells up to 6 months after exposure [29]. Microglia also becomes more active: the number of $Iba1^+$ cells and $GFAP^+$ astrocytes increases, and their morphology changes; there appear more postsynaptic protein PSD-95 and MAP-2 because of the malfunctioning Rac1-cofilin signaling pathway in the hippocampus and cerebral cortex [26, 29], while the level of tau protein there grows up [35] and the number and complexity of myelinated axons goes down [36]; the density of microvessels changes, and the drop in the activity of most proteins needed for production of ATP disrupts the function of mitochondria [29]. Some evidence suggests that the changes in neurogenesis and neuroinflammation may disappear earlier than the changes in animal behavior [33]. There is also evidence of an opposite situation when the number of activated microglia cells in the hippocampus remains increased and the number of astrocytes decreased in the term of up to 24 months, when behavioral deviations cease to manifest [30].

For most of the described effects, the early-age acute irradiation threshold dose is 0.3–0.5 Gy [32, 34]. However, some changes are induced with lower doses. Acute irradiation at the dose of 0.1 Gy raised the expression of proinflammatory cytokines in the hippocampus [31]. Having received a dose from 0.1 Gy prenatal, at the age of 4–15 weeks mice were more active socially in tests assessing social memory and sociability, and the Morris water maze test revealed dose-dependent changes in behavior strategies that signal of spatial memory disruptions [34]. A dose of 0.1 Gy received by mice on the 10th day after birth caused a small but persistent (registered for 6 months) depletion of the pool of proliferating cells in the dentate gyrus: the number of $Sox2^+$ type-2 cells increased 1 week after irradiation and the number of proliferating $PCNA^+$ cells decreased after 6 months. In case of adult mice, same dose increased the density of mature $NeuN^+$ neurons after 6 months. At the same time, the signs of mitochondrial homeostasis activation were more vivid in the animals irradiated at the age of 10 weeks, while the area of microvessels in the hippocampus of these subjects was found to diminish, which indicates a possible protective effect of a 0.1 Gy dose that depends on the age at the time of exposure [29].

A single 1 Gy dose of Y rays given to 10-days-old mice translated, in their adulthood, into a significantly smaller number of $GFAP^+$ type-1 stem cells with radial glial-like morphology in the subgranular zone of the dentate gyrus, while a dose from 0.5 Gy caused a dose-dependent drop in the proliferating $PCNA^+$ cells, and a dose from 0.1 Gy triggered a dose-dependent decline in the proliferating $Ki67^+$ precursors, which means disruption of neurogenesis in this area of the brain in adulthood [26]. The described changes concerning stem and proliferating cells led to a dose-dependent decrease in the number of mature neurons in dentate gyrus: by 21% for a dose of 0.1 Gy, by 26% for a dose of 0.5 Gy, and by 37% for a dose of 1 Gy [26].

In another study, mice were irradiated while newborn, and examination of proteome of their hippocampus and cerebral cortex 7 months after irradiation revealed a dose-dependent increase in the number of deregulated proteins for the doses from 0.02 to 1 Gy, and the doses of 0.5 and 1 Gy produced different profile of proteins with impaired regulation than lower doses [26].

In the course of 2 years, a one-time exposure of 10-week-old mice to Y rays (doses 0.063 Gy, 0.125 Gy, 0.5 Gy) triggered the following changes in sensorimotor and locomotor parameters: at the age 4 months, the animals that received 0.5 Gy had a decreased acoustic startle response; at the age of 12–18 months, the speed of movement decreased, same as the total distance traveled in the open field test; and a dose of 0.063 Gy, on the contrary, led to a slight improvement in the sensorimotor reaction and exploratory behavior at the age of 18 months [30]. However, only the doses of 0.125 Gy and 0.5 Gy (but not 0.063 Gy) caused manifestation of quantitative and morphological signs of the increased immune activity registered at the age of 24 months. In the cases of mice irradiated at 0.125 and 0.5 Gy, examination of morphology revealed a smaller number of $GFAP^+$ astrocytes in the dentate gyrus, and these astrocytes had fewer endings and nodes, and decreased branch length. A dose of 0.5 Gy increased the number of $Iba1^+$ microglial cells, but the cells had an amoeba-like shape and fewer endings,

nodes, intersections, with shorter branch length. The dose of 0.063 Gy, on the contrary, produced a neuroprotective effect at the 24-month mark: hyper-ramification of microglial cells and astrocytes was noted [30].

In another study, researchers report an opposite situation: they examined mice that received 0.1 Gy while newborn 6 months after irradiation and registered a significant increase in the number of $GFAP^+$ astrocytes in the hippocampus hilus, while larger numbers of $CD11b^+$ cells of activated microglia and greater concentration of pro-inflammatory cytokine TNF in the hippocampus were observed only in the subjects irradiated at 1 Gy [26].

Irradiation with Y rays in the range from 0.05 through 0.5 Gy revealed a dose-dependent change in the number of apoptotic cells, but proliferation arrest of neuroblasts required a threshold dose of 0.2 Gy (and, as the dose increased, the number of $Ki67^+$ cells decreased and the time of proliferation arrest increased), while the dose of 0.5 Gy decreased the proportion of immature Dcx^+ neurons [37]. The dose of 0.01 Gy triggered a slight decrease in the expression of TSPO in the endothelial cells of hippocampus vessels and in the ependymal cells in the short term after irradiation; higher doses (up to 2 Gy) brought no noticeable changes [38].

There are other adverse factors that may play an important role in the combined effect together with the low doses of radiation: for example, a single dose of 0.1–0.2 Gy of ionizing radiation coupled with ketamine in 10-day-old mice led to cognitive impairments in their adulthood, which was not the case for radiation alone [39].

Overall, the results of experimental and epidemiological studies summarized in the review [3] confirm capability of low doses of ionizing radiation to adversely affect cognitive function. It is important to factor in age both at the time of exposure and at the time of examination, since some effects appear immediately after irradiation and gradually fade away, while other effects develop over time.

There are many works investigating the effects of cosmic radiation simulated with heavy particles. One of them has shown the probability of alteration of cognitive functions to be dose-dependent in case of exposure to ^{28}Si or ^{56}Fe with doses ranging from 0.01 to 0.1 Gy [40]. High-energy particles and neutrons radiation exposure was found to cause effects similar to those produced by the Y rays: suppression of neurogenesis in the hippocampus region [41], long term persistence of signs of microglia activation [42], disruption of the synaptic transmission in hippocampus region [43], disruption of the functional links between hippocampus and peripheral cortex [42], decline of the mitochondrial functions and changes in the expression of a number of proteins [44]. As a result, animals that received doses in the range from 0.05 to 0.6 Gy exhibit certain cognitive dysfunctions both in the short and long term periods after irradiation: deteriorating ability to recognize and switch attention, impaired spatial memory, episodic memory, executive function deficiency, increased anxiety level [45]. In some cases, behavioral changes were detected 12–15 months after irradiation [42].

Different cognitive functions are mediated by different brain structures and may have different sensitivity to radiation. For example, irradiation with ^{56}Fe particles enables male C57Bl mice to better solve a hippocampal-dependent task (discrimination learning) without changing the effectiveness for a striatum-dependent task (rule-based learning) [46].

There is much less experimental data on the effects of chronic or fractionated radiation. Most studies involved a single session of acute irradiation, while clinically and environmentally significant situations mainly imply chronic or fractionated exposure.

Mice chronically irradiated with a neutron-photon mixed field at a dose of 0.18 Gy (dose rate — 1 mGy/day) showed decreased excitability of hippocampal neurons and impaired long-term potentiation of hippocampus and cerebral cortex, learning and memory disorders [47], as well as impaired synaptic plasticity in the hippocampus-prefrontal cortex axis [48]. Fractionated X ray irradiation at a cumulative dose of 0.5 Gy makes behavior more anxious and causes changes in motor activity [49], as is the case with acute exposure.

Probably, the effects of chronic and fractionated irradiation in general are also based on the disruption of neurogenesis (as acute irradiation at a dose of 2 Gy or fractionated irradiation at the same cumulative dose) [50], impaired synaptic transmission, decreased number of synapses and changes in the electrophysiological parameters of the hippocampal and cortical neurons [47, 48, 51], as well as activation of microglia [52]. It has been shown that fractionated exposure to low doses of ionizing radiation causes dose-specific changes in the global genomic methylation of different regions of a mouse's brain against the background of changes in the emotional state and increased anxiety, impaired coordination of movements in walking [49]. Compared to fractionated irradiation (20 fractions, 0.1 Gy each), acute irradiation with Y rays at a dose of 2 Gy triggered a more pronounced increase in the number of activated microglia cells and a decrease in the number of neuronal progenitor cells [52]. However, chronic bombardment with heavy particles (doses of 0.4–0.5 Gy) that simulated galactic cosmic radiation, had a more pronounced effect on the change of electrophysiological properties of hippocampal pyramidal cells in mice than acute irradiation [51]. Fractionated exposure to Y rays translated into damage to DNA in the tissues of frontal cortex and cerebellum that increased after each fraction, although in the hippocampal tissue, this indicator has grown only after the first fraction [49].

The available publications contain no data on the experiments designed to assess the effect of chronic or fractionated irradiation at low doses (cumulative dose up to 0.1 Gy). There are confirmed effects of acute irradiation at low doses and the comparable effects of fractionated and acute irradiation at moderate doses, but these do not eliminate the possibility of reaction from the CNS to chronic exposure at low doses. According to the report by UNSCEAR [53], such exposure causes changes in the immune system regulation mechanisms, and one of the described effects of ionizing radiation on CNS is pro-inflammatory activation of microglia. Other known effects of low doses include cellular-level DNA damage, unstable chromosomal aberrations, apoptosis of the most radiosensitive cells [54], which can potentially affect neurogenesis, especially in the critical periods of development of the brain.

Experimental studies have shown that in some cases, gender conditions the effect of exposure: for example, irradiation with 28Si slows neurogenesis in the long term, but this is a male-only effect, females remain unaffected [41]. In a study that simulated acute or chronic galactic radiation, the "object in updated location" test revealed persistent disruptions in formation and reconsolidation of hippocampal-dependent memory in female mice but not in male, while female subjects were better at recognition of the new objects than male, and only the chronically irradiated males showed increased aggressiveness in the tube dominance test [51].

Some experimental data support the hypothesis about the potential capability of ionizing radiation to increase the risk of

neurodegenerative changes. Inadequate chronic activation of microglia is observed both after irradiation and in cases of depression, Alzheimer's disease, Parkinson's disease [55]. Ionizing radiation at low and moderate doses can trigger molecular mechanisms that support development of the Alzheimer's disease [29], such mechanisms associated with oxidative stress, increased number of amyloid plaques in the brain [24], and accumulation of the tau protein [35]. In mice with ApoE deficiency used as a model of Alzheimer's disease, chronic irradiation for 300 days at cumulative doses of 0.3 Gy and 6.0 Gy caused changes in the number of proteins associated with control of synaptic plasticity, calcium-dependent signaling and brain metabolism [56]. However, there were also differences: signaling of the Rac1-cofilin pathway was activated only at a lower dose of 0.1 mg/day, and at the same level of exposure the amount of activated microglia in the hippocampus and expression of TNF and lipid peroxidation decreased. Thus, several molecular targets for low dose chronic radiation overlap with those in Alzheimer's pathology [56].

CONCLUSION

Currently, there is an extensive amount of information about the effect of ionizing radiation on the brain and higher nervous activity. High doses of ionizing radiation are an established risk factor for cognitive impairment, but the results of epidemiological studies assessing the effect of moderate and low doses on the human CNS are ambiguous.

Experimental animal studies have revealed such effects of irradiation as disruption of the learning and memory functions, increased anxiety level, and locomotion disorders. It has been established that the main causes of development of radiation-induced effects on the part of the CNS upon exposure to sparsely ionizing radiation at doses above 0.5 Gy are violation of normal neurogenesis and suppression of proliferation of neuronal stem cells, as well as pro-inflammatory activation of microglia. Other identified effects include violation of the blood-brain barrier permeability, changes in the synaptic transmission, balance disorders of neurotransmitters, etc. Active stages of brain formation during intrauterine and early postnatal development are the periods when ionizing radiation can do most damage. Then, the threshold dose level for acute exposure to Y rays is 0.2–0.3 Gy.

There are significantly less data on the effects of low doses of radiation and effects of fractionated and chronic exposure. The available papers show that acute irradiation at doses of about 0.1 Gy can have a multidirectional effect, producing both mild adverse effects on higher nervous activity and the brain, and a neuroprotective effect, depending on the age at the time of exposure, time after exposure and other factors. Fractionated X ray irradiation at the doses from 0.5 to 2 Gy can also trigger changes in the higher nervous activity; as for the potential effects of prolonged exposure to low dose ionizing radiation, there are no experimental data.

For the purposes of improving radiation safety and development of pathogenetic means of prevention and treatment of radiation-induced CNS disorders, further research efforts should be aimed at studying chronic exposure and assessment of both the functions of the higher nervous activity and morphofunctional indicators of the brain, as well as establishing causal relationships between chronic exposure and its adverse effects on the part of CNS in the long term post-exposure.

References

1. Kovalchuk A, Kolb B. Low dose radiation effects on the brain — from mechanisms and behavioral outcomes to mitigation strategies. Cell Cycle. 2017; 16 (13): 1266–70. PubMed PMID: 28656797.
2. Britten RA, Wellman LL, Sanford LD. Progressive increase in the complexity and translatability of rodent testing to assess space-radiation induced cognitive impairment. Neurosci Biobehav Rev. 2021; 126: 159–74. PubMed PMID: 33766676.
3. Pasqual E, Boussin F, Bazyka D, Nordenskjold A, Yamada M, Ozasa K, et al. Cognitive effects of low dose of ionizing radiation — Lessons learned and research gaps from epidemiological and biological studies. Environ Int. 2021; 147: 106295. PubMed PMID: 33341586.
4. Sources, effects and risks of ionizing radiation. UNSCEAR 2012 Report. United Nations sales publication E.16.IX.1. 2015. Available from: https://www.unscear.org/docs/reports/2012/UNSCEAR2012Report_15-08936_eBook_website.pdf.
5. Stewart FA, Akleyev AV, Hauer-Jensen M, Hendry JH, Kleiman NJ, Macvittie TJ, et al. ICRP publication 118: ICRP statement on tissue reactions and early and late effects of radiation in normal tissues and organs--threshold doses for tissue reactions in a radiation protection context. Ann ICRP. 2012; (1-2): 1–322. DOI: 10.1016/j.icrp.2012.02.001.
6. Sources, effects and risks of ionizing radiation. Volume II: Scientific annex B. UNSCEAR 2013 Report. United Nations sales publication E.14.IX.2. 2013. Available from: https://www.unscear.org/docs/publications/2013/UNSCEAR_2013_Report_Vol.II.pdf.
7. Report № 183. Radiation exposure in space and the potential for central nervous system effects: Phase II. 2019. Available from: https://www.researchgate.net/publication/337440807_Radiation_Exposure_in_Space_and_the_Potential_for_Central_Nervous_System_Effects_Phase_II
8. Tanguturi SK, Alexander BM. Neurologic complications of radiation therapy. Neurol Clin. 2018; 36 (3): 599–625. PubMed PMID: 30072073.
9. Gorbunov NV, Kiang JG. brain damage and patterns of neurovascular disorder after ionizing irradiation. Complications in radiotherapy and radiation combined injury. Radiat Res. 2021; 196 (1): 1–16. PubMed PMID: 33979447.
10. Sultana N, Sun C, Katsube T, Wang B. Biomarkers of brain damage induced by radiotherapy. dose response. 2020; 18 (3): 1559325820938279. PubMed PMID: 32694960.
11. Hall P, Adami HO, Trichopoulos D, Pedersen NL, Lagiou P, Ekbom A et al. Effect of low doses of ionising radiation in infancy on cognitive function in adulthood: Swedish population based cohort study. BMJ. 2004; 328 (7430): 19. PubMed PMID.
12. Burtovaya EYu, Kantina TEh, Belova MV, Akleev AV. Kognitivnye narusheniya u lic, podvergshihsya radiacionnomu vozdejstviyu v period prenatal'nogo razvitiya. Zhurnal nevrologii i psihiatrii im. C. C. Korsakova. 2015; 115 (4): 20–23. Russian.
13. Pasqual E, Bosch de Basea M, López-Vicente M, Thierry-Chef I, Cardis E. Neurodevelopmental effects of low dose ionizing radiation exposure: A systematic review of the epidemiological evidence. Environ Int. 2020; 136: 105371. PubMed PMID: 32007921.
14. Azizova TV, Bannikova MV, Grigoryeva ES, Rybkina VL, Hamada N. Occupational exposure to chronic ionizing radiation increases risk of Parkinson's disease incidence in Russian Mayak workers. Int J Epidemiol. 2020; 49 (2): 435–47. PubMed PMID: 31722376.
15. Laurent O, Samson E, Caër-Lorho S, Fournier L, Laurier D, Leuraud K. Updated Mortality Analysis of SELTINE, the French Cohort of Nuclear Workers, 1968–2014. Cancers (Basel). 2022; 15 (1): 79. PubMed PMID: 36612076.
16. Ishihara K, Kato N, Misumi M, Kitamura H, Hida A, Yamada M. Radiation effects on late-life neurocognitive function in childhood atomic bomb survivors: a radiation effects research foundation

adult health study. Radiat Res. 2022; 197 (4): 403–7. PubMed PMID: 35042238.
17. Kinoshita H, Tanaka K, Nakao R, Iso F, Honda S, Tanaka G, et al. Comparison of mental cognitive function of A-bomb survivors and non-A-bomb survivors in Nagasaki. Psychiatry Clin Neurosci. 2019; 73 (9): 594. PubMed PMID: 31206900.
18. Lopes J, Leuraud K, Klokov D, Durand C, Bernier MO, Baudin C. Risk of developing non-cancerous central nervous system diseases due to ionizing radiation exposure during adulthood: systematic review and meta-analyses. Brain Sci. 2022; 12 (8): 984. PubMed PMID: 35892428.
19. Loganovsky K, Marazziti D. Mental health and neuropsychiatric aftermath 35 years after the chernobyl catastrophe: current state and future perspectives. Clin Neuropsychiatry. 2021; 18 (2): 101–6. PubMed PMID.
20. Collett G, Craenen K, Young W, Gilhooly M, Anderson RM. The psychological consequences of (perceived) ionizing radiation exposure: a review on its role in radiation-induced cognitive dysfunction. Int J Radiat Biol. 2020; 96 (9): 1104–18. PubMed PMID: 32716221.
21. Lopes J, Baudin C, Leuraud K, Klokov D, Bernier MO. Ionizing radiation exposure during adulthood and risk of developing central nervous system tumors: systematic review and meta-analysis. Sci Rep. 2022; 12 (1): 16209. PubMed PMID: 36171442.
22. Little MP, Wakeford R, Bouffler SD, Abalo K, Hauptmann M, Hamada N, et al. Review of the risk of cancer following low and moderate doses of sparsely ionising radiation received in early life in groups with individually estimated doses. Environ Int. 2022; 159: 106983. PubMed PMID.
23. Perez WD, Perez-Torres CJ. Neurocognitive and radiological changes after cranial radiation therapy in humans and rodents: a systematic review. Int J Radiat Biol. 2023; 99 (2): 119–37. PubMed PMID: 35511499.
24. Severyukhin YS, Lalkovičová M, Utina DM, Lyakhova KN, Kolesnikova IA, Ermolaeva ME, et al. Comparative analysis of behavioral reactions and morphological changes in the rat brain after exposure to ionizing radiation with different physical characteristics. Cell Mol Neurobiol. 2023; 43 (1): 339–53. PubMed PMID: 34982311.
25. Njamnshi AK, Ahidjo N, Ngarka L, Nfor LN, Mengnjo MK, Njamnshi WY, et al. Characterization of the cognitive and motor changes revealed by the elevated plus maze in an experimental rat model of radiation-induced brain injury. Adv Biomed Res. 2020; 9: 72. PubMed PMID: 33816391.
26. Kempf SJ, Casciati A, Buratovic S, Janik D, von Toerne C, Ueffing M, et al. The cognitive defects of neonatally irradiated mice are accompanied by changed synaptic plasticity, adult neurogenesis and neuroinflammation. Mol Neurodegener. 2014; 9: 57. PubMed PMID.
27. Cacao E, Kapukotuwa S, Cucinotta FA. Modeling reveals the dependence of hippocampal neurogenesis radiosensitivity on age and strain of rats. Front Neurosci. 2018; 12: 980. PubMed PMID.
28. Serrano C, Dos Santos M, Kereselidze D, Beugnies L, Lestaevel P, Poirier R, et al. Targeted dorsal dentate gyrus or whole brain irradiation in juvenile mice differently affects spatial memory and adult hippocampal neurogenesis. Biology (Basel). 2021; 10 (3): 192. PubMed PMID: 33806303.
29. Casciati A, Dobos K, Antonelli F, Benedek A, Kempf SJ, Bellés M, et al. Age-related effects of X-ray irradiation on mouse hippocampus. Oncotarget. 2016; 7 (19): 28040–58. PubMed PMID: 27057631.
30. Ung MC, Garrett L, Dalke C, Leitner V, Dragosa D, Hladik D, et al. Dose-dependent long-term effects of a single radiation event on behaviour and glial cells. Int J Radiat Biol. 2021; 97 (2): 156–69. PubMed PMID: 33264576.
31. Acharya MM, Patel NH, Craver BM, Tran KK, Giedzinski E, Tseng BP, et al. Consequences of low dose ionizing radiation exposure on the hippocampal microenvironment. PLoS One. 2015; 10 (6): e0128316. PubMed PMID: 26042591.
32. Eriksson P, Buratovic S, Fredriksson A, Stenerlöw B, Sundell-Bergman S. Neonatal exposure to whole body ionizing radiation induces adult neurobehavioural defects: Critical period, dose--response effects and strain and sex comparison. Behav Brain Res. 2016; 304: 11–9. PubMed PMID: 26876140.
33. Liu Y, Ma H, Wang Y, Ren B, Liu L, Sun A, et al. Neonatal exposure to low-dose X-ray causes behavioral defects and abnormal hippocampal development in mice. IUBMB Life. 2023; 75 (6): 530–47. PubMed PMID: 36629313.
34. Verreet T, Rangarajan JR, Quintens R, Verslegers M, Lo AC, Govaerts K, et al. Persistent Impact of in utero irradiation on mouse brain structure and function characterized by mr imaging and behavioral analysis. Front Behav Neurosci. 2016; 10: 83. PubMed PMID: 27199692.
35. Buratovic S, Stenerlöw B, Fredriksson A, Sundell-Bergman S, Viberg H, Eriksson P. Neonatal exposure to a moderate dose of ionizing radiation causes behavioural defects and altered levels of tau protein in mice. Neurotoxicology. 2014; 45: 48–55. PubMed PMID: 25265567.
36. Mouton L, Etienne O, Feat-Vetel J, Barrière DA, Pérès EA, Boumezbeur F, et al. Noninvasive assessment of neurodevelopmental disorders after in utero irradiation in mice: an in vivo anatomical and diffusion mri study. Radiat Res. 2021; 195 (6): 568–83. PubMed PMID: 33826744.
37. Barazzuol L, Hopkins SR, Ju L, Jeggo PA. Distinct response of adult neural stem cells to low versus high dose ionising radiation. DNA Repair (Amst). 2019; 76: 70–75. PubMed PMID: 30822688.
38. Betlazar C, Middleton RJ, Howell N, Storer B, Davis E, Davies J, et al. Mitochondrial Translocator protein (TSPO) expression in the brain after whole body gamma irradiation. Front Cell Dev Biol. 2021; 9: 715444. PubMed PMID: 34760884.
39. Hladik D, Buratovic S, Von Toerne C, Azimzadeh O, Subedi P, Philipp J, et al. Combined Treatment with low-dose ionizing radiation and ketamine induces adverse changes in CA1 neuronal structure in male murine hippocampi. Int J Mol Sci. 2019; 20 (23): 6103. PubMed PMID: 31817026.
40. Matar M, Gokoglu SA, Prelich MT, Gallo CA, Iqbal AK, Britten RA, et al. Machine Learning models to predict cognitive impairment of rodents subjected to space radiation. Front Syst Neurosci. 2021; 15: 713131. PubMed PMID: 34588962.
41. Whoolery CW, Walker AK, Richardson DR, Lucero MJ, Reynolds RP, Beddow DH, et al. Whole-Body exposure to 28Si-Radiation dose-dependently disrupts dentate gyrus neurogenesis and proliferation in the short term and new neuron survival and contextual fear conditioning in the long term. Radiat Res. 2017; 188 (5): 532–51. PubMed PMID: 28945526.
42. Parihar VK, Maroso M, Syage A, Allen BD, Angulo MC, Soltesz I, et al. Persistent nature of alterations in cognition and neuronal circuit excitability after exposure to simulated cosmic radiation in mice. Exp Neurol. 2018; 305: 44–55. PubMed PMID: 29540322.
43. Klein PM, Alaghband Y, Doan NL, Ru N, Drayson OGG, Baulch JE, et al. Acute, Low-dose neutron exposures adversely impact central nervous system function. Int J Mol Sci. 2021; 22 (16): 9020. PubMed PMID: 34445726.
44. Laiakis EC, Pinheiro M, Nguyen T, Nguyen H, Beheshti A, Dutta SM, et al. Quantitative proteomic analytic approaches to identify metabolic changes in the medial prefrontal cortex of rats exposed to space radiation. Front Physiol. 2022; 13: 971282. PubMed PMID: 36091373.
45. Britten RA, Jewell JS, Duncan VD, Hadley MM, Macadat E, Musto AE, et al. Impaired attentional set-shifting performance after exposure to 5 cgy of 600 mev/n 28si particles. Radiat Res. 2018; 189 (3): 273–82. PubMed PMID: 29309264.
46. Soler I, Yun S, Reynolds RP, Whoolery CW, Tran FH, Kumar PL, et al. Multi-domain touchscreen-based cognitive assessment of C57BL/6J female mice shows whole-body exposure to 56Fe particle space radiation in maturity improves discrimination learning yet impairs stimulus-response rule-based habit learning. Front Behav Neurosci. 2021; 15: 722780. PubMed PMID: 34707486.
47. Acharya MM, Baulch JE, Klein PM, Baddour AAD, Apodaca LA, Kramár EA, et al. New Concerns for neurocognitive function during deep space exposures to chronic, low dose-rate, neutron radiation. eNeuro. 2019; 6 (4): ENEURO.0094-19.2019. PubMed PMID: 31383727.
48. Krishnan B, Natarajan C, Bourne KZ, Alikhani L, Wang J, Sowa A, et al. Chronic low dose neutron exposure results in altered neurotransmission properties of the hippocampus-prefrontal cortex axis in both mice and rats. Int J Mol Sci. 2021; 22 (7): 3668. PubMed PMID: 33915974.

49. Koturbash I, Jadavji NM, Kutanzi K, Rodriguez-Juarez R, Kogosov D, Metz GAS, et al. Fractionated low-dose exposure to ionizing radiation leads to DNA damage, epigenetic dysregulation, and behavioral impairment. Environ Epigenet. 2017; 2 (4): dvw025. PubMed PMID: 29492301.
50. Peng S, Yang B, Duan MY, Liu ZW, Wang WF, Zhang XZ, et al. The disparity of impairment of neurogenesis and cognition after acute or fractionated radiation exposure in adolescent BALB/c mice. Dose Response. 2019; 17 (1): 1559325818822574. PubMed PMID: 30670940.
51. Alaghband Y, Klein PM, Kramár EA, Cranston MN, Perry BC, Shelerud LM, et al. Galactic cosmic radiation exposure causes multifaceted neurocognitive impairments. Cell Mol Life Sci. 2023; 80 (1): 29. PubMed PMID: 36607431.
52. Schmal Z, Rübe CE. Region-specific effects of fractionated low-dose versus single-dose radiation on hippocampal neurogenesis and neuroinflammation. Cancers (Basel). 2022; 14 (22): 5477. PubMed PMID: 36428572.
53. Biological Mechanisms of Radiation Actions at Low doses. A white paper to guide the Scientific Committee's future programme of work. United Nations Scientific Committee on the Effects of Atomic Radiation, United Nations. 2012. Available from: https://www.unscear.org/docs/reports/Biological_mechanisms_WP_12-57831.pdf.
54. Koterov AN, Vajson AA. Biologicheskie i medicinskie ehffekty izlucheniya s nizkoj LPEh dlya razlichnyh diapazonov doz. Medicinskaya radiologiya i radiacionnaya bezopasnost'. 2015; 60 (3): 5–31.
55. Boyd A, Byrne S, Middleton RJ, Banati RB, Liu GJ. Control of neuroinflammation through radiation-induced microglial changes. Cells. 2021; 10 (9): 2381. PubMed PMID: 34572030.
56. Kempf SJ, Janik D, Barjaktarovic Z, Braga-Tanaka I 3rd, Tanaka S, Neff F, et al. Chronic low-dose-rate ionising radiation affects the hippocampal phosphoproteome in the ApoE-/- Alzheimer's mouse model. Oncotarget. 2016; 7 (44): 71817–32. PubMed PMID: 27708245.

Литература

1. Kovalchuk A, Kolb B. Low dose radiation effects on the brain — from mechanisms and behavioral outcomes to mitigation strategies. Cell Cycle. 2017; 16 (13): 1266–70. PubMed PMID: 28656797.
2. Britten RA, Wellman LL, Sanford LD. Progressive increase in the complexity and translatability of rodent testing to assess space-radiation induced cognitive impairment. Neurosci Biobehav Rev. 2021; 126: 159–74. PubMed PMID: 33766676.
3. Pasqual E, Boussin F, Bazyka D, Nordenskjold A, Yamada M, Ozasa K, et al. Cognitive effects of low dose of ionizing radiation — Lessons learned and research gaps from epidemiological and biological studies. Environ Int. 2021; 147: 106295. PubMed PMID: 33341586.
4. Sources, effects and risks of ionizing radiation. UNSCEAR 2012 Report. United Nations sales publication E.16.IX.1. 2015. Available from: https://www.unscear.org/docs/reports/2012/UNSCEAR2012Report_15-08936_eBook_website.pdf.
5. Stewart FA, Akleyev AV, Hauer-Jensen M, Hendry JH, Kleiman NJ, Macvittie TJ, et al. ICRP publication 118: ICRP statement on tissue reactions and early and late effects of radiation in normal tissues and organs--threshold doses for tissue reactions in a radiation protection context. Ann ICRP. 2012; (1-2): 1–322. DOI: 10.1016/j.icrp.2012.02.001.
6. Sources, effects and risks of ionizing radiation. Volume II: Scientific annex B. UNSCEAR 2013 Report. United Nations sales publication E.14.IX.2. 2013. Available from: https://www.unscear.org/docs/publications/2013/UNSCEAR_2013_Report_Vol.II.pdf.
7. Report № 183. Radiation exposure in space and the potential for central nervous system effects: Phase II. 2019. Available from: https://www.researchgate.net/publication/337440807_Radiation_Exposure_in_Space_and_the_Potential_for_Central_Nervous_System_Effects_Phase_II
8. Tanguturi SK, Alexander BM. Neurologic complications of radiation therapy. Neurol Clin. 2018; 36 (3): 599–625. PubMed PMID: 30072073.
9. Gorbunov NV, Kiang JG. brain damage and patterns of neurovascular disorder after ionizing irradiation. Complications in radiotherapy and radiation combined injury. Radiat Res. 2021; 196 (1): 1–16. PubMed PMID: 33979447.
10. Sultana N, Sun C, Katsube T, Wang B. Biomarkers of brain damage induced by radiotherapy. dose response. 2020; 18 (3): 1559325820938279. PubMed PMID: 32694960.
11. Hall P, Adami HO, Trichopoulos D, Pedersen NL, Lagiou P, Ekbom A et al. Effect of low doses of ionising radiation in infancy on cognitive function in adulthood: Swedish population based cohort study. BMJ. 2004; 328 (7430): 19. PubMed PMID.
12. Буртовая Е. Ю., Кантина Т. Э., Белова М. В., Аклеев А. В. Когнитивные нарушения у лиц, подвергшихся радиационному воздействию в период пренатального развития. Журнал неврологии и психиатрии им. С. С. Корсакова. 2015; 115 (4): 20–23.
13. Pasqual E, Bosch de Basea M, López-Vicente M, Thierry-Chef I, Cardis E. Neurodevelopmental effects of low dose ionizing radiation exposure: A systematic review of the epidemiological evidence. Environ Int. 2020; 136: 105371. PubMed PMID: 32007921.
14. Azizova TV, Bannikova MV, Grigoryeva ES, Rybkina VL, Hamada N. Occupational exposure to chronic ionizing radiation increases risk of Parkinson's disease incidence in Russian Mayak workers. Int J Epidemiol. 2020; 49 (2): 435–47. PubMed PMID: 31722376.
15. Laurent O, Samson E, Caër-Lorho S, Fournier L, Laurier D, Leuraud K. Updated Mortality Analysis of SELTINE, the French Cohort of Nuclear Workers, 1968–2014. Cancers (Basel). 2022; 15 (1): 79. PubMed PMID: 36612076.
16. Ishihara K, Kato N, Misumi M, Kitamura H, Hida A, Yamada M. Radiation effects on late-life neurocognitive function in childhood atomic bomb survivors: a radiation effects research foundation adult health study. Radiat Res. 2022; 197 (4): 403–7. PubMed PMID: 35042238.
17. Kinoshita H, Tanaka K, Nakao R, Iso F, Honda S, Tanaka G, et al. Comparison of mental cognitive function of A-bomb survivors and non-A-bomb survivors in Nagasaki. Psychiatry Clin Neurosci. 2019; 73 (9): 594. PubMed PMID: 31206900.
18. Lopes J, Leuraud K, Klokov D, Durand C, Bernier MO, Baudin C. Risk of developing non-cancerous central nervous system diseases due to ionizing radiation exposure during adulthood: systematic review and meta-analyses. Brain Sci. 2022; 12 (8): 984. PubMed PMID: 35892428.
19. Loganovsky K, Marazziti D. Mental health and neuropsychiatric aftermath 35 years after the chernobyl catastrophe: current state and future perspectives. Clin Neuropsychiatry. 2021; 18 (2): 101–6. PubMed PMID.
20. Collett G, Craenen K, Young W, Gilhooly M, Anderson RM. The psychological consequences of (perceived) ionizing radiation exposure: a review on its role in radiation-induced cognitive dysfunction. Int J Radiat Biol. 2020; 96 (9): 1104–18. PubMed PMID: 32716221.
21. Lopes J, Baudin C, Leuraud K, Klokov D, Bernier MO. Ionizing radiation exposure during adulthood and risk of developing central nervous system tumors: systematic review and meta-analysis. Sci Rep. 2022; 12 (1): 16209. PubMed PMID: 36171442.
22. Little MP, Wakeford R, Bouffler SD, Abalo K, Hauptmann M, Hamada N, et al. Review of the risk of cancer following low and moderate doses of sparsely ionising radiation received in early life in groups with individually estimated doses. Environ Int. 2022; 159: 106983. PubMed PMID.
23. Perez WD, Perez-Torres CJ. Neurocognitive and radiological changes after cranial radiation therapy in humans and rodents: a systematic review. Int J Radiat Biol. 2023; 99 (2): 119–37. PubMed PMID: 35511499.
24. Severyukhin YS, Lalkovičová M, Utina DM, Lyakhova KN, Kolesnikova IA, Ermolaeva ME, et al. Comparative analysis of behavioral reactions and morphological changes in the rat

brain after exposure to ionizing radiation with different physical characteristics. Cell Mol Neurobiol. 2023; 43 (1): 339–53. PubMed PMID: 34982311.
25. Njamnshi AK, Ahidjo N, Ngarka L, Nfor LN, Mengnjo MK, Njamnshi WY, et al. Characterization of the cognitive and motor changes revealed by the elevated plus maze in an experimental rat model of radiation-induced brain injury. Adv Biomed Res. 2020; 9: 72. PubMed PMID: 33816391.
26. Kempf SJ, Casciati A, Buratovic S, Janik D, von Toerne C, Ueffing M, et al. The cognitive defects of neonatally irradiated mice are accompanied by changed synaptic plasticity, adult neurogenesis and neuroinflammation. Mol Neurodegener. 2014; 9: 57. PubMed PMID.
27. Cacao E, Kapukotuwa S, Cucinotta FA. Modeling reveals the dependence of hippocampal neurogenesis radiosensitivity on age and strain of rats. Front Neurosci. 2018; 12: 980. PubMed PMID.
28. Serrano C, Dos Santos M, Kereselidze D, Beugnies L, Lestaevel P, Poirier R, et al. Targeted dorsal dentate gyrus or whole brain irradiation in juvenile mice differently affects spatial memory and adult hippocampal neurogenesis. Biology (Basel). 2021; 10 (3): 192. PubMed PMID: 33806303.
29. Casciati A, Dobos K, Antonelli F, Benedek A, Kempf SJ, Bellés M, et al. Age-related effects of X-ray irradiation on mouse hippocampus. Oncotarget. 2016; 7 (19): 28040–58. PubMed PMID: 27057631.
30. Ung MC, Garrett L, Dalke C, Leitner V, Dragosa D, Hladik D, et al. Dose-dependent long-term effects of a single radiation event on behaviour and glial cells. Int J Radiat Biol. 2021; 97 (2): 156–69. PubMed PMID: 33264576.
31. Acharya MM, Patel NH, Craver BM, Tran KK, Giedzinski E, Tseng BP, et al. Consequences of low dose ionizing radiation exposure on the hippocampal microenvironment. PLoS One. 2015; 10 (6): e0128316. PubMed PMID: 26042591.
32. Eriksson P, Buratovic S, Fredriksson A, Stenerlöw B, Sundell-Bergman S. Neonatal exposure to whole body ionizing radiation induces adult neurobehavioural defects: Critical period, dose--response effects and strain and sex comparison. Behav Brain Res. 2016; 304: 11–9. PubMed PMID: 26876140.
33. Liu Y, Ma H, Wang Y, Ren B, Liu L, Sun A, et al. Neonatal exposure to low-dose X-ray causes behavioral defects and abnormal hippocampal development in mice. IUBMB Life. 2023; 75 (6): 530–47. PubMed PMID: 36629313.
34. Verreet T, Rangarajan JR, Quintens R, Verslegers M, Lo AC, Govaerts K, et al. Persistent Impact of in utero irradiation on mouse brain structure and function characterized by mr imaging and behavioral analysis. Front Behav Neurosci. 2016; 10: 83. PubMed PMID: 27199692.
35. Buratovic S, Stenerlöw B, Fredriksson A, Sundell-Bergman S, Viberg H, Eriksson P. Neonatal exposure to a moderate dose of ionizing radiation causes behavioural defects and altered levels of tau protein in mice. Neurotoxicology. 2014; 45: 48–55. PubMed PMID: 25265567.
36. Mouton L, Etienne O, Feat-Vetel J, Barrière DA, Pérès EA, Boumezbeur F, et al. Noninvasive assessment of neurodevelopmental disorders after in utero irradiation in mice: an in vivo anatomical and diffusion mri study. Radiat Res. 2021; 195 (6): 568–83. PubMed PMID: 33826744.
37. Barazzuol L, Hopkins SR, Ju L, Jeggo PA. Distinct response of adult neural stem cells to low versus high dose ionising radiation. DNA Repair (Amst). 2019; 76: 70–75. PubMed PMID: 30822688.
38. Betlazar C, Middleton RJ, Howell N, Storer B, Davis E, Davies J, et al. Mitochondrial Translocator protein (TSPO) expression in the brain after whole body gamma irradiation. Front Cell Dev Biol. 2021; 9: 715444. PubMed PMID: 34760884.
39. Hladik D, Buratovic S, Von Toerne C, Azimzadeh O, Subedi P, Philipp J, et al. Combined Treatment with low-dose ionizing radiation and ketamine induces adverse changes in CA1 neuronal structure in male murine hippocampi. Int J Mol Sci. 2019; 20 (23): 6103. PubMed PMID: 31817026.
40. Matar M, Gokoglu SA, Prelich MT, Gallo CA, Iqbal AK, Britten RA, et al. Machine Learning models to predict cognitive impairment of rodents subjected to space radiation. Front Syst Neurosci. 2021; 15: 713131. PubMed PMID: 34588962.
41. Whoolery CW, Walker AK, Richardson DR, Lucero MJ, Reynolds RP, Beddow DH, et al. Whole-Body exposure to 28Si-Radiation dose-dependently disrupts dentate gyrus neurogenesis and proliferation in the short term and new neuron survival and contextual fear conditioning in the long term. Radiat Res. 2017; 188 (5): 532–51. PubMed PMID: 28945526.
42. Parihar VK, Maroso M, Syage A, Allen BD, Angulo MC, Soltesz I, et al. Persistent nature of alterations in cognition and neuronal circuit excitability after exposure to simulated cosmic radiation in mice. Exp Neurol. 2018; 305: 44–55. PubMed PMID: 29540322.
43. Klein PM, Alaghband Y, Doan NL, Ru N, Drayson OGG, Baulch JE, et al. Acute, Low-dose neutron exposures adversely impact central nervous system function. Int J Mol Sci. 2021; 22 (16): 9020. PubMed PMID: 34445726.
44. Laiakis EC, Pinheiro M, Nguyen T, Nguyen H, Beheshti A, Dutta SM, et al. Quantitative proteomic analytic approaches to identify metabolic changes in the medial prefrontal cortex of rats exposed to space radiation. Front Physiol. 2022; 13: 971282. PubMed PMID: 36091373.
45. Britten RA, Jewell JS, Duncan VD, Hadley MM, Macadat E, Musto AE, et al. Impaired attentional set-shifting performance after exposure to 5 cgy of 600 mev/n 28si particles. Radiat Res. 2018; 189 (3): 273–82. PubMed PMID: 29309264.
46. Soler I, Yun S, Reynolds RP, Whoolery CW, Tran FH, Kumar PL, et al. Multi-domain touchscreen-based cognitive assessment of C57BL/6J female mice shows whole-body exposure to 56Fe particle space radiation in maturity improves discrimination learning yet impairs stimulus-response rule-based habit learning. Front Behav Neurosci. 2021; 15: 722780. PubMed PMID: 34707486.
47. Acharya MM, Baulch JE, Klein PM, Baddour AAD, Apodaca LA, Kramár EA, et al. New Concerns for neurocognitive function during deep space exposures to chronic, low dose-rate, neutron radiation. eNeuro. 2019; 6 (4): ENEURO.0094-19.2019. PubMed PMID: 31383727.
48. Krishnan B, Natarajan C, Bourne KZ, Alikhani L, Wang J, Sowa A, et al. Chronic low dose neutron exposure results in altered neurotransmission properties of the hippocampus-prefrontal cortex axis in both mice and rats. Int J Mol Sci. 2021; 22 (7): 3668. PubMed PMID: 33915974.
49. Koturbash I, Jadavji NM, Kutanzi K, Rodriguez-Juarez R, Kogosov D, Metz GAS, et al. Fractionated low-dose exposure to ionizing radiation leads to DNA damage, epigenetic dysregulation, and behavioral impairment. Environ Epigenet. 2017; 2 (4): dvw025. PubMed PMID: 29492301.
50. Peng S, Yang B, Duan MY, Liu ZW, Wang WF, Zhang XZ, et al. The disparity of impairment of neurogenesis and cognition after acute or fractionated radiation exposure in adolescent BALB/c mice. Dose Response. 2019; 17 (1): 1559325818822574. PubMed PMID: 30670940.
51. Alaghband Y, Klein PM, Kramár EA, Cranston MN, Perry BC, Shelerud LM, et al. Galactic cosmic radiation exposure causes multifaceted neurocognitive impairments. Cell Mol Life Sci. 2023; 80 (1): 29. PubMed PMID: 36607431.
52. Schmal Z, Rübe CE. Region-specific effects of fractionated low-dose versus single-dose radiation on hippocampal neurogenesis and neuroinflammation. Cancers (Basel). 2022; 14 (22): 5477. PubMed PMID: 36428572.
53. Biological Mechanisms of Radiation Actions at Low doses. A white paper to guide the Scientific Committee's future programme of work. United Nations Scientific Committee on the Effects of Atomic Radiation, United Nations. 2012. Available from: https://www.unscear.org/docs/reports/Biological_mechanisms_WP_12-57831.pdf.
54. Котеров А. Н., Вайсон А. А. Биологические и медицинские эффекты излучения с низкой ЛПЭ для различных диапазонов доз. Медицинская радиология и радиационная безопасность. 2015; 60 (3): 5–31.
55. Boyd A, Byrne S, Middleton RJ, Banati RB, Liu GJ. Control of neuroinflammation through radiation-induced microglial changes. Cells. 2021; 10 (9): 2381. PubMed PMID: 34572030.
56. Kempf SJ, Janik D, Barjaktarovic Z, Braga-Tanaka I 3rd, Tanaka S, Neff F, et al. Chronic low-dose-rate ionising radiation affects the hippocampal phosphoproteome in the ApoE-/- Alzheimer's mouse model. Oncotarget. 2016; 7 (44): 71817–32. PubMed PMID: 27708245.

CURRENT UNDERSTANDING OF EPIDEMIOLOGY AND PATHOGENESIS OF MULTISYSTEM INFLAMMATORY SYNDROME ASSOCIATED WITH SARS-COV-2 IN CHILDREN

Konstantinova YuE[1]✉, Vilnitz AA[1,2], Bekhtereva MK[1,2], Alekseeva LA[1], Glotov OS[1], Egorova ES[1]

[1] Pediatric Research and Clinical Center for Infectious Diseases of Federal Medical Biological Agency, Saint-Petersburg, Russia

[2] Saint Petersburg State Pediatric Medical University, Saint-Petersburg, Russia

The review is dedicated to matters related to epidemiology and pathogenesis of multisystem inflammatory syndrome associated with SARS-CoV-2 in children (MIS-C). The majority of the reviewed reports are focused on immunopathogenesis of the disease. The causes of the syndrome related to the features of the virus are listed in the paper, the association with circulating variants is described. The role of the SARS-CoV-2 surface protein as superantigen is considered. The literature data on the likelihood of MIS-C development according to the antibody-dependent enhancement pattern are discussed. The factors of cellular and humoral immune response contributing to hyperinflammation are addressed. Sporadic papers describing genetic mutations that can play a certain role in the MIS-C pathogenesis are provided. Furthermore, the association of vaccination against novel coronavirus infection with the likelihood of MIS-C in vaccinated individuals is discussed.

Keywords: children, multisystem inflammatory syndrome, pathogenesis, SARS-CoV-2, COVID-19

Author contribution: Konstantinova YuE, Alekseeva LA, Glotov OS, Egorova ES — search for literature, manuscript writing and editing, approval of the final version of the article; Vilnitz AA, Bekhtereva MK — concept development, search for literature, manuscript writing and editing, approval of the final version of the article.

✉ **Correspondence should be addressed:** Yulia E. Konstantinova
Professora Popova, 9, Saint Petersburg, 197022, Russia; yulia.konstantinova23@mail.ru

Received: 25.08.2023 **Accepted:** 10.09.2023 **Published online:** 30.09.2023

DOI: 10.47183/mes.2023.040

СОВРЕМЕННЫЕ ПРЕДСТАВЛЕНИЯ ОБ ЭПИДЕМИОЛОГИИ И ПАТОГЕНЕЗЕ МУЛЬТИСИСТЕМНОГО ВОСПАЛИТЕЛЬНОГО СИНДРОМА У ДЕТЕЙ, АССОЦИИРОВАННОГО С SARS-COV-2

Ю. Е. Константинова[1]✉, А. А. Вильниц[1,2], М. К. Бехтерева[1,2], Л. А. Алексеева[1], О. С. Глотов[1], Е. С. Егорова[1]

[1] Детский научно-клинический центр инфекционных болезней Федерального медико-биологического агентства, Санкт-Петербург, Россия

[2] Санкт-Петербургский государственный педиатрический университет, Санкт-Петербург, Россия

Обзор посвящен вопросам эпидемиологии и патогенеза мультисистемного воспалительного синдрома у детей, ассоциированного с SARS-CoV-2 (МВС-Д). Наибольшее число проанализированных публикаций посвящено иммунопатогенезу заболевания. В статье перечислены возможные причины возникновения синдрома, связанные с особенностями вируса, описана связь с циркулирующими вариантами. Рассмотрена роль поверхностного белка SARS-CoV-2 как суперантигена. Приведено обсуждение литературных данных о возможности развития МВС-Д по механизму антителозависимого усиления инфекции. Разобраны факторы клеточного и гуморального иммунного ответа, способствующие развитию гипервоспалительного ответа. Представлены единичные работы, описывающие генетические мутации, которые могут играть определенную роль в патогенезе МВС-Д. Помимо этого рассмотрена связь между вакцинацией против новой коронавирусной инфекции и вероятностью развития МВС-Д у привитых.

Ключевые слова: дети, мультисистемный воспалительный синдром, патогенез, SARS-CoV-2, COVID-19

Вклад авторов: Ю. Е. Константинова, Л. А. Алексеева, О. С. Глотов, Е. С. Егорова — поиск литературы, подготовка и редактирование текста, утверждение окончательного варианта статьи; А. А. Вильниц, М. К. Бехтерева — разработка концепции, поиск литературы, подготовка и редактирование текста, утверждение окончательного варианта статьи.

✉ **Для корреспонденции:** Юлия Евгеньевна Константинова
ул. Профессора Попова, д. 9, г. Санкт-Петербург, 197022, Россия; yulia.konstantinova23@mail.ru

Статья получена: 25.08.2023 **Статья принята к печати:** 10.09.2023 **Опубликована онлайн:** 30.09.2023

DOI: 10.47183/mes.2023.040

The multisystem inflammatory syndrome associated with SARS-CoV-2 in children (MIS-C) is the condition occurring within 2–6 weeks after novel coronavirus infection caused by SARS-CoV-2 (COVID-19), it is characterized by severe inflammation affecting two or more organs or systems (mostly skin, mucous membranes, cardiovascular system, gastrointestinal tract). According to the data reported by various authors, 36–80% of patients are admitted to intensive care units (ICU), 10–20% of children need mechanical ventilation (MV), about 1% need extracorporeal membrane oxygenation (ECMO) [1–3]. Researchers still have no consensus whether MIS-C is a complication of COVID-19 or a distinct nosological entity.

MIS-C was first reported in school-age children by researchers from the UK in the beginning of the COVID-19 pandemic [4]. To date, the development of this syndrome has been reported in patients of various age cohorts, including newborns and young adults, however, MIS-C is most often found in children and adolescents [5, 6].

Today, criteria issued by the World Health Organization (WHO) [7] also provided in domestic guidelines [8] are used to diagnose MIS-C in most countries of the world, including the Russian Federation. According to these criteria, MIS-C occurs 2–6 weeks after recovery from COVID-19, most often in children and adolescents aged 0–19. It is characterized by pyretic fever (≥ 3 days), involvement of two or more organs or systems, elevated levels of inflammatory markers, and no information about the presence of infectious agents capable of causing such symptoms [7].

As defined by the US Centers for Disease Control and Prevention (CDC), MIS-C is a clinically severe disorder characterized by fever, elevated levels of inflammatory markers, and impaired function of several organs and systems, which requires hospitalization of the patient. It develops against the background of recent confirmed or probable COVID-19, while there is no other possible explanation of the disease clinical manifestations [9].

Etiology

Regardless of the MIS-C definition used, both options imply that the disease occurs due to prior SARS-CoV-2 infection regardless of the previous COVID-19 severity. The detection of specific immunoglobulins G (IgG) against novel coronavirus in the majority of patients is evident of the association between the disease developed and previous COVID-19. The presence of acute infection markers (IgM against SARS-CoV-2 and extraction of SARS-CoV-2 RNA) was reported only in 5–10% of sick children. These patients were clinically consistent with the MIS-C criteria, and the more thorough questioning showed that children had recently had COVID-19 or were in contact with COVID-19 patients [10].

In the beginning of the pandemic the evidence of contact with the COVID-19 patient within four weeks before developing the symptoms was enough to diagnose MIS-C as one of the criteria due to high incidence of the infection. Meanwhile, additional information is currently required to determine the association between MIS-C and previous COVID-19, which is due to a number of reasons. After three years from the beginning of the pandemic more than 80% of the population have IgG against SARS-CoV-2; IgM fade away within 3–4 weeks since the moment of infection and most often are not detected in the midst of MIS-C, that is why serological tests are not representative in such cases [11].

Second, the number of COVID-19 cases is decreasing, COVID-19 is becoming a seasonal respiratory infection by integrating into the structure of numerous viral infections manifested by respiratory tract involvement. As for daily practice, etiological decoding of uncomplicated acute respiratory tract infections is extremely rare, especially in outpatient practice, which is explained by both economic reasons and the results' negligible impact on the treatment tactics. That is why patients are less frequently tested for SARS-CoV-2.

Third, MIS-C is similar to other disorders characterized by severe inflammatory response (staphylococcal or streptococcal toxic shock syndrome, hemophagocytic syndrome, Kawasaki disease (KD), bacterial sepsis, etc.) in terms of clinical manifestations, which makes it more difficult to diagnose the syndrome [12, 13]. The case reports of viral infection (adenovirus, cytomegalovirus, Epstein–Barr virus) with the course similar to multisystem inflammatory syndrome were found in the literature before the pandemic, however, pathogenesis of this condition was also poorly understood. This resulted in controversy in the scientific community regarding the role of other infectious agents in the MIS-C development [14–16].

The researchers assumed the role of additional infectious agent in the MIS-C realization [17]. The authors of the report considered the probability that additional infectious agent acted as a trigger in patients having the history of COVID-19. Superinfection can trigger an acute inflammatory episode of MIS-C. Furthermore, despite the fact that no signs of the herpesvirus reactivation or persistent viral or bacterial infection have been found in the patients' peripheral blood, this theory also requires further research.

Understanding the causes of MIS-C is essential for development of optimal tactics for therapeutic interventions in patients with this disorder. Despite the symptoms' similarity, the MIS-C treatment is dramatically different from therapy of the number of conditions, such as sepsis, with which it is most often necessary to carry out differential diagnosis. Exclusion of bacterial pathogens that are significant for the syndrome development makes it possible to avoid antibacterial therapy; the symptoms are stopped after administration of high-dose intravenous immunoglobulins, systemic glucocorticoids, and, in rare cases, inhibitors of interleukin-6 (IL6) and interleukin-1 (IL1) receptor antagonists. By analogy with the KD therapy, acetylsalicylic acid is prescribed to prevent thromboembolic complications [8]. Untimely diagnosis results in delayed prescription of essential therapy, thereby adversely affecting the disease outcomes and prognosis.

Epidemiology

Since etiological diagnosis of MIS-C is difficult, and clinically the syndrome has no pathognomonic signs and is similar to other disorders characterized by severe inflammation, true MIS-C incidence in the population is likely to be underestimated. Foreign research has shown that the prevalence of the syndrome is 2 cases per 100,000 population under the age of 21 years [1] or less than 1% of children having a history of COVID-19 [2].

A total of 230 MIS-C cases were reported in Europe and the UK by 15 May 2020 (within a month after the first reported case), among which two (one in the UK and one in France) were fatal (0.87%) [18].

According to the data posted on the CDC official website (as at 3 July 2023), a total of 9499 MIS-C cases were reported in the USA, 79 children died (0.83%). The syndrome detection rate varied significantly from state to state. The largest number of cases was reported in such states, as California (more than 800) and Texas (600–800). About 46% of patients were children aged 5–11, among them boys prevailed (60%). About 57% of patients were of Hispanic ancestry (2358 children) or were African Americans of non-Hispanic ancestry (2720 individuals) [8].

The Public Health Agency of Canada reported 269 MIS-C cases between 11 March 2020 and 2 October 2021. The association with previous COVID-19 was confirmed by epidemiology data or laboratory tests only in 142 individuals (53%). The average age of patients was 6 years, among them boys prevailed (58%). A total of 36% of patients needed admission to ICU [19].

Following identification of various SARS-CoV-2 variants, there had been emerging evidence of the relationship between certain virus variants and the MIS-C detection rate. According to the data provided by CDC, the largest number of cases in the USA was reported between October 2020 and May 2021 following the rise in COVID-19 incidence caused by the "alpha" variant. The second "wave" of MIS-C took place in September–November 2021 during circulation of the "delta" variant, and the third one occurred between December 2021 and March 2022, immediately after the incidence peak caused by the "omicron" variant. Sporadic MIS-C cases have been reported since February 2023 [8].

The studies conducted in Canada have also revealed several incidence peaks: peak in May 2020 associated with the Wuhan variant and two waves, between November 2020 to March 2021 and in May 2021, caused by "alpha" variant [18].

Comparative analysis of the MIS-C incidence in the UK conducted by the research team [20] showed that number of the disease cases caused by "delta" variant was 56% lower before the start of mass vaccination and 66% lower after the start of mass vaccination relative to the wave caused by "alpha" variant; the number of cases caused by "omicron" variant was 95% lower.

Similar data were obtained in Australia. The Australian Paediatric Active Enhanced Disease Surveillance network (PAEDS) revealed only 95 MIS-C cases between 1 May 2020 and 30 April 2022. In New South Wales, Queensland

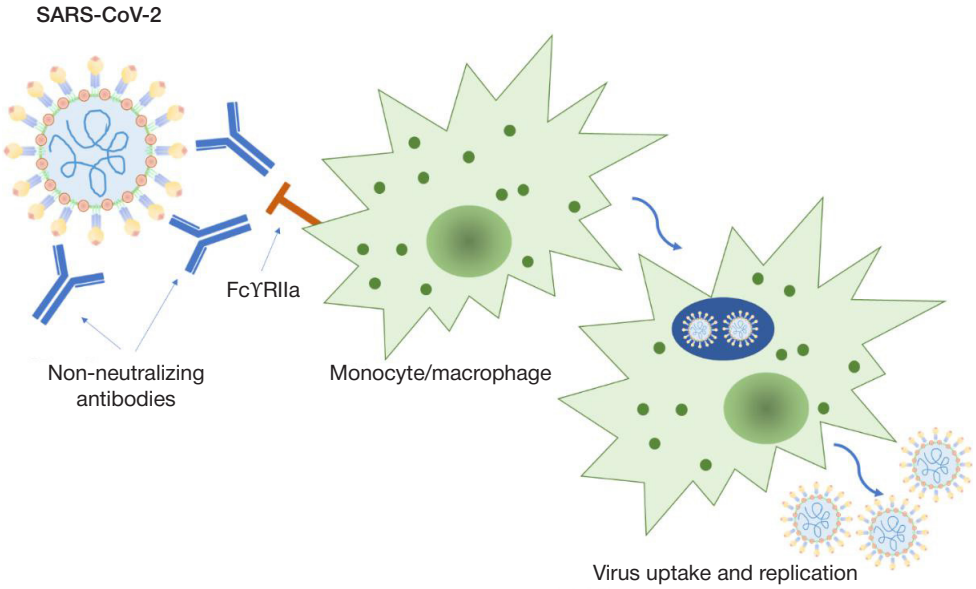

Fig. 1. Schematic representation of antibody-dependent enhancement: binding of SARS-CoV-2 by non-neutralizing antibodies → presentation of the virus to the cell → virus uptake into the monocyte/macrophage → virus replication in the cell → release of SARS-CoV-2 copies. Adapted from [32]

and Victoria the following number of cases was reported: 10 (3–26) MIS-C cases per 10,000 visits during the period before the emergence of "delta" variant (4 cases), 5 (4–7) cases per 10,000 visits during the period of "delta" variant circulation (30 cases), 0.8 (0–1) cases per 10,000 visits during circulation of "omicron" variant (61 cases) [21, 22].

Dependence of the MIS-C rate on the COVID-10 incidence peaks is an indirect evidence of the SARS-CoV-2 etiologic role in the syndrome pathogenesis, and the risk of the syndrome is likely to be associated with its genetic variant.

There are no official data on the rate of MIS-C in Russia. The majority of domestic publications are represented by case reports and reviews [23–25]. The researchers analyzed the data of 122 children with MIS-C aged 8.9 (5.3; 11.8), among them more than a half were boys (56.6%). A total of 45.1% of patients were admitted to ICU [26].

Pathogenesis

Multiple studies are focused on explaining the mechanisms underlying the MIS-C development. Since MIS-C was similar to KD, macrophage activation syndrome, and cytokine release syndrome in terms of clinical features, it was hypothesized that MIS-C resulted from hyperimmune response to the virus (as in the above conditions) in the beginning of the pandemic. However, most researchers tend to think that the MIS-C development mechanism differs from that of the above conditions [7, 12, 18, 27].

Currently, several theories of the MIS-C pathogenesis are discussed, among which the most popular are as follows: abnormal innate immune response to infection resulting from the cross-reaction between viral antigens and antigens of the host; response to the ongoing virus replication in the unrecognized viral reservoirs; superantigen theory; antibody-dependent enhancement (ADE). Researchers do not rule out the impact of genetic or epigenetic predisposition. Actually, it is more likely that there are concurrent mechanisms underlying the MIS-C development [28–31].

The theory of ADE associated with the SARS-CoV-2 infection was one of the first hypotheses. Since the detection rate of specific antibodies against SARS-CoV-2 was higher than the rate of viral RNA detection by PCR, it was suggested that antibodies against SARS-CoV-2 could be among the disease triggers. The non-neutralizing antibodies (nNAb) are produced after the first exposure to novel coronavirus. Some nNAb target specific region of viral spike protein (S-protein),

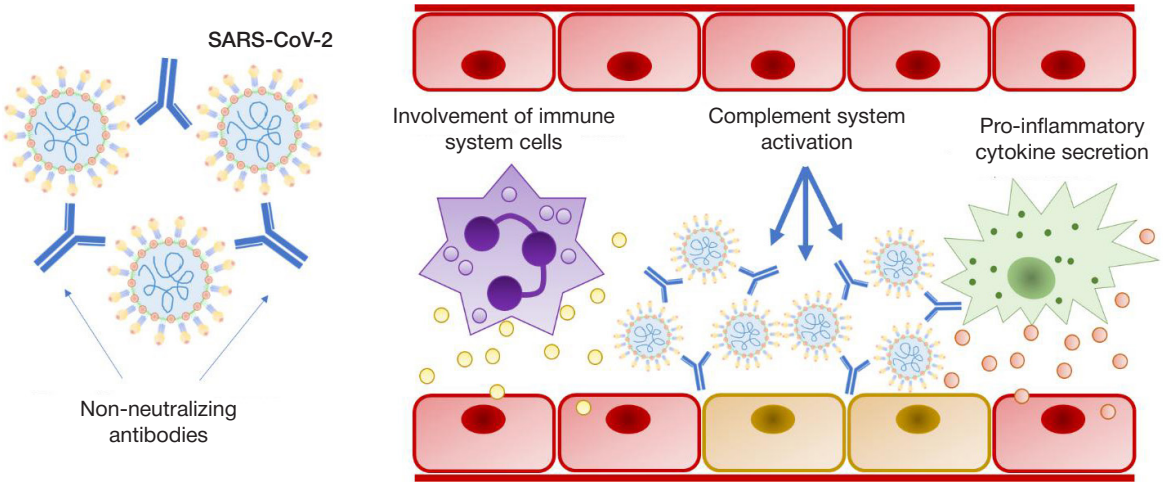

Fig. 2. Schematic representation of antibody-dependent enhancement: binding of SARS-CoV-2 by non-neutralizing antibodies → immune complexes' formation and deposition in the tissues → hyperimmune response. Adapted from [32]

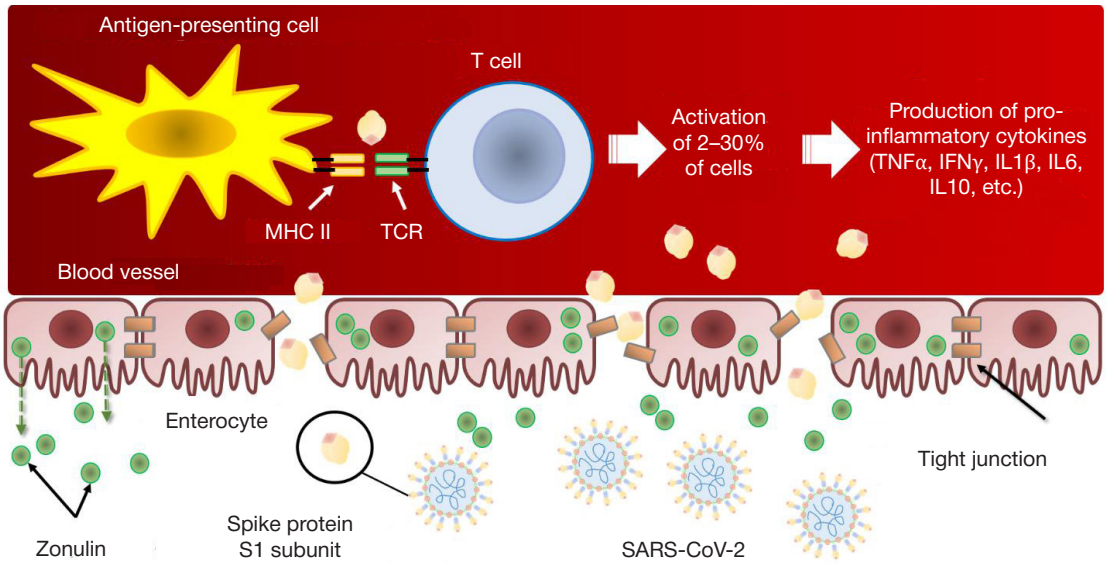

Fig. 3. Schematic representation of superantigen theory as MIS-C pathogenesis: SARS-CoV-2 persistence in the gut → zonulin release → disruption of intercellular contacts and increased intestinal permeability → viral S-protein S1 subunit entry in the bloodstream (as superantigen) → bonding of MHC II molecules found on the antigen-presenting cells with S1 subunit of the virus and T cell activation via TCR → hyperimmune response. Modified and adapted from [35, 37]

that is why MIS-C can develop according to the scenario of the ADE syndrome leading to viral replication in macrophages and disruption of numerous human cells (Fig. 1).

After binding to the macrophage Fc receptors, the virus-antibody complexes settle in tissues and lead to abnormal immune response regulation and enhanced cytokine secretion after the complement activation. Active production of inflammatory mediators contributes to the increased blood vessel permeability, fever, shock, and severe multiple organ damage (Fig. 2).

Meanwhile, as data on SARS-CoV-2 accumulated, it was found that the virus did not infect macrophages, that is why the ADE type involving Fc receptors was unlikely, and low affinity nNAb were produced in small amounts, hardly recognized the virus and did not bind to it [28, 33–34].

The hypothesis about the role of superantigens is based on the MIS-C clinical similarity to toxic shock syndrome caused by bacterial exo- and endotoxins. Superantigen can cause nonspecific activation of the large number of T cells, which, in turn, also produce pro-inflammatory cytokines and chemokines, thereby initiating autoimmune inflammation. High similarity of the SARS-CoV-2 spike protein subunit 1, S1 (responsible for binding of the virus to the host cell receptor), and the fragment of staphylococcal enterotoxin B, the superantigen, was revealed (Fig. 3). Assessment of peripheral blood samples from patients with MIS-C by immunosequencing revealed the *TRBV11-2* gene expansion that was correlated to the MIS-C severity and the serum levels of cytokines, which was consistent with the features of immune response caused by superantigen. The long-term persistence of SARS-CoV-2 in the gut of patients with MIS-C and circulation of the viral protein S1 subunits support this theory [35, 36].

The reports show that prolonged SARS-CoV-2 persistence in the gastrointestinal tract of children with MIS-C resulted in the release of zonulin (intestinal permeability marker) followed by the SARS-CoV-2 antigens entry in bloodstream and the development of hyperinflammation [37]. The data obtained by the authors are consistent with the other study results: genetic factors (expansion and activation of the *TRBV11-2+* gene) alters the diversity of the T cell receptors in children with MIS-C, which, in turn, can be induced by superantigen [38, 39].

Genetic analysis showed that enrichment of rare pathological variants affecting inflammatory and autoimmune pathways, such as dominant-negative mutations in the Notch1 NUMB and NUMBL regulators resulting in the Notch1 regulation enhancement, was observed in patients with MIS-C [40]. The Notch1 signal transmission to Tregs induced CD22, thereby causing their mTORC1-dependent destabilization and systemic inflammation enhancement.

It has been proven that in individuals with KD the virus can play a role of trigger by binding to antibodies and forming the immune complexes that settle on the blood vessel walls and cause inflammatory response through binding to Fc receptors or complement system activation. The genes involved in antigen production (*FCGR2A*, the gene encoding lymphoid tyrosine kinase, and the gene encoding the CD40 ligand) are responsible for this process. The gene encoding inositol 1,4,5-trisphosphate 3-kinase C (ITPKC) regulating cell activation is responsible for cellular response associated with KD. Similar mechanisms can underly the MIS-C pathogenesis [41]. The research team [42] analyzed three groups of patients (a total of 20 individuals) in order to reveal the differences and clarify the disease pathogenetic features: individuals with MIS-C ($n = 6$), mild and severe COVID-19 ($n = 5$ and $n = 9$, respectively). The authors determined the cytokine profiles (IFNγ, IL10, IL6, IL8, and TNFα) and the levels of soluble complement complex C5b-9, they also assessed the abundance of schizocytes in peripheral blood smears considering clinical data. The analysis showed that the total of TNFα and IL10 levels was significantly higher in patients with MIS-C than in patients with severe COVID-19. The elevated levels of these cytokines are indirect evidence of impaired innate immunity. In the discussion section the authors note that moderate increase in the levels of IL1, IL2, and IL6 is observed in individuals with KD. However, TNFα levels are likely to play a key role in pathogenesis of both MIS-C and KD. The levels of soluble complement complex C5b-9 were significantly higher in children with severe COVID-19, slightly lower in patients with MIS-C, and within normal range in patients with mild COVID-19. Schizocytes were found in peripheral blood smears in 67% of individuals with mild COVID-19, 80% of patients with severe COVID-19, and 100% of patients with MIS-C. Elevated levels of soluble complement complex C5b-9 are indicative of the presence of blood vessel damage in the MIS-C pathogenesis [42].

Cytokines and chemokines play a vitally important role in initiation, prolongation and suppression of immune response to any infection, including COVID-19. Studies have revealed elevated blood levels of IL6 in patients with severe MIS-C, however, the values did not exceed that observed in children with sepsis. In addition to IL1 and IL8, the levels of which are slightly elevated in MIS-C relative to KD, a significantly increased production of TNFα, IFNγ, and IL10 relative to KD is observed in individuals with MIS-C. The IL17 inflammatory mediator plays a more prominent role in pathogenesis of KD than that of MIS-C. It is important to note that the cytokine and chemokine levels can vary considerably between the studies involving various ratios of age cohorts, sample collection terms and diagnostic methods [43–47].

It is well-known that the increase in the levels of autoantibodies is typical for various autoimmune and inflammatory disorders, it also occurs in response to some viral infections. Studies revealed elevated levels of autoantibodies in patients with MIS-C [48]. Three autoantigens were identified as ones associated with MIS-C: UBE3A, ECE1, and RBM38. Another eight autoantigens were earlier reported in individuals with other disorders (ATP4A, TROVE2 of two types, KLHL12, FAM84A, HK1, MAOA, and CTDP1). The authors have found tissue-specific autoantigens in such organs, as the gut, heart, endothelium, and skeletal muscles, which explains clinical symptoms from these organs in MIS-C.

Cardiovascular system is a major target organ in MIS-C. Heart disorders in the form of valvulitis, coronary artery dilation and aneurysms, myocardial dysfunction, and fulminant myocarditis are observed in patients. The researchers make various assumptions to explain the rate of cardiac disorders. Thus, myocardial damage is most likely to result from binding of the virus to the ACE-2 receptors found on endothelial cells of arteries and veins and direct infection of cardiomyocytes by the virus [49–51]. Furthermore, the release of inflammatory cytokines also contributes to the vascular matrix disruption and loss of blood vessel structural integrity, thereby leading to coronary artery dilation and aneurysm formation [43]. Pathological examination of autopsy samples from patients with MIS-C confirms the presence of inflammatory infiltration in the myocardium and demonstrates high viral load in the patients' cardiac muscle [52, 53]. The research team assessed the results of heart MRI in four patients with MIS-C and revealed diffuse myocardial edema with no signs of replacement fibrosis or focal necrosis [54].

Vaccination against COVID-19 and MIS-C

Great attention is paid to the probability of developing MIS-C after vaccination against COVID-19 due to the emergence of sporadic reports of the syndrome development following vaccination against novel coronavirus infection. The paper [55] reports two cases of MIS-C following administration of the BNT162b2 vaccine (based on mRNA encoding the SARS-CoV-2 spike protein) in Virginia state (USA). A 15-year-old girl developed clinical symptoms of the disease six days after vaccination, however, it was later confirmed that she had a history of COVID-19 (the virus was not extracted by PCR, however, specific antibodies (IgG) against the SARS-CoV-2 nucleocapsid protein were detected along with no antibodies against S-protein). A 17-year-old girl was the second patient, who developed clinical symptoms of MIS-C seven days after vaccination. Novel coronavirus was also not extracted from nasopharyngeal discharge by PCR. There were specific antibodies (IgG) against S-protein and no antibodies against nucleocapsid protein, that is why it was impossible to confirm or disprove the likelihood of previous COVID-19. Both teenagers received therapy with normal human immunoglobulin for intravenous administration and systemic glucocorticoids, they were discharged from hospital when healthy.

A total of 52 MIS-C cases in children aged 0–17 for the period between 1 August 2021 and 1 February 2022 were assessed in Denmark. Among them one case occurred in a fully vaccinated adolescent. A 17-year-old girl developed MIS-C four months after administration of the second dose of BNT162b2 vaccine and five weeks after the confirmed breakthrough infection caused by SARS-CoV-2. The rate of MIS-C was 1 case per 3400 unvaccinated children (95% CI: 2600–4600) and 1 case per 9900 vaccinated individuals (95% CI: 1800–390,000) [56].

Ambiguity of the mechanisms underlying the development of MIS-C and the risk of this syndrome in vaccinated children led to the debate regarding the development of tactics for vaccination of patients having a history of MIS-C against SARS-CoV-2. In this context an international study involving 273 children having a history of MIS-C from 32 countries was performed. There were no reports of recurrent MIS-C or any other serious side effects of vaccination against SARS-CoV-2 in this group of children [57].

CONCLUSION

While etiological role of SARS-CoV-2 in the development of MIS-C is almost beyond doubt, there are still many unresolved issues related to the syndrome pathogenesis. Today, work continues on defining the role of immune mechanisms in the MIS-C development and course, various aspects related to innate and adaptive immunity are clarified. Further research on the MIS-C pathogenesis is essential for optimization of diagnostic and therapeutic measures contributing to prevention of severe effects of this disorder.

References

1. Dufort EM, Koumans EH, Chow EJ, Rosenthal EM, Muse A, Rowlands J, et al. Multisystem inflammatory syndrome in children in New York State. N Engl J Med. 2020; 383 (4): 347–58.
2. Feldstein LR, Tenforde MW, Friedman KG, Newhams M, Rose EB, Dapul H, et al. Characteristics and outcomes of US children and adolescents with multisystem inflammatory syndrome in children (MIS-C) compared with severe acute COVID-19. Jama. 2021; 325 (11): 1074–87.
3. CDC [Internet]. Information for Healthcare Providers about Multisystem Inflammatory Syndrome in Children (MIS-C) [cited 2023 Jul 29]. Available from: https://www.cdc.gov/mis/ MIS-C/hcp_cstecdc/index.html.
4. Riphagen S, Gomez X, Gonzalez-Martinez C, Wilkinson N, Theocharis P. Hyperinflammatory shock in children during COVID-19 pandemic. Lancet. 2020; 395 (10237): 1607–8.
5. Kunal S, Ish P, Sakthivel P, Malhotra N, Gupta K. The emerging threat of multisystem inflammatory syndrome in adults (MIS-A) in COVID-19: a systematic review. Heart & Lung. 2022; (54): 7–18.
6. Shaiba LA, More K, Hadid A, Almaghrabi R, Al Marri M, Alnamnakani M, et al. Multisystemic inflammatory syndrome in neonates: a systematic review. Neonatology. 2022; 119 (4): 405–17.
7. World Health Organization, et al. Multisystem inflammatory

syndrome in children and adolescents with COVID-19: scientific brief. 2020 May 15. World Health Organization. 2020. Available from: WHO/2019-nCoV/Sci_Brief/Multisystem_Syndrome_Children/2020.1.
8. Metodicheskie rekomendacii "Osobennosti klinicheskih projavlenij i lechenija zabolevanija, vyzvannogo novoj koronavirusnoj infekciej (COVID-19) u detej. Versija 2 (03.07.2020)", utv. Minzdravom Rossii. Russian.
9. CDC [Internet]. Health Department-Reported Cases of Multisystem Inflammatory Syndrome in Children (MIS-C) in the United States [cited 2023 Jul 29]. Available from: https://covid.cdc.gov/covid-data-tracker/#mis-national-surveillance.
10. Jiang L, Tang K, Levin M, Irfan O, Morris SK, Wilson K, et al. COVID-19 and multisystem inflammatory syndrome in children and adolescents. Lancet Infect Dis. 2020; 20 (11): 276–88.
11. Sadykov MN, Ziatdinov VB, Reshetnikova ID, Hakimov NM, Lopushov DV, Isaeva GSh. Izuchenie urovnja i struktury populjacionnogo immuniteta k SARS-CoV2 u naselenija Respubliki Tatarstan v period vtorogo pika rasprostranenija COVID-19. Jepidemiologija i vakcinoprofilaktika. 2021; 20 (5): 39–51. Russian.
12. Hoste L, Van Paemel R, Haerynck F. Multisystem inflammatory syndrome in children related to COVID-19: a systematic review. Eur J Pediatr. 2021; (180): 2019–34.
13. Kostik MM, Bregel LV, Avrusin IS, Dondurei EA, Matyunova AE, Efremova OS, et al. Distinguishing between multisystem inflammatory syndrome associated with COVID-19 in children and the Kawasaki disease: development of preliminary criteria based on the data of the retrospective Multicenter Cohort Study. Front Pediatr. 2021; (9): 787353.
14. Diwakar K, Sarangi T, Srivastava P, Tanti SK, Swaroop S. Human adenovirus infection causing hyperinflammatory syndrome mimicking multisystem inflammatory syndrome in children (MIS-C): a case report. Cureus. 2023; 15 (6): e40239.
15. Fabi M, Dondi A, Andreozzi L, Frazzoni L, Biserni GB, Ghiazza F, et al. Kawasaki disease, multisystem inflammatory syndrome in children, and adenoviral infection: a scoring system to guide differential diagnosis. Eur J Pediatr. 2023 Aug 19. Available from: https://link.springer.com/article/10.1007/s00431-023-05142-6.
16. Spivack T, Chawla R, Marik PE. Epstein-Barr virus-associated hemophagocytic syndrome mimicking severe sepsis. J Emerg Trauma Shock. 2008; 1 (2): 119–22.
17. Ramaswamy A, Brodsky NN, Sumida TS, Comi M, Asashima H, Hoehn KB, et al. Immune dysregulation and autoreactivity correlate with disease severity in SARS-CoV-2-associated multisystem inflammatory syndrome in children. Immunity. 2021; 54 (5): 1083–95.
18. Rapid Risk Assessment. Paediatric inflammatory multisystem syndrome and SARS-CoV-2 infection in children. European Centre for Disease Prevention and Control. 2020.
19. El Tal T, Morin MP, Morris SK, Farrar DS, Berard RA, Kakkar F, et al. Paediatric inflammatory multisystem syndrome in Canada: population-based surveillance and role of SARS-CoV-2 linkage. Pediatr Res. 2023 Jun 5: 1–10. Available from: https://www.nature.com/articles/s41390-023-02668-1.
20. Cohen JM, Carter MJ, Cheung CR, Ladhani S. Lower risk of multisystem inflammatory syndrome in children with the delta and omicron variants of severe acute respiratory syndrome coronavirus 2. Clinical Infectious Diseases. 2023; 76 (3): 518–21.
21. Lopez L, Burgner D, Glover C, Carr J, Clark J, Boast A, et al. Lower risk of multi-system inflammatory syndrome in children (MIS-C) with the omicron variant. Lancet Reg Health West Pac. 2022; (27): 100604.
22. Lopez L, Burgner D, Glover C, Carr J, Clark J, Boast A, et al. Corrigendum to “Lower risk of multi-system inflammatory syndrome in children (MIS-C) with the omicron variant”. Lancet Reg Health West Pac. 2023; (35): 100808.
23. Skudarnov EV, Vyhodceva GI, Novikova LM, Maljuga OM, Kirichjok EJu, Skudarnova AP, et al. Kliniko-laboratornye aspekty mul'tisistemnogo vospalitel'nogo sindroma, associirovannogo s COVID-19 u detej. Bjulleten' medicinskoj nauki. 2022; 2 (26): 61–6. Russian.
24. Avtandiljan LL, Fedulova AA, Parazjan AS, Arzumanjan AI, Gadzhiahmedova JeI. Klinicheskij sluchaj: mul'tisistemnyj vospalitel'nyj sindrom u detej, associirovannyj s COVID-19. Universum: medicina i farmakologija. 2021; 6 (78): 7–11. Russian.
25. Lobzin JuV, Vilnic AA, Kostik MM, Behtereva MK, Uskov AN, Skripchenko NV, et al. Pediatricheskij mul'tisistemnyj vospalitel'nyj sindrom, associirovannyj s novoj koronavirusnoj infekciej: nereshennye problemy. Zhurnal infektologii. 2021; 13 (1): 13–20. Russian.
26. Kostik MM, Bregel LV, Avrusin IS, Efremova OS, Belozerov KE, Dondurei EA, et al. Heart involvement in multisystem inflammatory syndrome, associated with COVID-19 in children: the retrospective multicenter cohort data. Front Pediatr. 2022; (10): 829420.
27. Lee PI, Hsueh PR. Multisystem inflammatory syndrome in children: A dysregulated autoimmune disorder following COVID-19. J Microbiol Immunol Infect. 2023; (56): 236–45.
28. Filippatos F, Tatsi EB, Michos A. Immunology of multisystem inflammatory syndrome after COVID-19 in children: a review of the current evidence. Int J Mol Sci. 2023; 24 (6): 5711.
29. Osmanov IM, Hegaj IM, Trunina II, Chebotareva TA, Cheburkin AA, Shumilov PV. Immunopatogenez mul'tisistemnogo vospalitel'nogo sindroma, svjazannogo s COVID-19, u detej. Immunologija. 2022; 43 (2): 217–23. Russian.
30. Dubrovina JuA, Legonkova TI, Vodneva LM, Shtykova ON, Shpakovskaja KS, Melnikova VM, Artjomenkova EI. Mul'tisistemnyj vospalitel'nyj sindrom u detej, perenesshih COVID-19. Vestnik Smolenskoj gosudarstvennoj medicinskoj akademii. 2022; 21 (3): 133–41. Russian.
31. Hacuk AS, Romanova KR, Samodova OV. Mul'tisistemnyj vospalitel'nyj sindrom, associirovannyj s SARS-CoV-2, u detej: jetiopatogenez, klinicheskaja kartina, diagnostika, lechenie (obzor). Zhurnal mediko-biologicheskih issledovanij. 2022; 10 (4), 371–9. Russian.
32. Lee WS, Wheatley AK, Kent SJ, DeKosky BJ. Antibody-dependent enhancement and SARS-CoV-2 vaccines and therapies. Nat Microbiol. 2020; 5 (10): 1185–91.
33. Katzelnick LC, Gresh L, Halloran ME, Mercado JC, Kuan G, Gordon A, et al. Antibody-dependent enhancement of severe dengue disease in humans. Science. 2017; 358 (6365): 929–32.
34. Khan S, Siddique R, Shereen MA, Ali A, Liu J, Bai Q, et al. Emergence of a novel coronavirus, severe acute respiratory syndrome coronavirus 2: biology and therapeutic options. J Clin Microbiol. 2020; 58 (5): 00187-20.
35. Noval Rivas M, Porritt RA, Cheng MH, Bahar I, Arditi M, et al. Multisystem inflammatory syndrome in children and long COVID: the SARS-CoV-2 viral superantigen hypothesis. Front Immunol. 2022; (13): 941009.
36. Porritt RA, Paschold L, Rivas MN, Cheng MH, Yonker LM, Chandnani H, et al. HLA class I-associated expansion of TRBV11-2 T cells in multisystem inflammatory syndrome in children. J Clin Invest. 2021; 131 (10): 146614.
37. Yonker LM, Gilboa T, Ogata AF, Senussi Y, Lazarovits R, Boribong BP, et al. Multisystem inflammatory syndrome in children is driven by zonulin-dependent loss of gut mucosal barrier. J Clin Invest. 2021; 131 (14): 149633.
38. Moreews M, Le Gouge K, Khaldi-Plassart S, Pescarmona R, Mathieu AL, Malcus C, et al. Polyclonal expansion of TCR Vβ 21.3+ CD4+ and CD8+ T cells is a hallmark of multisystem inflammatory syndrome in children. Sci Immunol. 2021; 6 (59): eabh1516.
39. Malik A, Tóth EN, Teng MS, Hurst J, Watt E, Wise L, et al. Distorted TCR repertoires define multisystem inflammatory syndrome in children. PLoS One. 2022; 17 (10): 274–89.
40. Benamar M, Chen Q, Chou J, Julé AM, Boudra R, Contini P, et al. The Notch1/CD22 signaling axis disrupts Treg function in SARS-CoV-2–associated multisystem inflammatory syndrome in children. J Clin Invest. 2023; 133 (1): 163235.
41. Khor CC, Davila S, Breunis WB, Lee YC, Shimizu C, Wright VJ, et al. Genome-wide association study identifies FCGR2A as a susceptibility locus for Kawasaki disease. Nat Genet. 2011; 43 (12): 1241–6.
42. Diorio C, Henrickson SE, Vella LA, McNerney KO, Chase J, Burudpakdee C, et al. Multisystem inflammatory syndrome in children and COVID-19 are distinct presentations of SARS–CoV-2. J Clin Invest. 2020; 130 (11): 5967–75.
43. Zou H, Lu J, Liu J, Wong JHY, Cheng S, Li Q, et al. Characteristics

of pediatric multi-system inflammatory syndrome (PMIS) associated with COVID-19: a meta-analysis and insights into pathogenesis. Int J Infect Dis. 2021; (102): 319–26.
44. Bautista-Rodriguez C, Sanchez-de-Toledo J, Clark BC, Herberg J, Bajolle F, Randanne PC, et al. Multisystem inflammatory syndrome in children: an international survey. Pediatrics. 2021; 147 (2): e2020024554.
45. Sharma C, Ganigara M, Galeotti C, Burns J, Berganza FM, Hayes DA, et al. Multisystem inflammatory syndrome in children and Kawasaki disease: a critical comparison. Nat Rev Rheumatol. 2021; 17 (12): 731–48.
46. Ouldali N, Pouletty M, Mariani P, Beyler C, Blachier A, Bonacorsi S, et al. Emergence of Kawasaki disease related to SARS-CoV-2 infection in an epicentre of the French COVID-19 epidemic: a time-series analysis. Lancet Child Adolesc Health. 2020; 4 (9): 662–8.
47. Consiglio CR, Cotugno N, Sardh F, Pou C, Amodio D, Rodriguez L, et al. The immunology of multisystem inflammatory syndrome in children with COVID-19. Cell. 2020; 183 (4): 968-981.
48. Porritt RA, Binek A, Paschold L, Rivas MN, McArdle A, Yonker LM, et al. The autoimmune signature of hyperinflammatory multisystem inflammatory syndrome in children. J Clin Invest. 2021; 131 (20): e151520.
49. Hoffmann M, Kleine-Weber H, Schroeder S, Krüger N, Herrler T, Erichsen S, et al. SARS-CoV-2 cell entry depends on ACE2 and TMPRSS2 and is blocked by a clinically proven protease inhibitor. Cell. 2020; 181 (2): 271–80.
50. Zhou T, Tsybovsky Y, Gorman J, Rapp M, Cerutti G, Chuang GY, et al. Cryo-EM structures of SARS-CoV-2 spike without and with ACE2 reveal a pH-dependent switch to mediate endosomal positioning of receptor-binding domains. Cell host & microbe. 2020; 28 (6): 867–79.
51. Shikov AE, Barbitoff YA, Glotov AS, Danilova MM, Tonyan ZN, Nasykhova YA, et al. Analysis of the spectrum of ACE2 variation suggests a possible influence of rare and common variants on susceptibility to COVID-19 and severity of outcome. Front Genet. 2020; (11): 551220.
52. Zhao Y, Patel J, Huang Y, Yin L, Tang L. Cardiac markers of multisystem inflammatory syndrome in children (MIS-C) in COVID-19 patients: a meta-analysis. Am J Emerg Med. 2021; (49): 62–70.
53. Ahmed M, Advani S, Moreira A, Zoretic S, Martinez J, Chorath K, et al. Multisystem inflammatory syndrome in children: a systematic review. EClinicalMedicine. 2020; (26):100527.
54. Blondiaux E, Parisot P, Redheuil A, Tzaroukian L, Levy Y, Sileo C, et al. Cardiac MRI in children with multisystem inflammatory syndrome associated with COVID-19. Radiology. 2020; 297 (3): 283–8.
55. Jain E, Donowitz JR, Aarons E, Marshall BC, Miller MP, et al. Multisystem inflammatory syndrome in children after SARS-CoV-2 vaccination. Emerging Infectious Diseases. 2022; 28 (5): 990–3.
56. Nygaard U, Holm M, Hartling UB, Glenthøj J, Schmidt LS, Nordly SB, et al. Incidence and clinical phenotype of multisystem inflammatory syndrome in children after infection with the SARS-CoV-2 delta variant by vaccination status: a Danish nationwide prospective cohort study. Lancet Child Adolesc Health. 2022; 6 (7): 459–65.
57. Hoste L, Soriano-Arandes A, Buddingh EP, Whittaker E, Belot A, Ulloa-Gutierrez R, et al. Severe acute respiratory syndrome coronavirus 2 vaccination in children with a history of multisystem inflammatory syndrome in children: an international survey. J Pediatr. 2022; (248): 114–18.

Литература

1. Dufort EM, Koumans EH, Chow EJ, Rosenthal EM, Muse A, Rowlands J, et al. Multisystem inflammatory syndrome in children in New York State. N Engl J Med. 2020; 383 (4): 347–58.
2. Feldstein LR, Tenforde MW, Friedman KG, Newhams M, Rose EB, Dapul H, et al. Characteristics and outcomes of US children and adolescents with multisystem inflammatory syndrome in children (MIS-C) compared with severe acute COVID-19. Jama. 2021; 325 (11): 1074–87.
3. CDC [Internet]. Information for Healthcare Providers about Multisystem Inflammatory Syndrome in Children (MIS-C) [cited 2023 Jul 29]. Available from: https://www.cdc.gov/mis/ MIS-C/hcp_cstecdc/index.html.
4. Riphagen S, Gomez X, Gonzalez-Martinez C, Wilkinson N, Theocharis P. Hyperinflammatory shock in children during COVID-19 pandemic. Lancet. 2020; 395 (10237): 1607–8.
5. Kunal S, Ish P, Sakthivel P, Malhotra N, Gupta K. The emerging threat of multisystem inflammatory syndrome in adults (MIS-A) in COVID-19: a systematic review. Heart & Lung. 2022; (54): 7–18.
6. Shaiba LA, More K, Hadid A, Almaghrabi R, Al Marri M, Alnamnakani M, et al. Multisystemic inflammatory syndrome in neonates: a systematic review. Neonatology. 2022; 119 (4): 405–17.
7. World Health Organization, et al. Multisystem inflammatory syndrome in children and adolescents with COVID-19: scientific brief. 2020 May 15. World Health Organization. 2020. Available from: WHO/2019-nCoV/Sci_Brief/Multisystem_Syndrome_Children/2020.1.
8. Методические рекомендации «Особенности клинических проявлений и лечения заболевания, вызванного новой коронавирусной инфекцией (COVID-19) у детей. Версия 2 (03.07.2020)», утв. Минздравом России.
9. CDC [Internet]. Health Department-Reported Cases of Multisystem Inflammatory Syndrome in Children (MIS-C) in the United States [cited 2023 Jul 29]. Available from: https://covid.cdc.gov/covid-data-tracker/#mis-national-surveillance.
10. Jiang L, Tang K, Levin M, Irfan O, Morris SK, Wilson K, et al. COVID-19 and multisystem inflammatory syndrome in children and adolescents. Lancet Infect Dis. 2020; 20 (11): 276–88.
11. Садыков М. Н., Зиатдинов В. Б., Решетникова И. Д., Хакимов Н. М., Лопушов Д. В., Исаева Г. Ш. Изучение уровня и структуры популяционного иммунитета к SARS-CoV2 у населения Республики Татарстан в период второго пика распространения COVID-19. Эпидемиология и вакцинопрофилактика. 2021; 20 (5): 39–51.
12. Hoste L, Van Paemel R, Haerynck F. Multisystem inflammatory syndrome in children related to COVID-19: a systematic review. Eur J Pediatr. 2021; (180): 2019–34.
13. Kostik MM, Bregel LV, Avrusin IS, Dondurei EA, Matyunova AE, Efremova OS, et al. Distinguishing between multisystem inflammatory syndrome associated with COVID-19 in children and the Kawasaki disease: development of preliminary criteria based on the data of the retrospective Multicenter Cohort Study. Front Pediatr. 2021; (9): 787353.
14. Diwakar K, Sarangi T, Srivastava P, Tanti SK, Swaroop S. Human adenovirus infection causing hyperinflammatory syndrome mimicking multisystem inflammatory syndrome in children (MIS-C): a case report. Cureus. 2023; 15 (6): e40239.
15. Fabi M, Dondi A, Andreozzi L, Frazzoni L, Biserni GB, Ghiazza F, et al. Kawasaki disease, multisystem inflammatory syndrome in children, and adenoviral infection: a scoring system to guide differential diagnosis. Eur J Pediatr. 2023 Aug 19. Available from: https://link.springer.com/article/10.1007/s00431-023-05142-6.
16. Spivack T, Chawla R, Marik PE. Epstein-Barr virus-associated hemophagocytic syndrome mimicking severe sepsis. J Emerg Trauma Shock. 2008; 1 (2): 119–22.
17. Ramaswamy A, Brodsky NN, Sumida TS, Comi M, Asashima H, Hoehn KB, et al. Immune dysregulation and autoreactivity correlate with disease severity in SARS-CoV-2-associated multisystem inflammatory syndrome in children. Immunity. 2021; 54 (5): 1083–95.
18. Rapid Risk Assessment. Paediatric inflammatory multisystem syndrome and SARS-CoV-2 infection in children. European Centre for Disease Prevention and Control. 2020.

19. El Tal T, Morin MP, Morris SK, Farrar DS, Berard RA, Kakkar F, et al. Paediatric inflammatory multisystem syndrome in Canada: population-based surveillance and role of SARS-CoV-2 linkage. Pediatr Res. 2023 Jun 5: 1–10. Available from: https://www.nature.com/articles/s41390-023-02668-1.
20. Cohen JM, Carter MJ, Cheung CR, Ladhani S. Lower risk of multisystem inflammatory syndrome in children with the delta and omicron variants of severe acute respiratory syndrome coronavirus 2. Clinical Infectious Diseases. 2023; 76 (3): 518–21.
21. Lopez L, Burgner D, Glover C, Carr J, Clark J, Boast A, et al. Lower risk of multi-system inflammatory syndrome in children (MIS-C) with the omicron variant. Lancet Reg Health West Pac. 2022; (27): 100604.
22. Lopez L, Burgner D, Glover C, Carr J, Clark J, Boast A, et al. Corrigendum to “Lower risk of multi-system inflammatory syndrome in children (MIS-C) with the omicron variant”. Lancet Reg Health West Pac. 2023; (35): 100808.
23. Скударнов Е. В., Выходцева Г. И., Новикова Л. М., Малюга О. М., Киричёк Е. Ю., Скударнова А. П. и др. Клинико-лабораторные аспекты мультисистемного воспалительного синдрома, ассоциированного с COVID-19 у детей. Бюллетень медицинской науки. 2022; 2 (26): 61–6.
24. Автандилян Л. Л., Федулова А. А., Паразян А. С., Арзуманян А. И., Гаджиахмедова Э. И. Клинический случай: мультисистемный воспалительный синдром у детей, ассоциированный с COVID-19. Universum: медицина и фармакология. 2021; 6 (78): 7–11.
25. Лобзин Ю. В., Вильниц А. А., Костик М. М., Бехтерева М. К., Усков А. Н., Скрипченко Н. В. и др. Педиатрический мультисистемный воспалительный синдром, ассоциированный с новой коронавирусной инфекцией: нерешенные проблемы. Журнал инфектологии. 2021; 13 (1): 13–20.
26. Kostik MM, Bregel LV, Avrusin IS, Efremova OS, Belozerov KE, Dondurei EA, et al. Heart involvement in multisystem inflammatory syndrome, associated with COVID-19 in children: the retrospective multicenter cohort data. Front Pediatr. 2022; (10): 829420.
27. Lee PI, Hsueh PR. Multisystem inflammatory syndrome in children: A dysregulated autoimmune disorder following COVID-19. J Microbiol Immunol Infect. 2023; (56): 236–45.
28. Filippatos F, Tatsi EB, Michos A. Immunology of multisystem inflammatory syndrome after COVID-19 in children: a review of the current evidence. Int J Mol Sci. 2023; 24 (6): 5711.
29. Османов И. М., Хегай И. М., Трунина И. И., Чеботарева Т. А., Чебуркин А. А., Шумилов, П. В. Иммунопатогенез мультисистемного воспалительного синдрома, связанного с COVID-19, у детей. Иммунология. 2022; 43 (2): 217–23.
30. Дубровина Ю. А., Легонькова Т. И., Воднева Л. М., Штыкова О. Н., Шпаковская К. С., Мельникова В. М., Артёменкова Е. И. Мультисистемный воспалительный синдром у детей, перенесших COVID-19. Вестник Смоленской государственной медицинской академии. 2022; 21 (3): 133–41.
31. Хацук А. С., Романова К. Р., Самодова О. В. Мультисистемный воспалительный синдром, ассоциированный с SARS-CoV-2, у детей: этиопатогенез, клиническая картина, диагностика, лечение (обзор). Журнал медико-биологических исследований. 2022; 10 (4): 371–9.
32. Lee WS, Wheatley AK, Kent SJ, DeKosky BJ. Antibody-dependent enhancement and SARS-CoV-2 vaccines and therapies. Nat Microbiol. 2020; 5 (10): 1185–91.
33. Katzelnick LC, Gresh L, Halloran ME, Mercado JC, Kuan G, Gordon A, et al. Antibody-dependent enhancement of severe dengue disease in humans. Science. 2017; 358 (6365): 929–32.
34. Khan S, Siddique R, Shereen MA, Ali A, Liu J, Bai Q, et al. Emergence of a novel coronavirus, severe acute respiratory syndrome coronavirus 2: biology and therapeutic options. J Clin Microbiol. 2020; 58 (5): 00187-20.
35. Noval Rivas M, Porritt RA, Cheng MH, Bahar I, Arditi M, et al. Multisystem inflammatory syndrome in children and long COVID: the SARS-CoV-2 viral superantigen hypothesis. Front Immunol. 2022; (13): 941009.
36. Porritt RA, Paschold L, Rivas MN, Cheng MH, Yonker LM, Chandnani H, et al. HLA class I-associated expansion of TRBV11-2 T cells in multisystem inflammatory syndrome in children. J Clin Invest. 2021; 131 (10): 146614.
37. Yonker LM, Gilboa T, Ogata AF, Senussi Y, Lazarovits R, Boribong BP, et al. Multisystem inflammatory syndrome in children is driven by zonulin-dependent loss of gut mucosal barrier. J Clin Invest. 2021; 131 (14): 149633.
38. Moreews M, Le Gouge K, Khaldi-Plassart S, Pescarmona R, Mathieu AL, Malcus C, et al. Polyclonal expansion of TCR Vβ 21.3+ CD4+ and CD8+ T cells is a hallmark of multisystem inflammatory syndrome in children. Sci Immunol. 2021; 6 (59): eabh1516.
39. Malik A, Tóth EN, Teng MS, Hurst J, Watt E, Wise L, et al. Distorted TCR repertoires define multisystem inflammatory syndrome in children. PLoS One. 2022; 17 (10): 274–89.
40. Benamar M, Chen Q, Chou J, Julé AM, Boudra R, Contini P, et al. The Notch1/CD22 signaling axis disrupts Treg function in SARS-CoV-2–associated multisystem inflammatory syndrome in children. J Clin Invest. 2023; 133 (1): 163235.
41. Khor CC, Davila S, Breunis WB, Lee YC, Shimizu C, Wright VJ, et al. Genome-wide association study identifies FCGR2A as a susceptibility locus for Kawasaki disease. Nat Genet. 2011; 43 (12): 1241–6.
42. Diorio C, Henrickson SE, Vella LA, McNerney KO, Chase J, Burudpakdee C, et al. Multisystem inflammatory syndrome in children and COVID-19 are distinct presentations of SARS–CoV-2. J Clin Invest. 2020; 130 (11): 5967–75.
43. Zou H, Lu J, Liu J, Wong JHY, Cheng S, Li Q, et al. Characteristics of pediatric multi-system inflammatory syndrome (PMIS) associated with COVID-19: a meta-analysis and insights into pathogenesis. Int J Infect Dis. 2021; (102): 319–26.
44. Bautista-Rodriguez C, Sanchez-de-Toledo J, Clark BC, Herberg J, Bajolle F, Randanne PC, et al. Multisystem inflammatory syndrome in children: an international survey. Pediatrics. 2021; 147 (2): e2020024554.
45. Sharma C, Ganigara M, Galeotti C, Burns J, Berganza FM, Hayes DA, et al. Multisystem inflammatory syndrome in children and Kawasaki disease: a critical comparison. Nat Rev Rheumatol. 2021; 17 (12): 731–48.
46. Ouldali N, Pouletty M, Mariani P, Beyler C, Blachier A, Bonacorsi S, et al. Emergence of Kawasaki disease related to SARS-CoV-2 infection in an epicentre of the French COVID-19 epidemic: a time-series analysis. Lancet Child Adolesc Health. 2020; 4 (9): 662–8.
47. Consiglio CR, Cotugno N, Sardh F, Pou C, Amodio D, Rodriguez L, et al. The immunology of multisystem inflammatory syndrome in children with COVID-19. Cell. 2020; 183 (4): 968-981.
48. Porritt RA, Binek A, Paschold L, Rivas MN, McArdle A, Yonker LM, et al. The autoimmune signature of hyperinflammatory multisystem inflammatory syndrome in children. J Clin Invest. 2021; 131 (20): e151520.
49. Hoffmann M, Kleine-Weber H, Schroeder S, Krüger N, Herrler T, Erichsen S, et al. SARS-CoV-2 cell entry depends on ACE2 and TMPRSS2 and is blocked by a clinically proven protease inhibitor. Cell. 2020; 181 (2): 271–80.
50. Zhou T, Tsybovsky Y, Gorman J, Rapp M, Cerutti G, Chuang GY, et al. Cryo-EM structures of SARS-CoV-2 spike without and with ACE2 reveal a pH-dependent switch to mediate endosomal positioning of receptor-binding domains. Cell host & microbe. 2020; 28 (6): 867–79.
51. Shikov AE, Barbitoff YA, Glotov AS, Danilova MM, Tonyan ZN, Nasykhova YA, et al. Analysis of the spectrum of ACE2 variation suggests a possible influence of rare and common variants on susceptibility to COVID-19 and severity of outcome. Front Genet. 2020; (11): 551220.
52. Zhao Y, Patel J, Huang Y, Yin L, Tang L. Cardiac markers of multisystem inflammatory syndrome in children (MIS-C) in COVID-19 patients: a meta-analysis. Am J Emerg Med. 2021; (49): 62–70.
53. Ahmed M, Advani S, Moreira A, Zoretic S, Martinez J, Chorath K, et al. Multisystem inflammatory syndrome in children: a systematic review. EClinicalMedicine. 2020; (26):100527.
54. Blondiaux E, Parisot P, Redheuil A, Tzaroukian L, Levy Y, Sileo C, et al. Cardiac MRI in children with multisystem inflammatory syndrome associated with COVID-19. Radiology. 2020; 297 (3):

283–8.
55. Jain E, Donowitz JR, Aarons E, Marshall BC, Miller MP, et al. Multisystem inflammatory syndrome in children after SARS-CoV-2 vaccination. Emerging Infectious Diseases. 2022; 28 (5): 990–3.
56. Nygaard U, Holm M, Hartling UB, Glenthøj J, Schmidt LS, Nordly SB, et al. Incidence and clinical phenotype of multisystem inflammatory syndrome in children after infection with the SARS-CoV-2 delta variant by vaccination status: a Danish nationwide prospective cohort study. Lancet Child Adolesc Health. 2022; 6 (7): 459–65.
57. Hoste L, Soriano-Arandes A, Buddingh EP, Whittaker E, Belot A, Ulloa-Gutierrez R, et al. Severe acute respiratory syndrome coronavirus 2 vaccination in children with a history of multisystem inflammatory syndrome in children: an international survey. J Pediatr. 2022; (248): 114–18.

NAVIGATED TRANSCRANIAL MAGNETIC STIMULATION: BRIEF REVIEW OF ENGINEERING SOLUTIONS

Zemlyakov IYu[2] ✉, Bureev ASh[1,2], Golobokova EV[1,2], Zhdanov DS[1,2], Kosteley YaV[1,2]

[1] National Research Tomsk State University, Tomsk, Russia

[2] National Medical Research Center of Rehabilitation and Balneology of Federal Medical Biological Agency, Moscow, Russia

Transcranial magnetic stimulation (TMS) stands out among the rapidly developing methods for clinical rehabilitation of patients after cerebral vascular accidents. The method is widely used not only in post-stroke rehabilitation, but also in sports medicine, psychiatry and other fields of medicine. However, there is an unresolved issue related to precise targeting and holding the magnetic field focus on the points of interest in the brain when performing TMS. Unprecise magnetic field focus localization may result in the emergence of side effects during the TMS session. The review provides the existing solutions of these problems, comparison of the commercially available navigation devices for TMS, analysis of their composition and operation algorithms; promising directions of developing hardware for TMS navigation are proposed.

Keywords: transcranial magnetic stimulation, technology overview, medical robots, neuroimaging, positioning

Funding: the study was performed as part of the State Assignment 84.007.22.800 "Construction and Clinical Approbation of Experimental Rehabilitation Robotic Hardware and Software Complex with Biological Feedback for Correction of Motor Deficits in Post-stroke Patients".

Acknowledgments: we would like to thank N.G. Abdulkina, Deputy General Director at the National Medical Research Center of Rehabilitation and Balneology of FMBA of Russia, for support of the research team; A.B. Vorozhtsov, Vice-Rector for Science and Innovation at the National Research Tomsk State University, for assistance with the development of research in the field of medical robotics.

Author contribution: Zemlyakov IYu — manuscript writing, drawing conclusions; Zhdanov DS — review of experimental design for nTMS systems; Bureev ASh — review of the principles of construction and performance of the commercially available nTMS complexes; Kosteley YaV — search for information about the available nTMS complexes; Golobokova EV — search for information about the directions of development and designs for nTMS systems.

Compliance with ethical standards: the study was approved by the Ethics Committee of the National Medical Research Center of Rehabilitation and Balneology of FMBA of Russia (protocol № 1 of 6 July 2022).

✉ **Correspondence should be addressed:** Ivan Yu. Zemlyakov
Rosy Luxemburg, 1, Tomsk, 634009, Russia; i_y_zem@mail.ru

Received: 03.08.2023 **Accepted:** 09.09.2023 **Published online:** 30.09.2023

DOI: 10.47183/mes.2023.038

НАВИГАЦИОННАЯ ТРАНСКРАНИАЛЬНАЯ МАГНИТНАЯ СТИМУЛЯЦИЯ: КРАТКИЙ ОБЗОР ТЕХНИЧЕСКИХ РЕШЕНИЙ

И. Ю. Земляков[2] ✉, А. Ш. Буреев[1,2], Е. В. Голобокова[1,2], Д. С. Жданов[1,2], Я. В. Костелей[1,2]

[1] Национальный исследовательский Томский государственный университет, Томск, Россия

[2] Научно-клинический центр медицинской реабилитации и курортологии Федерального медико-биологического агентства, Москва, Россия

В числе активно развивающихся методов клинической реабилитации больных после мозговых сосудистых катастроф особо выделяется транскраниальная магнитная стимуляция (ТМС). Метод широко применяют не только для постинсультной реабилитации, но и в спортивной медицине, психиатрии и других областях медицины. При этом существует нерешенная проблема, связанная с четким наведением и удержанием фокуса магнитного поля при ТМС на точках интереса в головном мозге. Из-за нечеткой локализации фокуса магнитного поля возможно возникновение побочных воздействий во время сеанса ТМС. В обзоре представлены существующие варианты решения данных проблем, сопоставлены присутствующие на рынке устройства для навигации ТМС, проанализированы состав и алгоритмы их работы, предложены перспективные направления развития технического обеспечения навигации ТМС.

Ключевые слова: транскраниальная магнитная стимуляция, обзор технологии, медицинские роботы, нейровизуализация, позиционирование

Финансирование: результаты получены при выполнении государственного задания 84.007.22.800 «Создание и клиническая апробация экспериментального образца реабилитационного роботизированного аппаратно-программного комплекса с биологической обратной связью для коррекции двигательных нарушений у больных, перенесших инсульт».

Благодарности: заместителю генерального директора ФГБУ ФНКЦ МРиК ФМБА России Абдулкиной Н. Г. за поддержку научного коллектива; проректору по научной и инновационной деятельности НИ ТГУ Ворожцову А. Б. за помощь в развитии исследований в области медицинской робототехники.

Вклад авторов: И. Ю. Земляков — написание статьи, формулировка выводов и заключения; Д. С. Жданов — анализ экспериментальных разработок для систем нТМС; А. Ш. Буреев — анализ принципов построения и работы серийно выпускаемых комплексов нТМС; Я. В. Костелей — поиск информации о выпускаемых комплексах нТМС; Е. В. Голобокова — поиск информации о направлениях развития и разработках для систем нТМС.

Соблюдение этических стандартов: исследование одобрено этическим комитетом ФГБУ ФНКЦ МРиК ФМБА России (протокол № 1от 06 июля 2022 г.).

✉ **Для корреспонденции:** Иван Юрьевич Земляков
ул. Розы Люксембург, д. 1, г. Томск, 634009, Россия; i_y_zem@mail.ru

Статья получена: 03.08.2023 **Статья принята к печати:** 09.09.2023 **Опубликована онлайн:** 30.09.2023

DOI: 10.47183/mes.2023.038

Transcranial magnetic stimulation (TMS) is an actively developed method for clinical neuromodulation and rehabilitation of ischemic patients. It is based on the brain tissue exposure to short pulses of high-intensity electromagnetic field (up to 4 T or more) generated by the induction effector (inductor or coil) [1, 2]. This results in the neuronal membrane depolarization and excitation [3]. Accumulation and analysis of clinical data on the results of using TMS have resulted in the expanded list of accessible defects, clarified parameters of using TMS in various clinical situations [2, 4]. Furthermore, TMS is used in sports medicine as a motor system stimulation method [5], in psychiatry for diagnosis and treatment of various conditions,

and шт other fields of medicine [6]. However, there are still a number of not completely resolved or controversial issues related to localization of the TMS magnetic field focus, desired intensity of exposure, and many other themes [5, 7].

Thus, impossibility to accurately match the stimulation point coordinates to the central nervous system anatomical structures is an important challenge faced when mapping motor areas using TMS [8]. The head and brain size and shape, localization of anatomical structures are unique. This makes the process of inductor positioning relative to the stimulation area challenging.

According to the Talairach coordinate system, individual differences in motor areas are 1.5–2 cm; these can be larger when considered relative to external reference points on the skull. This is also true for Broca's area localization [9], i. e. unique macroanatomy of the brain cannot be adequately defined using an anatomical atlas or a proportional coordinate grid. The navigated TMS (nTMS) method, in which the inductor spatial orientation is set based on the magnetic resonance imaging (MRI) data analysis, has been proposed to address the problem of inductor positioning [8, 10]. The use of this method to a significant extent solves the problem of coil positioning when performing therapeutic and/or diagnostic TMS.

The motor threshold testing for the motor response to the lowest possible stimulation level resulting in contraction of appropriate muscles is considered to be a standard criterion for assessment of the efficiency of the TMS effect on the excitable brain structures. It has been shown that even a slight shift of the inductor relative to the optimal point of exposure can significantly reduce the stimulation efficiency [7, 8, 10, 11–13]. Furthermore, any serial patient's exposure requires high reproducibility. Given its weight and size characteristics, manual holding of the coil in a predetermined position when the session duration is 10 min or more makes these tasks almost impossible, while these require technical execution [8, 10]. However, analysis of information taken from the available databases and catalogues has shown that despite huge number of reports of the nTMS clinical use, the data on engineering solutions for the method and the trends in their development are limited and fragmented. In this review we try to discuss the existing solutions and possible prospects of nTMS development from a technical perspective.

Main principles of navigated TMS functioning

The use of the stereoscopic technical vision system in combination with constructing a 3D model of the brain based on MRI scans turned out to be the most effective solution for matching the point of exposure in the brain to specific tags on the skull, magnetic field focus, and spatial position of the inductor [14]. The study performed by these authors was based on the 3D inductor positioning relative to a solid model of the brain with a stereoscopic video system using a common coordinate grid (Figure).

Two sets of procedures are executed to implement this scheme: initial cycle of nTMS session preparation and the repeating inductor position adjustment cycle. The algorithm for initial cycle shown on the left (Figure) includes the following operations:

1) constructing a 3D model of the brain based on the set of primary T1-weighted (T1W) MRI images;

2) MRI image segmentation and constructing a 3D model of the patient's brain using the BET algorithm [15]. False positive results are automatically deleted, while false negatives are added interactively. The brain surface and structures are reconstructed using flat contours;

3) determining the target area in the brain model relative to the skull considering the features of magnetic field focus and the distance to inductor ensuring the required magnetic field density;

4) recognition and localization of the patient's head using optical tags or any other method. The inductor coil localization and position are recognized the same way;

5) aligning the model of the brain, skull and inductor oriented towards the target area using the coordinate grid;

6) moving the inductor into the estimated baseline position depending on the patient's head position. Preparation for the nTMS session is complete.

In real-world settings it is necessary to consider the change in the patient's posture and his/her head move out of the calculated coordinates. In this case a software module for the repeating cycles of inductor position adjustment is responsible for correction of errors in the nTMS system. This algorithm shown on the right (Figure) includes the following operations:

1) periodic detection of the inductor and patient's head position by the technical vision system and recalculation of current coordinates relative to baseline values. If no discrepancies are found, no action is taken;

2) recalculation of coordinates and the direction of the inductor axis in case of inconsistency between the baseline and current relative position of the inductor and the model of the brain aimed to compensate the error indicated;

3) generation of the message about the need to navigate the inductor to a new position;

4) control recalculation to test whether the new position of inductor is matched to the target area;

5) recalculation and image output in absolute coordinates with the new position of inductor relative to the bias of the brain 3D model .

Efficiency of the described nTMS functioning algorithm has been confirmed by the experiments involving a human skull phantom and head MRI data of the healthy individual. The algorithm showed a trend toward flexibility, safety, accuracy, and time saving [14]. The system included a TMS unit, electromyography system, electroencephalography system, rack with inductor, and a computerized navigation system. The average errors of coordinate selection resulted mainly from the errors of MRI images: the errors on axes X, Y, and Z were 5 mm, 3 mm, and 3 mm, respectively. Later this approach was implemented in other models of nTMS systems [16].

It has been shown, that the TMS-induced electroencephalography (EEG) shows high reproducibility (correlation coefficient r = 0.85) within 200 ms before the stimulus termination given the exposure parameters are constant. Even a 10 mm shift of inductor results in significant EEG changes. The use of nTMS is the only possible way to ensure stability of the evoked effects [7].

However, there are nTMS errors that are yielded by the sources of errors:

1) individual features of magnetic field distribution across the cortex depending on the brain tissue state;

2) errors of brain MRI scan and appropriate distortion of the brain 3D model;

3) shift of focus due to patient's head movement after setting the focus;

4) errors of magnetic field generation by the coil.

The impact of such error on the joint position of the inductor and the head, as well as on the magnetic field, was analyzed based on the simplified and realistic models of the head [11]. Modeling involved the use of the SimNIBS computer subroutine library [12] and the sets of T1-weighted fat-suppressed and

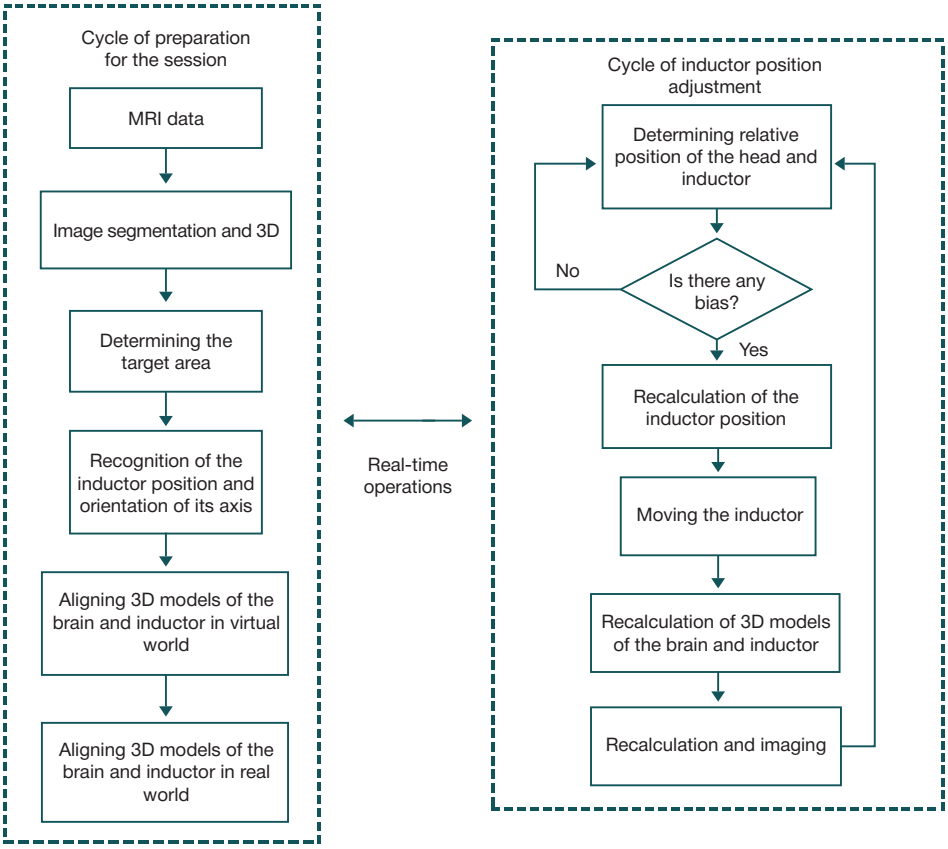

Fig. The nTMS system operation algorithm

T2-weighted MRI images with the 1 mm3/voxel resolution. The average bias of joint spatial position was within 2.2–3.6 mm and 1°. The errors were related to the MRI images with the average bias of 1.5–1.9 mm at the error of 0.2–0.4° and bias of 0.5–0.8 mm at the error of 0.1–0.2° for the models used. When assessing the magnetic field bias, the average accuracy of positioning, assessing the field orientation and peak value was within the ranges of 1.5–5.0 mm, 0.9–4.8°, and 4.4–8.5%. The modeling results showed a significantly reduced inductor positioning error during nTMS relative to standard recommendations, such as "over the projection of the upper third of the cerebral cortex motor area", and shift of inductor position relative to the external tags on the head measured in centimeters [13].

Commercially available nTMS complexes

Today, the following models of nTMS units implementing standard solutions are mass-produced (Table). The units are built on similar schemes based on the technical vision system (TVS). Optical tags or characteristic areas of face and head are used as orientation elements. The inductor position is changed directly using a robotic manipulator, while indirect changes are made in manual mode by following the signals of the nTMS control system.

The VISOR 2 nTMS system uses a 3D model of the brain constructed based on MRI images [17]. If no such model is available, simplified models are used. TVS tracks optical trackers positioned on the head and inductor. As a result, the 3D model of the brain and the inductor are pinned to the system of external tags in the three-dimensional coordinate grid. The physician follows the commands of the system to position the inductor in space. With a certain skill, the coordinate bias determined is about 2 mm. The VISOR2 system can be operated in combination with compatible TMS complexes, including the domestic Neuro-MC/B complex.

The TMS Navigator navigation system (LOCALITE; Germany) is also based on using technical vision to pin a 3D model of the brain, images of the patient's head and inductor obtained using video cameras to the three-dimensional navigation grid with optical trackers [18]. The algorithm for accurate matching of these objects to audio indication of the inductor position bias ensures the magnetic flux focus retention. For targeted stimulation, the system allows registration of four inductors of different types. It is possible to calculate the amount of energy that would be delivered to the target point. In the Robotic Edition version of the system, automatic inductor positioning aimed at compensating the patient's movements is performed using optical feedback.

The TMS Robot robotic system (Axilum Robotics; France) is implemented as a construct that combines a seven-degree-of-freedom manipulator, inductor, control unit, and a chair for the patient [19]. The principles of functioning, determining the coordinates of patient's head, target area, and inductor are similar to the listed above. After constructing a 3D model of the brain and assessing the head position, a TVS manipulator positions the inductor to ensure a precise focused effect. The patient's head movements are automatically compensated by moving the inductor. Manipulator and the chair have nine position sensors, which ensure baseline positioning accuracy of at least 1 mm along all axes; when the head moves, the inductor orientation is restored with the accuracy of at least 0.1 mm. This positioning system is used in combination with the Syneika One neuronavigation system.

The Syneika One neuronavigation system (SYNEIKA; France) is an integrated device that ensures coil navigation based on the data of the patient's brain 3D model [20]. The coil positioning and orientation are accomplished using

Table. Comparison of some existing navigation devices for TMS

System	VISOR2	TMS Navigator	TMS Robot	Syneika One	NBS eXimia Nexstim	Brainsight TMS Navigation	PowerMAG View!
Contractor	ANT Neuro, Netherlands	LOCALITE, Germany	Axium Robotics, France	SYNEIKA, France	Nexstim Ltd., Finland	Brainbox, UK	Jali Medical, USA
Optical navigation (type)	Yes	Yes, trackers	Other sensor type	Other sensor type	Yes, trackers	Yes, trackers	Yes, trackers
Manipulator available	No	Yes	Yes	No	No	No	No
Coil position adjustment	Indirect	Direct	Direct		Indirect	Indirect	Indirect
Chair for the patient	No	Yes	Yes	No	Yes	Yes	Yes
Features					Modeling of magnetic field distribution	Can be assembled of modules	Enables functional brain mapping

options of the described above Axilum Robotics TMS-Robot complex [19]. The TMS-Robot robotic rack guided by Syneika One moves the coil through space, thereby ensuring precise targeting the stimulation area and compensating possible head motion. There are no data on the sensor types used to assess the head and inductor position in the reports available.

TMS-Cobot, manufactured by the same company but implemented as a mobile device, represents a more simple and space-saving solution compared to TMS Robot [21]. The inductor positioning accuracy is 2 mm. The possibility of tracking the head position by optical system is preserved, however, it only supports the patient's head upper hemisphere due to smaller manipulator size. This device is not equipped with its own system for the brain 3D model construction and spatial navigation, it also has to operate under the control of external neuronavigator, such as Syneika One.

The NBS eXimia Nexstim complex (Nexstim Ltd.; Finland) designed in mid 2000s continues to evolve [22, 23]. The complex has advanced software allowing one to construct a high-precision 3D model of the brain consisting of more than 20,000 elements, control its representation and ensure targeted effect using a large touch screen monitor. An option of modeling the magnetic field distribution considering individual brain structure features is a hallmark of the system. Robotic devices are not used for targeting and retaining the coil when the patient moves. The inductor installation on the rack and spatial orientation are done manually following the targeting system instructions. Bias of the effect targeting does not exceed 10 mm.

The Brainsight TMS Navigation neuronavigation series (Brainbox; UK) to be used in combination with the DuoMAG XT series transcranial magnetic stimulator supporting the induced EEG recording [24] has become quite widespread. The market offers the Brainslight TMS Navigator and Brainslight TMS Chair integrated systems. The possibility of assembling specialized complexes of distinct modules is an interesting feature of the company's products.

The PowerMAG View! and ANT Neuro visor2 (Jali Medical; USA) neuronavigation systems, which use optical tags fixed on the patient's head with an elastic band as reference points for stereoscopic system, are used for research and diagnosis [25]. A 3D model of the brain is usually constructed based on MRI data, there is an option for functional brain mapping. The patient is seated in a chair with his head on the headrest. A simple rack is used to attach the inductor.

The NetBrain Neuronavigator 9000 complex (EB Neuro; Italy) is designed to be used in combination with the TMC STM 9000 Magnetic Stimulator manufactured by the same company [26]. The manufacturer positions the complex as a low-end device that nevertheless has advanced characteristics: bias of matching a 3D model of the brain to the coordinates of optical tags on the patient's head using the stereoscopic system can be less than 1 mm. The complex is operated using the Galileo software allowing one to communicate with the TMS unit and construct a 3D model of the brain, as well as to record the procedure and manage the patient's data. The patient reclines in a chair, and the TMS inductor is attached to the rack. The coil positioning and orientation in space are performed based on the prompts generated by the neuronavigation system.

The SimGuide Navigated TMC neuronavigation software package (MagSim Co Ltd; UK) is designed to work with the Horizon 3.0, Horizon Performance, and Horizon Lite units for transcranial therapy manufactured by the same company [27]. In all cases, a high-resolution stereoscopic system and the patient's elastic helmet with optical tags are used for spatial alignment of the head, 3D model of the brain, and the inductor mounted on the rack.

Similar features are offered by the Neuronavigated TMS system for visualization of anatomic and functional features based on the MRI data (SEBERS Medical; USA, Germany) [28]. One software suite enables communication with five types of M-series TMS units manufactured by the same company. The coil installation and orientation are performed using the stereoscopic system. The effect control is ensured by recording evoked EMG potentials using a wireless dual-channel electromyography unit.

It should be noted that the majority of commercially available nTMS systems use magnetic stimulation devices manufactured by third-party companies. The clinical data analysis [4–6] shows that the use of nTMS improves the efficiency of magnetotherapy course, since it ensures proper localization and high reproducibility of the effect, although there are alternative opinions [29]. However, these systems have not yet been widely introduced in domestic practice. Perhaps, this is due to the fact that nTMS systems are expensive, and the use of such systems requires medical personnel to have certain skills and knowledge in the field of computer engineering.

Experimental nTMS systems

The patient's semi-recumbent position with his/her head on the headrest is the simplest solution for nTMS realization [7, 16, 13, 22, 23]. This ensures head motion limitation, and the inductor orientation and retention can be ensured by the rack or by hand. However, this solution prevents exposure of the occipital areas. The alternative is a sitting position (if possible), however,

in this case there is a problem of the TMS effect focus retention associated with unrestricted mobility of the head during the session that can be solved by using a robotic coil positioning system [19, 20].

Experimental nTMS systems capable of tracking the patient's movements emerged about 15 years ago [30]. A robotic manipulator moved the inductor to follow the arbitrary trajectory along the axes X and Y within the range of 90 cm at angles of ± 45°, while the Z axis rotation was within the range of 360°. The error of installing the inductor with the weight of 1.5 kg did not exceed 1 mm on all axes. The inductor bias did not exceed 50 μm/min in any plain: it was 1 mm during the 20 min TMS session, which was not critical.

A simplified nTMS system has been described, in which the physician selects the TMS inductor position based on the patient's skull shape only (the output of TVS operation) [31]. The method proposed reduces the amount of data used to construct a 3D model of the brain approximately by an order, however, the risk of effect focusing errors is increased due to individual features of anatomical structure.

The precision nTMS system described by other authors is based on the scheme of the object coordinate recognition that is based on the high-resolution TVS, reflective trackers, and 3D model of the patient's brain constructed using the MRI data [32]. The use of infrared illumination at the wavelength of 850 nm that has partially solved the problem of the impact of hair on the scull model construction is the distinctive feature.

The use of trackers mounted on the patient's head and inductor makes it difficult to prepare for the nTMS session. As an alternative, it is suggested to estimate the head position using the characteristic face areas [33], however, this complicates construction of TVS and related software used to link the data from video cameras, 3D model of the brain, and position of inductor. At the same time, this solution accelerates and simplifies the TMS procedure, eliminates errors associated with the tracker bias.

The more simple nTMS variant involving orientation towards characteristic face areas uses only the skull model constructed based on the TVS data [34]. The inductor orientation is performed based on the scaled anatomical atlas data instead on the brain 3D model constructed using MRI.

When the patient has thick hair, the error of the skull model constructing using TVS and determining the compliance of the brain 3D model constructed can be reduced using the elastic cap that fits tightly on the head or the band with a picture of a chessboard with the elements of known size [35]. However, we believe that this solution represents the variant of using optical trackers with appropriate bias.

The virtual reality systems combining 3D models of the brain, skull, and inductor in a unified coordinate system are used to help the physician during the nTMS session [36]. This makes it possible to control fine-tuning of the inductor position without special skills using the minimalistic graphical and audio interface. The proposed approach turned out to be the least time-consuming in all proposed conditions relative to conventional neuronavigation. However, the latter showed higher targeting accuracy ($p < 0.001$).

When the virtual reality system is supplemented by the image of inductor specifying the magnetic field vector and density [37], the operator has to place the inductor coil in proper position and set the stimulation parameters, other operation will be performed in the automated mode. As a result, clarity of the created exposure scheme, reduction in time required for the session preparation, and simplification of all operations can be observed.

Reduction of the magnetic field side effects on the brain structures adjacent to the exposure focus during the TMS session is an important problem. This problem can be solved by using a figure-eight coil focusing the maximum field strength at the intersection of magnetic flux vectors [38]. As a result, the effect strength range is expanded and the focusing accuracy is increased, thereby reducing the risk of side effects and complications. However, the magnetic field generation system turns out to be rather bulky, requires precision production, and the shape of the target spot turns out to be unpredictable when the source is defocused, like the magnetic field strength in it.

It has been shown that the fixed-position dual centrosymmetric inductors form a dual focus exposure area [39]. This makes it possible to change the focus coordinate within a broad range by controlling the angle of their orientation only before the TMS session.

CONCLUSION

Certainly, it is impossible to provide multiple options and examples of implementation related to the technical background of navigated TMS. However, here we can highlight several areas for development of the method technical background.

First, this is improvement of the software part of constructing 3D models of the patient's brain and skull (head). It seems particularly challenging to increase accuracy of constructing a 3D image of brain tissues based on MRI data: resolution of the high-field MRI scanners enables recognition of objects sized 1–2 mm in increments of 5 mm with an angle error of ± 1° in the images, which is due to the apparatus table motion precision. Therefore, a properly working and adjusted scanner allows one to acquire a series of brain slices with an accuracy of about 1 mm, which is enough for the majority of applications. In rare cases when higher image resolution is required, one of the well-known nonlinear image interpolation methods can be used, however, correctness of such solution is questionable.

Second, it is improvement of the TMS inductor positioning and orientation accuracy. The experience of constructing a 3D model of the brain shows that positioning of the inductor axis with the angle accuracy of ±1° and the coordinates' uncertainty of ± 1 mm on all axes can be enough. It should be noted that the "spot" of magnetic field focus represents a bundle of tension lines (that of figure-eight coil is a circle with a diameter of 5–8 mm and blurry margins) [40]. Adjacent brain structures can be affected, but this can be perceived as the method inevitable cost. The use of the oriented two by two inductors of varying size, magnetic safety screens or magnetic field replicators enables improvement of the focusing accuracy [41].

Third, it is abandoning the handy elements simplifying recognition of the patient's skull position, which include various optical reflectors and probes mounted in pre-defined sites on the patient's head. In addition to the fact that installation of such elements results in inevitable installation accuracy errors, this requires the continuous use of disposables. We believe that aligning 3D models of the patient's brain and head using the clearly distinguishable face elements that are present in both cases (nose, eye sockets, brow ridges, and ears) is the most promising.

Fourth, it is the use of available variants of the control means realization and ensuring safety during the TMS session. This includes preliminary calculation of the field strength in the inductor focus with its indirect control during exposure. In our opinion, the effect strength control circuit is also essential that can be implemented in the form of the automated regulatory link based on the EEG and/or EMG data or in the form of the

component of verbal biological feedback via control enabling manual magnetic flux intensity adjustment within certain limits by the patient.

Fifth, it is considerable simplification and acceleration of preparation for the nTMS session due to emerging options and experimental virtual reality systems enabling overlapping of 3D models of the brain, skull, and inductor in the common three-dimensional space considering the magnetic field effect vector.

And finally it is the need for reliable hardware and software implementation of the robotic manipulator used to ensure retention of the inductor focus on the pre-specified brain area regardless of the patient's position. The majority of available nTMS construction variants provide for the patient is in supine or semi-recumbent position, which makes it difficult to place the inductor over the patient's head occipital part. The use of the chair to sit the patient requires installation of the headrest at least for approximate fixation of the head in proper position. However, the headrest inevitably distorts the magnetic field shape, even if made of non-magnetic materials. The only variant is the patient's posture with the head bent to the chest, however, the possibility of the head free motion makes it rather difficult to ensure the inductor focus retention via robotic manipulator control.

In general it should be noted that the nTMS method has evolved considerably in the past 15 years in terms of both methodology and technical background. Despite the fact that the majority of originally existing problems have been solved completely or partially, it is necessary to resume the search for variants of increasing the method efficacy, ensuring its safety, and reducing the cost of hardware.

References

1. Barker AT, Jalinous R, Freeston IL. Non-invasive magnetic stimulation of human motor cortex. Lancet. 1985; (May 11): 1 (8437): 1106–7. DOI: 10.1016/s0140-6736(85)92413-4. PMID: 2860322.
2. Bakulin IS, Poydasheva AG, Lagoda DYu, Suponeva NA, Piradov MA. Perspektivy razvitiya terapevticheskoy transkranial'noy magnitnoy stimulyatsii. Nervnye bolezni. 2021; 4: 3–17. DOI: 10.24412/2226-0757-2021-12371. Russian.
3. Sorokina ND, Zherdeva AS, Selitsky GV et al. Neurophysiological methods for assessing different forms of migraine. Neurosci Behav Physi. 2022; 52: 202–6. DOI: 10.1007/s11055-022-01224-4.
4. Suponeva NA, Bakulin IS, Poydasheva AG, Piradov MA. Safety of transcranial magnetic stimulation: review of international guidelines and new findings. Neuromuscular Diseases. 2017; 7 (2): 21–36. DOI: 10.17650/2222-8721-2017-7-2-21-36. Russian.
5. Komlev IO, Kislenko AS. Transkranial'naya magnitnaya stimulyatsiya: sovremennoe sostoyanie i perspektivy ispol'zovaniya v sporte (obzor). Aktual'nye voprosy fizicheskoy kul'tury i sporta. 2016; 16: 146–52. Russian.
6. Mosolov SN, Tsukarzi EE, Egorov AYu, Gorelik AL, Naryshkin AG. Transkranial'naya magnitnaya stimulyatsiya. In: Aleksandrovskiy Yu. A., Neznanov N. G., redaktory. Psikhiatriya. Kratkoe izdanie: natsional'noe rukovodstvo. M.: GEOTAR-Media, 2021; s. 749–53. Russian.
7. Kuhnke P, Numssen O, Völler J, Weise K, Hartwigsen G. Dosage optimization for transcranial magnetic stimulation based on cortical field thresholds. Clinical Neurophysiology, 2023; 148: 87. DOI: 10.1016/j.clinph.2023.02.104.
8. Chervyakov AV, Piradov MA, Savitskaya NG, Chernikova LA, Kremneva EI. Novyy shag k personifitsirovannoy meditsine. Navigatsionnaya sistema transkranial'noy magnitnoy stimulyatsii (NBS eXimia Nexstim). Annaly klinicheskoy i eksperimental'noy nevrologii. 2012; 6 (3): 37–46. Russian.
9. Mtui E., Gryuner G., Dokeri P. Klinicheskaya neyroanatomiya i nevrologiya po Fitsdzheral'du. M.: Izd-vo Panfilova; 2018. 388 s. Russian.
10. Ruohonen J, Karhu J. Navigated transcranial magnetic stimulation. Neurophysiol Clin. 2010; 40 (1): 7–17. DOI: 10.1016/j.neucli.2010.01.006. PMID: 20230931.
11. Makarov SN, Wartman WA, Daneshzand M, Fujimoto K, Raij T, Nummenmaa A. A software toolkit for TMS electric-field modeling with boundary element fast multipole method: An efficient MATLAB implementation. Journal of Neural Engineering. 2020; 17 (4). DOI: 10.1088/1741-2552/ab85b3.
12. SimNIBS 4. 2020 Jun. [cited 2023 May 6]. Available from: https://simnibs.github.io/simnibs/.
13. Ragimova AA, Petelin DS, Zakharova NV, Kozhokaru AB, i dr. Primenenie transkranial'noy magnitnoy stimulyatsii v psikhiatricheskoy i psikhonevrologicheskoy praktike. M.: Izd-vo Sechenovskogo Universiteta, 2022; 150 s. Russian.
14. Liu S, Shi L, Wang D, Chen J, Jiang Z, Wang W, et al. Mri-guided navigation and positioning solution for repetitive transcranial magnetic stimulation. Biomedical Engineering: Applications, Basis and Communications. 2013; 25 (1): 1350012. DOI: 10.4015/s1016237213500129.
15. Smith SM. Fast robust automated brain extraction. Hum Brain Mapp. 2002; 17 (3): 143–55. DOI: 10.1002/hbm.10062. PMID: 12391568; PMCID: PMC6871816.
16. Nieminen AE, Nieminen JO, Stenroos M, Novikov P, Nazarova M, Vaalto S, et al. Accuracy and precision of navigated transcranial magnetic stimulation. J Neural Eng. 2022; 19 (6). DOI: 10.1088/1741-2552/aca71a. PMID: 36541458.
17. VISOR2 navigation system for transcranial magnetic stimulation [cited 2023 Apr 30]. Available from: https://neurosoft.com/ru/catalog/equipment/90329. Russian.
18. TMS-Navigator. [cited 2023 May 6]. Available from: https://www.localite.de/en/products/tms-navigator/.
19. Robotic Assistant for Transcranial Magnetic Stimulation (TMS). [cited 2023 May 7]. Available from: https://www.axilumrobotics.com/en/tms-robot/?noredirect=en-US.
20. Neuronavigation for Transcranial Magnetic Stimulation TMS [cited 2023 September 2]. Available from: https://www.syneika.fr/en/.
21. TMS-Cobot Features. Setting a new standard for Transcranial Magnetic Stimulation with collaborative robotics [cited 2023 May 7]. Available from: https://www.axilumrobotics.com/en/tms-cobot-features/?noredirect=en-US.
22. Unmatched accuracy in TMS [cited 2023 September 2]. Available from: https://www.nexstim.com.
23. Rukovodstvo pol'zovatelya Nexstim® NBS System 5. Nexstim Plc. 2014; 228 c. Russian.
24. BRAINBOX TMS Transcranial Magnetic Stimulation [cited 2023 September 2]. Available from: https://brainbox-neuro.com/techniques/tms.
25. Jali Medical Neuronavigation Applications [cited 2023 September 2]. Available from: https://www.jalimedical.com/neuronavigation.php.
26. STM 9000 New Frontier in Magnetic Stimulation. Infomed Medzintechnik GmbH. 2018; 4.
27. Magstim TMS Therapy [cited 2023 September 2]. Available from: https://www.magstim.com/row-en/product-category/therapy/.
28. SEBERS Medical Neuronavigated TMS [cited 2023 September 2]. Available from: https://sebersmedical.com/product/neuronavigated-tms/.
29. Jeltema H-R, Ohlerth A-K, Wit A, Wagemakers M, Rofes A, Bastiaanse R, et al. Comparing navigated transcranial magnetic stimulation mapping and "gold standard" direct cortical stimulation mapping in neurosurgery: a systematic review. Neurosurgical Review. 2021; 44 (4): 1903–20. DOI: 44.10.1007/s10143-020-01397-x.
30. Okada A, Nishikawa A, Fukushima T, Taniguchi K, Miyazaki F, Sekino M, et al. Magnetic navigation system for home use of repetitive transcranial magnetic stimulation (rTMS). 2012 ICME International Conference on Complex Medical Engineering (CME).

Kobe, Japan. 2012; p. 112–8. DOI: 10.1109/iccme.2012.6275591.
31. Shin S, Kim S, Seo Y, An J, Kim H, Chung S, et al. Development of stereo camera module using webcam for navigation Transcranial Magnetic Stimulation system. 5th International Conference on BioMedical Engineering and Informatics 16–18 October 2012. 2012; p. 113–6. DOI: 10.1109/bmei.2012.6513167.
32. Bo W, Chjitsan C, Kun C, Bin Y, inventors; Shenyang Keen Technology Co. Ltd., assignee. The navigation positional device of a kind of transcranial magnetic stimulation device and localization method. China patent CN106110507A. 2016 Jul 26.
33. Tsun S, Bo W, Shanan C, inventors; Wuhan Capital Association Hong Kang Polytron Technologies Inc., assignee. Transcranial magnetic stimulation diagnosis and treatment navigation system based on camera. China patent CN110896611A. 2020 Mar 3.
34. Gangliang Z, Tianzai J, Zhengyi Y, Xuefeng L, Liang M, inventors; Shenyang Institute of Automation of CAS, assignee. Position and posture positioning device, method and equipment of transcranial magnetic stimulation coil for brain atlas navigation. China patent CN114073820A. 2022 Feb 22.
35. Schütz L, Weber E, Niu W, Daniel B, Mcnab J, Navab N, et al. Audiovisual augmentation for coil positioning in transcranial magnetic stimulation. Computer Methods in Biomechanics and Biomedical Engineering Imaging & Visualization. 2023; 11 (4): 1130–5. DOI: 10.1080/21681163.2022.2154277.
36. Jijun W, Yingying T, Wenyao Z, Yifeng X, Tianhong Z, inventors; Shanghai Mental Health Center (shanghai Psychological Counseling Training Center), assignee. Accurate transcranial magnetic stimulation online navigation method based on augmented reality. China patent CN111249622A. 2020 Jan 17.
37. Peng Z, Manhua L, Xin W, Jingxin W, Xiaotao L, inventors; Hunan Huayi Electromagnetic Medicine Research Institute Co Ltd., assignee. Transcranial magnetic stimulation device, transcranial magnetic stimulation system and transcranial magnetic stimulation method. China patent CN114225223A. 2021 Dec 31.
38. Peng Z, Manhua L, Xin W, Jingxin W, Yibo L, inventors; Hunan Huayi Electromagnetic Medicine Research Institute Co Ltd., assignee. Transcranial magnetic stimulation system and method. China patent CN114146315A. 2021 Dec 31.
39. Qiyong G, Haoyang X, Xiaoqi H, Su L, inventors; West China Hospital of Sichuan University, assignee. Electromagnetic navigation system and method for TMS coil. China patent CN113350698A. 2021 Mar 31.
40. Kvartalnyy MA, Davydov MV, Lynkov LM, Sagay Maruf G. Modeliruyushchie usloviya transkranial'noy magnitnoy stimulyatsii mozga v zavisimosti ot vida induktora. Doklady BGUIR — Belorusskiy gosudarstvennyy universitet informatiki i radiotekhniki. 2015; 94 (8): 57–63. Russian.
41. Samuylov IV, Kaydak MN, Sagay MGG, Belan VA. Vliyanie ekranov na raspredeleniya impul'snykh magnitnykh poley pri transkranial'noy magnitnoy stimulyatsii. Doklady belorusskogo gosudarstvennogo universiteta informatiki i radioelektroniki. 2016; 101 (7): 159–63. Russian.

Литература

1. Barker AT, Jalinous R, Freeston IL. Non-invasive magnetic stimulation of human motor cortex. Lancet. 1985; (May 11): 1 (8437): 1106–7. DOI: 10.1016/s0140-6736(85)92413-4. PMID: 2860322.
2. Бакулин И. С., Пойдашева А. Г., Лагода Д. Ю., Супонева Н. А., Пирадов М. А. Перспективы развития терапевтической транскраниальной магнитной стимуляции. Нервные болезни. 2021; 4: 3–17. DOI: 10.24412/2226-0757-2021-12371.
3. Sorokina ND, Zherdeva AS, Selitsky GV et al. Neurophysiological methods for assessing different forms of migraine. Neurosci Behav Physi. 2022; 52: 202–6. DOI: 10.1007/s11055-022-01224-4.
4. Супонева Н. А., Бакулин И. С., Пойдашева А. Г., Пирадов М. А. Безопасность транскраниальной магнитной стимуляции: обзор международных рекомендаций и новые данные. Нервно-мышечные болезни. 2017; 7 (2): 21–36. DOI: 10.17650/2222-8721-2017-7-2-21-36.
5. Комлев И. О., Кисленко А. С. Транскраниальная магнитная стимуляция: современное состояние и перспективы использования в спорте (обзор). Актуальные вопросы физической культуры и спорта. 2016; 16: 146–52.
6. Мосолов С. Н., Цукарзи Э. Э., Егоров А. Ю., Горелик А. Л., Нарышкин А. Г. Транскраниальная магнитная стимуляция. В книге: Александровский Ю. А., Незнанов Н. Г., редакторы. Психиатрия. Краткое издание: национальное руководство. М.: ГЭОТАР-Медиа, 2021; с. 749–53.
7. Kuhnke P, Numssen O, Völler J, Weise K, Hartwigsen G. Dosage optimization for transcranial magnetic stimulation based on cortical field thresholds. Clinical Neurophysiology. 2023; 148: 87. DOI: 10.1016/j.clinph.2023.02.104.
8. Червяков А. В., Пирадов М. А., Савицкая Н. Г., Черникова Л. А., Кремнева Е. И. Новый шаг к персонифицированной медицине. Навигационная система транскраниальной магнитной стимуляции (NBS eXimia Nexstim). Анналы клинической и экспериментальной неврологии. 2012; 6 (3): 37–46.
9. Мтуи Э., Грюнер Г., Докери П. Клиническая нейроанатомия и неврология по Фицджеральду. М.: Изд-во Панфилова, 2018; 388 с.
10. Ruohonen J, Karhu J. Navigated transcranial magnetic stimulation. Neurophysiol Clin. 2010; 40 (1): 7–17. DOI: 10.1016/j.neucli.2010.01.006. PMID: 20230931.
11. Makarov SN, Wartman WA, Daneshzand M, Fujimoto K, Raij T, Nummenmaa A. A software toolkit for TMS electric-field modeling with boundary element fast multipole method: An efficient MATLAB implementation. Journal of Neural Engineering. 2020; 17 (4). DOI: 10.1088/1741-2552/ab85b3.
12. SimNIBS 4. 2020 Jun. [cited 2023 May 6]. Available from: https://simnibs.github.io/simnibs/.
13. Рагимова А. А., Петелин Д. С., Захарова Н. В., Кожокару А. Б. и др. Применение транскраниальной магнитной стимуляции в психиатрической и психоневрологической практике. М.: Изд-во Сеченовского Университета, 2022; 150 с.
14. Liu S, Shi L, Wang D, Chen J, Jiang Z, Wang W, et al. Mri-guided navigation and positioning solution for repetitive transcranial magnetic stimulation. Biomedical Engineering: Applications, Basis and Communications. 2013; 25 (1): 1350012. DOI: 10.4015/s1016237213500129.
15. Smith SM. Fast robust automated brain extraction. Hum Brain Mapp. 2002; 17 (3): 143–55. DOI: 10.1002/hbm.10062. PMID: 12391568; PMCID: PMC6871816.
16. Nieminen AE, Nieminen JO, Stenroos M, Novikov P, Nazarova M, Vaalto S, et al. Accuracy and precision of navigated transcranial magnetic stimulation. J Neural Eng. 2022; 19 (6). DOI: 10.1088/1741-2552/aca71a. PMID: 36541458.
17. VISOR2 система навигации при транскраниальной магнитной стимуляции [последнее цитирование 30 апреля 2023 г.]. Доступно по ссылке: https://neurosoft.com/ru/catalog/equipment/90329.
18. TMS-Navigator. [cited 2023 May 6]. Available from: https://www.localite.de/en/products/tms-navigator/.
19. Robotic Assistant for Transcranial Magnetic Stimulation (TMS) [cited 2023 May 7]. Available from: https://www.axilumrobotics.com/en/tms-robot/?noredirect=en-US.
20. Neuronavigation for Transcranial Magnetic Stimulation TMS. [cited 2023 September 2]. Available from: https://www.syneika.fr/en/.
21. TMS-Cobot Features. Setting a new standard for Transcranial Magnetic Stimulation with collaborative robotics [cited 2023 May 7]. Available from: https://www.axilumrobotics.com/en/tms-cobot-features/?noredirect=en-US.
22. Unmatched accuracy in TMS [cited 2023 September 2]. Available from: https://www.nexstim.com.
23. Руководство пользователя Nexstim® NBS System 5. Nexstim Plc, 2014; 228 с.
24. BRAINBOX TMS Transcranial Magnetic Stimulation [cited 2023 September 2]. Available from: https://brainbox-neuro.com/

techniques/tms.

25. Jali Medical Neuronavigation Applications [cited 2023 September 2]. Available from: https://www.jalimedical.com/neuronavigation.php.
26. STM 9000 New Frontier in Magnetic Stimulation. Infomed Medzintechnik GmbH. 2018; 4.
27. Magstim TMS Therapy [cited 2023 September 2]. Available from: https://www.magstim.com/row-en/product-category/therapy/.
28. SEBERS Medical Neuronavigated TMS [cited 2023 September 2]. Available from: https://sebersmedical.com/product/neuronavigated-tms/.
29. Jeltema H-R, Ohlerth A-K, Wit A, Wagemakers M, Rofes A, Bastiaanse R, et al. Comparing navigated transcranial magnetic stimulation mapping and “gold standard” direct cortical stimulation mapping in neurosurgery: a systematic review. Neurosurgical Review. 2021; 44 (4): 1903–20. DOI: 44.10.1007/s10143-020-01397-x.
30. Okada A, Nishikawa A, Fukushima T, Taniguchi K, Miyazaki F, Sekino M, et al. Magnetic navigation system for home use of repetitive transcranial magnetic stimulation (rTMS). 2012 ICME International Conference on Complex Medical Engineering (CME). Kobe, Japan. 2012; p. 112–8. DOI: 10.1109/iccme.2012.6275591.
31. Shin S, Kim S, Seo Y, An J, Kim H, Chung S, et al. Development of stereo camera module using webcam for navigation Transcranial Magnetic Stimulation system. 5th International Conference on BioMedical Engineering and Informatics 16–18 October 2012. 2012; p. 113–6. DOI: 10.1109/bmei.2012.6513167.
32. Bo W, Chjitsan C, Kun C, Bin Y, inventors; Shenyang Keen Technology Co. Ltd., assignee. The navigation positional device of a kind of transcranial magnetic stimulation device and localization method. China patent CN106110507A. 2016 Jul 26.
33. Tsun S, Bo W, Shanan C, inventors; Wuhan Capital Association Hong Kang Polytron Technologies Inc., assignee. Transcranial magnetic stimulation diagnosis and treatment navigation system based on camera. China patent CN110896611A. 2020 Mar 3.
34. Gangliang Z, Tianzai J, Zhengyi Y, Xuefeng L, Liang M, inventors; Shenyang Institute of Automation of CAS, assignee. Position and posture positioning device, method and equipment of transcranial magnetic stimulation coil for brain atlas navigation. China patent CN114073820A. 2022 Feb 22.
35. Schütz L, Weber E, Niu W, Daniel B, Mcnab J, Navab N, et al. Audiovisual augmentation for coil positioning in transcranial magnetic stimulation. Computer Methods in Biomechanics and Biomedical Engineering Imaging & Visualization. 2023; 11 (4): 1130–5. DOI: 10.1080/21681163.2022.2154277.
36. Jijun W, Yingying T, Wenyao Z, Yifeng X, Tianhong Z, inventors; Shanghai Mental Health Center (shanghai Psychological Counseling Training Center), assignee. Accurate transcranial magnetic stimulation online navigation method based on augmented reality. China patent CN111249622A. 2020 Jan 17.
37. Peng Z, Manhua L, Xin W, Jingxin W, Xiaotao L, inventors; Hunan Huayi Electromagnetic Medicine Research Institute Co Ltd., assignee. Transcranial magnetic stimulation device, transcranial magnetic stimulation system and transcranial magnetic stimulation method. China patent CN114225223A. 2021 Dec 31.
38. Peng Z, Manhua L, Xin W, Jingxin W, Yibo L, inventors; Hunan Huayi Electromagnetic Medicine Research Institute Co Ltd., assignee. Transcranial magnetic stimulation system and method. China patent CN114146315A. 2021 Dec 31.
39. Qiyong G, Haoyang X, Xiaoqi H, Su L, inventors; West China Hospital of Sichuan University, assignee. Electromagnetic navigation system and method for TMS coil. China patent CN113350698A. 2021 Mar 31.
40. Квартальный М. А., Давыдов М. В., Лыньков Л. М., Сагай Маруф Г. Моделирующие условия транскраниальной магнитной стимуляции мозга в зависимости от вида индуктора. Доклады БГУИР — Белорусский государственный университет информатики и радиотехники. 2015; 94 (8): 57–63.
41. Самуйлов И. В., Кайдак М. Н., Сагай М. Г. Г., Белан В. А. Влияние экранов на распределения импульсных магнитных полей при транскраниальной магнитной стимуляции. Доклады белорусского государственного университета информатики и радиоэлектроники. 2016; 101 (7): 159–63.

POLYMORPHISM OF INTERLEUKIN CONTROL GENES AND RISK OF NEOPLASMS IN EXPOSED INDIVIDUALS

Blinova EA[1,2]✉, Yanishevskaya MA[1], Akleyev AV[1,2]

[1] Urals Research Center for Radiation Medicine of Federal Medical and Biological Agency, Chelyabinsk, Russia
[2] Chelyabinsk State University, Chelyabinsk, Russia

Factors of the immune system, including secreted pro-inflammatory interleukins, enable tumor control. However, against the background of prolonged chronic inflammation, they can trigger oncogenesis. Polymorphic variants in the coding and regulatory regions of cytokine genes can affect gene expression, mRNA stability, structure and activity of the protein product, with consequences on the levels of cells and body as a whole. This study aimed to search for the relation between polymorphic variants of interleukin genes *IL1b* (rs1143634), *IL2* (rs2069762), *IL4* (rs2070874), *IL6* (rs1800795), *IL8* (rs4073), *IL10* (rs1800871) and risk of cancer, and to analyze the effect of polymorphic loci on concentration of serum interleukins. The study involved 585 persons chronically exposed to radiation. We established association of polymorphic *IL4* site (rs2070874) with concentration of serum *IL4* in individuals with chronic low dose-rate exposure of the red bone marrow 1.17 to 3507 mGy (mean value — 566 mGy). The content of serum IL4 in people with C/T and T/T genotypes (as per the dominant model) was significantly lower than in those with C/C genotype (p = 0.02). Polymorphic sites rs1143634, rs2069762, rs2070874, rs1800795, rs4073, rs1800871 were not found to be associated with the risk of malignant neoplasms in exposed individuals.

Keywords: SNP, immune system, malignant neoplasms, chronic radiation exposure, long-term effects.

Funding: the study received funding in the context of the Federal Target Program "Ensuring nuclear and radiation safety in 2016-2020 and up to 2030" (State Contract #11.313.21.2 of June 15, 2021).

Author contribution: Blinova EA — generalization of primary material, analysis and discussion of results, article text authoring; Yanishevskaya MA — statistical processing of primary data; Akleyev AV — study planning, article editing.

Compliance with the ethical standards: the study was approved by the Ethics Committee of the Urals Research Center for Radiation Medicine of the FMBA of Russia (Minutes #4 of June 8, 2023). All procedures on humans performed in the context of the study conform to the requirements of the 1964 Helsinki Declaration and its subsequent amendments or comparable ethical standards. Each participant of the study signed the voluntary informed consent form.

✉ **Correspondence should be addressed:** Evgenia Andreevna Blinova
Vorovskogo, 68, korp. A, Chelyabinsk, 454141, Russia; blinova@urcrm.ru

Received: 09.06.2023 **Accepted:** 20.07.2023 **Published online:** 12.08.2023

DOI: 10.47183/mes.2023.024

ПОЛИМОРФИЗМ ГЕНОВ КОНТРОЛЯ ИНТЕРЛЕЙКИНОВ И РИСК РАЗВИТИЯ ОПУХОЛЕВЫХ ЗАБОЛЕВАНИЙ У ОБЛУЧЕННЫХ ЛИЦ

Е. А. Блинова[1,2]✉, М. А. Янишевская[1], А. В. Аклеев[1,2]

[1] Уральский научно-практический центр радиационной медицины Федерального медико-биологического агентства, Челябинск, Россия
[2] Челябинский государственный университет, Челябинск, Россия

Факторы иммунной системы, в том числе секретируемые провоспалительные интерлейкины, обеспечивают противоопухолевый надзор, однако в случае длительного хронического воспаления могут приводить к активации онкогенеза. Полиморфные варианты, располагающиеся в кодирующих и регуляторных областях генов цитокинов, могут влиять на экспрессию гена, стабильность мРНК, структуру и активность белкового продукта, что в свою очередь отражается на клеточном и организменном уровнях. Целью работы было провести поиск связи полиморфных вариантов генов интерлейкинов *IL1b* (rs1143634), *IL2* (rs2069762), *IL4* (rs2070874), *IL6* (rs1800795), *IL8* (rs4073), *IL10* (rs1800871) с риском развития онкологических заболеваний, а также проанализировать влияние полиморфных локусов на концентрацию сывороточных интерлейкинов. В исследовании приняли участие 585 человек, подвергшихся хроническому радиационному воздействию. Была выявлена связь полиморфного участка *IL4* (rs2070874) с концентрацией сывороточного *IL4* у лиц, подвергшихся хроническому низкоинтенсивному радиационному воздействию в диапазоне доз на красный костный мозг (ККМ) от 1,17 до 3507 мГр. Содержание сывороточного *IL4* у носителей генотипов C/T и T/T в соответствии с доминантной моделью было статистически значимо ниже, чем у носителей генотипа C/C (p = 0,02). Не выявлено связи полиморфных участков rs1143634, rs2069762, rs2070874, rs1800795, rs4073, rs1800871 с риском развития злокачественных новообразований у облученных лиц.

Ключевые слова: SNP, иммунная система, злокачественные новообразования, хроническое радиационное воздействие, отдаленные последствия

Финансирование: финансирование осуществлялось в рамках Федеральной целевой программы «Обеспечение ядерной и радиационной безопасности на 2016–2020 годы и на период до 2030 года» (Государственный контракт № 11.313.21.2 от 15 июня 2021 г.).

Вклад авторов: Е. А. Блинова — обобщение первичного материала, анализ и обсуждение результатов, подготовка текста статьи; М. А. Янишевская — статистическая обработка первичных данных; А. В. Аклеев — планирование исследования, редактирование статьи.

Соблюдение этических стандартов: исследование одобрено этическим комитетом УНПЦ РМ ФМБА России (протокол № 4 от 8 июня 2023 г.). Все процедуры, выполненные в исследовании с участием людей, соответствуют требованиям Хельсинкской декларации 1964 г. и ее последующим изменениям или сопоставимым нормам этики. Каждый участник исследования подписал добровольное информированное согласие.

✉ **Для корреспонденции:** Евгения Андреевна Блинова
ул. Воровского, д. 68, корп. А, г. Челябинск, 454141, Россия; blinova@urcrm.ru

Статья получена: 09.06.2023 **Статья принята к печати:** 20.07.2023 **Опубликована онлайн:** 12.08.2023

DOI: 10.47183/mes.2023.024

Interleukins play an important regulatory role in antitumor immunity. They enable mediator interaction of the immune system cells and regulate various processes, such as activation of immunocompetent cells, apoptosis, cell cycle and differentiation of immunocompetent cells. For example, *IL1* boosts proliferation of $CD4^+$ cells and binding of natural killer cells (NK cells) to tumor cells; it also induces production of *IL2*, which, in turn, supports proliferation of dendritic cells, and infiltration of the tumor by dendritic cells correlates with the effectiveness of antitumor immunity [1]. In addition, the antitumor response regulated by Th1 through secretion of proinflammatory cytokines *IL2*, TNFα, and IFNγ, promotes not only priming and activation of cytotoxic T cells but also antitumor activity of macrophages and NK cells [2]. *IL4* is instrumental to the development of pro-inflammatory reactions. It enables proliferation of NK cells and activated T cells, enhances their antitumor effect, regulates activated anti-inflammatory macrophages that help eliminate cancer cells [3]. It is also believed to be directly capable of suppressing tumor growth by arresting the cell cycle [1]. At the same time, macrophages themselves can secrete *IL10*, which improves immune suppression by disrupting the activity of effector T cells and inhibiting maturation of dendritic cells [2]. *IL6* possesses a strong pro-inflammatory capability and it can suppress tumor growth, but in some cases it is produced by tumor cells, and then it promotes growth of myelomas and some types of tumor cells [4]. There is little data on the antitumor activity of *IL8*, however, it is known to attract and functionally modulate neutrophils and macrophages into tumor foci, and high levels of *IL8*, on the contrary, contribute to cancer progression and metastasis through various mechanisms, including proangiogenesis and maintenance of conditions for development of cancer stem cells [5].

Pro-inflammatory factors, including secreted pro-inflammatory cytokines, help suppress tumor, but with a prolonged chronic inflammation in the background, they can trigger oncogenesis [6].

Inflammation is known to play an important role in the development of cancer at different stages of carcinogenesis: it promotes genomic instability, epigenetic modifications, induction of proliferation of cancer cells, enhancement of anti-apoptotic signals, stimulation of angiogenesis [7]. At least 25% of cancer cases are associated with chronic inflammation [2, 8].

The possible causes of chronic inflammation are microbial infection, autoimmune disorders, obesity, immune dysfunction, as well as environmental factors. Several studies have shown that in the long run, radiation exposure promotes development of chronic inflammation [9]. In particular, the survivors of Hiroshima and Nagasaki bombings had the Th1/Th2 balance broken in the long term, which lead to chronic inflammation [10]. Moreover, among the exposed in Japan, greater dose meant higher level of such pro-inflammatory markers as C-reactive protein, *IL6,* INFγ, TNFα and *IL10* [11, 12]. Chernobyl accident liquidators had their cytokine profiles changing in the long run, with levels of INFγ and TNFα growing up [13]. Prolonged exposure to low and medium doses of radiation can also cause chronic inflammation. In particular, after 60–75 years, residents of the villages on the Techa River, which is contaminated with radioactive waste, exhibit changes in quantitative and functional indicators of systemic immunity [14] and pro-inflammatory changes in the cytokine profile [15].

Polymorphic variants in coding, regulatory and non-coding sites of genes, as well as in intergenic regions, can affect gene expression, mRNA stability, structure and activity of the protein product and, subsequently, alter the functional state at the levels of cells and body as a whole [16]. Some studies have established the connection between polymorphic sites in interleukin genes and risk of oncogenesis. Polymorphism of rs2069762 (-330T>G) in the *IL2* gene's promoter site is associated with a predisposition to several types of cancer, such as bladder cancer [17], nasopharyngeal carcinoma [18], and non-Hodgkin's lymphoma [19]. A meta-analysis of studies has found that polymorphism of rs2070874 (-33T>C) in the *IL4* gene raises the risk of leukemia and oral cancer [20]. Polymorphism of rs1800795 in the IL6 gene has been shown to play an important role in the pathogenesis of several types of cancer, including cervical cancer, colorectal cancer and breast cancer [21]. Polymorphism of rs4073 (-251A>T) in the *IL8* anti-inflammatory cytokine gene was found to increase the risk of gastric cancer [22]. All these data point to the modifying effect of polymorphic loci in interleukin genes manifesting during oncotransformation of the cell. However, despite the existing connection with the pathological condition, it is quite difficult to establish the functional significance of the identified polymorphism for the development of the disease, especially in the case of such a multifactorial pathology as cancer. One of the possible patterns of influence is alteration of the gene's expression activity, which affects concentration of the final product. In this connection, this study is a search for a relation between polymorphic variants of interleukin genes *IL1b* (rs1143634), *IL2* (rs2069762), *IL4* (rs2070874), *IL6* (rs1800795), *IL8* (rs4073), *IL10* (rs1800871) and the risk of cancer development, as well as an analysis of the effect polymorphic loci have on concentration of serum interleukins in people chronically exposed to radiation.

METHODS

Characteristics of the examined individuals

The study involved people chronically affected by low dose-rate exposure over the period from 1949 through 1960, the source being radioactive wastes discharged from Mayak Production Association to the Techa River (Southern Urals, Russia) [23]. We searched for an association between polymorphic alleles and genotypes *IL1b* (rs1143634), *IL2* (rs2069762), *IL4* (rs2070874), *IL6* (rs1800795), *IL8* (rs4073), IL10 (rs1800871) and the risk of development of solid malignant neoplasms (SMN), as well as effect said alleles and genotypes have on the concentration of serum interleukins. The exposed individuals included in the study have had their state monitored at the clinical department of the Urals Research Center for Radiation Medicine (URCRM) for many years. The criteria for inclusion in the study were residence from January 1, 1950 to December 31, 1960 in one of the Techa riverside villages, and calculated individual doses to the red bone marrow (RBM), thymus and peripheral lymphoid organs. Applicants whose residence in radiation-contaminated areas could not be confirmed were excluded from the study. Additional exclusion criteria were applied to individuals without SMN that donated samples for the serum interleukins analysis: they were not supposed to have autoimmune, acute or chronic inflammatory diseases diagnosed at the time of examination, as well as hemoblastosis, renal or hepatic insufficiency, acute cerebral circulatory disorders during the last three months, oncological diseases, and take antibiotics, glucocorticoids, cytostatics. At the Biophysics laboratory of the URCRM, all study participants had their individual absorbed radiation doses calculated for RBM and soft tissues, the calculations enabled by the Techa River Dosimetry System (TRDS 2016) [24].

All in all, the study involved 585 individuals who were chronically exposed to radiation. They were divided into two

Table 1. Characteristics of participants of the study

Indicator		Exposed with MN (*n* = 207)	Exposed without MN (*n* = 378)
Gender, *n* (%)	male female	81 (39,13) 126 (60,87)	127 (33,60) 251 (66,40)
Ethnic group, *n* (%)	Slavs Turks	98 (47,34) 109 (52,66)	153 (40,48) 225 (59,52)
Age at the time of examination, years[1] M ± SD (min–max)		75,71 ± 7,32 (55–95)	77,79 ± 7,33 (57–98)
Absorbed dose to RBM, mGy M ± SE (min–max)[2]		566,27 ±42,84 (1,17–3507,08)	700,39 ± 32,37 (0,70–3393,51)
Absorbed dose to soft tissues, mGy M ± SE (min–max)[2]		97,35 ± 8,67 (0,13–740,78)	99,90 ± 5,68 (0,05–622,40)

Note: [1] — mean value ± standard deviation (min–max); 2 — mean value ± standard error (min–max).

groups: 207 people with a history of malignant neoplasms (MN) of various localizations made up the "Exposed with MN" group, and 378 practically healthy people formed the "Exposed without MN" (control) group. Table 1 presents the detailed characteristics of the examined individuals.

The solid MN diagnosed had the following localizations: digestive system — 70 persons (ICD-10 code C00.2, C02.1, C04.9, C06.9, C15.9, C16.9, C18.4, C19, C22.9, C25.9, Q15.9); female reproductive system — 66 people (ICD-10 C50, C53.9, C54.9, C57.4); respiratory system — 25 people (ICD-10 Z85.22, C32.9, C33, C34); urinary system — 16 man (ICD code-10 C67.9, C68.9); endocrine system — 10 people (ICD code-10 C73); male reproductive system — 9 people (ICD code-10 C61); integumentary system — 9 people (ICD code-10 C43.9, C44.90), vision system — 2 people (C69.90).

DNA isolation and genotyping

Genomic DNA (gDNA) was isolated from whole blood using the commercially available ExtractDNA Blood & Cells column system (Eurogen; Russia) following the standard protocol based on the manufacturer's recommendations. To assess the purity of the gDNA preparations, we used the NanoDrop 2000 spectrophotometer (Thermo Scientific; USA); the control value was the ratio of 260 and 280 nm (A260/280) wavelengths.

For amplification, we used the StepOnePlus™ Real-Time PCR System (Applied Biosystems; USA) and a set for genotyping polymorphic markers for *IL1b* (rs1143634), *IL2* (rs2069762), *IL4* (rs2070874), *IL6* (rs1800795), *IL8* (rs4073), *IL10* (rs1800871) (TestGen; Russia). The 10 µl of reaction mixture contained 4 µl of the PCR mixture, 3 µl of deionized water, 2 µl of Taq polymerase and 1 µl of the studied gDNA sample. StepOne Software v2.1 (Applied Biosystems; USA) was used to analyze the genotyping data.

Assessment of the serum interleukin concentration

We employed EIA and used the Lazurite automatic analyzer (DYNEX Technologies; USA) and corresponding test systems (Vector-Best; Russia) to assess the concentration of serum interleukins (IL1β, IL2, IL4, IL6, IL8, IL10). Participants donated blood samples fasting, through a puncture in the median cubital vein; samples were collected into a vacuum tube with a coagulation activator (SiO_2), in the amount of 9 ml. The serum was separated after 45–60 minutes of blood incubation at 20–25 °C and subsequent 10-minute centrifugation at 1500 rpm. Then the serum was frozen once at –20 °C and kept frozen until analyzed. The concentration of cytokines in serum was expressed in pg/ml.

Statistical data processing

For statistical processing, we used the STATISTICA v.12.0 software package (IBM, USA), as well as online calculators Medstatistics (https://medstatistic.ru/) and GeneCalc (https://gene-calc.pl/hardy-weinberg-page). The significance of differences in the frequency of distribution of alleles and genotypes in the study groups was established with the help of the chi-squared test with Yates's correction for multiple comparisons. Intergroup differences in serum interleukin concentrations were assessed using the nonparametric Mann–Whitney U test. We searched for links between the studied polymorphisms and the risk of MN development in two genetic models: dominant (combined comparison of heterozygous and variant homozygous genotypes with a reference homozygous genotype) and recessive (combined comparison of heterozygous and reference homozygous genotypes with a variant homozygous genotype). To assess the relation between polymorphic gene sites and the risk of MN development, we calculated the odds ratio (OR) and the 95% confidence interval (95% CI) as per the formula suggested in the literature [25]. Associations with $p < 0.05$ were considered statistically significant.

RESULTS

Table 2 presents genotype distribution for polymorphic loci rs1143634, rs2069762, rs2070874, rs1800795, rs4073, rs1800871. Hardy–Weinberg law held true for all the polymorphic loci studied.

Seeking to determine the possible effect of polymorphic sites of *IL1b* (rs1143634), *IL2* (rs2069762), *IL4* (rs2070874), *IL6* (rs1800795), *IL8* (rs4073), *IL10* (rs1800871) on the concentration of interleukins in the "Exposed without MN" group, we investigated concentration of the corresponding serum interleukins in people with different genotypes (Table 3). We found that, by polymorphic site rs2070874 in the *IL4* gene, those carrying minor allele rs2070874*T (genotypes C/T and T/T) had significantly less *IL4* in blood serum compared to the carriers dominant genotype C/C ($p = 0.02$). At 90% significance (registrable trend), carriers of minor allele rs1143634*T (genotypes C/T and T/T) of the *IL1* gene had smaller concentration of serum *IL1* compared with carriers of the C/C genotype ($p = 0.054$). For the remaining polymorphic loci, we discovered no significant changes in the concentration of serum interleukins in carriers of different genotypes.

In the context of this study, we found the remaining polymorphic sites of interleukin genes do not influence serum interleukin concentrations, but our previous research revealed the effect rs2069762 in the *IL2* gene has on the number

Table 2. Occurrence of genotypes of the studied SNPs in exposed individuals with and without MN

Gene/SNP	Genotype	Groups								Compared models (dominant/ recessive)	OR (95% CI)	*p*4
		Exposed with MN				Exposed without MN						
		Frequency of genotypes, %										
		Quantity (%)	Ho[1]	He[2]	pHWE3	Quantity (%)	Ho	He	pHWE			
IL1b rs1143634	C/C	95 (59.75)	0.35	0.35	0.96	203 (61.52)	0.34	0.34	0.94	C/C vs C/T+T/T	1.08 (0.73–1.59)	0.71
	C/T	55 (34.59)				113 (34.24)				C/T+C/C vs T/T	1.35 (0.57–3.20)	0.49
	T/T	9 (5.66)				14 (4.24)						
IL2 rs2069762	A/A	37 (44.05)	0.46	0.44	0.88	131 (39.94)	0.47	0.46	0.98	A/A vs A/C+C/C	0.84 (0.52–1.37)	0.5
	A/C	39 (46.43)				154 (46.95)				A/C+A/A vs C/C	0.70 (0.31–1.55)	0.36
	C/C	8 (9.52)				43 (13.11)						
IL4 rs2070874	C/C	74 (47.44)	0.46	0.42	0.55	164 (50.00)	0.41	0.42	0.87	C/C vs C/T+T/T	1.11 (0.76–1.62)	0.6
	C/T	71 (45.51)				133 (40.55)				C/T+C/C vs T/T	0.73 (0.36–1.49)	0.37
	T/T	11 (7.05)				31 (9.45)						
IL6 rs1800795	G/G	34 (34.69)	0.48	0.48	0.99	106 (35.22)	0.48	0.48	0.99	G/G vs G/C+C/C	1.02 (0.63–1.65)	0.92
	G/C	47 (47.96)				145 (48.17)				G/C+G/G vs C/C	1.05 (0.58–1.93)	0.87
	C/C	17 (17.35)				50 (16.61)						
IL8 rs4073	T/T	36 (29.03)	0.51	0.49	0.96	101 (32.27)	0.47	0.49	0.67	T/T vs T/A+A/A	1.16 (0.74–1.83)	0.51
	T/A	63 (50.81)				147 (46.96)				T/A+T/T vs A/A	0.96 (0.57–1.62)	0.89
	A/A	25 (20.16)				65 (20.77)						
IL10 rs1800871	C/C	70 (47.95)	0.45	0.42	0.74	108 (52.43)	0.39	0.4	0.85	C/C vs C/T+T/T	1.20 (0.78–1.83)	0.41
	C/T	65 (44.52)				80 (38.83)				C/T+C/C vs T/T	0.85 (0.39–1.86)	0.68
	T/T	11 (7.53)				18 (8.74)						

Note: [1] — observed heterozygosity; 2 — expected heterozygosity; 3 — significance of deviation from the Hardy-Weinberg law (at $p > 0.05$); 4 — significance of the odds ratio indicator (OR).

of T lymphocytes and T NK cells ($CD3^+CD16^+56^+$ phenotype) in exposed individuals, as well as the effect of rs1800795 in the *IL6* gene on the number of T helpers [26]. Therefore, we looked into the relationship of the studied polymorphic loci and the risk of cancer in the exposed individuals. For this substudy we considered two genetic models, recessive and dominant. However, as shown in Table 2, we found no association with oncological diseases for any of the studied polymorphic loci.

DISCUSSION

A possible link between a particular polymorphic site and cancer risk may be the effect this polymorphism has on the structure of the protein, if located in the coding region of the gene, or its concentration, if located in the intron and promoter regions of the gene. For example, rs2069762 polymorphism is located in the site of binding of transcription factor and promoter region of the *IL2* gene, and it affects expression of IL2 [27].

In our studies involving individuals affected by chronic low dose-rate exposure (dose to RBM from 1.17 to 3507 mGr, mean value — 566 mGr), we identified a significant drop of serum content of *IL4* in carriers of the C/T and T/T genotypes compared with carriers of the dominant C/C genotype by polymorphic site of rs2070874.

Polymorphic site of rs2070874 is located in the 5'-untranslated region (5'UTR) of the *IL4* gene. This region is involved in control of efficiency of protein translation, since it manages binding of the transcription factor, RNA polymerase, and formation of the initiating ribosomal complex [28, 29]. It is possible that substitution in this region can affect the efficiency of the translation process and the final concentration of *IL4*.

In addition, carriers of minor allele rs1143634*T (genotypes C/T and T/T) of the *IL1* gene had smaller serum *IL1* concentration than carriers of the C/C genotype (90% significance). The rs1143634 polymorphic site is a synonymous variant, it can cause disturbance of mRNA splicing, which probably manifests as a change in the concentration of the protein product [30]. No published papers available describe any effect of the identified polymorphic sites on the concentration of serum products.

Several studies have found a link between polymorphic loci of *IL2* (rs2069762), *IL4* (rs2070874), *IL6* (rs1800795), *IL8* (rs4073) and the risk of development of MN of various localizations. Thus, rs2069762 is associated with a predisposition to bladder cancer [17], nasopharyngeal carcinoma [18] and non-Hodgkin's lymphoma [19]; rs2070874 — with risk of leukemia and oral cancer [20]; rs1800795 — with cervical cancer, colorectal cancer and breast cancer [21]; rs4073 — with increased risk of stomach cancer [22]. Moreover, polymorphism and oncogenic

Table 3. Indicators of systemic immunity in carriers of various genotypes of the studied SNPs, "Exposed without MN" group

Indicator	Model	Genotype1	Mean value of the indicator (SE)	p^2
IL1b rs1143634 (*n* = 246)				
IL1 content, pg/ml	Dominant	C/C (160) C/T+T/T (86)	41,05 (8,88) 30,21 (8,61)	0,054
	Recessive	C/C+C/T (239) T/T (7)	38,00 (6,69) 12,06 (5,64)	0,39
IL2 rs2069762 (*n* = 234)				
IL2 content, pg/ml	Dominant	A/A (98) A/C+C/C (136)	10,52 (1,07) 10,11 (1,09)	0,56
	Recessive	A/A+A/C (205) C/C (29)	10,38 (0,85) 9,58 (1,74)	0,92
IL4 rs2070874 (*n* = 240)				
IL4 content, pg/ml	Dominant	C/C (130) C/T+T/T (110)	5,16 (0,50) 4,13 (0,56)	0,02*
	Recessive	C/T+C/C (217) T/T (23)	4,56 (0,37) 4,99 (1,74)	0,64
IL6 rs1800795 (*n* = 114)				
IL6 content, pg/ml	Dominant	G/G (42) G/C+C/C (72)	24,00 (11,37) 16,24 (5,79)	0,84
	Recessive	G/C+G/G (93) C/C (21)	22,12 (6,73) 5,76 (2,89)	0,13
IL8 rs4073 (*n* = 231)				
IL8 content, pg/ml	Dominant	T/T (79) T/A+A/A (152)	6,36 (1,45) 7,94 (1,55)	0,58
	Recessive	T/A+T/T (189) A/A (42)	7,82 (1,34) 5,53 (1,56)	0,67
IL10 rs1800871 (*n* = 166)				
IL10 content, pg/ml	Dominant	C/C (88) C/T+T/T (78)	17,52 (2,02) 16,83 (2,61)	0,5
	Recessive	C/T+C/C (151) T/T (15)	16,50 (1,65) 24,23 (6,81)	0,4

Note: [1] — number in parentheses after name of the genotype is the number of its carriers among the participants; 2 — significance by Mann–Whitney U test; * — significance at $p > 0.05$, Mann–Whitney U test, IL content (pg/ml), between carriers of different genotypes.

factors were found to produce a joint effect. For example, rs1800795*G allele in the *IL6* gene was an additional squamous cell lung cancer risk factor in men who had been smoking for less than 35 years [16]. However, in our studies, we have not established the relationship between loci of *IL1b* (rs1143634), *IL2* (rs2069762), *IL4* (rs2070874, *IL6* (rs1800795), *IL8* (rs4073), *IL10* (rs1800871) and the MN development risk in persons chronically exposed to radiation. Likely, the reason therefor is heterogeneity of the MN considered in the study. It is important to remember that carcinogenesis is a multi-stage process involving various signaling pathways and protective systems of the body regulated by a large number of genes and gene networks, and therefore it is necessary to continue searching for genetic markers of MN development.

CONCLUSIONS

Our study revealed the link between polymorphic site of *IL4* (rs2070874) and concentration of serum *IL4*. Carriers of the C/T and T/T genotypes, dominant model, had significantly smaller *IL4* content than carriers of the C/C genotype. At the same time, we established no relation between polymorphic loci of *IL1b* (rs1143634), *IL2* (rs2069762), *IL4* (rs2070874), *IL6* (rs1800795), *IL8* (rs4073), *IL10* (rs1800871) and MN development risk in chronically exposed people with the dose to RBM ranging from 0.70 to 3,393 mGy (mean value — 700 mGy). However, as we have shown, presence of polymorphic sites in interleukin genes can affect individual indicators of the immune system and thereby modify the response to radiation exposure.

References

1. Teletaeva GM. Citokiny i protivoopuxolevyj immunitet. Prakticheskaya onkologiya. 2007; 8 (4): 211–18. Russian.
2. Gonzalez H, Hagerling C, Werb Z. Roles of the immune system in cancer: from tumor initiation to metastatic progression. Genes Dev. 2018; 32 (19–20): 1267–84.
3. Mantovani A, Marchesi F, Malesci A, Laghi L, Allavena P. Tumour-associated macrophages as treatment targets in oncology. Nat Rev Clin Oncol. 2017; 14 (7): 399–416.
4. Kumari N, Dwarakanath BS, Das A, Bhatt AN. Role of interleukin-6 in cancer progression and therapeutic resistance. Tum our Biol. 2016; 37 (9): 11553–72.
5. Teijeira A, Garasa S, Ochoa MC, Villalba M, Olivera I, Cirella A, et al. IL8, Neutrophils, and NETs in a collusion against cancer immunity and immunotherapy. Clin Cancer Res. 2021; 27 (9): 2383v93.
6. Briukhovetska D, Dörr J, Endres S, Libby P, Dinarello CA, Kobold S. Interleukins in cancer: from biology to therapy. Nat Rev Cancer. 2021; 21 (8): 481–99.

7. Hanahan D, Weinberg RA. Hallmarks of cancer: the next generation. Cell. 2011, 144: 646–74.
8. Coussens LM, Werb Z. Inflammation and cancer. Nature. 2002; 420: 860–7.
9. Lumniczky K, Impens N, Armengol G, Candeias S, Georgakilas AG, Hornhardt S, et al. Low dose ionizing radiation effects on the immune system. Environment International. 2021; 149: 106212.
10. I. Shigematsu C. Kamada Ito N. Effects of A-bomb radiation on the human body. Tokyo: Harwood academic publishers. Bunkodo Co., 1995; 419 s.
11. Hayashi T, Kusunoki Y, Hakoda M, Morishita Y, Kubo Y, Maki M, et al. Radiation dose-dependent increases in inflammatory response markers in A-bomb survivors. International Journal of Radiation Biology. 2003; 79 (2): 129–36.
12. Hayashi T, Morishita Y, Kubo Y, Kusunoki Y, Hayashi I, Kasagi F, et al. Long-term effects of radiation dose on inflammatory markers in atomic bomb survivors. The American Journal of Medicine. 2005; 118 (1): 83–86.
13. Senyuk OF, Kavsan VM, Müller WE, Schröder HC. Long-term effects of low-dose irradiation on human health. Cellular and Molecular Biology. 2002; 48 (4): 393–409.
14. Akleev AA. Immunnyj status cheloveka v otdalennom periode xronicheskogo radiacionnogo vozdejstviya. Medicinskaya radiologiya i radiacionnaya bezopasnost'. 2020; 65 (4): 29–35. Russian.
15. Kodinceva EA, Akleev AA, Blinova EA. Citokinovyj profil' lic, podvergshixsya xronicheskomu radiacionnomu vozdejstviyu, v otdalennye sroki posle oblucheniya. Radiacionnaya biologiya. Radioehkologiya. 2021; 61 (5): 506–14. Russian.
16. Gordeeva LA, Mun SA, Voronina EN, Polenok EG, Magatina AD, Titov VA, i dr. Associacii polimorfizma v genax citokinov s riskom ploskokletochnogo raka legkogo u muzhchin v zavisimosti ot dlitel'nosti kureniya. Ehkologicheskaya genetika. 2018; 16 (1): 60–69. Russian.
17. Shen Y, Liu Y, Liu S, Zhang A. The association between –330T/G polymorphism of interleukin 2 gene and bladder cancer. DNA and Cell Biology. 2012; 31: 983–7.
18. Wei YS, Lan Y, Zhang L, Wang JC. Association of the interleukin-2 polymorphisms with interleukin-2 serum levels and risk of nasopharyngeal carcinoma. DNA and cell biology. 2010; 29 (7): 363–8.
19. Song H, Chen L, Cha Z, Bai J. Interleukin 2 gene polymorphisms are associated with non-Hodgkin lymphoma. DNA Cell Biol. 2012; 31 (7): 1279–84.
20. Jia Y, Xie X, Shi X, Li S. Associations of common IL4 gene polymorphisms with cancer risk: A meta-analysis. Mol Med Rep. 2017; 16 (2): 1927–45.
21. Peng X, Shi J, Sun W, Ruan X, Guo Y, Zhao L, et al. Genetic polymorphisms of IL-6 promoter in cancer susceptibility and prognosis: a meta-analysis. Oncotarget. 2018; 9 (15): 12351–64.
22. Moghimi M, Alireza Dastgheib S, Heiranizadeh N, Zare M, Sheikhpour E, H. Neamatzadeh H. Association of IL-8 –251T>A (rs4073) polymorphism with susceptibility to gastric cancer: a systematic review and meta-analysis based on 33 case-control studies. Gastroenterol. 2020; 57 (01): 91–99.
23. Akleev AV, Kiselev MF, redaktory. Mediko-biologicheskie i ehkologicheskie posledstviya radioaktivnogo zagryazneniya reki Techa. M.: Vtoraya tipografiya FU «Medbioehkstrem», 2001; 531 s. Russian.
24. Degteva MO, Nape BA, Tolstyx EI, Shishkina EA, Bugrov NG, Krestinina LYu, i dr. Raspredelenie individual'nyx doz v kogorte lyudej, obluchennyx v rezul'tate radioaktivnogo zagryazneniya reki Techi. Medicinskaya radiologiya i radiacionnaya bezopasnost'. 2019; 64 (3): 46–53. Russian.
25. Bland JM. Statistics Notes: The odds ratio. BMJ. 2000; 320 (7247): 1468.
26. Akleev AA, Blinova EA, Akleev AV. Odnonukleotidnye polimorfizmy kak biomarkery otdalennyx radiacionno-inducirovannyx izmenenij sistemnogo immuniteta. Patogenez. 2021; 19 (3): 38–49. Russian.
27. Jain J, Valge-Archer VE, Rao A. Analysis of the AP-1 sites in the IL-2 promoter. J Immunol. 1992; 148 (4): 1240–50.
28. Hinnebusch AG, Ivanov IP, Sonenberg N. Translational control by 5'-untranslated regions of eukaryotic mRNAs. Science. 2016; 352 (6292): 1413–6.
29. Robert F, Pelletier J. Exploring the impact of single-nucleotide polymorphisms on translation. Front Genet. 2018; 9: 507.
30. Mueller WF, Larsen LS, Garibaldi A, Hatfield GW, Hertel KJ. The Silent Sway of Splicing by Synonymous Substitutions. The Journal of biological chemistry. 2015; 290 (46): 27700–11.

Литература

1. Телетаева Г. М. Цитокины и противоопухолевый иммунитет. Практическая онкология. 2007; 8 (4): 211–18.
2. Gonzalez H, Hagerling C, Werb Z. Roles of the immune system in cancer: from tumor initiation to metastatic progression. Genes Dev. 2018; 32 (19–20): 1267–84.
3. Mantovani A, Marchesi F, Malesci A, Laghi L, Allavena P. Tumour-associated macrophages as treatment targets in oncology. Nat Rev Clin Oncol. 2017; 14 (7): 399–416.
4. Kumari N, Dwarakanath BS, Das A, Bhatt AN. Role of interleukin-6 in cancer progression and therapeutic resistance. Tum our Biol. 2016; 37 (9): 11553–72.
5. Teijeira A, Garasa S, Ochoa MC, Villalba M, Olivera I, Cirella A, et al. IL8, Neutrophils, and NETs in a collusion against cancer immunity and immunotherapy. Clin Cancer Res. 2021; 27 (9): 2383v93.
6. Briukhovetska D, Dörr J, Endres S, Libby P, Dinarello CA, Kobold S. Interleukins in cancer: from biology to therapy. Nat Rev Cancer. 2021; 21 (8): 481–99.
7. Hanahan D, Weinberg RA. Hallmarks of cancer: the next generation. Cell. 2011, 144: 646–74.
8. Coussens LM, Werb Z. Inflammation and cancer. Nature. 2002; 420: 860–7.
9. Lumniczky K, Impens N, Armengol G, Candeias S, Georgakilas AG, Hornhardt S, et al. Low dose ionizing radiation effects on the immune system. Environment International. 2021; 149: 106212.
10. I. Shigematsu C. Kamada Ito N. Effects of A-bomb radiation on the human body. Tokyo: Harwood academic publishers. Bunkodo Co., 1995; 419 s.
11. Hayashi T, Kusunoki Y, Hakoda M, Morishita Y, Kubo Y, Maki M, et al. Radiation dose-dependent increases in inflammatory response markers in A-bomb survivors. International Journal of Radiation Biology. 2003; 79 (2): 129–36.
12. Hayashi T, Morishita Y, Kubo Y, Kusunoki Y, Hayashi I, Kasagi F, et al. Long-term effects of radiation dose on inflammatory markers in atomic bomb survivors. The American Journal of Medicine. 2005; 118 (1): 83–86.
13. Senyuk OF, Kavsan VM, Müller WE, Schröder HC. Long-term effects of low-dose irradiation on human health. Cellular and Molecular Biology. 2002; 48 (4): 393–409.
14. Аклеев А. А. Иммунный статус человека в отдаленном периоде хронического радиационного воздействия. Медицинская радиология и радиационная безопасность. 2020; 65 (4): 29–35.
15. Кодинцева Е. А., Аклеев А. А., Блинова Е. А. Цитокиновый профиль лиц, подвергшихся хроническому радиационному воздействию, в отдаленные сроки после облучения. Радиационная биология. Радиоэкология. 2021; 61 (5): 506–14.
16. Гордеева Л. А., Мун С. А., Воронина Е. Н., Поленок Е. Г., Магатина А. Д., Титов В. А. и др. Ассоциации полиморфизма в генах цитокинов с риском плоскоклеточного рака легкого у мужчин в зависимости от длительности курения. Экологическая генетика. 2018; 16 (1): 60–69.
17. Shen Y, Liu Y, Liu S, Zhang A. The association between –330T/G polymorphism of interleukin 2 gene and bladder cancer. DNA and Cell Biology. 2012; 31: 983–7.
18. Wei YS, Lan Y, Zhang L, Wang JC. Association of the interleukin-2 polymorphisms with interleukin-2 serum levels and risk of nasopharyngeal carcinoma. DNA and cell biology. 2010; 29 (7):

363–8.
19. Song H, Chen L, Cha Z, Bai J. Interleukin 2 gene polymorphisms are associated with non-Hodgkin lymphoma. DNA Cell Biol. 2012; 31 (7): 1279–84.
20. Jia Y, Xie X, Shi X, Li S. Associations of common IL4 gene polymorphisms with cancer risk: A meta-analysis. Mol Med Rep. 2017; 16 (2): 1927–45.
21. Peng X, Shi J, Sun W, Ruan X, Guo Y, Zhao L, et al. Genetic polymorphisms of IL-6 promoter in cancer susceptibility and prognosis: a meta-analysis. Oncotarget. 2018; 9 (15): 12351–64.
22. Moghimi M, Alireza Dastgheib S, Heiranizadeh N, Zare M, Sheikhpour E, H. Neamatzadeh H. Association of IL-8 –251T>A (rs4073) polymorphism with susceptibility to gastric cancer: a systematic review and meta-analysis based on 33 case-control studies. Gastroenterol. 2020; 57 (01): 91–99.
23. Аклеев А. В., Киселев М. Ф., редакторы. Медико-биологические и экологические последствия радиоактивного загрязнения реки Теча. М.: Вторая типография ФУ «Медбиоэкстрем», 2001; 531 с.
24. Дегтева М. О., Напье Б. А., Толстых Е. И., Шишкина Е. А., Бугров Н. Г., Крестинина Л. Ю., и др. Распределение индивидуальных доз в когорте людей, облученных в результате радиоактивного загрязнения реки Течи. Медицинская радиология и радиационная безопасность. 2019; 64 (3): 46–53.
25. Bland JM. Statistics Notes: The odds ratio. BMJ. 2000; 320 (7247): 1468.
26. Аклеев А. А., Блинова Е. А., Аклеев А. В. Однонуклеотидные полиморфизмы как биомаркеры отдаленных радиационно-индуцированных изменений системного иммунитета. Патогенез. 2021; 19 (3): 38–49.
27. Jain J, Valge-Archer VE, Rao A. Analysis of the AP-1 sites in the IL-2 promoter. J Immunol. 1992; 148 (4): 1240–50.
28. Hinnebusch AG, Ivanov IP, Sonenberg N. Translational control by 5'-untranslated regions of eukaryotic mRNAs. Science. 2016; 352 (6292): 1413–6.
29. Robert F, Pelletier J. Exploring the impact of single-nucleotide polymorphisms on translation. Front Genet. 2018; 9: 507.
30. Mueller WF, Larsen LS, Garibaldi A, Hatfield GW, Hertel KJ. The Silent Sway of Splicing by Synonymous Substitutions. The Journal of biological chemistry. 2015; 290 (46): 27700–11.

THE EFFECT OF CHRONIC EXPOSURE ON THE FOXP3 CONCENTRATION IN LYSATES OF THE MITOGEN-STIMULATED MONONUCLEAR CELLS

Kodintseva EA[1,2] ✉, Akleyev AA[3]

[1] Urals Research Center for Radiation Medicine of Federal Medical and Biological Agency, Chelyabinsk, Russia

[2] Chelyabinsk State University, Chelyabinsk, Russia

[3] South-Ural State Medical University, Chelyabinsk, Russia

Disruptions of the Treg differentiation and functioning processes can play one of the crucial roles in the pathogenesis of radiation-induced malignant neoplasms in residents of the Techa riverside villages, who were chronically exposed in the low-to-medium dose range with predominant damage to the red bone marrow (RBM). This study aimed to determine the effect of radiation exposure, gender, age at the time of examination, and ethnicity on concentration of FOXP3 protein in lysates of mitogen-stimulated peripheral blood mononuclear cells in chronically exposed individuals in the period of cancer effects development. The main group consisted of 30 people aged 67–80 years, predominantly female and Turks. The comparison group included 10 unexposed individuals of similar age, gender, and ethnicity. In the main group, the mean dose to RBM was 867 mGr, to the thymus and peripheral lymphoid organs — 125 mGr. After 24-hour *in vitro* PHA stimulation, mononuclears were lysed, and the concentrations of the total protein and FOXP3 (using quantitative enzyme immunoassay) were measured. Among the different dose groups, there were no significant differences in FOXP3 concentration in mitogen-stimulated mononuclears (prior to the stimulation: 0 pg/ml in the comparison group and 3.50 ± 1.50 (0–27.19) pg/ml in the main group at $p = 0.349$; after the stimulation, respectively: 1.54 ± 1.51 (0–15.16) pg/ml and 9.71 ± 3.86 (0–77.92) pg/ml, $p = 0.512$). The variability of individual values is slightly higher in the main group than in the comparison group. Preliminary results allow concluding that the dose to RBM, thymus and peripheral lymphoid organs, age at the time of examination, gender, and ethnicity have no statistically significant effect on the concentration of FOXP3 protein in the lysates of the mitogen-stimulated peripheral blood mononuclear cells of chronically exposed people.

Keywords: chronic radiation exposure, the Techa River, intracellular concentration, FOXP3 transcription factor, peripheral blood mononuclear cells, Phytohemagglutinin

Funding: this study was carried out in the framework of state assignment of the FMBA of Russia, subject "State of human cellular immunity during realization of long-term effects of chronic radiation exposure."

Acknowledgments: authors thank Startsev NV, Head of the "Human Being" Database Department of the Urals Research Center for Radiation Medicine of the FMBA of Russia, for the data provided; Litvinenko NP, senior laboratory assistant at the Laboratory of Molecular Cellular Radiobiology of the Urals Research Center for Radiation Medicine of the FMBA of Russia, for assistance in conducting the experiment.

Author contribution: Kodintseva EA — study concept and design, experimental work, analysis and statistical processing of the data, article authoring; Akleev AA — study concept, interpretation of the results, article editing.

Compliance with ethical standards: the study was approved by the Ethics Committee of the Urals Research Center for Radiation Medicine of the FMBA of Russia (Minutes #3 of June 8, 2023). Participants of the study signed a voluntary informed consent in conformity with the 2013 Declaration of Helsinki.

✉ **Correspondence should be addressed:** Ekaterina A. Kodintseva
Vorovskogo, 68A, Chelyabinsk, 454141, Russia; ovcharova.cat@mail.ru

Received: 31.07.2023 **Accepted:** 22.08.2023 **Published online:** 28.09.2023

DOI: 10.47183/mes.2023.032

ВЛИЯНИЕ ХРОНИЧЕСКОГО ОБЛУЧЕНИЯ НА КОНЦЕНТРАЦИЮ БЕЛКА FOXP3 В ЛИЗАТАХ МИТОГЕН-СТИМУЛИРОВАННЫХ МОНОНУКЛЕАРОВ КРОВИ

Е. А. Кодинцева[1,2] ✉, А. А. Аклеев[3]

[1] Уральский научно-практический центр радиационной медицины Федерального медико-биологического агентства, Челябинск, Россия

[2] Челябинский государственный университет, Челябинск, Россия

[3] Южно-Уральский государственный медицинский университет Министерства здравоохранения Российской Федерации, Челябинск, Россия

Нарушения процессов дифференцировки и функционирования Treg могут быть одним из важнейших звеньев в патогенезе радиационно-индуцированных злокачественных новообразований у людей из когорты реки Течи, хронически облученных в диапазоне малых и средних доз с преимущественным поражением красного костного мозга (ККМ). Целью работы было определить влияние радиационного воздействия, пола, возраста на момент обследования и этнической принадлежности на концентрацию белка FOXP3 в лизатах митоген-стимулированных мононуклеарных клеток периферической крови у хронически облученных людей в период реализации канцерогенных эффектов. Основную группу составили 30 человек в возрасте 67–80 лет, среди них преобладали женщины и лица тюркской этнической группы. В группу сравнения вошли 10 необлученных человек аналогичного возраста, пола, этнической группы. В основной группе средняя доза облучения ККМ составила 867 мГр; тимуса и периферических лимфоидных органов — 125 мГр. После 24-часовой стимуляции ФГА *in vitro* мононуклеары лизировали, измеряли концентрацию общего белка и количественным иммуноферментным анализом — концентрацию FOXP3. Концентрация белка FOXP3 в митоген-стимулированных мононоуклеарах статистически значимо не различалась у людей из разных дозовых групп (до стимуляции: 0 пг/мл в группе сравнения и 3,50 ± 1,50 (0–27,19) пг/мл в основной группе при $p = 0,349$; после стимуляции, соответственно: 1,54 ± 1,51 (0–15,16) пг/мл и 9,71 ± 3,86 (0–77,92) пг/мл, $p = 0,512$). Вариабельность индивидуальных значений несколько выше у людей из основной группы, чем в группе сравнения. По предварительным результатам, статистически значимого влияния дозы облучения ККМ, тимуса и периферических лимфоидных органов, возраста на момент обследования, а также пола, этнической принадлежности на концентрацию белка FOXP3 в лизатах митоген-стимулированных мононоуклеаров периферической крови хронически облученных людей не выявлено.

Ключевые слова: хроническое радиационное воздействие, река Теча, внутриклеточная концентрация, фактор транскрипции FOXP3, мононуклеарные клетки периферической крови, фитогемагглютинин

Финансирование: научно-исследовательская работа выполнена в рамках государственного задания ФМБА России по теме «Состояние клеточного иммунитета человека в период реализации отдаленных эффектов хронического радиационного воздействия».

Благодарности: заведующему отделом Базы данных «Человек» ФГБУН УНПЦ РМ ФМБА России Н. В. Старцеву за предоставленые данные, старшему лаборанту лаборатории молекулярно-клеточной радиобиологии Н. П. Литвиненко ФГБУН УНПЦ РМ ФМБА России за помощь в проведении эксперимента.

Вклад авторов: Е. А. Кодинцева — разработка концепции и дизайна исследования, экспериментальная работа, анализ и статистическая обработка данных, написание статьи; А. А. Аклеев — разработка концепции исследования, интерпретация результатов, редактирование статьи.

Соблюдение этических стандартов: исследование одобрено этическим комитетом ФГБУН УНПЦ РМ ФМБА России (протокол № 3 от 8 июня 2023 г.). Участники исследования подписали добровольное информированное согласие в рамках Хельсинкской декларации 2013 г.

✉ **Для корреспонденции:** Екатерина Александровна Кодинцева
ул. Воровского, д. 68А, г. Челябинск, 454141, Россия; ovcharova.cat@mail.ru

Статья получена: 31.07.2023 **Статья принята к печати:** 22.08.2023 **Опубликована онлайн:** 28.09.2023

DOI: 10.47183/mes.2023.032

Today, the search for markers of individual radiosensitivity in the context of realization of long-term effects of radiation exposure is an urgent problem for modern radiobiology [1–3]. Radiation-induced carcinogenesis is one of the most significant effects of human exposure to ionizing radiation; its pathogenetic mechanisms are being actively investigated. There are various cohorts of people that run an increased long-term oncopathology risk after radiation exposure: survivors of atomic bombings [4], liquidators of radiation accidents [5], professionals working with sources of radiation [6], population living in radiation-contaminated areas [7, 8]. A particular cohort that belongs to this list are the residents of the Techa riverside villages. For them, the risks of morbidity and mortality from malignant tumors and leukemias are increased [9].

In the context of ensuring the optimal medical monitoring for persons running an increased risk of malignant neoplasms (MN), it is important to identify and verify the markers of predisposition to the development of radiation-induced oncopathology that enables optimization of approaches to the formation of high-risk groups in cohorts of people affected by radiation exposure [2]. Immunity indicators, primarily those characterizing the state of T-cells in the long term after radiation exposure, can be considered as such markers. For example, many of the mentioned residents of the Techa riverside villages had chronic radiation syndrome (CRS), and 65 years after the start of the exposure, they exhibited decreasing absolute numbers of $CD3^+$, $CD4^+$ and $CD8^+$ lymphocytes in peripheral blood, and increasing serum concentrations of IL4 and TNFα, compared to people of the same age and gender who received comparable doses but had no CRS in their medical histories [10].

In the context of pathogenetic mechanisms of radiation-induced carcinogenesis, a heterogeneous subpopulation of T-regulatory cells (Treg or $CD3^+CD4^+CD25^+FOXP3^+$ lymphocytes [11]) is particularly interesting. The FOXP3 transcription factor is specific to Treg; it supports control of differentiation and functioning of this subpopulation of lymphocytes [12]. It may be feasible to establish the level of this protein as one of the potential markers of predisposition to radiation-induced human oncopathology in the long term after chronic radiation exposure that predominantly involved damage to the central organ of hematopoiesis, the red bone marrow (RBM). The *FOXP3* gene dominantly controls the function of Treg, and its continuous expression guarantees that these cells fully preserve their suppressive ability [11]. The FOXP3 transcription factor represses IL2 transcription, increases expression of CD25 and other Treg markers. The mechanisms of Treg-mediated suppression are still a subject of discussion, but it is known that the regulation of FOXP3 protein expression is crucial for the control over immune responses, including antitumor immune surveillance [12].

Normally, FOXP3 protein interacts with the key transcription factors of T-lymphocytes, including NFAT, NFkB and AML1/Runx1, and others. Transcriptional and epigenetic regulation enables control over the *FOXP3* gene expression; a change therein entails alterations in the phenotype of T-cells and their functions [12]. In humans, expression of the *FOXP3* gene in most $CD4^+$-T-cells can be caused by prolonged stimulation of the T-cell receptor, with most $FOXP3^+$ T-cells having a low level of FOXP3 factor [12]. Transcription of the *FOXP3* gene can be initiated in effector T-cells upon antigen recognition during inflammation [13]. Due to their ability to inhibit antitumor immunity, Tregs promote development and progression of tumors. High infiltration of tumor tissue by Treg cells is associated with poor survival rate among patients with various types of MN [14]. The regulatory functions of Tregs infiltrating a tumor are realized via the COX2/PGE2 signalling pathway [15]. Currently, Tregs are being actively investigated as potential targets for oncotherapy [14], but there are few studies that cover modulating effects of ionizing radiation on the Treg cells' phenotype and functions, including expression of the *FOXP3* gene, concentrations and functional activity of the FOXP3 transcription factor [16].

The plasticity of Treg subpopulation, participation of the FOXP3 transcription factor in Treg differentiation, as well as the role of regulatory T-cells in radiation-induced carcinogenesis underpin the relevance of counting the FOXP3 protein in peripheral blood mononuclears donated by people from the Techa river cohort.

This study aimed to investigate the effect of radiation exposure, gender, age at the time of examination, and ethnicity, on concentration of the FOXP3 protein in lysates of mitogen-stimulated peripheral blood mononuclear cells sampled from chronically exposed residents of the Techa riverside villages at the time of realization of carcinogenic effects.

METHODS

We studied the blood samples donated by permanent residents of the Techa riverside villages that were chronically exposed to low dose rate radiation mainly from bone-seeking radionuclides (targeting RBM) at the premises of the Urals Research Center for Radiation Medicine of the FMBA of Russia. The dose of radiation received by each patient was assessed using the TRDS-2016 dosimetry system [17].

Before donating the blood, all patients underwent a medical examination in accordance with the established procedure. The inclusion criteria were: absence of acute inflammatory diseases, absence of exacerbations of chronic inflammatory diseases; absence of renal or hepatic insufficiency. The exclusion criteria were: acute cerebral circulation disruption incidents or traumatic brain injuries within three months before the study; confirmed oncological and autoimmune diseases; courses of hormone, antibiotic, chemo- and (or) radiotherapy; medical procedures using ionizing radiation within six months before the study.

The exposed group (main group) comprised 30 persons aged 67–80 years, the mean age being 72.4 ± 0.5 years. The mean accumulated RBM dose in this group was 876 ± 136 mGr, with the values ranging from 87 to 3716 mGr. The

Table. Concentrations of FOXP3 transcription factor in MNC lysates after mitogenic stimulation

Concentration, pg/ml		Comparison group, RBM: less than 0.07 Gy, *n* = 10	Main group, RBM dose: (0.07–3.72) Gy, *n* = 30	Subgroups of the main group, RBM dose:		
				from 0.07 to 0.49 Gy, *n* = 10	from 0.50 to 0.84 Gy, *n* = 10	from 0.85 to 3.72 Gy, *n* = 10
FOXP3 after 24 hours of incubation	without PHA	0	3.50 ± 1.50 (0–27.19)	2.63 ± 2.63 (0–26.33)	6.78 ± 3.52 (0–27.19)	1.09 ± 0.78 (0–7.32)
	with PHA	1.54 ± 1.51 (0–15.16)	9.71 ± 3.86 (0–77.92)	5.97 ± 4.88 (0–48.84)	13.42 ± 8.00 (0–77.92)	9.73 ± 7.28 (0–73.2)

Note: The data are presented as M ± SE (min–max).

mean dose accumulated by thymus and peripheral lymphoid organs was 125 ± 20 mGr, the range of values spanning from 28 to 446 mGr.

To study dose dependencies, we divided the main group into three subgroups similar in age, gender and ethnic makeup but different in the RBM doses received: minimal (0.07 through 0.49 Gy), moderate (0.50 through 0.84 Gy) and high (0.85 through 3.72 Gy). These subgroups were called dose groups; there were no statistically significant differences in qualitative characteristics between them and the comparison group.

The comparison group consisted of 10 people aged 63–82 years, none of whom was exposed to radiation in the context of industrial activities. The mean age in this group was 71.2 ± 2.0 years, mean accumulated RBM dose — 27 ± 4 mGr (values from 15 to 49 mGr), and the mean dose accumulated by thymus and peripheral lymphoid organs — 12 ± 3 mGr (values from 2 to 34 mGr).

Women were more numerous in both groups: 73.3% (22 persons) in the main group and 90.0% (9 people) in the comparison group. Eighty percent (24 individuals) of the main group participants were of Turkic origin, and in the comparison group this value was 70.0% (7 people). We found no significant differences in the age, gender, and ethnic composition of the main and comparison groups.

Fasting blood samples (4 ml) were taken under a standard protocol [18], from the ulnar vein, in the morning, into vacuettes containing sodium heparin. The fraction of mononuclear cells (MNCs) was isolated at the density gradient of 1.077 g/cm^3 (Biolot; Russia), washed twice with the modified Dulbecco′s phosphate buffered saline (Biolot; Russia). The incubation of MNCs lasted 24 hours at 37.0 ± 0.5 °C; for the process, we used the RPMI-1640 medium (HEPES 25 mM, $NaHCO_3$ 24 mM) (Paneco; Russia) with vitamins (Paneco; Russia) and L-glutamine 2 mM (Paneco; Russia), to which 10% fetal calf serum (Biolot; Russia) was added. Phytohemagglutinin-P (PHA) (Paneco; Russia) was added to the test sample of MNCs at the final concentration of 20 μg/ml, and the control sample of MNCs was completed with purified water in the amount equal to that of the mitogen solution. After stimulation, MNCs were precipitated, supernatant removed, and the samples were stored at minus 80 °C until the next stage. The thawing temperature was 2–8 °C; we induced hemolysis of erythrocyte impurities with a cooled ammonium chloride solution with pH 7.2–7.4 [19]. MNCs were washed with a cold phosphate-salt buffer (pH 7.4) (Sigma-Aldrich; USA). The concentration of cells was estimated using the Countess II FL (Thermo Scientific; USA) cell counter. We lysed the MNCs by freezing the samples three times at minus 20 °C and then defrosting them at room temperature as per recommendations of the manufacturer of the enzyme immunoassay test system (ELISA). Total protein content in cell lysates was determined in reaction with bicynchonicic acid (Merck test system; USA) in a 96-well tablet, with the help of a Lazurite analyzer (Dynex Technologies Inc.; USA). We relied on quantitative ELISA (Blue gene test system; China) to establish the content of FOXP3 transcription factor in the samples; the counting enabled by the same analyzer and followed by recalculation of the result for 1 μg of total protein in the sample. SigmaPlot software (demo version; SYSTAT Software, USA) was used for statistical data analysis. The normality of frequency distribution in the samples was checked with the help of the Kolmogorov-Smirnov test. The actual distribution was abnormal in all samples. For maximum clarity (the median value is zero in cases when concentration of the FOXP3 transcription factor in all or most of the samples is below the minimum detection limit of the ELISA system), we expressed the descriptive statistics data as arithmetic mean (M), error of mean (m) and a range of values (min–max). Datasets were compared using the Mann Whitney U-test, and for quality indicators we used the chi-squared test. Spearman's rank correlation coefficient enabled correlation analysis; the differences or relationships were considered significant at 95% confidence level.

RESULTS

The table below shows the results of quantification of the FOXP3 transcription factor in lymphocyte lysates after 24-hour incubation with PHA and without mitogen.

Comparing the main group, the three dose groups and the comparison group, we identified no significant differences in concentrations of the FOXP3 protein in MNC lysates incubated for 24 hours with PHA and without mitogen. The respective values were as follows: main group — p = 0.349 before stimulation, p = 0.512 after stimulation; three dose subgroups — p = 0.706, p = 0.257, p = 0.450 before stimulation, and p = 0.940, p = 0.326, p = 0.597 after stimulation (ascending order by the RBM dose).

In the groups of chronically exposed individuals with different accumulated doses, intracellular concentration of the FOXP3 transcription factor after *in vitro* mitogenic stimulation of the MNCs was slightly higher than in the comparison group.

Analyzing dose dependencies, we found no significant relationships between concentration of the FOXP3 transcription factor in the MNC lysates (stimulated (SR = 0.13; p = 0.414) and not stimulated (SR = 0.18; p = 0.263) with mitogen for 24 hours) and RBM and thymus/peripheral lymphoid organ doses (before stimulation: SR = 0.23, p = 0.183; after stimulation: SR = 0.09, p = 0.602).

We detected no effect of gender (before stimulation: SR = –0.08, p = 0.609, after stimulation: SR = –0.03, p = 0.856), age at the time of examination (before stimulation: SR = 0.02, p = 0.915; after stimulation: SR = 0.11, p = 0.484), ethnicity (before stimulation: SR = 0.05, p = 0.767; after stimulation: SR = –0.01, p = 0.966) on the studied indicators neither in the main group nor in the control group. Spearman's rank correlation was used for this analysis.

DISCUSSION

Radiation-induced carcinogenesis implies long-term realization of the effects. The reason behind this specificity is the complex of factors of non-radiation nature that affect the exposed individual, including the MN risk factors. A body that received sublethal doses activates compensatory adaptive mechanisms, which, when they function adequately, prevent oncotransformation of normal cells [10]. Immunocompetent cells are the main effectors of antitumor immune surveillance; MN pathogenesis largely depends on the disruptions of their activity [20].

The Techa floodplain was contaminated with radionuclides as a result of the Mayak Production Association activity; practically healthy residents of that area have been exposed to low dose rate ionizing radiation for many years and in the long term, they have persistent changes in the immune status, with such in the T-cell component of the immunity being most drastic. Accordingly, previous studies have reported decreased quantities of peripheral blood leukocytes (mainly because of neutrophils and lymphocytes), higher lysosomal activity of neutrophils, some suppression of the intracellular oxygen-dependent monocyte metabolism [1], and inclination of the

cytokine system towards a pro-inflammatory response [21].

On the one hand, regulatory T-cells can directly inhibit activity of cytotoxic T-cells, and on the other hand, they can be recruited or induced by the oncotransformed cells and cells of the tumor microenvironment, which allows them to avoid attack from the immune system. Treg lymphocytes can interfere with the activation and differentiation of $CD4^+$ and $CD8^+$ T cells, induce reactivity against autologous and tumor antigens [11].

In the tumor microenvironment, Tregs induction and differentiation occurs from T-lymphocytes with a strong immunosuppressive function, which suppress antitumor immunity and thus support tumor appearance and development. Tregs from the tumor microenvironment, in turn, can suppress the function of immune effector cells (using various mechanisms); they play an important part in the tumor's effort to elude immune surveillance [22–25]. Such Tregs can secrete TGFß, IL10, and IL35 [26], which inhibit antitumor immune response, suppress antigenic presentation in the dendritic cells as well as the T-helper function, and generate tumor-specific $CD8^+$ cytotoxic T-lymphocytes. The expression of IL10 and IL35 cytokines differs among subpopulations of the tumor microenvironment Treg cells; synergistically, they promote depletion of intratumor T-cells by regulating the expression of several inhibitory receptors [27]. Tregs are capable of direct cytolysis of other cells through secretion of perforin and granzymes, and they also synthesize and produce cyclic adenosine phosphate, thus affecting the metabolism of other cells [11, 14].

Data from mice experiments show that the share of tumor and splenic Tges grows after local irradiation at doses of 10 and 20 Gy, and the dose of 1.25 Gy (whole irradiation) brings down the total amount of $CD4^+$*FOXP3*$^+$-Treg in the lymph nodes [28].

In humans, ionizing radiation decreased the viability of human $CD4^+$ lymphocytes, and this effect is dose-dependent. There is evidence of a higher radioresistance of Tregs compared to $CD4^+$ lymphocytes, as well as of a dose-dependent reduction of expression of the *FOXP3* gene in Treg when the received doses are 0.940 Gy and 1.875 Gy. Compared to regular $CD4^+$ lymphocytes, natural (nTreg) and TGFß-induced (iTreg) regulatory T-cells exhibit increased resistance to radiation at a dose of 10 Gy. Forty-eight hours after exposure to this dose, the expression of *FOXP3* gene decreases in nTreg and in iTreg (more pronounced). After *in vitro* irradiation, the expression of *FOXP3* gene in iTreg goes down, but it does not affect differentiation into T-helpers of the first or second type. In $CD4^+CD25^+$-iTreg, the expression of the *T-BET* gene involved in the differentiation of cells into first type T-helpers was low before and after irradiation at a dose of 10 Gy, and the expression of the *GATA3* gene involved in the differentiation of lymphocytes into second type T-helpers decreased 48 hours after such exposure. Irradiation changes the expression of characteristic iTreg molecules. Exposed to ionizing radiation, iTregs increase the expression of *LAG-3* gene, decrease that of CD25 and CTLA-4 molecules and the ability of the cells to inhibit proliferation of $CD3^+CD8^+$ lymphocytes weakens [16].

The data from this study allow assuming functional integrity of the peripheral blood Tregs (in practically or conditionally healthy individuals) in the long term; inter alia, they preserve the ability to differentiate effected by the *FOXP3* gene and its key transcription factor, FOXP3 protein. The possible reason therefor is the high adaptive potential of the human immune and hematopoietic system, which realizes in the long term after chronic low-intensity radiation exposure with RBM as the primary target [1, 10, 21]. However, the presented data disallow excluding the possibility of aberrant local immune responses with participation of Tregs at the MN initiation stage in the exposed patients from the high oncological risk cohort. This problem requires a more thorough investigation.

The results of this study are generally consistent with the current scientific knowledge; its contribution thereto is information about the reaction of MNCs isolated from the peripheral blood of the chronically exposed people to *in vitro* mitogenic stimulation at the time of realization of carcinogenic effects of radiation in the studied population cohort.

CONCLUSIONS

Comparison of the main (chronically exposed) and comparison (not exposed) groups revealed no significant differences in the concentrations of the FOXP3 transcription factors in MNC lysates after 24 hours of incubation with mitogen and without PHA. Likewise, we found no evidence of the effect of RBM doses and doses to thymus and peripheral lymphoid organs to intracellular concentrations of the FOXP3 transcription factor in human peripheral blood MNCs after mitogen stimulation. There were no significant correlations between gender, age at the time of examination, ethnicity of the examined people and concentration of the FOXP3 protein in lysates of mitogen-stimulated MNCs. In the samples from practically healthy chronically irradiated people, we registered high variability of intracellular concentrations of the FOXP3 transcription factor after *in vitro* MNCs stimulation by mitogen, which indirectly confirms the hypothesis of presence of latent and, apparently, compensated functional changes in the mature immunocompetent cells. This indicator can be considered as one of the potential markers enabling assessment of individual radiosensitivity under chronic exposure to low and moderate doses with RBM as the primary target organ. It is necessary to further study the key transcription factors involved in differentiation of immunocompetent cells and ensuring their normal functioning in chronically irradiated population, as well investigate their role in radiation-induced carcinogenesis.

References

1. Akleev AA. Immunnyj status cheloveka v otdalennom periode xronicheskogo radiacionnogo vozdejstviya. Medicinskaya radiologiya i radiacionnaya bezopasnost'. 2020; 4 (65): 29–35. DOI: 10.12737/1024-6177-2020-65-4-29-35. Russian.
2. Akleyev AV. Specific features of medical care provision to the population of the Techa riverside settlements. Journal of Radiological Protection. 2021; 41 (4): S342. DOI: 10.1088/1361-6498/ac0c02.
3. Rybkina VL, Bannikova MV, Adamova GV, Dörr H, Scherthan H, Azizova TV. Immunological Markers of Chronic Occupational Radiation Exposure. Health Physics. 2018; 115 (1): 108–13. DOI: 10.1097/HP.0000000000000855.
4. Ozasa K, Cullings HM, Ohishi W, Hida A, Grant EJ. Epidemiological studies of atomic bomb radiation at the Radiation Effects Research Foundation. International Journal of Radiation Biology. 2019; 95 (7): 879–91. DOI: 10.1080/09553002.2019.1569778.
5. Bazyka DA, Prysyazhnyuk AY, Gudzenko NA, Fuzik MM, Trotsyuk NK, Babkina NG, et al. Late oncological aftereffects of radiation exposure caused by the chornobyl accident. Probl Radiac Med Radiobiol. 2022; 27: 138–49. English, Ukrainian. DOI:

10.33145/2304-8336-2022-27-138-149.
6. Adliene D, Griciene B, Skovorodko K, Laurikaitiene J, Puiso J. Occupational radiation exposure of health professionals and cancer risk assessment for Lithuanian nuclear medicine workers. Environmental Research. 2020; 183: 109–44. DOI: 10.1016/j.envres.2020.109144.
7. Krestinina LYu, Silkin SS, Mikryukova LD, Epifanova SB, Akleev AV. Risk zabolevaemosti solidnymi zlokachestvennymi novoobrazovaniyami v Ural'skoj kogorte avarijno-obluchennogo naseleniya: 1956–2017. Radiacionnaya gigiena. 2020; 13 (3): 6–17. DOI: 10.21514/1998-426X-2020-13-3-6-17. Russian.
8. Drozdovitch V. Radiation exposure to the thyroid after the chernobyl accident. Frontiers in Endocrinology (Lausanne). 2021 Jan [cited 2023 Apr 20]; 11: 569041. Available from: https://pubmed.ncbi.nlm.nih.gov/33469445/. DOI: 10.3389/fendo.2020.569041.
9. Krestinina LYu, Silkin SS, Degteva MO, Akleev AV. Risk smerti ot boleznej sistemy krovoobrashheniya v Ural'skoj kogorte avarijno-obluchennogo naseleniya za 1950-2015 gody. Radiacionnaya gigiena. 2019; 12 (1): 52–61. DOI: 10.21514/1998-426X-2019-12-1-52-61. Russian.
10. Akleev AA, Dolgushin II. Osobennosti immunnogo statusa u lyudej, perenesshih hronicheskij luchevoj sindrom, v otdalennye sroki. Radiaciya i risk. 2018; 27 (2): 7666–85. DOI: 10.21870/0131-3878-2018-27-2-76-85. Russian.
11. Li C, Jiang P, Wei S, Xu X, Wang J. Regulatory T cells in tumor microenvironment: new mechanisms, potential therapeutic strategies and future prospects. Molecular Cancer. 2020 Jul [cited 2023 Apr 20]; 19 (1): 116. Available from: https://pubmed.ncbi.nlm.nih.gov/32680511/ DOI: 10.1186/s12943-020-01234-1.
12. Ono M. Control of regulatory T–cell differentiation and function by T–cell receptor signalling and Foxp3 transcription factor complexes. Immunology. 2020; 160 (1): 24–37. DOI: 10.1111/imm.13178
13. Bending D, Paduraru A, Ducker CB, Prieto Martin P, Crompton T, Ono M. A temporally dynamic Foxp3 autoregulatory transcriptional circuit controls the effector Treg programme. EMBO Journal. 2018 Aug [cited 2023 Apr 20]; 37: e99013. Available from: https://pubmed.ncbi.nlm.nih.gov/29991564/. DOI: 10.15252/embj.201899013
14. Ohue Y, Nishikawa H. Regulatory T (Treg) cells in cancer: Can Treg cells be a new therapeutic target? Cancer Science. 2019; 110 (7): 2080–9. DOI:10.1111/cas.14069.
15. Emel S, Mehmet S. Epigenetical targeting of the FOXP3 gene by S-adenosylmethionine diminishes the suppressive capacity of regulatory T cells ex vivo and alters the expression profiles. Journal of Immunotherapy. 2019; 42 (1): 11–22. DOI: 10.1097/CJI.0000000000000247.
16. Beauford SS, Kumari A, Garnett-Benson C. Ionizing radiation modulates the phenotype and function of human CD4+ induced regulatory T cells. BMC Immunology. 2020 Apr [cited 2023 Apr 20]; 21 (1): 18. Available from: https://pubmed.ncbi.nlm.nih.gov/32299365/ DOI: 10.1186/s12865-020-00349-w, DOI: 10.1186/s12865-020-00363-y.
17. Degteva MO, Napier BA, Tolstykh EI, Shishkina EA, Bougrov NG, Krestinina LYu, i dr. Raspredelenie individual'nyh doz v kogorte lyudej, obluchennyh v rezul'tate radioaktivnogo zagryazneniya reki Techi. Medicinskaya radiologiya i radiacionnaya bezopasnost'. 2019; 64 (3): 46–53. DOI: 10.12737/article_5cf2364cb49523.98590475. Russian.
18. Kishkun AA. Klinicheskaya laboratornaya diagnostika: uchebnoe posobie. M.: GEhOTAR-Media, 2019; 1000 s. Russian.
19. Klaus Dzh, redaktor. Limfocity: metody. M.: Mir, 1990; 395 s. Russian.
20. Slepov YuK, Laushkin MA, Deev RV. Gipoteza o roli immunnoj sistemy v kancerogeneze. Geny & Kletki. 2021; 16 (1): 82–91. DOI: 10.23868/202104013. Russian.
21. Kodintseva EA, Akleyev AA, Blinova EA. Citokinovyj profil' lic, podvergshihsya hronicheskomu radiacionnomu vozdejstviyu, v otdalennye sroki posle oblucheniya. Radiacionnaya biologiya. Radioehkologiya. 2021; 5 (61): 506–14. DOI: 10.31857/S0869803121050076. Russian.
22. Sakaguchi S, Mikami N, Wing JB, Tanaka A, Ichiyama K, Ohkura N. Regulatory T cells and human disease. Annual Review of Immunology. 2020; 38: 541–66. DOI: 10.1146/annurev-immunol-042718-041717.
23. Toker A, Ohashi PS. Expression of costimulatory and inhibitory receptors in FoxP3(+) regulatory T cells within the tumor microenvironment: implications for combination immunotherapy approaches. Advances in Cancer Research. 2019; 144: 193–261. DOI: 10.1016/bs.acr.2019.05.001.
24. Campbell C, Rudensky A. Roles of regulatory T cells in tissue pathophysiology and metabolism. Cell Metabolism. 2020; 31: 18–25. DOI: 10.1016/j.cmet.2019.09.010.
25. Cuadrado E, van den Biggelaar M, de Kivit S, Chen YY, Slot M, Doubal I, Meijer A, van Lier RAW, Borst J, Amsen D. Proteomic analyses of human regulatory T cells reveal adaptations in signaling pathways that protect cellular identity. Immunity. 2018; 48: 1046–6. DOI: 10.1016/j.immuni.2018.04.008.
26. Sullivan JA, Tomita Y, Jankowska-Gan E, Lema DA, Arvedson MP, Nair A et al. Treg-cell-derived IL-35-coated extracellular vesicles promote infectious tolerance. Cell Reports. 2020; 30: 1039–51. DOI: 10.1016/j.celrep.2019.12.081.
27. Sawant DV, Yano H, Chikina M, Zhang Q, Liao M, Liu C et al. Adaptive plasticity of IL-10(+) and IL-35(+) Treg cells cooperatively promotes tumor T cell exhaustion. Nature Immunology. 2019; 20: 724–35. DOI: 10.1038/s41590-019-0346-9.
28. Muroyama Y, Nirschl TR, Kochel CM, Lopez-Bujanda Z, Theodros D, Mao W, et al. Stereotactic Radiotherapy Increases Functionally Suppressive Regulatory T Cells in the Tumor Microenvironment. Cancer Immunology Research. 2017; 5 (11): 992–1004. DOI: 10.1158/2326-6066.

Литература

1. Аклеев А. А. Иммунный статус человека в отдаленном периоде хронического радиационного воздействия. Медицинская радиология и радиационная безопасность. 2020; 4 (65): 29–35. DOI: 10.12737/1024-6177-2020-65-4-29-35.
2. Akleyev AV. Specific features of medical care provision to the population of the Techa riverside settlements. Journal of Radiological Protection. 2021; 41 (4): S342. DOI: 10.1088/1361-6498/ac0c02.
3. Rybkina VL, Bannikova MV, Adamova GV, Dörr H, Scherthan H, Azizova TV. Immunological Markers of Chronic Occupational Radiation Exposure. Health Physics. 2018; 115 (1): 108–13. DOI: 10.1097/HP.0000000000000855.
4. Ozasa K, Cullings HM, Ohishi W, Hida A, Grant EJ. Epidemiological studies of atomic bomb radiation at the Radiation Effects Research Foundation. International Journal of Radiation Biology. 2019; 95 (7): 879–91. DOI: 10.1080/09553002.2019.1569778.
5. Bazyka DA, Prysyazhnyuk AY, Gudzenko NA, Fuzik MM, Trotsyuk NK, Babkina NG, et al. Late oncological aftereffects of radiation exposure caused by the chornobyl accident. Probl Radiac Med Radiobiol. 2022; 27: 138–49. English, Ukrainian. DOI: 10.33145/2304-8336-2022-27-138-149.
6. Adliene D, Griciene B, Skovorodko K, Laurikaitiene J, Puiso J. Occupational radiation exposure of health professionals and cancer risk assessment for Lithuanian nuclear medicine workers. Environmental Research. 2020; 183: 109–44. DOI: 10.1016/j.envres.2020.109144.
7. Крестинина Л. Ю., Силкин С. С., Микрюкова Л. Д., Епифанова С. Б., Аклеев А. В. Риск заболеваемости солидными злокачественными новообразованиями в Уральской когорте аварийно-облученного населения: 1956–2017. Радиационная гигиена. 2020; 13 (3): 6–17. DOI: 10.21514/1998-426X-2020-13-3-6-17.
8. Drozdovitch V. Radiation exposure to the thyroid after the chernobyl accident. Frontiers in Endocrinology (Lausanne). 2021 Jan [cited 2023 Apr 20]; 11: 569041. Available from: https://pubmed.ncbi.nlm.nih.gov/33469445/. DOI: 10.3389/fendo.2020.569041.
9. Крестинина Л. Ю., Силкин С. С., Дегтева М. О., Аклеев А. В. Риск смерти от болезней системы кровообращения в Уральской когорте аварийно-облученного населения за 1950-2015

годы. Радиационная гигиена. 2019; 12 (1): 52–61. DOI: 10.21514/1998-426X-2019-12-1-52-61.
10. Аклеев А. А., Долгушин И. И. Особенности иммунного статуса у людей, перенесших хронический лучевой синдром, в отдалтнные сроки. Радиация и риск. 2018; 27 (2): 7666–85. DOI: 10.21870/0131-3878-2018-27-2-76-85.
11. Li C, Jiang P, Wei S, Xu X, Wang J. Regulatory T cells in tumor microenvironment: new mechanisms, potential therapeutic strategies and future prospects. Molecular Cancer. 2020 Jul [cited 2023 Apr 20]; 19 (1): 116. Available from: https://pubmed.ncbi.nlm.nih.gov/32680511/ DOI: 10.1186/s12943-020-01234-1.
12. Ono M. Control of regulatory T–cell differentiation and function by T–cell receptor signalling and Foxp3 transcription factor complexes. Immunology. 2020; 160 (1): 24–37. DOI: 10.1111/imm.13178
13. Bending D, Paduraru A, Ducker CB, Prieto Martin P, Crompton T, Ono M. A temporally dynamic Foxp3 autoregulatory transcriptional circuit controls the effector Treg programme. EMBO Journal. 2018 Aug [cited 2023 Apr 20]; 37: e99013. Available from: https://pubmed.ncbi.nlm.nih.gov/29991564/. DOI: 10.15252/embj.201899013.
14. Ohue Y, Nishikawa H. Regulatory T (Treg) cells in cancer: Can Treg cells be a new therapeutic target? Cancer Science. 2019; 110 (7): 2080–9. DOI:10.1111/cas.14069.
15. Emel S, Mehmet S. Epigenetical targeting of the FOXP3 gene by S-adenosylmethionine diminishes the suppressive capacity of regulatory T cells ex vivo and alters the expression profiles. Journal of Immunotherapy. 2019; 42 (1): 11–22. DOI: 10.1097/CJI.0000000000000247.
16. Beauford SS, Kumari A, Garnett-Benson C. Ionizing radiation modulates the phenotype and function of human CD4+ induced regulatory T cells. BMC Immunology. 2020 Apr [cited 2023 Apr 20]; 21 (1): 18. Available from: https://pubmed.ncbi.nlm.nih.gov/32299365/ DOI: 10.1186/s12865-020-00349-w, DOI: 10.1186/s12865-020-00363-y.
17. Дегтева М. О., Напье Б. А., Толстых Е. И., Шишкина Е. А., Бугров Н. Г., Крестинина Л. Ю. и др. В. Распределение индивидуальных доз в когорте людей, облученных в результате радиоактивного загрязнения реки Течи. Медицинская радиология и радиационная безопасность. 2019; 64 (3): 46–53. DOI: 10.12737/article_5cf2364cb49523.98590475.
18. Кишкун А. А. Клиническая лабораторная диагностика: учебное пособие. М.: ГЭОТАР-Медиа, 2019; 1000 с.
19. Клаус Дж., редактор. Лимфоциты: методы. М.: Мир, 1990; 395 с.
20. Слепов Ю. К., Лаушкин М. А., Деев Р. В. Гипотеза о роли иммунной системы в канцерогенезе. Гены & Клетки. 2021; 16 (1): 82–91. DOI: 10.23868/202104013.
21. Кодинцева Е. А., Аклеев А. А., Блинова Е. А. Цитокиновый профиль лиц, подвергшихся хроническому радиационному воздействию, в отдаленные сроки после облучения. Радиационная биология. Радиоэкология. 2021; 5 (61): 506–14. DOI: 10.31857/S0869803121050076.
22. Sakaguchi S, Mikami N, Wing JB, Tanaka A, Ichiyama K, Ohkura N. Regulatory T cells and human disease. Annual Review of Immunology. 2020; 38: 541–66. DOI: 10.1146/annurev-immunol-042718-041717.
23. Toker A, Ohashi PS. Expression of costimulatory and inhibitory receptors in FoxP3(+) regulatory T cells within the tumor microenvironment: implications for combination immunotherapy approaches. Advances in Cancer Research. 2019; 144: 193–261. DOI: 10.1016/bs.acr.2019.05.001.
24. Campbell C, Rudensky A. Roles of regulatory T cells in tissue pathophysiology and metabolism. Cell Metabolism. 2020; 31: 18–25. DOI: 10.1016/j.cmet.2019.09.010.
25. Cuadrado E, van den Biggelaar M, de Kivit S, Chen YY, Slot M, Doubal I, Meijer A, van Lier RAW, Borst J, Amsen D. Proteomic analyses of human regulatory T cells reveal adaptations in signaling pathways that protect cellular identity. Immunity. 2018; 48: 1046–6. DOI: 10.1016/j.immuni.2018.04.008.
26. Sullivan JA, Tomita Y, Jankowska-Gan E, Lema DA, Arvedson MP, Nair A et al. Treg-cell-derived IL-35-coated extracellular vesicles promote infectious tolerance. Cell Reports. 2020; 30: 1039–51. DOI: 10.1016/j.celrep.2019.12.081.
27. Sawant DV, Yano H, Chikina M, Zhang Q, Liao M, Liu C et al. Adaptive plasticity of IL-10(+) and IL-35(+) Treg cells cooperatively promotes tumor T cell exhaustion. Nature Immunology. 2019; 20: 724–35. DOI: 10.1038/s41590-019-0346-9.
28. Muroyama Y, Nirschl TR, Kochel CM, Lopez-Bujanda Z, Theodros D, Mao W, et al. Stereotactic Radiotherapy Increases Functionally Suppressive Regulatory T Cells in the Tumor Microenvironment. Cancer Immunology Research. 2017; 5 (11): 992–1004. DOI: 10.1158/2326-6066.

COMPUTATIONAL RED BONE MARROW DOSIMETRY PHANTOM OF A ONE-YEAR-OLD CHILD ENABLING ASSESSMENT OF EXPOSURE DUE TO INCORPORATED BETA EMITTERS

Sharagin PA[1]✉, Shishkina EA[1,2], Tolstykh EI[1]

[1] Urals Research Center for Radiation Medicine of Federal Medical and Biological Agency, Chelyabinsk, Russia

[2] Chelyabinsk State University, Chelyabinsk, Russia

For residents of territories along the Techa River that was contaminated with radioactive substances in the 1950s, bone-seeking beta-emitting ^{89,90}Sr were the main source of internal exposure of active (red) bone marrow (AM). The dose of these radionuclides conditions the severity of leukemia risk for them. Improvement of the methods of internal AM dosimetry is an important task. Computational 3D phantoms of the skeleton sites are a component of the solution for this task. Simulation of radiation transfer in a heterogeneous bone model allows estimating the dose conversion factors from radionuclide activity to AM dose. This manuscript continues the series of papers covering the development of a set of computational phantoms of a reference human being of different age. The objective of the study was to develop a computational phantom of a one-year-old child skeleton for internal AM dosimetry (exposure due to incorporated beta emitters). Using the original SPSD (stochastic parametric skeletal dosimetry) model, we develop voxel 3D models of skeletal sites. Skeleton sites with active hematopoiesis were modeled as a set of phantoms of simple geometries. Distribution of AM throughout the skeleton and parameters of the phantoms were assessed on the basis of the published results of measurement done in real bones of children aged 9 months to 2 years. The generated computational phantom of a one-year-old child consisted of 39 segments. It simulates the structure of the bone tissue, location of AM, and population variability of the skeleton microstructure and size parameters.

Keywords: trabecular bone, cortical bone, bone marrow dosimetry, computational phantoms, Sr

Funding: the work was part of the Federal Target Program "Ensuring Nuclear and Radiation Safety for 2016-2020 and up to 2035", with financial support from the Federal Medical Biological Agency of Russia.

Author contribution: Sharagin PA — data generation, analysis, interpretation, manuscript authoring and editing; Tolstykh EI — study methodology development, manuscript editing; Shishkina EA — conceptualization, manuscript editing.

✉ **Correspondence should be addressed:** Pavel A. Sharagin
Vorovsky, 68 A, Chelyabinsk, 454141, Russia; sharagin@urcrm.ru

Received: 14.06.2023 **Accepted:** 23.08.2023 **Published online:** 26.09.2023

DOI: 10.47183/mes.2023.030

ВЫЧИСЛИТЕЛЬНЫЙ ФАНТОМ ДЛЯ ДОЗИМЕТРИИ КРАСНОГО КОСТНОГО МОЗГА ГОДОВАЛОГО РЕБЕНКА ОТ ИНКОРПОРИРОВАННЫХ БЕТА-ИЗЛУЧАТЕЛЕЙ

П. А. Шарагин[1]✉, Е. А. Шишкина[1,2], Е. И. Толстых[1]

[1] Уральский научно-практический центр радиационной медицины Федерального медико-биологического агентства, Челябинск, Россия

[2] Челябинский государственный университет, Челябинск, Россия

Остеотропные бета-излучающие изотопы стронция (^{89,90}Sr) были основными источниками внутреннего облучения красного костного мозга (ККМ) для жителей прибрежных территорий реки Течи, подвергшейся радиоактивному загрязнению в 1950-е годы. Именно с дозой этих частиц связан повышенный риск лейкозов в когорте жителей ее прибрежных территорий. Важной задачей является совершенствование внутренней дозиметрии облучения ККМ. Она включает в себя разработку вычислительных фантомов, представляющих собой трехмерные модели участков скелета. Имитация переноса излучения в гетерогенной модели кости позволяет оценить коэффициенты перехода от активности радионуклида в кости к дозе на ККМ. Эта статья является продолжением работы по созданию набора вычислительных фантомов скелета людей разного возраста. Целью работы было разработать вычислительный фантом скелета годовалого ребенка для внутренней дозиметрии ККМ от инкорпорированных бета-излучателей. С помощью оригинальной методики SPSD (stochastic parametric skeletal dosimetry) создавали трехмерные модели участков скелета в воксельной форме. Участки скелета с активным гемопоэзом моделировали как набор фантомов простой геометрической формы. Распределение ККМ в скелете, а также параметры фантомов оценивали на основе опубликованных результатов измерений реальных костей детей в возрасте от 9 месяцев до 2 лет. Для годовалого ребенка был сгенерирован вычислительный фантом, состоящий из 39 сегментов. Он имитирует структуру костной ткани и положение ККМ, а также популяционную вариабельность параметров микроструктуры и размеров скелета.

Ключевые слова: трабекулярная кость, кортикальная кость, дозиметрия костного мозга, вычислительные фантомы, Sr

Финансирование: работа выполнена в рамках реализации Федеральной целевой программы «Федеральная целевая программа «Обеспечение ядерной и радиационной безопасности на 2016–2020 годы и на период до 2035 года» и при финансовой поддержке Федерального медико-биологического агентства России.

Вклад авторов: П. А. Шарагин — получение, анализ и интерпретацию данных, написание и редактирование статьи; Е. И. Толстых — разработка методики исследования, редактирование статьи; Е. А. Шишкина — разработка концепции, редактирование статьи.

✉ **Для корреспонденции:** Павел Алексеевич Шарагин
ул. Воровского, д. 68 А, г. Челябинск, 454141, Россия; sharagin@urcrm.ru

Статья получена: 14.06.2023 **Статья принята к печати:** 23.08.2023 **Опубликована онлайн:** 26.09.2023

DOI: 10.47183/mes.2023.030

Radionuclide incorporation in a human body could lead to internal exposure of tissues and organs. One of the most radiosensitive organs is the haematopoietically active bone marrow (AM). Found inside skeletal cavities, AM cells are the main target for bone-seeking radionuclides that accumulate in mineralized bone tissue. The most dangerous of the radionuclides are ^{89,90}Sr. These very radionuclides were the key source of AM exposure for the residents of the Techa riverside settlements, contaminated with radioactive substances in the 1950s. Mean AM dose absorbed in the course of a lifetime in the Techa River Cohort members was 0.35 Gy, but in some people it exceeded 1 Gy and could reach 7 Gy, which resulted in a chronic radiation

syndrome development and raised the risk of leukemia [1–4]. The contribution to the AM dose was 61–94% and 2.5–3.2% of ^{90}Sr and ^{89}Sr, respectively [5]. Among the exposed individuals are people of various ages, including small children. Dose assessment for the exposed population could help to prepare for potential radiation emergencies. The methods of dosimetric modeling that were used previously to estimate AM dose are outdated [6]. More accurate data on AM doses received by the members of the Southern Urals population exposed to radiation cohort (SUPER cohort) would allow better assessment of the radiation-related risks of leukemias [7]. Estimation of the AM doses requires assessment of the radionuclide specific activity in the source tissue and calculation of the dose conversion factor (*DF*) from specific activity of a radionuclide in the source to the absorbed dose rate in a target.

Biokinetic models that describe distribution and transfer of a radionuclide through the tissues of the body after its ingress are used to estimate radionuclide specific activity [5]. *DF* is calculated using dosimetric modeling. It involves simulating the transfer of radiation resulting from strontium isotopes decay in the source tissue (bone) and energy absorption in AM (the target tissue), taking into account the exposure geometry. That is why an important part of dosimetric modeling is the elaboration of computational bone phantoms. They are surrogates of the real body tissues (AM and bone) that describe the geometry of source and target tissues and allow simulation of radiation transfer. It should be noted that the current approaches to modeling shape and structure of the bone are based on the analysis of postmortem computed tomography (CT) images of individual bone segments [6, 8–12]. The use of autopsy material limits the number of samples used to estimate the parameters of phantoms and makes it impossible to account for individual variability of size of human bones.

An original parametric method of stochastic modeling of bone structures, SPSD modeling (SPSD — stochastic parametric skeletal dosimetry), was developed at the Urals Research Center for Radiation Medicine [13]. SPSD modeling implies determination of parameters of the phantoms based on numerous published bone measurements. It allows accounting for the uncertainties due to the variability of skeletons in different people. The inside of a computational bone phantom is filled with spongiosa, which is a combination of trabecular bone and AM. And its outside bears a dense layer of cortical bone. The trabecular bone is modeled as a grid of rod-like trabeculae. Such model is a simplified representation of a real bone, yet it is suitable for internal dosimetry of bone-seeking beta-emitters [13]. The previously published numerical experiments [14, 15] demonstrate adequacy of the model; these experiments yielded energy dependences for SPSD phantoms that were compared to the published data [12].

The current study is devoted to the elaboration of a computational phantom of a one-year-old child's skeleton. It is the next step in the series of studies on the development of a set of computational phantoms of a reference man of different age. Previously, we published a paper covering the development of the computational phantom of a newborn's skeleton [16].

The objective of the study is the elaboration of a computational phantom of skeleton of a one-year-old child to estimate AM doses due to beta-emitting radionuclides incorporated in the bone.

METHODS

The phantoms were created using the original SPSD method. For dosimetric modeling, we selected only the skeletal sites with active hematopoiesis. A set of hematopoietic sites were identified based on the published data on AM distribution inside the skeleton [17]. SPSD phantom of skeletal hematopoietic sites consists of a set of smaller phantoms, which are basic phantoms of bone segment (BPS) of simple geometry. They describe individual sites of the skeletal bones. The approach to determination of BPS parameters (based on the previously published data) is given below.

We studied papers in peer-reviewed journals, atlases, manuals, monographs and dissertations as sources of data on dimensional characteristics of bones of a one-year-old child. This set was completed with electronic resources containing collections of X-ray images. The measurements of people/samples that the authors qualified as healthy without diseases leading to bone deformation were collected for the analysis. The ethnicities considered were Caucasians and Mongoloids, as these groups are common in the Ural region. The age of the children ranged from 9 months to 2 years.

Relying on the published data, for every hematopoietic site we assessed linear dimensions and thickness of the cortical bone layer (*Ct.Th.*), as well as bone microarchitecture characteristics: trabeculae thickness (*Tb.Th.*), trabecular separation (*Tb.Sp*), bone volume fraction of spongiosa (*BV/TV*). The linear skeletal bone measurements obtained using callipers, osteometric boards, ultrasound and X-ray examinations, and CT were studied. Histomorphometry and micro-CT data were used to assess the parameters of trabecular bone (*Tb.Th.*, *Tb.Sp*, *BV/TV*) and cortical layer thickness.

Averaged estimates of bone characteristics were taken as parameters for digital phantoms. If published papers containing data on individual measurements were available, we combined them and calculated arithmetic means and standard deviations (SD). When the data on the study of the groups of people were averaged, then for each group we used a weighting factor, (W_N), that factored in the number (N) of samples: $W_N = 1$ if $N \geq 25$; $W_N = N/25$ if $N < 25$. The methods of selection and analysis of the published data were described in detail in previous publications [18–21].

Having acquired the datasets presenting population-average characteristics of bone size and shape, we divided each hematopoietic site into small segments of simple geometric shape with homogeneous bone microarchitecture and cortical layer thickness. Such segmentation allows accounting for heterogeneity of structure of trabecular and cortical bone inside a single hematopoietic site and simplifies modeling. The process of segmentation has been described in detail in [18, 19].

Each phantom includes descriptions of the modeled media and geometry of source and target tissues. Bone marrow (BM) and mineralized bone tissue (part of trabecular and cortical bone) are the media constituting BPS. Chemical composition and density of the modeled media were determined based on the previously published data [22] and applied for all phantoms of a one-year-old child.

For each segment a voxel BPS was generated in the Trabecula [23] software. Depending on the position of the center of the voxel in the phantom, voxels imitate either mineralized bone or bone marrow (BM). We regarded trabecular bone (TB) and cortical bone (CB) as source tissues, and bone marrow (BM) as a detector tissue. BM was uniformly distributed between trabeculae inside the BPS. Voxel sizes differed phantom to phantom, but did not exceed 70% of the trabecula thickness [23, 24]. In the modeled phantoms, the size of the voxel varied in the range from 50 to 200 μm. Trabecula software automatically calculated the volumes of source and detector tissues for each BPS.

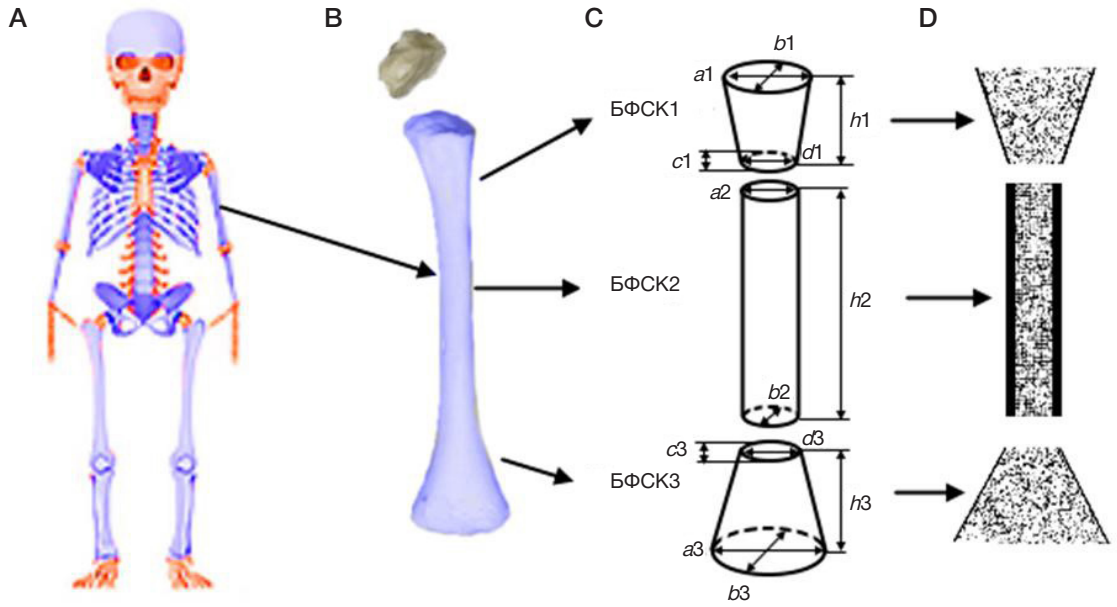

Fig. Segmentation of a hematopoietic site of a one-year-old child's skeleton using the example of humerus. **A**. Skeleton of a one-year-old child (active hematopoietic sites are highlighted blue). **B**. Humerus. **C**. *Pattern* of division of the bone into BPSs and their dimensions. **D**. BPS of humerus in voxel representation, a sectional view (*black* voxels imitate bone, *white* — BM)

Hematopoietic sites of a one-year-old child, division into segments and modeled BPS are demonstrated on the example of the humerus (Figure).

To simulate population variability of dimensions and microstructure characteristics, we generated 12 SPSs (supplementary phantoms) for each BPS with mean parameter values. The parameters of these SPSs were selected at random, within the range of their individual variability (within the limits of minimum and maximum values of the measurements).

RESULTS

The main hematopoietic sites in a one-year-old child's skeleton and the AM mass fraction therein, were determined in accordance with the MRI data [17] (Table 1).

According to Table 1, skeleton of a one-year-old child includes 13 hematopoietic sites for modeling. The AM mass fraction therein ranges from 0.9 to 28.7% of its total mass fraction in the body.

As is the case with a newborn [16], the following parts of the skeleton were not modeled: epiphysis of the tubular bone, sternum, craniofacial bones and vertebral processes (cervical, thoracic, lumbar), because, according the published data [26–31], they either contain very little AM or consist of cartilage tissue.

Table 2 presents chemical composition of the modeled media; we selected the values based on the ICRP data [22] for adults.

The density of mineralized bone tissue was calculated based on the published measurement results of the cortical bone density of one-year-old children [25]; it made up 1.70 g/cm^3. As for the red bone marrow, its density was taken as equal to that of water, 1 g/cm^3 [16].

The parameters of spongiosa were also determined based on the published data; their analysis and calculation of population-average spongiosa parameters were described in detail in [21]. Table 3 presents the values of the BPSs micro-architecture parameters of a one-year-old child.

Table 4 presents linear dimensions and cortical layer thickness assumed for BPSs of a one-year-old child.

The phantom of hematopoietic sites of a newborn's skeleton consists of 39 BPSs (Table 4). Depending on the shape of the simulated hematopoietic sites, we used different amount of BPSs to describe them: from 1 (ribs) to 9 (sacrum).

Table 1. AM mass fraction (% of the total AM mass fraction in the skeleton) in the main hematopoietic sites of a one-year-old child's skeleton [15].

№	Hematopoietic site	AM mass fraction, %
1	Femur	8.1
2	Humeri	5.2
3	Sacrum	5.1
4	Tibia bones	8.7
5	Pelvic bones	13.1
6	Skull	28.7
7	Clavicle	0.9
8	Scapula	2.7
9	Ribs	8.2
10	Radius and ulna	2.6
11	Cervical vertebrae	2.1
12	Thoracic vertebrae	8.3
13	Lumbar vertebrae	6.4

Table 2. Chemical composition of the modeled media (all BPS)

Chemical composition, relative untis		
Chemical element	Bone	Bone marrow
H	0.035	0.105
C	0.16	0.414
N	0.042	0.034
O	0.445	0.439
Na	0.003	0.001
Mg	0.002	0.002
P	0.095	0.002
S	0.003	0.002
Ca	0.215	–

For the most part, BPSs were modeled by cylinders and rectangular parallelepipeds. The size of the phantoms varies widely, from 2.7 to 35.8 mm. Phantoms describing spinal column have no cortical layer due to the fact that the ossification process is incomplete (Table 4). Bodies of femur and tibia have the highest values of *Ct.Th.* for the BPS of a one-year-old child: 2.3 mm. In the first year of life, bones of the cranial vault ossify intensively and the fontanelles close up, therefore, as opposed to those of a newborn, BPSs representing cranial vault of a one-year-old child are covered with a cortical bone layer. The spongiosa parameters differed significantly for different BPSs. The *BV/TV* ratio in BPSs varies from 14 to 52%, *Tb.Th.* value — from 0.09 to 0.29 mm, *Tb.Sp* value — from 0.48 to 0.98 mm (Table 3).

Individual variability of the BPSs dimensional parameters on the average made up 14%, with the highest value belonging to the scapula acromion (42%) and the lowest — to the acetabulum of pubic bone (3%). On the average variability of the cortical layer thickness made up 20%, with the maximum 47% variability for iliac ala. The mean variability of spongiosa parameters was 25%, with minimum and maximum values 9% and 52%, respectively.

The variability values were used to model the SPSs. Their volumes vary widely; they can be 3-fold larger or smaller than those of the BPSs. Further on, we shall calculate DF both for BPSs and SPSs. Mean square deviation of DF calculated for SPSs from those calculated for BPS will characterize the population variability of the DF.

DISCUSSION

In the study devoted to the modeling of a newborn's skeleton [16], we have demonstrated that the weight of the generated phantoms correspond to the weight of real bones. We could not make such a comparison for the phantom of a one-year-old child's skeleton due to lack of data on weight of the respective wet bones in the available literature. However, it is interesting to compare skeletal phantoms of a one-year-old child and a newborn. In general, the former includes more BPSs than the latter, which counts 34 of them. This is due to the ossification and increase in the size of sacrum, which required additional segmentation of the ilium. At the same time, in the bones of hands and feet, yellow bone marrow replaces AM already in the first year of life, which means these segments are not modeled when a one-year-old child's phantom is elaborated.

Naturally, the volume of similar BPSs increases with age, along with the size of the bones. The comparison of the volume of the phantoms of the skeletal sites of a newborn and one-year old child based on the example of distal femur, clavicle, cervical and lumbar vertebral bodies is given in table 5.

The volume of BPSs in the phantom of a one-year-old child is significantly higher than in that of a newborn (Table 5). The volumes of the modeled media also increase in the vast majority of phantoms. Interestingly, if the source tissue volume (TB and CB) increases 1.5 times on the average, the volume of the target tissue increases in 4.5 times. The drop in the volume of trabecular bone (TB) in the lumbar vertebral body phantoms

Table 3. Spongiosa parameters assumed for BPSs of a one-year-old child [32–42] (CV is given in parentheses, %)

Hematopoietic site	*BV/TV*, %	*Tb.Th.*, mm	*Tb.Sp*, mm
Femur	22 (32)	0.16 (38)	0.54 (20)
Humeri	22 (32)	0.17 (17)	0.58 (47)
Ribs	29 (34)	0.23 (35)	0.51 (14)
Tibia	20 (15)	0.09 (9)	0.74 (11)
Pelvis	23 (13)	0.12 (20)	0.48 (23)
Skull	52 (10)	0.29 (31)	0.57 (35)
Clavicle*	29 (31)	0.15 (13)	0.80 (25)
Ulna and radii*	16 (31)	0.13 (15)	0.77 (16)
Scapulae*	22 (36)	0.19 (52)	0.96 (23)
Cervical vertebrae	20 (20)	0.18 (13)	0.60 (20)
Thoracic vertebrae + Lumbar vertebrae + Sacrum	14 (29)	0.10 (42)	0.60 (20)

Note: * — spongiosa parameters calculated based on measurements of similar bones or data for other ages; the method of calculation has been described previously [20].

Table 4. Linear dimensions and cortical layer thickness assumed for BPSs of a one-year-old child

Hematopoietic site	Segment	Shape[1]	Parameters of phantom, mm (CV in parentheses, %)[2]						References
			h	*a*	*b*	*c*	*d*	*Ct.Th.*	
Femur	Diaphysis[4]	c	30	11.2 (7)	11.2 (7)			2.3 (17)	43–47
	Proximal end	dc	35.8 (4)	34 (12)	18 (8)	11.2 (7)	11.2 (7)	0.7 (17)	
	Distal end	dc	35.8 (4)	34 (12)	18 (8)	11.2 (7)	11.2 (7)	0.6 (17)	
Humeri	Diaphysis[4]	c	30	9.1 (13)	9.1 (13)			1.6 (19)	43, 45, 47, 48
	Proximal end	dc	16 (13)	19.8 (13)	19.8 13)	9.1 (13)	9.1 (13)	0.5 (20)	
	Distal end	dc	16 (13)	19.8 (16)	9.1 (13)	9.1 (13)	9.1 (13)	0.4 (20)	
Ribs	Ribs[4]	p	8.7 (32)	30	3.9 (35)			0.5 (33)	49, 50
Sacrum	Body of the 1st vertebra	p	9.2 (20)	25.2 (10)	12.5 (10)				51–55
	Body of the 2nd vertebra	p	9.2 (20)	20.2 (10)	10 (10)				
	Body of the 3rd vertebra	p	8.3 (20)	15.1(10)	8.8 (10)				
	Body of the 4th vertebra	p	5.5 (20)	15.1 (10)	8.8 (10)				
	Body of the 5th vertebra	p	5.5 (20)	12.6 (10)	5 (10)				
	Ala of the 1st vertebra	p	9.2 (20)	10.7 (10)	12.5 (10)				
	Ala of the 2nd vertebra	p	9.2 (20)	8 (10)	10 (10)				
	Ala of the 3rd vertebra	p	8.3 (20)	8 (10)	8.8 (10)				
	Ala of the 4th vertebra	p	5.5 (20)	5.4 (9)	8.8 (10)				
Tibia bones	Fibula[4]	c	30	4.4 (11)	4.4 (11)			1.2 (17)	56
	Tibia diaphysis[4]	c	30	9 (13)	9 (13)			2.3 (9)	55–58
	Tibia proximal end	dc	38.9 (6)	27.2 (12)	15.2 (18)	9 (13)	9 (13)	0.5 (14)	
	Tibia distal end	dc	22.3 (6)	16.8 (23)	16.8 (23)	9 (13)	9 (13)	0.5 (14)	
Pelvic bones	Iliac bone part 1[3]	p	5 (18)	30	30			1.2 (33) 0.5 (47)	59–64
	Iliac bone part[2]	p	5 (18)	30	30			0.4 (30)	
	Acetabular part of iliac bone	dc	14.5 (10)	26.1 (9)	10 (30)	23.6 (22)	17.8 (40)	0.4 (30)	
	Acetabular part of pubic bone	c	4.8 (15)	15.5 (3)	10.9 (7)	7.7 (11)	7.7 (11)	0.4 (30)	
	Pubic ramus superior	c	19.3 (15)	7.7 (11)	7.7 (11)			0.4 (30)	
	Acetabular part of ischium	p	17.5 (15)	17.5 (15)	17.8 (30)	17.5 (15)		0.4 (3)	
	Ischium tuberosity	c	13 (15)	11.7 (15)	11.9 (15)			0.4 (3)	
Skull	Flat bones[4]	p	2.7 (30)	30	30			0.7 (29)	65–68
Clavicle	Body	c	42.2 (11)	7.2 (10)	5.2 (10)			0.9 (10)	69–72
	Sternum end	dc	7.4 (11)	14.1 (10)	12.7 (9)	7.2 (10)	5.2 (10)	0.4 (10)	
	Acromial end	dc	7.4 (11)	12.1 (10)	7.2 (19)	7.2 (10)	5.2(10)	0.4 (10)	
Radius and ulna	Diaphysis[4]	c	30	5.3 (6)	5.3 (6)			1.1 (13)	46, 56, 57
	End	dc	16.2 (6)	8 (6)	5.3 (6)	5.3 (6)	5.3 (6)	0.4 (29)	
Scapula	Glenoid	c	6.8 (26)	17.5 (18)	10.2 (29)			0.5 (29)	73–77
	Acromion	p	7 (19)	16 (41)	13 (42)			0.4 (13)	
	Body[4]	p	2.7 (13)	30	30			0.4 (13)	
Cervical vertebrae	Vertebral body	c	5.8 (9)	9.7 (7)	12.6 (7)				78, 79
Thoracic vertebrae	Vertebral body	c	8 (15)	11.9 (13)	15 (23)				78, 80
Lumbar vertebrae	Vertebral body	c	9.6 (16)	9.6 (16)	21 (3)				78, 53

Note: [1] — the shape of a phantom was designated as follows: *c* — cylinder, dc — deformed cylinder, *p* — rectangular parallelepiped, *e* — ellipsoid; [2] — dimensions of the BPSs: *h* — height; *a* — major axis (c), major axis for a larger base (dc) or side a (r); *b* — minor axis (c), minor axis for a larger base (dc) or side b (r); *c* — major axis for smaller base (dc); *d* — minor axis for smaller base (dc); for ellipsoid (e), *a*, *b*, *c* are the axes; [3] — different cortical layer thickness values were taken for inner (medial) and outer (gluteal) surfaces of this segment of the iliac bone (see Figure); [4] — BPS simulated only part of a modeled bone segment when dimensions thereof significantly exceeded 30 mm, since in such cases from the point of view of dosimetry it makes no sense to model the entire segment [13, 16].

Table 5. Comparison of the volumes of BPSs, newborn and one-year-old child

BPSs	Modeled media	Volume of the modeled structure, cm^3		
		Newborn	One-year-old	One-year-old / newborn
Tibia distal end	*BM*	1.36	6.53	4.80
	TB	0.79	1.88	2.38
	CB	0.37	1.41	3.81
	Entire BPS	2.52	9.82	3.90
Clavicle sternal end	*BM*	0.19	0.35	1.84
	TB	0.08	0.14	1.75
	CB	0.05	0.09	1.80
	Entire BPS	0.32	0.58	1.81
Lumbar vertebra body	*BM*	0.36	1.32	3.67
	TB	0.29	0.2	0.69
	Entire BPS	0.65	1.52	2.34
Cervical vertebra body	*BM*	0.06	0.45	7.50
	TB	0.08	0.11	1.38
	Entire BPS	0.14	0.56	4.00

is explained by the decreasing BV/TV ratio: according to the published data, it goes down from 0.45 to 0.14 (Table 3). In most BPSs, the volume of CB increases significantly, 2.3-fold on the average, in the first year of life, with the exception of BPSs of vertebral bodies. On the average, the total volume of BPSs for a one-year-old child is 2.4 times larger than that for a newborn.

CONCLUSIONS

As a result of this study computational phantoms of the main sites of a one-year-old child's skeleton with active hematopoiesis were created. We developed these phantoms using the same methods as for the phantoms of a newborn. The generated phantoms simulate bone tissue structure and population variability of the size of individual bone structure. The presented phantom of a one-year-old child will be used to calculate DF for ^{89,90}Sr, which in turn are necessary to estimate refined factors linking individual intake of the radionuclide and the AM dose, which will help to improve dose estimates for residents of the Ural region. It should be noted that the phantom developed with the help of SPSD could be used to calculate DF for other bone-seeking beta emitters, including those used in radionuclide therapy, such as ^{89}Sr, ^{32}P, ^{186}Re, ^{188}Re, ^{117}mSn. Our plans include generation of SPSD skeletal phantoms for other age groups: 5-year, 10-year, 15-year old children and adults. SPSD phantoms can be used for dosimetry of incorporated bone-seeking beta-emitters in the population in situations when the environment is contaminated with radionuclides.

References

1. Degteva MO, Shagina NB, Vorobiova MI, Shishkina EA, Tolstykh EI, Akleyev AV. Contemporary Understanding of Radioactive Contamination of the Techa River in 1949-1956. Radiats Biol Radioecol. 2016; 56 (5): 523–34.PMID: 30703313. Russian.
2. Krestinina LY, Epifanova S, Silkin S, Mikryukova L, Degteva M, Shagina N, et al. Chronic low-dose exposure in the Techa River Cohort: risk of mortality from circulatory diseases. Radiat Environ Biophys. 2013; 52 (1): 47–57. DOI: 10.1007/s00411-012-0438-5. Epub 2012 Nov 4.
3. Akleev AV. Hronicheskij luchevoj sindrom u zhitelej pribrezhnyh sel reki Techa. Chelyabinsk: Kniga, 2012; 464 s. Russian.
4. Preston DL, Sokolnikov ME, Krestinina LY, Stram DO. Estimates of radiation effects on cancer risks in the mayak worker, Techa river and atomic bomb survivor studies. Radiat Prot Dosimetry. 2017; 173 (1–3): 26–31. DOI: 10.1093/rpd/ncw316.
5. Degteva MO, Napier BA, Tolstykh EI, et al. Enhancements in the Techa river dosimetry system: TRDS-2016D Code for reconstruction of deterministic estimates of dose from environmental exposures. Health Phys. 2019; 117 (4): 378–87. DOI: 10.1097/HP.0000000000001067.
6. Spiers FW, Beddoe AH, Whitwell JR. Mean skeletal dose factors for beta-particle emitters in human bone. Part I: volume-seeking radionuclides. The British journal of radiology. 1978; 51 (608): 622–7.
7. Silkin SS, Krestinina LYu, Starcev NV, Akleev AV. Ural'skaya kogorta avarijno-obluchennogo naseleniya. Medicina ehkstremal'nyh situacij. 2019; 21 (3): 393–402. Russian.
8. O'Reilly SE, DeWeese LS, Maynard MR, Rajon DA, Wayson MB, Marshall EL, et al. An 13 image-based skeletal dosimetry model for the ICRP reference adult female-internal electron 14 sources. Phys Med Biol. 2016 Dec 21; 61 (24): 8794–824. Epub 2016 Nov 29.
9. Xu XG, Chao TC, Bozkurt A. VIP-Man: an image-based whole-body adult male model constructed from color photographs of the Visible Human Project for multi-particle Monte Carlo calculations. Health Phys. 2000; 78 (5): 476–86. DOI: 10.1097/00004032-200005000-00003. PMID: 10772019.
10. Shah AP, Bolch WE, Rajon DA, Patton PW, Jokisch DW. A paired-image radiation transport model for skeletal dosimetry. J Nucl Med. 2005; 46 (2): 344–53. PMID: 15695796.
11. Pafundi D. Image-based skeletal tissues and electron dosimetry models for the ICRP reference pediatric age series. A dissertation presented to the graduate schools of the University of Florida in partial fulfillment of the requirements for the degree of doctor of the philosophy. University of Florida. 2009.
12. Hough M, Johnson P, Rajon D, Jokisch D, Lee C, Bolch W. An image-based skeletal dosimetry model for the ICRP reference adult male–internal electron sources. Phys Med Biol. 2011; 56 (8): 2309–46. DOI: 10.1088/0031-9155/56/8/001.
13. Degteva MO, Tolstykh EI, Shishkina EA, Sharagin PA, Zalyapin VI, Volchkova AYu, et al. PLoS One. 2021; 16 (10): e0257605.

DOI: 10.1371/journal.pone.0257605. PMID: 34648511; PMCID: PMC8516275.PlosOne.
14. Dyogteva MO, Shishkina EA, Tolstykh EI, Zalyapin VI, Sharagin PA, Smit MA, i dr. Metodologicheskij podhod k razrabotke dozimetricheskih modelej skeleta cheloveka dlya beta-izluchayushhih radionuklidov. Radiacionnaya gigiena. 2019; 12 (2). DOI: 10.21514/1998-426X-2019-12-2-66-75. Russian.
15. Volchkova AYu, Sharagin PA, Shishkina EA. Internal bone marrow dosimetry: the effect of the exposure due to 90Sr incorporated in the adjacent bone segments. Bulletin of the South Ural State University. Ser. Mathematical Modelling, Programming & Computer Software. 2022; 15 (4): 44–58. DOI: 10.14529/mmp220404.
16. Sharagin PA, Shishkina EA, Tolstykh EI. Vychislitel'nyj fantom dlya dozimetrii krasnogo kostnogo mozga novorozhdennogo rebenka ot inkorporirovannyh beta-izluchatelej. Medicina ehkstremal'nyh situacij. 2022; (4): 74–82. DOI: 10.47183/mes.2022.045. Russian.
17. Cristy M. Active bone marrow distribution as a function of age in humans. Phys Med Biol. 1981; 26 (3): 389–400.
18. Sharagin PA, Shishkina EA, Tolstykh EI, Volchkova AYu, Smith MA, Degteva MO. Segmentation of hematopoietic sites of human skeleton for calculations of dose to active marrow exposed to bone-seeking radionuclides. RAD Conference Proceedings. 2018; (3): 154–8. DOI: 10.21175/RadProc.2018.33.
19. Sharagin PA, Tolstykh EI, Shishkina EA, Degteva MO. Dozimetricheskoe modelirovanie kosti dlya osteotropnyh beta-izluchayushhih radionuklidov: razmernye parametry i segmentaciya. V sbornike: Materialy mezhdunarodnoj nauchnoj konferencii “Sovremennye problemy radiobiologii”. Belarus', Gomel', 23-24 sentyabrya 2021; s. 200–204. Russian.
20. Tolstykh EI, Sharagin PA, Shishkina EA, Degteva MO. Formirovanie doz oblucheniya krasnogo kostnogo mozga cheloveka ot 89,90Sr, ocenka parametrov trabekulyarnoj kosti dlya dozimetricheskogo modelirovaniya. V sbornike: Materialy mezhdunarodnoj nauchnoj konferencii “Sovremennye problemy radiobiologii”. Belarus', Gomel', 23–24 sentyabrya 2021; s. 176–179. Russian.
21. Tolstykh EI, Sharagin PA, Shishkina EA, Volchkova AYu, Degteva MO. Anatomo-morfologicheskij bazis dlya dozimetricheskogo modelirovaniya trabekulyarnoj kosti cheloveka s ispol'zovaniem stoxasticheskogo parametricheskogo podhoda. Klinicheskij vestnik GNC FMBC im. A. I. Burnazyana. 2022; 3: 25–40. Russian.
22. Valentin J. Basic anatomical and physiological data for use in radiological protection: reference values. Annals of the ICRP. Annals of the ICRP. 2002; 32 (3–4): 1–277.
23. Shishkina EA, Timofeev YS, Volchkova AY, Sharagin PA, Zalyapin VI, Degteva MO, et al. Trabecula: a random generator of computational phantoms for bone marrow dosimetry. Health Phys. 2020; 118 (1): 53–59. DOI: 10.1097/HP.0000000000001127.
24. Zalyapin VI, Timofeev YuS, Shishkina EA. A parametric stochastic model of bone geometry. Bulletin of Southern Urals State University, Issue «Mathematical Modelling. Programming & Computer Software» (SUSU MMCS) 2018; 11 (2): 44–57. DOI: 10.14529/mmp180204.
25. Robinson RA. Chemical analysis and electron microscopy of bone. In: Rodahl K, Nicholson JT, Brown EM editors. Bone as a tissue. New York: McGraw-Hill, 1960; p. 186–250.
26. Vogler JB 3rd, Murphy WA. Bone marrow imaging. Radiology. 1988; 168 (3): 679–93.
27. Vande Berg BC, Malghem J, Lecouvet FE, Maldague B. Magnetic resonance imaging of the normal bone marrow. Skeletal Radiology. 1998; 27: 471–83.
28. Vande Berg BC, Malghem J, Lecouvet FE, Maldague B. Magnetic resonance imaging of normal bone marrow. Eur Radiol. 1998; 8 (8): 1327–34.
29. Taccone A, Oddone M, Dell'Acqua AD, Occhi M, Ciccone MA. MRI "road–map" of normal age-related bone marrow. II. Thorax, pelvis and extremities. Pediatr Radiol. 1995; 25 (8): 596–606; PubMed PMID: 8570312.
30. Taccone A, Oddone M, Occhi M, Dell'Acqua AD, Ciccone MA. MRI "road–map" of normal age-related bone marrow. I. Cranial bone and spine. Pediatr Radiol. 1995; 25 (8): 588–95; PubMed PMID: 8570311.
31. Cunningham C, Scheuer L, Black S. Developmental juvenile osteology. Elsevier Academic Press, 2016.
32. Ryan TM, Krovitz GE. Trabecular bone ontogeny in the human proximal femur. J Hum Evol. 2006; 51 (6): 591–602.
33. Milovanovic P, Djonic D, Hahn M, Amling M, Busse B, Djuric M. Region-dependent patterns of trabecular bone growth in the human proximal femur: A study of 3D bone microarchitecture from early postnatal to late childhood period. Am J Phys Anthropol. 2017; 164 (2): 281–91. DOI: 10.1002/ajpa.23268. Epub 2017 Jun 20.
34. Saers JP, Cazorla-Bak Y, Shaw CN, Stock JT, Ryan TM. Trabecular bone structural variation throughout the human lower limb. J Hum Evol. 2016; 97: 97–108. DOI: 10.1016/j.jhevol.2016.05.012.
35. Ryan TM, Raichlen DA, Gosman JH. Structural and mechanical changes in trabecular bone during early development in the human femur and humerus. In: Building bones: bone formation and development in anthropology. Cambridge University Press, 2017; p. 281–302. Available from: https://doi.org/10.1017/9781316388907.013.
36. Byers S, Moore AJ, Byard RW, Fazzalari NL. Quantitative histomorphometric analysis of the human growth plate from birth to adolescence. Bone. 2000; 27 (4): 495–501.
37. Gosman JH, Ketcham RA. Patterns in ontogeny of human trabecular bone from SunWatch Village in the Prehistoric Ohio Valley: general features of microarchitectural change. Am J Phys Anthropol. 2009; 138 (3): 318–32. DOI: 10.1002/ajpa.20931. PubMed PMID: 18785633.
38. Volpato V. Bone endostructure morphogenesis of the human ilium. Comptes rendus Palévol. 2008; 7: 463–71. DOI: 10.1016/j.crpv.2008.06.001.
39. Glorieux FH, Travers R, Taylor A, Bowen JR, Rauch F, Norman M, et al. Normative data for iliac bone histomorphometry in growing children. Bone. 2000; 26 (2): 103–9.
40. Rodriguez-Florez N, Ibrahim A, Hutchinson JC, Borghi A, James G, Arthurs OJ, et al. Cranial bone structure in children with sagittal craniosynostosis: relationship with surgical outcomes. J Plast Reconstr Aesthet Surg. 2017; 70 (11): 1589–97. DOI: 10.1016/j.bjps.2017.06.017.
41. Hough M, Johnson P, Rajon D, Jokisch D, Lee C, Bolch W. An image-based skeletal dosimetry model for the ICRP reference adult male—internal electron sources. Phys Med Biol. 2011; 56 (8): 2309–46.
42. Acquaah F, Robson Brown KA, Ahmed F, Jeffery N, Abel RL. Early trabecular development in human vertebrae: overproduction, constructive regression, and refinement. Front Endocrinol (Lausanne). 2015; 6: 67. DOI: 10.3389/fendo.2015.00067. eCollection 2015.
43. Florence JL. Linear and cortical bone dimensions as indicators of health status in subadults from the Milwaukee County Poor Farm Cemetery. M.A., University of Colorado at Denver, 2007.
44. Miles AEW. Growth cuves of immature bones from a scottish island population of sixteenth to mid-nineteenth century: limb-bone diaphyses and some bones of the hand and foot. International Journal of Osteoarcheology. 1994; 4: 121–36.
45. Maresh MM. Measurements from roentgenograms. In: McCammon RW, editor. Human Growth and Development. Springfield, IL: Charles C. Thomas, 1970; p. 157–200.
46. Dhavale N, Halcrow SE, Buckley HR, Tayles N, Domett KM, Gray AR. Linear and appositional growth in infants and children from the prehistoric settlement of Ban Non Wat, Northeast Thailand: evaluating biological responses to agricultural intensification in Southeast Asia. Journal of Archaeological Science: Reports. 2017; 11: 435–46.
47. Svadovsky VS. Age-related bone remodeling. Moscow, 1961.
48. Danforth ME, Wrobel GD, Armstrong CW, Swanson D. Juvenile age estimation using diaphyseal long bone lengths among ancient Maya populations. Latin American Antiquity. 2017; 20 (1): 3–13.
49. Beresheim AC, Pfeiffer S, Grynpas M. Ontogenetic changes to bone microstructure in an archaeologically derived sample of human ribs. J Anat. 2019. DOI: 10.1111/joa.13116
50. Pfeiffer S. Cortical Bone Histology in Juveniles. Available from: https://www.researchgate.net/publication/303179375_Cortical_bone_histology_in_Juveniles
51. Hresko AM, Hinchcliff EM, Deckey DG, Hresko MT. Developmental

sacral morphology: MR study from infancy to skeletal maturity. Eur Spine J. 2020. Available from: https://doi.org/10.1007/s00586-020-06350-6.
52. Kuznecov LE. Perelomy taza u detej: morfologiya, biomexanika, diagnostika. M.: Folium, 1994. Russian.
53. Mavrych V, Bolgova O, Ganguly P, Kashchenko S. Age-related changes of lumbar vertebral body morphometry. Austin J Anat. 2014; 1 (3): 7.
54. Dimeglio A, Bonnel F, Canavese F. The Growing Spine. In: Jean Marc Vital, Derek Thomas Cawley, editors. Spinal Anatomy. Modern Concepts. Springer, 2020; p. 25–52.
55. Andronevsky A. Anatomy rebenka. Buharest: Meridian, 1970.
56. Bernert Zs, Évinger S, Hajdu T. New data on the biological age estimation of children using bone measurements based on historical populations from the Carpathian Basin. Annales Historico-Naturales Musei Nationalis Hungarici. 2007; 99: 199–206.
57. Gindhart PS. Growth standards for the tibia and radius in children aged one month through eighteen years. Am J Phys Anthrop. 1973; 39: 41–48.
58. Lopez-Costas O, Rissech C, Trancho G, Turbón D. Postnatal ontogenesis of the tibia. Implications for age and sex estimation. Forensic Sci Int. 2012; 214 (1–3): 207.e1–11. DOI: 10.1016/j.forsciint.2011.07.038. Epub 2011 Aug 20. PubMed PMID: 21862250.
59. Blake KAS. An investigation of sex determination from the subadult pelvis: a morphometric analysis. Doctoral Dissertation, University of Pittsburgh. 2011.
60. Cunningham CA, Black SM. Iliac cortical thickness in the neonate - the gradient effect. J Anat. 2009; 215 (3): 364–70. DOI: 10.1111/j.1469-7580.2009.01112.x.
61. Cunningham CA, Black SM. Anticipating bipedalism: trabecular organization in the newborn ilium. J Anat. 2009; 214 (6): 817–29. DOI: 10.1111/j.1469-7580.2009.01073.x
62. Corron L, Marchal F, Condemi S, Chaumoître K, Adalian P. A New Approach of Juvenile Age Estimation using Measurements of the Ilium and Multivariate Adaptive Regression Splines (MARS) Models for Better Age Prediction. Forensic Sci. 2017; 62 (1): 18–29. DOI: 10.1111/1556-4029.13224.
63. Parfitt AM, Travers R, Rauch F, Glorieux FH. Structural and cellular changes during bone growth in healthy children. Bone. 2000; 27 (4): 487–94. PMID: 11033443.
64. Schnitzler CM, Mesquita JM, Pettifor JM. Cortical bone development in black and white South African children: iliac crest histomorphometry. Bone. 2009; 44 (4): 603–11. DOI: 10.1016/j.bone.2008.12.009.
65. De Boer HH, Van der Merwe AE, Soerdjbalie-Maikoe VV. Human cranial vault thickness in a contemporary sample of 1097 autopsy cases: relation to body weight, stature, age, sex and ancestry. Int J Legal Med. 2016; 130 (5): 1371–7. DOI: 10.1007/s00414-016-1324-5.
66. Margulies S, Coats B. Experimental injury biomechanics of the pediatric head and brain. Chapter 4. In: Crandall JR, Myers BS, Meaney DF, Schmidtke SZ, editors. Pediatric Injury Biomechanics Springer Science + Business Media New York. 2013; p. 157–190.
67. Li Z, Park BK, Liu W, Zhang J, Reed MP, Rupp JD, et al. A statistical skull geometry model for children 0–3 years old. PLoS One. 2015 May 18; 10 (5): e0127322. DOI: 10.1371/journal.pone.0127322. eCollection 2015.
68. Rodriguez-Florez N, Ibrahim A, Hutchinson JC, Borghi A, James G, Arthurs OJ, et al. Cranial bone structure in children with sagittal craniosynostosis: Relationship with surgical outcomes. J Plast Reconstr Aesthet Surg. 2017; 70 (11): 1589–97. DOI: 10.1016/j.bjps.2017.06.017.
69. McGraw MA, Mehlman CT, Lindsell CJ, Kirby CL. Postnatal growth of the clavicle: birth to eighteen years of age. Journal of Pediatric Orthopedics. 2009; 29: 937.
70. Bleuze MM, Wheeler SM, Williams LJ, Dupras TL. Growth of the pectoral girdle in a sample of juveniles from the kellis 2 cemetery, Dakhleh Oasis, Egypt. Am J Hum Biol. 2016; 28 (5): 636–45.
71. Black SM, Scheuer JL. Age changes in the clavicle: from the early neonatal period to skeletal maturity. International Journal of Osteoarchaeology. 1996; 6: 425–34.
72. Bernat A, Huysmans T, Van Glabbeek F, Sijbers J, Gielen J, Van Tongel A. The anatomy of the clavicle: a three-dimensional cadaveric study. Clin Anat. 2014; 27 (5): 712–23.
73. Vallois HV. L'omoplate humaine. Bulletin de la Sociétié d'Anthropolgie de Paris. 1946; 7: 16–99.
74. Saunders S, Hoppa R, Southern R. Diaphyseal growth in a nineteenth-century skeletal sample of subadults from St Thomas' Church, Belleville, Ontario. International Journal of Osteoarchaeology. 1993; 3: 265–81.
75. Rissech C, Black S. Scapular development from neonatal period to skeletal maturity. A preliminary study. Int J Osteoarchaeol. 2007; 17: 451–64.
76. Cardoso HFV, Spake L, Humphrey LT. Age estimation of immature human skeletal remains from the dimensions of the girdle bones in the postnatal period. Am J Phys Anthropol. 2017; 163 (4): 772–83. DOI: 10.1002/ajpa.23248. Epub 2017 May 24. PubMed PMID: 28542741.
77. Badr El Dine F, Hassan H. Ontogenetic study of the scapula among some Egyptians: Forensic implications in age and sex estimation using Multidetector Computed Tomography, Egyptian Journal of Forensic Sciences. 2015; 6 (2): 56–77.
78. Kneissel M, Roschger P, Steiner W, Schamall D, Kalchhauser G, Boyde A, et al. Cancellous Bone Structure in the Growing and Aging Lumbar Spine in a Historic Nubian Population. Calcif Tissue Int. 1997; 61: 95–100.
79. Johnson KT, Al-Holou WN, Anderson RC, Wilson TJ, Karnati T, Ibrahim M, et al. Morphometric analysis of the developing pediatric cervical spine. J Neurosurg Pediatr. 2016; 18 (3): 377–89. DOI: 10.3171/2016.3. PEDS1612. Epub 2016 May 27. PubMed PMID: 27231821.
80. Comeau A. Age-related changes in geometric characteristics of the pediatric thoracic cage and comparison of thorax shape with a pediatric CPR Manikin. PhD thesis. 2010.

Литература

1. Degteva MO, Shagina NB, Vorobiova MI, Shishkina EA, Tolstykh EI, Akleyev AV. Contemporary Understanding of Radioactive Contamination of the Techa River in 1949-1956. Radiats Biol Radioecol. 2016; 56 (5): 523–34.PMID: 30703313. Russian.
2. Krestinina LY, Epifanova S, Silkin S, Mikryukova L, Degteva M, Shagina N, et al. Chronic low-dose exposure in the Techa River Cohort: risk of mortality from circulatory diseases. Radiat Environ Biophys. 2013; 52 (1): 47–57. DOI: 10.1007/s00411-012-0438-5. Epub 2012 Nov 4.
3. Аклеев А. В. Хронический лучевой синдром у жителей прибрежных сел реки Теча. Челябинск: Книга, 2012; 464 с.
4. Preston DL, Sokolnikov ME, Krestinina LY, Stram DO. Estimates of radiation effects on cancer risks in the mayak worker, Techa river and atomic bomb survivor studies. Radiat Prot Dosimetry. 2017; 173 (1–3): 26–31. DOI: 10.1093/rpd/ncw316.
5. Degteva MO, Napier BA, Tolstykh EI, et al. Enhancements in the Techa river dosimetry system: TRDS-2016D Code for reconstruction of deterministic estimates of dose from environmental exposures. Health Phys. 2019; 117 (4): 378–87. DOI: 10.1097/HP.0000000000001067.
6. Spiers FW, Beddoe AH, Whitwell JR. Mean skeletal dose factors for beta-particle emitters in human bone. Part I: volume-seeking radionuclides. The British journal of radiology. 1978; 51 (608): 622–7.
7. Силкин С. С., Крестинина Л. Ю., Старцев Н. В, Аклеев А. В. Уральская когорта аварийно-облученного населения. Медицина экстремальных ситуаций. 2019; 21 (3): 393–402.
8. O'Reilly SE, DeWeese LS, Maynard MR, Rajon DA, Wayson MB, Marshall EL, et al. An 13 image-based skeletal dosimetry model for the ICRP reference adult female-internal electron 14 sources. Phys Med Biol. 2016 Dec 21; 61 (24): 8794–824. Epub 2016 Nov 29.
9. Xu XG, Chao TC, Bozkurt A. VIP-Man: an image-based whole-body adult male model constructed from color photographs of the Visible Human Project for multi-particle Monte Carlo calculations.

Health Phys. 2000; 78 (5): 476–86. DOI: 10.1097/00004032-200005000-00003. PMID: 10772019.
10. Shah AP, Bolch WE, Rajon DA, Patton PW, Jokisch DW. A paired-image radiation transport model for skeletal dosimetry. J Nucl Med. 2005; 46 (2): 344–53. PMID: 15695796.
11. Pafundi D. Image-based skeletal tissues and electron dosimetry models for the ICRP reference pediatric age series. A dissertation presented to the graduate schools of the University of Florida in partial fulfillment of the requirements for the degree of doctor of the philosophy. University of Florida. 2009.
12. Hough M, Johnson P, Rajon D, Jokisch D, Lee C, Bolch W. An image-based skeletal dosimetry model for the ICRP reference adult male–internal electron sources. Phys Med Biol. 2011; 56 (8): 2309–46. DOI: 10.1088/0031-9155/56/8/001.
13. Degteva MO, Tolstykh EI, Shishkina EA, Sharagin PA, Zalyapin VI, Volchkova AYu, et al. PLoS One. 2021; 16 (10): e0257605. DOI: 10.1371/journal.pone.0257605. PMID: 34648511; PMCID: PMC8516275.PlosOne.
14. Дёгтева М. О., Шишкина Е. А., Толстых Е. И., Заляпин В. И., Шарагин П. А., Смит М. А., и др. Методологический подход к разработке дозиметрических моделей скелета человека для бета-излучающих радионуклидов. Радиационная гигиена. 2019; 12 (2). DOI: 10.21514/1998-426X-2019-12-2-66-75.
15. Volchkova AYu, Sharagin PA, Shishkina EA. Internal bone marrow dosimetry: the effect of the exposure due to 90Sr incorporated in the adjacent bone segments. Bulletin of the South Ural State University. Ser. Mathematical Modelling, Programming & Computer Software. 2022; 15 (4): 44–58. DOI: 10.14529/mmp220404.
16. Шарагин П. А., Шишкина Е. А., Толстых Е. И. Вычислительный фантом для дозиметрии красного костного мозга новорожденного ребенка от инкорпорированных бета-излучателей. Медицина экстремальных ситуаций. 2022; (4): 74–82. DOI: 10.47183/mes.2022.045.
17. Cristy M. Active bone marrow distribution as a function of age in humans. Phys Med Biol. 1981; 26 (3): 389–400.
18. Sharagin PA, Shishkina EA, Tolstykh EI, Volchkova AYu, Smith MA, Degteva MO. Segmentation of hematopoietic sites of human skeleton for calculations of dose to active marrow exposed to bone-seeking radionuclides. RAD Conference Proceedings. 2018; (3): 154–8. DOI: 10.21175/RadProc.2018.33.
19. Шарагин П. А., Толстых Е. И., Шишкина Е. А., Дегтева М. О. Дозиметрическое моделирование кости для остеотропных бета-излучающих радионуклидов: размерные параметры и сегментация. В сборнике: Материалы международной научной конференции “Современные проблемы радиобиологии”. Беларусь, Гомель, 23-24 сентября 2021; с. 200–204.
20. Толстых Е. И., Шарагин П. А., Шишкина Е. А., Дегтева М. О. Формирование доз облучения красного костного мозга человека от 89,90Sr, оценка параметров трабекулярной кости для дозиметрического моделирования. В сборнике: Материалы международной научной конференции “Современные проблемы радиобиологии”. Беларусь, Гомель, 23–24 сентября 2021; с. 176–179.
21. Толстых Е. И., Шарагин П. А., Шишкина Е. А., Волчкова А. Ю. Дегтева М. О. Анатомо-морфологический базис для дозиметрического моделирования трабекулярной кости человека с использованием стохастического параметрического подхода. Клинический вестник ГНЦ ФМБЦ им. А. И. Бурназяна. 2022; 3: 25–40.
22. Valentin J. Basic anatomical and physiological data for use in radiological protection: reference values. Annals of the ICRP. Annals of the ICRP. 2002; 32 (3–4): 1–277.
23. Shishkina EA, Timofeev YS, Volchkova AY, Sharagin PA, Zalyapin VI, Degteva MO, et al. Trabecula: a random generator of computational phantoms for bone marrow dosimetry. Health Phys. 2020; 118 (1): 53–59. DOI: 10.1097/HP.0000000000001127.
24. Zalyapin VI, Timofeev YuS, Shishkina EA. A parametric stochastic model of bone geometry. Bulletin of Southern Urals State University, Issue «Mathematical Modelling. Programming & Computer Software» (SUSU MMCS) 2018; 11 (2): 44–57. DOI: 10.14529/mmp180204.
25. Robinson RA. Chemical analysis and electron microscopy of bone. In: Rodahl K, Nicholson JT, Brown EM editors. Bone as a tissue. New York: McGraw-Hill, 1960; p. 186–250.
26. Vogler JB 3rd, Murphy WA. Bone marrow imaging. Radiology. 1988; 168 (3): 679–93.
27. Vande Berg BC, Malghem J, Lecouvet FE, Maldague B. Magnetic resonance imaging of the normal bone marrow. Skeletal Radiology. 1998; 27: 471–83.
28. Vande Berg BC, Malghem J, Lecouvet FE, Maldague B. Magnetic resonance imaging of normal bone marrow. Eur Radiol. 1998; 8 (8): 1327–34.
29. Taccone A, Oddone M, Dell'Acqua AD, Occhi M, Ciccone MA. MRI "road–map" of normal age-related bone marrow. II. Thorax, pelvis and extremities. Pediatr Radiol. 1995; 25 (8): 596–606; PubMed PMID: 8570312.
30. Taccone A, Oddone M, Occhi M, Dell'Acqua AD, Ciccone MA. MRI "road–map" of normal age-related bone marrow. I. Cranial bone and spine. Pediatr Radiol. 1995; 25 (8): 588–95; PubMed PMID: 8570311.
31. Cunningham C, Scheuer L, Black S. Developmental juvenile osteology. Elsevier Academic Press, 2016.
32. Ryan TM, Krovitz GE. Trabecular bone ontogeny in the human proximal femur. J Hum Evol. 2006; 51 (6): 591–602.
33. Milovanovic P, Djonic D, Hahn M, Amling M, Busse B, Djuric M. Region-dependent patterns of trabecular bone growth in the human proximal femur: A study of 3D bone microarchitecture from early postnatal to late childhood period. Am J Phys Anthropol. 2017; 164 (2): 281–91. DOI: 10.1002/ajpa.23268. Epub 2017 Jun 20.
34. Saers JP, Cazorla-Bak Y, Shaw CN, Stock JT, Ryan TM. Trabecular bone structural variation throughout the human lower limb. J Hum Evol. 2016; 97: 97–108. DOI: 10.1016/j.jhevol.2016.05.012.
35. Ryan TM, Raichlen DA, Gosman JH. Structural and mechanical changes in trabecular bone during early development in the human femur and humerus. In: Building bones: bone formation and development in anthropology. Cambridge University Press, 2017; p. 281–302. Available from: https://doi.org/10.1017/9781316388907.013.
36. Byers S, Moore AJ, Byard RW, Fazzalari NL. Quantitative histomorphometric analysis of the human growth plate from birth to adolescence. Bone. 2000; 27 (4): 495–501.
37. Gosman JH, Ketcham RA. Patterns in ontogeny of human trabecular bone from SunWatch Village in the Prehistoric Ohio Valley: general features of microarchitectural change. Am J Phys Anthropol. 2009; 138 (3): 318–32. DOI: 10.1002/ajpa.20931. PubMed PMID: 18785633.
38. Volpato V. Bone endostructure morphogenesis of the human ilium. Comptes rendus Palévol. 2008; 7: 463–71. DOI: 10.1016/j.crpv.2008.06.001.
39. Glorieux FH, Travers R, Taylor A, Bowen JR, Rauch F, Norman M, et al. Normative data for iliac bone histomorphometry in growing children. Bone. 2000; 26 (2): 103–9.
40. Rodriguez-Florez N, Ibrahim A, Hutchinson JC, Borghi A, James G, Arthurs OJ, et al. Cranial bone structure in children with sagittal craniosynostosis: relationship with surgical outcomes. J Plast Reconstr Aesthet Surg. 2017; 70 (11): 1589–97. DOI: 10.1016/j.bjps.2017.06.017.
41. Hough M, Johnson P, Rajon D, Jokisch D, Lee C, Bolch W. An image-based skeletal dosimetry model for the ICRP reference adult male—internal electron sources. Phys Med Biol. 2011; 56 (8): 2309–46.
42. Acquaah F, Robson Brown KA, Ahmed F, Jeffery N, Abel RL. Early trabecular development in human vertebrae: overproduction, constructive regression, and refinement. Front Endocrinol (Lausanne). 2015; 6: 67. DOI: 10.3389/fendo.2015.00067. eCollection 2015.
43. Florence JL. Linear and cortical bone dimensions as indicators of health status in subadults from the Milwaukee County Poor Farm Cemetery. M.A., University of Colorado at Denver, 2007.
44. Miles AEW. Growth cuves of immature bones from a scottish island population of sixteenth to mid-nineteenth century: limb-bone diaphyses and some bones of the hand and foot. International Journal of Osteoarcheology. 1994; 4: 121–36.
45. Maresh MM. Measurements from roentgenograms. In: McCammon RW, editor. Human Growth and Development.

Springfield, IL: Charles C. Thomas, 1970; p. 157–200.
46. Dhavale N, Halcrow SE, Buckley HR, Tayles N, Domett KM, Gray AR. Linear and appositional growth in infants and children from the prehistoric settlement of Ban Non Wat, Northeast Thailand: evaluating biological responses to agricultural intensification in Southeast Asia. Journal of Archaeological Science: Reports. 2017; 11: 435–46.
47. Svadovsky VS. Age-related bone remodeling. Moscow, 1961.
48. Danforth ME, Wrobel GD, Armstrong CW, Swanson D. Juvenile age estimation using diaphyseal long bone lengths among ancient Maya populations. Latin American Antiquity. 2017; 20 (1): 3–13.
49. Beresheim AC, Pfeiffer S, Grynpas M. Ontogenetic changes to bone microstructure in an archaeologically derived sample of human ribs. J Anat. 2019. DOI: 10.1111/joa.13116
50. Pfeiffer S. Cortical Bone Histology in Juveniles. Available from: https://www.researchgate.net/publication/303179375_Cortical_bone_histology_in_Juveniles
51. Hresko AM, Hinchcliff EM, Deckey DG, Hresko MT. Developmental sacral morphology: MR study from infancy to skeletal maturity. Eur Spine J. 2020. Available from: https://doi.org/10.1007/s00586-020-06350-6.
52. Кузнецов Л. Е. Переломы таза у детей: морфология, биомеханика, диагностика. М.: Фолиум, 1994.
53. Mavrych V, Bolgova O, Ganguly P, Kashchenko S. Age-related changes of lumbar vertebral body morphometry. Austin J Anat. 2014; 1 (3): 7.
54. Dimeglio A, Bonnel F, Canavese F. The Growing Spine. In: Jean Marc Vital, Derek Thomas Cawley, editors. Spinal Anatomy. Modern Concepts. Springer, 2020; p. 25–52.
55. Андроневский А. Анатомия ребенка. Бухарест: Меридиан, 1970.
56. Bernert Zs, Évinger S, Hajdu T. New data on the biological age estimation of children using bone measurements based on historical populations from the Carpathian Basin. Annales Historico-Naturales Musei Nationalis Hungarici. 2007; 99: 199–206.
57. Gindhart PS. Growth standards for the tibia and radius in children aged one month through eighteen years. Am J Phys Anthrop. 1973; 39: 41–48.
58. Lopez-Costas O, Rissech C, Trancho G, Turbón D. Postnatal ontogenesis of the tibia. Implications for age and sex estimation. Forensic Sci Int. 2012; 214 (1–3): 207.e1–11. DOI: 10.1016/j.forsciint.2011.07.038. Epub 2011 Aug 20. PubMed PMID: 21862250.
59. Blake KAS. An investigation of sex determination from the subadult pelvis: a morphometric analysis. Doctoral Dissertation, University of Pittsburgh. 2011.
60. Cunningham CA, Black SM. Iliac cortical thickness in the neonate - the gradient effect. J Anat. 2009; 215 (3): 364–70. DOI: 10.1111/j.1469-7580.2009.01112.x.
61. Cunningham CA, Black SM. Anticipating bipedalism: trabecular organization in the newborn ilium. J Anat. 2009; 214 (6): 817–29. DOI: 10.1111/j.1469-7580.2009.01073.x
62. Corron L, Marchal F, Condemi S, Chaumoître K, Adalian P. A New Approach of Juvenile Age Estimation using Measurements of the Ilium and Multivariate Adaptive Regression Splines (MARS) Models for Better Age Prediction. Forensic Sci. 2017; 62 (1): 18–29. DOI: 10.1111/1556-4029.13224.
63. Parfitt AM, Travers R, Rauch F, Glorieux FH. Structural and cellular changes during bone growth in healthy children. Bone. 2000; 27 (4): 487–94. PMID: 11033443.
64. Schnitzler CM, Mesquita JM, Pettifor JM. Cortical bone development in black and white South African children: iliac crest histomorphometry. Bone. 2009; 44 (4): 603–11. DOI: 10.1016/j.bone.2008.12.009.
65. De Boer HH, Van der Merwe AE, Soerdjbalie-Maikoe VV. Human cranial vault thickness in a contemporary sample of 1097 autopsy cases: relation to body weight, stature, age, sex and ancestry. Int J Legal Med. 2016; 130 (5): 1371–7. DOI: 10.1007/s00414-016-1324-5.
66. Margulies S, Coats B. Experimental injury biomechanics of the pediatric head and brain. Chapter 4. In: Crandall JR, Myers BS, Meaney DF, Schmidtke SZ, editors. Pediatric Injury Biomechanics Springer Science + Business Media New York. 2013; p. 157–190.
67. Li Z, Park BK, Liu W, Zhang J, Reed MP, Rupp JD, et al. A statistical skull geometry model for children 0–3 years old. PLoS One. 2015 May 18; 10 (5): e0127322. DOI: 10.1371/journal.pone.0127322. eCollection 2015.
68. Rodriguez-Florez N, Ibrahim A, Hutchinson JC, Borghi A, James G, Arthurs OJ, et al. Cranial bone structure in children with sagittal craniosynostosis: Relationship with surgical outcomes. J Plast Reconstr Aesthet Surg. 2017; 70 (11): 1589–97. DOI: 10.1016/j.bjps.2017.06.017.
69. McGraw MA, Mehlman CT, Lindsell CJ, Kirby CL. Postnatal growth of the clavicle: birth to eighteen years of age. Journal of Pediatric Orthopedics. 2009; 29: 937.
70. Bleuze MM, Wheeler SM, Williams LJ, Dupras TL. Growth of the pectoral girdle in a sample of juveniles from the kellis 2 cemetery, Dakhleh Oasis, Egypt. Am J Hum Biol. 2016; 28 (5): 636–45.
71. Black SM, Scheuer JL. Age changes in the clavicle: from the early neonatal period to skeletal maturity. International Journal of Osteoarchaeology. 1996; 6: 425–34.
72. Bernat A, Huysmans T, Van Glabbeek F, Sijbers J, Gielen J, Van Tongel A. The anatomy of the clavicle: a three-dimensional cadaveric study. Clin Anat. 2014; 27 (5): 712–23.
73. Vallois HV. L'omoplate humaine. Bulletin de la Sociétié d'Anthropolgie de Paris. 1946; 7: 16–99.
74. Saunders S, Hoppa R, Southern R. Diaphyseal growth in a nineteenth-century skeletal sample of subadults from St Thomas' Church, Belleville, Ontario. International Journal of Osteoarchaeology. 1993; 3: 265–81.
75. Rissech C, Black S. Scapular development from neonatal period to skeletal maturity. A preliminary study. Int J Osteoarchaeol. 2007; 17: 451–64.
76. Cardoso HFV, Spake L, Humphrey LT. Age estimation of immature human skeletal remains from the dimensions of the girdle bones in the postnatal period. Am J Phys Anthropol. 2017; 163 (4): 772–83. DOI: 10.1002/ajpa.23248. Epub 2017 May 24. PubMed PMID: 28542741.
77. Badr El Dine F, Hassan H. Ontogenetic study of the scapula among some Egyptians: Forensic implications in age and sex estimation using Multidetector Computed Tomography, Egyptian Journal of Forensic Sciences. 2015; 6 (2): 56–77.
78. Kneissel M, Roschger P, Steiner W, Schamall D, Kalchhauser G, Boyde A, et al. Cancellous Bone Structure in the Growing and Aging Lumbar Spine in a Historic Nubian Population. Calcif Tissue Int. 1997; 61: 95–100.
79. Johnson KT, Al-Holou WN, Anderson RC, Wilson TJ, Karnati T, Ibrahim M, et al. Morphometric analysis of the developing pediatric cervical spine. J Neurosurg Pediatr. 2016; 18 (3): 377–89. DOI: 10.3171/2016.3. PEDS1612. Epub 2016 May 27. PubMed PMID: 27231821.
80. Comeau A. Age-related changes in geometric characteristics of the pediatric thoracic cage and comparison of thorax shape with a pediatric CPR Manikin. PhD thesis. 2010.

DEVELOPING AND EVALUATING THE EFFECTIVENESS OF WOUND-HEALING COMPOUNDS BASED ON CATIONIC PEPTIDES AND FULLERENE

Galkina AA[1] ✉, Bolyakina DK[1], Shatilova AV[1], Shatilov AA[1], Babikhina MO[1], Golomidova AK[2], Andreev SM[1], Shershakova NN[1], Khaitov MR[1,3]

[1] National Research Center — Institute of Immunology of Federal Medical Biological Agency, Moscow, Russia

[2] Federal Research Centre "Fundamentals of Biotechnology" of the Russian Academy of Sciences, Moscow, Russia

[3] Pirogov Russian National Research Medical University, Moscow, Russia

Skin and soft tissue infections following surgical procedures are usually caused by a broad range of bacteria and are the major cause of septic complications and hospital mortality. Treatment of such wounds is a challenge often resulting from the transition from acute to chronic inflammation due to persistence of pathogenic microflora in the wound tissue. The study was aimed to assess the wound-healing activity of the ointment composition based on the dispersion of fullerene C60 (AFD) in the in vivo model of skin wound, to estimate the effects of AFD on the expression of cytokines as markers of regenerative processes, to determine antibacterial activity of the developed cationic peptides. AFD was obtained by tangential ultrafiltration and used to make an ointment composition. The BALB/c mice were used to model the skin injury. The cationic peptides (CPs) were synthesized by the solid-phase method using the Fmoc technology. Antibacterial effects of CPs and AFD were estimated by colony counting. It was found that the AFD-based ointment exerted wound-healing and anti-inflammatory activity. The minimum bactericidal concentrations (MBC) of the CPs most active against the *E. coli* Dh5α strain, AB-1, AB-2, AB-3, and ST-10, were 1.15, 0.11, 0.74, and 0.74 mM, respectively, while MBC of ampicillin was 0.7 mM. We assume that constructing the hybrid compounds/fullerene C60 conjugates with active CPs will be a promising area of the development of drugs for treatment of wounds complicated by bacterial infection.

Keywords: fullerene C60 aqua dispersion, regenerative activity, cationic peptides, antibacterial activity

Funding: the study was conducted as part of the State Assignment of FMBA "Fullerene-21" (code 612.017.1:616.9).

Author contribution: Galkina AA — setting up methodology, laboratory tests, manuscript writing; Bolyakina DK — laboratory tests; Shatilova AV, Shatilov AA, Babikhina MO — laboratory tests; Golomidova AK — setting up methodology; Shershakova NN — setting up methodology, study concept, manuscript writing, research supervision; Andreev SM — setting up methodology, study concept, research supervision; Khaitov MR — study concept, research supervision.

Compliance with ethical standards: the study was approved by the Bioethics Commission of the Institute of Immunology of FMBA of Russia (order № 102 of November 2015) and conducted in accordance with the Directive 2010/63/EU for animal experiments and the Regulations Regarding Research Involving Laboratory Animals in the National Research Center — Institute of Immunology of FMBA of Russia.

✉ **Correspondence should be addressed:** Anastasiia A. Galkina
Kashirskoe sh., 24, Moscow, 115522, Russia; anastasia.a.galkina@gmail.com

Received: 28.07.2023 **Accepted:** 05.09.2023 **Published online:** 29.09.2023

DOI: 10.47183/mes.2023.036

РАЗРАБОТКА И ОЦЕНКА ЭФФЕКТИВНОСТИ РАНОЗАЖИВЛЯЮЩИХ СОЕДИНЕНИЙ НА ОСНОВЕ КАТИОННЫХ ПЕПТИДОВ И ФУЛЛЕРЕНА

А. А. Галкина[1] ✉, Д. К. Болякина[1], А. В. Шатилова[1], А. А. Шатилов[1], М. О. Бабихина[1], А. К. Голомидова[2], С. М. Андреев[1], Н. Н. Шершакова[1], М. Р. Хаитов[1,3]

[1] Государственный научный центр «Институт иммунологии» Федерального медико-биологического агентства, Москва, Россия

[2] Федеральный исследовательский центр «Фундаментальные основы биотехнологии» Российской академии наук, Москва, Россия

[3] Российский национальный исследовательский медицинский университет имени Н. И. Пирогова, Москва, Россия

Инфекции кожи и мягких тканей при хирургических манипуляциях обычно вызваны широким спектром бактериальных микроорганизмов, и служат основной причиной септических осложнений и госпитальной смертности. Лечение таких ран является очень сложной проблемой, часто обусловленной переходом воспалительного процесса в хроническую стадию в связи с наличием устойчивой патогенной микрофлоры в раневой ткани. Целью работы было проанализировать ранозаживляющую активность мазевой композиции на основе водной дисперсии фуллерена С60 (ВДФ) на модели кожной травмы *in vivo*, оценить влияние ВДФ на экспрессию цитокинов как маркеров регенеративных процессов, определить антибактериальную активность разработанных нами катионных пептидов. ВДФ получали методом тангенциальной ультрафильтрации, а затем на ее основе готовили мазевую композицию. Моделирование кожной травмы проводили с использованием мышей линии BALB/c. Синтез катионных пептидов (КП) осуществляли твердофазным методом, используя Fmoc-технологию. Антибактериальную активность КП и ВДФ оценивали методом подсчета колоний. Установлено, что мазь на основе ВДФ обладала ранозаживляющей и противовоспалительной активностью. У наиболее активных КП, АВ-1, АВ-2, АВ-3 и ST-10 минимальная бактерицидная концентрация (МБК) в отношении бактериального штамма *E. coli* Dh5α составляла 1,15, 0,11, 0,74 и 0,74 мМ, соответственно, при МБК ампициллина 0,7 мМ. Мы предполагаем, что создание гибридных соединений/конъюгатов фуллерена С60 с активными КП будет перспективным направлением в разработке лекарственных средств для терапии раневых поражений, осложненных бактериальной инфекцией.

Ключевые слова: водный раствор фуллерена С60, ранозаживляющая активность, катионные пептиды, антибактериальная активность

Финансирование: исследование выполнено в рамках государственного задания ФМБА «Фуллерен-21» (код 612.017.1:616.9).

Вклад авторов: А. А. Галкина — постановка методики, лабораторные исследования, написание статьи; Д. К. Болякина — лабораторные исследования; А. В. Шатилова, А. А. Шатилов, М. О. Бабихина — лабораторные исследования; А. К. Голомидова — постановка методики; Н. Н. Шершакова — постановка методики, концепция исследования, написание статьи, научное руководство; С. М. Андреев — постановка методики, концепция исследования, научное руководство; М. Р. Хаитов — концепция исследования, научное руководство.

Соблюдение этических стандартов: исследование одобрено комиссией по биоэтике Института иммунологии ФМБА России (приказ № 102 ноябрь 2015 г.), проведено в соответствии с Директивой ЕС 2010/63/ЕС для экспериментов на животных и Правилами исследовательской работы с лабораторными животными в ФГБУ ГНЦ «Институт иммунологии» ФМБА России.

✉ **Для корреспонденции:** Анастасия Андреевна Галкина
Каширское ш., д. 24, г. Москва, 115522, Россия; anastasia.a.galkina@gmail.com

Статья получена: 28.07.2023 **Статья принята к печати:** 05.09.2023 **Опубликована онлайн:** 29.09.2023

DOI: 10.47183/mes.2023.036

Skin wound healing is a complex process involving cells of various types and multiple regulatory factors, and abnormal wound healing can result in scarring and the transition from acute to chronic inflammation. Scars can restrict movements, cause pain and itching; scars can be the cause of physiological stress in case they remain visible and cannot be hidden by clothing or makeup, thereby seriously affecting the person's self-confidence and quality of life. Removal and treatment of scars remain a pressing issue, since, despite the diversity of available treatment methods, the methods' efficacy is quite low. The total volume of the global market in this field was 19.6 billion dollars in 2019. It is expected that it will grow by 11.5% in the next decade [1].

Comorbidities, such as diabetes mellitus, hypertension, and other vascular and autoimmune disorders, can hinder effective treatment of the wound healing process complications [2]. Bacterial superinfections play an important role in chronification of inflammation.

All wounds are to some extent contaminated with microorganisms being a part of saprophytic skin microflora. The type and abundance of such microorganisms vary depending on the wound type [3]. *Pseudomonas aeruginosa*, *Staphylococcus aureus*, *Klebsiella pneumoniae*, *Enterococcus faecalis*, and *Acinetobacter baumannii* are the most common bacterial species causing wound infection [4]. It is well-known that wound infections constitute a third of cases of nosocomial infections in surgical patients and cause 70–80% of deaths from wounds [5]. Chronic wounds affect the patients' quality of life, along with the increased morbidity and mortality, and represent a huge financial burden on health systems all over the world, since such wounds are associated with the expenses for long-term hospital stay, diagnostic tests, antibiotics, and sometimes invasive surgery [6, 7]. That is why wound healing is a serious health problem that requires the development of safe and effective therapeutic agents.

The drugs for wound healing are based on adsorbents, anti-inflammatory components, antibiotics or dexpanthenol that stimulates regeneration processes. The search for new approaches to healing wounds complicated by bacterial infection has become a pressing issue due to the alarming increase in resistance to conventional antimicrobial drugs. Among alternative antimicrobial agents, special attention is paid to cationic antimicrobial peptides (CAMPs) [8].

Cationic peptides (CPs) attract much attention as transporters and biologically active substances due to high affinity for cell membranes and specific structure enabling mass spectrometry analysis and wide possibilities to design the variety of such molecules. CPs are widespread in nature and found in all mammals, especially in the skin, where they play a protective role against pathogenic microorganisms. Cationic antimicrobial peptides, or host defense peptides, are a heterogeneous group of short positively charged peptides, mostly amphiphilic. These peptides are secreted by immune (for example, neutrophils and macrophages [9]) and epithelial cells of vertebrates and invertebrates to ensure protection against microbial invasion [10]. The shortcomings of using peptides as potential antimicrobial drugs for treatment include a very complex structure that hampers synthesis and the CPs' proteolytic instability. It has been assumed, that the CAMP conjugation with other biologically active molecules, such as other peptides, polypeptides, proteins, and antibiotics in general, can contribute to improvement of antimicrobial properties and provide the basis for the development of drugs possessing multiple biological activities. In particular, the development of drugs with low toxicity combining antibacterial and anti-inflammatory effects and showing low probability of developing resistance would contribute significantly to both fundamental research and practical healthcare.

Since CAMPs show proteolytic instability, we believe that it seems promising to use such molecules, as fullerene C60, as carriers for peptides.

Fullerene C60 is a carbon-based molecule that has a shape of truncated icosahedron and possesses strong antioxidant activity. It is well-known that the fullerene C60 water-soluble forms have multiple biological effects, including antiviral, anti-inflammatory, anti-allergy, and regenerative effects [11, 12]. An *in vivo* model of wound healing process has shown that some covalent fullerene C60 derivatives accelerate wound healing and prevent inflammatory cell infiltration [13].

It is known that fullerene C60 is insoluble in aqueous media, which is clearly a significant obstacle to its extensive use in medicine. We have earlier developed a unique scalable technology to obtain stable aqueous dispersion of fullerene C60, enabling assessment of its biological activity [14]. It should be noted that this technology does not involve the use of organic solvents, ultrasonic processing or heating, which ensures bio-compatibility and safety of the resulting solution. Our method makes it possible to generate highly concentrated stable AFD with the concentration of at least 1 g/l.

The main purpose of the study was to assess the wound-healing activity of the AFD-based ointment composition in the experimental model of wound inflammation, as well as to estimate the effects of AFD on the expression of marker genes involved in regeneration, analyze the CP antibacterial activity, and assess the prospects of creating the CP- and fullerene C60-based complexes for treatment of wounds.

METHODS

AFD-based composition

The AFD-containing ointment (composition: AFD, vaseline, sucrose palmitate in the ratio of 40 : 36 : 24 (by weight)) for *in vivo* treatment of wounds was prepared using the IKA 25 digital homogenizer IKA 25 as a mixing device ("AFD ointment"). The fullerene C60 aqueous dispersion was acquired by the dialysis method [14]. This bio-compatible method does not involve the use of toxic organic solvents, ultrasonic processing or heating. At the same time, it ensures high yield of fullerene C60 during transition from crystals into solution (the concentration of sterile fullerene C60 solution was 1 mg/mL). The hydrodynamic particle size determined by the dynamic light scattering method was 100–200 nm.

In vivo model of wound inflammation

Female BALB/c mice aged 4–6 weeks (Stolbovaya breeding nursery; Moscow, Russia) were used to model the wound healing process [15]. The following housing conditions were used for animals: ambient temperature 18–26 °C; automatic 12 h ligh/dark cycle; relative humidity 30–70%. All animals had unlimited access to drinking water and food. The animals were anesthetized with 4% isoflurane solution for 2 min via airways and topically administered 0.5% lidocaine solution prior to making the incised wounds. To model the surgical wound, a skin fragment (1 × 1 cm) was excised from the back of the BALB/c mouse. The AFD ointment was applied to the wound surface (40 μg of C60/mouse) 24 h after the surgical procedure ("AFD ointment" group). The widely used therapeutic agent, cream for treatment of surgical wounds, was used as positive control ("C+" group). The ointment containing phosphate

buffered saline (PBS) instead of AFD was used as negative control ("PBS" group). The "intact" group (with no skin wounds) was also used as negative control. The listed above preparations were used once a day for 11 days. On day 12 mice were euthanized by cervical dislocation, and skin samples were collected for quantitative RT-PCR.

Assessment of wound healing efficiency

The skin wound healing rate was assessed by measuring the wound area in the longitudinal and transverse directions (mm) every day and calculating the wound area using the following formula:

$$S_{el} = \varpi ab,$$

where S_{el} — area of an ellipse, a — semi-major axis (half of the longer diameter or transverse dimension), b — semiaxis (half of the shorter diameter or longitudinal dimension).

The wound healing efficiency (X) was calculated as percentage using the following formula:

$$X = (1 - S_f/S_i) \times 100\%,$$

где S_f — final wound area, S_i — initial wound area [16].

Real-time polymerase chain reaction

Total RNA was extracted from skin samples using the RNeasy Mini Kit (Qiagen, Courtaboeuf; France) in accordance with the manufacturer's instructions; cDNA was synthesized using the Reverta-L kit (InterLabService; Russia). The reverse transcription product was amplified by the real-time polymerase chain reaction (RT-PCR) using the iCycler iQ real-time PCR detection system (Bio-Rad Laboratories; USA) and the PCR Mix kit (Syntol; Russia).

The calculations to determine relative gene expression were performed using the comparative Ct method (ΔCt) against mHPRT.

Relative quantification by RT-PCR was used to detect changes in the expression of target genes relative to the reference gene represented by murine *hprt* gene. Quantitative PCR results for mRNA expression were compared as ΔCt values calculated using the following formula: ratio (reference/target) = $2^{Ct(hprt)-Ct(target\ gene)}$ [17].

Assessment of antibacterial effects of AFD and cationic peptides

Antibacterial activity of AFD and the synthesized peptides was assessed *in vitro* on the example of the *E. coli Dh5*α strain by colony counting relative to the well-known antibiotic ampicillin selected as positive control. In the method the bacterial suspension was incubated with various CAMP concentrations in the LB liquid medium for 4 h at 37 °C, then it was applied dropwise to the surface of the dried agar medium. The culture was incubated overnight at 37 °C.

It is important to note that the abovementioned *E. coli* strain is not pathogenic and shows no resistance to antibiotics. Activity of peptides against the selected strain was assessed based on the determined minimum bactericidal concentration.

Cationic peptide synthesis

Peptides were synthesized by the solid-phase method in the automated PS3 Peptide Synthesizer (Gyros Protein Technologies Inc.; USA) according to the Fmoc-chemistry protocol using the N-hydroxybenzotriazole and diisopropylcarbodiimide (HOBt/DIC) mixture as a condensing agent. The starting Fmoc-aminoacyl polymers and the Rink Amide ChemMatrix gel-type resin were used for synthesis. The side carboxyl and hydroxyl groups of amino acids were protected by the tert-butyl group (t-Bu), the lysine ε-amino group by Boc, the cysteine SH-group by Trt, the arginine guanidinium functional group by Pbf, and the carboxyl and hydroxyl groups of amino acids by tert-butyl ethers. The standard cycle included washing (DMF), removal of Fmoc protection (20% 4-methylpiperidine in DMF), preliminary Fmoc amino acid (DIC/HOBt) activation and condensation on the DMF/N-methylpyrrolidone medium with the twofold carboxyl component excess (~0.5–1 h). The extent of the reaction was controlled using the Kaiser Test (ninhydrin test), the condensation reaction was repeated when necessary (0.5 h). The terminal peptides were cleaved from the polymer with trifluoroacetic acid in the presence of scavengers (triisopropylsilane, ethanediol, water, dimethyl sulfide). The raw product was precipitated with the dry methyl tert-butyl ether, then the peptide was extracted with the acetic acid aqueous solution, and the extract was lyophilized (VirTis AdVantage 2.0 EL freeze dryer; SP Scientific, USA). The peptides were purified by preparative HPLC chromatography (LC-20 Shimadzu; Japan) on the reversed phase column (C18) using acetonitrile — 0.1% trifluoroacetic acid aqueous solution as a mobile phase (gradient elution). The resulting peptides were tested for homogeneity by capillary zone electrophoresis in the Kapel-105M system (Lumex; Russia) with photometric detection at 226 nm. Molecular weight was analyzed using the Microflex™ LT MALDI-TOF mass spectrometer (Bruker Daltonic; USA).

Statistical analysis

Statistical analysis was performed using the Statistica 8.0 software (StatSoft Inc.; USA). Significance was determined based on Student's t-test. The differences were considered significant at $p < 0.05$. The data were presented as mean ± standard error.

RESULTS

In vivo assessment of the AFD regenerative effect in the model of wound inflammation

Analysis of the AFD-based ointment regenerative activity relative to commercial drug ("C+", positive control) was performed using the model of wound healing. Visual assessment of the wound healing process by measuring the lesion area was carried out individually for each mouse. The baseline average lesion area was 143.5 ± 6.1 mm^2 ("before treatment" group). On the last day of the experiment the lesion area by groups was as follows: "no treatment" — 44.4 ± 6.5 mm^2, "AFD ointment" — 14.8 ± 2.7 mm^2, "C+" — 26.0 ± 2.6 mm^2. These values show that healing of wounds treated with AFD was effective, and the healing rate was comparable with that of the positive control group and even slightly superior to the latter. Since visual assessment of healing was a subjective parameter, statistical analysis of wound area was performed in the groups that revealed significant differences between the values of the "AFD ointment" and "C+" groups, which, in turn, differed from the values of the "PBS" group. It was found that the residual wound area was the least when the AFD-based ointment was used for surgical wound treatment.

Assessment of the expression of pathogenetically significant genes

Expression of a number of genes was analyzed to assess the AFD capability of affecting the pathogenetically significant factors of

Table. List of cationic peptides showing antibacterial activity against *E. coli Dh5*α

Peptide	Structure	Charge	Molecular weight, Da
AB–1	Linear	+ 8	1736
AB–3	Linear	+ 12	3328
AB–4	Dendrimeric	+ 11	2758
ST–10	Dendrimeric	+ 8	2749

regenerative process. The expression of genes in murine skin with wounds treated/not treated with AFD was determined by real-time PCR. It was shown that the expression of such pro-inflammatory factor, as *tnf*α produced in response to pathogen entry and tissue damage that stimulates local inflammatory response, was significantly lower in all experimental groups, where animals received AFD, than in the group of animals that received no therapy ("PBS"). The expression of genes encoding other pro-inflammatory cytokines, such as *il6* and *il1a*, was also significantly lower in mice with wounds treated with AFD than in animals that received no therapy. Furthermore, we have revealed the fullerene C60 capability of enhancing the expression of HMGB1 factor that violates the collagen synthesis and can ensure scarless tissue healing observed when treating the wound with AFD.

Thus, our findings suggest that fullerene C60 can inhibit the expression of genes encoding pro-inflammatory cytokines, which results in the pro-inflammatory effect of this substance that is likely to contribute to the healing process acceleration.

Cationic peptide design

CPs are widespread in nature and produced by almost all organisms as part of the nonspecific immune system. These compounds were initially considered as potential substitutes for antibiotics, however, it was found out that the compounds had a broader spectrum of therapeutic effects, including the effects on viruses, bacteria, and microbial biofilms. The naturally occurring CPs are linear molecules consisting of up to 50 amino acids having a high share of hydrophobic and cationic residues. This makes the molecules to fold into amphipathic structures to form α-helices and β-sheets. Such peptides form specific loop conformations due to high cysteine content and disulfide bond formation. The charges of the vast majority of natural antimicrobial CPs vary between +3 and +9. The mechanism underlying their effects is associated primarily with the cell membrane damage [18]. Today, technology makes it possible to build the structures which are quite different from natural constructs in terms of topology, including the non-naturally occurring dendrimeric structures. The amino acid sequence construction included building the construct with low toxicity, which was stable in the serum medium. Furthermore, the structure had to demonstrate high efficiency of transfection stimulation. The plan also involved building modular constructs. One of such modules is the N-terminal supercationic fragment represented by the arginine and/or lysine residues, which is essential for interaction with the nucleic acid and the cell surface. The central module is represented by the hydrophobic core consisting of the lysine residues and short hydrophobic/amphiphilic inserts. The C-terminal module also forms a hydrophobic fragment ensuring additional affinity for cell membrane, it contains the cysteine residue with a free thiol group intended for reporter label attachment.

Hydrophobic interactions between the aliphatic chains of lipid membranes and the peptide hydrophobic residues play an important role in the mechanism underlying membrane damage, which contributes to its incorporation in the membrane bilayer through various interactions, such as pore formation. In the carpet model, the cationic peptide is directed in parallel to the cell to cover it and saturate via interaction with the outer phospholipid layer of the membrane. After the threshold value is achieved, the peptides start spinning and embed in the membrane causing its permeabilization. The branched structures, dendrimeric CPs, are of special interest. It should be noted that these show higher resistance to proteolytic enzymes along with lower toxicity compared to the linear peptides with similar amino acid composition. At the same time these show stronger binding to cells due to cooperative effects resulting from the fact that the molecule has several chains. Our early experiments demonstrated their high permeability through cell membranes enabling using such peptides as carriers for cell transfection, transfer of genes and other biologically active compounds [19].

Assessment of antibacterial effects of AFD and cationic peptides

When assessing antibacterial activity of AFD and CPs, we showed that AFD possessed no bactericidal activity and was unable to inhibit bacterial growth. Then we analyzed a number of CPs, which were expected to possess potential antibacterial activity based on their structural features. Thus, among 35 linear and dendrimeric CAMPs with the molecular weight not exceeding 4.5 kDa we had synthesized, four cationic peptides, specifically linear peptides AB-1, AB-3 and dendrimeric peptides AB-4, ST-10, to various extent inhibited growth of the *E. coli Dh5a* microbial culture and showed some bactericidal activity against this strain (Table).

Minimum bactericidal concentrations (MBC) of the cationic peptides, i.e. the lowest concentrations killing all bacteria under standard experimental conditions, were determined by colony counting.

Thus, MBC of the AB-1 peptide was 1.15 mM. It should be noted that the AB-1 peptide concentration of 0.23 mM (five times lower compared to bactericidal concentration) showed no significant activity against this bacterial culture, which was indicative of the extremely narrow operative range of peptide concentrations (Fig. 1).

The AB-3 peptide has higher bactericidal activity against the *E. coli Dh5*a strain than AB-1 (Fig. 2).

MBC of this peptide was 0.11 mM. Meanwhile, activity of appropriate ampicillin doses was about 6 times lower. MBC of ampicillin was 0.74 mM.

The studied AB-4 peptide exerted considerable bactericidal activity that was comparable with that of control antibiotic (ampicillin). MBC of this peptide was 0.74 mM (Fig. 3).

MBC of the ST-10 dendrimeric peptide was 0.74 mM (Fig. 4).

The above concentration was the least concentration that killed almost 100% of cells. It should be noted that the level of activity exerted by the ST-10 peptide was slightly higher compared to the control sample of ampicillin antibiotic. Thus, with comparable concentrations of 0.15 mM and the same *E. coli* dilution (1 : 10) it is evident that the number of bacterial colonies detected in the culture treated with the ST-10 peptide

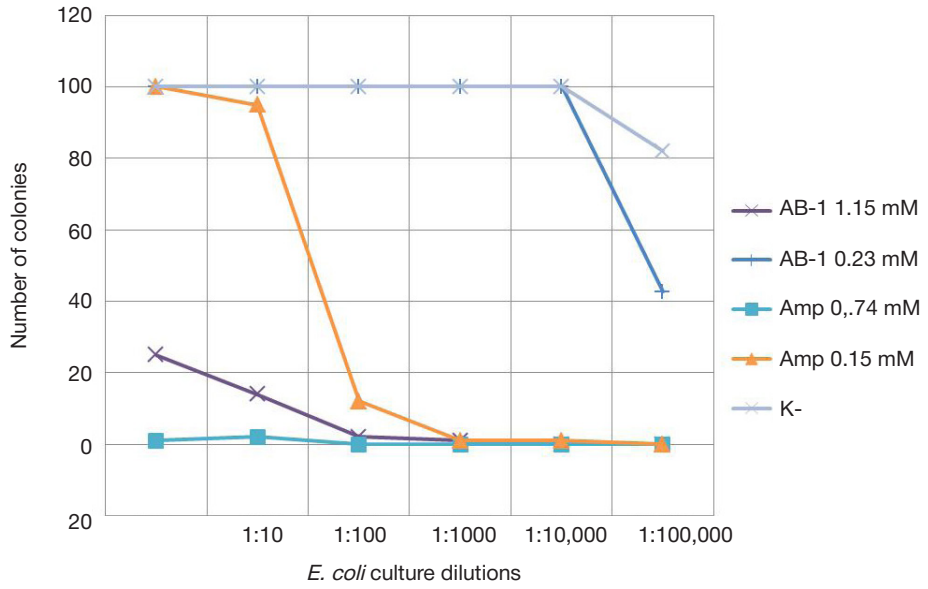

Fig. 1. Bacterial growth intensity under exposure to the AB-1 peptide

is considerably lower than in the culture treated with ampicillin (16 and 95, respectively). Therefore, the effect of bacterial culture growth inhibition under exposure to 0.15 mM of peptide and antibiotic was more prominent in ST-10.

DISCUSSION

In the majority of cases wounds are associated with bleeding from the damaged blood vessels and the release of inflammatory mediators, such as serotonin, histamine, vasoactive substances, and cytokines, into the surrounding tissues. Normal wound healing includes the following phases: inflammation, proliferation, maturation, and remodeling. To determine the AFD regenerative effects, we assessed the expression of a number of marker genes, such as *tnf*α, *il-6* and *il-1*α, involved in regenerative process by RT-PCR. Elevated expression of these cytokines is observed during the inflammatory phase of wound healing. It is well-known that TNFα stimulates production of not only IL1, IL6, but also other pro-inflammatory cytokines [20, 21]. IL6 is one of the most important mediators of the acute phase of inflammation. It is known that delayed wound epithelization is observed in mice with IL6 deficiency. However, excess IL6 levels serve as a signal for fibroblast proliferation suppression during the late wound healing phase and lead to scar formation [22]. As for IL1a, it has been earlier shown that it stimulates collagenase production, and overexpression of this cytokine can be associated with abnormal wound healing due to collagen breakdown. The moderate *il1a* expression increase later mediates keratinocyte proliferation in the wound area [23]. Low levels of *il1a* are observed in the wound fluid from acute wounds, while fluid from surgical wounds shows elevated levels of *il1a*.

Thus, suppression of the *tnf*α, *il6*, and *il1a* expression under exposure to fullerene C60 suggests that it not only possesses anti-inflammatory effect, but is also capable of preventing wound chronization [15]. We have earlier shown antiallergy effects of AFD with inhibition of Th1 cytokines in the model of atopic dermatitis, along with the elevated expression of genes *Foxp3* and *FLG* (filaggrin) [24]. Therefore, AFD has shown its ability to suppress inflammation associated with not

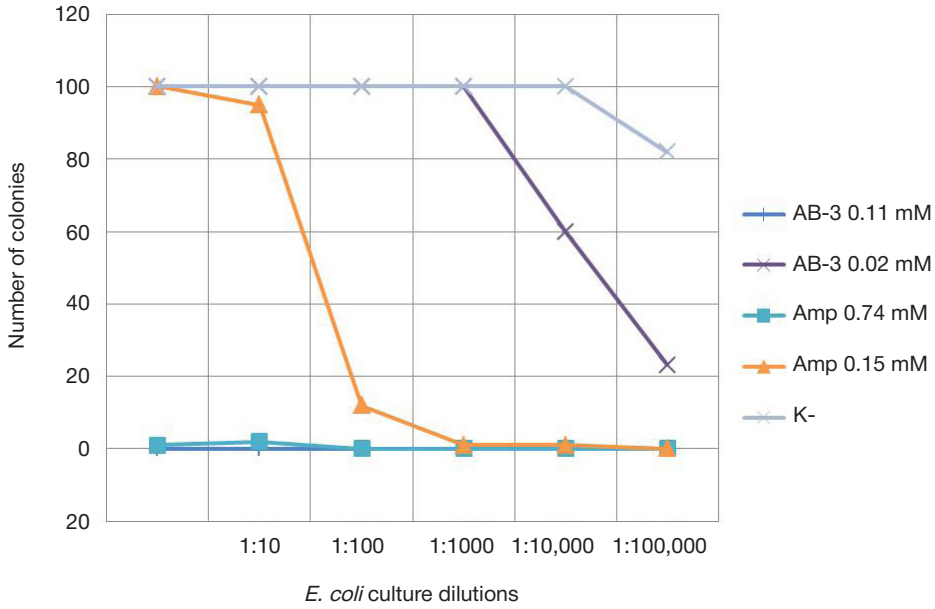

Fig. 2. Bacterial growth intensity under exposure to the AB-3 peptide

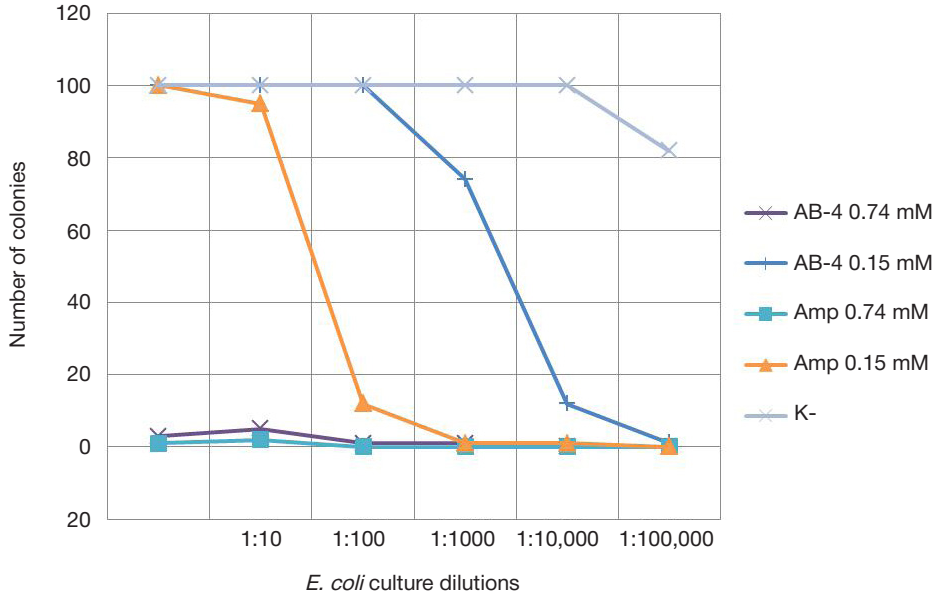

Fig. 3. Bacterial growth intensity under exposure to the AB-4 peptide

only wounds, but also allergy. This makes AFD a promising compound for treatment of inflammatory skin disorders.

Wound healing is often accompanied by accession of secondary bacterial infection. It is well-known that CAMPs have a broad range of antimicrobial and immunomodulatory effects against Gram positive and Gram negative bacteria, biofilms, viruses, fungi, and parasites; CAMPs are also effective against multidrug-resistant strains. It is important to note that the likelihood of developing resistance to cationic peptides is extremely low and requires multiple mutations, including that mediating changes in the cell wall structure, due to fast bactericidal action of CAMPs and the diversity of mechanisms of action and targets [25–27]. The above makes CAMPs promising compounds for the development of the CAMP-based antibacterial drugs. Understanding of how the antimicrobial peptide properties depend on the amino acid sequence will make it possible to timely respond to the emergence of new antibiotic-resistant bacterial strains in the future due to targeted reconstruction of peptide sequences [28].

We have created the library of CAMPs supposed to possess high antimicrobial activity and have low toxicity within the framework of current research. When developing the CP panel, we relied on the databases of already known peptides and the literature data on the CP biological (antibacterial) activity. Thus, the peptide sequences were constructed considering the content of positively charged amino acids, hydrophobic amino acids. Furthermore, both linear and dendrimeric molecules were obtained when constructing the sequences.

Thus, by defining some rules for creating cationic peptides showing antibacterial activity we look forward to creating more active CPs. The AFD anti-inflammatory activity makes the idea of developing hybrid molecules based on CPs and AFD perspective.

CONCLUSIONS

As result of the research, we have developed and synthesized CPs possessing antibacterial effects. Thus, we believe that the AB-1, AB-2, AB-3, and ST-10 peptides are promising in terms of developing antimicrobial drugs on their basis. During further studies we plan to develop hybrid compounds based on the CPs and fullerene C60 to combine the anti-inflammatory and wound-healing effects with antibacterial activity. Fullerene can

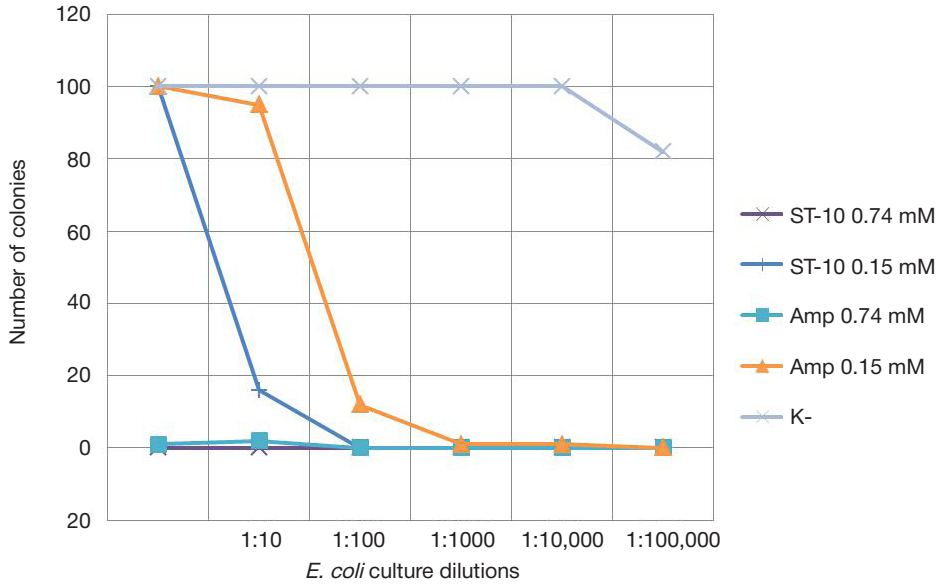

Fig. 4. Bacterial growth intensity under exposure to the ST-10 peptide

play a role of carrier platform for CPs. Since the area of the spherical fullerene molecule is rather large, up to 4–8 peptide molecules can be attached to it. Such multivalent structure is less prone to biodegradation, and antimicrobial activity can be increased due to cooperative effect, simultaneous attachment of several CP chains to the bacterial cell membrane. It should also be considered that fullerene C60 itself and its amino acid adducts can permeate through biological membranes.

References

1. The report "Scar Treatment Market Size, Share & Trends Analysis Report By Scar Type, By Product, By End Use And Segment Forecasts, 2019–2026". GLOBE NEWSWIRE. New York, 2019.
2. Beyene RT, Derryberry SL Jr, Barbul A. The Effect of Comorbidities on Wound Healing. Surg Clin North Am. 2020; 100 (4): 695–705. DOI: 10.1016/j.suc.2020.05.002. Epub 2020 Jun 17. PMID: 32681870.
3. Sachdeva C, Satyamoorthy K, Murali TS. Microbial Interplay in Skin and Chronic Wounds. Curr Clin Micro Rpt. 2022; 9: 21–31. DOI: 10.1007/s40588-022-00180-4.
4. Huszczynski SM, Lam JS, Khursigara CM. The Role of Pseudomonas aeruginosa Lipopolysaccharide in Bacterial Pathogenesis and Physiology. Pathogens. 2019; 9: 6. DOI: 10.3390/pathogens9010006.
5. Puca V, Marulli RZ, Grande R, Vitale I, Niro A, Molinaro G, et al. Microbial Species Isolated from Infected Wounds and Antimicrobial Resistance Analysis: Data Emerging from a Three–Years Retrospective Study. Antibiotics (Basel). 2021; 10 (10): 1162. PubMed PMID: 34680743; PubMed PMCID: PMC8532735.
6. Prohorov DV, Shherbenyova AA, Ngema MV, Ispiryan MB, Kuznecova MYu. Sovremennye metody kompleksnogo lecheniya i profilaktiki rubcov kozhi. Krymskij terapevticheskij zhurnal. 2021; 1: 26–31. Russian.
7. Puca V, Traini T, Guarnieri S, Carradori S, Sisto F, Macchione N, et al. The Antibiofilm Effect of a Medical Device Containing TIAB on Microorganisms Associated with Surgical Site Infection. Molecules. 2019; 24 (12): 2280. PubMed PMID: 31248162; PubMed PMCID: PMC6630542.
8. Geitani R, Ayoub Moubareck C, Touqui L, Karam Sarkis D. Cationic antimicrobial peptides: alternatives and/or adjuvants to antibiotics active against methicillin-resistant Staphylococcus aureus and multidrug-resistant Pseudomonas aeruginosa. BMC Microbiol. 2019; 19 (1): 54.
9. Samanta I, Bandyopadhyay S. Streptococcus. In: Antimicrobial Resistance in Agriculture. United States Cambridge: Academic Press in an imprint of Elsevier, 2020; p. 217–232.
10. Mookherjee N, Anderson MA, Haagsman HP, Davidson DJ. Antimicrobial host defence peptides: functions and clinical potential. Nat Rev Drug Discov. 2020; 19: 311–32. DOI: 10.1038/s41573-019-0058-8.
11. Bosi S, Da Ros T, Spalluto G, Prato M. Fullerene derivatives: an attractive tool for biological applications. Eur J Med Chem. 2003; 38 (11–12): 913–23. PubMed PMID: 14642323.
12. Gharbi N, Pressac M, Hadchouel M, Szwarc H, Wilson SR, Moussa F. Fullerene is a powerful antioxidant in vivo with no acute or subacute toxicity. Nano Lett. 2005; 5 (12): 2578–85. PubMed PMID: 16351219.
13. Zhou Z, Joslin S, Dellinger A, Ehrich M, Brooks B, Ren Q, et al. A novel class of compounds with cutaneous wound healing properties. J Biomed Nanotechnol. 2010; 6 (5): 605–11. PubMed PMID: 21329053.
14. Andreev S, Purgina D, Bashkatova E, Garshev A, Maerle A, Andreev I, et al. Study of fullerene aqueous dispersion prepared by novel dialysis method: simple way to fullerene aqueous solution. Fullerenes Nanotubes and Carbon Nanostructures. 2015; 23: 792–800.
15. Shershakova NN, Andreev SM, Tomchuk AA, Makarova EA, Nikonova AA, Turetskiy EA, et al. Wound healing activity of aqueous dispersion of fullerene C60 produced by "green technology". Nanomedicine. 2023; 47: 102619. Epub 2022 Oct 19.
16. Molchanova VI, Chikalovec IV, Chernikov OV, Popov AM, Krivoshapko ON, Lukyanov PA. Sravnitel'noe izuchenie biologicheskoj aktivnosti bioglikanov iz dal'nevostochnoj midii crenomytilus grayanus. Tixookeanskij medicinskij zhurnal. 2012; 1 (47): 47–50. Russian.
17. Livak KJ, Schmittgen TD. Analysis of relative gene expression data using real–time quantitative PCR and the 2(–Delta Delta C(T)) method. Methods. 2001; 25 (4): 402–8. PubMed PMID: 11846609.
18. Shamova OV, Zharkova MS, Chernov AN, Vladimirova EV, Suxareva MS, Komlev AS. i dr. Antimikrobnye peptidy vrozhdennogo immuniteta kak prototipy novyx sredstv bor'by s antibiotikorezistentnymi bakteriyami. Rossijskij zhurnal personalizirovannoj mediciny. 2021; 1 (1): 146–72. Russian.
19. Kozhikhova KV, Shilovskiy IP, Shatilov AA, Timofeeva AV, Turetskiy EA, Vishniakova LI, et al. Linear and dendrimeric antiviral peptides: Design, chemical synthesis and activity against human respiratory syncytial virus. J. Mater. Chemistry B. 2020; 8 (13): 2607–17. DOI: 10.1039/c9tb02485a.
20. Werner S, Grose R. Regulation of wound healing by growth factors and cytokines. Physiol Rev. 2003; 83 (3): 835–70. PubMed PMID: 12843410.
21. Ashcroft GS, Jeong MJ, Ashworth JJ, Hardman M, Jin W, Moutsopoulos N, et al. Tumor necrosis factor-alpha (TNF-α) is a therapeutic target for impaired cutaneous wound healing. Wound Repair Regen. 2012; 20 (1): 38–49. Epub 2011 Dec 8. PubMed PMID: 22151742; PubMed PMCID: PMC3287056.
22. Stockmann C, Kirmse S, Helfrich I, Weidemann A, Takeda N, Doedens A, et al. A wound size–dependent effect of myeloid cell–derived vascular endothelial growth factor on wound healing. J Invest Dermatol. 2011; 131 (3): 797–801. Epub 2010 Nov 25. PubMed PMID: 21107350.
23. Robertson FM, Pellegrini AE, Ross MR, Oberyszyn AS, Boros LG, Bijur GN, et al. Interleukin-1alpha gene expression during wound healing. Wound Rep Reg. 1995; 3 (4): 473–84. PubMed PMID: 17147659.
24. Shershakova N, Baraboshkina E, Andreev S, Purgina D, Struchkova I, Kamyshnikov O, et al. Anti–inflammatory effect of fullerene C60 in a mice model of atopic dermatitis. J Nanobiotechnology. 2016; 14: 8. PubMed PMID: 26810232; PubMed PMCID: PMC4727272.
25. Spohn R, Daruka L, Lázár V. et al. Integrated evolutionary analysis reveals antimicrobial peptides with limited resistance. Nat Commun. 2019; 10 (1): 4538. PubMed PMID: 31586049; PubMed PMCID: PMC6778101.
26. Jangir PK, Ogunlana L, MacLean RC. Evolutionary constraints on the acquisition of antimicrobial peptide resistance in bacterial pathogens. Trends Microbiol. 2021; 29 (12): 1058–1061. Epub 2021 Apr 6. PubMed PMID: 33836929. PubMed PMID: 32355003; PubMed PMCID: PMC8097767.
27. Lazzaro BP, Zasloff M, Rolff J. Antimicrobial peptides: application informed by evolution. Science. 2020; 368 (6490): eaau5480. PubMed PMID: 32355003; PubMed PMCID: PMC8097767.
28. Falanga A, Del Genio V, Galdiero S. Peptides and Dendrimers: How to Combat Viral and Bacterial Infections. Pharmaceutics. 2021; 13 (1): 101.

Литература

1. The report "Scar Treatment Market Size, Share & Trends Analysis Report By Scar Type, By Product, By End Use And Segment Forecasts, 2019–2026". GLOBE NEWSWIRE. New York, 2019.
2. Beyene RT, Derryberry SL Jr, Barbul A. The Effect of Comorbidities on Wound Healing. Surg Clin North Am. 2020; 100 (4): 695–705. DOI: 10.1016/j.suc.2020.05.002. Epub 2020 Jun 17. PMID: 32681870.
3. Sachdeva C, Satyamoorthy K, Murali TS. Microbial Interplay in Skin and Chronic Wounds. Curr Clin Micro Rpt. 2022; 9: 21–31. DOI: 10.1007/s40588-022-00180-4.
4. Huszczynski SM, Lam JS, Khursigara CM. The Role of Pseudomonas aeruginosa Lipopolysaccharide in Bacterial Pathogenesis and Physiology. Pathogens. 2019; 9: 6. DOI: 10.3390/pathogens9010006.
5. Puca V, Marulli RZ, Grande R, Vitale I, Niro A, Molinaro G, et al. Microbial Species Isolated from Infected Wounds and Antimicrobial Resistance Analysis: Data Emerging from a Three–Years Retrospective Study. Antibiotics (Basel). 2021; 10 (10): 1162. PubMed PMID: 34680743; PubMed PMCID: PMC8532735.
6. Прохоров Д. В., Щербенёва А. А., Нгема М. В., Испирьян М. Б., Кузнецова М. Ю. Современные методы комплексного лечения и профилактики рубцов кожи. Крымский терапевтический журнал. 2021; 1: 26–31.
7. Puca V, Traini T, Guarnieri S, Carradori S, Sisto F, Macchione N, et al. The Antibiofilm Effect of a Medical Device Containing TIAB on Microorganisms Associated with Surgical Site Infection. Molecules. 2019; 24 (12): 2280. PubMed PMID: 31248162; PubMed PMCID: PMC6630542.
8. Geitani R, Ayoub Moubareck C, Touqui L, Karam Sarkis D. Cationic antimicrobial peptides: alternatives and/or adjuvants to antibiotics active against methicillin-resistant Staphylococcus aureus and multidrug-resistant Pseudomonas aeruginosa. BMC Microbiol. 2019; 19 (1): 54.
9. Samanta I, Bandyopadhyay S. Streptococcus. In: Antimicrobial Resistance in Agriculture. United States Cambridge: Academic Press in an imprint of Elsevier, 2020; p. 217–232.
10. Mookherjee N, Anderson MA, Haagsman HP, Davidson DJ. Antimicrobial host defence peptides: functions and clinical potential. Nat Rev Drug Discov. 2020; 19: 311–32. DOI: 10.1038/s41573-019-0058-8.
11. Bosi S, Da Ros T, Spalluto G, Prato M. Fullerene derivatives: an attractive tool for biological applications. Eur J Med Chem. 2003; 38 (11–12): 913–23. PubMed PMID: 14642323.
12. Gharbi N, Pressac M, Hadchouel M, Szwarc H, Wilson SR, Moussa F. Fullerene is a powerful antioxidant in vivo with no acute or subacute toxicity. Nano Lett. 2005; 5 (12): 2578–85. PubMed PMID: 16351219.
13. Zhou Z, Joslin S, Dellinger A, Ehrich M, Brooks B, Ren Q, et al. A novel class of compounds with cutaneous wound healing properties. J Biomed Nanotechnol. 2010; 6 (5): 605–11. PubMed PMID: 21329053.
14. Andreev S, Purgina D, Bashkatova E, Garshev A, Maerle A, Andreev I, et al. Study of fullerene aqueous dispersion prepared by novel dialysis method: simple way to fullerene aqueous solution. Fullerenes Nanotubes and Carbon Nanostructures. 2015; 23: 792–800.
15. Shershakova NN, Andreev SM, Tomchuk AA, Makarova EA, Nikonova AA, Turetskiy EA, et al. Wound healing activity of aqueous dispersion of fullerene C60 produced by "green technology". Nanomedicine. 2023; 47: 102619. Epub 2022 Oct 19.
16. Молчанова В. И., Чикаловец И. В., Черников О. В., Попов А. М., Кривошапко О. Н., Лукьянов П. А. Сравнительное изучение биологической активности биогликанов из дальневосточной мидии crenomytilus grayanus. Тихоокеанский медицинский журнал. 2012; 1 (47): 47–50.
17. Livak KJ, Schmittgen TD. Analysis of relative gene expression data using real–time quantitative PCR and the 2(–Delta Delta C(T)) method. Methods. 2001; 25 (4): 402–8. PubMed PMID: 11846609.
18. Шамова О. В., Жаркова М. С., Чернов А. Н., Владимирова Е. В., Сухарева М. С., Комлев А. С. и др. Антимикробные пептиды врожденного иммунитета как прототипы новых средств борьбы с антибиотикорезистентными бактериями. Российский журнал персонализированной медицины. 2021; 1 (1): 146–72.
19. Kozhikhova KV, Shilovskiy IP, Shatilov AA, Timofeeva AV, Turetskiy EA, Vishniakova LI, et al. Linear and dendrimeric antiviral peptides: Design, chemical synthesis and activity against human respiratory syncytial virus. J. Mater. Chemistry B. 2020; 8 (13): 2607–17. DOI: 10.1039/c9tb02485a.
20. Werner S, Grose R. Regulation of wound healing by growth factors and cytokines. Physiol Rev. 2003; 83 (3): 835–70. PubMed PMID: 12843410.
21. Ashcroft GS, Jeong MJ, Ashworth JJ, Hardman M, Jin W, Moutsopoulos N, et al. Tumor necrosis factor-alpha (TNF-α) is a therapeutic target for impaired cutaneous wound healing. Wound Repair Regen. 2012; 20 (1): 38–49. Epub 2011 Dec 8. PubMed PMID: 22151742; PubMed PMCID: PMC3287056.
22. Stockmann C, Kirmse S, Helfrich I, Weidemann A, Takeda N, Doedens A, et al. A wound size–dependent effect of myeloid cell–derived vascular endothelial growth factor on wound healing. J Invest Dermatol. 2011; 131 (3): 797–801. Epub 2010 Nov 25. PubMed PMID: 21107350.
23. Robertson FM, Pellegrini AE, Ross MR, Oberyszyn AS, Boros LG, Bijur GN, et al. Interleukin-1alpha gene expression during wound healing. Wound Rep Reg. 1995; 3 (4): 473–84. PubMed PMID: 17147659.
24. Shershakova N, Baraboshkina E, Andreev S, Purgina D, Struchkova I, Kamyshnikov O, et al. Anti–inflammatory effect of fullerene C60 in a mice model of atopic dermatitis. J Nanobiotechnology. 2016; 14: 8. PubMed PMID: 26810232; PubMed PMCID: PMC4727272.
25. Spohn R, Daruka L, Lázár V. et al. Integrated evolutionary analysis reveals antimicrobial peptides with limited resistance. Nat Commun. 2019; 10 (1): 4538. PubMed PMID: 31586049; PubMed PMCID: PMC6778101.
26. Jangir PK, Ogunlana L, MacLean RC. Evolutionary constraints on the acquisition of antimicrobial peptide resistance in bacterial pathogens. Trends Microbiol. 2021; 29 (12): 1058–1061. Epub 2021 Apr 6. PubMed PMID: 33836929. PubMed PMID: 32355003; PubMed PMCID: PMC8097767.
27. Lazzaro BP, Zasloff M, Rolff J. Antimicrobial peptides: application informed by evolution. Science. 2020; 368 (6490): eaau5480. PubMed PMID: 32355003; PubMed PMCID: PMC8097767.
28. Falanga A, Del Genio V, Galdiero S. Peptides and Dendrimers: How to Combat Viral and Bacterial Infections. Pharmaceutics. 2021; 13 (1): 101.

FEATURES OF USING A LYMPHOCYTE TEST FOR BIOLOGICAL DOSIMETRY IN THE EARLY PERIOD AFTER EXPOSURE

Sedankin MK ✉, Gudkov EA, Soloviev VYu, Mershin LYu

Burnasyan Federal Medical Biophysical Center of Federal Medical Biological Agency, Moscow, Russia

When eliminating the consequences of large-scale radiation accidents, primary triage of victims is of key importance during the early phase of medical evacuation. Information about lymphocyte counts (blood test) per unit of peripheral blood volume can be used for this purpose. The study was aimed to validate the method of using a lymphocyte test for prediction of acute radiation injury severity in the first days after the exposure associated with the radiation mass casualty incident, given peripheral blood was tested once. We performed correlation analysis of the data of laboratory studies focused on quantifying lymphocytes in peripheral blood of victims during the first days following the Chernobyl disaster and other radiation accidents on the territory of the countries of the former USSR (115 individuals), including radiation accidents with gamma neutron radiation (20 individuals). It was found that with the lymphocyte concentration of 0.2–1.0 × 10^9/L on day 2 after exposure, the absolute error of estimated dose was ±1.5 Gy in case of gamma exposure and ±1.3 Gy in case of exposure to gamma neutron radiation. When the lymphocyte concentration exceeds 1.0 × 10^9/L, mild acute radiation syndrome (ARS) is predicted, given the average dose is below 2.0 Gy; when the lymphocyte concentration is less than 0.2 × 10^9/L< the estimated average dose exceeds 4.0 Gy, which corresponds to severe or extremely severe ARS. Thanks to the lymphocyte test accessibility and simplicity, this biological dosimetry method can occupy a worthy position in the diagnosis of radiation injury associated with large-scale accidents, since the results of cytogenetic tests are not available within first days after the accident.

Keywords: radiation dose, lymphocytes, acute radiation syndrome, radiation accident, radiological accident, nuclear accident, biological dosimetry

Author contribution: Sedankin MK — study concept and design, manuscript writing, literature review, approval of the final version of the article; Gudkov EA — study concept and design, data acquisition, data interpretation, computation tool development; Soloviev VYu — general management, study concept and design, manuscript writing; Mershin LYu — editing, data interpretation, computation tool optimization.

✉ **Correspondence should be addressed:** Mikhail K. Sedankin
Zhivopisnaya, 46, Moscow, 123098, Russia; msedankin@yandex.ru

Received: 10.08.2023 **Accepted:** 11.09.2023 **Published online:** 28.09.2023

DOI: 10.47183/mes.2023.034

ОСОБЕННОСТИ ИСПОЛЬЗОВАНИЯ ЛИМФОЦИТАРНОГО ТЕСТА ДЛЯ БИОЛОГИЧЕСКОЙ ДОЗИМЕТРИИ В РАННИЕ СРОКИ ПОСЛЕ ОБЛУЧЕНИЯ

М. К. Седанкин ✉, Е. А. Гудков, В. Ю. Соловьев, Л. Ю. Мершин

Федеральный медико-биологический центр имени А. И. Бурназяна Федерального медико-биологического агентства, Москва, Россия

При ликвидации последствий крупномасштабных радиационных аварий на ранних этапах медицинской эвакуации ключевое значение имеет первичная медицинская сортировка пострадавших. Для этой цели может быть использована информация о количестве лимфоцитов (анализ крови) в единице объема периферической крови. Целью исследования было провалидировать метод использования лимфоцитарного теста для прогнозирования степени тяжести острого лучевого поражения в первые дни после облучения при массовых радиационных поражениях при условии однократного анализа периферической крови. Проводили корреляционный анализ данных клинико-лабораторных исследований числа лимфоцитов в периферической крови пострадавших в первые дни после облучения при аварии на ЧАЭС и других радиационных инцидентах на территориях стран бывшего СССР (115 человек), в том числе в радиационных инцидентах с гамма-нейтронным облучением (20 человек). Установлено, что при концентрации лимфоцитов 0,2–1,0 × 10^9/л на 2-е сутки после облучения абсолютная погрешность оценки дозы составляет ±1,5 Гр при воздействии гамма-лучей и ±1,3 Гр — при воздействии гамма-нейтронного излучения. При концентрации лимфоцитов более 1,0 × 10^9/л в обоих случаях прогнозируется легкая степень острой лучевой болезни (ОЛБ) при средней дозе менее 2,0 Гр; при концентрации лимфоцитов менее 0,2 × 10^9/л оценка средней дозы составляет более 4,0 Гр, что соответствует тяжелой или крайне тяжелой степени ОЛБ. Благодаря доступности и простоте лимфоцитарного теста, этот метод биологической дозиметрии способен занять важное место в диагностике радиационных поражений при крупномасштабных авариях, в связи с тем что результаты цитогенетических тестов недоступны в течение первых дней после инцидента.

Ключевые слова: доза облучения, лимфоциты, острая лучевая болезнь, радиационная авария, радиологический инцидент, ядерный инцидент, биологическая дозиметрия

Вклад авторов: М. К. Седанкин — дизайн и концепция исследования, написание статьи, обзор литературы, утверждение окончательного варианта статьи; Е. А. Гудков — дизайн и концепция исследования, сбор материала, интерпретация данных, разработка инструмента математических расчетов; В. Ю. Соловьев — общее руководство, дизайн и концепция исследования, написание статьи; Л. Ю. Мершин — редактирование, интерпретация данных, оптимизация инструмента математических расчетов.

✉ **Для корреспонденции:** Михаил Константинович Седанкин
ул. Живописная, д. 46, г. Москва, 123098, Россия; msedankin@yandex.ru

Статья получена: 10.08.2023 **Статья принята к печати:** 11.09.2023 **Опубликована онлайн:** 28.09.2023

DOI: 10.47183/mes.2023.034

When eliminating the consequences of large-scale radiation accidents, primary triage of victims is of key importance in the early phase of medical evacuation. Provided victims have no personal dosimeters, information about primary response to exposure considering personal data on the exposure conditions and/or blood testing can be used for this purpose. The results of summarizing information about clinical manifestations of primary response to exposure and their prognostic value for assessment of radiation injury severity are provided in many papers [1–6]. Thus, actual knowledge about the symptoms of primary response in victims of the Chernobyl disaster (1986) and other radiation accidents was analyzed [5, 6]. It has been shown that among all symptoms of primary response to exposure, the time to emesis following the exposure is the most informative one. However, in some cases these data can be of low prognostic value, for example, due to the fact that victims

could use antiemetics [2, 7] or other reasons (head injuries, psychoemotional disorders, etc.). In this regard, information about lymphocyte counts per unit of peripheral blood volume, i.e. the so-called lymphocyte test (white blood cell count), can be an additional source of information about the radiation injury severity.

Peripheral blood cell counts are an important biomarker of radiation exposure. The lymphocyte test, i.e. measuring absolute lymphocyte counts and the dynamics of their changes in victims' blood, is of special prognostic value. Measuring absolute lymphocyte counts is the fastest and easiest laboratory test for radiation dose estimation within 24 h after the exposure. Physicians initially used a nomogram developed by G.A. Andrews to predict the radiation injury severity. Detection of low absolute lymphocyte counts or a progressive decrease in lymphocyte counts within certain time

Table 1. Peripheral blood lymphocyte counts ($\times 10^9$/L) on day 2 after exposure in victims of the Chernobyl disaster (1986) and other radiation accidents (according to the data from the database on acute radiation injury in humans compiled by the State Research Center — Burnasyan Federal Medical Biophysical Center of Federal Medical Biological Agency), amended and reworked from the earlier published paper [13]. The cases of exposure to gamma neutron radiation are allocated separately

Unique patient identifier	Dose, Gy	Lymphocyte counts, $\times 10^9$/L	Unique patient identifier	Dose, Gy	Lymphocyte counts, $\times 10^9$/L	Unique patient identifier	Dose, Gy	Lymphocyte counts, $\times 10^9$/L
Gamma radiation (95 individuals)								
1001	7.5	0.117	1055	5.3	0.522	1096	3.7	0.342
1005	5.2	0.165	1056	3.6	0.41	1097	1	0.662
1007	5.5	0.325	1057	3	0.516	1098	2	0.63
1011	6.3	0.081	1058	3	0.437	1099	5.6	1.2
1013	6.3	0.108	1059	5.8	0.54	1100	2.6	0.48
1018	2.7	0.229	1060	6.1	0.432	1101	3.2	0.841
1019	4.6	0.216	1061	4.4	0.513	1102	1.2	1.597
1021	4.7	0.164	1062	7	0.483	1103	1.9	0.817
1022	7.1	0.162	1063	1.1	0.51	1105	1.5	0.557
1024	2.3	0.365	1065	3.1	1.008	1106	2.3	0.69
1025	6	0.637	1066	1	0.884	1107	0.7	1.128
1028	7.3	0.376	1067	2.6	0.75	1108	2.3	0.756
1030	6.4	0.189	1068	4.6	0.293	1140	0.3	1.092
1031	7.7	0.399	1070	1.2	0.56	3033	7.7	0.296
1032	4.2	0.754	1071	5.4	0.128	3034	4	0.285
1033	3.9	0.636	1072	3.6	0.45	3035	6	0.222
1035	4	0.532	1073	3.5	2.52	3038	1.3	0.98
1037	2.8	0.566	1075	1.4	1.162	3044	1.7	1.155
1039	4.3	0.852	1078	0.3	1.842	3048	2.6	0.405
1040	1.7	0.612	1079	0.6	2.12	3050	2.3	0.484
1041	3.1	0.344	1081	1.2	1.275	3051	3	0.438
1042	6.3	0.357	1082	1.2	2.352	3052	3	0.7
1043	4.7	0.281	1083	1.9	0.989	3053	3	0.335
1044	3.7	0.609	1084	1.1	1.058	3067	2.3	1.044
1047	3.2	0.744	1085	3.3	0.3	3068	3	0.728
1048	2	0.924	1087	3.5	0.378	3069	3.5	0.504
1049	2.1	0.235	1089	1.7	0.846	3077	0.85	1.107
1050	3.3	0.897	1090	1.2	0.74	3078	0.9	1.26
1051	1.8	0.943	1091	1.2	0.608	3082	2.1	0.697
1052	4.3	0.436	1092	2.7	0.72	3083	1.3	1.798
1053	2.8	0.594	1094	6.6	0.684	3084	2.1	0.91
1054	3.6	0.456	1095	2.2	0.923			
Gamma neutron radiation (20 individuals)								
3008	3.8	0.352	3036	3.3	0.067	3065	2.25	0.504
3010	0.9	1.564	3037	3.7	0.269	3071	3.7	0.93
3011	0.5	1.222	3040	5.8	0.204	3073	5	0.08
3020	4	0.396	3042	4.1	0.259	3079	2.1	1.147
3025	2.5	0.423	3043	3	0.551	3081	1.5	0.774
3027	1.1	1.071	3045	5.5	0.444	3086	1.9	0.769
3030	3.6	0.403	3046	7.4	0.072			

Table 2. Dose estimation based on the time between blood tests and the ratio of lymphocyte concentrations L_2/L_1 within 2–18 h after exposure

L_2/L_1	Time between measurements, h				
	4	6	8	10	12
0.8	8	5.4	4	3.2	2.7
0.7	>12	8.6	6.4	5.1	4.3
0.6	>12	>12	9.2	7.4	6.1
0.5	>12	>12	>12	10	8.3

period indicates probable exposure to a high radiation dose, which follows classical lymphocyte depletion curves [8].

Generally, the use of lymphocyte test is based on the fact that the average concentration of lymphocytes in peripheral blood remains more or less constant during the period between days 2 and 9 following a substantial decrease within the first 24 h after the exposure. The guidelines on the lymphocyte test practical use are based on these patterns. The correlation between peripheral blood lymphocyte counts/concentrations and the dose received was thoroughly investigated in the population of victims of the Chernobyl accident (1986) and other radiation accidents [9]. It has been shown that the highest correlation between the dose and the average peripheral blood lymphocyte concentration is observed on days 3–6 after exposure. However, the earlier period is not discussed in this paper.

However, in practice situations are possible when only one blood test performed in the first days after exposure is reported for the victim. According to the domestic literature, this time range is insufficiently studied. Further research is needed to raise the lymphocyte test informativity in this time period.

Dose estimation based on only one blood test performed within the first 24 h is not very informative, since there is a high degree of uncertainty. This issue is poorly understood in terms of statistics. The literature provides data on assessing injury severity within the first days or hours after the radiation accident [10, 11]. The radiation injury severity can be predicted based on the victim's absolute peripheral blood lymphocyte counts within the first two days after exposure in accordance with the guidelines issued by the IAEA and the WHO [12].

Currently, it is important to develop and improve the lymphocyte test as a biological dosimetry method in order to assess and predict the severity of injury in victims of radiation accidents in the first days after the accidents during the early phase of medical evacuation and subsequent echelon care.

The study was aimed to validate the method of using a lymphocyte test within two days after the exposure to predict the severity of injury associated with the radiation mass casualty incident, given peripheral blood was tested once, based on the use of laboratory data on victims of radiation incidents on taken from the database on ARS compiled by the State Research Center — Burnasyan Federal Medical Biophysical Center of Federal Medical Biological Agency.

METHODS

The study involved the use of clinical data from the database on ARS compiled by the State Research Center — Burnasyan Federal Medical Biophysical Center of Federal Medical Biological Agency as background information [13]. The populations of victims of the Chernobyl disaster (77 individuals) and other radiation accidents (38 individuals), who received the exposure doses not exceeding 8 Gy were considered (Table 1). Correlation analysis was used as a research method.

We assessed the relationship between the absorbed dose and the concentration of lymphocytes in peripheral blood of

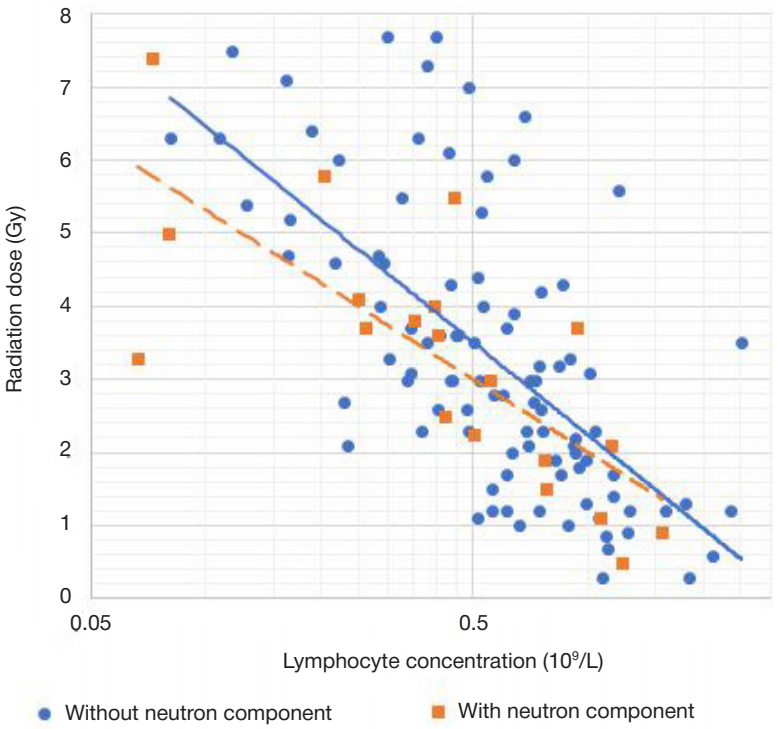

Fig. Radiation dose (Gy) as a function of lymphocyte counts (×10^9/L) on day 2 after exposure. Markers indicate baseline data (separately for groups exposed to gamma and gamma neutron radiation), and lines indicate the observed trends

Table 3. Estimated uncertainty of the received dose (Gy) and radiation injury severity based on peripheral blood lymphocyte concentration on day 2 and the average value on days 3–6 after exposure (based on the data from [9])

Lymphocyte concentrations, $\times 10^9$/L	Days after exposure			
	Gamma radiation		Gamma neutron radiation	
	2	3–6	2	3–6
< 0.2	II–IV	III–IV	II–IV	III–IV
0.3	4.4 (3–5.9) II–III	5.8 (4.2–7.4) III–IV	3.7 (2.6–4.9) II–III	4.5 (3.0–6.0) II–III
0.4	3.9 (2.5–5.4) II–III	5 (3.3–6.6) II–IV	3.3 (2.2–4.4) II–III	3.7 (2.2–5.2) II–III
0.5	3.5 (2.1–5) II–III	4.3 (2.7–5.9) II–III	3 (1.9–4.1) I–III	3.1 (1.7–4.6) I–III
0.6	3.2 (1.7–4.6) I–III	3.8 (2.2–5.4) II–III	2.7 (1.6–3.9) I–II	2.6 (1.3–4.0) I–II
0.8	2.6 (1.2–4.1) I–III	3 (1.4–4.6) I–III	2.3 (1.2–3.4) I–II	1.8 (0.7–3.0) I–II
1	2.2 (0.8–3.7) до II	2.3 (0.7–3.9) I–II	2 (0.9–3.1) до II	1.1 (0.2–2.0) до II

victims on day 2 after exposure for the data considered, we also determined the correlation between these parameters. The cases of combined exposure to gamma neutron radiation were considered separately. The results are provided in Figure and Table 3.

RESULTS

The earlier published report showed that the concentration of lymphocytes in peripheral blood decreased approximately exponentially during the first day after exposure to the clinically significant dose range [10]. The constant of the lymphocyte concentration decrease rate between hours 2 and 18 after exposure is correlated to the radiation dose D, which enables estimation of this dose based on two time points of blood testing [11]:

$$D = -(k/\Delta T) \times \ln(L_1/L_2) \quad (1)$$

where L_1 and L_2 — lymphocyte counts in blood samples collected at time points t_1 and t_2 after exposure ($t_2 > t_1$), $\Delta T = t_2 - t_1$ — time between blood samples, and the constant $k = 144$. Similar to the data provided in the paper [11], using the formula provided makes it possible to estimate absorbed dose according to two blood tests (Table 2).

The data provided in Table 2 were used to assess the correlation between the absorbed dose and the lymphocyte counts in peripheral blood of victims on day 2 after exposure (Figure). Statistical processing made it possible to estimate uncertainty of the radiation injury severity predicted based on one blood test performed on day 2 after exposure (Table 3). For comparison, the table also provides the values predicted based on the average lymphocyte counts on days 3–6 after exposure.

DUSCUSSION

It should be noted that in case of gamma neutron exposure the predicted dose is on average 10–15% lower than in case of gamma exposure.

Turning to the issue of the possibility of using one blood test performed within the first 24 h after exposure, the results of the study can be used that show that individual fluctuations of peripheral blood lymphocyte counts in healthy people constitute about + 20% of the average value at long-term follow-up [11]. That is why the data of previous blood testing cannot be considered as a reliable guide to refine the prediction. The ratio (1), where the data of first lymphocyte count measurement L1 are represented by the data of the victim's blood testing performed a few days before exposure and the $\Delta T = t - 2$ parameter, where t is an interval between the time of exposure and blood testing performed within the period between hours 2 and 18 after exposure, can be used for dose estimation.

The concentration parameters of blood can be of lower significance due to multiple clinical problems not related to radiation exposure and the spread of biological parameters: the fact of infusion and transfusion therapy, non-radiation-induced injuries, ethnicity, age, health status, and gender of the assessed victims, parameter reduction or elevation using drugs, etc. [14, 15]. That is why establishing preliminary diagnosis based on the lymphocyte test only, without taking into account other data and the listed above reasons, can result in biased estimated dose or radiation injury severity.

CONCLUSIONS

Validation of information about the peripheral blood lymphocyte counts on day 2 after exposure made it possible to adjust the predicted radiation injury severity: 1) when peripheral blood lymphocyte concentration is below 0.2×10^9/L, severe (grade III) or extremely severe (grade IV) ARS is predicted; 2) when the lymphocyte concentrations are within the range of $0.2–1.0 \times 10^9$/L, the estimated dose absolute error is ±1.5 Gy in case of gamma exposure and ±1.3 Gy in case of gamma neutron exposure. Victims are diagnosed with moderate (grade II) or severe (grade III) radiation injury, it is necessary to start treatment in a specialized hospital as soon as possible; 3) when the peripheral blood lymphocyte concentration exceeds 1.0×10^9/L, mild (grade I) to moderate (grade II) ARS can be predicted. As compared with the method reported in the paper [9], this test enables prediction of radiation dose based on the data of only one blood test performed on day 2 after exposure. This may be preferable in cases of large-scale radiation accidents and incidents, when the medical resources available are not enough for full-fledged diagnosis of the ARS severity. The lymphocyte test remains one of the most simple and accessible biological dosimetry methods, which defines its role in the diagnosis of radiation injury associated with large-scale accidents, when no cytogenetic test results are available in the first days after the incident. Prediction accuracy can be improved in the future with additional sources of information about the lymphocyte concentration in the first days after exposure.

References

1. Flynn DF, Goans RE. Nuclear Terrorism: triage and medical management of radiation and combined-injury casualties. Surgical Clinics. 2006; 86 (3): 601–35. DOI: 10.1016/j.suc.2006.03.005.
2. Waselenko JK, MacVittie TJ, Blakely WF, Pesik N, Wiley AL, Dickerson WE, et al. Medical management of the acute radiation syndrome: recommendations of the strategic National Stockpile Radiation Working Group. Annals of Internal Medicine. 2004; 140 (12): 1037–14. DOI: 10.7326/0003-4819-140-12-200406150-00015.
3. Iddins CJ, Davis JE, Goans RE, Case C. Radiological and nuclear terrorism. Oncologic Emergency Medicine. 2021; 543–10. DOI: 10.1007/978-3-030-67123-5_42.
4. Baranov AE. Ostraya luchevaya bolezn': biologicheskaya dozimetriya, rannyaya diagnostika i lechenie, ishody i otdalennye posledstviya. V knige: Barabanova AV, Baranov AE, Bushmanov AYu, Gus'kova AK. Radiacionnye porazheniya cheloveka. Izbrannye klinicheskie lekcii, metodicheskoe posobie. M.: Slovo, 2007; 53–31. Russian.
5. Solovev VYu, Samojlov AS, Lebedev AO, Sedankin MK, Gudkov EA. Ispol'zovanie informacii o vremeni razvitiya rvoty pri pervichnoj sortirovke postradavshih v radiacionnyh avariyah. Mediko-biologicheskie i social'no-psihologicheskie problemy bezopasnosti v chrezvychajnyh situaciyah. 2021; (1): 14–7. DOI: 10.25016/2541-7487-2021-0-1-14-21. Russian.
6. Solovev VYu, Krasnyuk VI, Fatkina SS. Baza dannyh po ostrym luchevym porazheniyam cheloveka. Soobshhenie 4. Zakonomernosti formirovaniya pervichnoj reakcii pri otnositel'no ravnomernom avarijnom obluchenii. Medicinskaya radiologiya i radiacionnaya bezopasnost'. 2014; 59 (4): 32–8. Russian.
7. Fliedner TM, Friesecke I, Beyrer K, editors. Medical management of radiation accidents: manual on the acute radiation syndrome. British Inst of Radiology. 2001; 65.
8. Andrews GA, Auxier JA, Lushbaugh CC. The Importance of dosimetry to the medical management of persons accidentally exposed to high levels of radiation. In: Personnel dosimetry for radiation accidents. Proceedings of an International Atomic Energy Agency symposium. Vienna: International Atomic Energy Agency. 1965; 3–16
9. Lebedev AO, Samojlov AS, Solovyov VYu, Baranova NN, Gudkov EA. Osobennosti ispol'zovaniya limfocitarnogo testa dlya prognozirovaniya stepeni tyazhesti ostrogo luchevogo porazheniya. Medicina katastrof. 2021; (3): 29–4. DOI: 10.33266/2070-1004-2021-3-29-33. Russian.
10. Goans RE, Holloway EC, Berger ME, Ricks RC. Early Dose Assessment Following Severe Radiation Accidents. Health Physics. 1997; 72 (4): 513–8.
11. Parker DD, Parker JC. Estimating radiation dose from time to emesis and lymphocyte depletion. Health Physics. 2007; 93 (6): 701–4. DOI: 10.1097/01.HP.0000275289.45882.29.
12. Obshhie procedury medicinskogo reagirovaniya pri yadernoj ili radiologicheskoj avarijnoj situacii. Seriya «Avarijnaya gotovnost' i reagirovanie», IAEA-EPR-MEDICAL. Vena: MAGATEh, 2009; 327 c.
13. Samoilov AS, Soloviev VYu, editors. ATLAS. Acute radiation syndrome. M.: SRC-FMBC, 2019; 232.
14. Obrador E, Salvador-Palmer R, Villaescusa JI, Gallego E, Pellicer B, Estrela JM, Montoro A. Nuclear and Radiological Emergencies: Biological Effects, Countermeasures and Biodosimetry. Antioxidants. 2022; 11 (6): 1098–51. DOI: 10.3390/antiox11061098.
15. Hu S, Blakely WF, Cucinotta FA. HEMODOSE: a biodosimetry tool based on multi-type blood cell counts. Health physics. 2015; 109 (1): 54–68. DOI: 10.1097/HP.0000000000000029568.

Литература

1. Flynn DF, Goans RE. Nuclear Terrorism: triage and medical management of radiation and combined-injury casualties. Surgical Clinics. 2006; 86 (3): 601–35. DOI: 10.1016/j.suc.2006.03.005.
2. Waselenko JK, MacVittie TJ, Blakely WF, Pesik N, Wiley AL, Dickerson WE, et al. Medical management of the acute radiation syndrome: recommendations of the strategic National Stockpile Radiation Working Group. Annals of Internal Medicine. 2004; 140 (12): 1037–14. DOI: 10.7326/0003-4819-140-12-200406150-00015.
3. Iddins CJ, Davis JE, Goans RE, Case C. Radiological and nuclear terrorism. Oncologic Emergency Medicine. 2021; 543–10. DOI: 10.1007/978-3-030-67123-5_42.
4. Баранов А. Е. Острая лучевая болезнь: биологическая дозиметрия, ранняя диагностика и лечение, исходы и отдаленные последствия. В книге: Барабанова А. В., Баранов А. Е., Бушманов А. Ю., Гуськова А. К. Радиационные поражения человека. Избранные клинические лекции, методическое пособие. М.: Слово, 2007; 53–31.
5. Соловьев В. Ю., Самойлов А. С., Лебедев А. О., Седанкин М. К., Гудков Е. А. Использование информации о времени развития рвоты при первичной сортировке пострадавших в радиационных авариях. Медико-биологические и социально-психологические проблемы безопасности в чрезвычайных ситуациях. 2021; (1): 14–7. DOI: 10.25016/2541-7487-2021-0-1-14-21.
6. Соловьев В. Ю., Краснюк В. И., Фатькина С. С. База данных по острым лучевым поражениям человека. Сообщение 4. Закономерности формирования первичной реакции при относительно равномерном аварийном облучении. Медицинская радиология и радиационная безопасность. 2014; 59 (4): 32–8.
7. Fliedner TM, Friesecke I, Beyrer K, editors. Medical management of radiation accidents: manual on the acute radiation syndrome. British Inst of Radiology, 2001.
8. Andrews GA, Auxier JA, Lushbaugh CC. The Importance of dosimetry to the medical management of persons accidentally exposed to high levels of radiation. In: Personnel dosimetry for radiation accidents. Proceedings of an International Atomic Energy Agency symposium. Vienna: International Atomic Energy Agency. 1965; 3–16
9. Лебедев А. О., Самойлов А. С., Соловьёв В. Ю., Баранова Н. Н., Гудков Е. А. Особенности использования лимфоцитарного теста для прогнозирования степени тяжести острого лучевого поражения. Медицина катастроф. 2021; (3): 29–4. DOI: 10.33266/2070-1004-2021-3-29-33.
10. Goans RE, Holloway EC, Berger ME, Ricks RC. Early Dose Assessment Following Severe Radiation Accidents. Health Physics. 1997; 72 (4): 513–8.
11. Parker DD, Parker JC. Estimating radiation dose from time to emesis and lymphocyte depletion. Health Physics. 2007; 93 (6): 701–4. DOI: 10.1097/01.HP.0000275289.45882.29.
12. Общие процедуры медицинского реагирования при ядерной или радиологической аварийной ситуации. Серия «Аварийная готовность и реагирование», IAEA-EPR-MEDICAL. Вена: МАГАТЭ, 2009; 327 с.
13. Samoilov AS, Soloviev VYu, editors. ATLAS. Acute radiation syndrome. M.: SRC-FMBC, 2019; 232.
14. Obrador E, Salvador-Palmer R, Villaescusa JI, Gallego E, Pellicer B, Estrela JM, Montoro A. Nuclear and Radiological Emergencies: Biological Effects, Countermeasures and Biodosimetry. Antioxidants. 2022; 11 (6): 1098–51. DOI: 10.3390/antiox11061098.
15. Hu S, Blakely WF, Cucinotta FA. HEMODOSE: a biodosimetry tool based on multi-type blood cell counts. Health physics. 2015; 109 (1): 54–68. DOI: 10.1097/HP.0000000000000029568.

FEATURES OF EEG MICROSTATE ANALYSIS IN POST-STROKE APHASIA

Gulyaev SA[1,2] ✉, Khanukhova LM[2], Garmash AA[1]

[1] Institute for Physics and Engineering in Biomedicine, National Research Nuclear University MEPhI, Moscow, Russia

[2] La Salute Clinic, Moscow, Russia

Knowledge about the specificity of changes in the activity of neural networks associated with realization of thought processes can be used to construct the personalized medical rehabilitation systems. This approach is of particular interest for people with the speech function disturbance due to stroke, since the development of aphasia with the loss of speech leads to severe social maladaptation that worsens the disease outcome. The study was aimed to assess the functional activity of individual neural networks based on the theory of combining the EEG microstate identification technique with the method of determining spatial localization by solving the EEG inverse problem in 27 individuals (15 males and 12 females) with an average age of 52 years, who had speech impairment due to acute atherothrombotic stroke. Mathematical analysis of the scalp bioelectrical activity multichannel recording from the system for EEG microstate model isolation was carried out under changing environmental conditions caused by the auditory-speech load together with the EEG inverse problem solution for each subject. It was found that the speech disorder development depends not only on the fact of damage to brain structures, but also on the deep functional restructuring of both neural streams involved in implementation of brain function and the entire speech connectome. The disease with a predominant motor disorder, that has shown the possibility of transferring functions to the intact hemisphere prefrontal structures, in contrast to sensory disorders representing global changes in the entire speech connectome, can probably be considered the most favorable variant of aphasia.

Keywords: electroencephalography, speech function, brain rhythms, diagnostics, rehabilitation, cerebral stroke, aphasia

Author contributions: the authors contributed equally to the study.

Compliance with ethical standards: the study was approved based on the contract between the National Research Nuclear University MEPhI and La Salute Clinic (protocol № 09-01/23 of 09 January 2023), approved by the ethics committee of the National Research Nuclear University MEPhI (protocol of 25 May 2023), and conducted in accordance with the principles of biomedical ethics set out in the Declaration of Helsinki (1964) and its subsequent updates.

✉ **Correspondence should be addressed:** Sergey A. Gulyaev
Ramenki, 31, k. 136, Moscow, 119607, Russia; s.gulyaev73@gmail.com

Received: 20.06.2023 **Accepted:** 22.07.2023 **Published online:** 13.08.2023

DOI: 10.47183/mes.2023.025

ОСОБЕННОСТИ АНАЛИЗА ЭЭГ-МИКРОСОСТОЯНИЙ ПРИ ПОСТИНСУЛЬТНОЙ АФАЗИИ

С. А. Гуляев[1,2] ✉, Л. М. Ханухова[2], А. А. Гармаш[1]

[1] Инженерно-физический институт биомедицины Национального исследовательского ядерного университета «МИФИ», Москва, Россия

[2] Общество с ограниченной ответственностью «Клиника Ла Салюте», Москва, Россия

Знания о специфичности изменений активности нейронных сетей, связанных с реализацией мыслительного процесса, могут быть использованы в построении систем персонализированной медицинской реабилитации. Особый интерес данный подход представляет для лиц, потерявших речевую функцию в результате развития церебрального инсульта, так как развитие афазии с потерей речевой коммуникации приводит к выраженной социальной дезадаптации, ухудшающей прогноз заболевания. Целью исследования было определить функциональную активность отдельных нейронных сетей, основываясь на теории комбинированной технологии определения ЭЭГ-микросостояний с методикой определения пространственной локализации с помощью решения обратной задачи ЭЭГ у 27 человек (15 мужчин и 12 женщин) со средним возрастом — 52 года, с нарушением речевой функции вследствие развития острого атеротромботического инсульта. Для всех обследованных был осуществлен математический анализ многоканальной записи скальповой биоэлектрической активности с системы выделения модели ЭЭГ-микростостояний с решением обратной задачи ЭЭГ для каждого из них в изменяемых внешних условиях, вызванных проведением слухо-речевой нагрузки. Обнаружено, что развитие речевых нарушений зависит не только от самого факта повреждения мозговых структур, но и от выраженной функциональной перестройки как отдельных нейронных сетей, вовлеченных в реализацию мозговой функции, так и всего речевого коннектома. Наиболее благоприятным вариантом афазий, вероятно, можно считать заболевание с преобладанием моторных нарушений, демонстрировавшее возможность передачи функций на префронтальные структуры интактного полушария, в то время как сенсорные нарушения представляли глобальные изменения всего речевого коннектома.

Ключевые слова: электроэнцефалография, речевая функция, мозговые ритмы, диагностика, реабилитация, мозговой инсульт, афазия

Вклад авторов: все авторы внесли равнозначный вклад в данное исследование.

Соблюдение этических стандартов: исследование одобрено на основании договора ИФИБ НИЯУ МИФИ и ООО «Клиника Ла Салюте» (протокол № 09-01/23 от 09 января 2023 г.) и этическим комитетом НИЯУ МИФИ (протокол от 25 мая 2023 г.), проведено в соответствии с принципами биомедицинской этики, сформулированными в Хельсинкской декларации 1964 г. и ее последующих обновлениях.

✉ **Для корреспонденции:** Сергей Александрович Гуляев
Раменки, д. 31, к. 136, г. Москва, 119607, Россия; s.gulyaev73@gmail.com

Статья получена: 20.06.2023 **Статья принята к печати:** 22.07.2023 **Опубликована онлайн:** 13.08.2023

DOI: 10.47183/mes.2023.025

Speech represents a higher cognitive function closely linked to the person's integration into society, that is why speech impairment is among severe conditions resulting in profound social maladaptation and therefore worsening the outcome of rehabilitation.

The first research into post-stroke aphasia reported by P. Broca and C. Wernicke revealed the major speech centers of the human brain and paved the way to the disorder objective diagnosis [1, 2]. In 1980s, the doctrine of two-stream model providing the basis for the functional speech connectome, which made it possible to objectively assess the aphatic disorders diversity and explain the features of speech function rehabilitation in the post-stroke period, was developed based on the new data obtained using the dynamically developing

magnetic resonance imaging techniques [3]. It was this theory that triggered an interest in monitoring the subdominant hemisphere prefrontal cortical structures' involvement in the process of speech function restoration [4, 5], thereby allowing the group of European experts to recommend the use of neurostimulation applied to these areas as one of the rehabilitation methods aimed at restoring speech in the post-stroke period [6].

However, determining the features of speech organization is currently a major technological challenge posed by the characteristics of modern medical equipment. The widely used method of functional magnetic resonance imaging (fMRI) demonstrates the changes in the nervous tissue oxygen consumption resulting from the increase in metabolic activity associated with the nervous tissue excitation, which lead to the pronounced temporal delay preventing recording of the characteristics of information transmission between various nerve centers responsible for speech function realization.

This is especially important in the context of post-stroke speech impairment rehabilitation [7], since the patient-centered approach to the lost function restoration is more effective than the use of standardized and formalized technologies.

The synaptic connection activity recording that forms the basis of electroencephalography (EEG) and magnetoencephalography (MEG) makes it possible to reveal rapid excitation processes. However, MEG systems are not mainstream enough yet and are virtually non-existent in the clinics. Furthermore the existing EEG technique that is based on the principles proposed by H. Jasper in 1940–1954 [8] has some serious technical limitations hampering assessment of activity in distinct brain structures. These limitations are related to the visual and phenomenological analysis technology not allowing one to obtain information about the association between the recorded activity and the brain's anatomical structures comparable to that provided by neuroimaging methods, since the technology deals only with the total activity values of multiple nervous system structures.

However, the concept of EEG microstates is considered to be a solution. In 1998, D. Lehmman identified certain overall scalp potential variants and concluded that electrical activity of the brain detected by routine EEG could be represented by the repeating sequence of individual fixed time patterns of biopotential distribution over the scalp related to the activity of some finite number of neural networks producing rhythmic activity within a limited period of time [9, 10]. It was also concluded that the duration of single microstate could be interpreted as an indicator of the underlying neuronal assembly preservation and stability, while frequency of occurrence could be interpreted as activity (activation) of the underlying neural generators during execution of certain brain function. Further investigation of this phenomenon showed that four most representative configurations belonged to the EEG microstate classes A, B, C, D and were related to the activity of the brain's default mode network structures, while changes in external verbal conditions affected the duration, occurrence and coverage of microstates due to involvement of other neuronal pools related to realization of the overall function of the brain [11, 12].

Subsequent research has confirmed that measurement of EEG microstates is sensitive to the neuronal activity changes in the cortical areas responsible for modality-specific processing via certain tasks (state-dependent effects) [13]. Assessment of intersubjective and intrasubjective relationships between the features of microstates in 29 healthy subjects has shown that the dynamics of microstates can reflect transitions between the global states characterized by selective inhibition of certain intracortical areas and have functional and behavioral effects on sensory processing and cognitive functions [14]. In 2021, the use of similar technique in the subjects being in the wakeful rest state made it possible to conclude that memories were consolidated by the brain mainly during the "offline" periods, when an individual was not engaged in task execution and when his/her attention was not focused on executing certain task [15].

The above reports allowed one to formulate the concept of using the EEG microstate model as a tool to help identify distinct components of the entire continuous EEG recording that were associated with the functional activity of certain neuronal groups. However, identification of spatial relationships between certain EEG microstates and anatomical structures these were produced by was still an outstanding issue.

In 1994–1997, the EEG inverse problem solution system was proposed that was based on the technique involving matching the dipole localization and the layered head model that was referred to as low resolution electromagnetic tomography (LORETA) and solved the problem of the EEG signal source cortical localization. Starting from 1999, the method was supplemented by quantitative neuroanatomy based on the digitized Talairach Atlas provided by the Brain Imaging Centre of the Montreal Neurological Institute (MNI). The combination of these innovations brought LORETA to the level comparable to that of conventional functional imaging methods, such as PET and fMRI [12, 16]. In 2008, it was shown that LORETA provided the best solution for single source localization in terms of both zero localization error and false sources compared to other software products using similar techniques to solve the EEG inverse problem [17]. In 2014, simultaneous fMRI-EEG studies aimed at determining the relationship between the default mode network (DMN) activity and the power of the EEG frequency bands suggested that the LORETA technique used to determine the EEG power of the alpha, beta, delta, and theta frequency bands in the region of interest helped reveal a close relationship between the spontaneous BOLD fluctuations in the brain's default mode networks and various EEG rhythms. The use of the technique also suggests that individual neural network is characterized by specific "electrophysiological signature" produced by the combination of various brain rhythms [18]. However, as early as in 2010, the differences in organization of stimulation paradigms used in EEG and fMRI experiments were noted, and the question arose whether it was possible to effectively localize the evoked EEG activity using the constantly changing intensity of the features occurring in the natural stimuli presented within rather long time periods. In particular, there was a question whether the aspects of the stimulus-driven EEG signal would be localized along with appropriate fMRI BOLD signal [19]. Today, EEG source reconstruction includes the process, in which the best results are achieved using conditional functional models [20] resembling the technique proposed in 2014 [21], in which the number of conditional neural networks involved in realization of the studied function would be comparable with the number and activity of microstates identified during the EEG test.

Thus, the current development of EEG analysis technologies makes it possible to obtain a new tool for exploration of the brain cortical structures' functional activity that can be used to assess the status of higher neural functions, such as speech, and determine the possibility of function restoration in individuals with various types of speech impairment developed due to the disease [22, 23].

The study was aimed to determine the functional activity of individual neural networks based on the theory of combining the EEG microstate identification technique with the method of determining spatial localization by solving the EEG inverse problem in individuals with speech function impairment due to acute cerebrovascular accident.

METHODS

A total of 27 individuals (15 males and 12 females) were assessed, who contacted La Salute Clinic for treatment and rehabilitation after ischemic (atherothrombotic) stroke in the area supplied by the left middle cerebral artery that was followed by the development of persistent neurological deficit (cerebral stroke), one of the syndromes of which was aphasia. Inclusion criteria: Russian speakers with the left hemisphere dominance confirmed by the development of post-stroke aphasia; no problems with speech production before the disease.

Exclusion criteria for the study group: traumatic brain injury with functional impairment, mental disorder; constant use of psychoactive substances (ongoing or prior); verified diagnosis of epilepsy; dysarthria due to neurological disorder.

As a result, the study group included individuals with an average age of 52 years (minimum — 21 years, maximum — 68 years; Mo — 49 years, Me — 54 years; 1st quartile — 46 years, 3rd quartile — 61 years). In all of them both the fact of damage to speech connectome and the speech disorder with predominance of motor, sensory or total (mixed) speech impairment itself (motor variant of the disorder was found in 11 subjects, 9 subjects had a sensory variant, while in 7 subjects we failed to identify the aphasic disorder predominant type) were considered. No epileptic seizures were reported in the surveyed patients, no specific epileptiform activity in perifocal areas of the cerebral infarction lesion was recorded. The degree of functional impairment according to the Rankin scale did not exceed 3 in all patients.

All participants underwent an EEG at relative rest (passive relaxed wakefulness with no auditory-speech load) and under a load (listening to a short story in the passive relaxed wakefulness state with eyes closed). A total of 54 tests were performed, and the results were used for further analysis.

Characteristics of methods

The T1-weighted and T2-weighted MRI in the suppression and diffusion nodes showed that the average lesion volume was 82 cm3 (Me — 30.8; 1st quartile — 1, 3rd quartile — 176). EEG was recorded in a darkened, relatively soundproof room in the relaxed wakefulness state with eyes closed. Recording was performed using the 52-channel EEG system (Medical Computer Systems, Zelenograd, Russia). The analog-to-digital converter sampling rate was 500 Hz. The tests involved the use of the electrode placement scheme with an average reference allowing one to obtain equal values of the recorded voltage and scalp biopotential. The native signal bandwidth was 0.5–70 Hz, with the inclusion of the 50 Hz notch network filter.

No recording was performed within the first minute after connecting the volunteer to the device in order to suppress physiological artifacts associated with disadaptation and the need to become habituated to the test. The total electrode resistance, impedance, was controlled within the limits of 10 kOm and constantly checked during the entire study in accordance with the manufacturer's guidelines.

The loading test involved assessment under auditory-speech load in the form of listening to one short story (the same for all subjects) in the native language (Russian) taken from the open access online library. This made it possible to create the conditions of the altered state comparable with the passive relaxed wakefulness state based on common characteristics, but determined by activation of only one cognitive function (speech in this case) having a relatively well understood cortical analyzer architecture [24].

The listening test was selected due to minimization of muscle activity and as a test able to activate the maximum number of speech centers including both gnosis centers of speech and the centers responsible for generation of imagined speech.

Subsequent data acquisition, processing, and analysis were performed in several phases. The first phase involved minimization of artifacts. For that the by-standing electrical devices that generated parasitic electromagnetic fields were switched off, interface impedance was controlled, temperature in the room was adjusted, and parasitic movements of the

Table 1. Registration of the EEG activity frequency characteristics over the areas of the main speech centers

	Predominance of motor impaiment			
	Broca's area oscillation frequency (areas 44, 45 on the left)	Wernicke's area oscillation frequency (areas 39, 40 on the left)	Intact hemisphere prefrontal cortex oscillation frequency (areas 8, 9, 10, 11, 12, 13, 14, 24, 25, 32, 44, 45, 46, and 47)	
Average	0	15,6 ± 6,5	19,3 ± 1,9	*
	Predominance of sensory impairment			
	Broca's area oscillation frequency (areas 44,45 on the left)	Wernicke's area oscillation frequency (areas 39,40 on the left)	Intact hemisphere prefrontal cortex oscillation frequency (areas 8, 9, 10, 11, 12, 13, 14, 24, 25, 32, 44, 45, 46, and 47)	
Average	17,0 ±1,2	0	0	*
	Total (mixed) variants			
	Broca's area oscillation frequency (areas 44, 45 on the left)	Wernicke's area oscillation frequency (areas 39, 40 on the left)	Intact hemisphere prefrontal cortex oscillation frequency (areas 8, 9, 10, 11, 12, 13, 14, 24, 25, 32, 44, 45, 46, and 47)	
Average	13,5 ± 2,5	16,3 ± 2,9	18,0 ± 4,6	**

Note: (ANOVA-test), * — $p < 0.001$; ** — $p > 0.05$.

Table 2. Changes in the characteristics of EEG microstates relative to their contribution to formation of the head's overall bioelectric field

Major syndrome	Class/test	A	B	C	D	I	II
Motor	Load	0,04	0,06	0,02	0,05	0,06	0,07
	No load	0,16	0,11	0,12	0,2	0,17	0,24
	p	*	**	*	**	*	*
Sensory	Load	0,22	0,26	0,05	0,21	0,14	0,12
	No load	0,19	0,11	0,12	0,1	0,37	0,11
	p	**	*	**	*	**	**
Total (mixed)	Load	0,18	0,17	0,09	0,05	0,09	0,43
	No load	0,23	0,13	0,26	0,11	0,09	0,18
	p	**	**	*	**	**	**

Note: *t*-test, * — $p < 0.05$; ** — $p > 0.05$.

muscles were minimized. During the second phase the resulting data pool was subjected to standardization of basic assembly to create a common electrode space, as well as to artifact removal via extraction of independent signal components. This made it possible to purify the native signal of various physiological artifacts that had not been eliminated by filtration. During the third phase the EEG signal segmentation was performed to extract individual EEG microstates by clustering and allocating six classes of individual microstates (conventional A, B, C, D and two (I and II) extra ones, considering of their variability). The final phase of the study involved analysis of the activity source localization for each of the allocated EEG microstate classes using the EEG inverse problem solution algorithm implemented in the sLORETA v. 20210701 software package (University of Zurich; Switzerland).

The results provided information about six distinct classes of EEG microstates, including the following characteristics: 1) microstate lifetime (duration) in seconds; 2) frequency of microstate recording per 1 s (occurrence); 3) contribution of EEG microstate to the structure of the scalp energy total energy spectral characteristics (coverage); 4) localization of the main cortical structure generating the EEG microstate according to the Brodmann area atlas (atlas issued by the Montreal Neurological Institute, MNI).

Statistical processing of the results was performed in accordance with the earlier reported guidelines [25] using the GNU-PSPP software (v. GNU PSPP ver. 1.6.2-g78a33a) for OC Linux Mate 10.10. The Shapiro–Wilk normality test, Pearson correlation coefficients, and analysis of variance (ANOVA) with Bonferroni correction for the small number of independent samples were used. The Student's t-test was used for paired samples with normal distribution. The same degree of freedom was used for all calculations, the significance level was set as $\alpha < 0.05$.

RESULTS

Changes in frequency characteristics of EEG signal recorded over the main speech centers

The results of rhythmic activity localization over the areas of the main speech centers identified by spatial fixation of the EEG electrodes' position matched the characteristics of anatomic lesion, patient's diagnosis and MRI findings (Table 1). An EEG test involving the use of the technology for extraction of individual EEG microstates combined with the EEG inverse problem solution showed that it was impossible to record rhythmic phenomena over the affected areas of individuals with severe anatomical defects since the area's neural network was disrupted, and the rhythmic phenomena, specifically those recorded in slow activity ranges, were reduced by the tissues surrounding the primary focus. At the same time, in cases of the dominant hemisphere Broca's area (areas 44,

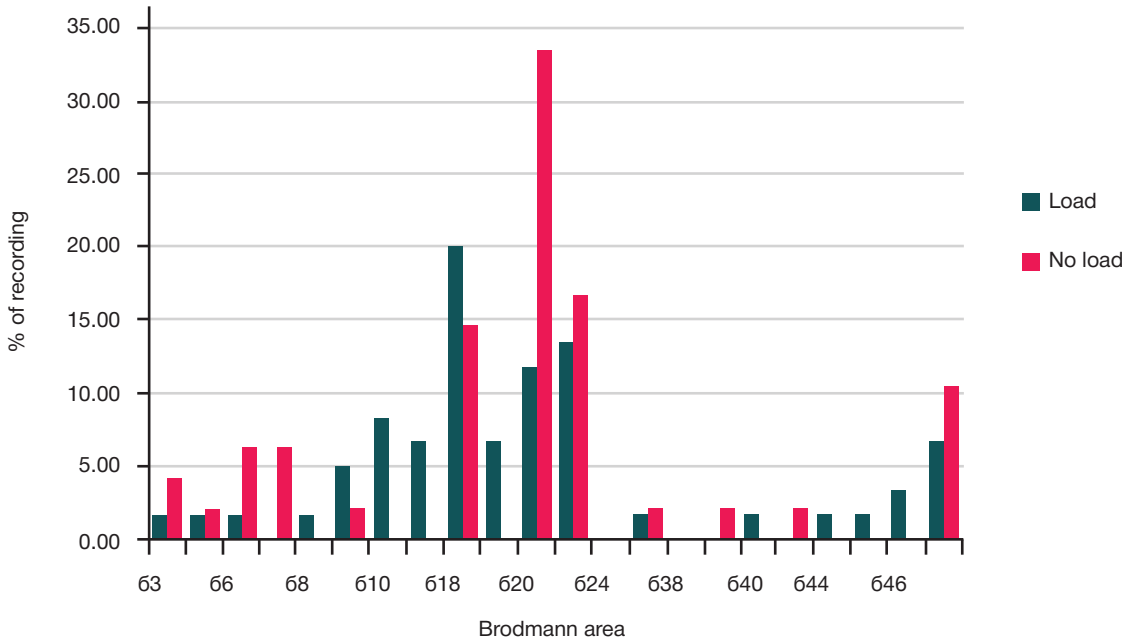

Fig. 1. Histogram of EEG activity (in %) over individual Brodmann areas in cases of motor aphasic disorder variant predominance, $p < 0.05$ (Pearson's test)

Table 3. Changes in the characteristics of EEG microstates relative to their frequency of occurrence per 1 s

Major syndrome	Class/test	A	B	C	D	I	II
Motor	Load	3,2	3,4	1,9	1	2,4	3,3
	No load	2,3	1,9	3	3	4,4	3,1
	p	**	**	**	**	**	**
Sensory	Load	4,3	4,7	1	5,8	4,3	2,3
	No load	30,2	15,7	19,6	18,6	30,2	20,8
	p	*	*	*	*	*	*
Total (mixed)	Load	2,5	1,8	2,2	1,3	2,8	5,3
	No load	36,8	46,7	50,3	44,5	33,8	26,5
	p	*	**	*	**	*	**

Note: *t*-test, * — $p < 0.05$; ** — $p > 0.05$.

45) anatomical disruption, the expected changes in rhythmic activity were recorded over the intact hemisphere prefrontal cortical structures. Such activity was observed in the same frequency range (17–24 Hz); it showed signs of activation response to auditory-speech load (Fig. 1). However, as stated above, it was almost diffuse and arouse in all structures of the intact hemisphere prefrontal cortex (areas 8, 9, 10, 11, 12, 13, 14, 24, 25, 32, 44, 45, 46 и 47).

A lesion in the Wernicke's area (Fig. 2) and disruption of sensory areas (39, 40) made it impossible to identify rhythmic phenomena over the Wernicke's area, which was expected due to neural network disruption in this area, and the intact hemisphere structures. Rhythmic EEG phenomena were recorded over the Broca's area only, however, there was no activation response to speech-auditory load.

In individuals with the total (mixed) variant of impairment (Fig. 3), rhythmic phenomena arose in the affected hemisphere over both Broca's and Wernicke's areas, but these findings had low significance (ANOVA test > 0.05), which suggested incomplete injury of both major speech centers. However, low significance resulted probably from limitations of both applied technique and relatively low number of observations.

Charasteristics of distinct EEG microstates

Analysis of the EEG microstate characteristics under auditory-speech load allowed us to find out that these characteristics showed significant differences ($p < 0.05$) in their contributions to overall scalp potential (except for classes B and D) in individuals with predominant motor aphasia. At the same time, in individuals with sensory aphasia, this indicator, by contrast, showed a significant response to the load. In individuals with total aphasia, significant differences were reported for class C only (Tables 2–4), which was considered as a sign of both structural damage to certain neuronal assemblies and information processing disorder prevailing in cases of sensory aphasia.

There were no significant responses to the loading test in terms of occurrence and duration of individual EEG microstates in individuals with motor impairment, however, individuals with prevailing sensory or total impairment showed significant changes of these characteristics, especially in cases of sensory impairment (for almost all indentified classes) and cases of total impairment (for classes A and I).

DISCUSSION

Interpretation of the data obtained needs to be further discussed. Thus, splitting the entire continuous EEG recording into a sequence of individual EEG microstates allows the researcher not only to consider common characteristics of total postsynaptic activity, but also to indentify distinct components of such activity associated with the activity of individual neural structures, thereby making it possible to create an affordable

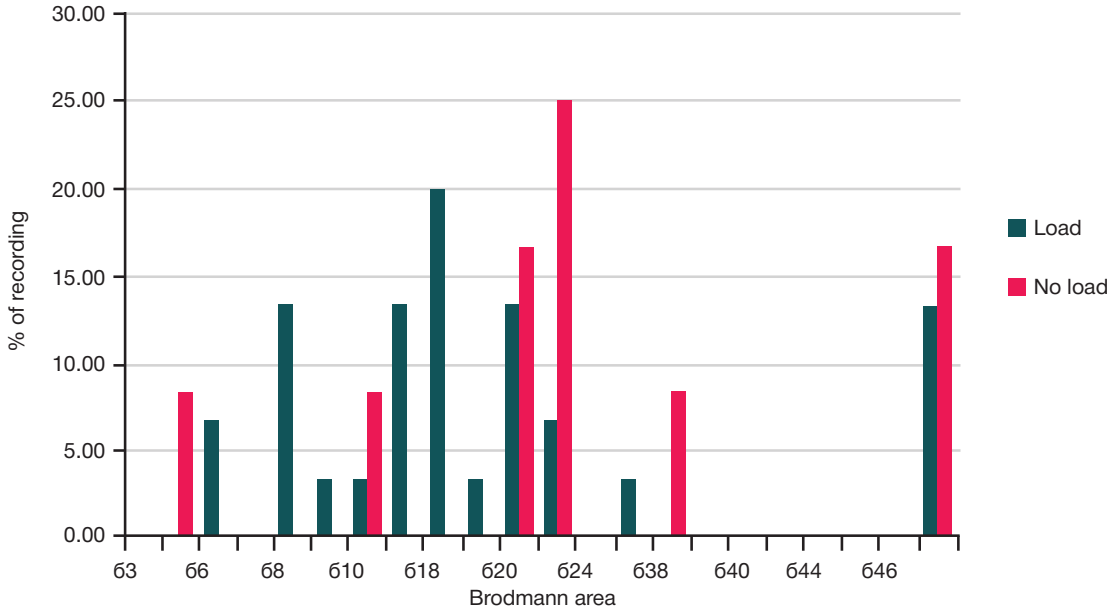

Fig. 2. Histogram of EEG activity (in %) over individual Brodmann areas in cases of sensory aphasic disorder variant predominance, $p < 0.05$ (Pearson's test)

Table 4. Changes in the characteristics of EEG microstates relative to their duration in 1 s

Major syndrome	Class/test	A	B	C	D	I	II
Motor	Load	0,04	0,06	0,02	0,05	0,06	0,07
	No load	0,05	0,04	0,03	0,05	0,04	0,07
	p	**	**	**	**	**	**
Sensory	Load	0,05	0,06	0,04	0,04	0,03	0,04
	No load	0,01	0,01	0,01	0,01	0,01	0,01
	p	**	*	**	*	**	**
Total (mixed)	Load	0,06	0,08	0,05	0,04	0,03	0,1
	No load	0,02	0,01	0,02	0,01	0,01	0,02
	p	*	*	**	**	*	**

Note: *t*-test, * — $p < 0.05$; ** — $p > 0.05$.

system for neurophysiological diagnosis of certain brain functions, particularly speech [26].

The study results obtained by conducting the functional loading test involving listening for different variants of aphasia show differences in both nature of rhythmic phenomena recorded on the scalp surface and spatial localization of these phenomena, which can be interpreted from the perspective of consistent various neural networks' participation in the speech function realization [13].

The development of speech impairment resulting from cerebral stroke is due to both infarction affecting various brain structures [7] and functional rearrangement of the neural networks system, which is reflected by changes in the EEG microstate characteristics [14] that may become the key factors to assess objectively the speech functional state and the changes in speech function resulting from the disorder. In our study this was confirmed by changes in characteristics of individual EEG microstates.

Thus, in cases of predominant motor impairment (preserved auditory information receipt systems), was observed the transfer of the speech production function to the intact hemisphere prefrontal cortex. But this answer was presented as the general response observed over the entire surface of the prefrontal cortex, not only within the limits of the well-formed neural centers (44, 45 Brodman's fields).

In sensory variant of aphasia, the changes in bioelectrical activity showed no variants of transferring the affected function to the contralateral (intact) hemisphere, which was manifested in identification of non-specific rhythmic phenomena, and demonstrated disruption of the sequence of class C and D EEG microstates that was considered to be associated with the structures responsible for tertiary information processing in tertiary areas (Brodmann's areas 6 and 7) [24, 27]. That is why sensory variant of aphasia could be characterized not only as profound impairment of certain brain networks' activity, but also as a more severe damage to the entire connectome system affecting both ventral stream responsible for information acquisition and the lateral one responsible for processing and comprehension. However, total variants of aphasia were associated with the less pronounced changes; the EEG microstate analysis revealed predominant involvement of the speech ventral stream structures and preserved tertiary structures responsible for constructive analysis [28].

In all cases of aphasia, the most interesting was the activity increase over the Brodmann areas 47 and, consequently, 37, showing maximum representation in individuals with predominant sensory aphasia. Their activity suggests involvement of phylogenetically older mechanisms underlying auditory tone perception that are found in children aged 2–5 and apes. This leads to the assumption that conventional system of phonemes and morphemes, the speech function can be replaced by the system of auditory tone perception and musical tone (onomatopoetic) reproduction, as reported in the number of studies focused on rehabilitation of feral

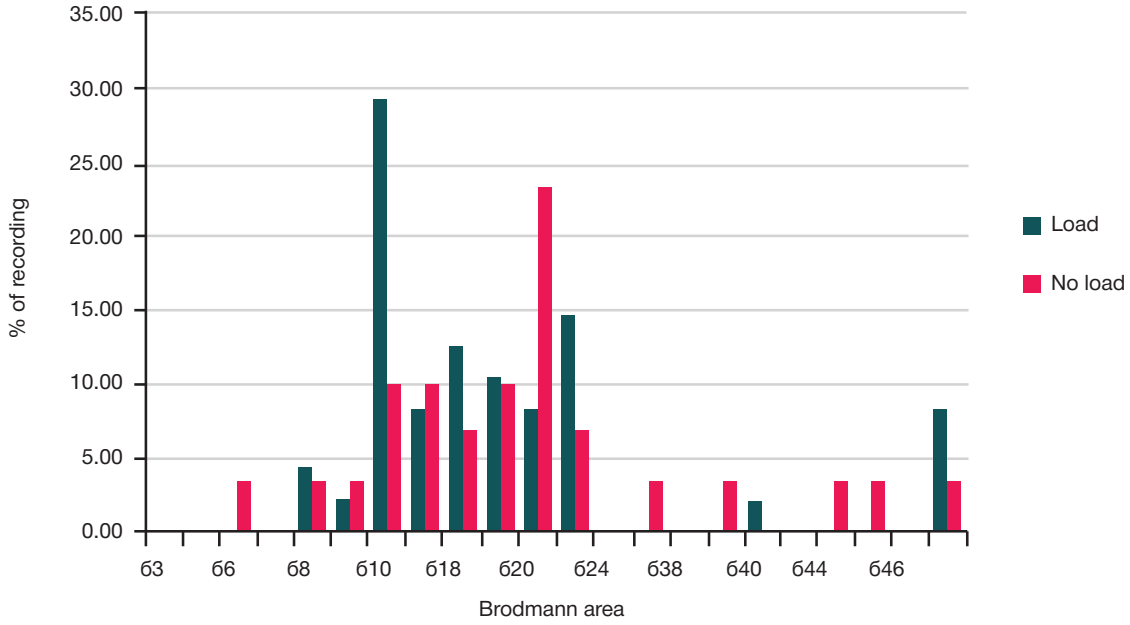

Fig. 3. Histogram of EEG activity (in %) in cases of total (mixed) aphasic disorder variant predominance, $p < 0.05$ (Pearson's test)

children and children with autism spectrum disorders, who failed to develop a normal human speech system [29, 30].

Limitations of the study

The study limitations are related to a relatively small number of observations (27 individuals) forcing us to adjust statistical data when performing calculations, as well as to the features of EEG technique applied associated with the scalp electrode positioning. The use of the medium-density EEG montage (10–10 system) did not put any meaningful restrictions relative to the 10–5 system or any other high-density EEG system, since it enabled acquisition of native data with the lower number of nonspecific physical artifacts occurring in high-density systems due to short interelectrode distances.

CONCLUSIONS

The study has shown that recording of the brain bioelectrical activity using modern computing power and mathematical methods optimization allows one to record individual bioelectrical phenomena closely related to the distinct brain structures' responses to the presented functional load. This opens up new prospects for creating diagnostic systems to study functional links between distinct higher nervous functions. Today, affordability is one of the benefits of the proposed method, since modern digital EEG does not require expensive equipment or maintenance provided by special repair and engineering units. Furthermore, it is not demanding to housing conditions, which enables its wide introduction in both research centers and medical institutions providing treatment and rehabilitation services to the population. The proposed brain bioelectrical activity processing system can provide the basis for the development of new diagnostic systems for human thought processes assessment, thereby allowing to expand the human body capabilities in the context of growing perceived information amount, as well as to provide new approaches to rehabilitation of higher nervous functions impaired due to the disease.

References

1. Broca P. Remarks on the Seat of Spoken Language, Followed by a Case of Aphasia (1861). Neuropsychology Review. 2011; 21 (3) 15: 227–9. Available from: https://doi.org/ 10.1007/s11065-011-9174-x.
2. Wernicke C. Grundriss der Psychiatrie in klinischen Vorlesungen. Theil II, Die paranoischen Zustände. Leipzig: Verlag von Georg Thieme. American Journal of Psychiatry.1897; 53 (4): 581–3. Available from: https://doi.org/ 10.1176/ajp.53.4.581.
3. Mishkin M Ungerleider LG Contribution of striate inputs to the visuospatial functions of parieto-preoccipital cortex in monkeys. Behav Brain Res. 1982; 6 (1): 57–77. Available from: https://doi.org/10.1016/0166-4328(82)90081-x.
4. Sul B, Kim JS, Hong BY, Lee KB, Hwang WS, Kim YK, et al. The Prognosis and Recovery of Aphasia Related to Stroke Lesion. Ann Rehabil Med. 2016; 40 (5): 786–93. Available from: https://doi.org/ 10.5535/arm.2016.40.5.786.
5. Harvey DY, Podell J, Turkeltaub PE, Faseyitan O, Coslett HB, Hamilton RH. Functional Reorganization of Right Prefrontal Cortex Underlies Sustained Naming Improvements in Chronic Aphasia via Repetitive Transcranial Magnetic Stimulation. Cogn Behav Neurol. 2017; 30 (4): 133–44. Available from: https://doi.org/ 10.1097/WNN.0000000000000141.
6. Lefaucheur JP, Antal A, Ayache SS, Benninger DH, Brunelin J, Cogiamanian F, et al. Evidence-based guidelines on the therapeutic use of transcranial direct current stimulation (tDCS). Clin Neurophysiol. 2017; 128 (1): 56–92. Available from: https://doi.org/ 10.1016/j.clinph.2016.10.087.
7. Lefaucheur JP, Aleman A, Baeken C, Benninger DH, Brunelin J, Di Lazzaro V, et al. Evidence-based guidelines on the therapeutic use of repetitive transcranial magnetic stimulation (rTMS): An update (2014–2018). Clin Neurophysiol. 2020; 131 (2): 474–528. Available from: https://doi.org/ 10.1016/j.clinph.2019.11.002.
8. Penfield W, Roberts L. Speech and Brain Mechanisms Princeton University Press, 2014, 302 p. Available from: https://doi.org/10.1515/9781400854677.192.
9. Michel CM, Koenig T. EEG microstates as a tool for studying the temporal dynamics of whole-brain neuronal networks: A review. Neuroimage. 2018; 180 (Pt B): 577–93. Available from: https://doi.org/ 10.1016/j.neuroimage.2017.11.062.
10. Mishra A, Englitz B, Cohen MX. EEG microstates as a continuous phenomenon. Neuroimage. 2020; 208: 116454. Available from: https://doi.org/ 10.1016/j.neuroimage.2019.116454. Epub 2019 Dec 10.
11. Milz P, Faber PL, Lehmann D, Koenig T, Kochi K, Pascual-Marqui RD. The functional significance of EEG microstates--Associations with modalities of thinking. Neuroimage. 2016; 125: 643–56. Available from: https://doi.org/ 10.1016/j.neuroimage.2015.08.023.
12. Milz P, Pascual-Marqui RD, Lehmann D, Faber PL. Modalities of Thinking: State and Trait Effects on Cross-Frequency Functional Independent Brain Networks. Brain Topogr. 2016; 29 (3): 477–90. Available from: https://doi.org/ 10.1007/s10548-016-0469-3.
13. Seitzman BA, Abell M, Bartley SC, Erickson MA, Bolbecker AR, Hetrick WP. Cognitive manipulation of brain electric microstates. Neuroimage. 2017; 146: 533–43. Available from: https://doi.org/ 10.1016/j.neuroimage.2016.10.002.
14. Croce P, Quercia A, Costa S, Zappasodi F. EEG microstates associated with intra- and inter-subject alpha variability. Sci Rep. 2020; 10 (1): 2469. Available from: https://doi.org/ 10.1038/s41598-020-58787-w.
15. Poskanzer C, Denis D, Herrick A, Stickgold R. Using EEG microstates to examine post-encoding quiet rest and subsequent word-pair memory. Neurobiol Learn Mem. 2021; 181: 107424. Available from: https://doi.org/ 10.1016/j.nlm.2021.107424.
16. Pascual-Marqui RD, Esslen M, Kochi K, Lehmann D. Functional imaging with low-resolution brain electromagnetic tomography (LORETA): a review. Methods Find Exp Clin Pharmacol. 2002; 24 Suppl C: 91–5. PMID: 12575492.
17. Grech R, Cassar T, Muscat J, Camilleri KP, Fabri SG, Zervakis M, et al. Review on solving the inverse problem in EEG source analysis. J Neuroeng Rehabil. 2008; 5: 25. Available from: https://doi.org/ 10.1186/1743-0003-5-25.
18. Neuner I, Arrubla J, Werner CJ, Hitz K, Boers F, Kawohl W, et al. The default mode network and EEG regional spectral power: a simultaneous fMRI-EEG study. PLoS One. 2014; 9 (2): e88214. Available from: https://doi.org/ 10.1371/journal.pone.0088214.
19. Whittingstall K, Bartels A, Singh V, Kwon S, Logothetis NK. Integration of EEG source imaging and fMRI during continuous viewing of natural movies. Magn Reson Imaging. 2010; 28 (8): 1135–42. Available from: https://doi.org/ 10.1016/j.mri.2010.03.042.
20. Abreu R, Soares JF, Lima AC, Sousa L, Batista S, Castelo-Branco M, et al. Optimizing EEG Source Reconstruction with Concurrent fMRI-Derived Spatial Priors. Brain Topogr. 2022; 35 (3): 282–301. Available from: https://doi.org/ 10.1007/s10548-022-00891-3. Epub 2022 Feb 10.
21. Thatcher RW, North DM, Biver CJ. LORETA EEG phase reset of the default mode network. Front Hum Neurosci. 2014; 8: 529. Available from: https://doi.org/ 10.3389/fnhum.2014.00529.
22. Gulyaev SA. EEG Microstate Analysis and the EEG Inverse Problem

Solution as a Tool for Diagnosing Cognitive Dysfunctions in Individuals Who Have Had a Mild Form of COVID-19. Hum Physiol. 2022; 48 (5): 587–597. DOI: 10.1134/S0362119722600217. Epub 2022 Oct 13. PMID: 36258795; PMCID: PMC9559548.
23. Gulyaev SA. Neurophysiological Solution of the Inverse Problem of EEG Research at Rest and under Conditions of Auditory-Speech Load. J Evol Biochem Phys. 2022; 58: 585–97. Available from: https://doi.org/10.1134/S0022093022020259
24. Johnson F, Beeke S, Best W. Searching for active ingredients in rehabilitation: applying the taxonomy of behaviour change techniques to a conversation therapy for aphasia. Disabil Rehabil. 2021; 43 (18): 2550–60. Available from: https://doi.org/ 10.1080/09638288.2019.1703147.
25. Sarter M, Fritschy JM. Reporting statistical methods and statistical results in EJN. Eur J Neurosci. 2008; 28 (12): 2363–4. Available from: https://doi.org/10.1111/j.1460-9568.2008.06581.x.
26. Gulyaev SA, Lelyuk VG. Neurophysiological isolation of individual rhythmic brain activity arising from auditory-speech load. Brain Netw Modul. 2023; 2 (2): 47–52. Available from: https://doi.org/ 10.4103/2773-2398.379340.
27. Seitzman BA, Abell M, Bartley SC, Erickson MA, Bolbecker AR, Hetrick WP. Cognitive manipulation of brain electric microstates. Neuroimage. 2017; 146: 533–43. Available from: https://doi.org/ 10.1016/j.neuroimage.2016.10.002. Epub 2016 Oct 11.
28. Poskanzer C, Denis D, Herrick A, Stickgold R. Using EEG microstates to examine post-encoding quiet rest and subsequent word-pair memory. Neurobiol Learn Mem. 2021; 181: 107424. Available from: https://doi.org/ 10.1016/j.nlm.2021.107424. Epub 2021 Mar 22.
29. Zuk NJ, Murphy JW, Reilly RB, Lalor EC. Envelope reconstruction of speech and music highlights stronger tracking of speech at low frequencies. PLoS Comput Biol. 2021; 17 (9): e1009358. Available from: https://doi.org/ 10.1371/journal.pcbi.1009358.
30. Schoen SA, Lane SJ, Mailloux Z, May-Benson T, Parham LD, Smith Roley S, et al. A systematic review of ayres sensory integration intervention for children with autism. Autism Res. 2019; 12 (1): 6–19. DOI: 10.1002/aur.2046. Epub 2018 Dec 12. PMID: 30548827; PMCID: PMC6590432.

Литература

1. Broca P. Remarks on the Seat of Spoken Language, Followed by a Case of Aphasia (1861). Neuropsychology Review. 2011; 21 (3) 15: 227–9. Available from: https://doi.org/ 10.1007/s11065-011-9174-x.
2. Wernicke C. Grundriss der Psychiatrie in klinischen Vorlesungen. Theil II, Die paranoischen Zustände. Leipzig: Verlag von Georg Thieme. American Journal of Psychiatry.1897; 53 (4): 581–3. Available from: https://doi.org/ 10.1176/ajp.53.4.581.
3. Mishkin M Ungerleider LG Contribution of striate inputs to the visuospatial functions of parieto-preoccipital cortex in monkeys. Behav Brain Res. 1982; 6 (1): 57–77. Available from: https://doi.org/10.1016/0166-4328(82)90081-x.
4. Sul B, Kim JS, Hong BY, Lee KB, Hwang WS, Kim YK, et al. The Prognosis and Recovery of Aphasia Related to Stroke Lesion. Ann Rehabil Med. 2016; 40 (5): 786–93. Available from: https://doi.org/ 10.5535/arm.2016.40.5.786.
5. Harvey DY, Podell J, Turkeltaub PE, Faseyitan O, Coslett HB, Hamilton RH. Functional Reorganization of Right Prefrontal Cortex Underlies Sustained Naming Improvements in Chronic Aphasia via Repetitive Transcranial Magnetic Stimulation. Cogn Behav Neurol. 2017; 30 (4): 133–44. Available from: https://doi.org/ 10.1097/WNN.0000000000000141.
6. Lefaucheur JP, Antal A, Ayache SS, Benninger DH, Brunelin J, Cogiamanian F, et al. Evidence-based guidelines on the therapeutic use of transcranial direct current stimulation (tDCS). Clin Neurophysiol. 2017; 128 (1): 56–92. Available from: https://doi.org/ 10.1016/j.clinph.2016.10.087.
7. Lefaucheur JP, Aleman A, Baeken C, Benninger DH, Brunelin J, Di Lazzaro V, et al. Evidence-based guidelines on the therapeutic use of repetitive transcranial magnetic stimulation (rTMS): An update (2014–2018). Clin Neurophysiol. 2020; 131 (2): 474–528. Available from: https://doi.org/ 10.1016/j.clinph.2019.11.002.
8. Пенфильд В., Робертс Л. Речь и мозговые механизмы. М.: Медицина, 1964; 260 с.
9. Michel CM, Koenig T. EEG microstates as a tool for studying the temporal dynamics of whole-brain neuronal networks: A review. Neuroimage. 2018; 180 (Pt B): 577–93. Available from: https://doi.org/ 10.1016/j.neuroimage.2017.11.062.
10. Mishra A, Englitz B, Cohen MX. EEG microstates as a continuous phenomenon. Neuroimage. 2020; 208: 116454. Available from: https://doi.org/ 10.1016/j.neuroimage.2019.116454. Epub 2019 Dec 10.
11. Milz P, Faber PL, Lehmann D, Koenig T, Kochi K, Pascual-Marqui RD. The functional significance of EEG microstates--Associations with modalities of thinking. Neuroimage. 2016; 125: 643–56. Available from: https://doi.org/ 10.1016/j.neuroimage.2015.08.023.
12. Milz P, Pascual-Marqui RD, Lehmann D, Faber PL. Modalities of Thinking: State and Trait Effects on Cross-Frequency Functional Independent Brain Networks. Brain Topogr. 2016; 29 (3): 477–90. Available from: https://doi.org/ 10.1007/s10548-016-0469-3.
13. Seitzman BA, Abell M, Bartley SC, Erickson MA, Bolbecker AR, Hetrick WP. Cognitive manipulation of brain electric microstates. Neuroimage. 2017; 146: 533–43. Available from: https://doi.org/ 10.1016/j.neuroimage.2016.10.002.
14. Croce P, Quercia A, Costa S, Zappasodi F. EEG microstates associated with intra- and inter-subject alpha variability. Sci Rep. 2020; 10 (1): 2469. Available from: https://doi.org/ 10.1038/s41598-020-58787-w.
15. Poskanzer C, Denis D, Herrick A, Stickgold R. Using EEG microstates to examine post-encoding quiet rest and subsequent word-pair memory. Neurobiol Learn Mem. 2021; 181: 107424. Available from: https://doi.org/ 10.1016/j.nlm.2021.107424.
16. Pascual-Marqui RD, Esslen M, Kochi K, Lehmann D. Functional imaging with low-resolution brain electromagnetic tomography (LORETA): a review. Methods Find Exp Clin Pharmacol. 2002; 24 Suppl C: 91–5. PMID: 12575492.
17. Grech R, Cassar T, Muscat J, Camilleri KP, Fabri SG, Zervakis M, et al. Review on solving the inverse problem in EEG source analysis. J Neuroeng Rehabil. 2008; 5: 25. Available from: https://doi.org/ 10.1186/1743-0003-5-25.
18. Neuner I, Arrubla J, Werner CJ, Hitz K, Boers F, Kawohl W, et al. The default mode network and EEG regional spectral power: a simultaneous fMRI-EEG study. PLoS One. 2014; 9 (2): e88214. Available from: https://doi.org/ 10.1371/journal.pone.0088214.
19. Whittingstall K, Bartels A, Singh V, Kwon S, Logothetis NK. Integration of EEG source imaging and fMRI during continuous viewing of natural movies. Magn Reson Imaging. 2010; 28 (8): 1135–42. Available from: https://doi.org/ 10.1016/j.mri.2010.03.042.
20. Abreu R, Soares JF, Lima AC, Sousa L, Batista S, Castelo-Branco M, et al. Optimizing EEG Source Reconstruction with Concurrent fMRI-Derived Spatial Priors. Brain Topogr. 2022; 35 (3): 282–301. Available from: https://doi.org/ 10.1007/s10548-022-00891-3. Epub 2022 Feb 10.
21. Thatcher RW, North DM, Biver CJ. LORETA EEG phase reset of the default mode network. Front Hum Neurosci. 2014; 8: 529. Available from: https://doi.org/ 10.3389/fnhum.2014.00529.
22. Gulyaev SA. EEG Microstate Analysis and the EEG Inverse Problem Solution as a Tool for Diagnosing Cognitive Dysfunctions in Individuals Who Have Had a Mild Form of COVID-19. Hum Physiol. 2022; 48 (5): 587–597. DOI: 10.1134/S0362119722600217. Epub 2022 Oct 13. PMID: 36258795; PMCID: PMC9559548.
23. Gulyaev SA. Neurophysiological Solution of the Inverse Problem of EEG Research at Rest and under Conditions of Auditory-Speech Load. J Evol Biochem Phys. 2022; 58: 585–97. Available from: https://doi.org/10.1134/S0022093022020259
24. Johnson F, Beeke S, Best W. Searching for active ingredients in rehabilitation: applying the taxonomy of behaviour change

techniques to a conversation therapy for aphasia. Disabil Rehabil. 2021; 43 (18): 2550–60. Available from: https://doi.org/10.1080/09638288.2019.1703147.

25. Sarter M, Fritschy JM. Reporting statistical methods and statistical results in EJN. Eur J Neurosci. 2008; 28 (12): 2363–4. Available from: https://doi.org/10.1111/j.1460-9568.2008.06581.x.
26. Gulyaev SA, Lelyuk VG. Neurophysiological isolation of individual rhythmic brain activity arising from auditory-speech load. Brain Netw Modul. 2023; 2 (2): 47–52. Available from: https://doi.org/10.4103/2773-2398.379340.
27. Seitzman BA, Abell M, Bartley SC, Erickson MA, Bolbecker AR, Hetrick WP. Cognitive manipulation of brain electric microstates. Neuroimage. 2017; 146: 533–43. Available from: https://doi.org/10.1016/j.neuroimage.2016.10.002. Epub 2016 Oct 11.
28. Poskanzer C, Denis D, Herrick A, Stickgold R. Using EEG microstates to examine post-encoding quiet rest and subsequent word-pair memory. Neurobiol Learn Mem. 2021; 181: 107424. Available from: https://doi.org/ 10.1016/j.nlm.2021.107424. Epub 2021 Mar 22.
29. Zuk NJ, Murphy JW, Reilly RB, Lalor EC. Envelope reconstruction of speech and music highlights stronger tracking of speech at low frequencies. PLoS Comput Biol. 2021; 17 (9): e1009358. Available from: https://doi.org/ 10.1371/journal.pcbi.1009358.
30. Schoen SA, Lane SJ, Mailloux Z, May-Benson T, Parham LD, Smith Roley S, et al. A systematic review of ayres sensory integration intervention for children with autism. Autism Res. 2019; 12 (1): 6–19. DOI: 10.1002/aur.2046. Epub 2018 Dec 12. PMID: 30548827; PMCID: PMC6590432.

ESTIMATION OF MUTAGENIC POTENTIAL OF THE VALPROIC ACID DERIVATIVE CONTAINING A TERTIARY AMINO GROUP

Zolotoverkhaja EA ✉, Kubarskaya LG, Bespalov AYa, Melekhova AS

Golikov Research Clinical Center of Toxicology of Federal Medical and Biological Agency, Saint-Petersburg, Russia

The model of severe poisoning with acetylcholinesterase inhibitors has shown the possibility of drug treatment of toxic effects with valproic acid containing a tertiary amino group. The study was aimed to assess potential mutagenic effects of the valproic acid derivative containing a tertiary amino group when studing its safety. Testing for toxicophores and assessment of the mutagenic effect probability were perfomed using the QSAR Toolbox offline software (v4.5 SP1). The Ames test with and without metabolic activation was used to estimate mutagenic potential of valproic acid containing a tertiary amino group *in vitro*. The computer prediction results predicted that the test substance would show no mutagenic effects in the Ames test. These data were confirmed by the *in vitro* Ames test for a broad range of concentrations of valproic acid containing a tertiary amino group (0.02–5.0 mg/mL). The concentrations of valproic acid containing a tertiary amino group exceeding 1.58 mg/mL have a bacteriostatic effect on the TA 100 *S. typhimurium* strain and the WP2 uvr A pKM 101c *E. coli* strain. Thus, the valproic acid derivative containing a tertiary amino group possesses no mutagenic effect, it can be recommended for further preclinical trials of therapeutic efficacy and safety.

Keywords: valproic acid, acetylcholinesterase inhibitors, computer prediction, mutagenicity, Ames test, anticholinergics

Funding: the study was performed as part of the State Assignment “Assessment of Effiacy and Safety of the Valproic Acid Amino Ester Substance as an Agent for Drug Treatment of the Toxin-Induced Seizures”, R&D project № 121041500281-1.

Author contribution: Zolotoverkhaja EA — study planning, *in silico* analysis, statistical analysis and data interpretation, manuscript writing; Kubarskaya LG — *in vitro* experiments, data acquisition and analysis; Bespalov AYa — synthesis of the test compound, data interpretation, manuscript editing; Melekhova AS — manuscript editing, preparing supportive documents for publishing.

Compliance with ethical standards: the study was performed *in silico* and *in vitro*, no approval by the Ethics Committee was required.

✉ **Correspondence should be addressed:** Ekaterina A. Zolotoverkhaja
Bekhtereva, 1, Saint-Petersburg, 192019, Russia; e.zolotoverkhaja@yandex.ru

Received: 20.06.2023 **Accepted:** 23.08.2023 **Published online:** 15.09.2023

DOI: 10.47183/mes.2023.027

ОЦЕНКА МУТАГЕННОГО ПОТЕНЦИАЛА ПРОИЗВОДНОГО ВАЛЬПРОЕВОЙ КИСЛОТЫ С ТРЕТИЧНОЙ АМИНОГРУППОЙ

Е. А. Золотоверхая ✉, Л. Г. Кубарская, А. Я. Беспалов, А. С. Мелехова

Научно-клинический центр токсикологии имени С. Н. Голикова Федерального медико-биологического агентства, Санкт-Петербург, Россия

Моделирование тяжелого отравления ингибиторами ацетилхолинэстеразы показало возможность фармакологической терапии токсических проявлений препаратом вальпроевой кислоты с третичной аминогруппой. Целью работы было исследовать потенциальную мутагенную активность вальпроевой кислоты с третичной аминогруппой в рамках изучения ее безопасности. Анализ наличия токсикофоров и оценку вероятности проявления мутагенности выполняли с использованием автономного программного обеспечения QSAR Toolbox (v4.5 SP1). Для оценки мутагенного потенциала вальпроевой кислоты с третичной аминогруппой *in vitro* использовали тест Эймса с метаболической активацией и без. Результаты компьютерного прогнозирования предсказали отсутствие мутагенного действия изучаемой субстанции в тесте Эймса. Данные были подтверждены в тесте Эймса *in vitro* для широкого диапазона концентраций вальпроевой кислоты с третичной аминогруппой (0,02–5,0 мг/мл). В концентрации выше 1,58 мг/мл вальпроевая кислота с третичной аминогруппой обладает бактериостатическим действием на штаммы *S. typhimurium* TA 100 и *E. coli* WP2 uvr A pKM 101. Таким образом, производное вальпроевой кислоты с третичной аминогруппой не обладает потенциальным мутагенным действием, его можно рекомендовать для дальнейшего исследования терапевтической эффективности и безопасности в доклинических исследованиях.

Ключевые слова: вальпроевая кислота, ингибиторы ацетилхолинэстеразы, компьютерное прогнозирование, мутагенность, тест Эймса, холиноблокаторы

Финансирование: работа выполнена в рамках государственного задания НИР «Изучение эффективности и безопасности субстанции аминоэфира вальпроевой кислоты как лекарственного препарата фармакотерапии токсического судорожного синдрома», номер НИОКТР 121041500281-1.

Вклад авторов: Е. А. Золотоверхая — планирование исследования, проведение анализа *in silico*, статистическая обработка и интерпретация данных, подготовка рукописи; Л. Г. Кубарская: проведение экспериментов *in vitro*, сбор и анализ данных; А. Я. Беспалов — синтез исследуемого вещества, интерпретация результатов исследования, редактирование статьи; А. С. Мелехова — редактирование статьи, подготовка сопроводительных документов для опубликования.

Соблюдение этических стандартов: исследование выполнено *in silico* и *in vitro* на бактериальных штаммах, одобрение этического комитета не требуется.

✉ **Для корреспонденции:** Екатерина Андреевна Золотоверхая
ул. Бехтерева, д. 1, г. Санкт-Петербург, 192019, Россия; e.zolotoverkhaja@yandex.ru

Статья получена: 20.06.2023 **Статья принята к печати:** 23.08.2023 **Опубликована онлайн:** 15.09.2023

DOI: 10.47183/mes.2023.027

Organophosphorus compounds and carbamates are the commonly used insecticides that inhibit cholinesterase activity, causing acute muscarinic toxicity symptoms and some symptoms of nicotine-like toxicity [1]. Furthermore, reversible acetylcholinesterase inhibitors are more and more often used for pharmacological support of patients with neurodegenerative diseases [2, 3]. The increasing adoption of acetylcholinesterase inhibitors as insecticides and pharmacological agents increases the risk of household and industrial poisoning requiring immediate medical intervention. When the levels of exposure are high, cholinesterase inhibition quickly leads to accumulation of acetylcholine neurotransmitter, the endogenous ligand of muscarinic and nicotinic receptors [4]. The sudden and rapid increase in acetylcholine levels in synapses results in hyperstimulation of cholinergic receptors and the symptoms of cholinergic crisis. Atropine is most commonly

used as an antidote to poisoning, including poisoning with acetylcholinesterase inhibitors [5]. Insufficient protective effect of atropine associated with the lack of nicotinolytic effect, along with the risk of excessive atropinization during care provision, necessitates the need to develop drugs with minimum toxicity possessing central anticholinergic activity.

A neuromodulator drug, (1-methylpiperidin-4-yl)-2-propylpentanoate hydrochloride (valproic acid derivative containing a tertiary amino group), was synthesized in the Golikov Research Clinical Center of Toxicology of FMBA of Russia [6]. The rat models of severe carbamate poisoning showed diverse pharmacological effects of this drug, it had both anticholinergic and anticonvulsant effects [7].

At the initial stage of the study of the pharmacologically active compound toxic effects, the computer prediction methods are used in silico before conducting in vitro and in vivo experiments. Potential mutagenic activity should be assessed when studying the test substance safety. In case mutagenic potential of the new compound has been revealed, it is necessary to consider the presence of functional groups determining the toxic effects, along with the available experimental data on the compounds with similar structure [8]. For that the specially developed software is used that makes it possible to assess genotoxic potential of promising pharmacologically active compounds based on the analysis of structural similarity and the presence of toxicophores [9]. The Ames test is used for primary screening aimed to assess the new drugs' mutagenic potential in vitro [10].

The study was aimed to assess potential mutagenic effects of the valproic acid derivative containing a tertiary amino group using the in silico and in vitro tests.

METHODS

Research object

The research object was represented by (1-methylpiperidin-4-yl)-2-propylpentanoate hydrochloride (valproic acid derivative containing a tertiary amino group), synthesized in the Drug Synthesis Laboratory, Golikov Research Clinical Center of Toxicology of FMBA of Russia. An in silico study was performed using the following SMILES formula of the test compound: CCCC(CCC)C(=O)OC1CCN(C)CC1.

In silico mutagenicity assessment

Analysis of the structural fragments indicative of potential genotoxicity of the tertiary amino group-containing valproic acid derivative, identification of probable mechanisms underlying mutagenic effects, and estimation of the probability of mutagenic effects in the Ames test based on the available experimental data on the compounds with similar structure were performed using the QSAR Toolbox offline software (v4.5 SP1).

Bacterial reverse mutations in S. typhimurium TA 1535, TA 1537, TA 98, TA 100 with or without metabolic activation and E. coli WP2 uvr A pKM 101 with or without metabolic activation were considered to be the study endpoints.

The following profilers available for the selected endpoints were chosen as algorithms for identification of the studied compound specific features, i.e. for profiling: "DNA alert for Ames assay, chromosomal aberrations, and micronucleus test according to the protocol developed by the Laboratory of Mathematical Chemistry, Burgas, Bulgaria" ("DNA alert for AMES, CA, and MNT by OASIS"), "in vitro mutagenicity alert (for Ames test) according to the protocol developed by Istituto Superiore di Sanità (Rome, Italy)" ("*in vitro* mutagenicity alert (Ames) by ISS"), "DNA binding according to the protocol developed by the Organization for Economic Co-operation and Development" ("DNA binding by OECD"), and "DNA binding according to the protocol developed by the Laboratory of Mathematical Chemistry, Burgas, Bulgaria" ("DNA binding by OASIS").

The primary sample of chemical substances similar to the valproic acid derivative containing a tertiary amino group, which was based on structure, was compiled based on the presence of the following functional groups: branched alkane containing a tertiary carbon or tertiary amine or an ester derived from a carboxylic acid or tertiary aliphatic amine.

The categories were clarified based on the specific DNA binding mechanism determined for the valproic acid derivative containing a tertiary amino group in accordance with the algorithm "DNA alert for Ames assay, chromosomal aberrations, and micronucleus test according to the protocol developed by the Laboratory of Mathematical Chemistry, Burgas, Bulgaria (OASIS)" ("DNA alert for AMES, CA, and MNT by OASIS"). This algorithm considers probable genotoxicity (for example, genetic mutations in *in vivo* and *in vitro* tests, DNA damage and/or reparation, DNA and/or protein damage in the liver, chromosomal aberrations, transgenic rodent mutations) and carcinogenicity. Categorization by the substance structure was performed using the organic functional group profiler developed by the U.S. Environmental Protection Agency (US EPA).

Ames assay

The test was performed using the MPF™ Penta 1 kit (Xenometrix; Switzerland) containing all necessary microbiological media and supplements, appropriate bacterial strain, positive controls, components of the S9 rat liver microsomal fraction. Three repetitions were carried out for each concentration of the valproic acid derivative containing a tertiary amino group. The test variants involving metabolic activation of the system by the Aroclor 1254 induced rat liver homogenate S9 microsomal fraction with the NADP cofactor and glucose-6-phosphate or no activation by the S9 microsomal fraction were used.

The concentration range was selected using an overnight S. typhimurium TA98 culture to choose the test compound maximum concentration, at which no cytotoxic effects would be observed, as well as to estimate drug solubility in experimental conditions. Sterile water for injection was used as a solvent. The test concentrations used for preliminary testing were as follows: 0.01 mg/mL, 0.02 mg/mL, 0.05 mg/mL, 0.16 mg/mL, 0.50 mg/mL, 1.58 mg/mL, and 5.00 mg/mL. The signs of cytotoxicity were determined based on no bacterial growth at certain concentration of the test compound.

Data analysis

Significance of differences between binomial distributions in the Ames test was determined using the cumulative binomial [11, 12]. The cumulative binomial probability (B-value) exceeding 0.99 indicated that the study result was associated with mutagenic effects of the drug with the probability ≥ 99%. In addition to probability, we assessed the factor by which the number of revertant colonies exceeded the baseline. The baseline was calculated as a sum of the average number of spontaneous reversions (revertants in the negative control sample) and the standard deviation. When the number exceeded the baseline less than twice, the result was considered to be non-significant and was not considered as positive. When the concentration-dependent effect or the baseline value exceeded more than

Table 1. Results of testing the valproic acid amino ester containing a tertiary amino group using the Ames assay involving no activation by microsomal fraction (M ± SD)

Test substance	Concentration	Strains				
		TA98	TA100	TA1535	TA1537	*E. coli* Combo
Valproic acid amino ether	0.02 mg/mL	0.7 ± 0.6	5.7 ± 1.2	2.7 ± 1.5	0.0 ± 0.0	5.7 ± 2.0
	0.05 mg/mL	0.7 ± 0.6	5.3 ± 2.1	0.0 ± 0.0	1.7 ± 0.6	7.3 ± 0.6
	0.16 mg/mL	0.7 ± 0.6	7.7 ± 2.1	0.3 ± 0.6	1.0 ± 0.0	6.0 ± 1.0
	0.50 mg/mL	1.0 ± 0.0	5.3 ± 3.2	1.0 ± 1.0	1.0 ± 0.0	8.0 ± 2.0
	1.58 mg/mL	0.3 ± 0.6	4.3 ± 0.6	0.7 ± 1.2	1.7 ± 2.1	3.3 ± 1.2
	5.00 mg/mL	1.3 ± 2.3	1.7 ± 2.1#	0.0 ± 0.0	1.0 ± 1.0	0.0 ± 0.0#
Negative control	0	1.2 ± 1.2	7.6 ± 3.2	1.3 ± 1.2	1.6 ± 2.6	6.2 ± 3.9
Negative control baseline	–	2.4	10.8	2.5	4.2	10.1
Positive control for TA 98 strain	2.0 µg/mL	47.6 ± 1.1	–	–	–	–
Positive control for TA 100 strain	0.1 µg/mL	–	46.3 ± 2.5	–	–	–
Positive control for TA1535 strain	100 µg/mL	–	–	48.0 ± 0.0	–	–
Positive control for TA1537 strain	15 µg/mL	–	–	–	48.0 ± 0.0	–
Positive control for *E. coli* Combo strains	2.0 µg/mL	-	-	-	-	34.0 ± 3.7

Note: # — decrease in the level of spontaneous reversions (B-value ≤ 0.01)

twice was revealed, the test drug was classified as mutagen. The data considerably lower than the level of spontaneous reversions (B-value ≤ 0.01) can be indicative of the drug citotoxic effect.

RESULTS

In silico mutagenicity assessment

No experimental data of the studies of the valproic acid derivative containing a tertiary amino group were found in the databases used by the QSAR Toolbox (v4.5 SP1), the drug was assigned no CAS number.

Profiling based on nonspecific endpoints revealed no "in vitro mutagenicity alert (Ames) by ISS" and "DNA alert for AMES, CA, and MNT by OASIS" for the systems with and without metabolic activation. The use of general mechanistic approach based on the "DNA binding by OASIS" algorithm revealed no alerts, while the "DNA binding by OECD" algorithm alerted to probable mono-nucleophilic substitution reaction yielding the reactive iminium ion.

Initial sample of chemical substances similar to the test valproic acid derivative based on the "organic functional groups" criterion that were taken from the European Chemicals Agency database included 12,963 compounds. Among them 2,300 compounds had the data for the endpoint "assessment of bacterial reverse mutations in *S. typhimurium* TA 1535, TA 1537, TA 98, TA 100 showing or not showing metabolic activation" and 299 had the data for the endpoint "assessment of bacterial reverse mutations in *E. coli* WP2 uvr A pKM 101 showing or not showing metabolic activation".

Subsequent selection of analogues was based on the specific DNA binding mechanisms identified for the valproic acid derivative. Among analogues, for which experimental data were available, chemical substances were found showing both positive and negative results of the Ames assay involving *S. typhimurium* TA 1535, TA 1537, TA 98, TA 100 and *E. coli* WP2 uvr A pKM 101. Furthermore, the program warned that there were chemical substances different from the test substance in the database. In this regard the "DNA alert for AMES, CA, and MNT by OASIS", "organic functional groups" developed by the U.S. Environmental Protection Agency (US EPA) and "structural similarity" profilers were used to refine the database. As a result, 80 chemical compounds with similar structure and DNA binding type, for which experimental data of the Ames assay involving S. typhimurium TA 1535, TA 1537, TA 98, TA 100 were available, were selected, along with 33 chemical compounds with similar structure and DNA binding type, for which experimental data of the Ames assay involving *E. coli* WP2 uvr A pKM 101 with and without metabolic activation were available. None of the analogues showed mutagenic effects in the Ames test. In silico prediction based on the test results of five most close analogues with the significance level of 0.00412 predicted no mutagenic effects exerted by the valproic acid amino ester in the Ames test involving *S. typhimurium* TA 1535, TA 1537, TA 98, TA 100 and E. coli WP2 uvr A pKM 101 with and without metabolic activation.

Determining the substance concentration range of interest

The valproic acid derivative containing a tertiary amino group exerted no cytotoxic effects in the studied concentration range. All the studied concentrations remained soluble under the conditions of preliminary testing. That is why the Ames assay was performed in the concentration range of 0.02–5 mg/mL with a half an order increment (0.02 mg/mL, 0.05 mg/mL, 0.16 mg/mL, 0.50 mg/mL, 1.58 mg/mL, 5.00 mg/mL).

Results of the test without metabolic activation of the system

Table 1 provides the mean and standard deviation (M ± SD) for the number of wells with revertant colonies in a series of three iterations of 48 wells per each studied concentration of the valproic acid amino ester substance, positive and negative controls in the system without microsomal fraction activation.

Standard mutagens were used as positive controls: 2-nitrofluorene (2.0 µg/mL for the TA98 strain), 4-nitroquinoline-N-oxide (0.1 µg/mL for the TA100 strain), N4-aminocytidine (100 µg/mL for the TA1535 strain), 9-aminoacridine (15 µg/mL

Table 2. Results of testing the valproic acid amino ester containing a tertiary amino group using the Ames assay involving activation by S9 microsomal fraction (M ± SD)

Test substance	Concentration	Strains				
		TA98	TA100	TA1535	TA1537	*E. coli* Combo
Valproic acid amino ether	0.02 mg/mL	0.7 ± 0.6	8.7 ± 3.2	1.0 ± 0.0	1.3 ± 0.6	10.0 ± 1.0
	0.05 mg/mL	0.7 ± 1.2	8.0 ± 0.0	1.3 ± 1.2	1.7 ± 1.5	8.3 ± 1.5
	0.16 mg/mL	1.0 ± 1.0	10.0 ± 3.6	2.3 ± 2.3	0.7 ± 0.6	8.0 ± 3.0
	0.50 mg/mL	1.3 ± 1.2	13.0 ± 1.0	1.3 ± 0.6	2.7 ± 0.6	8.0 ± 0.0
	1.58 mg/mL	3.0 ± 2.0	17.3 ± 1.5	1.3 ± 0.6	0.7 ± 0.6	0.7 ± 0.6#
	5.00 mg/mL	0.0 ± 0.0	1.3 ± 0.6#	0.3 ± 0.6	0.7 ± 0.6	0.0 ± 0.0#
Negative control	0	1.0 ± 1.2	8.4 ± 2.6	1.5 ± 1.2	0.8 ± 0.8	7.2 ± 4.2
Negative control baseline	–	2.2	11.0	2.7	1.6	11.4
2-aminoanthracene	1.0 μg/mL	47.9 ± 0.5	–	–	–	–
2-aminoanthracene	2.5 μg/mL	–	48.0 ± 0.2	43.8 ± 3.1	41.3 ± 7.1	–
2-aminoanthracene	400 μg/mL	–	–	–	–	30.0 ± 8.1

Note: # — decrease in the level of spontaneous reversions (B-value ≤ 0.01)

for the TA1537 strain), 4-nitroquinoline-N-oxide (2.0 μg/mL for the wp2 uvrA and wp2 [pKM101] strains). These mutagens effectively induced reverse mutations in bacterial cells. The average number of the negative control revertant colonies for all strains did not exceed the maximum permissible value.

The findings showed that the valproic acid amino ester concentrations of 0.02 mg/mL, 0.05 mg/mL, 0.16 mg/mL, 0.5 mg/mL, 1.58 mg/mL, and 5.00 mg/mL did not induce mutations in the system without metabolic activation.

The decrease in the number of revertant colonies relative to the level of spontaneous reversions in the negative control sample of this strain and the number of revertant colonies at lower test substance concentrations was reported for the TA100 strain of *S. typhimurium* and the mixture of *E. coli* strains wp2 uvrA and wp2 [pKM101] (*E. coli* Combo) at the valproic acid amino ester concentration of 5.0 mg/mL in the system without metabolic activation. B-value was below 0.01, which could indicate that the valproic acid amino ester concentrations exceeding 5.0 had a bacteriostatic effect on these strains.

Results of the test with metabolic activation of the system by microsomal fraction (+S9)

Table 2 provides the mean for the number of revertant colonies and standard deviation (M ± SD) of three iterations per strain in the system with activation by the S9 microsomal fraction.

Various 2-aminoanthracene concentrations were used as positive controls for all strains. Testing of substances in the presence of S9 microsomal fraction showed that the average number of mutant colonies in the sections containing a positive control exceeded the minimum permissible value. The average number of colonies with reverse mutations in the sections containing a negative control did not exceed the maximum permissible value in the presence of S9 microsomal fraction.

The valproic acid amino ester did not induce mutations in the studied concentration range in the system with metabolic activation.

The decrease in the number of revertant colonies relative to the level of spontaneous reversions in the negative control sample of this strain and the number of revertant colonies at lower test substance concentrations was reported for the TA100 strain of S. typhimurium at the valproic acid amino ester concentration of 5.0 mg/mL and for the *E. coli* Combo mixture of strains at the valproic acid derivative concentrations of 1.58 mg/mL and 5.0 mg/mL in the system with metabolic activation. B-value was below 0.01, which could confirm the hypothesis that the valproic acid derivative concentration exceeding 1.58 mg/mL had a cytotoxic effect on these strains.

DISCUSSION

The QSAR Toolbox (v4.5 SP1) uses more than 50 databases of chemical substances and contains information on approximately 100,000 compounds. The studied valproic acid containing a tertiary amino group was not found in the databases used, which meant that there were no results of open-label trials of this substance.

Metabolic activation of the relatively inert functional groups into electrophilic reactive intermediates is considered to be an essential event in etiology of many side effects caused by drug intake. That is why assessment of biochemical reactivity of functional groups and structural motifs of potential pharmacological substances is important from a safety standpoint. And the alerts obtained by profiling should be considered when planning further preclinical and clinical trials [13].

The mechanistic profilers used in our study involve alerts that are based on the chemistry of the reactions associated with genotoxicity and on the hypothesis that electrophilic potential of a chemical is associated with genotoxic properties [14]. According to the “DNA binding by OASIS” algorithm, chemical structure of valproic acid containing a tertiary amino group is not associated with genotoxicity, however, the “DNA binding by OECD” algorithm alerts to probable mono-nucleophilic substitution reaction yielding the reactive iminium ion as a potential DNA adduct formation pathway [15].

DNA adduct formation can weaken a bond between the nitrogenous base and deoxyribose and result in the base loss (depurination or depyrimidination). Such DNA modification results in generation of the unstable apurinic/apyrimidinic site (AP site). The lack of appropriate base in the DNA matrix may result in blocking of DNA and RNA polymerases, as well as in single nucleotide substitutions and deletions/insertions. Chemical reactivity of AP sites causes DNA breaks, as well as DNA–protein and DNA–DNA crosslinks, thereby contributing to high mutagenicity and cytotoxicity of such damage [16].

In addition to probable genotoxicity, metabolic reactions yielding the reactive iminium ions can result in organ-specific toxicity. Neurotoxic effects of haloperidol, which, like the valproic acid derivative, has 4-piperidinyl in its molecular structure, are considered to be associated with the pyridine derivative formation, while the iminium ion is an intermediate of this process. However, loperamide that also has 4-piperidinyl in

its structure and forms a pyridine derivative via metabolization involving cytochrome CYP3A4 possesses no neurotoxic effects [15]. The differences between safety profiles of haloperidol and loperamide support the view that not all compounds involved in the same bioactivation patterns cause similar toxic effects. The fact that the valproic acid derivative is through bioactivation yielding DNA adducts and organ-specific toxic metabolites, including neurotoxic ones, should be considered when studying the substance pharmacokinetics.

Assessment of the probability of mutagenic effects in the Ames test using the QSAR Toolbox (v4.5 SP1) software with the significance level set at 0.00412 makes it possible to predict that the valproic acid derivative containing a tertiary amino group would show no mutagenic effects in the Ames test involving *S. typhimurium* TA 1535, TA 1537, TA 98, TA 100 and *E. coli* WP2 uvr A pKM 101 with or without metabolic activation.

Such assessment is consistent with the results of our *in vitro* study. According to the results, the concentrations of valproic acid containing a tertiary amino group of 0.02 mg/mL, 0.05 mg/mL, 0.16 mg/mL, 0.5 mg/mL, 1.58 mg/mL, and 5.00 mg/mL did not indice frameshift mutations (*S. typhimurium* strains TA98 and TA1537) and base-pair substitutions (S. typhimurium strains TA100, TA1535 and *E. coli* strains wp2 uvrA and wp2 [pKM101]) in the Ames assay without metabolic activation. The test system supplementation with the metabolic fraction of the liver did not affect the test substance genotoxic effects.

It is interesting to note cytotoxic effects of the concentration of valproic acid containing a tertiary amino group exceeding 1.58 mg/mL on the TA 100 *S. typhimurium* strain and WP2 uvr A pKM 101 *E. coli* strain in the tests both with and without metabolic activation. On the one hand, such an effect can mask mutagenic effects of the test substance high concentrations. On the other hand, cytotoxic effects can be associated with generation of DNA adducts resulting from metabolic activation, along with generation of AP sites and interstrand cross-links in the DNA molecule. However, cytotoxic effects of the valproic acid derivative containing a tertiary amino group have been also shown in the Ames test with metabolic activation, which contradicts this statement.

CONCLUSIONS

The results of the in silico and in vitro Ames test show that the valproic acid derivative containing a tertiary amino group possesses no mutagenicity. This pharmacologically active compound can be recommended for further preclinical trials of therapeutic efficacy and safety. However, it is important to note, that cytotoxic effects of valproic acid containing a tertiary amino group on some bacterial strains can mask its mutagenic effects when the concentration is high. Considering cytotoxic effects and the possibility of DNA adduct formation, it is necessary to study probable carcinogenic and cytotoxic effects using the tests involving mammalian cells and the experiments involving animal models.

References

1. Petrov AN, Sofronov GA, Nechiporenko SP, Somin IN. Antidoty fosfororganicheskikh otravlyayushchikh veshchestv. Rossiyskiy khimicheskiy zhurnal. 2004; 48 (2): 110–116. Russian.
2. Marucci G, Buccioni M, Ben DD, Lambertucci C, Volpini R, Amenta F. Efficacy of acetylcholinesterase inhibitors in Alzheimer's disease. Neuropharmacology. 2021; 190: 108352. PubMed PMID: 33035532.
3. Birks JS, Grimley Evans J. Rivastigmine for Alzheimer's disease. Cochrane Database Syst Rev. 2015; 4: CD001191. PubMed PMID: 25858345.
4. Zorina VN, Evdokimova EA, Reynyuk VL. Metody profilaktiki i terapii sudorozhnogo sindroma pri otravlenii konvul'santami kholinergicheskogo ryada. Meditsina ekstremal'nykh situatsiy. 2022; (2): 14–21. Russian.
5. Connors NJ, Harnett ZH, Hoffman RS. Comparison of current recommended regimens of atropinization in organophosphate poisoning. J Med Toxicol. 2014; 10 (2): 143–7.
6. Bespalov AYa, Prokopenko LI, Gorchakova TL, Petrov AN, Zaytseva MA, i dr, avtory; Federal'noe gosudarstvennoe byudzhetnoe uchrezhdenie nauki «Institut toksikologii Federal'nogo mediko-biologicheskogo agentstva», patentoobladatel'. Gidrokhlorid (1-metilpiperidin-4-il)-2-propilpentanoata, obladayushchiy kholinoliticheskoy i protivosudorozhnoy aktivnost'yu. Patent RF № 2714135. 12.02.2020. Russian.
7. Melekhova AS, Petrov AN, Bespalov AYa, Belskaya AV, Melnikova MV, Zatsepin EP, i dr. Eksperimental'naya farmakoterapiya sudorozhnogo sindroma pri modelirovanii tyazhelogo otravleniya karbamatom. Medlayn.ru. 2019; 20: 294–306. Russian.
8. Snodin DJ. Genotoxic limpurities: from structural alerts to qualification. Organic process research and development. 2010; 14 (4): 960–976.
9. Fukuchi J, Kitazawa A, Hirabayashi K, Honma M. A practice of expert review by read-across using QSAR Toolbox. Mutagenesis. 2019; 34 (1): 49–54.
10. Mortelmans K, Zeiger E. The Ames Salmonella/microsome mutagenicity assay. Mutat Res. 2000; 455 (1–2): 29–60. PubMed PMID: 11113466.
11. Heringa MB, Harmsen DJ, Beerendonk EF, Reus AA, Krul CA, Metz DH, et al. Formation and removal of genotoxic activity during UV/H(2)O(2)-GAC treatment of drinking water. Water Res. 2011; 45 (1): 366–374. PubMed PMID: 20828782.
12. Piegorsch WW, Simmons SJ, Margolin BH, Zeiger E, Gidrol XM, Gee P. Statistical modeling and analyses of a base-specific Salmonella mutagenicity assay. Mutat Res. 2000; 467 (1): 11–19. PubMed PMID: 10771267.
13. Benigni R. In silico assessment of genotoxicity. Combinations of sensitive structural alerts minimize false negative predictions for all genotoxicity endpoints and can single out chemicals for which experimentation can be avoided. Regulatory Toxicology and Pharmacology. 2021; 126: 105042.
14. Ashby J, Tennant RW. Definitive relationships among chemical structure, carcinogenicity and mutagenicity for 301 chemicals tested by the U.S. NTP. Mutat Res. 1991; 257 (3): 229–306.
15. Kalgutkar AS, Gardner I, Obach RS, Shaffer CL, Callegari E, Henne KR, et al. A comprehensive listing of bioactivation pathways of organic functional groups. Curr Drug Metab. 2005; 6 (3): 161–225 PubMed PMID: 15975040.
16. Phillips DH, Arlt VM. Genotoxicity: damage to DNA and its consequences. EXS. 2009; 99: 87–110. PubMed PMID: 19157059.

Литература

1. Петров А. Н., Софронов Г. А., Нечипоренко С. П., Сомин И. Н. Антидоты фосфорорганических отравляющих веществ. Российский химический журнал. 2004; 48 (2): 110–116.
2. Marucci G, Buccioni M, Ben DD, Lambertucci C, Volpini R, Amenta F. Efficacy of acetylcholinesterase inhibitors in Alzheimer's disease. Neuropharmacology. 2021; 190: 108352. PubMed

PMID: 33035532.
3. Birks JS, Grimley Evans J. Rivastigmine for Alzheimer's disease. Cochrane Database Syst Rev. 2015; 4: CD001191. PubMed PMID: 25858345.
4. Зорина В. Н., Евдокимова Е. А., Рейнюк В. Л. Методы профилактики и терапии судорожного синдрома при отравлении конвульсантами холинергического ряда. Медицина экстремальных ситуаций. 2022; (2): 14–21.
5. Connors NJ, Harnett ZH, Hoffman RS. Comparison of current recommended regimens of atropinization in organophosphate poisoning. J Med Toxicol. 2014; 10 (2): 143–7.
6. Беспалов А. Я., Прокопенко Л. И., Горчакова Т. Л., Петров А. Н., Зайцева М. А. и др., авторы; Федеральное государственное бюджетное учреждение науки «Институт токсикологии Федерального медико-биологического агентства», патентообладатель. Гидрохлорид (1-метилпиперидин-4-ил)-2-пропилпентаноата, обладающий холинолитической и противосудорожной активностью. Патент РФ № 2714135. 12.02.2020.
7. Мелехова А. С., Петров А. Н., Беспалов А. Я., Бельская А. В., Мельникова М. В., Зацепин Э. П. и др. Экспериментальная фармакотерапия судорожного синдрома при моделировании тяжелого отравления карбаматом. Медлайн.ру. 2019; 20: 294–306.
8. Snodin DJ. Genotoxic limpurities: from structural alerts to qualification. Organic process research and development. 2010; 14 (4): 960–976.
9. Fukuchi J, Kitazawa A, Hirabayashi K, Honma M. A practice of expert review by read-across using QSAR Toolbox. Mutagenesis. 2019; 34 (1): 49–54.
10. Mortelmans K, Zeiger E. The Ames Salmonella/microsome mutagenicity assay. Mutat Res. 2000; 455 (1–2): 29–60. PubMed PMID: 11113466.
11. Heringa MB, Harmsen DJ, Beerendonk EF, Reus AA, Krul CA, Metz DH, et al. Formation and removal of genotoxic activity during UV/H(2)O(2)-GAC treatment of drinking water. Water Res. 2011; 45 (1): 366–374. PubMed PMID: 20828782.
12. Piegorsch WW, Simmons SJ, Margolin BH, Zeiger E, Gidrol XM, Gee P. Statistical modeling and analyses of a base-specific Salmonella mutagenicity assay. Mutat Res. 2000; 467 (1): 11–19. PubMed PMID: 10771267.
13. Benigni R. In silico assessment of genotoxicity. Combinations of sensitive structural alerts minimize false negative predictions for all genotoxicity endpoints and can single out chemicals for which experimentation can be avoided. Regulatory Toxicology and Pharmacology. 2021; 126: 105042.
14. Ashby J, Tennant RW. Definitive relationships among chemical structure, carcinogenicity and mutagenicity for 301 chemicals tested by the U.S. NTP. Mutat Res. 1991; 257 (3): 229–306.
15. Kalgutkar AS, Gardner I, Obach RS, Shaffer CL, Callegari E, Henne KR, et al. A comprehensive listing of bioactivation pathways of organic functional groups. Curr Drug Metab. 2005; 6 (3): 161–225 PubMed PMID: 15975040.
16. Phillips DH, Arlt VM. Genotoxicity: damage to DNA and its consequences. EXS. 2009; 99: 87–110. PubMed PMID: 19157059.

IDENTIFICATION OF STAPHYLOCOCCAL ENTEROTOXIN B IN DAIRY PRODUCTS BY IMMUNOCHROMATOGRAPHY WITH VISUAL AND DIGITAL VIDEO DETECTION

Yarkov SP ✉, Tretyakov SI, Shilenko IV, Ishkov YuN, Styazhkin KK

State Scientific Research Institute of Biological Engineering of Federal Medical Biological Agency, Moscow, Russia

Detection of staphylococcal enterotoxins in food products is an important task of food poisoning prevention. The study was aimed to develop immunochromatography tests (ICTs) for detection of staphylococcal enterotoxins A (SEA) and be B (SEB), as well as to improve sensitivity of immunochromatography detection of staphylococcal enterotoxins (by the example of SEB) in dairy products relative to visual assessment by recording the analysis results with digital video recorders (DVR) using the principle of processing digital immunochromatogram images acquired using illumination in various spectral ranges. ICTs for detection of enterotoxins were designed as sandwich tests based on highly specific monoclonal antibodies (MABs) against staphylococcal enterotoxins. Milk, cream, sour cream, cheese artificially contaminated with SEB were analyzed. The analysis results were recorded visually or by DVR. DVR of immunochromatograms of the enterotoxin-containing dairy products acquired using illumination with white light in the wavelength range of 400–800 nm ensures a 4-fold increase in the SEB detection sensitivity, while that involving illumination with green light in the wavelength range having its maximum at 525 nm ensures a 4–8-fold increase relative to visual recording. The use of the "Reflecom" and "Zondazh" digital video immunochromatogram analyzers multiplies sensitivity of SEB detection by immunochromatography when assessing dairy products relative to visual recording.

Keywords: staphylococcal enterotoxin types A and B, immunochromatography, video digital registration of results, dairy products

Funding: the study was conducted as part of the State Assignment of the Federal Medical Biological Agency of Russia (GK № 42.001.22.6).

Author contribution: Yarkov SP — concept, part in developing the "Zondazh" unit, planning the experiments and analysis of the results, manuscript draft; Tretyakov SI — developing immunochromatography tests, experiments with dairy products, analysis of the study results; Shilenko IV — developing immunochromatography tests, experimental procedure, analysis of the results; Ishkov YuN — day-to-day research management, manuscript editing; Styazhkin KK — general management, manuscript editing.

✉ **Correspondence should be addressed:** Sergey P. Yarkov
Volokolamskoe sh., 75, korp. 1, Moscow, 125424, Russia; diasol@dol.ru

Received: 24.08.2023 **Accepted:** 18.09.2023 **Published online:** 30.09.2023

DOI: 10.47183/mes.2023.039

ВЫЯВЛЕНИЕ СТАФИЛОКОККОВОГО ЭНТЕРОТОКСИНА ТИПА В В МОЛОЧНОЙ ПРОДУКЦИИ ИММУНОХРОМАТОГРАФИЕЙ С ВИЗУАЛЬНОЙ И ВИДЕОЦИФРОВОЙ ДЕТЕКЦИЕЙ

С. П. Ярков ✉, С. И. Третьяков, И. В. Шиленко, Ю. Н. Ишков, К. К. Стяжкин

Государственный научно-исследовательский институт биологического приборостроения Федерального медико-биологического агентства, Москва, Россия

Выявление стафилококковых энтеротоксинов в продуктах питания является важной задачей профилактики пищевых отравлений. Целью исследования были разработка иммунохроматографических тестов (ИХТ) для обнаружения стафилококковых энтеротоксинов типов А (SEA) и В (SEB), а также повышение чувствительности иммунохроматографического выявления стафилококковых энтеротоксинов (на примере SEB) в молочных продуктах по сравнению с визуальным наблюдением за счет регистрации результатов анализа приборами видеоцифровой регистрации (ВЦР), использующими принцип обработки цифровых изображений иммунохроматограмм при освещении в различных спектральных диапазонах. ИХТ для выявления энтеротоксинов были сконструированы в «сэндвич»-формате на основе высокоспецифичных моноклональных антител (МКА) к стафилококковым энтеротоксинам. Анализу подвергались молоко, сливки, сметана, сыр, искусственно контаминированные SEB. Результаты анализа фиксировали визуально и с помощью ВЦР. Осуществление ВЦР иммунохроматограмм молочных продуктов, содержащих энтеротоксин, при освещении белым светом в диапазоне длин волн 400–800 нм повышает чувствительность выявления SEB в 4 раза, а при освещении зеленым в диапазоне спектра при максимуме длины волны 525 нм — в 4–8 раз по сравнению с визуальной регистрацией. Использование видеоцифровых анализаторов иммунохроматограмм «Рефлеком» и «Зондаж» кратно повышает чувствительность выявления SEB иммунохроматографическим методом при анализе молочных продуктов по сравнению с визуальным методом регистрации.

Ключевые слова: стафилококковые энтеротоксины типов А и В, иммунохроматография, видеоцифровая регистрация результатов, молочные продукты

Финансирование: исследования проводили в рамках государственного заказа Федерального медико-биологического агентства России (ГК № 42.001.22.6).

Вклад авторов: С. П. Ярков — идея, участие в создании прибора «Зондаж», планирование экспериментов и анализ результатов, подготовка черновика рукописи; С. И. Третьяков — создание иммунохроматографических тестов, эксперименты с молочными продуктами, анализ результатов исследования; И. В. Шиленко — создание иммунохроматографических тестов, проведение экспериментов, анализ полученных результатов; Ю. Н. Ишков — текущее руководство исследованиями, правка рукописи; К. К. Стяжкин — общее редактирование рукописи и руководство.

✉ **Для корреспонденции:** Сергей Петрович Ярков
Волоколамское шоссе, д. 75, корпус 1, г. Москва, 125424, Россия; diasol@dol.ru

Статья получена: 24.08.2023 **Статья принята к печати:** 18.09.2023 **Опубликована онлайн:** 30.09.2023

DOI: 10.47183/mes.2023.039

Staphylococcal enterotoxins produced by the Staphylococcus aureus Gram-positive bacterial strains cause food poisoning of varying severity in humans [1–3]. Ingestion of infected food is the main root of staphylococcal enterotoxin entry. According to the guidelines of Rospotrebnadzor MUK 4.2.2429-08 "Method to Determine Staphylococcal Enterotoxins in Food Products" and amendment (MUK 4.2.2879-11) [4, 5], food products with the toxin levels ≥ 100 μg/kg of product are considered to be toxicogenic in the Russian Federation. The same norms are set forth by the U.S. Food and Drug Administration (FDA) [6]. Immunochromatography tests (ICTs) are widely used for detection of staphylococcal enterotoxins in raw materials and processed foods, along with enzyme-linked immunosorbent assay. The ICT efficiency for detection of SEA [7], SEA and SEB

Fig. 1. Zondazh reflectometer-fluorimeter

in food products has been shown [8]. Undoubted advantages of ICT are as follows: compact test system design, quick and simple procedure, possible visual assessment of the results. At the same time, the issue of increasing ICT sensitivity is extremely relevant. Such studies focused on the staphylococcal enterotoxin detection by using silver ions and bifunctional gold nanoparticles have been conducted [9, 10].

Given the above, the study was aimed to develop domestic ICTs for detection of staphylococcal enterotoxins A and B, as well as to demonstrate the possibility of improving sensitivity of the above enterotoxin detection relative to visual recording of the results by using digital video immunochromatography analyzers based on processing of immunochromatogram digital images acquired using illumination in various spectral ranges.

METHODS

The procedure of producing ICTs for detection of SEB and the materials used have been previous reported [10]. ICTs for detection of SEA were constructed by the same method using various combinations of MABs produced by the 329D9B3, 329D9B3 and 329A11F6 clones (Table.1). MABs produced by the 357E10E9 and 357A8C1 clones (48th CSRI of the Defence Ministry; Russia) were used to manufacture ICTs for detection of SEB. MABs S222, S643 were produced by RCMDT (Russia). Colloidal gold nanoparticles (CGNs) with an average diameter of 30 nm conjugated to MABs were used in ICTs, and the SEB preparation was used as a concomitant (SRCAMB of Rospotrebnadzor; Russia). The following domestic dairy products were also used: cow's milk, 3.2% fat (GOST 31450-2013), cream, 10% fat (GOST 31450-2013), thermostatic sour cream, 10% fat (GOST 31452-2012), "Rossiysky" cheese, 50% fat (GOST 314521-2012).

Sample preparation for analysis was performed as follows. A total of 1 mL of the toxin-containing dairy product was placed in the 2 ml microcentrifuge tube, added 50 μL of the 0.5 M citrate buffer (pH = 3.0) and mixed by quick shaking. Samples were centrifuged at 4000 g for 15 min. The sample separated, and sedimentation of milk fat on the test tube bottom occurred. A total of 200 μL were collected from the upper transparent liquid layer and mixed with 200 μL of the concentrated buffer solution for immunochromatography analysis (GosNIIBP of FMBA of Russia; Russia). A total of 140 μL were collected from the resulting sample and applied to ICT. The following procedure was used for cheese samples. A total of 1 g of finely grated cheese was placed in the 10 mL test tube, added 1.0 mL of sterile buffer saline and shaken in vibration shaker for 1 min at maximum speed. Holding the test tube at an angle, wet cheese was squeezed by pressing against the test tube wall with a spatula, so that the liquid could drain into the 2 mL centrifuge tube. Samples were centrifuged at 4000 g for 15 min. A total of 200 μL of transparent supernatant fluid were collected and mixed with the concentrated buffer solution in a volume ratio of 1 : 1 for immunochromatography analysis. Then 140 μL of the resulting mixture were applied to ICT. After 25 min the analysis results were recorded visually or using DVR.

The Reflecom digital video immunochromatography analyzer (Sinteco-Complex; Russia) was used for DVR of chromatograms. Measurements were also conducted with the Zondazh reflectometer-fluorimeter (GosNIIBP of FMBA of Russia; Russia) (Fig. 1). The Zondazh experimental DVR reflectometer-fluorimeter model makes it possible to record intensity of light reflected from the immunochromatography test analytical zone or control zone in four spectral ranges: white — 400–800 nm, red — 650 nm, green — 525 nm, blue — 470 nm. The instrument spectral range enables recording of not only CGN conjugates, but also submicron latex particles of different color often used as a dispersed phase in ICTs. When operated in the luminescence intensity measurement mode, the Zondazh unit enables recording of luminescence

Table 1. ICT analytical properties when detecting SEA and SEB using visual recording of the results

Analyte	Sensitivity, ng/mL	Immunochromatography time, min	Combinations of MABs
SEA (variant I)	50	22	329D9B3 / 329D9B3
SEA (variant II)	25	7	329A11F6 / 329D9B3
SEA (variant II)	10	25	329A11F6 / 329D9B3
SEB (variant I)	10	25	357E10E9 / 357A8C1
SEB (variant II)	16	25	S222 / S643

Note: there were no cross-reactions between SEA and SEB concentrations 100 times higher than the corresponding ICT sensitivity; the toxin solutions were prepared using a buffer solution for immunochromatography analysis.

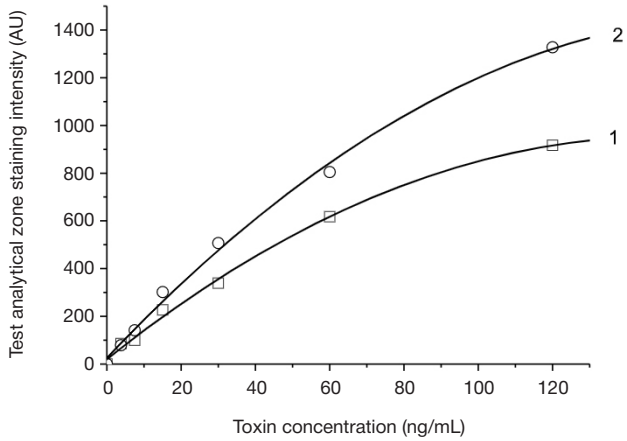

Fig. 2. Graphs of the relationship between the test analytical zone staining intensity and the SEB concentration in buffer solution measured using the Zondazh reflectometer-fluorimeter: 1 — illumination with white light (λ = 400–800 nm); 2 — illumination with green light (λmax = 525 nm). Chromatography time 25 min

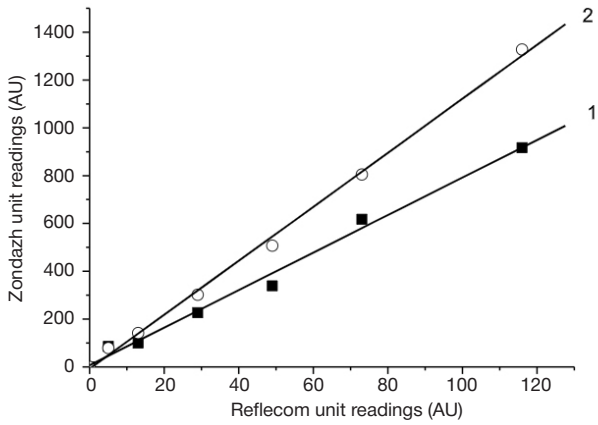

Fig. 3. Graphs of the correlation between the readings of the Reflecom and Zondazh reflectometers used to measure the test analytical zone staining intensity in the SEB concentration range of 0–120 ng/mL. 1 — illumination with white light, 2 — illumination with green light, correlation coefficients of linear relationships R = 0.995 and R = 0.999, respectively

chromatograms, it ensures luminescence excitation wavelength of 380 nm and emission recording wavelength of 490 nm. The instrument operation principle is based on reflectometry of digital chromatogram images or luminescence intensity recording when used in luminescence tests. Light-emitting diodes were used as light sources. A solid state video camera was used as an image receiver.

The unit ensures calculation of the integral intensity of the analyzed and control ICT areas along with the automated baseline correction. When performing DVR with the Zondazh reflectometer-fluorimeter, the increase in the intensity of the test analytical zone staining over the average background value obtained during the blank experiment considering the measurement error at the 95% confidence level was considered to be a criterion of positive result:

$$[X_{av} - t_s \times SE]_{signal} \geq [X_{av} + t_s \times SE]_{background},$$

where $X_{av.}$ was the mean of n measurements, t_s was the Student's t-distribution coefficient for n measurements, SE was the standard error at the 95 % confidence level.

RESULTS

Immunochromatography tests for detection of staphylococcal enterotoxins were designed as sandwich-format tests using MABs. The operation principle of sandwich-format ICTs has been extensively described in the literature [7–10]. A liquid sample potentially containing antigens of toxins is applied to the substrate for sample application. Liquid moves through the multimembrane composites due to influence of capillary forces. First, the CGN conjugate with specific antibodies is solubilized. It is cherry-colored, therefore its movement through the membrane can be visually traced. Moreover, when there is analyte antigen, antigenic immune complex is formed in the sample that starts moving across the test membrane with the fluid flow along with excess conjugate. Then the immune complex is immobilized on the test membrane by specific antibodies in the analytical zone (AZ) to form a “sandwich”, and the unbound antibodies of the conjugate are immobilized by antibodies in the control zone (CZ) of the test strip, which results in the emergence of two stained lines. When there is no antigen in the sample, no antigenic immune complex is formed, therefore only one visible line is formed due to binding of the conjugate antibodies and the CZ antibodies (antispecies antibodies against the conjugate antibodies) in the CZ only.

Two ICT options for SEA detection and two for SEB detection were produced based on various combinations of MABs. The ICT sensitivity was dependent on the immunochromatography assay time, it increased as the process progressed throughout 25 min (Table 1).

ICT for detection of SEB variant I was selected for further research due to higher sensitivity shown during the 25 min assay.

Graphs of the relationships of the Zondazh reflectometer-fluorimeter readings obtained during recording immunochromatograms of SEB diluted in the test buffer illuminated with various spectral ranges were plotted based on the data obtained (Fig. 2). The curves were well approximated by fitting with the following polynomials: $Y = 20.49 + 12.43X - 0.041X^2$ (white light) and $Y = 25.91 + 16.44X - 0.047X^2$ (green light); covariation coefficient $R^2 = 0.996$ in both cases. Such relationships are typical for immunochromatograms of SEB [9].

As can be seen in the graphs showing the correlation between the readings of the Reflecom digital video immunochromatography analyzer and the Zondazh reflectometer-fluorimeter yielded when assessing immunochromatograms of SEB, there is a linear correlation between the readings of these instruments (Fig. 3).

Readings of the instruments depending on the SEB concentration in the artificially contaminated dairy products yielded after immunochromatography are provided in Table 2.

DISCUSSION

Enzyme-linked immunosorbent assay (ELISA) with photometry or luminescence detection is recommended by the regulatory documents on detection of enterotoxins in food products [4, 5] as an express method. Facilitation of immunochromatography analysis relative to ELISA is achieved due to rejection of additional processing, washing, incubation with the signal-enhancing substrate, as well as to visual assessment of the results. When CGNs are used as labels, typical ICT time is 10–25 min, and the method sensitivity for protein toxins is usually within the range of 1–100 ng/mL, depending on the toxin type. Since immunochemical reactions on the membrane are nonequilibrium, ICT is considered to be inferior to ELISA in terms of sensitivity. At the same time, there are practices and methods to increase the ICT sensitivity to 0.1 ng/mL when used for protein antigens, however, this requires using additional reagents or luminescent labels together with instrumental recording, which significantly increases the analysis time.

In our studies DVR of the ICT results was used to obtain quantitative data along with visual recording. DVR of

Table 2. The test analytical zone staining intensity depending on the SEB concentration and the light spectral range measured using DVR instruments

SEB cocentration, ng/mL	Staining intensity, AU		
	Reflecom digital video immunochromatography analyzer White light λ = 400–800 nm	Zondajzh reflectometer-fluorimeter	
		White light λ = 400–800 nm	Green light λ_{max} = 525 nm
Milk, 3.2% fat, according to GOST 31450-2013			
0	0.0 ± 0.0	77 ± 4	118 ± 5
3.8	0.0 ± 0.0	80 ± 9	135 ± 7
7.5	0.0 ± 0.0	88 ± 5	156 ± 7
15	0.8 ± 0.1	124 ± 12	250 ± 6
30	1.9 ± 0.2	156 ± 8	303 ± 9
60	3.0 ± 0.2	544 ± 17	729 ± 8
Cream, 10% fat, according to GOST 31451-2012			
0	0.0 ± 0.0	93 ± 8	119 ± 6
3.8	0.0 ± 0.0	119 ± 10	139 ± 10
7.5	0.1 ± 0.1	117 ± 8	138 ± 15
15	0.8 ± 0.1	254 ± 11	272 ± 15
30	2.7 ± 0.2	293 ± 6	571 ± 7
60	3.1 ± 0.2	410 ± 12	510 ± 8
120	6.2 ± 0.3	597 ± 8	968 ± 10
240	8.2 ± 0.3	824 ± 11	120 ± 9
Sour cream, 10% fat, according to GOST 31452-2012			
0	0.0 ± 0.0	97 ± 13	120 ± 5
3.8	0.0 ± 0.0	123 ± 20	354 ± 34
7.5	0.5 ± 0.1	326 ± 16	610 ± 8
15	1.8 ± 0.1	533 ± 18	954 ± 39
30	2.9 ± 0.2	704 ± 8	1037 ± 2
Cheese, 50% fat, according to GOST 314521-2012			
0	0.0 ± 0.0	77 ± 6	118 ± 4
3.8	0.0 ± 0.0	80 ± 12	104 ± 10
7.5	0.4 ± 0.1	91 ± 8	128 ± 4
15	0.8 ± 0.1	187 ± 2	237 ± 3
30	1.2 ± 0.1	384 ± 10	291 ± 12
60	2.4 ± 0.2	541 ± 15	616 ± 13
120	4.4 ± 0.2	723 ± 14	825 ± 14

Note: the instrument readings provided in the table are mean values of five measurements. The error represents a standard error at the 95 % confidence level 95%, multiplied by the coefficient ts = 2.776 of Student's t-distribution for four degrees of freedom. Calculations were performed using MS Excel.

immunochromatograms is a common method to obtain semi-quantitative and quantitative immunochromatography analysis results when performing laboratory diagnosis of disorders [11]. DVR is based on assessing digital immunochromatogram images using specialized software that enables determination of integrated intensity of light absorbed by the analytical and control zones formed by the stained particles of the CGN conjugate with specific antibodies. A maximum contrast between the membrane background and the stained zone of chromatograms is required to achieve maximum recording sensitivity. Considering the fact that CGNs and their conjugates have broad structureless absorption bands within the range of 500–600 nm, the contrast must depend on the immunochromatogram illumination spectral composition. Based on subtractive color perception theory, a red object illuminated by green light looks almost black. Since there is too little green in red, the red object would absorb the majority of green photons and reflect almost nothing. Red would lose very much in saturation and tone, it would become brown, gray or even black [12]. Illumination of SEB immunochromatograms with green light (λmax = 525 nm) ensures a more intense signal during DVR compared to illumination with white light (Fig. 2). The readings of two different instruments using the same signal processing principle are linearly correlated. Furthermore, DVR response is stronger when using illumination in green spectral range (Fig. 3). The same relationships are observed when performing analysis of artificially contaminated dairy products after sample preparation for immunochromatography analysis (Table 2). The pooled data on the sensitivity of SEB detection using illumination of immunochromatograms in various spectral ranges are shown in the chart (Fig. 4). DVR of immunochromatograms of the enterotoxin-containing dairy products involving the use of illumination with white light four times increases the SEB detection sensitivity, while illumination with green spectral range 4–8 times increases sensitivity compared to visual recording.

It can be expected that the patterns of SEB detection in dairy products would be preserved when performing SEA analysis, considering structural similarity of these proteins.

The analyte-containing matrix has a great impact on the possibility of chromatography analysis and sensitivity [13, 14].

To obtain appropriate results, it is necessary to concentrate a protein enterotoxin in the low-viscosity hydrophilic phase with pH = 5.5–7.0 that is optimal for immunochemical reaction. Such phase would move well through the ICT nitrocellulose membrane and ensure immunochemical binding of reagents. As for dairy products, it is necessary to separate the serum containing proteins (such as staphylococcal enterotoxin) and the milk fat globules by centrifugation. When the product fat content is low, the product can be analyzed directly with no sample preparation. Thus, the results of assessing milk (3.2% fat) with or without sample preparation are almost the same. However, sample preparation involving sample dilution and incomplete toxin extraction to the hydrophilic phase reduces overall sensitivity of the analysis.

Our findings confirm the possibility of using ICT for detection of staphylococcal enterotoxins in dairy products, and the staphylococcal enterotoxin detection sensitivity achieved by using DVR is 3.8–7.5 ng/mL. These values enable the analysis meeting regulatory requirements that the levels of enterotoxins in food products should not exceed 100 ng/g of product.

CONCLUSIONS

We have developed ICTs based on MABs for detection of SEA and SEB showing sensitivity of 10 ng/mL for each toxin when conducting immunochromatography in buffer solutions for 25 min (visual assessment of the results). ICTs show no cross-reactions when used for analysis of enterotoxins A and B with the 100-fold increased concentration of enterotoxin of other type. DVR of enterotoxin-containing dairy product immunochromatograms involving the use of illumination with white light four times increases the SEB detection sensitivity, while illumination with green spectral range results in the 4–8 times increased sensitivity compared to visual recording.

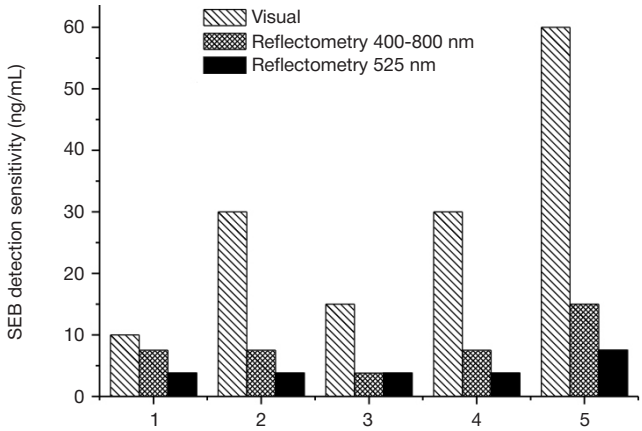

Fig. 4. Chart reflecting sensitivity of SEB detection in dairy products using visual recording of the results or instrumental recording with the Zondazh reflectometer-fluorimeter. 1 — SEB solution in buffer; 2 — milk, 3.2% fat; 3 — cream, 10% fat; 4 — sour cream, 10% fat; 5 — cheese, 50% fat

References

1. Pinchuk IV, Beswick EJ, Reyes VE. Staphylococcal enterotoxins. Toxins. 2010; 2 (8): 2177–97. DOI: 10.3390/toxins 2082177.
2. Savini F, Romano A, Giacometti F, Indio V, Pitti M, Decastelli L, et al. Investigation of a Staphylococcus aureus sequence type 72 food poisoning outbreak associated with food-handler contamination in Italy. Zoonoses Public Health. 2023; 70: 411–9.
3. Goudsmit A, Markowicz S, Lali S-E, Cherif1 S. Food poisoning due to a TSST1-producing Staphylococcus aureus. ID Cases. 2021; DOI: 10.1016/j.idcr.2021.e01272.
4. MUK 4.2.2429-08 «Metod opredeleniya stafilokokkovykh enterotoksinov v pishchevykh produktakh» [cited 2023 July 4]. Available from: https://files.stroyinf.ru/Data2/1/4293829/4293829076.htm#i183860/. Russian.
5. MUK 4.2.2879-11 «Metody opredeleniya stafilokokkovykh enterotoksinov v pishchevykh produktakh». Dopolneniya i izmeneniya 1 k MUK 4.2.2429-08 [cited 2023 July 4]. Available from: https://files.stroyinf.ru/Data2/0/4294809/4294809581.htm. Russian.
6. Bennett RW, Halt JM. Bacterial Analytical Manual online. US Food and Drug Administration. 2011 [cited 2023 July 6]. Available from: http://www.fda.gov/Food/ScienceResearch/LaboratoryMethods/BacteriologicalAnalyticalManualBAM/default.htm].
7. Lyubavina IA, Brovko FA, Valyakina TI, Vertiev YuV, Grishin EV. Metody ekspress-analiza stafilokokkovogo enterotoksina A v produktakh pitaniya. Bioorganicheskaya khimiya. Russian.
8. Eremkin AV, Ipatov SS, Kuklina GV, Pechenkin DV, Kytmanov AA, Tikhvinskaya OV, et al. Development of Elisa Test-Systems and Immune-Chromatographic Reagent Panel Designed for the Detection of Staphylococcal Enterotoxins of A and B Types. Problems of Particularly Dangerous Infections. 2021; 2: 94–9. DOI: 10.21055/0370-1069-2021-2-94-99. Russian.
9. Yarkov SP, Tretyakov SI, Shaulina EK, Brovkina AN, Khramov EN. Elevation the sensitivity of immunochromatographic tests to identify the causative agent of anthrax and staphylococcal enterotoxin type b based on silver amplification and instrumental recording. Extreme Medicine. 2019; 21 (3):455–63. Russian.
10. Yarkov SP, Tretyakov SI. Lateral flow test for the detection of staphylococcal enterotoxin type b using bifunctional gold nanoparticles. International research journal. 2021; 10 (112): 113–20. DOI: 10.23670/IRJ.2021.112.10.019. Russian.
11. Urusov AE, Jerdev AV, Starovoitova TA, Vengerov YuYu, Dzantiev BB. The device registration of immune chromatographic express-tests. Russian Clinical Laboratory Diagnostics. 2016; 61 (3): 173–9. DOI: 10.18821/0869-2084-2016-3-173-179. Russian.
12. Artyushin LF. Osnovy` vosproizvedeniya czveta v fotografii, kino i poligrafii. M.: Iskusstvo, 1970; 548 s. Russian.
13. Dzantiev BB, Byzova NA, Urusov AE, Zherdev AV. Immunochromatographic methods in food analysis. TrAC Trends in Analytical Chemistry. 2014; 55: 81–93.
14. Zherdev AV, Dzantiev BB. Ways to reach lower detection limits of lateral flow immunoassays. Journal of Analytical Chemistry. 2022; 77 (4): 298–311. DOI: 10.5772/intechopen.76926.

Литература

1. Pinchuk IV, Beswick EJ, Reyes VE. Staphylococcal enterotoxins. Toxins. 2010; 2 (8): 2177–97. DOI: 10.3390/toxins 2082177.
2. Savini F, Romano A, Giacometti F, Indio V, Pitti M, Decastelli L, et al. Investigation of a Staphylococcus aureus sequence type 72 food poisoning outbreak associated with food-handler contamination in Italy. Zoonoses Public Health. 2023; 70: 411–9.
3. Goudsmit A, Markowicz S, Lali S-E, Cherif1 S. Food poisoning due to a TSST1-producing Staphylococcus aureus. ID Cases. 2021; DOI: 10.1016/j.idcr.2021.e01272.
4. МУК 4.2.2429-08 «Метод определения стафилококковых энтеротоксинов в пищевых продуктах» [последнее цитирование 4 июля 2023 г.]. Доступно по ссылке: https://files.stroyinf.ru/

Data2/1/4293829/4293829076.htm#i183860/.
5. МУК 4.2.2879-11 «Методы определения стафилококковых энтеротоксинов в пищевых продуктах». Дополнения и изменения 1 к МУК 4.2.2429-08 [последнее цитирование 4 июля 2023 г.]. Доступно по ссылке: https://files.stroyinf.ru/Data2/0/4294809/4294809581.htm.
6. Bennett RW, Halt JM. Bacterial Analytical Manual online. US Food and Drug Administration. 2011 [cited 2023 July 6]. Available from: http://www.fda.gov/Food/ScienceResearch/LaboratoryMethods/BacteriologicalAnalyticalManualBAM/default.htm].
7. Любавина И. А., Бровко Ф. А., Валякина Т. И., Вертиев Ю. В., Гришин Е. В. Методы экспресс-анализа стафилококкового энтеротоксина А в продуктах питания. Биоорганическая химия. 2014; 40 (2): 186–95. DOI: 10.7868/S0132342314020109.
8. Еремкин А. В., Ипатов С. С., Куклина Г. В., Печёнкин Д. В., Кытманов А. А., Тихвинская О.В., и др. Разработка иммуноферментных тест-систем и иммунохроматографических наборов реагентов, предназначенных для выявления стафилококковых энтеротоксинов типов А и В. Проблемы особо опасных инфекций. 2021; 2: 94–9. DOI: 10.21055/0370-1069-2021-2-94-99.
9. Ярков С. П., Третьяков С. И., Шаулина Е. К., Бровкина А. Н., Храмов Е. Н. Повышение чувствительности иммунохроматографических тестов для выявления возбудителя сибирской язвы и стафилококкового энтеротоксина типа В на основе усиления серебром и инструментальной регистрации. Медицина экстремальных ситуаций. 2019; 21 (3): 455–63.
10. Ярков С. П., Третьяков С. И. Иммунохроматографический анализ для выявления стафилококкового энтеротоксина типа В с использованием бифункциональных наночастиц золота. Международный научно-исследовательский журнал. 2021; 10 (112): 113–20. DOI: 10.23670/IRJ.2021.112.10.019.
11. Урусов А. Е., Жердев А. В., Старовойтова Т. А., Венгеров Ю. Ю., Дзантиев Б. Б. Приборная регистрация иммунохроматографических экспресс-тестов. Клиническая лабораторная диагностика. 2016; 61 (3): 173–9. DOI: 10.18821/0869-2084-2016-3-173-179.
12. Артюшин Л. Ф. Основы воспроизведения цвета в фотографии, кино и полиграфии. М.: Искусство, 1970; 548 с.
13. Dzantiev BB, Byzova NA, Urusov AE, Zherdev AV. Immunochromatographic methods in food analysis. TrAC Trends in Analytical Chemistry. 2014; 55: 81–93.
14. Zherdev AV, Dzantiev BB. Ways to reach lower detection limits of lateral flow immunoassays. Journal of Analytical Chemistry. 2022; 77 (4): 298–311. DOI: 10.5772/intechopen.76926.

HEART DISEASE IN YOUNG ELITE ATHLETES HAVING A HISTORY OF COVID-19

Makarov LM[1,2,3] ✉, Komolyatova VN[1,2], Kiselyova II[1], Besportochny DA[1], Akopyan AG[1], Dmitrieva AV[1], Aksyonova NV[1]

[1] Federal Scientific and Clinical Center for Children and Adolescents of Federal Medical Biological Agency, Moscow, Russia

[2] Russian Medical Academy of Continuous Professional Education of the Ministry of Healthcare of the Russian Federation, Moscow, Russia

[3] Academy of Postgraduate Education, Federal Scientific and Clinical Center of Federal Medical Biological Agency, Moscow, Russia

The impact of coronavirus infection (SARS-CoV-2) on cardiac output in underage athletes is uncertain. The study was aimed to determine heart disease in young elite athletes having a history of COVID-19 (SARS-CoV-2). A retrospective analysis of the results of the developed three-phase medical assessment of 236 elite athletes aged 14–17 (16 ± 1), who had had SARS-CoV-2 infection, was performed. The first phase of assessment involved examination, ECG, ECHO, bicycle ergometry (BEM), creatine kinase and creatine kinase MB tests. During the second phase 22 athletes (9.3%) underwent a more thorough assessment that included Holter monitoring (HM) with heart rate turbulence (HRT), microvolt T–wave alternans (MTWA), heart rate variability (HRV) estimation, signal averaged ECG (SAECG), determination of myocardial damage biochemical markers (troponin, NTproBNP) due to alterations revealed. Seven athletes (32%) having alterations revealed during this phase were referred to gadolinium enhancement cardiac magnetic resonance imaging (MRI) (the third phase). Myopericarditis was diagnosed in four cases (1.7% of 236) based on the results. Thus, low myocardial involvement (below 2%) has been revealed in young elite athletes, who have a history of SARS-CoV-2 infection. Cardiovascular assessment algorithm has been developed for such athletes. Detection of cardiac arrhythmias by ECG, BEM, and HM is the most informative. SAECG, HRV, HRT, and MTWA can be used as additional methods to determine indications for MRI as a gold standard of the diagnosis of myocarditis.

Keywords: coronavirus infection, SARS-CoV2, myocarditis, young elite athlete, noninvasive electrocardiology

Funding: the study was supported by grant № 37B/CSM FMBA Rossii/22 of 10.08.2022.

Author contribution: Makarov LM — study concept and design, manuscript writing, conclusions; Komolyatova VN — data analysis by statistical and mathematical methods, literature data acquisition; Kiselyova II — clinical assessment of athletes, literature data acquisition; Besportochny DA — instrumental assessment, working on graphics; Akopyan AG, Dmitrieva AV — instrumental assessment; Aksyonova NV — selection of populations for assessment.

Compliance with ethical standards: the study was approved by the Ethics Commitee of the Pirogov Russian National Research Medical University (protocol № 217 of 18 April 2022) and conducted in accordance with the framework legislation "On Protection of Public Health"; the informed consent to examination was submitted by all participants.

✉ **Correspondence should be addressed:** Leonid M. Makarov
Moskvorechye, 20, Moscow, 115409, Russia; dr.leonidmakarov@mail.ru

Received: 27.07.2023 **Accepted:** 23.08.2023 **Published online:** 30.09.2023

DOI: 10.47183/mes.2023.042

ПОРАЖЕНИЕ СЕРДЦА У ЮНЫХ ЭЛИТНЫХ СПОРТСМЕНОВ, ПЕРЕНЕСШИХ COVID-19

Л. М. Макаров[1,2,3] ✉, В. Н. Комолятова[1,2], И. И. Киселева[1], Д. А. Беспорточный[1], А. Г. Акопян[1], А. В. Дмитриева[1], Н. В. Аксенова[1]

[1] Федеральный научно-клинический центр детей и подростков Федерального медико-биологического агентства, Москва, Россия

[2] Российская медицинская академия непрерывного профессионального образования Министерства здравоохранения России, Москва, Россия

[3] Академия постдипломного образования Федерального научно-клинического центра Федерального медико-биологического агентства, Москва, Россия

Влияние коронавирусной инфекции (SARS-CoV-2) на состояние сердца у несовершеннолетних спортсменов остается неопределенным. Целью работы было определение поражения сердца юных элитных спортсменов, перенесших инфекции COVID-19 (SARS-CoV-2). Проведен ретроспективный анализ результатов разработанного трехэтапного медицинского обследования 236 элитных спортсменов 14–17 (16 ± 1) лет, перенесших инфекцию SARS-CoV-2. Первый этап обследования включал осмотр, ЭКГ, ЭХО-КГ, велоэргометрию (ВЭМ), оценку КФК и КФК-МВ. В связи с выявленными изменениями 22-м спортсменам (9,3%) на втором этапе проводили более углубленное обследование, включающее холтеровское мониторирование (ХМ) с оценкой турбулентности ритма сердца (ТРС), микровольтной альтернации Т-зубца (МАТ) и вариабельности ритма сердца (ВРС), ЭКГ высокого разрешения (ЭКГ ВР), определение биохимических маркеров поражения миокарда: тропонин, NTproBNP. Семь спортсменов (32%) с выявленными на этом этапе изменениями были направлены на проведение магнитно-резонансной томографии (МРТ) сердца с контрастированием гадолинием (третий этап). По ее результатам в четырех случаях (1,7% из 236) был поставлен диагноз миоперикардит. Таким образом, отмечена низкая (менее 2%) вовлеченность поражения миокарда у юных элитных спортсменов, перенесших инфекцию SARS-CoV-2. Разработан алгоритм обследования сердца таких спортсменов. Наиболее информативно выявление аритмий сердца с помощью ЭКГ, ВЭМ и ХМ. Дополнительными методами определения показаний к МРТ сердца как золотому стандарту диагностики миокардита могут быть методы ЭКГ ВР, ВРС, ТРС и МАТ.

Ключевые слова: коронавирусная инфекция, SARS-CoV-2, миокардит, юные элитные спортсмены, неинвазивная электрокардиология

Финансирование: исследование выполнено по гранту No 37В /ЦСМ ФМБА России/22 от 10.08.2022.

Вклад авторов: Л. М. Макаров — концепция и дизайн исследования, написание текста рукописи, формулировка выводов; В. Н. Комолятова — анализ данных с помощью статистических и математических методов, сбор данных литературы, формулировка выводов; И. И. Киселева — клиническое обследование спортсменов, сбор данных литературы; Д. А. Беспорточный — проведение инструментальных исследований, работа с графическим материалом; А. Г. Акопян, А. В. Дмитриева — проведение инструментальных исследований; Н. В. Аксенова — отбор групп обследования.

Соблюдение этических стандартов: исследование одобрено этическим комитетом РНИМУ им. Н. И. Пирогова (протокол № 217 от 18 апреля 2022 г.), проведено в соответствии с требованиями Основ законодательства «Об охране здоровья граждан»; все участники подписали информированное согласие на обследование.

✉ **Для корреспонденции:** Леонид Михайлович Макаров
Москворечье, д. 20, г. Москва, 115409, Россия; dr.leonidmakarov@mail.ru

Статья получена: 27.07.2023 **Статья принята к печати:** 23.08.2023 **Опубликована онлайн:** 30.09.2023

DOI: 10.47183/mes.2023.042

Today, there are extensive data on cardiovascular disease, primarily myocarditis, in patients having a history of COVID-19 (SARS-CoV-2), including in athletes [1–6]. It is well-known that myocarditis often causes sudden cardiac death (SCD) in sports [7–9].

However, the data on the prevalence and clinical significance of heart disease in athletes, who had had the SARS-CoV-2 infection, varied significantly (1.4–56%) depending on the disease assessment criteria, diagnostic methods applied, and other aspects of the study design [3–5]. Cardiac MRI is the gold standard of detecting the heart disease following previous infection [1]. However, this method is costly and cannot be used as a screening tool. The search for additional markers and factors is an extremely topical task, which will make it possible to clarify the category of individuals in need of this procedure. The so-called "triad" testing (ECG, ECHO, troponin measurement) is the most widely used protocol for cardiovascular testing after having SARS-CoV-2 infection in the world [2–6]. Myocarditis of any etiology is a major cause of sudden death in athletes [7-9]. Abnormal "triad" testing results probably associated with SARS-CoV-2 affecting the heart were obtained using ECHO in 24 (0.9%) out 2556, using 12-lead ECG in 21 (0.7%) out 2999, and using troponin measurement in 24 (0.9%) out of 2719 [10].

The study was aimed to determine heart involvement in the elite athletes of higher sports mastery having a history of COVID-19 (SARS-CoV-2).

METHODS

Inclusion criteria: athletes' age 14–17 years; self-reported previous SARS-CoV-2 infection or medical documents confirming the history of SARS-CoV-2 infection; cardiac check-up conducted as part of in-depth medical assessment in the Center for Syncope and Cardiac Arrhythmias, Federal Scientific and Clinical Center for Children and Adolescents of FMBA of Russia.

Exclusion criteria: athletes' age under 14 and over 17 years; no in-depth medical assessment results.

To conduct retrospective analysis of the cardiovascular system assessment results, 236 medical histories of young elite athletes aged 14–17 (16 ± 1), who had reported having SARS-CoV-2 infection between September 1, 2021 and June 31, 2022, out 1505 were selected based on the inclusion criteria. All athletes had cardiac check-up conducted as part of in-depth medical assessment in the Center for Syncope and Cardiac Arrhythmias, Federal Scientific and Clinical Center for Children and Adolescents of FMBA of Russia. The time between infection and check-up was 1–6 months.

The examination program consisted of three phases. During the first phase the following was performed in all athletes as part of in-depth medical assessment: history taking and gathering complaints, examination involving measuring blood pressure, auscultation, cardiac percussion, 12-lead ECG (Mac 5500; GE Healthcare, USA), ECHO (Vivid T8, GE Healthcare, USA) and bicycle ergometry or BEM (CardioSoft 6.5; GE Healthcare, USA), extended biochemical profile. When performing analysis of medical documents, emphasis was placed on previous coronavirus infection, specific symptoms of infection (loss of taste and smell), common symptoms of intoxication associated with infection, duration of fever and the disease. Complaints of palpitation and dyspnea that were non-specific for coronavirus infection, as well as the decreased athletic performance, abnormal heart murmurs, and heart failure assessment were also taken into account. The analysis of previous 12-lead ECG was performed based on the Seattle criteria [11] and International recommendations [12] for the athletes' ECG analysis; heart rhythm disturbances and the signs of metabolic and ischemic myocardial alterations (T wave, ST segment, QT interval alterations).

ECHO was performed in accordance with the standard protocol involving assessing contractility of myocardium and heart chambers, hemodynamic parameters. Heart dimensions were estimated against body surface area and compared with normal age- and gender-related values considering z-scores of deviations [13]. BEM was performed in accordance with PWC 170 involving assessment of ECG and blood pressure during each phase of the test and the recovery period [14]. The creatine kinase and creatine kinase MB fraction levels were assessed in biochemical profiles of all athletes. The creatine kinase levels of 26–174 U/L and creatine kinase MB levels of 0–24 U/L were considered to be normal.

When detecting abnormalities during the first phase, the athlete was referred to the second-phase assessment that also included signal averaged ECG (SAECG) with ventricular late potentials detection: tot fQRS (normal values are below 114 ms), Last 40 (normal values are over 38 ms), and RMS40 (normal values are over 20 Hz) [14], Holter monitoring with estimation of arrhythmia and the dynamics of ventricular repolarization indicators (ST, T, QT alterations). When assessing the results of Holter monitoring, emphasis was on the signs of electrical myocardial instability: reduced heart rate variability or HRV (values below SDNN 100 ms, pNN50 below 15%) [15], episodes of microvolt T-wave alternans (above 55 μV) [16], reduced heart rate turbulence (onset over 0% and slope over 6 ms/RR) [17].

At this stage biochemical markers of myocardial damage were also determined: troponin (normal values are below 9 ng/mL) and N-terminal pro-B-type natriuretic peptide (NT-proBNP, normal values are below 125 pg/mL) levels.

When detecting abnormalities during this phase, the athlete was referred to the third-phase assessment involving the gadolinium enhancement cardiac magnetic resonance imaging (MRI).

Statistical data analysis was performed using the Statistica software package for Windows, ver. 7.0 (StatSoft; USA). Nonparametric statistical methods were used for data analysis, the differences were considered significant at $p < 0.05$.

RESULTS

The algorithm and results of the three-phase assessment of underage athletes having a history of SARS-CoV-2 infection are provided in Figure. The majority of athletes had mild and even more often asymptomatic (positive PCR tests performed during the pre-competition examination) SARS-CoV-2 infection, only one athlete developed pneumonia and needed hospital admission. None of the athletes had heart abnormalities according to the data of physical examination. During the first phase, cardiovascular system alterations that required in-depth assessment were found in 22 athletes (9.3%) based on the ECG, BEM, and ECHO data (Table 1). The combinations of several abnormalities were observed in six athletes. We revealed no relationship between the SARS-CoV-2 infection severity according to medical history and the need for second-stage assessment. As mentioned above, one athlete was earlier hospitalized with the COVID-19-associated pneumonia, however, cardiac check-up revealed no heart involvement.

The levels of creatine kinase were estimated in all athletes during the first phase of assessment. The group that needed second-phase assessment had significantly higher total

Table 1. Cardiovascular system alterations in underage elite athletes having a history of SARS-CoV-2 revealed during the first-phase assessment (see Figure). AVB — atrioventricular block; BEM — bicycle ergometry; PVC — ventricular extrasystole; LVEDD — left ventricular end-diastolic diameter; QTc — QT interval corrected using Bazett's formula (QT/√RR)

Alterations detected	*n* of athletes (% of all group)
Ventricular extrasystole on the resting ECG	2 (0.8%)
AVB, 2nd degree, Mobitz I, on the resting ECG	1 (0.4%)
QTc exceeding 460 ms on the resting ECG	5 (2.1%)
Reduced LV contractility and increased LVEDD	2 (0.8%)
PVC on BEM	18 (7.6%)
T wave inversion on BEM	8 (3.3%)

creatine kinase levels (525 [155, 684] vs. 325 [74, 422] U/L, $p < 0.05$) and creatine kinase MB levels (27 [5, 34] vs. 21 [7, 24] U/L, $p < 0.05$). No cases of elevated troponin or natriuretic peptide (NT-proBNP) levels were revealed during the second phase.

Ventricular late potentials were reported in two athletes (9%) out of 22 based on all three HRECG parameters (tot fQRS — 122 ± 5 ms whereas normal values are below 114 ms, Last 40 — 42 ± 5 ms whereas normal values exceed 38 ms, RMS40 — 18 ± 3 Hz whereas normal values exceed 20 Hz). The presence of these electrical myocardial instability signs suggested possible post-COVID myocarditis and allowed us to refer the athletes to MRI.

HM revealed sinus bradycardia in almost all athletes, only three athletes (16%) out of 22 had HR exceeding normal (sinus tachycardia) [15]. Reduced HRV was reported in two of them. One athlete had his HR back to normal after a month of rest, therefore, sinus tachycardia revealed by HM was considered as a sign of overtraining. None of 18 athletes showing exercise-induced ventricular extrasystole during BEM showed frequent ventricular extrasystoles during HM; the extrasystole rate varied between single extrasystoles and 105 extrasystoles per day (less than 1%), it was associated with elevated HR in the diurnal cycle (diurnal type). Reduced heart rate turbulence, the indicator associated with malignant extrasystole against the background of possible myocardial involvement, was revealed in two athletes out of 18 (11.1%). A short run of nonsustained ventricular tachycardia of three QRS complexes was recorded during HM in the morning in one athlete, who also needed MRI. HM revealed the values of microvolt T-wave alternans exceeding 55 μV in three patients with exercise-induced ventricular extrasystole. All eight athletes, who showed abnormal ventricular repolarization (negative T waves) during BEM (Table 1), had similar episodes during HM in the form of deep T-wave inversion, mainly against the background of sinus tachycardia. The analysis of previous check-ups of these athletes revealed similar alterations found during the in-depth medical assessment performed before the infection in three individuals (37.5%), thereby allowing us to exclude post-COVID-19 alterations. The patients with the combination of abnormal ventricular repolarization and exercise-induced ventricular extrasystole were referred to MRI. Thus, after the second phase of assessment seven athletes (32%) out of 22 were referred to the contrast-enhanced cardiac MRI (Table 2) that was performed in six of them. One athlete failed to provide MRI results, and his further sports fate is unknown. Myopericarditis was diagnosed in four athletes (1.7% of 236) based on MRI results. MRI revealed no alterations in the athlete, who had shown a run of nonsustained ventricular tachycardia. Four athletes with confirmed myocarditis were suspended from training for six months in accordance with the existing guidelines [18].

Table 2. Results of third-phase assessment of athletes having a history of SARS-CoV-2 infection (contrast-enhanced heart MRI). AVB – atrioventricular block; HRC — heart rate variability; BEM — bicycle ergometry; VT — ventricular tachycardia; PVC — ventricular extrasystole; LVEDD — left ventricular end-diastolic diameter; MTWA — microvolt T wave alternans; MRI — magnetic resonance imaging; HRT — heart rate turbulence; EF — ejection fraction; HM — Holter monitoring

	Age, gender, sports	ECG	ECHO	BEM	HM	MRI
1	17, f, field hockey	Tachycardia, QT prolongation (QTc > 460 ms)	normal	Abnormal ventricular repolarization, exercise-induced PVC	Tachycardia, abnormal ventricular repolarization, rare PVC, reduced HRT, MTWA	Data confirming subacute myopericarditis
2	16, f, badminton	PVC	normal	PVC during testing	MTWA, tachycardia, reduced HRV	No alterations detected
3	16, m, hockey	AVB, 2nd degree, Mobitz I	normal	AVB,1st degree, at the beginning of the test and during the recovery period	Frequent episodes of AVB, 2nd degree, Mobitz I and II	Acute myopericarditis
4	15, m, boxing	Abnormal ventricular repolarization (ST depression up to 0.5 mm in V4-V6)	Reduced contractility (EF 53%), diastolic dysfunction	Abnormal ventricular repolarization worsens under load	Abnormal ventricular repolarization	No data
5	16, m, volleyball	QT prolongation (QTc > 460 ms)	LV dilatation (LVEDD up to 61 mm), normal EF	normal	Tachycardia, reduced HRV, 1st degree AVB, episodes of 2nd degree AVB	Data confirming acute myocarditis
6	15, f, artistic gymnastics	normal	normal	Abnormal ventricular repolarization, exercise-induced PVC	Abnormal ventricular repolarization, rare PVC, reduced HRT	Data confirming myopericarditis
7	16, m, swimming	normal	normal	Abnormal ventricular repolarization	Run of polymorphic VT, MTWA	No alterations detected

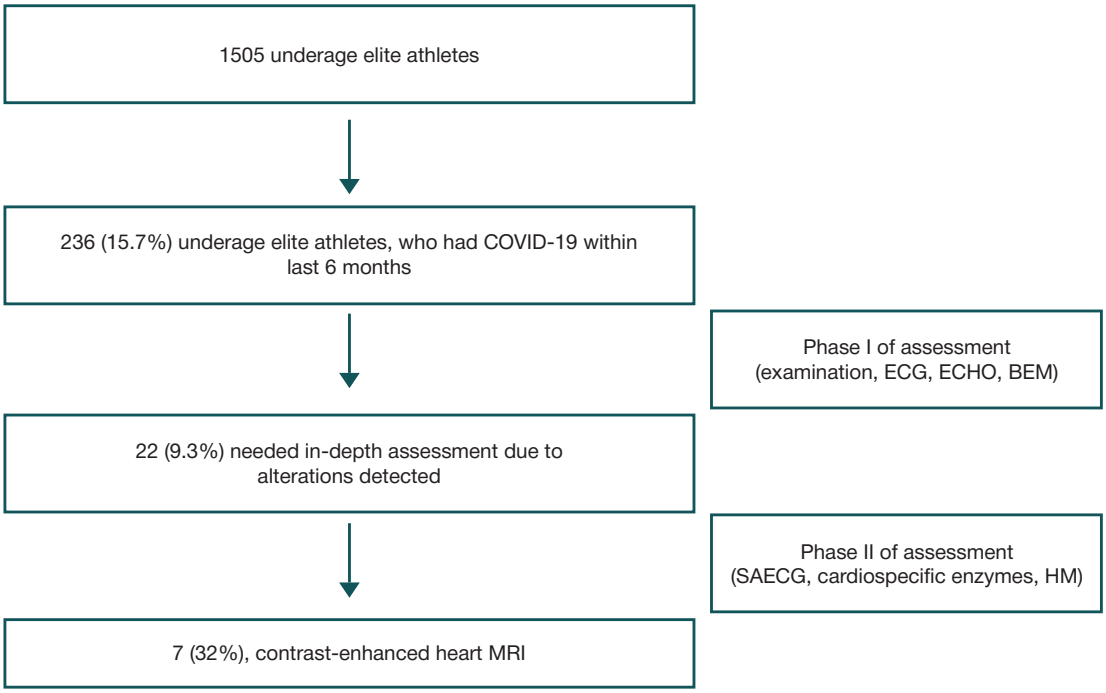

Fig. Algorithm and results of the three-phase assessment of underage elite athletes aged 14–17, who have had SARS-CoV-2 infection

DISCUSSION

Complications of SARS-CoV-2 infection affecting all systems of the body are reported in athletes. Cardiovascular system turned out to be the most vulnerable [18]. However, the prevalence and clinical manifestations of heart involvement in athletes having a history of SARS-CoV-2 infection vary considerably between studies [2–5, 18, 19]. Our findings showed that the prevalence of myocardial inflammation following previous SARS-CoV-2 infection in young athletes turned out to be low (1.7%) relative to the data of the sample of adult patients with severe disease (non-athletes, average age 64 years, 33% females) [20]. According to our data, reduced left ventricle contractility was observed in only one young athlete; unfortunately, he failed to provide the data of MRI he was recommended. In general, according to some reports, the detection rate of definite or probable heart involvement in young athletes was 2.7% [10], which was significantly lower compared to adult patients [1].

The symptoms of previous infections usually did not determine the course severity and complications. Thus, in one of the studies the clinically significant disease symptoms were reported in 27% of athletes, while myocarditis was found in 46% [4]. Other authors reported symptoms in 70–77% of cases, while no cases of myocarditis were revealed [2, 19]. Similar data were obtained during our study: among 236 athletes, only one had moderate disease. He was admitted to hospital due to pneumonia, but later had no cardiovascular alterations. In contrast, all athletes with confirmed myopericarditis had mild novel coronavirus infection (loss of taste or smell only). The fact of previous novel coronavirus infection is not always the cause of cardiac abnormalities detected. Such alterations in young elite athletes are often caused by the “overtraining” syndrome [21]. It is sometimes difficult to reveal the relationship between the alterations detected and previous infection, the analysis of previous assessment is often helpful. In our study, the analysis of previous documents in three athletes with abnormal repolarization during exertion out of eight made it possible to exclude coronavirus infection as the cause of alterations detected. One female athlete (patient 2; Table 2) had a combination of ventricular extrasystole, sinus tachycardia, and reduced HRV, however, no alterations were revealed by MRI. HR and HRV were back to normal after the short rest.

The so-called “triad” testing (ECG, ECHO, troponin measurement) is the most widely used protocol for detection of cardiac involvement after having SARS-CoV-2 infection in the world [18]. That is why our study involved assessment of troponin levels during the second phase, however, no cases of elevated levels were revealed. Perhaps, this is due to the fact that the time between the infection and the check-up was 1–6 months, despite elevated troponin levels can persist within 52 ± 17 days after the infection [22]. In one of the largest studies focused on assessing the course and effects on the heart of young athletes having a history of acute coronavirus infection, abnormal results of the “triad” testing probably associated with the heart disease after SARS-CoV-2 were detected by ECHO in 24 individuals (0.9%) out of 2556, by 12-lead ECG in 21 individuals (0.7%) out of 2999, by troponin measurement in 24 individuals (0.9%) out of 2719. A total of 65 athletes had at least one abnormal test, two athletes had two abnormal tests (ECG, ECHO), none of the athletes had three normal tests [10]. Myocarditis following previous SARS-CoV-2 infection was revealed in 81 athletes (2.7%) based on the “triad” testing and MRI, in 56 athletes (1.9%) the alterations detected were not associated with previous infection. According to the study, the “triad” testing turned out to be a highly sensitive marker of heart involvement in patients having a history of SARS-CoV-2 infection (OR: 37.4; CI: 13.3–105.3) [10]. We believe that the “triad” testing can be useful for detection of heart involvement in athletes, since in our study 75% of individuals with confirmed myocarditis had abnormalities on ECG and 25% had abnormalities on ECHO. One more study of athletes having a history of COVID-19 has shown that MRI was 7.4 more informative in terms of detecting heart involvement than other tests [23]. However, the value of MRI as a tool for mass screening of all athletes, who have had SARS-CoV-2 infection, is still unknown [18].

In our study, ECG, BEM, and HM were the most informative tests for detection of heart involvement before conducting MRI

(Table 1). In our opinion, such noninvasive electrocardiology methods, as SAECG and assessment of heart rate turbulence and variability, can be used as additional informative methods.

The wider use of MRI and additional methods for assessment of athletes having a history of SARS-CoV-2 infection will enable a more accurate determination of the heart disease prevalence in this group, since the issue of efficiency and informativeness of MRI-based screening in all athletes, who have had SARS-CoV-2 infection, relative to the study based on certain indications is a matter of debate [10]. The diversity of clinical manifestations, lack of strong associations between the previous infection severity and the development of complications raise many questions about the possibility of admitting athletes having a history of SARS-CoV-2 infection to training.

Retrospective design and lack of possibility to compare the levels of anti-SARS-CoV-2 antibodies and PCR tests at the disease onset with the later detected alterations, as well as short follow-up period not allowing one to estimate the long-term follow-up history, are the study limitations. The association of the disease with the athletes' anthropometric data, experience in athletics, training stage, previous injuries, etc., was not included in the analysis, which can be considered in further studies.

CONCLUSIONS

Low prevalence (up to 2%) of hearth involvement after the infection is observed in underage elite athletes having a history of SARS-CoV-2 infection. A three-phase algorithm for assessment of cardiovascular system in athletes, who have had SARS-CoV-2 infection, has been developed. Detection of cardiac arrhythmia by ECG, bicycle ergometry or Holter monitoring is the most informative in terms of determining probable heart involvement in young athletes. Detection of ventricular late potentials by SAECG, as well as reduced heart rate variability and turbulence, microvolt T-wave alternans, can be considered as additional methods to determine indications for MRI. Gadolinium enhancement cardiac MRI is the gold standard of myocardial involvement diagnosis in underage elite athletes having a history of SARS-CoV-2. However, the value of this method as a tool for mandatory screening of all convalescent athletes is still a matter of debate.

References

1. Clerkin KJ, Fried JA, Raikhelkar J, et al. COVID-19 and Cardiovascular Disease. Circulation. 2020; 141: 1648–55.
2. Brito D, Meester S, Yanamala N, Patel HB, Balcik BJ, Casaclang-Verzosa G, et al. High prevalence of pericardial involvement in college student athletes recovering from COVID-19. JACC Cardiovasc Imaging. 2021; 14: 541–55.
3. Clark DE, Parikh A, Dendy JM, Diamond AB, George-Durrett K, Fish FA, et al. COVID-19 myocardial pathology evaluation in athletes with cardiac magnetic resonance (COMPETE CMR). Circulation. 2021; 143: 609–12.
4. Rajpal S, Tong MS, Borchers J, Zareba KM, Obarski TP, Simonetti OP, et al. Cardiovascular magnetic resonance findings in competitive athletes recovering from COVID-19 infection. JAMA cardiology. 2021; 6: 116–8.
5. Starekova J, Bluemke DA, Bradham WS, Eckhartd LL, Grist TM, Kusmirek JE, et al. Evaluation for myocarditis in competitive student athletes recovering from coronavirus disease 2019 with cardiac magnetic resonance imaging. JAMA Cardiology. 2021; 6 (8): 945–50.
6. Puntmann VO, Carerj ML, Wieters I, Fahim M, Arendt C, Hoffmann J, et al. Outcomes of cardiovascular magnetic resonance imaging in patients recently recovered from coronavirus disease 2019 (COVID- 19). JAMA Cardiology. 2020; 5: 1265–73.
7. Makarov L. Sudden cardiac death in young athletes. In: P. Magnusson, J.A. LeQuang, editors. Sudden Cardiac Death. IntechOpen (London, UK). 2020; 51–62. DOI: 10.5772/intechopen.90627.
8. Harmon KG, Asif IM, Maleszewski JJ, Owens DS, Prutkin JM, Salerno JC, et al. Incidence, cause, and comparative frequency of sudden cardiac death in national collegiate athletic association athletes: A decade in review. Circulation. 2015; 132: 10–19.
9. Peterson DF, Kucera K, Thomas LC, Maleszewski J, Siebert D, Lopez-Anderson M, et al. Etiology and incidence of sudden cardiac arrest and death in young competitive athletes in the USA: a 4-year prospective study.Br J Sports Med. 2021; 55 (21): 1196–203.
10. Moulson N, Petek BJ, Drezner JA, Harmon KG, Kliethermes SA, Patel MR, et al. Outcomes Registry for Cardiac Conditions in Athletes Investigators.SARS-CoV-2 cardiac involvement in young competitive athletes. Circulation. 2021; 144: 256–66.
11. Drezner J, Ackerman M, Anderson J, Ashley E, Asplund G, Baggish A, et al. Electrocardiographic interpretation in athletes: the 'Seattle criteria'. Br J Sports Med. 2013; 47 (3): 122–4.
12. Sharma S, Drezner J, Baggish A, Papadakis M, Wilson M, Prutkin J, et al. International Recommendations for Electrocardiographic Interpretation in Athletes. JACC. 2017; 69 (8): 1057–75.
13. Kampmann C, Wiethoff CM, Wenzel A, Stolz G, Betancor M, Wippermann CF, et al. Normal values of M mode echocardiographic measurements of more than 2000 healthy infants and children in central Europe. Heart. 2000; 83 (6): 667–72.
14. Makarov LM. ECG v pediatrii. 3-e izdanie. M.: Medpraktika-M, 2013; 696 s. Russian.
15. Makarov LM, Komoljatova VN, Kuprijanova OO, Pervova EV, Rjabykina GV, Sobolev AV, i dr. Nacional'nye rossijskie rekomendacii po primeneniju metodiki holterovskogo monitorirovanija v klinicheskoj praktike. Rossijskij kardiologicheskij zhurnal. 2014; (2): 6–71. Russian.
16. Makarov L, Komoliatova V. Microvolt T-wave alternans during Holter monitoring in children and adolescents. Ann Noninvasive Electrocardiol. 2010; 15 (2): 138–44.
17. Makarov LM. Holterovskoe monitorirovanie. 4-e izdanie. M.: Medpraktika-M, 2017; 504 s. Russian.
18. Gluckman TJ, Bhave NM, Allenet LA, Chung EH, Spatz ES, et al. ACC expert consensus decision pathway on cardiovascular sequelae of COVID-19 in adults: myocarditis and other myocardial involvement, post-acute sequelae of SARS-CoV-2 infection, and return to play: a report of the American College of Cardiology solution set oversight committee. J Am Coll Cardiol. 2022; 79: 1717–56.
19. Małek ŁA, Marczak M, Miłosz-Wieczorek B, Konopka M, Braksator W, Drygas W, et al. Cardiac involvement in consecutive elite athletes recovered from Covid-19: a magnetic resonance study. J Magn Reson Imaging. 2021; 53: 1723–9.
20. Daher A, Balfanz P, Cornelissen C, et al. Follow up of patients with severe coronavirus disease 2019 (COVID-19): pulmonary and extrapulmonary disease sequelae. Respir Med. 2020; 174: 106197.
21. Makarov LM, Komolyatova VN, Aksenova NV. Analiz prichin otvodov ot zanjatij sportom junyh jelitnyh sportsmenov. Ros. vestn. perinatol. i pediatr. 2020; 65: (6): 65–71. Russian.
22. Hanneman K, Houbois C, Schoffel A, et al. Combined cardiac fluorodeoxyglucose-positron emission tomography/magnetic resonance imaging assessment of myocardial injury in patients who recently recovered from COVID-19. /JAMA Cardiol. 2022; 7 (3): 298–308.
23. Daniels CJ, Rajpal S, Greenshields JT, Rosenthal GL, Chung EH, Terrin M, et al. Prevalence of clinical and subclinical myocarditis in competitive athletes with recent SARS-CoV-2 infection results from the big ten COVID-19 cardiac registry. JAMA Cardiology. 2021; 6 (9): 1078–87.

Литература

1. Clerkin KJ, Fried JA, Raikhelkar J, et al. COVID-19 and Cardiovascular Disease. Circulation. 2020; 141: 1648–55.
2. Brito D, Meester S, Yanamala N, Patel HB, Balcik BJ, Casaclang-Verzosa G, et al. High prevalence of pericardial involvement in college student athletes recovering from COVID-19. JACC Cardiovasc Imaging. 2021; 14: 541–55.
3. Clark DE, Parikh A, Dendy JM, Diamond AB, George-Durrett K, Fish FA, et al. COVID-19 myocardial pathology evaluation in athletes with cardiac magnetic resonance (COMPETE CMR). Circulation. 2021; 143: 609–12.
4. Rajpal S, Tong MS, Borchers J, Zareba KM, Obarski TP, Simonetti OP, et al. Cardiovascular magnetic resonance findings in competitive athletes recovering from COVID-19 infection. JAMA cardiology. 2021; 6: 116–8.
5. Starekova J, Bluemke DA, Bradham WS, Eckhartd LL, Grist TM, Kusmirek JE, et al. Evaluation for myocarditis in competitive student athletes recovering from coronavirus disease 2019 with cardiac magnetic resonance imaging. JAMA Cardiology. 2021; 6 (8): 945–50.
6. Puntmann VO, Carerj ML, Wieters I, Fahim M, Arendt C, Hoffmann J, et al. Outcomes of cardiovascular magnetic resonance imaging in patients recently recovered from coronavirus disease 2019 (COVID- 19). JAMA Cardiology. 2020; 5: 1265–73.
7. Makarov L. Sudden cardiac death in young athletes. In: P. Magnusson, J.A. LeQuang, editors. Sudden Cardiac Death. IntechOpen (London, UK). 2020; 51–62. DOI: 10.5772/intechopen.90627.
8. Harmon KG, Asif IM, Maleszewski JJ, Owens DS, Prutkin JM, Salerno JC, et al. Incidence, cause, and comparative frequency of sudden cardiac death in national collegiate athletic association athletes: A decade in review. Circulation. 2015; 132: 10–19.
9. Peterson DF, Kucera K, Thomas LC, Maleszewski J, Siebert D, Lopez-Anderson M, et al. Etiology and incidence of sudden cardiac arrest and death in young competitive athletes in the USA: a 4-year prospective study.Br J Sports Med. 2021; 55 (21): 1196–203.
10. Moulson N, Petek BJ, Drezner JA, Harmon KG, Kliethermes SA, Patel MR, et al. Outcomes Registry for Cardiac Conditions in Athletes Investigators.SARS-CoV-2 cardiac involvement in young competitive athletes. Circulation. 2021; 144: 256–66.
11. Drezner J, Ackerman M, Anderson J, Ashley E, Asplund G, Baggish A, et al. Electrocardiographic interpretation in athletes: the 'Seattle criteria'. Br J Sports Med. 2013; 47 (3): 122–4.
12. Sharma S, Drezner J, Baggish A, Papadakis M, Wilson M, Prutkin J, et al. International Recommendations for Electrocardiographic Interpretation in Athletes. JACC. 2017; 69 (8): 1057–75.
13. Kampmann C, Wiethoff CM, Wenzel A, Stolz G, Betancor M, Wippermann CF, et al. Normal values of M mode echocardiographic measurements of more than 2000 healthy infants and children in central Europe. Heart. 2000; 83 (6): 667–72.
14. Макаров Л. М. ЭКГ в педиатрии. 3-е издание. М.: Медпрактика-М, 2013; 696 с.
15. Макаров Л. М., Комолятова В. Н., Куприянова О. О., Первова Е. В., Рябыкина Г. В., Соболев А. В., и др. Национальные российские рекомендации по применению методики холтеровского мониторирования в клинической практике. Российский кардиологический журнал. 2014; (2): 6–71.
16. Makarov L, Komoliatova V. Microvolt T-wave alternans during Holter monitoring in children and adolescents. Ann Noninvasive Electrocardiol. 2010; 15 (2): 138–44.
17. Макаров Л. М. Холтеровское мониторирование. 4-е издание. М.: Медпрактика-М, 2017; 504 с.
18. Gluckman TJ, Bhave NM, Allenet LA, Chung EH, Spatz ES, et al. ACC expert consensus decision pathway on cardiovascular sequelae of COVID-19 in adults: myocarditis and other myocardial involvement, post-acute sequelae of SARS-CoV-2 infection, and return to play: a report of the American College of Cardiology solution set oversight committee. J Am Coll Cardiol. 2022; 79: 1717–56.
19. Małek ŁA, Marczak M, Miłosz-Wieczorek B, Konopka M, Braksator W, Drygas W, et al. Cardiac involvement in consecutive elite athletes recovered from Covid-19: a magnetic resonance study. J Magn Reson Imaging. 2021; 53: 1723–9.
20. Daher A, Balfanz P, Cornelissen C, et al. Follow up of patients with severe coronavirus disease 2019 (COVID-19): pulmonary and extrapulmonary disease sequelae. Respir Med. 2020; 174: 106197.
21. Макаров Л. М., Комолятова В. Н., Аксенова Н. В. Анализ причин отводов от занятий спортом юных элитных спортсменов. Рос. вестн. перинатол. и педиатр. 2020; 65: (6): 65–71.
22. Hanneman K, Houbois C, Schoffel A, et al. Combined cardiac fluorodeoxyglucose-positron emission tomography/magnetic resonance imaging assessment of myocardial injury in patients who recently recovered from COVID-19. /JAMA Cardiol. 2022; 7 (3): 298–308.
23. Daniels CJ, Rajpal S, Greenshields JT, Rosenthal GL, Chung EH, Terrin M, et al. Prevalence of clinical and subclinical myocarditis in competitive athletes with recent SARS-CoV-2 infection results from the big ten COVID-19 cardiac registry. JAMA Cardiology. 2021; 6 (9): 1078–87.

RELATIONSHIP BETWEEN THE ATHLETE'S PRE-START STATE PARAMETERS AND PHYSIOLOGICAL RESPONSE TO STANDARDIZED LOAD

Chikov AE[1,2] ✉, Kutsalo AL[1], Kiselev AD[1], Vladimirov VV[1], Krylova MV[1], Medvedev DS[3], Kaplun DI[4], Shpakovskaya II[4]

[1] Research Institute of Hygiene, Occupational Pathology and Human Ecology of the Federal Medical Biological Agency, Saint Petersburg, Russia

[2] Almazov National Medical Research Centre, Saint Petersburg, Russia

[3] Saint Petersburg Institute of Bioregulation and Gerontology, Saint Petersburg, Russia

[4] Saint Petersburg Electrotechnical University "LETI", Saint Petersburg, Russia

Intense physical work is characterized by activity of physiological mechanisms as interrelated components joint for physical exertion. Definition of a set of individual and typological patterns of the physiological mechanisms' activity answers the questions related to improvement of the athlete's potential realization efficiency, definition of the limiting components and body's reserve capacity, training load management. The study was aimed to assess the relationship between the responses of physiological mechanisms associated with standardized physical exertion and the pre-start state parameters. The athlete was through the step incremental test with the treadmill involving recording of the gas exchange parameters and heart rate to study physiological patterns. The physiological response parameters were calculated relative to the key phases of the exercise test: pre-start state, aerobic and anaerobic thresholds, peak exertion, rapid and slow recovery phases. The mathematical model "Horseshoe of Rest" characterizing the athlete's pre-start state before performing the test was constructed using the T-SNE dimensionality reduction algorithms. The model enables estimation of the release of non-metabolic CO_2 throughout the testing period (MIC — 0.29) and the exertion period (MIC — 0.35).

Keywords: athlete, physical activity, pre-start state, modeling of energy supply, threshold of anaerobic metabolism, physiological response, standardized load

Author contribution: Chikov AE — analysis of the results; Kiselev AD, Vladimirov VV — manuscript writing, literature review; Kutsalo AL, Medvedev DS — discussion of the results, manuscript writing; Krylova MV — data preparation for analysis; Kaplun DI, Shpakovskaya II — data processing, constructing the pre-start state model.

Compliance with the ethical standards: the study was approved by the Ethics Committee of the Research Institute of Hygiene, Occupational Pathology and Human Ecology of FMBA of Russia (protocol № 2 of 1 March 2021).

✉ **Correspondence should be addressed:** Alexander E. Chikov
Zavodskaja, zd. 6/2, korp. 93, gp. Kuzmolovskij, 188663, Russia; chikov.alexandr@yandex.ru

Received: 21.08.2023 **Accepted:** 17.09.2023 **Published online:** 30.09.2023

DOI: 10.47183/mes.2023.037

ВЗАИМОСВЯЗЬ ПОКАЗАТЕЛЕЙ «ПРЕДСТАРТОВОГО» СОСТОЯНИЯ СПОРТСМЕНА С ФИЗИОЛОГИЧЕСКОЙ РЕАКЦИЕЙ НА СТАНДАРТИЗИРОВАННУЮ НАГРУЗКУ

А. Е. Чиков[1,2] ✉, А. Л. Куцало[1], А. Д. Киселев[1], В. В. Владимиров[1], М. В. Крылова[1], Д. С. Медведев[3], Д. И. Каплун[4], И. И. Шпаковская[4]

[1] Научно-исследовательский институт гигиены, профпатологии и экологии человека ФМБА России, Санкт-Петербург, Россия

[2] Национальный медицинский исследовательский центр имени В. А. Алмазова Минздрава России, Санкт-Петербург, Россия

[3] Санкт-Петербургский Институт биорегуляции и геронтологии, Санкт-Петербург, Россия

[4] Санкт-Петербургский государственный электротехнический университет «ЛЭТИ» имени В. И. Ульянова (Ленина), Санкт-Петербург, Россия

Интенсивная физическая работа характеризуется активностью физиологических механизмов как взаимосвязанных компонентов, объединенных для выполнения физической нагрузки. Определение набора индивидуально-типологических паттернов активности физиологических механизмов отвечает на вопросы, связанные с повышением эффективности реализации потенциала спортсмена, определением лимитирующих звеньев и резервных возможностей организма, управлением тренировочной нагрузкой. Целью работы было изучение взаимосвязи реакции физиологических механизмов при выполнении стандартизированной физической нагрузки с показателями «предстартового» состояния. Для исследования физиологических закономерностей спортсмен выполнял ступенчато-возрастающий тест на беговой дорожке с фиксацией показателей газообмена, частоты сердечных сокращений. Расчет показателей физиологических реакций производили относительно ключевых фаз нагрузочного тестирования: «предстартового» состояния, аэробного и анаэробного порогов, пика нагрузки, фаз быстрого и медленного восстановления. С использованием алгоритмов понижения размерности T-SNE была разработана математическая модель «Подкова_покоя», характеризующая «предстартовое» состояние спортсмена перед выполнением теста. Модель позволяет оценить уровень выделения неметаболического CO_2 за весь период тестирования (MIC — 0,29) и за период нагрузки (MIC — 0,35).

Ключевые слова: спортсмен, физическая нагрузка, «предстартовое» состояние, моделирование энергообеспечения, порог анаэробного обмена, физиологическая реакция, стандартизированная нагрузка

Вклад авторов: А. Е. Чиков — анализ результатов исследования; А.Д. Киселёв, В. В. Владимиров — подготовка текста статьи, анализ литературных источников; А. Л. Куцало, Д. С. Медведев — обсуждение результатов исследования, подготовка текста статьи; М. В. Крылова — подготовка данных к анализу; Д. И. Каплун, И. И. Шпаковская — обработка данных, разработка модели предтестового состояния.

Соблюдение этических стандартов: исследование одобрено этическим комитетом ФГУП «НИИ ГПЭЧ» ФМБА России (протокол № 2 от 01 марта 2021 г.).

✉ **Для корреспонденции:** Александр Евгеньевич Чиков
ул. Заводская, зд. 6/2, корп. 93, гп. Кузьмоловский, 188663, Россия; chikov.alexandr@yandex.ru

Статья получена: 21.08.2023 **Статья принята к печати:** 17.09.2023 **Опубликована онлайн:** 30.09.2023

DOI: 10.47183/mes.2023.037

Regular muscle work of considerable volume and intensity is ensured by the coordinated activity of various physiological mechanisms reflecting the systemic nature of the response to exertion [1–3]. In this context physiological mechanisms and appropriate responses mean the set of interrelated components and their responses to the standardized incremental exercise to failure. Each physiological mechanism has a common architecture and is distinguished by the characteristics of its components, to which, in our opinion, it is appropriate to attribute the sources of energy supply (aerobic, lactatic and alactic ATP resynthesis pathways) and the factors of their realization characterizing the dynamic and processual aspects of energy supply (performance, capacity, rate of deployment and switching between various ATP resynthesis pathways). These physiological mechanisms provide the leading functional system (LFS) that is responsible for the goal-directed activity realization at the whole-body level [4, 5]. Performing the activity requires an adequate (depending on the exercise characteristics) level of body's physiological reserves. Energy generation is ensured by the coordinated activity of the cardiovascular, respiratory, muscular, nervous, hemic systems, etc. [6]. The required physical performance intensity can be ensured by the adequate energy generation level only [7, 8]. Definition of a set of individual and typological patterns of the physiological mechanisms' activity answers a number of questions related to improvement of the athlete's potential realization efficiency, definition of the limiting components and body's reserve capacity, training load management aimed at ensuring health preservation and professional longevity [9–11]. Due to complex organization of physiological patterns associated with muscle work, assessing such patterns using mathematical modeling and machine learning algorithms seems to be promising [12–15]. For example, there are a number of successful solutions for prediction of lactate threshold in amateur runners using recurrent neural networks [12, 16].

It should be noted that the functional system development involving cortical influences begins even before the start of intense physical exertion (competitions or exercise testing to failure) (pre-start state). We believe that the correlation of pre-start state with physiological response to physical exertion is important, since it will make it possible to predict in advance the responses of body's systems.

The study was aimed to assess the relationship between the responses of physiological mechanisms associated with standardized physical exertion and the athlete's pre-start state.

METHODS

The study involved althetes aged 24.7 ± 4.0, who specialized in complex-coordination and cyclic sports and were first-class sportsmen or candidates for master of sport. The athletes were tested in the preparatory period of the annual training cycle. Assessment results of 1495 athletes were used to build the models. The subjects were through standardized exercise testing in the form of the treadmill incremental exercise. The exercise testing protocol was as follows: first stage — 5 km/h, stage duration — 2 min, speed increment at each stage —1.5 km/h. The following primary parameters were recorded within 3 min before testing (pre-start state), during testing and during the recovery period (15 min) using the Oxycon Pro ergospirometry system (Erich Jaeger; Germany): heart rate (HR, bpm), minute ventilation (VE, L/min), oxygen uptake (VO_2, L/min) and carbon dioxide production (VCO_2, L/min), respiratory exchange ratio (RER), oxygen pulse (O_2HR, mL/beat), respiratory oxygen equivalent (EqO_2) and carbon dioxide equivalent ($EqCO_2$). The criterion for stopping was the athlete's failure or reaching a maximum estimated HR (heart rate) calculated according to the following formula:

$$HR_{max} = 220 - \text{age}.$$

Failure when doing exercises was reported in 1358 athletes, 137 athletes were stopped after reaching the maximum HR.

When assessing physiological responses, parameters in the following phases of exercise testing were taken into account:

1) pre-start state;
2) aerobic threshold;
3) anaerobic thershold;
4) rapid recovery phase.

Phases two, three, and four were set using the AT_Inter tool [16] using a recommender system to determine the aerobic and anaerobic thresholds and the rapid recovery phase by conventional methods and machine learning methods (cluster analysis) [8]. More than 100 indicators characterizing the body's physiological responses to the standardized physical exertion were calculated based on primary parameters.

Data processing was performed using Python 3 and scikit-learn libraries (open-source machine learning libraries). The Maximal Information Coefficient (MIC) was used to estimate nonlinear relationships between the parameters [17]. The indicator's range is 0–1, where 0 corresponds to statistical

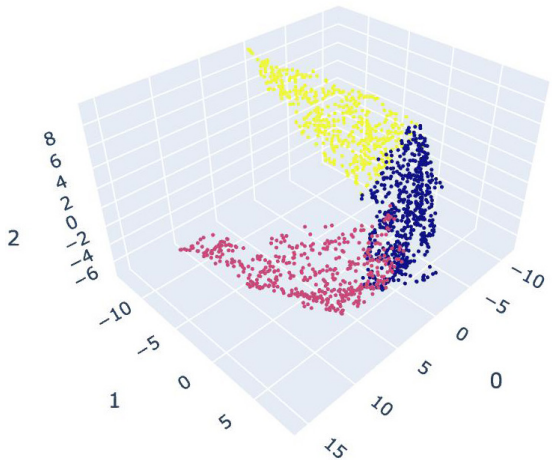

Fig. The "Horsechoe of Rest" model of pre-start state

Table 1. Values of the assessed athletes' pre-start state primary parameters

Parameter	Mean	Error of the mean
HR	86.1	12.9
VE	15.7	3
VO_2	519.1	98.6
VCO_2	417.6	86.3
O_2HR	6.1	1.3
EqO_2	27.1	3.4
$EqCO_2$	33.6	3.5

Table 2. Correlation between non-metabolic CO_2 and characteristic 2 of the "Horsechoe of Rest" model

Parameter	Coordinate 2
CO_2_non_physiol_total	0.29
CO_2_non_physiol_L	0.35

independence and 1 corresponds to dependencies between parameters. The critically significant level of the relationship used in the study is 0.2 at $p < 0.05$.

RESULTS

The athlete's body state in the first phase of exercise testing is characterized by changes in the function of body's physiological systems, such as cardiovascular and respiratory systems, resulting from cortical influences associated with the upcoming intense physical exertion (Table 1).

The correlation analysis revealed no significant correlations between the pre-start state primary parameters and the indicators of body's physiological response to the standardized physical exertion ($p > 0.05$). That is why we decided to use the dimensionality reduction t-SNE algorithm for reduction to three-dimensional map in order to build a "Horsechoe of Rest" model characterizing the pre-start state (Figure). The t-SNE algorithm (t-distributed Stochastic Neighbor Embedding) is a nonlinear dimension reduction technique [18, 19]. The main idea of the method is the search for the multidimensional feature space projection onto a plane, from n-dimensional space to three-dimensional, i.e. the search is performed for new data representation, with which the neighborhood observations are preserved [20]. Primary parameters of the pre-start state were input to the described algorithm. The new synthetic characteristics 0, 1 and 2, which accumulated information from original characteristics but had no clear interpretation, were the output. Each point of the "Horsechoe of Rest" model corresponded to one observation having characteristics 0, 1 and 2 (Figure). All observations formed a horseshoe indicating that there was a pattern inherent to the athletes' pre-start state.

The MIC value was calculated to evaluate the non-linear relationship between the parameters obtained during the major phases of testing and the interpretation of new synthetic characteristics 0, 1 and 2. The findings showed that coordinates 0 and 1 showed no significant correlations (the maximum correlation values did not reach the critically significant level, MIC = 0.2) with the exercise testing results. The characteristic 2 showed a significant correlation with the non-metabolic carbon dioxide emission: 1) over the period of testing (CO_2_non_physiol_total); 2) over the period of exertion (CO_2_non_physiol_L). MIC was 0.29 and 0.35, respectively (Table 2). Non-metabolic CO_2 was calculated for the period of exertion and the recovery period as the amount of carbon dioxide emitted that exceeded the level at RER 0 > 1.

DISCUSSION

The non-metabolic CO_2 associated with intense physical exertion is generated due to activity of anaerobic lactic mechanism and neutralization of its metabolites by buffer systems, specifically by plasma bicarbonate. Thus, the pre-start state parameters allow one to judge the activity of this mechanism and the systems maintaining homeostasis via CO_2 removal from the lungs, neutralization of increased acidity by buffer systems of blood, primarily by bicarbonate and hemoglobin systems, involving carbonic anhydrase [21]. CO_2 removal also depends on individual perfusion characteristics of the lung alveoli [22, 23].

The literature provides very little data on the role and significance of CO_2 emission for assessment of physical performance [24]. The majority of researchers pay attention to the maximum oxygen uptake and uptake at the aerobic threshold level when evaluating physical performance. However, the athlete's body capacity depends not only on the consumed amount of O_2 as an equivalent of energy production, but also on the parameters limiting physical performance, specifically on CO_2 emission as an integral indicator of the anaerobic mechanism activity [25]. It is well-known that the increase in CO_2 levels and the decrease in pH to the known values resulting from the anaerobic lactate mechanism activity stimulate the LFS, and the values moving out of the optimal range inhibit the system due to inhibition of the enzyme systems' activity, reduced nerve impulse transmission speed, muscle contractility, etc. [26–28].

CONCLUSIONS

The relationship between the new synthetic characteristic 2 and the values of non-metabolic carbon dioxide emission associated with the standardized physical exertion has been revealed based on the "Horsechoe of Rest" model developed. The non-metabolic CO_2 value is an integrated parameter of the anaerobic lactate mechanism activity and the mechanisms underlying utilization of its metabolites having a significant impact on the LFS [27]. In subsequent papers we are going to show the value of non-metabolic CO_2 for the duration of doing incremental exercises to failure and introduce the study results into the already constructed model [16] in order to determine individual and typological patterns of the physiological mechanisms' activity associated with the standardized physical exertion.

References

1. Ozhgibesova MA, Ganeeva ER, Kurilyak MM. Key mechanisms of muscle growth. Scientific Journal Scientific Review. Pedagogical sciences.2019; 4: 31–4. Russian.
2. Piuccoa T, Diefenthaelerb F, Prossera A, Binic R. Validity of different EMG analysis methods to identify aerobic and anaerobic thresholds in speed skaters. Journal of Electromyography and Kinesiology. 2020; 52.
3. Zignoli A, Fornasiero A, Stella F, Pellegrini B, Schena F, Biral F, et al. Expert-level classification of ventilatory thresholds from cardiopulmonary exercising test data with recurrent neural networks. European Journal of Sport Science. 2019; 19 (9): 1221–9.
4. Anokhin PK. Printsipial'nye voprosy obshchey teorii funktsional'nykh sistem. Printsipy sistemnoy organizatsii funktsiy. M.: Nauka; 1973. 120 s. Russian.
5. Bykov EV, Balberova OV, Kolomiets OI, Chipyshev AVCh. Correlation of functional testing data and results of competitive activities of athletes with different directions of physical activity. Scientific notes of the University. P.F. Lesgaft. 2018; 8: 32–8.

Russian.
6. Ham J-H, Park H-Y, Kim Y-H, Bae S-K, Ko B-H, Nam S-S. Development of an anaerobic threshold (HRLT, HRVT) estimation equation using the heart rate threshold (HRT) during the treadmill incremental exercise. J Exerc Nutrition Biochem. 2017; 21 (3): 43–9.
7. Kiselev AD. Modeling of elements of sports activities for the assessment and development of special performance. Physical education and sports training. 2021; 35: 72–80. Russian.
8. Wasserman K, Hansen JE, Sue DY, Stringer W, Sietsema K, X-G Sun, et al. Principles of Exercise Testing and Interpretation. 3rd ed. Lipincott Williams & Wilkins, 1999; p. 551.
9. Korzeniewski B. Regulation of ATP supply in mammalian skeletal muscle during resting state intensive work transition. Biophysical Chemistry. 2000; 83 (1): 19–34.
10. Sales MM, Sousa CV, Alves PM. Response to “A comprehensive integrative perspective of the anaerobic threshold engine”: the driver is not a part of an engine. Physiology & Behavior. 2019; 15.
11. Giovanelli N, Scaini S, Billat V, Lazzer S. A new field test to estimate the aerobic and anaerobic thresholds and maximum parameters. European Journal of Sport Science. 2020; 20 (4): 437–43.
12. Etxegaraia U, Portillo E, Irazusta J, Arriandiaga A, Cabanes I, et al. Estimation of lactate threshold with machine learning techniques in recreational runners. Applied Soft Computing. 2018; 63: 181–96.
13. Moxnes JF, Sandbakk Ø. Mathematical modelling of the oxygen uptake kinetics during whole-body endurance exercise and recovery. Mathematical and Computer Modelling of Dynamical Systems. 2018; 24 (1): 76–86.
14. Morton RH, Billat V. Modelling decremental ramps using 2- and 3-parameter "critical power" models. Journal of Sports Sciences. 2013; 31 (7): 731–5.
15. Lin C-W, Huang C-F, Wang J, Fu L-L, Mao T-Y. Detection of ventilatory thresholds using near-infrared spectroscopy with a polynomial regression model. Saudi Journal of Biological Sciences. 2020; 27 (6): 1637–42.
16. Chikov A, Egorov N, Medvedev D, Chikova S, Pavlov E, Drobintsev P, et al. Determination of the athletes' anaerobic threshold using machine learning methods. Biomedical Signal Processing and Control. 2022; 73: 47–53.
17. Reshef DN, Reshef YA, Finucane HK, Grossman SR, McVean G, Turnbaugh PJ, et al. Detecting novel associations in large data sets. Science. 2011; 334 (6062): 1518–24.
18. Van der Maaten L, Hinton G. Visualizing data using t-SNE. Journal of machine learning research. 2008; 9: 11.
19. James G, Witten D, Hastie T, Tibshirani R. An Introduction to Statistical Learning: with Applications in R / 1nd ed. Statistical Theory and Related Fields. 2021; 6 (1): 440.
20. McInnes L, Healy J, Melville J. Uniform manifold approximation and projection for dimension reduction. 2018 Feb. Available from: https://arxiv.org/abs/1802.03426.
21. Occhipinti R, Boron WF. Role of carbonic anhydrases and inhibitors in acid-base physiology: insights from mathematical modeling. International Journal of Molecular Sciences. 2019; 20 (15): 38–41.
22. Naumenko ZhK, Chernyak AV, Neklyudova GV, Chuchalin AG. Ventilation-perfusion ratio. Journal of Practical Pulmonology. 2018; 4: 86–90. Russian.
23. Ovsyannikov RYu, Lebedinsky KM. Choice of ultimate expiratory pressure with mechanical respiratory support (review). General resuscitation. 2022; 18 (6): 50–8. Russian.
24. Chesnokova NP, Ponukalina EV, Morrison VV, Bizenkova MN. Lecture 4. Physiology of blood gas transport and tissue oxygen supply. Scientific review. Medical sciences. 2017; 2: 40–2. Russian.
25. Torevsky VI, Litvak AL. The relationship between O2 consumption and blood supply of contracting muscles when working at different capacities in aerobic endurance trainees. Theory and practice of physical culture. 2006; 4: 49–54. Russian.
26. Anaev EKh. Lactat and lungs: from theory to practice. Pulmonology. 2014; 6: 108–14. Russian.
27. Mikhaylov SS. Biokhimiya dvigatel'noy deyatel'nosti. M.: Sport, 2016; 296 s. Russian.
28. Lazareva EA. Bioenergetic performance criteria for athletes specializing in various distances of athletics running. Features of the formation of a healthy lifestyle: factors and conditions. 2015; 179–82. Russian.

Литература

1. Ожгибесова М. А., Ганеева Е. Р., Куриляк М. М. Ключевые механизмы мышечного роста. Научное обозрение. Педагогические науки. 2019; 4: 31–4.
2. Piuccoa T, Diefenthaelerb F, Prossera A, Binic R. Validity of different EMG analysis methods to identify aerobic and anaerobic thresholds in speed skaters. Journal of Electromyography and Kinesiology. 2020; 52.
3. Zignoli A, Fornasiero A, Stella F, Pellegrini B, Schena F, Biral F, et al. Expert-level classification of ventilatory thresholds from cardiopulmonary exercising test data with recurrent neural networks. European Journal of Sport Science. 2019; 19 (9): 1221–9.
4. Анохин П. К. Принципиальные вопросы общей теории функциональных систем. Принципы системной организации функций. М.: Наука, 1973; 120 с.
5. Быков Е. В., Балберова О. В., Коломиец О. И., Чипышев А. В. Ч. Взаимосвязь данных функционального тестирования и результатов соревновательной деятельности спортсменов с различной направленностью физических нагрузок. Ученые записки университета им. П. Ф. Лесгафта. 2018; 8: 32–8.
6. Ham J-H, Park H-Y, Kim Y-H, Bae S-K, Ko B-H, Nam S-S. Development of an anaerobic threshold (HRLT, HRVT) estimation equation using the heart rate threshold (HRT) during the treadmill incremental exercise. J Exerc Nutrition Biochem. 2017; 21 (3): 43–9.
7. Киселев А. Д. Моделирование элементов спортивной деятельности для оценки и развития специальной работоспособности. Физическое воспитание и спортивная тренировка. 2021; 35: 72–80.
8. Wasserman K, Hansen JE, Sue DY, Stringer W, Sietsema K, X-G Sun, et al. Principles of Exercise Testing and Interpretation. 3rd ed. Lipincott Williams & Wilkins, 1999; p. 551.
9. Korzeniewski B. Regulation of ATP supply in mammalian skeletal muscle during resting state intensive work transition. Biophysical Chemistry. 2000; 83 (1): 19–34.
10. Sales MM, Sousa CV, Alves PM. Response to “A comprehensive integrative perspective of the anaerobic threshold engine”: the driver is not a part of an engine. Physiology & Behavior. 2019; 15.
11. Giovanelli N, Scaini S, Billat V, Lazzer S. A new field test to estimate the aerobic and anaerobic thresholds and maximum parameters. European Journal of Sport Science. 2020; 20 (4): 437–43.
12. Etxegaraia U, Portillo E, Irazusta J, Arriandiaga A, Cabanes I, et al. Estimation of lactate threshold with machine learning techniques in recreational runners. Applied Soft Computing. 2018; 63: 181–96.
13. Moxnes JF, Sandbakk Ø. Mathematical modelling of the oxygen uptake kinetics during whole-body endurance exercise and recovery. Mathematical and Computer Modelling of Dynamical Systems. 2018; 24 (1): 76–86.
14. Morton RH, Billat V. Modelling decremental ramps using 2- and 3-parameter "critical power" models. Journal of Sports Sciences. 2013; 31 (7): 731–5.
15. Lin C-W, Huang C-F, Wang J, Fu L-L, Mao T-Y. Detection of ventilatory thresholds using near-infrared spectroscopy with a polynomial regression model. Saudi Journal of Biological Sciences. 2020; 27 (6): 1637–42.
16. Chikov A, Egorov N, Medvedev D, Chikova S, Pavlov E, Drobintsev P, et al. Determination of the athletes' anaerobic threshold using machine learning methods. Biomedical Signal Processing and Control. 2022; 73: 47–53.
17. Reshef DN, Reshef YA, Finucane HK, Grossman SR, McVean G, Turnbaugh PJ, et al. Detecting novel associations in large data

sets. Science. 2011; 334 (6062): 1518–24.
18. Van der Maaten L, Hinton G. Visualizing data using t-SNE. Journal of machine learning research. 2008; 9: 11.
19. James G, Witten D, Hastie T, Tibshirani R. An Introduction to Statistical Learning: with Applications in R / 1nd ed. Statistical Theory and Related Fields. 2021; 6 (1): 440.
20. McInnes L, Healy J, Melville J. Uniform manifold approximation and projection for dimension reduction. 2018 Feb. Available from: https://arxiv.org/abs/1802.03426.
21. Occhipinti R, Boron WF. Role of carbonic anhydrases and inhibitors in acid-base physiology: insights from mathematical modeling. International Journal of Molecular Sciences. 2019; 20 (15): 38–41.
22. Науменко Ж. К., Черняк А. В., Неклюдова Г. В., Чучалин А. Г. Вентиляционно-перфузионное отношение. Практическая пульмонология. 2018; 4: 86–90.
23. Овсянников Р. Ю., Лебединский К. М. Выбор конечно-экспираторного давления при механической респираторной поддержке (обзор). Общая реаниматология. 2022; 18 (6): 50–8.
24. Чеснокова Н. П., Понукалина Е. В., Моррисон В. В., Бизенкова М. Н. Лекция 4. Физиология транспорта газов кровью и кислородного обеспечения тканей. Научное обозрение. Медицинские науки. 2017; 2: 40–2.
25. Тхоревский В. И., Литвак А. Л. Взаимосвязь между потреблением О2 и кровоснабжением сокращающихся мышц при работе разной мощности у лиц, тренирующих аэробную выносливость. Теория и практика физической культуры. 2006; 4: 49–54.
26. Анаев Э. Х. Лактат и легкие: от теории к практике. Пульмонология. 2014; 6: 108–14.
27. Михайлов С. С. Биохимия двигательной деятельности. М.: Спорт, 2016; 296 с.
28. Лазарева Э. А. Биоэнергетические критерии работоспособности спортсменов, специализирующихся на различных дистанциях легкоатлетического бега. Особенности формирования здорового образа жизни: факторы и условия. 2015; 179–82.

TRANSCRIPTION FACTORS IN HUMAN SKELETAL MUSCLE ASSOCIATED WITH SINGLE AND REGULAR STRENGTH EXERCISES

Lednev EM[1,2] ✉, Makhnovskii PA[2], Vepkhvadze TF[2], Sultanov RI[1], Zhelankin AV[1], Kanygina AV[1], Popov DV[1,2], Generozov EV[1]

[1] Lopukhin Federal Research and Clinical Center of Physical-Chemical Medicine of Federal Medical Biological Agency, Moscow, Russia

[2] Institute for Biomedical Problems of the Russian Academy of Sciences, Moscow, Russia

Skeletal muscle plasticity is the ability to change morphofunctional properties in response to changes in contractile activity. Strength training increases the size of muscle fibers and maximum strength with the activation of protein synthesis. Regulation of these changes at the gene level has not been investigated properly. This study aimed to identify transcription factors associated with changes in the transcriptome of the human skeletal muscle in the context of single and regular strength exercises. We assessed changes in the transcriptomic profile of *m. vastus lateralis* of 10 young men (mean age 23 (20.8 - 25.9) years) before and after 12-week leg extensor muscles strength training course, as well as before, 8 and 24 hours after a single exercise. Transcriptomic profiling involved RNA sequencing, search for binding motifs and the associated transcription factors. Bioinformatic methods of statistics, FastQC, GraphPad Prizm 8, DAVID, R enabled analysis of the data acquired. The strength training course resulted in the enrichment of the functional groups of genes "secreted proteins", "extracellular matrix" and "basal membrane" ($p < 0.05$). Transcriptomic responses and the associated transcription factors differed 8 and 24 hours after a single session as well as after regular training sessions. Transcription factors involved in adjustment to regular and one-time loads participate in myogenesis, angiogenesis, regulation of fiber phenotype, proteostasis and other processes. Thus, regulation of gene expression during adjustment to the resistance training loads is a complex process that involves many transcription factors with different functions. Investigation of the role played by these factors in the context of adjustment to exercising is a potentially rewarding task.

Keywords: gene expression, strength training, muscle plasticity, muscle fibers, hypertrophy

Funding: the study was supported financially by the Russian Science Foundation, Agreement № 21-15-00362 "Investigation of molecular genetic mechanisms of morphofunctional changes in human muscle fibers during high-intensity physical loads".

Author contribution: Lednev EM, Vepkhvadze TF — study design and conduct, muscle sampling; Makhnovskii PA, Sultanov RI and Kanygina AV — bioinformatic data analysis; Zhelankin AV, Lednev EM — laboratory research; Generozov EV, Popov DV — study design and conduct, data processing, article authoring.

Compliance with ethical standards: the study was approved by the Ethics Committee of the Lopukhin Federal Research and Clinical Center Of Physical-Chemical Medicine (Minutes № 202/06/01 of June 01, 2021). All participants signed the voluntary informed consent form.

✉ **Correspondence should be addressed:** Egor M. Lednev
Khoroshevskoe sh., 76A, Moscow, 123007, Russia ledhauz@gmail.com

Received: 21.07.2023 **Accepted:** 01.09.2023 **Published online:** 27.09.2023

DOI: 10.47183/mes.2023.031

ТРАНСКРИПЦИОННЫЕ ФАКТОРЫ В СКЕЛЕТНОЙ МЫШЦЕ ЧЕЛОВЕКА, АССОЦИИРОВАННЫЕ С ОДНОКРАТНЫМ И РЕГУЛЯРНЫМИ СИЛОВЫМИ УПРАЖНЕНИЯМИ

Е. М. Леднев[1,2] ✉, П. А. Махновский[2], Т. Ф. Вепхвадзе[2], Р. И. Султанов[1], А. В. Желанкин[1], А. В. Каныгина[1], Д. В. Попов[1,2], Э. В. Генерозов[1]

[1] Федеральный научно-клинический центр физико-химической медицины имени Ю. М. Лопухина Федерального медико-биологического агентства, Москва, Россия

[2] Институт медико-биологических проблем Российской академии наук, Москва, Россия

Пластичность скелетной мышцы — способность менять морфофункциональные свойства в ответ на изменение сократительной активности. Силовые тренировки ведут к увеличению размеров мышечных волокон и максимальной силы с активацией синтеза белков. Регуляция этих изменений на генном уровне мало изучена. Целью работы было выявить транскрипционные факторы, ассоциированные с изменением транскриптома скелетной мышцы человека при однократном и регулярных силовых упражнениях. Изменение транскриптомного профиля оценивали в *m. vastus lateralis* 10 молодых мужчин (возраст 23 (20,8–25,9) года) до и после 12-недельной силовой тренировки мышц-разгибателей ног, а также до, через 8 и 24 ч после однократного упражнения. Транскриптомные профили оценивали методом РНК секвенирования, поиска мотивов связывания и ассоциированных транскрипционных факторов. Использовали биоинформатические методы статистики, программы FastQC, GraphPad Prizm 8, DAVID, R. Длительная силовая тренировка привела к обогащению функциональных групп генов «секретируемые белки», «внеклеточный матрикс» и «базальная мембрана» ($p < 0,05$). Транскриптомные ответы и ассоциированные транскрипционные факторы различались через 8 и 24 ч после однократной нагрузки, а также после регулярных тренировок. Транскрипционные факторы, участвующие в адаптации к длительной и однократной нагрузке, участвуют в миогенезе, ангиогенезе, регуляции фенотипа волокон, протеостазе и иных процессах. Таким образом, регуляция экспрессии генов при адаптации к силовым нагрузкам — сложный процесс с участием множества транскрипционных факторов с разными функциями. Изучение роли этих факторов в адаптации скелетной мышцы к упражнениям является перспективной задачей.

Ключевые слова: экспрессия генов, силовая тренировка, мышечная пластичность, мышечные волокна, гипертрофия

Финансирование: исследование выполнено при финансовой поддержке Российского научного фонда, соглашение № 21-15-00362 «Исследование молекулярно-генетических механизмов морфофункциональных изменений мышечных волокон человека в ходе высокоинтенсивных физических нагрузок».

Вклад авторов: Е. М. Леднев, Т. Ф. Вепхвадзе — организация и проведение исследования, взятие мышечных биопсий; П. А. Махновский, Р. И. Султанов и А. В. Каныгина — биоинформатический анализ данных; А. В. Желанкин, Е. М. Леднев — выполнение лабораторных исследований; Э. В. Генерозов, Д. В. Попов — организация и проведение исследования, обработка данных, написание статьи.

Соблюдение этических стандартов: исследование одобрено этическим комитетом ФГБУ ФНКЦ ФХМ им. Ю. М. Лопухина ФМБА России (номер протокола № 202/06/01 от 01 июня 2021 г.). Все испытуемые подписали добровольное информированное согласие на участие в исследовании.

✉ **Для корреспонденции:** Егор Михайлович Леднев
Хорошевское шоссе, д. 76А, г. Москва, 123007, Россия; ledhauz@gmail.com

Статья получена: 21.07.2023 **Статья принята к печати:** 01.09.2023 **Опубликована онлайн:** 27.09.2023

DOI: 10.47183/mes.2023.031

Plasticity is one of the capabilities of skeletal muscles: they can change their morphofunctional characteristics in response to changes in the level of contractile activity. Investigation of the molecular mechanisms underpinning plasticity is a fundamental task. It also has a practical dimension in the context of optimization of training programs for amateur and professional athletes, as well as for prevention of the negative effect of various diseases on the skeletal muscles. On the one hand, a high-intensity physical load triggers transient increase of the mTORC1-dependent rate of muscle protein synthesis [1–3]; thus, practiced on a regular basis, such loads make muscle fibers and muscle in general grow bigger and stronger. On the other hand, a single session [4–7] and regular resistance training of varying duration [4, 6–11] alter the gene expression profile in the exercised skeletal muscle. The mechanisms regulating these alterations (in particular, transcription factors associated with changes in the transcriptomic profile) have not been sufficiently investigated.

This study aimed to search for transcription factors associated with changes in the transcriptome of human skeletal muscle in the context of single and regular strength exercises. For this purpose, we used RNA sequencing in order to detect changes in the transcriptomic profile of bioptic samples of *m. vastus lateralis*. The samples were taken from 10 young men before and after a 12-week leg extensor (knee joint) training course and 8 and 24 hours after a single exercise session (Fig. 1).

METHODS

Study design

The study involved 10 young men, median age — 23 years (20.8–25.9), median BMI — 22 (20.9–25.1) kg/m^2. The inclusion criteria were: perfect health; lack of acute and chronic diseases; lack of experience of long-term resistance training; lack of traumas and surgeries on the back and lower limbs. The exclusion criteria were: refusal to participate in the training sessions and test procedures; detection of adverse conditions in the context of training sessions or procedures (life- and health-threatening); violation of the recommended diet or practicing vicious habits during the experiment. For 12 weeks, the participants trained leg extensor muscles by doing the seated leg press exercise (both legs). They were surveyed before the experiment; all of the participants reported diverse diets with regular meals containing sufficient amounts of protein, fats and carbohydrates, and adequate volumes of water consumed through the day. The recommendation for them was to continue with their usual diets during the experiment. All participants were non-smokers before and during the study; they did not take bioactive supplements for 3–4 months before the experiment nor while involved therein. None of them was a vegetarian or a vegan. With regular resistance training sessions, it is not the magnitude of the load but doing each exercise to expressed fatigue (failure, inability to continue) that guarantees muscle growths [12]. At the same time, a training program optimal from the viewpoint of strength development includes 25 sets per session and at least 2 sessions a week [13,14]. Therefore, the participants of our study trained 3 times a week, with varying intensity: Monday — (65% MVC, to failure) × 3 sets, Wednesday — (50% MVC, 25 repetitions) × 4 sets, Friday — (75% MVC, to failure) × 4 sets. The participants were allowed 4 minutes of rest between the sets. In addition, each training session started with a warm up (50% MVC, 12 repetitions). All participants reported 8 hours of sleep a day (on average), none of them mentioned any changes in the sleeping patterns during the experiment. We recommended moderation in physical activity and keeping it at the customary level for 24 hours after each training sessions; also, the recommendation was to abstain from alcohol for 24–48 hours thereafter, when the body is restoring.

We took bioptic samples from *m. vastus lateralis* before the training part of the experiment (Fig. 1; B1). Two days later, the participants took an introductory session, and after another 2 days, we determined their MVC, which was a derivative of the maximum load at which the participant could fully extend both legs. We assessed the MVC every 2–3 weeks and after the training part of the experiment (Fig. 1; T2). Separately, we measured the MVC of the leg that was loaded later, during the test training session (TTS); this leg was selected at random in order to mitigate the dominant limb effect (Fig. 1; T1). After 4 days, the participants attended the TTS and did the seated leg press exercise with one leg (Fig. 1): warm-up (50% of the MVC, 12 repetitions) + (65% MVC, to failure) × 4 approaches). Bioptic samples were taken from both legs (donor muscle — *m. vastus lateralis*), loaded and not loaded, 8 and 24 hours after the session. Gene response may change several hours after exertion not only because of the muscle contractions, but also under the influence of systemic factors (circadian oscillations, nutrition, etc.) [15,16]. In our work, seeking to eliminate the

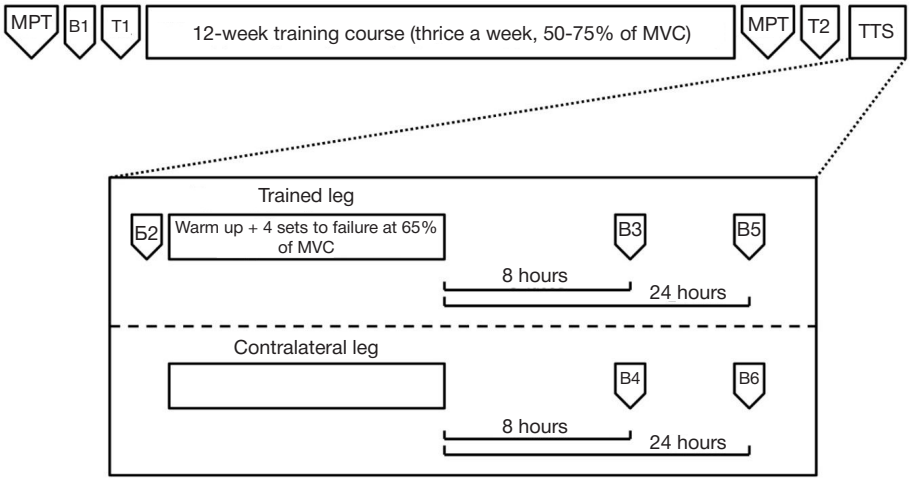

Fig. 1. Physiological experiment diagram. T1, T2 — testing the maximum voluntary contraction (MVC); TTS — test training session (single session with bioptic samples taken from both legs before and after exercising one leg); B1–B6 — sampling from the *m. vastus lateralis*. Biopsies B1, B2, B3, B5 were taken from the leg loaded during TTS. Biopsies B4 and B6 — from the contralateral leg (which was not loaded). Both legs were exercised during twelve-week training course

Table 1. Results of analysis of functional enrichment, genes that changed expression in *m. vastus lateralis* after a training course and a one-time physical load

Comparison	UniProt term	P_{adj}	Number of genes	Genes
After/before training course	Secreted	5,40E-12	39	*COL15A1, SPARC, PCOLCE2, LAMA4, HTRA1, F13A1, C1ORF54, CHRDL1, NID2, FSTL1, THBS4, SERPINA5, CNPY4, CTSK, PENK, S100A13, CCN1, PAMR1, POSTN, CD163, IGFBP3, LAMB1, RNASE1, PLXDC1, ASPN, FNDC5, MFAP5, COL1A1, SFRP4, SMOC2, COL3A1, COL1A2, FNDC1, TCN2, COL5A2, MGP, SAA1, S100A4, MASP1*
	Extracellular matrix	1,70E-06	14	*POSTN, COL15A1, SPARC, LAMA4, LAMB1, NID2, ASPN, THBS4, MFAP5, COL1A1, SMOC2, COL3A1, COL1A2, COL5A2*
	Basement membrane	0.0098	5	*SMOC2, SPARC, LAMA4, LAMB1, NID2*
Loaded/not loaded muscle, 8 hours after exercise	–	n.s.	–	–
Loaded/not loaded muscle, 24 hours after exercise	Cytoskeleton	0.0087	64	*RIPOR2, RIF1, WDR1, CBY1, HSPB1, HNRNPU, NR3C1, TUBA1C, TUBA1B, CSRP3, TUBA1A, SGCD, MPRIP, CEP250, CEP170, DYNLT1, TUBB, ANXA11, CSNK1D, PPP4R3B, ANK3, RANGAP1, MLF1, TUBA4A, ACTA2, KAT2B, KIF9, PALLD, EVL, EZR, PFN1, FKBP4, MACF1, DCTN4, CEP85L, PXN, UACA, AURKA, FGD4, TTC21B, FLNB, CEP192, FLNC, CCT5, MAP2K6, CEP350, RAB3IP, SYNJ2, PARVB, ARHGAP26, ARHGAP24, SEPTIN7, RAB10, DIAPH1, KITLG, TTLL4, ACTC1, APPBP2, KATNBL1, JMY, SPIRE1, PKN2, PTPN4, CALM2*

influence of systemic factors on gene expression after a one-time load, we evaluated the differences in the transcriptomic profile in samples taken from both the loaded and the not loaded (control) muscle of the contralateral limb.

All bioptic samples were taken after 30 minutes of rest in the supine position, from the middle third of *m. vastus lateralis*, under local anesthesia (2 ml of 2% lidocaine), using a 6 mm suction-modified Bergström needle [17]. The site of each subsequent sampling was 4 cm proximal to the previous one. The tissue samples were quickly cleaned of blood and connective tissue, frozen in liquid nitrogen and stored at –80 °C.

Transcriptomic analysis

Muscle tissue samples (~20 mg) were homogenized in a TissueLyser II homogenizer (Qiagen; Germany), two cycles of 1 minute each, at the frequency of 30 Hz; RNA was isolated with an RNeasy mini kit (Qiagen; Germany). We used a Qubit 3.0 fluorimeter (Thermo Scientific; USA) to measure concentration of the RNA, and a Bioanalyzer 2100 capillary electrophoresis device (Agilent; USA) to establish its integrity. RNA was cleaned of DNA contamination with the help of a Turbo DNA-free Kit (Thermo Scientific, USA). Double-stranded cDNA was synthesized in a Mint-2 kit (Eurogen; RF). The technology used to purify the resulting PCR product was SPRI, the process involved AMPure XP beads (Beckman-Coulter; USA); double-stranded cDNA was split in a ME220 focused-ultrasonicator (Covaris; USA) into double-stranded DNA fragments of 250 pn, strips of eight 50 µl tubes (Peak Incident Power 75W, Duty Factor 20%, Cycles per Burst 1000, Treatment Time 75 s). The resulting double-stranded cDNA fragments were also purified using the SPRI technology and AMPure XP beads (Beckman-Coulter; USA).

Universal DNA Library Prep Set (MGI-Tech; PRC) was used to prepare libraries for 10 ng fragments of the acquired double-stranded cDNA. The protocol included repair and phosphorylation of ends of the fragments, ligation of asymmetric adapters and 47 cycles of amplification of the ligation products for quantitative library development. RNA were sequenced in a DNBseq-G400 analyzer (MGI; PRC) as per the manufacturer's instructions, using reagents from the DNBSEQ-G400RS High-throughput Sequencing Set (PE100), read length — 100 nucleotides, depth — 50 million pairs of reads per sample.

Bioinformatic processing of the RNA sequencing data

We used the FastQC v0.11.9 software (Babraham Institute; UK) to control quality of the sequencing data. Low-quality reads and adapter sequences were removed from the analysis using the Trimomatic tool v0.39 (USADELLAB; USA), standard parameters. We mapped the paired reads to the reference human genome, version GRCh38.p13 (gencode v37), using STAR v2.7.4a (Cold Spring Harbor Laboratory, USA) with standard parameters. The number of unique reads aligned to known exons of each gene was determined using the featureCounts function of the Rsubread package (R programming language, Lucent Technologies, USA), with genome annotation gencode v37.

We used the DESeq2 package of the R programming language to find differentially expressed genes (DEGs) in the compared groups. The DEG registration threshold was Padj < 0.1 (BH-adjusted *p*-value). To analyze the functional enrichment of DEGs, we used DAVID tools (Frederick National Laboratory for Cancer Research; USA) and UniProt resources.

Searching for transcription factors potentially regulating gene expression in response to strength exercises, as well as the corresponding binding motifs, we analyzed promoter sites of DEGs (open chromatin sites around the transcription initiation start that were determined for skeletal muscle and reported earlier [18]). The search for motifs (and the associated transcription factors) was performed by the GeneXplain platform and the TRANSFAC v2022.1 positional weight matrix database, as described earlier [18]. The maximum enrichment (FEadj, adjusted odds ratio of site frequency with a confidence interval of 99%) was determined for each positional weight matrix (PWM) relative to a random set of 5000 promoters. The adjusted enrichment value (FEadj) > 1.5 for binding sites with transcription factors (binomial test) and FDR < 0.05 were selected as significance criteria.

Statistical processing

We used the GraphPad Prizm 8 program (GraphPad Software, Dotmatics; USA) and Wilcoxon test ($p < 0.05$) to assess changes in the MVC post training.

RESULTS

Twelve weeks of strength training increased the maximum voluntary contraction by 1.19 times ($p = 0.002$), which is

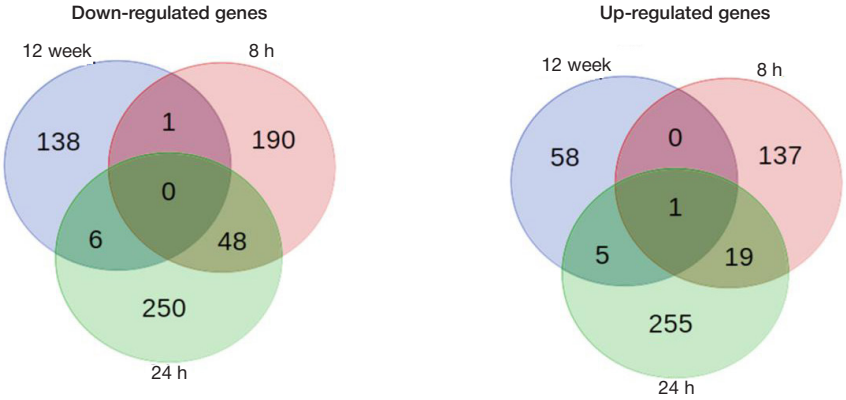

Fig. 2. Number of genes that changed expression in *m. vastus lateralis* after a 12-week training program and 8 and 24 hours after a single load. Venn diagrams show the number of mRNAs unique and common to different experimental conditions for genes that increased and decreased expression

comparable to the results of studies involving training with a similar design [19, 20]. The figure confirms effectiveness of the training program we selected.

The effect of regular strength training on changes in the basal transcriptome

Training changed expression of 209 genes, with the content of 145 mRNAs increasing and 64 mRNAs decreasing (comparison B2-B1; Figure 1). Functional enrichment analysis revealed significant enrichment for the functional terms "extracellular matrix", "secreted proteins", and "basement membrane". Among these genes, there were various collagens, calmodulin-like proteins and adhesion molecules (Table 1). This result, despite the minor character of alterations, is consistent with the findings of meta-analyses that reviewed transcriptome changes in response to regular strength training [21, 22]. On the one hand, activation of expression of protein genes of extracellular matrix is probably one of the mechanisms involved in the adjustment of the trained skeletal muscle to regular physical exertion. On the other hand, our and other studies report a relatively weak effect of prolonged strength training on the skeletal muscle transcriptome, even when training sessions are regular for 15 years or more [23]. This may be due to the fact that strength exercises, first of all, activate translation and not transcription.

Transcriptome change in response to a single session

Eight and twenty-four hours after a single session, the content of 396 and 584 mRNAs changed, respectively; more than half of them increased expression: 239 mRNAs and 304 mRNAs, respectively. There was little overlap between the sets of genes that changed expression 8 and 24 hours after a single session (Fig. 2). The analysis of enrichment revealed no functional categories 8 hours after the load. Nevertheless, we detected activation of expression of a number of genes known from previous studies as markers of early response to contractile activity (including during aerobic exercise): *ATF3*, *DDIT3*, *JUND*, *MAFF*, *NR4A3*, *VDR*, *PRKAG2*, *PPARGC1A*, etc. [22,24–26]. Genes that changed expression 24 hours after a single session were associated with the term "cytoskeleton" (Table 1). More than half of them increased expression and were represented by genes of motor proteins (alpha- and beta-tubulin, actins *ACTA2* and *ACTC1*, components of the kinesin-dynein complex KIF9 and *DYNLT1*), chaperones (*CRYAB1*, *HSPB1*), etc. It should be noted that some contractile activity response expression markers (*ATF3*, *DDIT3*, *VDR*, *PRKAG2*) remained activated during the post-exercise recovery period for up to 24 hours, which suggests their important role in regulating the response to physical exertion. Interestingly, there is even less overlap between gene response to a single exertion and regular training sessions (Fig. 2).

After a 12-week strength training program that involved both legs, we have registered a change in the transcriptomic profile of *m. vastus lateralis* that is comparable to that described earlier in similar studies. Using a test model, which was the exercise done with one leg, and comparing gene expression in the loaded and not loaded *m. vastus lateralis*, we, for the first time ever, managed to describe the transcriptomic response (on the 8th and 24th hours of recovery) in human skeletal muscle that is specific to strength exercises, i.e., this response was independent of circadian and systemic influences. There was only a slight overlap between the sets of genes that changed expression between different experimental conditions, which can be explained by the specific mechanisms of gene expression regulation peculiar to the said conditions.

Analysis of transcription factors associated with changes in gene expression

Figure 3 presents the results of search for transcription factors associated with changes in gene expression under the studied experimental conditions. Adjustment to regular strength training sessions triggered changes in basement gene expression in *m. vastus lateralis* that were associated with diverse families of transcription regulators; the most enriched of them were the poorly studied factors with zinc finger domains. In addition, we identified a number of factors that quite expectedly altered their activity after regular strength training sessions. Thus, activation of gene expression was associated with factors directly related to the contractile activity; for example, NFATC component of the Ca^{2+}–dependent calcineurin-NFAT signaling pathway [27]. NFATC1 is known to control muscle growth [28–30] and the ratio of muscle fiber types in mice, as well as suppress the activity of MyoD-dependent promoters [31].

DISCUSSION

Regular training sessions lead to activation of the expression of extracellular matrix genes, including genes encoding angiogenesis regulatory proteins. Among the transcription factors we found, potential regulators of angiogenesis are ERG and SOX18. ERG is known to regulate angiogenesis by controlling the expression of E-cadherin and the Wnt/β-catenin signaling pathway [27]. SOX18 is expressed mainly in endothelial cells; it regulates angiogenesis by activating their migration and proliferation, while the pattern of SOX18

TFs associated with up-regulated genes

	Training	+8 h	+24 h	
FOXJ2	1.51			FOX
FOXP1	1.95			FOX
RELA	1.50			NfkappaB-related
NFATC1	1.62			NFAT-related
NFATC3	1.65			NFAT-related
NFATC4	1.62			NFAT-related
STAT6	1.51			STAT
TBP	1.78		1.65	TBP-related
ZNF713	1.52			C2H2 zinc finger factors
ZFP3	1.61			C2H2 zinc finger factors
ZNF677	1.50			C2H2 zinc finger factors
ZBTB45	2.64			C2H2 zinc finger factors
ZNF362	2.21			C2H2 zinc finger factors
ZNF384	1.68			C2H2 zinc finger factors
ZNF260	1.89			C2H2 zinc finger factors
ZFP30	2.63			C2H2 zinc finger factors
ZNF354A	1.68			C2H2 zinc finger factors
ZNF611	2.31			C2H2 zinc finger factors
ZNF251	1.51			C2H2 zinc finger factors
ZNF224		1.63		C2H2 zinc finger factors
ZNF569		1.60		C2H2 zinc finger factors
ZNF16			2.08	C2H2 zinc finger factors
ZBTB11			1.53	C2H2 zinc finger factors
ERG	1.74			Ets-related
SOX18	1.52			SOX
HBP1		1.67		SOX
MEF2A	1.52			MADS box factors
POU6F1	1.70			POU
MSX2	1.50			NK
HOXA13	1.68			HOX
HOXA10	1.61			HOX
HOXA6		1.75		HOX
HOXB6		1.54		HOX
HOXB7		2.31		HOX
JUN		2.00		Jun-related
JUNB		1.95		Jun-related
JUND		1.86		Jun-related
BACH1		1.89		Jun-related
BACH2		2.02		Jun-related
FOS		1.97		Fos-related
FOSL2		2.34		Fos-related
ATF3		2.35		Fos-related
JDP2		1.87		Fos-related
MAF		1.79		Maf-related
MAFK		1.95		Maf-related
ATF4		2.21		ATF4
CREB1		1.52		CREB-related
MSC		1.68		Tal-related
TFAP4		1.51		BHLH-ZIP
ESR1		1.65		Steroid hormone receptors
PPARG		1.66		Thyroid hormone receptors
IRX3		1.98		TALE-type HD
PKNOX1		1.59		TALE-type HD
SATB1			1.56	HD-CUT
ETS2			1.76	Ets-related
GMEB2			1.68	GMEB
CEBPA	1.79		2.72	CEBP-related
CEBPB	1.78		1.64	CEBP-related
CEBPD	1.91		1.59	CEBP-related
CEBPG	1.51	1.98		CEBP-related
DDIT3		1.78		CEBP-related
DBP			1.59	CEBP-related
HLF			1.63	CEBP-related

TFs associated with down-regulated genes

	Training	+8 h	+24 h	
PKNOX1	1.52			TALE-type HD
TGIF1	1.64			TALE-type HD
TCF12	1.52			E2A
MYOG	1.60			MyoD-ASC-related
MYF5	1.86			MyoD-ASC-related
MSC	1.72			Tal-related
SOX13			1.87	SOX
SOX6		1.62		SOX
RELB		1.52		NfkappaB-related
TBP		1.76		TBP-related
FOXO1		1.60		FOX
FOXO4		1.56		FOX
FOXP1		1.69		FOX
FOXK1			1.83	FOX
ZBTB11	1.76			C2H2 zinc finger factors
ZNF770	1.56			C2H2 zinc finger factors
ZNF132		1.55		C2H2 zinc finger factors
RBAK			2.62	C2H2 zinc finger factors
ZNF263			1.63	C2H2 zinc finger factors
ZNF664			1.51	C2H2 zinc finger factors
ZNF774			1.54	C2H2 zinc finger factors
ZFP30			1.54	C2H2 zinc finger factors
ZNF341			1.58	C2H2 zinc finger factors
TEF			1.71	CEBP-related
DMRT2			2.10	DMRT
ARID3A			2.01	ARID-related

Fig. 3. Transcription factors (TFs) associated with genes that increased and decreased expression after regular strength training sessions (Training) and 8 hours and 24 hours after a single physical load. Shades of color and numbers indicate the amount of enrichment of the binding motif with the transcription factor in individual promoters of genes that have changed expression, relative to 5000 random genes that have not changed expression (see METHODS).

expression in endothelial cells coincides with VEGFA and its receptor [32]. We have expectedly found MEF2A, regulator of myogenesis, and MSX2 among the factors associated with gene expression growth. Unexpectedly, a drop in expression of some genes was associated with myogenic E-box-binding factors (MYOG, MYF5, MSC) controlling the differentiation of myoblasts at different stages. It can be assumed that increased activity of some myogenic factors and suppression of others is associated with a change in the phenotype of the muscle after training. Such strength training programs are known to predominantly increase the size of type II muscle fibers and have only a weak effect on the type I fibers [1].

It is difficult to assess the functions of other transcription factors associated with changes in the transcription profile in the context of regular strength training sessions. For example, FOXP1 was previously described as a transcription repressor, its overexpression causing atrophy and loss of muscle mass in mice [33]. In addition, FOXP1 inhibits the activity of MyoD [34]. RELA and STAT6 are known as regulators of inflammation, but they also play a role in the regulation of myogenesis and atrophy [35, 36].

Eight hours after a single session, the regulation of gene expression was primarily associated with factors of the bZIP class (families of early response factors JUN, FOS, MAF, etc.). Some of them (ATF4, AP-1 factors (FOS, JUN), DDIT3, CEBP) are known to be are activated against violation of proteostasis and EPR stress [37, 38]. Activation of these factors is quite expected, since high-intensity strength exercises cause pronounced metabolic and mechanical stress, however, these factors were not found to activate at later stages of recovery (24 hours) after a single session. On the contrary, dropping gene expression at the 8th hour of recovery was associated with factors of the FOXO family, which regulate the activity of the ubiquitin-proteasome system in the muscle [39–41].

Twenty-four hours after the exercise, the change in gene expression was associated with a small number of transcription factors: growth — mainly with the factors of the CEBP family, suppression — factors containing zinc finger domains, KRAB domain containing RBAK repressor in particular.

Thus, we have sufficient uniqueness of the sets of genes that changed expression in response to a 12-week

strength training course and a single training session, as well as the transcription factors associated with them. Apparently, the reason behind these findings is the availability of many signaling pathways regulating activation of various sets of transcription factors and their target genes in the basal state after a course of regular aerobic training and at different stages of recovery after a single training session. There are published papers that describe the role in regulation of myogenesis played by some transcription factors that we have predicted in our work, which indirectly confirms correctness of the bioinformatic analysis methods we use. The role of other transcription factors in the regulation of myogenesis is not so obvious. Investigation of the role played by these factors in the context of adjustment of a skeletal muscle to high-intensity exercises is a potentially rewarding task.

CONCLUSIONS

We have shown pronounced changes in the transcriptome of skeletal muscle in response to a single exercise session and a 12-week strength training course building up contractile capacities of the trained muscles. These changes are quite consistent with the results of other works that involved similar training routines. Notably, transcriptomic responses and the associated transcription factors differed markedly both 8 hours and 24 hours both after a single training session and after a 12-week regular exercising course. Our results indicate complexity of regulation of gene expression during adjustment to resistance loads, with the apparent reason therefore being the large number of processes involved in the regulation growth of muscle mass.

References

1. Vinogradova OL, Popov DV, Netreba AI, Cvirkun DV, Kurochkina NS, Bachinin AV, i dr. Optimizaciya processa fizicheskoj trenirovki: razrabotka novyh “shhadyashhih” podxodov k trenirovke silovyh vozmozhnostej, Fiziologiya cheloveka. 2013; 39: 71–85. Dostupno po ssylke: https://doi.org/10.7868/S0131164613050172. Russian.
2. Solsona R, Pavlin L, Bernardi H, Sanchez AMJ. Molecular regulation of skeletal muscle growth and organelle biosynthesis: Practical recommendations for exercise training. Int J Mol Sci. 2021; 22: 1–31. Available from: https://doi.org/10.3390/ijms22052741.
3. Mesquita PHC, Vann CG, Phillips SM, McKendry J, Young KC, Kavazis AN, et al. Skeletal muscle ribosome and mitochondrial biogenesis in response to different exercise training modalities. Front Physiol. 2021; 12. Available from: https://doi.org/10.3389/fphys.2021.725866.
4. Gordon PM, Liu D, Sartor MA, IglayReger HB, Pistilli EE, Gutmann L, et al. Resistance exercise training influences skeletal muscle immune activation: a microarray analysis. J Appl Physiol. 2012: 112: 443–53. Available from: https://doi.org/10.1152/japplphysiol.00860.2011.
5. Dickinson JM, D'Lugos AC, Naymik MA, Siniard AL, Wolfe AJ, Curtis DP, et al. Transcriptome response of human skeletal muscle to divergent exercise stimuli. J Appl Physiol. 2018; 124: 1529–40. Available from: https://doi.org/10.1152/japplphysiol.00014.2018.
6. Damas F, Ugrinowitsch C, Libardi CA, Jannig PR, Hector AJ, Mcglory C, et al. Resistance training in young men induces muscle transcriptome-wide changes associated with muscle structure and metabolism refining the response to exercise-induced stress. Eur J Appl Physiol. 2018; 118: 2607–16. Available from: https://doi.org/10.1007/s00421-018-3984-y.
7. Raue U, Trappe TA, Estrem ST, Qian HR, Helvering LM, Smith RC, et al. Transcriptome signature of resistance exercise adaptations: Mixed muscle and fiber type specific profiles in young and old adults. J Appl Physiol. 2012; 112: 1625–36. Available from: https://doi.org/10.1152/japplphysiol.00435.2011.
8. Lundberg TR, Fernandez-Gonzalo R, Gustafsson T, Tesch PA. Aerobic exercise does not compromise muscle hypertrophy response to short-term resistance training. J Appl Physiol. 2013; 114: 81–89. Available from: https://doi.org/10.1152/japplphysiol.01013.2012.
9. Liu D, Sartor MA, Nader GA, Gutmann L, Treutelaar MK, Pistilli EE, et al. Skeletal muscle gene expression in response to resistance exercise: Sex specific regulation. BMC Genomics. 2010; 11: 659. Available from: https://doi.org/10.1186/1471-2164-11-659.
10. Nascimento EBM, Hangelbroek RWJ, GHooiveld GJEJ, Hoeks J, Van Marken Lichtenbelt WD, Hesselink MHC, et al. Comparative transcriptome analysis of human skeletal muscle in response to cold acclimation and exercise training in human volunteers. BMC Med Genomics. 2020; 13: 1–11. Available from: https://doi.org/10.1186/s12920-020-00784-z.
11. Stepto NK, Coffey VG, Carey AL, Ponnampalam AP, Canny BJ, Powell D, et al. Global gene expression in skeletal muscle from well-trained strength and endurance athletes. Med Sci Sports Exerc. 2009; 41: 546–65. Available from: https://doi.org/10.1249/MSS.0b013e31818c6be9.
12. Schoenfeld BJ, Grgic J, Ogborn D, Krieger JW. Strength and hypertrophy adaptations between low- vs. High-load resistance training: A systematic review and meta-analysis. J Strength Cond Res. 2017; 31: 3508–23. Available from: https://doi.org/10.1519/JSC.0000000000002200.
13. Krieger JW. Single Vs. Multiple Sets of Resistance. J Strength Cond Res. 2010; 24: 1150–9. Available from: htpps://doi.org/10.1519/JSC.0b013e3181d4d36
14. Schoenfeld BJ, Ogborn D, Krieger JW. Effects of Resistance Training Frequency on Measures of Muscle Hypertrophy: A Systematic Review and Meta-Analysis. Sport Med. 2016; 46: 1689–97. Available from: https://doi.org/10.1007/s40279-016-0543-8.
15. Catoire M, Mensink M, Boekschoten MV, Hangelbroek R, Müller M, Schrauwen P, et al. Pronounced Effects of Acute Endurance Exercise on Gene Expression in Resting and Exercising Human Skeletal Muscle. PLoS One. 2012; 7. Available from: https://doi.org/10.1371/journal.pone.0051066.
16. Schroder EA, Harfmann BD, Zhang X, Srikuea R, England JH, Hodge BA, et al. Intrinsic muscle clock is necessary for musculoskeletal health. J Physiol. 2015; 593: 5387–404. Available from: https://doi.org/10.1113/JP271436.
17. Shanely AR, Zwetsloot KA, Travis Triplett N, Meaney MP, Farris GE, Nieman DC. Human skeletal muscle biopsy procedures using the modified Bergström technique. J Vis Exp. 2014; 1–8. Available from: https://doi.org/10.3791/51812.
18. Makhnovskii PA, Gusev OA, Bokov RO, Gazizova GR, Vepkhvadze TF, Lysenko EA, et al. Alternative transcription start sites contribute to acute-stress-induced transcriptome response in human skeletal muscle. Hum Genomics. 2022; 16: 1–13. Available from: https://doi.org/10.1186/s40246-022-00399-8.
19. Campos GER, Luecke TJ, Wendeln HK, Toma K, Hagerman FC, Murray TF et al. Muscular adaptations in response to three different resistance-training regimens: Specificity of repetition maximum training zones. Eur J Appl Physiol. 2002; 88: 50–60. Available from: https://doi.org/10.1007/s00421-002-0681-6.
20. Yapici H, Gülü M, Yagin FH, Ugurlu D, Comertpay E, Eroglu O et al. The effect of 8-weeks of combined resistance training and chocolate milk consumption on maximal strength, muscle thickness, peak power and lean mass, untrained, university-aged males. Front Physiol. 2023; 14: 1–11. Available from: https://doi.org/10.3389/fphys.2023.1148494.
21. Deane CS, Willis CRG, Phillips BE, Atherton PJ, Harries LW, Ames RM, et al. Transcriptomic meta-analysis of disuse muscle atrophy vs. resistance exercise-induced hypertrophy in young and older humans. J Cachexia Sarcopenia Muscle. 2021; 12: 629–45.

Available from: https://doi.org/10.1002/jcsm.12706.
22. Pillon NJ, Gabriel BM, Dollet L, Smith JAB, Sardón Puig L, Botella J, et al. Transcriptomic profiling of skeletal muscle adaptations to exercise and inactivity. Nat Commun. 2020; 11: 470. Available from: https://doi.org/10.1038/s41467-019-13869-w.
23. Chapman MA, Arif M, Emanuelsson EB, Reitzner SM, Lindholm ME, Mardinoglu A, et al. Skeletal Muscle Transcriptomic Comparison between Long-Term Trained and Untrained Men and Women. Cell Rep. 2020; 31. Available from: https://doi.org/10.1016/j.celrep.2020.107808.
24. Dzik KP, Grzywacz T, Łuszczyk M, Kujach S, Flis DJ, Kaczor JJ. Single bout of exercise triggers the increase of vitamin D blood concentration in adolescent trained boys: a pilot study. Sci Rep. 2022; 12: 1–10. Available from: https://doi.org/10.1038/s41598-022-05783-x.
25. Rundqvist HC, Montelius A, Osterlund T, Norman B, Esbjornsson M, Jansson E. Acute sprint exercise transcriptome in human skeletal muscle. PLoS One. 2019; 14: 1–24. Available from: https://doi.org/10.1371/journal.pone.0223024.
26. Makhnovskii PA, Bokov RO, Kolpakov FA, Popov DV. Transcriptomic signatures and upstream regulation in human skeletal muscle adapted to disuse and aerobic exercise. Int J Mol Sci. 2021; 22: 1–20. Available from: https://doi.org/10.3390/ijms22031208.
27. Birdsey GM, Shah AV, Dufton N, Reynolds LE, Almagro LO, Yang Y et al. The endothelial transcription factor erg promotes vascular stability and growth through Wnt/β-catenin signaling. Dev Cell. 2015; 32: 82–96. Available from: https://doi.org/10.1016/j.devcel.2014.11.016.
28. Sakuma K, Yamaguchi A. The functional role of calcineurin in hypertrophy, regeneration, and disorders of skeletal muscle. J Biomed Biotechnol. 2010; 2010. Available from: https://doi.org/10.1155/2010/721219.
29. Hudson MB, Price SR. Calcineurin: A poorly understood regulator of muscle mass. Int J Biochem Cell Biol. 2013; 45: 2173–8. Available from: https://doi.org/10.1016/j.biocel.2013.06.029.
30. Dunn SE, Burns JL, Michel RN. Calcineurin is required for skeletal muscle hypertrophy. J Biol Chem. 1999; 274: 21908–12. Available from: https://doi.org/10.1074/jbc.274.31.21908.
31. Ehlers ML, Celona B, Black BL. NFATc1 controls skeletal muscle fiber type and is a negative regulator of MyoD activity. Cell Rep. 2014; 8: 1639–48. Available from: https://doi.org/10.1016/j.celrep.2014.08.035.NFATc1.
32. Darby IA, Bisucci T, Raghoenath S, Olsson J, Muscat GEO, Koopman P. Sox18 is transiently expressed during angiogenesis in granulation tissue of skin wounds with an identical expression pattern to Flk-1 mRNA. Lab Investig. 2001; 81: 937–43. Available from: https://doi.org/10.1038/labinvest.3780304.
33. Neyroud D, Nosacka RL, Callaway CS, Trevino JG, Hu H, Judge SM, et al. FoxP1 is a transcriptional repressor associated with cancer cachexia that induces skeletal muscle wasting and weakness. J Cachexia Sarcopenia Muscle. 2021; 12: 421–42. Available from: https://doi.org/10.1002/jcsm.12666.
34. Wright WE, Li C, Zheng C, Tucker HO. FOXP1 Interacts with MyoD to Repress its Transcription and Myoblast Conversion. J Cell Signal. 2021; 2: 9–26.
35. Kurosaka M, Ogura Y, Sato S, Kohda K, Funabashi T. Transcription factor signal transducer and activator of transcription 6 (STAT6) is an inhibitory factor for adult myogenesis. Skelet Muscle. 2021; 11: 1–14. Available from: https://doi.org/10.1186/s13395-021-00271-8.
36. Yamaki T, Wu CL, Gustin M, Lim J, Jackman RW, Kandarian SC. Rel A/p65 is required for cytokine-induced myotube atrophy. Am J Physiol. Cell Physiol. 2012; 303: 135–43. Available from: https://doi.org/10.1152/ajpcell.00111.2012.
37. Arensdorf AM, Diedrichs D, Rutkowski DT. Regulation of the transcriptome by ER stress: Non-canonical mechanisms and physiological consequences. Front Genet. 2013; 4: 1–16. Available from: https://doi.org/10.3389/fgene.2013.00256.
38. Marafon BB, Pinto AP, Ropelle ER, de Moura LP, Cintra DE, Pauli JR, et al. Muscle endoplasmic reticulum stress in exercise. Acta Physiol. 2022; 235: e13799. Available from: https://doi.org/https://doi.org/10.1111/apha.13799.
39. Møller AB, Vendelbo MH, Schjerling P, Couppé C, Møller N, Kjær M et al. Immobilization decreases foxo3a phosphorylation and increases autophagy-related gene and protein expression in human skeletal muscle. Front Physiol. 2019; 10: 1–14. Available from: https://doi.org/10.3389/fphys.2019.00736.
40. Senf SM, Dodd SL, Judge AR. FOXO signaling is required for disuse muscle atrophy and is directly regulated by Hsp70. Am J Physiol. Cell Physiol. 2010; 298. Available from: https://doi.org/10.1152/ajpcell.00315.2009.
41. Sandri M, Sandri C, Gilbert A, Skurk C, Calabria E, Picard A et al. Foxo transcription factors induce the atrophy-related ubiquitin ligase atrogin-1 and cause skeletal muscle atrophy. Cell. 2004; 117: 399–412. Available from: https://doi.org/10.1016/S0092-8674(04)00400-3.

Литература

1. Виноградова О. Л., Попов Д. В., Нетреба А. И., Цвиркун Д. В., Курочкина Н. С., Бачинин А. В.и др. Оптимизация процесса физической тренировки: разработка новых “щадящих” подходов к тренировке силовых возможностей. Физиология человека. 2013; 39: 71–85. Доступно по ссылке: https://doi.org/10.7868/S0131164613050172.
2. Solsona R, Pavlin L, Bernardi H., Sanchez AMJ. Molecular regulation of skeletal muscle growth and organelle biosynthesis: Practical recommendations for exercise training. Int J Mol Sci. 2021; 22: 1–31. Available from: https://doi.org/10.3390/ijms22052741.
3. Mesquita PHC, Vann CG, Phillips SM, McKendry J, Young KC, Kavazis AN, et al. Skeletal muscle ribosome and mitochondrial biogenesis in response to different exercise training modalities. Front Physiol. 2021; 12. Available from: https://doi.org/10.3389/fphys.2021.725866.
4. Gordon PM, Liu D, Sartor MA, IglayReger HB, Pistilli EE, Gutmann L, et al. Resistance exercise training influences skeletal muscle immune activation: a microarray analysis. J Appl Physiol. 2012: 112: 443–53. Available from: https://doi.org/10.1152/japplphysiol.00860.2011.
5. Dickinson JM, D'Lugos AC, Naymik MA, Siniard AL, Wolfe AJ, Curtis DP, et al. Transcriptome response of human skeletal muscle to divergent exercise stimuli. J Appl Physiol. 2018; 124: 1529–40. Available from: https://doi.org/10.1152/japplphysiol.00014.2018.
6. Damas F, Ugrinowitsch C, Libardi CA, Jannig PR, Hector AJ, Mcglory C, et al. Resistance training in young men induces muscle transcriptome-wide changes associated with muscle structure and metabolism refining the response to exercise-induced stress. Eur J Appl Physiol. 2018; 118: 2607–16. Available from: https://doi.org/10.1007/s00421-018-3984-y.
7. Raue U, Trappe TA, Estrem ST, Qian HR, Helvering LM, Smith RC, et al. Transcriptome signature of resistance exercise adaptations: Mixed muscle and fiber type specific profiles in young and old adults. J Appl Physiol. 2012; 112: 1625–36. Available from: https://doi.org/10.1152/japplphysiol.00435.2011.
8. Lundberg TR, Fernandez-Gonzalo R, Gustafsson T, Tesch PA. Aerobic exercise does not compromise muscle hypertrophy response to short-term resistance training. J Appl Physiol. 2013; 114: 81–89. Available from: https://doi.org/10.1152/japplphysiol.01013.2012.
9. Liu D, Sartor MA, Nader GA, Gutmann L, Treutelaar MK, Pistilli EE, et al. Skeletal muscle gene expression in response to resistance exercise: Sex specific regulation. BMC Genomics. 2010; 11: 659. Available from: https://doi.org/10.1186/1471-2164-11-659.
10. Nascimento EBM, Hangelbroek RWJ, GHooiveld GJEJ, Hoeks J, Van Marken Lichtenbelt WD, Hesselink MHC, et al. Comparative transcriptome analysis of human skeletal muscle in response to cold acclimation and exercise training in human volunteers. BMC Med Genomics. 2020; 13: 1–11. Available from: https://doi.

org/10.1186/s12920-020-00784-z.
11. Stepto NK, Coffey VG, Carey AL, Ponnampalam AP, Canny BJ, Powell D, et al. Global gene expression in skeletal muscle from well-trained strength and endurance athletes. Med Sci Sports Exerc. 2009; 41: 546–65. Available from: https://doi.org/10.1249/MSS.0b013e31818c6be9.
12. Schoenfeld BJ, Grgic J, Ogborn D, Krieger JW. Strength and hypertrophy adaptations between low- vs. High-load resistance training: A systematic review and meta-analysis. J Strength Cond Res. 2017; 31: 3508–23. Available from: https://doi.org/10.1519/JSC.0000000000002200.
13. Krieger JW. Single Vs. Multiple Sets of Resistance. J Strength Cond Res. 2010; 24: 1150–9. Available from: htpps://doi.org/10.1519/JSC.0b013e3181d4d36
14. Schoenfeld BJ, Ogborn D, Krieger JW. Effects of Resistance Training Frequency on Measures of Muscle Hypertrophy: A Systematic Review and Meta-Analysis. Sport Med. 2016; 46: 1689–97. Available from: https://doi.org/10.1007/s40279-016-0543-8.
15. Catoire M, Mensink M, Boekschoten MV, Hangelbroek R, Müller M, Schrauwen P, et al. Pronounced Effects of Acute Endurance Exercise on Gene Expression in Resting and Exercising Human Skeletal Muscle. PLoS One. 2012; 7. Available from: https://doi.org/10.1371/journal.pone.0051066.
16. Schroder EA, Harfmann BD, Zhang X, Srikuea R, England JH, Hodge BA, et al. Intrinsic muscle clock is necessary for musculoskeletal health. J Physiol. 2015; 593: 5387–404. Available from: https://doi.org/10.1113/JP271436.
17. Shanely AR, Zwetsloot KA, Travis Triplett N, Meaney MP, Farris GE, Nieman DC. Human skeletal muscle biopsy procedures using the modified Bergström technique. J Vis Exp. 2014; 1–8. Available from: https://doi.org/10.3791/51812.
18. Makhnovskii PA, Gusev OA, Bokov RO, Gazizova GR, Vepkhvadze TF, Lysenko EA, et al. Alternative transcription start sites contribute to acute-stress-induced transcriptome response in human skeletal muscle. Hum Genomics. 2022; 16: 1–13. Available from: https://doi.org/10.1186/s40246-022-00399-8.
19. Campos GER, Luecke TJ, Wendeln HK, Toma K, Hagerman FC, Murray TF et al. Muscular adaptations in response to three different resistance-training regimens: Specificity of repetition maximum training zones. Eur J Appl Physiol. 2002; 88: 50–60. Available from: https://doi.org/10.1007/s00421-002-0681-6.
20. Yapici H, Gülü M, Yagin FH, Ugurlu D, Comertpay E, Eroglu O et al. The effect of 8-weeks of combined resistance training and chocolate milk consumption on maximal strength, muscle thickness, peak power and lean mass, untrained, university-aged males. Front Physiol. 2023; 14: 1–11. Available from: https://doi.org/10.3389/fphys.2023.1148494.
21. Deane CS, Willis CRG, Phillips BE, Atherton PJ, Harries LW, Ames RM, et al. Transcriptomic meta-analysis of disuse muscle atrophy vs. resistance exercise-induced hypertrophy in young and older humans. J Cachexia Sarcopenia Muscle. 2021; 12: 629–45. Available from: https://doi.org/10.1002/jcsm.12706.
22. Pillon NJ, Gabriel BM, Dollet L, Smith JAB, Sardón Puig L, Botella J, et al. Transcriptomic profiling of skeletal muscle adaptations to exercise and inactivity. Nat Commun. 2020; 11: 470. Available from: https://doi.org/10.1038/s41467-019-13869-w.
23. Chapman MA, Arif M, Emanuelsson EB, Reitzner SM, Lindholm ME, Mardinoglu A, et al. Skeletal Muscle Transcriptomic Comparison between Long-Term Trained and Untrained Men and Women. Cell Rep. 2020; 31. Available from: https://doi.org/10.1016/j.celrep.2020.107808.
24. Dzik KP, Grzywacz T, Łuszczyk M, Kujach S, Flis DJ, Kaczor JJ. Single bout of exercise triggers the increase of vitamin D blood concentration in adolescent trained boys: a pilot study. Sci Rep. 2022; 12: 1–10. Available from: https://doi.org/10.1038/s41598-022-05783-x.
25. Rundqvist HC, Montelius A, Osterlund T, Norman B, Esbjornsson M, Jansson E. Acute sprint exercise transcriptome in human skeletal muscle. PLoS One. 2019; 14: 1–24. Available from: https://doi.org/10.1371/journal.pone.0223024.
26. Makhnovskii PA, Bokov RO, Kolpakov FA, Popov DV. Transcriptomic signatures and upstream regulation in human skeletal muscle adapted to disuse and aerobic exercise. Int J Mol Sci. 2021; 22: 1–20. Available from: https://doi.org/10.3390/ijms22031208.
27. Birdsey GM, Shah AV, Dufton N, Reynolds LE, Almagro LO, Yang Y et al. The endothelial transcription factor erg promotes vascular stability and growth through Wnt/β-catenin signaling. Dev Cell. 2015; 32: 82–96. Available from: https://doi.org/10.1016/j.devcel.2014.11.016.
28. Sakuma K, Yamaguchi A. The functional role of calcineurin in hypertrophy, regeneration, and disorders of skeletal muscle. J Biomed Biotechnol. 2010; 2010. Available from: https://doi.org/10.1155/2010/721219.
29. Hudson MB, Price SR. Calcineurin: A poorly understood regulator of muscle mass. Int J Biochem Cell Biol. 2013; 45: 2173–8. Available from: https://doi.org/10.1016/j.biocel.2013.06.029.
30. Dunn SE, Burns JL, Michel RN. Calcineurin is required for skeletal muscle hypertrophy. J Biol Chem. 1999; 274: 21908–12. Available from: https://doi.org/10.1074/jbc.274.31.21908.
31. Ehlers ML, Celona B, Black BL. NFATc1 controls skeletal muscle fiber type and is a negative regulator of MyoD activity. Cell Rep. 2014; 8: 1639–48. Available from: https://doi.org/10.1016/j.celrep.2014.08.035.NFATc1.
32. Darby IA, Bisucci T, Raghoenath S, Olsson J, Muscat GEO, Koopman P. Sox18 is transiently expressed during angiogenesis in granulation tissue of skin wounds with an identical expression pattern to Flk-1 mRNA. Lab Investig. 2001; 81: 937–43. Available from: https://doi.org/10.1038/labinvest.3780304.
33. Neyroud D, Nosacka RL, Callaway CS, Trevino JG, Hu H, Judge SM, et al. FoxP1 is a transcriptional repressor associated with cancer cachexia that induces skeletal muscle wasting and weakness. J Cachexia Sarcopenia Muscle. 2021; 12: 421–42. Available from: https://doi.org/10.1002/jcsm.12666.
34. Wright WE, Li C, Zheng C, Tucker HO. FOXP1 Interacts with MyoD to Repress its Transcription and Myoblast Conversion. J Cell Signal. 2021; 2: 9–26.
35. Kurosaka M, Ogura Y, Sato S, Kohda K, Funabashi T. Transcription factor signal transducer and activator of transcription 6 (STAT6) is an inhibitory factor for adult myogenesis. Skelet Muscle. 2021; 11: 1–14. Available from: https://doi.org/10.1186/s13395-021-00271-8.
36. Yamaki T, Wu CL, Gustin M, Lim J, Jackman RW, Kandarian SC. Rel A/p65 is required for cytokine-induced myotube atrophy. Am J Physiol. Cell Physiol. 2012; 303: 135–43. Available from: https://doi.org/10.1152/ajpcell.00111.2012.
37. Arensdorf AM, Diedrichs D, Rutkowski DT. Regulation of the transcriptome by ER stress: Non-canonical mechanisms and physiological consequences. Front Genet. 2013; 4: 1–16. Available from: https://doi.org/10.3389/fgene.2013.00256.
38. Marafon BB, Pinto AP, Ropelle ER, de Moura LP, Cintra DE, Pauli JR, et al. Muscle endoplasmic reticulum stress in exercise. Acta Physiol. 2022; 235: e13799. Available from: https://doi.org/https://doi.org/10.1111/apha.13799.
39. Møller AB, Vendelbo MH, Schjerling P, Couppé C, Møller N, Kjær M et al. Immobilization decreases foxo3a phosphorylation and increases autophagy-related gene and protein expression in human skeletal muscle. Front Physiol. 2019; 10: 1–14. Available from: https://doi.org/10.3389/fphys.2019.00736.
40. Senf SM, Dodd SL, Judge AR. FOXO signaling is required for disuse muscle atrophy and is directly regulated by Hsp70. Am J Physiol. Cell Physiol. 2010; 298. Available from: https://doi.org/10.1152/ajpcell.00315.2009.
41. Sandri M, Sandri C, Gilbert A, Skurk C, Calabria E, Picard A et al. Foxo transcription factors induce the atrophy-related ubiquitin ligase atrogin-1 and cause skeletal muscle atrophy. Cell. 2004; 117: 399–412. Available from: https://doi.org/10.1016/S0092-8674(04)00400-3.

INITIAL ADMINISTRATION OF β_2-AGONISTS REDUCES THE RISK OF BRONCHOSPASM CAUSED BY β_1-BLOCKERS IN COMORBID CARDIORESPIRATORY PATHOLOGY

Smolyakova EV[1,2] ✉, Sinitsyn EA[2], Zykov KA[1,2]

[1] Evdokimov Moscow State University of Medicine and Dentistry, Moscow, Russia

[2] Pulmonology Research Institute of Federal Medical Biological Agency, Moscow, Russia

In the treatment of patients with cardiorespiratory pathology, it is often necessary to simultaneously administer drugs that affect β-adrenergic receptors: β_1-adrenoblockers and β_2-agonists. β_1-blockers can trigger a bronchospasm in patients with bronchoobstructive diseases, therefore, practitioners often decide not to prescribe them. This work aimed to evaluate functional parameters of patients with cardiovascular and bronchoobstructive diseases in the context of different sequences of administration of selective β_1-blockers (bisoprolol) and long-acting β_2-agonists (formoterol). This prospective, single-center 2-week pilot study involved 30 individuals suffering the aforementioned diseases. Using the envelopes method, we divided the patients into two groups of 15 people each. First group started therapy with a long-acting β_2-agonist, second group — with a selective β_1-adrenoblocker. While taking the β_1-adrenoblocker, patients underwent a four-hour spirometric test enabling assessment of the external respiration function parameters. The tests and assessments have shown that the value of FEV1 went down in 33.3% of those who started therapy with a selective β_1-adrenoblocker (bisoprolol 2.5 mg), and in the group that first took a long-acting β_2-agonist for a week and then added bisoprolol 2.5 mg to the regimen the said value dropped in 7% of patients only. Thus, preceding long-acting β_2-agonists, formoterol in particular, reduced the risk of bronchospastic incidents triggered by selective β_1-adrenoblocker (bisoprolol) in patients with cardiorespiratory pathology.

Keywords: cardiovascular diseases, bronchoobstructive diseases, cardiorespiratory pathology, β_1-adrenoblockers, β_2-agonists

Author contribution: Smolyakova EV — recruitment of patients, processing of the results, article authoring; Sinitsyn EA — discussion of the results; Zykov KA — patient treatment management, discussion of the study results, article authoring.

Compliance with ethical standards: the study was approved by the Ethics Committee of the National Medical Research Center for Cardiology named after academician Yevgeniy Chazov of the Ministry of Health of the Russian Federation (Minutes № 220 of October 31, 2016)

✉ **Correspondence should be addressed:** Ekaterina V. Smolyakova
Orekhovy bulvar, 28, 115682, Moscow, Russia; smolyakovak@mail.ru

Received: 21.07.2023 **Accepted:** 04.09.2023 **Published online:** 28.09.2023

DOI: 10.47183/mes.2023.033

ПРИ КОМОРБИДНОЙ КАРДИОРЕСПИРАТОРНОЙ ПАТОЛОГИИ ИНИЦИАЛЬНОЕ НАЗНАЧЕНИЕ β_2-АГОНИСТОВ СНИЖАЕТ РИСК БРОНХОСПАЗМА, ВЫЗВАННОГО β_1-АДРЕНОБЛОКАТОРАМИ

Е. В. Смолякова[1,2]✉, Е. А. Синицын[2], К. А. Зыков[1,2]

[1] Московский государственный медико-стоматологический университет имени А. И. Евдокимова, Москва, Россия

[2] Научно-исследовательский институт пульмонологии Федерального медико-биологического агентства, Москва, Россия

При лечении пациентов с кардиореспираторной патологией часто необходимо одновременное использование препаратов, воздействующих на β-адренорецепторы: β_1-адреноблокаторы и β_2-агонисты. Из-за возможности развития бронхоспазма у пациентов с бронхообструктивными заболеваниями на фоне использования β_1-адреноблокаторов, практикующие врачи нередко отказываются от их назначения. Целью работы было оценить функциональные параметры у пациентов с сердечно-сосудистыми и бронхообструктивными заболеваниями при различной последовательности назначения селективных β_1-адреноблокаторов (бисопролола) и β_2-агонистов длительного действия (формотерола). В пилотное одноцентровое проспективное исследование было включено 30 пациентов с сердечно-сосудистыми заболеваниями и бронхообструктивными заболеваниями, длительность исследования составила 2 недели. Пациенты методом «конвертов» были разделены на две группы по 15 человек. Первая группа пациентов начинала старт терапии с приема β_2-агониста длительного действия, а вторая группа — с приема селективного β_1-адреноблокатора. На фоне приема β_1-адреноблокатора пациентам проводили четырехчасовую спирометрическую пробу с оценкой параметров функции внешнего дыхания. Показано, что у начинающих старт терапии с приема селективного β_1-адреноблокатора (бисопролола 2,5 мг) снижение ОФВ1 происходило у 33,3% человек, в то время как у принимающих бисопролол 2,5 мг на фоне недельного приема β_2-агониста длительного действия процент выявленных случаев снижения ОФВ1 составил всего 7%.Таким образом, предварительное назначение β_2-агонистов длительного действия, в частности формотерола, снижало риск бронхоспастического действия селективного β_1-адреноблокатора — бисопролола у пациентов с кардиореспираторной патологией.

Ключевые слова: сердечно-сосудистые заболевания, бронхообструктивные заболевания, кардиореспираторная патология, β_1-адреноблокаторы, β_2-агонисты

Вклад авторов: Е. В. Смолякова — набор пациентов, обработка результатов, написание статьи; Е. А. Синицын — обсуждение результатов; К. А. Зыков — руководство лечением пациентов и обсуждение результатов исследования, написание статьи.

Соблюдение этических стандартов: исследование одобрено этическим комитетом ФГБУ «Национального медицинского исследовательского центра кардиологии им. ак. Е.И. Чазова» Минздрава России (протокол № 220 от 31 октября 2016 г.).

✉ **Для корреспонденции:** Екатерина Владимировна Смолякова
Ореховый бульвар, д. 28, 115682, г. Москва, Россия; smolyakovak@mail.ru

Статья получена: 21.07.2023 **Статья принята к печати:** 04.09.2023 **Опубликована онлайн:** 28.09.2023

DOI: 10.47183/mes.2023.033

Cardiovascular and bronchoobstructive diseases, namely bronchial asthma (BA) and chronic obstructive pulmonary disease (COPD), are among the main public health problems in people aged 40 and older [1]. The reasons behind the high prevalence of comorbidity of cardiovascular and bronchoobstructive pathologies are the common risk factors, pathophysiological processes that jointly aggravate the course of the diseases [2, 3]. From the epidemiological point of view,

cardiovascular diseases (CVD) are among the top reasons of death of patients with COPD and BA [4]. The drugs used to treat a cardiorespiratory pathology are β_1-blockers and β_2-agonists, which block or activate the adrenergic system. These drugs are not 100% selective, and the receptors are located close to each other; these factors translate into a possibility of cross-receptor interaction, which often leads to side effects and to suboptimal effect of the drugs on both conditions: underprescription or rejection of pathognomonic therapy [5].

β_1-Blockers are widely used in the treatment of CVD, the particular conditions being coronary heart disease, cardiac arrhythmia and heart failure [6]. There are two types of β-blockers: non-selective, which block both β_1- and β_2-adrenergic receptors, and selective (cardioselective) β_1-adrenoblockers, which act mainly on β_1-adrenergic receptors. Traditionally, there are concerns about prescribing β-blockers to patients with concomitant COPD and BA, since they can cause reduction of the vital lung capacity, bronchospasm, erosion of the efficacy of short-acting β_2-agonists taken to arrest an attack, same as erosion of the efficacy of long-acting β_2-agonists, which is the result of direct blockade of β_2-adrenergic receptors of bronchi's smooth muscles. Therefore, the preferred drugs should be cardioselective β_1-adrenoblockers [7, 8]. At that, it should be remembered that selectivity of β_1-blockers deteriorates as their dose grows up [9]. Even nebivolol, the selectivity of which is 1:22–46, does not eliminate the risks of bronchospasm because of uneven distribution of β-adrenergic receptors through organs and tissues.

In turn, β_2-agonists are the main symptomatic drugs for patients with a bronchoobstructive pathology. However, since there are β_2-adrenoreceptors in the heart, such drugs, especially their short-acting varieties, can indirectly (through activation of the sympathoadrenal system) provoke growth of blood pressure and heart rate in patients with comorbid CVDs, and, according to some authors, decrease of the concentration of potassium in the blood triggered by higher doses of β_2-agonists may be the cause of development of life-threatening arrhythmias [10].

At the same time, combined intake of selective β_1-adrenoblockers and β_2-agonists, through suppression of tachycardia and hypertension associated with high doses of β_2-agonists taken to arrest COPD and BA exacerbations, has shown capability to decrease the frequency of cardiovascular events. Some randomized trials, as well as a number of meta-analyses, have revealed a decreased CVD-associated mortality among COPD and BA patients taking β_1-adrenoblockers [11, 12]. There is also evidence suggesting that β_2-agonists can mitigate the risk of cardiovascular complications through reduction of the residual volume of air in the lungs, which translates into lighter inspiratory dyspnea [13]. Moreover, the right ventricular compliance indicators improve [13], and the pulmonary artery pressure goes down [14], which means fewer COPD and BA exacerbations raising the risk of cardiovascular diseases and mortality.

Thus, treatment of patients with a combined cardiorespiratory pathology often requires simultaneous administration of a selective β_1-adrenoblocker and a β_2-agonist. Today, medical professionals seek practical recommendations covering the order of prescription of these drugs if they need to be used together. It should be noted that currently, there are no evidence-based data on the comparative safety and efficacy of prescribing β-agonists first and β-adrenoblockers second in a regimen, nor is there evidence describing the approach involving initial prescription of β-adrenoblockers. This study aimed to determine the preferred sequence of administration of selective β_1-adrenoblockers (bisoprolol) and long-acting β_2-agonists (formoterol) in patients with cardiovascular and bronchoobstructive diseases based on the assessment of functional parameters.

METHODS

This work was a was pilot, single-center prospective study that involved 30 patients (66.97 ± 9.84 years, 18 male, 12 female). The inclusion criteria were: cardiovascular diseases — arterial

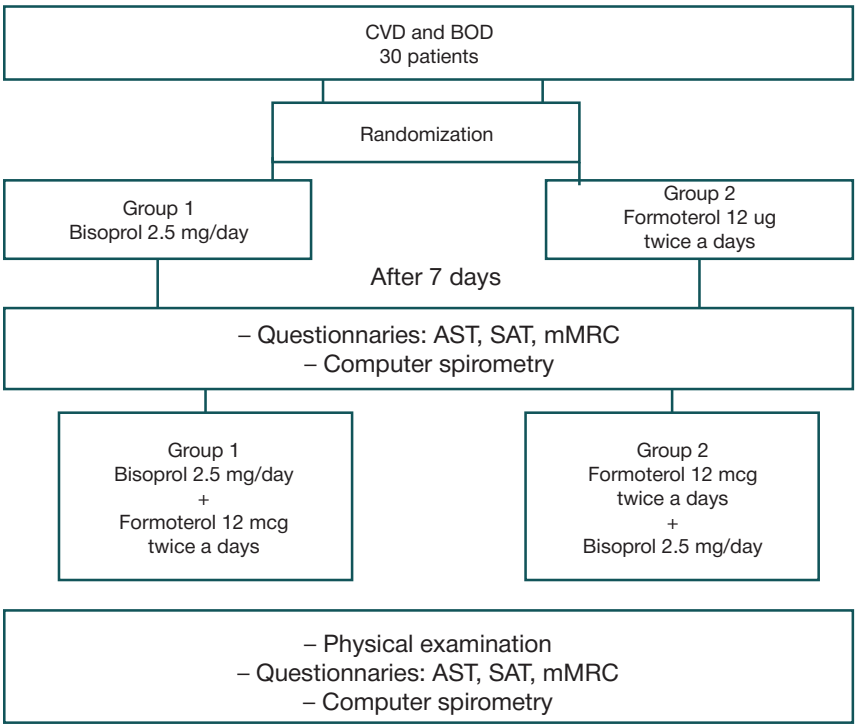

Fig. 1. Study design. BP — blood pressure; AST — Asthma Control Test; BOD — bronchoobstructive diseases; CAT — COPD Assessment Test, mMRC — modified Medical Research Council Dyspnea Scale

Table 1. Clinical characteristics of the patients with CVD and BOD, groups 1 and 2 (medical history data)

Patient characteristic	Patients with CVD and BOD (*n* = 15), group 1	Patients with CVD and BOD (*n* = 15), group 2
Age, years	65.9 ± 10	68 ± 10.3
Gender, male/female, %	46.7 / 53.3	73.5 / 26.5
AH, degrees I, II, III, %	0; 46.7; 53.3	0; 40%; 60.2.
CHD functional class, I, II, III, %	6.6; 40; 0	26.7; 13.3; 20
PICS, %	26.7	40
HA, %	46.7	26.7
BA, %	26.7	20
COPD, %	53.3	66.7
COPD + BS, %	20	13.3
ACT, points	17.00 [15.50; 20.00]	17.00 [13.00;18.00]
CAT, points	16.00 [14.00; 24.00]	22.00 [21.00; 25.00]
mMRC, points	2 [1.50; 3.00]	3.00 [2.00; 3.00]
CCA therapy, %	40	53.3
ACE inhibitors therapy, %	13.3	26.7
ARB therapy, %	73.5	60.2

Note: the data are given as M ± SD and % of the total number of patients; * — $p < 0.05$; AH – arterial hypertension; ACT — asthma control test; BA — bronchial asthma; CCA — calcium channel antagonists; ARB — angiotensin-2 receptor blockers; CHD — coronary heart disease; ACE inhibitors — angiotensin converting enzyme inhibitors; mMRC — modified medical research council dyspnea scale; HA — heart arrhythmia; PICS — post-infarction cardiosclerosis; CAT — COPD assessment test; COPD — chronic obstructive pulmonary disease.

hypertension, coronary heart disease, cardiac arrhythmia, — concomitant with bronchoobstructive diseases (BOD) — bronchial asthma, chronic obstructive pulmonary disease. All the patients were prescribed a selective β_1-adrenoblocker (bisoprolol) and a β_2-agonist (formoterol).

Using the envelopes method, we divided the patients into two groups comparable in age, gender, and therapy at the time of inclusion in the study. Tables 1 and 2 present clinical characteristics of the patients [15].

Patients of group 1 started therapy with a β_1-adrenoblocker, bisoprolol 2.5 mg, and for group 2, the initial drug was a long-acting β_2-agonist, formoterol 12 μg twice a day. A week later, group 1 began taking formoterol, group 2 — bisoprolol. Selection of the initial doses of the drugs was based on the preceding computer spirometry, specialized tests and questionnaires (Fig. 1). SuperSpiro spirometer enabled spirometry (MICRO MEDICAL; UK), and the acquired values were compared to the spirometry reference values developed by the European Coal and Steel Community (ECSC) in 1993.

In order to prevent the development of bronchospasm, all patients underwent a 4-hour spirometry before being prescribed the first dose of the β_1-adrenoblocker. This test allows evaluating the initial external respiration parameters (FVC — forced vital capacity, FEV1 — forced exhale volume in 1 s, FEV1/FVC) before taking the drug and 30 minutes, 90 minutes, 150 minutes and 240 minutes after taking bisoprolol 2.5 mg.

Participants of the study

A total of 30 patients (66.97 ± 9.84 years old, 18 male and 12 female) participated in the study. They were divided into two comparable groups of 15 people.

The inclusion criteria were: CVD and BOD, compensation stage, lack of any acute process at the time of screening for the study; confirmed BA diagnosed in accordance with the generally accepted clinical, laboratory and functional criteria (GINA 2017 [16]); COPD diagnosed in accordance with the GOLD 2017 criteria [17]; signature under the informed consent form confirming voluntary participation in the study.

The exclusion criteria were: severe CVD (acute cerebrovascular accident, myocardial infarction less than 6 months before inclusion in the study, unstable angina pectoris); exacerbation of COPD, BA less than 1 month before

Table 2. Clinical characteristics of the patients with CVD and BOD, groups 1 and 2 (laboratory and instrumental study data)

Patient characteristics	Patients with CVD and BOD (*n* = 15), group 1	Patients with CVD and BOD (*n* = 15), group 2
ECP, μg/l	21.9 ± 12.1	18.8 ± 15.2
CRP, mg/l	18.8 ± 15.2	5. 91 ± 7.5
ESR, mm/h	12.9 ± 10.8	13.7 ± 13.5
Leukocytes, 10^9/l	8.2 ± 1.8	7.9 ± 1.4
Erythrocytes, 10^9/l	5.2 ± 0.9	4.9 ± 0.4
Eosinophils, %	2.88 ± 2.07	3.99 ± 2.2
SBP/DBP, mmHg	128.8/79.8 ± 11/3.8	126.7/78 ± 8.8/5.5
HR, beats/min	70.9 ± 9	68.9 ± 10.1
FEV1, % of the reference value	73.2 ± 11.7	78.86 ± 17.3
FVC, % of the reference value	95.8 ± 19.6	96.7 ± 17.9

Note: the data are given as M ± SD; * — $p < 0.05$; DBP — diastolic blood pressure; FEV1 — forced expiratory volume, 1 s; SBP — systolic blood pressure; ESR — erythrocyte sedimentation rate; CRP — C-reactive protein; ECP — eosinophilic cationic protein; FVC — forced vital capacity; HR — heart rate.

inclusion in the study; contraindications to intake of selective β_1-adrenoblockers and β_2-agonists; oncological diseases; pregnancy, breastfeeding; clinical conditions that, according to the doctor, prevent participation in the study.

The study was conducted at the National Medical Research Centre of Cardiology named after Academician E.I. Chazov, in the department of hypertension. The length of the study was 2 weeks, its key outcome — evaluation of functional parameters of patients with comorbidities in the context of different sequences of administration of selective β_1-adrenoblockers and long-acting β_2-agonists.

Statistical analysis

This was a pilot study, therefore, we did estimate power of the sample. PSPP 1.2.0 (GNY project; USA) enabled statistical processing of the data, and Kolmogorov–Smirnov test — verification of the distribution hypotheses. For quantitative variables in the context of normal distribution, we used the mean ± standard deviation, and for nonparametric indicators — median and percentiles [25; 75]. The differences were considered significant at $p < 0.05$.

RESULTS

Four-hour spirometry revealed no significant (over 20% from the baseline) drop of the level of FVC and FEV1; overall, the participants in both groups reported no deterioration of condition, which was subjectively assessed with the help of ACT, CAT, mMRC questionnaires (Table 3). However, analysis of data of all patients has shown that in 29 patient out of 30, bisoprolol 2.5 mg/day triggered a reversible decrease of FEV1, maximum to 300 ml, which is down 17% from the baseline, the recovery to which occurred after a bronchodilation test with salbutamol 400 mg (Figure 2). In most cases, FEV1 drops (in absolute values and in % from the baseline) were registered 30 minutes and 240 minutes after initial administration of bisoprolol 2.5 mg. We included the drop values starting from 2% (Fig. 2) into the calculations, thus eliminating the possibility of measurement error.

Statistical processing of the patient data by groups revealed a greater percentage of FEV1 reduction cases in group 1 (33.3% of the participants), where the therapy began with a selective β_1-adrenoblocker (bisoprolol 2.5 mg). At the same time, in group 2, which received a long-acting β_2-agonist (formoterol 24 μg) as the initial drug and started taking bisoprolol 2.5 mg only after 7 days of bronchodilation therapy, the share of those whose FEV1 decreased was 7% (Fig. 3).

DISCUSSION

The problems of drug therapy aimed at combined cardiovascular and bronchopulmonary pathologies, COPD and BA in particular, remain relevant. The need for β_1-adrenoblockers in treatment of patients with bronchoobstructive diseases remains a debatable subject. A meta-analysis of observational studies that included 15 cohort studies with a follow-up period of up to 7.2 years, all of which investigated the use of β_1-adrenblockers in patients with CVD and BOD, has shown that these drugs significantly reduce mortality and exacerbations of BOD [18]. The results of this analysis is confirmed in two other major studies. One of them demonstrated that cardioselective β_1-adrenoblockers boost the response to β_2-agonists and cause no clinically significant side effects on the part of the respiratory system [7]; another reported that administration of β_1-adrenoblockers decreases overall mortality and sudden cardiac death by reducing heart rate and prolonging the diastolic period of the cardiac cycle, which improves myocardial perfusion [19]. Still, there are registered cases of decreasing vital lung capacity in the context of regimens that start the therapy with β_1-adrenoblockers. Our study confirms that: against the background of complete clinical well-being and lack of any deterioration of condition, as reported by the patients with CVD and BOD comorbidities, FEV1 reversibly dropped, in the extreme case — to 300 ml and 7% of the baseline. In an earlier paper, 4-hour spirometry has also revealed decreasing FEV1 in patients with cardiorespiratory pathology, and the share of those in whom the drop exceeded 20% from the baseline was 6.4%. However, authors of that work emphasized that long-term use of selective β_1-adrenoblockers (bisoprolol) did not translate into a significant FEV1 and FVC decrease that could be detected by spirometry [20].

Taking into account the results of our study, patients at high risk of bronchospasm who require prescription of a β_1-adrenoblocker can be recommended a 4-hour spirometry in a hospital setting. The test will help practitioners initiate administration of β-adrenoblockers, starting with small doses and continuing with their gradual titration.

Our study lacked statistical power to allow an unambiguous conclusion, yet, we demonstrated that it is advantageous to start therapy with a long-acting β_2-agonist, thus reducing the risk of a bronchospastic component in patients with CVD and BOD comorbidities that need constant and long-term administration of β_1-adrenoblockers. Of course, this suggestion should be backed with more extensive clinical studies, which would seek to ultimately determine the variability of FEV1 against the background of different tactics of simultaneous administration of selective β_1-adrenoblockers and β_2-agonists.

Study limitations

The limitation of this study is the small sample of patients. However, the results are significant, which raises the need for continued research of this subject matter with sufficient statistical power.

Table 3. Dynamics of indicators as registered with CAT, ACT, MRC questionnaires, patients with CVD and BOD comorbidities, both groups

	CVD and BOD, group 1		CVD and BOD, group 2	
	baseline	a week later	baseline	a week later
ACT, points	17 [15.50; 20.00]	20 [19.00; 23.00]	17.00 [13.00; 18.00]	19.00 [17.00; 21.00]*
CAT, points	16 [14.00; 24.00]	13 [9.00; 15.00]	22.00 [21.00; 25.00]	17.00 [14.50; 21.50]*
mMRC, points	2 [1.50; 3.00]	1 [1.00; 2.00]	3.00 [2.00; 3.00]	2.00 [1.00; 2.50]*

Note: * — $p < 0.05$.

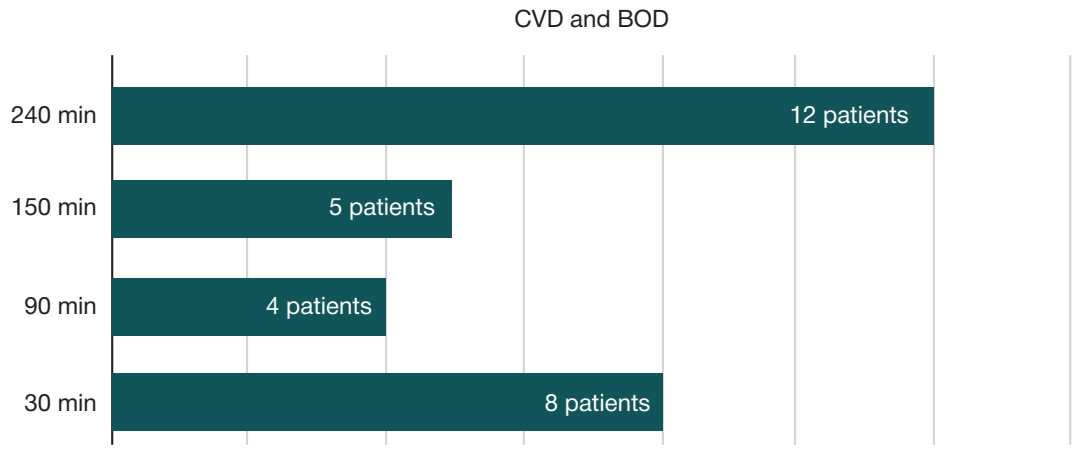

Fig. 2. Distribution of patients with the greatest FEV1 drop (in % from the reference values) at different time, CVD and BOD groups

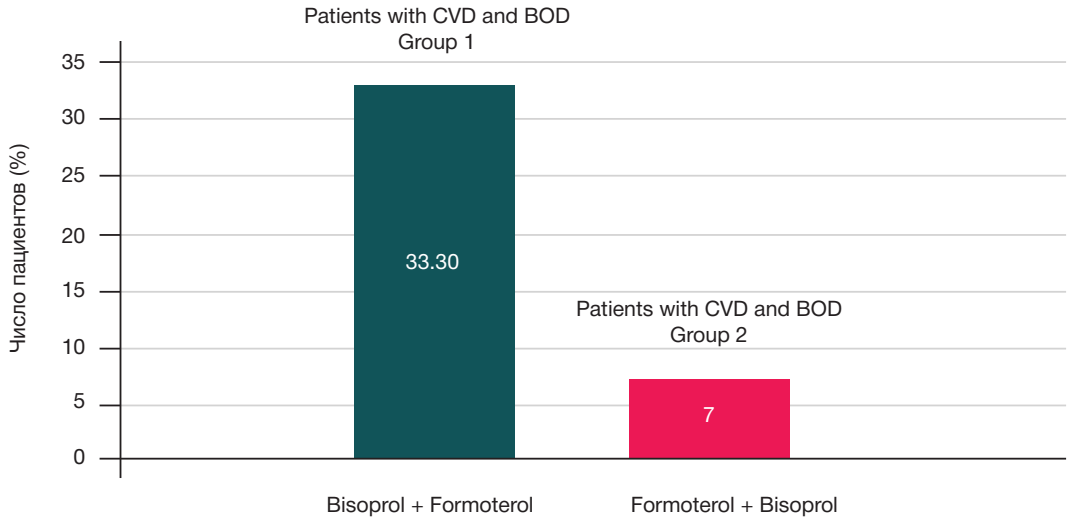

Fig. 3. Percentage of patients with CVD and BOD whose FEV1 decreased over 2% from the reference values

CONCLUSIONS

Despite the close pathogenetic relationships between CVD and BOD and availability of clinical recommendations covering these comorbidities, in everyday practice, medical professionals still face difficulties in selecting therapy for such patients. Our study has shown the importance of sequence in regimens involving both β_2-agonists and β_1-adrenoblockers. Starting the therapy with long-acting β_2-agonists, in particular formoterol, reduces the risk of bronchospastic effect of selective β_1-adrenoblocker, bisoprolol, in patients with a cardiorespiratory pathology. This phenomenon deserves attention and requires further studies on a larger sample of patients.

References

1. World Health Organization. 2022. Available from: https://www.who.int.
2. Ingebrigtsen TS, Marott JL, Vestbo J, Nordestgaard BG, Lange P. Coronary heart disease and heart failure in asthma, COPD and asthma-COPD overlap. BMJ Open Respir Res. 2020; 7 (1): e000470. DOI: 10.1136/bmjresp-2019-000470. PMID: 33371008; PMCID: PMC7011896.
3. Rabe KF, Hurst JR, Suissa S. Cardiovascular disease and COPD: dangerous liaisons? Eur Respir Rev. 2018; 27 (149): 180057. DOI: 10.1183/16000617.0057-2018. Erratum in: Eur Respir Rev. 2018; 27 (150): PMID: 30282634; PMCID: PMC9488649.
4. Shnoda M, Gajjar K, Ivanova V. COPD and Cardiovascular Disease: A Review of Association, Interrelationship, and Basic Principles for Integrated Management. Crit Care Nurs Q. 2021; 44 (1): 91–102. DOI: 10.1097/CNQ.0000000000000342. PMID: 33234862.
5. Arcoraci V, Squadrito F, Rottura M, Barbieri MA, Pallio G, Irrera N, et al. Beta-Blocker use in older hospitalized patients affected by heart failure and chronic obstructive pulmonary disease: an Italian survey from the REPOSI register. Front Cardiovasc Med. 2022; 9: 876693. DOI: 10.3389/fcvm.2022.876693. PMID: 35651906; PMCID: PMC9149000.
6. Nebieridze DV. Aktual'nye voprosy primeneniya β-adrenoblokatorov v razlichnyh klinicheskih situaciyah. Medicinskij sovet. 2018; 12: 12–17. DOI 10.21518/2079-701X-2018-12-12-17. Russian.
7. GOLD, 2023. Available from: https://goldcopd.org/2023-gold-report-2/.
8. GINA, 2023. Available from: https://ginasthma.org/2023-gina-main-report/.
9. Reiter MJ. Cardiovascular drug class specificity: beta-blockers. Prog Cardiovasc Dis. 2004; 47: 11–33.
10. Guhan AR, Cooper S, Oborne J, Lewis S, Bennett J, Tattersfield AE. Systemic effects of formoterol and salmeterol: a dose-response comparison in healthy subjects. Thorax. 2000; 55 (8): 650–6. DOI: 10.1136/thorax.55.8.650. PMID: 10899240; PMCID: PMC1745819.
11. Yang YL, Xiang ZJ, Xiang RL. Increasing the prescription rate of β-blockers is beneficial for patients with chronic obstructive pulmonary and cardiovascular disease. Eur Heart J. 2021; 42

(34): 3409. DOI: 10.1093/eurheartj/ehab239. PMID: 33948636.
12. Gulea C, Quint JK, Zakeri R. Clinical and methodological considerations when interpreting meta-analyses of beta-blocker use in patients with chronic obstructive pulmonary disease. Eur Heart J. 2021; 42 (34): 3407–8. DOI: 10.1093/eurheartj/ehab217. PMID: 33948644.
13. Santus P, Radovanovic D, Di Marco S, et al. Effect of indacaterol on lung deflation improves cardiac performance in hyperinflated COPD patients: an interventional, randomized, double-blind clinical trial. Int J Chron Obstruct Pulmon Dis. 2015; 10: 1917–23.
14. Cazzola M, Mantero A, Santus P, et al. Doppler echocardiographic assessment of the effects of inhaled long-acting β2-agonists on pulmonary artery pressure in COPD patients. Pulm Pharmacol Ther. 2007; 20: 258–64.
15. Smolyakova EV. Vliyanie terapii selektivnym β1-adrenoblokatorom i β2-agonistom na izmenenie harakteristik β-adrenoreceptorov u pacientov s kardiorespiratornoj patologiej (dissertaciya). 2019. Russian.
16. GINA, 2017. Available from: https://ginasthma.org/wp-content/uploads/2019/01/2017-GINA.pdf.
17. GOLD, 2017. Available from: https://goldcopd.org/wp-content/uploads/2017/02/wms-GOLD-2017-FINAL.pdf.
18. Du Q, Sun Y, Ding N, Lu L, Chen Y. Beta-blockers reduced the risk of mortality and exacerbation in patients with COPD: a meta-analysis of observational studies. PLoS One. 2014; 9 (11): e113048. DOI: 10.1371/journal.pone.0113048.
19. Gulea C, Zakeri R, Alderman V, Morgan A, Ross J, Quint JK. Beta-blocker therapy in patients with COPD: a systematic literature review and meta-analysis with multiple treatment comparison. Respir Res. 2021; 22 (1): 64. DOI: 10.1186/s12931-021-01661-8. PMID: 33622362; PMCID: PMC7903749.
20. Nazarov BM. Izuchenie bezopasnosti i ehffektivnosti lecheniya selektivnym β-adrenoblokatorom bol'nyh s serdechno-sosudistymi zabolevaniyami v sochetanii s bronhoobstruktivnymi zabolevaniyami (dissertaciya). 2014. Russian.

Литература

1. World Health Organization. 2022. Available from: https://www.who.int.
2. Ingebrigtsen TS, Marott JL, Vestbo J, Nordestgaard BG, Lange P. Coronary heart disease and heart failure in asthma, COPD and asthma-COPD overlap. BMJ Open Respir Res. 2020; 7 (1): e000470. DOI: 10.1136/bmjresp-2019-000470. PMID: 33371008; PMCID: PMC7011896.
3. Rabe KF, Hurst JR, Suissa S. Cardiovascular disease and COPD: dangerous liaisons? Eur Respir Rev. 2018; 27 (149): 180057. DOI: 10.1183/16000617.0057-2018. Erratum in: Eur Respir Rev. 2018; 27 (150): PMID: 30282634; PMCID: PMC9488649.
4. Shnoda M, Gajjar K, Ivanova V. COPD and Cardiovascular Disease: A Review of Association, Interrelationship, and Basic Principles for Integrated Management. Crit Care Nurs Q. 2021; 44 (1): 91–102. DOI: 10.1097/CNQ.0000000000000342. PMID: 33234862.
5. Arcoraci V, Squadrito F, Rottura M, Barbieri MA, Pallio G, Irrera N, et al. Beta-Blocker use in older hospitalized patients affected by heart failure and chronic obstructive pulmonary disease: an Italian survey from the REPOSI register. Front Cardiovasc Med. 2022; 9: 876693. DOI: 10.3389/fcvm.2022.876693. PMID: 35651906; PMCID: PMC9149000.
6. Небиеридзе Д. В. Актуальные вопросы применения β-адреноблокаторов в различных клинических ситуациях. Медицинский совет. 2018; 12: 12–17. DOI 10.21518/2079-701X-2018-12-12-17.
7. GOLD, 2023. Available from: https://goldcopd.org/2023-gold-report-2/.
8. GINA, 2023. Available from: https://ginasthma.org/2023-gina-main-report/.
9. Reiter MJ. Cardiovascular drug class specificity: beta-blockers. Prog Cardiovasc Dis. 2004; 47: 11–33.
10. Guhan AR, Cooper S, Oborne J, Lewis S, Bennett J, Tattersfield AE. Systemic effects of formoterol and salmeterol: a dose-response comparison in healthy subjects. Thorax. 2000; 55 (8): 650–6. DOI: 10.1136/thorax.55.8.650. PMID: 10899240; PMCID: PMC1745819.
11. Yang YL, Xiang ZJ, Xiang RL. Increasing the prescription rate of β-blockers is beneficial for patients with chronic obstructive pulmonary and cardiovascular disease. Eur Heart J. 2021; 42 (34): 3409. DOI: 10.1093/eurheartj/ehab239. PMID: 33948636.
12. Gulea C, Quint JK, Zakeri R. Clinical and methodological considerations when interpreting meta-analyses of beta-blocker use in patients with chronic obstructive pulmonary disease. Eur Heart J. 2021; 42 (34): 3407–8. DOI: 10.1093/eurheartj/ehab217. PMID: 33948644.
13. Santus P, Radovanovic D, Di Marco S, et al. Effect of indacaterol on lung deflation improves cardiac performance in hyperinflated COPD patients: an interventional, randomized, double-blind clinical trial. Int J Chron Obstruct Pulmon Dis. 2015; 10: 1917–23.
14. Cazzola M, Mantero A, Santus P, et al. Doppler echocardiographic assessment of the effects of inhaled long-acting β2-agonists on pulmonary artery pressure in COPD patients. Pulm Pharmacol Ther. 2007; 20: 258–64.
15. Смолякова Е. В. Влияние терапии селективным β1-адреноблокатором и β2-агонистом на изменение характеристик β-адренорецепторов у пациентов с кардиореспираторной патологией (диссертация). 2019.
16. GINA, 2017. Available from: https://ginasthma.org/wp-content/uploads/2019/01/2017-GINA.pdf.
17. GOLD, 2017. Available from: https://goldcopd.org/wp-content/uploads/2017/02/wms-GOLD-2017-FINAL.pdf.
18. Du Q, Sun Y, Ding N, Lu L, Chen Y. Beta-blockers reduced the risk of mortality and exacerbation in patients with COPD: a meta-analysis of observational studies. PLoS One. 2014; 9 (11): e113048. DOI: 10.1371/journal.pone.0113048.
19. Gulea C, Zakeri R, Alderman V, Morgan A, Ross J, Quint JK. Beta-blocker therapy in patients with COPD: a systematic literature review and meta-analysis with multiple treatment comparison. Respir Res. 2021; 22 (1): 64. DOI: 10.1186/s12931-021-01661-8. PMID: 33622362; PMCID: PMC7903749.
20. Назаров Б. М. Изучение безопасности и эффективности лечения селективным β-адреноблокатором больных с сердечно-сосудистыми заболеваниями в сочетании с бронхообструктивными заболеваниями (диссертация). 2014.

EFFECTS OF MILD HYPOTHERMIA ON THE CEREBRAL MICROVASCULAR TONE

Melnikova NN ✉

Pavlov Institute of Physiology, Russian Academy of Sciences, Saint Petersburg, Russia

Acute blood loss is associated with deterioration of blood circulation, including microcirculation. Clinical and experimental studies are focused on the search for the possibility of neutralizing the consequences of such impairment. The use of hypothermia is considered not only as a method to improve survival, but also as a method to improve cerebral microcirculation in hemorrhage. The study was aimed to assess the state of the rats' cerebral arteries in cases of mild hypothermic exposure after acute moderate blood loss. The study involving anesthetized Wistar rats was performed by vital microscopy. We assessed the responses of pial arteries (initial diameter 10–40 μm) in animals cooled to the rectal temperature of 34 °C under conditions of hemodynamic stability and when simulating blood loss (20% of total blood loss) in normothermic animals and animals with mild hypothermia. The findings showed that 3.5 h of exposure were associated with vasoconstriction in animals of all studied groups. Hypothermic state of the body was associated with initial decrease in the diameter by 9% of the baseline (24.9 ± 0.9 μm to 22.7 ± 0.7 μm; $p < 0.05$) followed by restoration of the diameter after 2 h (to 25.7 ± 1.7; $p > 0.05$). Blood loss was associated with the decrease in the diameter of cerebral blood vessels by 20–25% within the first hour (23.4 ± 0.7 μm to 17.6 ± 1.1 μm; $p < 0.001$) and no subsequent restoration (the diameter was 16.7 ± 0.8 μm after 3.5 h of monitoring). When using hypothermia, vasoconstriction following blood loss was 8–10% in the first 45 min of monitoring (22.6 ± 1.3 μm to 20.3 ± 1.2 μm; $p < 0.05$), then the constriction decrease was observed (the diameter was 21.4 ± 1.4 μm after 3.5 h of monitoring). It was concluded that the use of mild hypothermia resulted in the reduced vasoconstrictor effect of moderate blood loss on the pial microvessels.

Keywords: hypothermia, blood loss, cerebral vessels

Funding: the study was supported by the State Programme 47 GP "Scientific and Technological Development of the Russian Federation" (2019–2030), project 0134-2019-003.

Compliance with ethical standards: the study was approved by the Ethics Committee of the Commission for Care and Use of Laboratory Animals, Pavlov Institute of Physiology RAS (protocol № 05/10 of 10 May 2021) and conducted in accordance with the principles of the Declaration of Helsinki (2013).

✉ **Correspondence should be addressed:** Nadezhda N. Melnikova
nab. Makarova, 6, Saint Petersburg, 199034; melnn@mail.ru

Received: 30.06.2023 **Accepted:** 07.08.2023 **Published online:** 20.08.2023

DOI: 10.47183/mes.2023.026

ВЛИЯНИЕ ГИПОТЕРМИИ ЛЕГКОЙ СТЕПЕНИ НА СОСУДИСТЫЙ ТОНУС МИКРОЦИРКУЛЯТОРНОГО РУСЛА ГОЛОВНОГО МОЗГА

Н. Н. Мельникова ✉

Институт физиологии имени И. П. Павлова Российской академии наук, Санкт-Петербург, Россия

Острая кровопотеря сопровождается ухудшением кровообращения, в том числе, на микроциркуляторном уровне. В клинических и в экспериментальных исследованиях идет поиск возможности нивелировать последствия этих нарушений. Использование гипотермии рассматривают не только как один из способов повышения выживаемости, но и как средство для улучшения церебрального микроциркуляторного кровообращения при геморрагии. Целью исследования было изучить состояние артериальных церебральных сосудов крыс при воздействии легкой гипотермии после острой кровопотери средней степени. Исследование проведено на наркотизированных крысах линии Вистар с помощью методики прижизненного микроскопирования. Изучали реакции пиальных артерий (начальный диаметр 10–40 мкм) при охлаждении животных до ректальной температуры 34 °С в условиях гемодинамической стабильности и при моделировании кровопотери (20% от ОЦК) при нормотермии и при гипотермии легкой степени. Результаты исследования показали, что 3,5 ч экспозиции в изучаемых условиях сопровождались вазоконстрикцией у животных всех исследуемых групп. При гипотермическом состоянии организма наблюдали первоначальное уменьшение диаметра на 9% от уровня фона (от 24,9 ± 0,9 мкм до 22,7 ± 0,7 мкм; $p < 0,05$), а затем его восстановление через 2 ч (до 25,7 ± 1,7; $p > 0,05$). При кровопотере диаметр церебральных микрососудов уменьшался на протяжении первого часа на 20–25% (от 23,4 ± 0,7 мкм до 17,6 ± 1,1 мкм; $p < 0,001$) без дальнейшего восстановления (диаметр через 3,5 ч наблюдений составлял 16,7 ± 0,8 мкм). Вазоконстрикция при использовании гипотермии после кровопотери составила 8–10% за первые 45 мин наблюдений (от 22,6 ± 1,3 мкм до 20,3 ± 1,2 мкм; $p < 0,05$) с последующим уменьшением сокращения (диаметр через 3,5 ч наблюдений составлял 21,4 ± 1,4 мкм). Сделан вывод, что использование легкой гипотермии приводило к сокращению вазоконстрикторного влияния умеренной кровопотери на пиальные микрососуды.

Ключевые слова: гипотермия, кровопотеря, церебральные сосуды

Финансирование: работа выполнена при поддержке Госпрограммы 47 ГП «Научно-технологическое развитие Российской Федерации» (2019–2030), тема 0134-2019-003.

Соблюдение этических стандартов: исследование одобрено этическим комитетом Комиссии по контролю над содержанием и использованием лабораторных животных ФГБУН Института физиологии им. И. П. Павлова РАН (протокол № 05/10 от 10 мая 2021 г.), проведено в соответствии с принципами Хельсинской декларации 2013 г.

✉ **Для корреспонденции:** Надежда Николаевна Мельникова
наб. Макарова, д. 6, г. Санкт-Петербург, 199034; melnn@mail.ru

Статья получена: 30.06.2023 **Статья принята к печати:** 07.08.2023 **Опубликована онлайн:** 20.08.2023

DOI: 10.47183/mes.2023.026

Blood loss associated with trauma is a major factor of high mortality among both civilians and servicemen [1, 2]. In the majority of cases severe condition of the patient with hemorrhage is aggravated by accidental hypothermia [3–5].

According to the existing guidelines on treatment of traumatic bleeding, hypothermia should be avoided [6, 7]. However, in early 2000s the animal experiments were conducted as part of the number of foreign trials that involved simulation of hemorrhagic shock and the use of cooling. The majority of studies involving various animal species were focused on the effect of different temperatures on survival rate. Thus, in rats with lethal uncontrolled bleeding, cooling of the body surface to 34 and 30 °C resulted in the increased survival (119 and 132 min, respectively, vs. 51 min) compared to normothermic rats [8]. The same results were obtained for rats with controlled hemorrhagic shock cooled to 34 °C within 12 h and during resuscitation [9]. Therapeutic mild hypothermia (34 °C) and delayed fluid resuscitation improved survival of rats after uncontrolled hemorrhagic shock [10].

The swine models of hemorrhagic shock also showed improved survival associated with hypothermia. Thus, surface cooling to Tr 34 °C improves survival of pigs after prolonged controlled hemorrhagic shock and splenic rupture [11]. Deep hypothermia and cardiopulmonary bypass can improve survival in pigs with lethal uncontrolled hemorrhage [12]. The study of traumatic uncontrolled hemorrhagic shock in rabbits has shown that mild hypothermia (Tr 34 °C) after restoration of circulation improves early survival and the function of organs, not disturbing homeostasis [13].

Later attempts were made to explore neuroprotective mechanisms of hypothermia. One of the recent reviews provides evidence of the effectiveness of using therapeutic hypothermia during heart surgery, in traumatic brain injury and neonatal encephalopathy in both animal studies and clinical trials [14]. Prevention of irreversible neuronal necrosis and ischemic brain injury is the main result of using hypothermia.

The use of therapeutic hypothermia in clinical practice in cases of hemorrhagic shock and resuscitation may be effective in terms of reducing the levels of reactive oxygen species and decreasing vascular permeability [15], contributing to successful resuscitation of the patient. It has been proven that the use of therapeutic hypothermia (34 °C) in rats with controlled or uncontrolled hemorrhagic shock reduces blood loss and oxygen consumption and causes no coagulopathy [16]. The ovine model has shown that the use of mild hypothermia in healthy animals is associated with significantly reduced density of sublingual capillaries along with no pronounced changes in systemic hemodynamics [17].

Beneficial effects of mild hypothermia on the cerebral cortex microcirculation measured by multichannel laser flowmetry have been proven in the rabbit model of cardiac arrest [18]. A similar effect of cerebral microcirculation improvement was observed in rats subjected to early mild whole-body hypothermia during resuscitation from cardiac arrest [19]. At the same time, mild hypothermia reduced both cerebral blood flow in the pigs' microvessels, as well as the cerebral metabolism after blood circulation restoration relative to normothermic animals [20, 21]. The overall effect was as follows: the ratio of the need and oxygen supply to the brain improved during the period of hypothermia.

A pilot study focused on assessing the effects of hypothermia on microcirculation in severe hemorrhagic shock was performed in 2021 [22]. The study showed that despite the fact that hemorrhage caused severe microcirculation disorder in the sublingual area, intestinal villi and the kidney cortex of the sheep, further decrease of rectal temperature to 33–34 °C improved microcirculation in these areas.

In our previous study, immersion cooling of the body aggravated microcirculatory dysfunction cause by acute massive blood loss [23]. When the rats were cooled so fast, additive effects of hypothermia and hemorrhage on vasoconstrictor responses of cerebral microvessels were observed in the phase of moderate hypothermia. To determine the pattern of mutual effects of hypothermia and hemorrhage, we set a goal to explore the effects of mild hypothermia in rats with previously evoked moderate blood loss on the brain microcirculatory bed.

METHODS

The experiments involved male Wistar rats (n = 23) with the body weight of 280–310 g obtained from the Collection of Laboratory Mammals of Different Taxons (Pavlov Institute of Physiology RAS).

The animals were anesthetized with urethane solution (intraperitoneal aministration, 1000 mg/kg). To perform an in vivo study of cerebral microvessels, parietal craniotomy with the bone flap size of 7 × 5 mm was performed, and dura mater was removed within the window. A catheter filled with heparinized (40 U/ml) saline was placed in the left femoral artery for direct blood pressure measurement, and the right femoral artery was catheterized for blood collection. The rectal temperature (Tr) of 37–38 °C was maintained in the rats during the surgical procedure using an electric pad for small animals.

The animals were randomized into three groups during the experiments. Animals of group 1 (n = 7) were cooled to the rectal temperature of 34 °C, then this temperature was maintained throughout 3.5 h of the experiment. Animals of group 2 (n = 6) were used to simulate blood loss with the estimated rate of 20% of total blood volume, then the animals with the baseline Tr 37 °C were kept at the room temperature of 20–22 °C throughout 3.5 h of the experiment. After the evoked hemorrhage, animals of group 3 (n = 10) were cooled in the air to Tr 34 °C that had been maintained for 3.5 h.

Arterial blood was collected: 1.2 mL per 100 g of the animal's weight or 20% of total blood volume. This was equivalent to moderate blood loss, i.e. blood exfusion in the rat with the body weight of 300 g was 3.6 mL. Blood was collected for ≈10 min, the average exfusion rate was 0.36 mL/min.

Rats were cooled to Tr 34 °C in the air at standard room temperature by wetting a part of the animal's back and using the directional airflow produced by a domestic fan. The cooling duration was ≈ 30 min.

The order of exposures used during the experiment in each group is provided in Fig. 1.

Imaging and monitoring of the pial microcirculatory bed was performed using the vital microscopy system that included the LUMAM K-1 microscope (LOMO; Russia) with the contact dark-field lens and the ACUMEN AiP-B84A color video camera (ACUMEN Int. Corp.; Taiwan). The resulting image was subjected to computer processing in the Pinnacle Studio software package. The calibration measurement was performed using the OS-1 standard stage micrometer (scale division value 10 μm).

After preliminary procedures (cooling / exfusion / both) the responses of pial arteries were recorded every 15 min throughout 3.5 h of the experiment. The baseline microvessel diameter was 10–40 μm, and the majority of arteries were about 20–25 μm in diameter. Identical segments of blood vessels were measured 50–90 times within each series of the

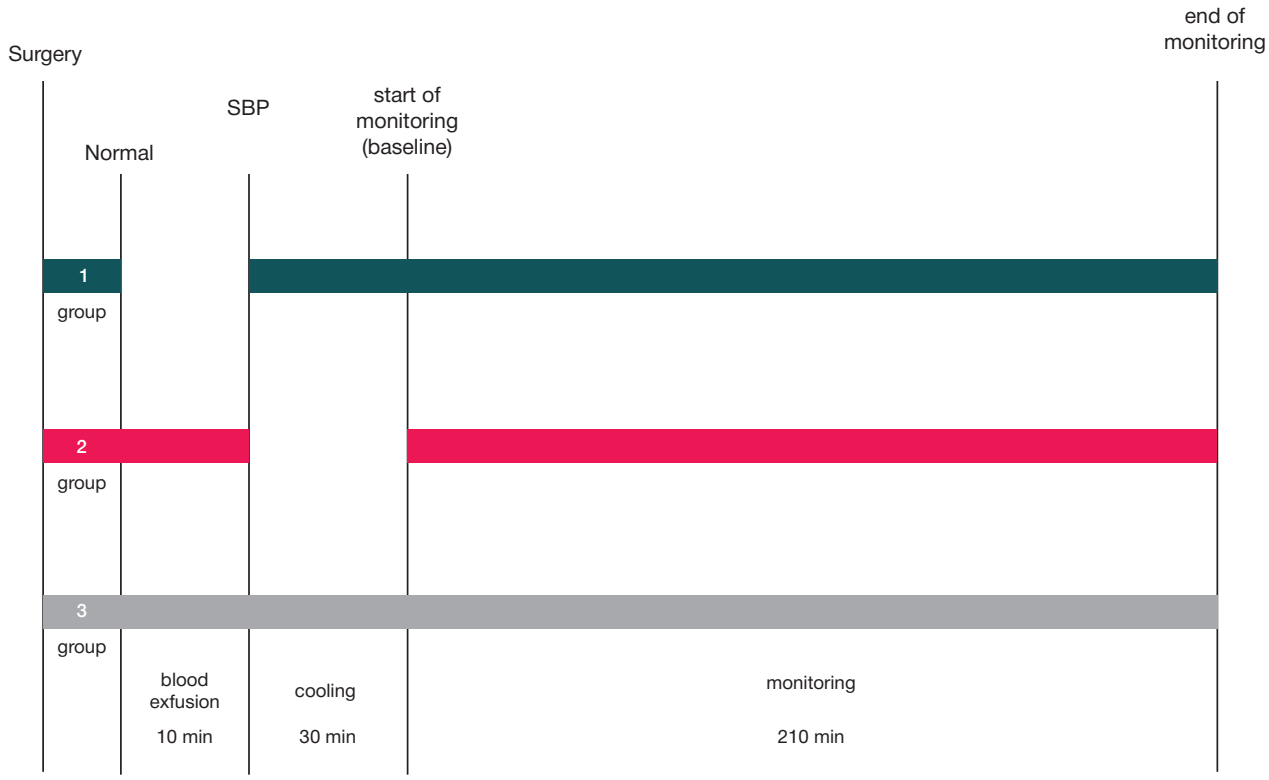

Fig. 1. Experimental design

experiment at each time period. After the end of the experiment animals were euthanized via urethane solution overdose.

Heart rate according to ECG, average blood pressure (direct measurement via femoral artery catheter) and respiratory rate (carbon sensor) were continuously recorded. The E-154 ADC (L-Card; Russia) was used to digitize analog signals and save these signals in computer memory.

Statistical processing of the results was performed using the STATISTICA 6.0 software package. Significance of intragroup differences was assessed using the nonparametric Wilcoxon test, while intergroup differences were revealed using the nonparametric Mann–Whitney U test. The significance level was set as $p < 0.05$. All experimental data were presented as mean ± standard error of the mean (M ± SE).

RESULTS

Indicators of the body's functional state before exposure (referred to as normal) were the same ($p > 0.05$) in all experimental groups (Table). In groups 2 and 3, preliminary blood exfusion equivalent to 20% of total blood volume resulted in rapid decrease in SBP by 60% ($p < 0.001$), slight decrease in HR by 5–7% ($p < 0.05$), while RR remained unchanged ($p > 0.05$). In groups 1 and 3, when Tr 34 °C (referred to as baseline) was achieved by the beginning of monitoring, SBP was 11% ($p < 0.05$) and 30% ($p < 0.001$) lower than normal, respectively, HR decreased by 16–17% ($p < 0.01$) in both groups, while RR decreased by 5% ($p > 0.05$) in group 1 and 24% ($p < 0.01$) in group 3. In group 2, when monitoring was begun (baseline), SBP increased by 29% ($p < 0.01$) of minimum SBP measured during blood collection, HR and RR slightly decreased ($p > 0.05$), and Tr was 37.1 ± 0.2 °C. Thus, by the beginning of monitoring (baseline) the animals' physiological parameters reached certain levels that were different from normal, after that the required for the experiment Tr of 34 °C was maintained in animals of groups 1 and 3 for 3.5 h, and animals of group 2 were kept at room temperature.

In group 1 (Fig. 2) in the 15th minute of hypothermia the rat's SBP slightly increased to 107.7 ± 5.7 mmHg ($p < 0.05$), but later it was within the range of 85–98 mmHg. HR of animals in this group was slightly higher compared to baseline within the first 1.5 h of monitoring, then in was at the baseline level, but did not increase to normal. The pairwise comparison of RR in group 1 revealed slight significant differences between the normal value and the values reported in animals with hypothermia ($p < 0.05$) throughout the experiment.

In group 2, Tr decreased throughout the experiment and reached 34.3 ± 0.3 °C by the end of monitoring (after 3.5 h). SBP grew evenly within 1 h to reach 80 mmHg ($p < 0.01$),

Table. Parameters of the rats' functional state before the beginning of monitoring

Groups	1	2	3	2	3	1	3	2
Parameters	Normal			Blood collection, min SBP		Beginning of monitoring (baseline)		
						Hypothermia, Tr 34 °C		Normothermia, Tr 37 °C
SBP	104.0 ± 6.4	107.5 ± 4.6	103.5 ± 4.9	42.7 ± 2.8***	39.0 ± 1.9***	92.2 ± 6.3*	72.4 ± 4.7***†††	55.0 ± 3.5***††
HR	458 ± 11.1	471.5 ± 10.8	450.4 ± 7.4	447.3 ± 11*	422.9 ± 13.1*	385.7 ± 6.8**	374.7 ± 8.7**	435.3 ± 14.5
RR	109.1 ± 3.2	103.3 ± 2.4	101.6 ± 5.6	101.0 ± 8.3	101.9 ± 10.5	103.4 ± 5.5	76.8 ± 6.2**†	95.7 ± 7.8

Note: * — $p < 0.05$, ** — $p < 0.01$, *** — $p < 0.001$ when comparing to normal; † — $p < 0.05$, †† — p — 0.01, ††† — $p < 0.001$ when comparing baseline values with the values recorded during blood collection.

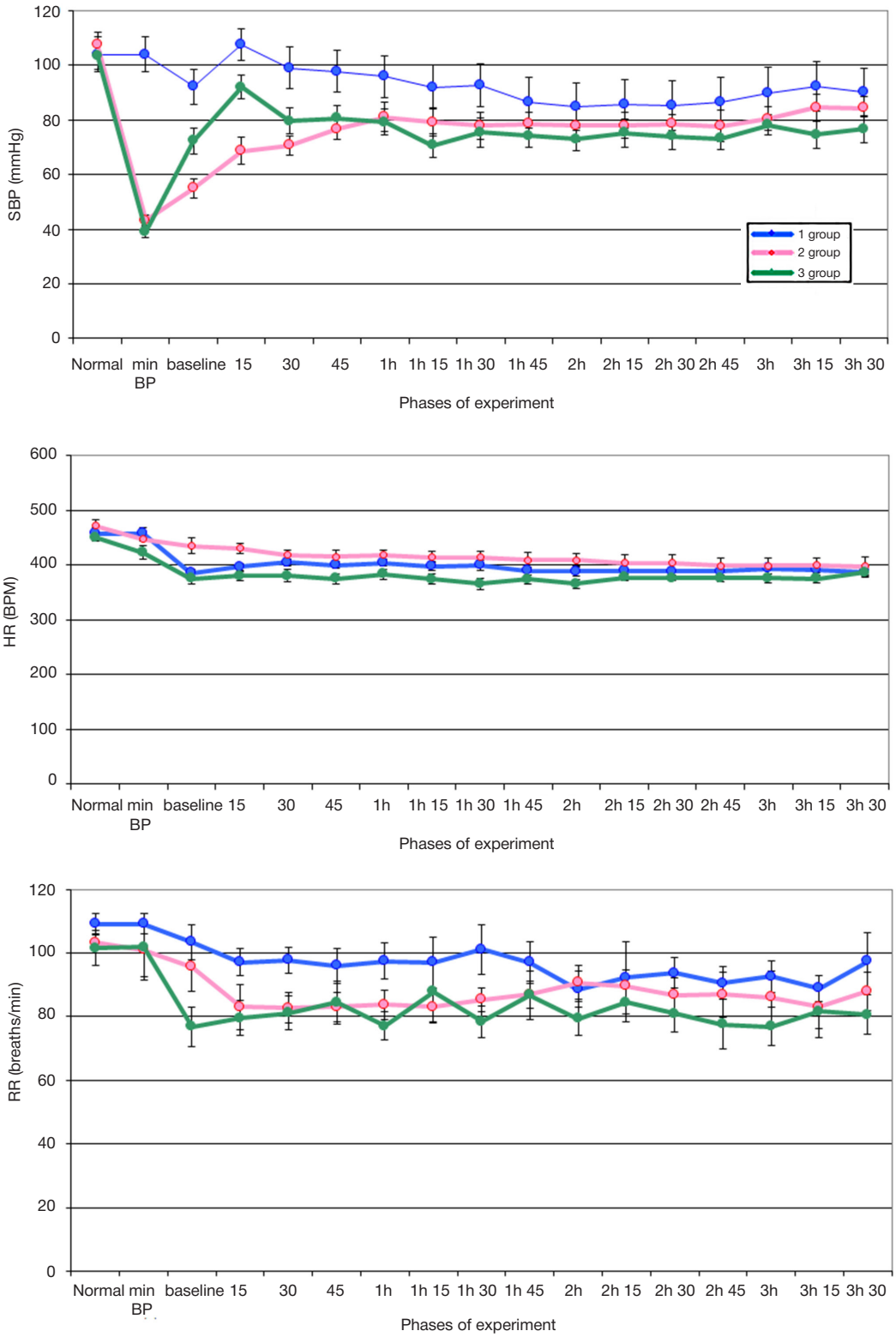

Fig. 2. Average blood pressure, heart rate and respiratory rate in rats during the experiment

after that it remained at this level till the end of monitoring. HR showed a downward trend throughout the period of monitoring, in the end of this period HR was 16% lower than normal and 9% lower than baseline ($p < 0.01$). RR was at the baseline level.

In group 3, SBP increased to 53.9 ± 3.7 mmHg by the beginning of cooling, it continued raising to 72.4 ± 4.7 mmHg at the point corresponding to the beginning of monitoring during further cooling and reached its maximum (92.1 ± 4.2 mmHg) after blood loss on the 15th minute of monitoring ($p < 0.001$). HR and RR were at the baseline level throughout the period of monitoring.

Fig. 3 provides the results of the direct measurement of pial artery diameter in μm.

During the stage of experiment between the animal's initial state and the baseline values reported at the beginning of monitoring the changes in diameter of blood vessels were calculated as a percentage of the initial diameter (normal). Vasoconstriction was observed in all three groups during

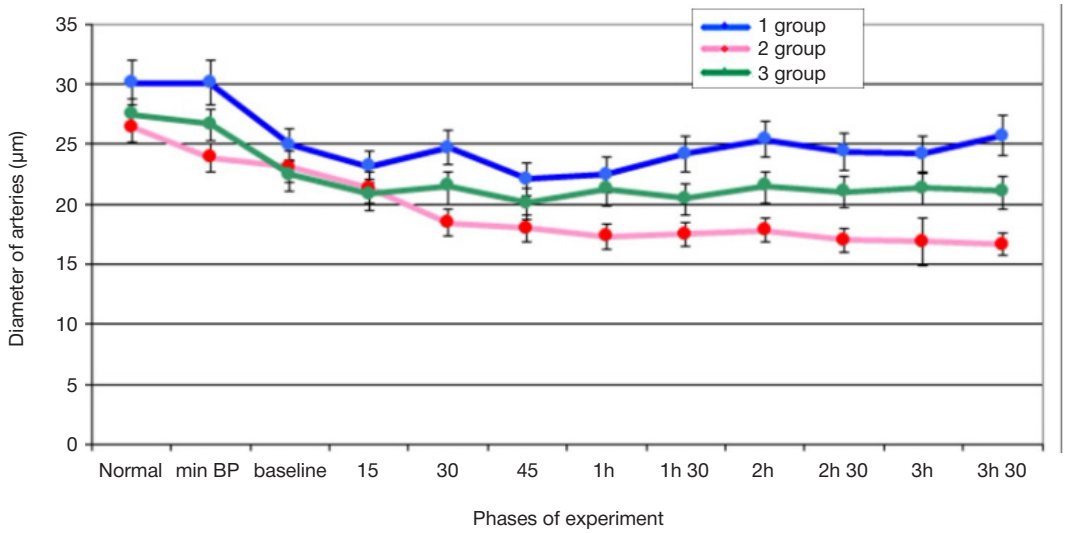

Fig. 3. Changes in the diameter of pial arteries at different stages of the experiment

both preliminary blood exfusion and cooling of animals. At the moment when SBP reached its minimum constriction of blood vessels was 9% in group 2 and 4% in group 3. After the animals were cooled by the beginning of monitoring, the decrease in the diameter was 17.2 ± 2.8% of normal in group 1 and 18.4 ± 2.3% in group 3 ($p < 0.001$).

The diameter of blood vessels reported at the beginning of this stage (baseline) was considered as 100% to objectively assess subsequent microcirculatory bed changes during the experiment. These changes are shown in Fig. 4. Persistent hypethermia (group 1) was associated with initial decrease in the diameter followed by the diameter restoration to the baseline level within 2 h. In group 2, the experiment involving monitoring at room temperature showed that the diameter of cerebral microvessels continued to decrease within the first hour and then remained at the level of 80% of baseline showing no trend towards restoration. Constriction of the arteries in animals of group 3 that experienced both blood loss and hypothermia was 2 times lower than in animals of group 2 in the first 45 min of monitoring, later this ratio increased.

DISCUSSION

The major factors of the acute hemorrhage syndrome include reduced total blood volume, changes in blood vessel tone and cardiac output reduction [7, 24]. It is believed that blood loss that constitutes 15% of total blood volume triggers a compensatory mechanism, however, this mechanism turns out to be untenable in terms of preventing progressive hypotension. Our study involved the use of the small animal model of moderate blood loss (average exfusion rate 0.36 mL/min) with the total blood loss of 20% of total blood volume that resulted in the SBP decrease to ≈ 40 mmHg. Later, slight blood pressure compensation was observed in normothermia: in group 2, SBP increased to 55 ± 3.5 mmHg by the beginning of monitoring and then gradually increased with time to reach 70–80 mmHg. Hypothermic exposure along with blood loss (group 3) resulted in the earlier and larger (up to 90 mmHg) compensatory increase in SBP. Such results suggest that in the conditions of acute blood loss that constituted 20% of total blood volume SBP compensation was achieved faster and more effectively in animals with mild hypothermia than in normothermic animals.

Undoubtedly, blood pressure is merely a means of the tissue energy supply and does not fully reflect the tissue hypoperfusion associated with acute loss of a portion of total blood volume. However, the state of tissue circulation can be roughly estimated based on the SBP changes. It is believed that capillary blood flow is preserved when SBP exceeds 80 mmHg, SBP below 55 mmHg is associated with the loss of organ blood flow autoregulation, and critical cerebral perfusion impairment occurs when SBP is below 35 mmHg [24]. In our study involving the use of hypothermia a faster SBP compensation to до 90 mmHg was observed, then SBP was maintained within the range of 75–80 mmHg. That is why it can be assumed that mild hypothermic exposure prevents or significantly reduces the risk of organ hypoxia.

The findings of our experimental study confirm that mild hypothermia with or without moderate blood loss definitely affects the changes in the state of microcirculatory bed in anesthetized rats. We revealed vasoconstriction relative to baselines in animals of all experimental groups (Fig. 3). Only slight differences in HR and RR throughout 3.5 h of monitoring were reported in animals of different experimental groups in the first 90 min, and in the final phase the values of these indicators were the same ($p > 0.05$). Furthermore, the differences in SBP between all groups by the end of monitoring were non-significant. Thus, it was shown that the 3.5 h exposure in hypothermic animals, normothermic animals with blood loss, and animals that experienced the combined effects of blood loss and hypothermia did not lead to significant differences in SBP, HR and RR in the final phase, but were associated with the changes in the diameter of pial arteries in animals of all studied groups.

The compensation to blood loss results also from the reflex sympathetically mediated arteriolar vasoconstriction induced by catecholamines acting on the α1 receptors [7]. Our study has shown that the spasm occurs not only in the peripheral, but also in the cerebral arteries, at least in the parietal cortex we have studied. It is believed that the key role in redistribution of blood needed to provide adequate blood supply of the brain tissue is played by the pial arteries [25].

We revealed microcirculatory disorders associated with hypothermia that took place since the very beginning of cooling. This was in line with the existing studies. Thus, when studying the effects of moderate hypothermia on the dynamics of microcirculatory bed in the zone of the tail vein projection in rats, vasoconstriction and reduced indicators of microcirculation were revealed [26]. The experiments on the cerebral arteries showed the same relationship: blood flow

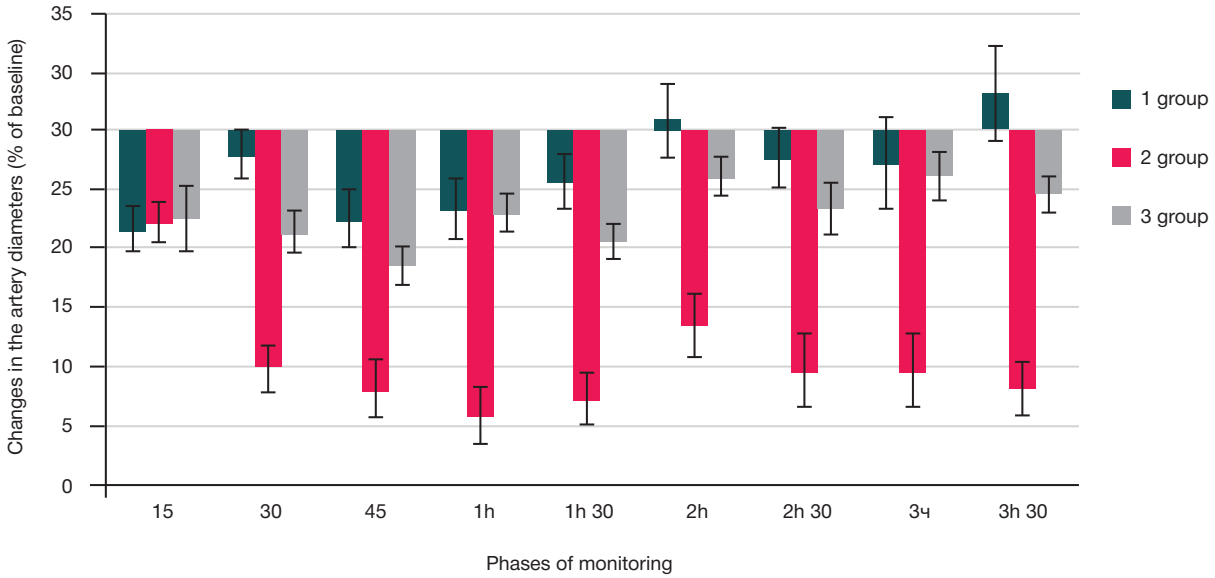

Fig. 4. Dynamic changes in the diameter of the rats' pial arteries relative to baseline in different experimental groups

in the cerebral microvessels progressively decreased during cooling [21]. Microcirculation can play a crucial role when the cell metabolism adjusts to the temperature fluctuations. The decrease of the temperature, and, therefore, metabolic rate, results in the constriction of precapillary resistance vessels, thereby reducing blood flow. This results in the less effective perfusion capability of microcirculation [20, 21]. However, these studies show that cooling did not lead to poorer supply of oxygen to the brain, since the oxygen concentration was stable or even elevated when the cerebral artery perfusion was reduced. This important fact suggests that the ratio of the need and oxygen supply to the brain is improved in hypothermia.

The relationship between hypothermia and hemorrhage was studied repeatedly under different conditions, however, the number of studies focused on assessing the impact of the systemic hypothermia effects on the cerebral microcirculatory bed in acute blood loss is low. The hemorrhagic shock models of different animal species have demonstrated improved survival associated with hypothermia [8–13]. The improvement of blood flow through cerebral microcirculation by means of mild hypothermia during cardiopulmonary resuscitation has been reported [18, 19, 27]. Our study has also shown that the use of mild hypothermia improves the state of the rats' cerebral cortex microcirculatory bed after moderate acute blood loss. This is consistent with the findings of the studies showing that systemic hypothermia provides protection against further impairment affecting microcirculatory beds of the kidneys, intestinal villi, and the sublingual space in hemorrhagic shock [22].

In our previous study, when the animals were subjected to continuous immersion cooling until the hypothermia-induced respiratory arrest was achieved, constriction of blood vessels by ≈ 20% of normal was observed during the period of deep hypothermia, while in animals with previously evoked blood loss (35% of total blood volume) that were further cooled constriction of blood vessels exceeded 30% [23]. In this study we did not use cooling to such low temperatures: animals of groups 1 and 3 were cooled only to Tr 34 °C, and blood exfusion was 20% of total blood volume. Constriction was less severe under such mild conditions, which was indicative of the direct relationship between the degree of vasoconstriction and the degree of the body's exposure to negative factors.

Neuroprotective mechanisms of hypothermia used after the cerebral microcirculation impairment are poorly understood. After reperfusion injury, mild hypothermia reduces the increased cerebral oxygen extraction ratio [19]. The review focused on the effects of therapeutic hypothermia in neurological disorders reports that reduced metabolic rate and the decrease in the brain's need for oxygen and glucose are the main mechanism underlying protective effects of hypothermia [28]. It can be assumed that it is the reduced need for oxygen that underlies compensation of reduced blood flow by hypothermia after the acute hemorrhagic exposure.

CONCLUSIONS

The findings suggest that mostly vasoconstrictor effects were observed in the pial microvessels of anesthetized rats under the conditions of mild hypothermia, hemorrhage constituting 20% of total blood volume or combined exposure to both. The use of mild hypothermia led to the significantly decreased vasoconstrictor effect of moderate acute blood loss on the cerebral microvessels. It should be noted that the current data on the use of hypothermia in the models of animal or human injury or hemorrhage are scarce, despite the large number of studies focused on the use of hypothermia in medical practice. Further research is needed to determine the possibility and most effective schemes of using hypothermia in injuries and hemorrhage.

References

1. Perlman R, Callum J, Laflamme C, Tien H, Nascimento B, Beckett A, Alam A. A recommended early goal-directed management guideline for the prevention of hypothermia-related transfusion, morbidity, and mortality in severely injured trauma patients. Crit Care. 2016; 20 (1): 107. PubMed PMID: 27095272.
2. Poh PY, Gagnon D, Romero SA, Convertino VA, Adams-Huet B, Crandall CG. Hemodynamic stability to surface warming and cooling during sustained and continuous simulated hemorrhage in humans. Shock. 2016; 46 (3 Suppl 1): 42–9. PubMed PMID: 27224744.
3. van Veelen MJ, Brodmann Maeder M. Hypothermia in trauma. Int J Environ Res Public Health. 2021; 18 (16): 8719. PubMed PMID: 34444466.
4. Rösli D, Schnüriger B, Candinas D, Haltmeier T. The impact of accidental hypothermia on mortality in trauma patients overall and patients with traumatic brain injury specifically: a systematic review and meta-analysis. World J Surg. 2020; 44 (12): 4106–17. PubMed PMID: 32860141.
5. Rauch S, Miller C, Bräuer A, Wallner B, Bock M, Paal P. Perioperative Hypothermia-A Narrative Review. Int J Environ Res Public Health. 2021; 18 (16): 8749. PubMed PMID: 34444504.
6. Grigorev EV, Lebedinskij KM, Shhegolev AV, Bobovnik SV, Bulanov AYu, Zabolotskix IB, i dr. Reanimaciya i intensivnaya terapiya pri ostroj massivnoj krovopotere u vzroslyx pacientov. Anesteziologiya i reanimatologiya. 2020; (1): 5–24. Russian.
7. Bonanno FG. Management of hemorrhagic shock: physiology approach, timing and strategies. J Clin Med. 2023; 12 (1): 260. PubMed PMID: 36615060.
8. Takasu A, Carrillo P, Stezoski SW, Safar P, Tisherman SA. Mild or moderate hypothermia but not increased oxygen breathing prolongs survival during lethal uncontrolled hemorrhagic shock in rats, with monitoring of visceral dysoxia. Crit Care Med. 1999; 27 (8): 1557–64. PubMed PMID: 10470764.
9. Wu X, Stezoski J, Safar P, Nozari A, Tisherman SA. After spontaneous hypothermia during hemorrhagic shock, continuing mild hypothermia (34 degrees C) improves early but not late survival in rats. J Trauma. 2003; 55 (2): 308–16. PubMed PMID: 12913642.
10. Hachimi-Idrissi S, Yang X, Nguyen DN, Huyghens L. Combination of therapeutic mild hypothermia and delayed fluid resuscitation improved survival after uncontrolled haemorrhagic shock in mechanically ventilated rats. Resuscitation. 2004: 62 (3): 303–10. PubMed PMID: 15325450.
11. Wu X, Kochanek PM, Cochran K, Nozari A, Henchir J, Stezoski SW, et al. Mild hypothermia improves survival after prolonged, traumatic hemorrhagic shock in pigs. J Trauma. 2005; 59 (2): 291–301. PubMed PMID: 16294067.
12. Alam HB, Rhee P, Honma K, Chen H, Ayuste EC, Lin T et al. Does the rate of rewarming from profound hypothermic arrest influence the outcome in a swine model of lethal hemorrhage? J Trauma. 2006; 60 (1): 134–46. PubMed PMID: 16456447.
13. Jiang SY, Zhao YY, Zhao XG. Potential role of therapeutic hypothermia in the salvage of traumatic hemorrhagic shock. Crit Care. 2013; 17 (3): 318. PubMed PMID: 23714428.
14. Hong JM, Choi ES, Park SY. Selective brain cooling: a new horizon of neuroprotection. Front Neurol. 2022; 20; 13: 873165. PubMed PMID: 35795804.
15. Childs EW, Udobi KF, Hunter FA. Hypothermia reduces microvascular permeability and reactive oxygen species expression after hemorrhagic shock. J Trauma. 2005; 58 (2): 271–7. PubMed PMID: 15706187.
16. Li T, Lin X, Zhu Y, Li L, Liu L. Short-term, mild hypothermia can increase the beneficial effect of permissive hypotension on uncontrolled hemorrhagic shock in rats. Anesthesiology. 2012; 116 (6): 1288–98. PubMed PMID: 22546964.
17. He X, Su F, Taccone FS, Maciel LK, Vincent JL. Cardiovascular and microvascular responses to mild hypothermia in an ovine model. Resuscitation. 2012; 83 (6): 760–6. PubMed PMID: 22155698.
18. Chun-Lin H, Jie W, Xiao-Xing L, Xing L, Yu-Jie L, Hong Z, et al. Effects of therapeutic hypothermia on coagulopathy and microcirculation after cardiopulmonary resuscitation in rabbits. Am J Emerg Med. 2011; 29 (9): 1103–10. PubMed PMID: 20951524.
19. Gong P, Zhao S, Wang J, Yang Z, Qian J, Wu X, et al. Mild hypothermia preserves cerebral cortex microcirculation after resuscitation in a rat model of cardiac arrest. Resuscitation. 2015; 97: 109–14. PubMed PMID: 26485658.
20. Wu J, Yuan W, Li J, Zhao Y, Li J, Li Z. Effects of mild hypothermia on cerebral large and small microvessels blood flow in a porcine model of cardiac arrest. Neurocrit Care. 2017; 27 (2): 297–303. PubMed PMID: 28405859.
21. Donadello K, Su F, Annoni F, Scolletta S, He X, Peluso L, et al. The effects of temperature management on brain microcirculation, oxygenation and metabolism. Brain Sci. 2022; 12 (10): 1422. PubMed PMID: 36291355.
22. Caminos Eguillor JF, Ferrara G, Kanoore Edul VS, Buscetti MG, Canales HS, Lattanzio B, et al. Effects of systemic hypothermia on microcirculation in conditions of hemodynamic stability and in hemorrhagic shock. Shock. 2021; 55 (5): 686–92. PubMed PMID: 32694390.
23. Melnikova NN. Vozdejstvie sistemnoj gipotermii na reakcii pial'nyx arterij pri ostroj massivnoj krovopotere u narkotizirovannyx krys linii Wistar. Zhurnal ehvolyucionnoj bioximii i fiziologii. 2022; 58 (5): 382–92. Russian.
24. Vasilev AG, Xajcev NV, Balashov AL, Balashov LD, Kravcova AA., Trashkov AP, i dr. O patogeneze sindroma ostroj krovopoteri. Pediatr. 2019; 10 (3): 93–100. Russian.
25. Markina LD, Shiryaeva EE, Markin VV. Morfofunkcional'nye osobennosti pial'nyx arterij zon smezhnogo krovosnabzheniya golovnogo mozga v usloviyax ostroj cirkulyatornoj gipoksii. Tixookeanskij medicinskij zhurnal. 2015; (1): 40–2. Russian.
26. Lycheva NA, Sedov AV, Makushkina DA, Shaxmatov II, Vdovin VM. Neprednamerennaya gipotermiya kak faktor narusheniya raboty mikrocirkulyatornogo rusla. Kazanskij medicinskij zhurnal. 2019; 100 (2): 252–6. Russian.
27. Yu H, Wang L, Zhang H, Wei W, Chen Y, Tang W. Effect of mild hypothermia on cerebral microcirculation in a murine cardiopulmonary resuscitation model. Microcirculation. 2019; 26 (6): e12537. PubMed PMID: 30801897.
28. Kurisu K, Kim JY, You J, Yenari MA. Therapeutic hypothermia and neuroprotection in acute neurological disease. Curr Med Chem. 2019; 26 (29): 5430–55. PubMed PMID: 31057103.

Литература

1. Perlman R, Callum J, Laflamme C, Tien H, Nascimento B, Beckett A, Alam A. A recommended early goal-directed management guideline for the prevention of hypothermia-related transfusion, morbidity, and mortality in severely injured trauma patients. Crit Care. 2016; 20 (1): 107. PubMed PMID: 27095272.
2. Poh PY, Gagnon D, Romero SA, Convertino VA, Adams-Huet B, Crandall CG. Hemodynamic stability to surface warming and cooling during sustained and continuous simulated hemorrhage in humans. Shock. 2016; 46 (3 Suppl 1): 42–9. PubMed PMID: 27224744.
3. van Veelen MJ, Brodmann Maeder M. Hypothermia in trauma. Int J Environ Res Public Health. 2021; 18 (16): 8719. PubMed PMID: 34444466.
4. Rösli D, Schnüriger B, Candinas D, Haltmeier T. The impact of accidental hypothermia on mortality in trauma patients overall and patients with traumatic brain injury specifically: a systematic review and meta-analysis. World J Surg. 2020; 44 (12): 4106–17. PubMed PMID: 32860141.
5. Rauch S, Miller C, Bräuer A, Wallner B, Bock M, Paal P. Perioperative Hypothermia-A Narrative Review. Int J Environ Res Public Health. 2021; 18 (16): 8749. PubMed PMID: 34444504.
6. Григорьев Е. В., Лебединский К. М., Щеголев А. В., Бобовник С. В.,

Буланов А. Ю., Заболотских И. Б. и др. Реанимация и интенсивная терапия при острой массивной кровопотере у взрослых пациентов. Анестезиология и реаниматология. 2020; (1): 5–24.
7. Bonanno FG. Management of hemorrhagic shock: physiology approach, timing and strategies. J Clin Med. 2023; 12 (1): 260. PubMed PMID: 36615060.
8. Takasu A, Carrillo P, Stezoski SW, Safar P, Tisherman SA. Mild or moderate hypothermia but not increased oxygen breathing prolongs survival during lethal uncontrolled hemorrhagic shock in rats, with monitoring of visceral dysoxia. Crit Care Med. 1999; 27 (8): 1557–64. PubMed PMID: 10470764.
9. Wu X, Stezoski J, Safar P, Nozari A, Tisherman SA. After spontaneous hypothermia during hemorrhagic shock, continuing mild hypothermia (34 degrees C) improves early but not late survival in rats. J Trauma. 2003; 55 (2): 308–16. PubMed PMID: 12913642.
10. Hachimi-Idrissi S, Yang X, Nguyen DN, Huyghens L. Combination of therapeutic mild hypothermia and delayed fluid resuscitation improved survival after uncontrolled haemorrhagic shock in mechanically ventilated rats. Resuscitation. 2004: 62 (3): 303–10. PubMed PMID: 15325450.
11. Wu X, Kochanek PM, Cochran K, Nozari A, Henchir J, Stezoski SW, et al. Mild hypothermia improves survival after prolonged, traumatic hemorrhagic shock in pigs. J Trauma. 2005; 59 (2): 291–301. PubMed PMID: 16294067.
12. Alam HB, Rhee P, Honma K, Chen H, Ayuste EC, Lin T et al. Does the rate of rewarming from profound hypothermic arrest influence the outcome in a swine model of lethal hemorrhage? J Trauma. 2006; 60 (1): 134–46. PubMed PMID: 16456447.
13. Jiang SY, Zhao YY, Zhao XG. Potential role of therapeutic hypothermia in the salvage of traumatic hemorrhagic shock. Crit Care. 2013; 17 (3): 318. PubMed PMID: 23714428.
14. Hong JM, Choi ES, Park SY. Selective brain cooling: a new horizon of neuroprotection. Front Neurol. 2022; 20; 13: 873165. PubMed PMID: 35795804.
15. Childs EW, Udobi KF, Hunter FA. Hypothermia reduces microvascular permeability and reactive oxygen species expression after hemorrhagic shock. J Trauma. 2005; 58 (2): 271–7. PubMed PMID: 15706187.
16. Li T, Lin X, Zhu Y, Li L, Liu L. Short-term, mild hypothermia can increase the beneficial effect of permissive hypotension on uncontrolled hemorrhagic shock in rats. Anesthesiology. 2012; 116 (6): 1288–98. PubMed PMID: 22546964.
17. He X, Su F, Taccone FS, Maciel LK, Vincent JL. Cardiovascular and microvascular responses to mild hypothermia in an ovine model. Resuscitation. 2012; 83 (6): 760–6. PubMed PMID: 22155698.
18. Chun-Lin H, Jie W, Xiao-Xing L, Xing L, Yu-Jie L, Hong Z, et al. Effects of therapeutic hypothermia on coagulopathy and microcirculation after cardiopulmonary resuscitation in rabbits. Am J Emerg Med. 2011; 29 (9): 1103–10. PubMed PMID: 20951524.
19. Gong P, Zhao S, Wang J, Yang Z, Qian J, Wu X, et al. Mild hypothermia preserves cerebral cortex microcirculation after resuscitation in a rat model of cardiac arrest. Resuscitation. 2015; 97: 109–14. PubMed PMID: 26485658.
20. Wu J, Yuan W, Li J, Zhao Y, Li J, Li Z. Effects of mild hypothermia on cerebral large and small microvessels blood flow in a porcine model of cardiac arrest. Neurocrit Care. 2017; 27 (2): 297–303. PubMed PMID: 28405859.
21. Donadello K, Su F, Annoni F, Scolletta S, He X, Peluso L, et al. The effects of temperature management on brain microcirculation, oxygenation and metabolism. Brain Sci. 2022; 12 (10): 1422. PubMed PMID: 36291355.
22. Caminos Eguillor JF, Ferrara G, Kanoore Edul VS, Buscetti MG, Canales HS, Lattanzio B, et al. Effects of systemic hypothermia on microcirculation in conditions of hemodynamic stability and in hemorrhagic shock. Shock. 2021; 55 (5): 686–92. PubMed PMID: 32694390.
23. Мельникова Н. Н. Воздействие системной гипотермии на реакции пиальных артерий при острой массивной кровопотере у наркотизированных крыс линии Wistar. Журнал эволюционной биохимии и физиологии. 2022; 58 (5): 382–92.
24. Васильев А. Г., Хайцев Н. В., Балашов А. Л., Балашов Л. Д., Кравцова А. А., Трашков А.П. и др. О патогенезе синдрома острой кровопотери. Педиатр. 2019; 10 (3): 93–100.
25. Маркина Л. Д., Ширяева Е. Е., Маркин В. В. Морфофункциональные особенности пиальных артерий зон смежного кровоснабжения головного мозга в условиях острой циркуляторной гипоксии. Тихоокеанский медицинский журнал. 2015; (1): 40–2.
26. Лычева Н. А., Седов А. В., Макушкина Д. А., Шахматов И. И., Вдовин В. М. Непреднамеренная гипотермия как фактор нарушения работы микроциркуляторного русла. Казанский медицинский журнал. 2019; 100 (2): 252–6.
27. Yu H, Wang L, Zhang H, Wei W, Chen Y, Tang W. Effect of mild hypothermia on cerebral microcirculation in a murine cardiopulmonary resuscitation model. Microcirculation. 2019; 26 (6): e12537. PubMed PMID: 30801897.
28. Kurisu K, Kim JY, You J, Yenari MA. Therapeutic hypothermia and neuroprotection in acute neurological disease. Curr Med Chem. 2019; 26 (29): 5430–55. PubMed PMID: 31057103.

FEATURES OF BIOELECTRIC ACTIVITY OF THE RETROSPLENIAL CORTEX

Gulyaev SA[1,2] ✉, Khanukhova LM[2], Garmash AA[1]

[1] Institute for Physics and Engineering in Biomedicine, National Research Nuclear University MEPhI, Moscow, Russia

[2] La Salute Clinic, Moscow, Russia

Human brain is one of the most difficult organs to study. The possibility of developing the technologies that have sufficient scientific accuracy and economic accessibility and never violate the moral and ethical standards of human society is of great interest. The study was aimed to study the possibility of assessing the retrosplenial cortex (RSC) structures' activity based on the EEG analysis of brain activity in the alpha frequency range in 36 healthy volunteers with an average age of 29.1 years, no acute central nervous system disorders or exacerbation of chronic central nervous system disorders, severe traumatic brain injuries, mental disorders or epilepsy. Significant source localizations were obtained by solving the EEG inverse problem that could be used for identification of the cerebral retrosplenial cortex structures' bioelectric activity. The use of such technology will allow us to expand the scope of the research focused on assessing the brain functional activity in both research and clinical centers, thereby paving the way for understanding the features of the brain structures' activity in physiologically normal conditions and in individuals with mental disorders caused by various functional alterations in the brain.

Keywords: electroencephalography, mathematical methods, retrosplenial cortex, bioelectrical activity of the brain

Author contributions: Gulyaev SA — study concept, clinical neurophysiological assessment, statistical analysis of the results; Khanukhova LM — research organization; Garmash AA — general management.

Compliance with ethical standards: the study was approved by the Ethics Committee of the National Research Nuclear University MEPhI (protocol № 05/23 of 25 May 2023) and conducted in accordance with the principles of biomedical ethics set out in the Declaration of Helsinki (1964) and its subsequent updates.

✉ **Correspondence should be addressed:** Sergey A. Gulyaev
Ramenki, 31, k. 136, Moscow, 119607, Russia; s.gulyaev73@gmail.com

Received: 27.06.2023 **Accepted:** 04.09.2023 **Published online:** 25.09.2023

DOI: 10.47183/mes.2023.028

ОСОБЕННОСТИ БИОЭЛЕКТРИЧЕСКОЙ АКТИВНОСТИ РЕТРОСПЛЕНИАЛЬНОЙ КОРЫ ГОЛОВНОГО МОЗГА

С. А. Гуляев[1,2] ✉, Л. М. Ханухова[2], А. А. Гармаш[1]

[1] Инженерно-физический институт биомедицины Национального исследовательского ядерного университета «МИФИ», Москва, Россия

[2] Клиника Ла Салюте, Москва, Россия

Головной мозг человека представляет собой один из самых сложных для исследования органов. Огромный интерес представляет возможность разработки технологий, обладающих достаточной научной точностью и экономической доступностью при полном соблюдении морально-этических норм человеческого сообщества. Целью работы было изучить возможность исследования активности структур ретроспленциальной коры (RSC) на основе ЭЭГ-анализа биоэлектрической активности головного мозга в альфа-диапазоне частот у 36 здоровых добровольцев возрастом в среднем 29,1 года, не имевших острых и хронических заболеваний центральной нервной системы в стадии обострения, тяжелых черепномозговых травм, психических заболеваний и эпилепсии. Получены статистически достоверные локализации источников с помощью решения обратной ЭЭГ-задачи, позволяющие использовать их для идентификации биоэлектрической активности структур ретроспленциальной коры головного мозга. Применение данной технологии позволит расширить объем исследований функциональной активности головного мозга как в научных, так и клинических учреждениях, создав условия для понимания особенностей работы мозговых структур в условиях физиологической нормы и при наличии психических заболеваний, основу которых составляют различные функциональные изменения головного мозга.

Ключевые слова: электроэнцефалография, математические методы, ретроспленциальная кора, биоэлектрическая активность головного мозга

Вклад авторов: С. А. Гуляев — идея проекта, реализация клинико-нейрофизиологического исследования, статистический анализ результатов; Л. М. Ханухова — организация исследования; А. А. Гармаш — общее руководство исследованием.

Соблюдение этических стандартов: исследование одобрено этическим комитетом НИЯУ МИФИ (протокол № 05/23 от 25 мая 2023 г.), проведено в соответствии с принципами биомедицинской этики, сформулированными в Хельсинкской декларации 1964 г. и ее последующими обновлениями.

✉ **Для корреспонденции:** Сергей Александрович Гуляев
Раменки, д. 31, к. 136, г. Москва, 119607, Россия; s.gulyaev73@gmail.com

Статья получена: 27.06.2023 **Статья принята к печати:** 04.09.2023 **Опубликована онлайн:** 25.09.2023

DOI: 10.47183/mes.2023.028

Human brain is one of the most difficult organs to study, which is due to the features of human anatomy, the need to comply with ethical standards, and the economic component of the use of advanced functional visualization methods: computed tomography (CT), positron emission tomography (PET), and magnetic resonance imaging (MRI). That is why the possibility of developing the research technologies that have sufficient scientific accuracy and economic accessibility and do not violate moral and ethical standards of modern society is of great interest.

Electroencephalography (EEG), developed in the beginning of the previous century, but given a new impulse with the development of mathematical data processing systems, has become one such technology [1–3].

In terms of EEG, brain activity is a combination of rhythmic phenomena reflecting the changes in the summed total of postsynaptic potentials. Alpha activity that is currently considered to be associated with the visual analyzer or visual cortex (VC) (Brodmann's areas 17, 18, 19) activity represents the most prominent and commonly recorded EEG phenomenon [4]. Occupying almost the entire occipital lobe, it produces strong occipital rhythmic activity with the frequency of 8–14 Hz that vanishes with eye opening; its association with the visual cortex shows conclusively that there are rhythmic phenomena

associated with the activity of other neural analyzers, the mu and kappa rhythms that have specific stimuli and do not respond to eye opening [5–9]. However, a number of studies [10, 11] have revealed alpha-activity heterogeneity in individuals with borderline disorders and mental deviations manifested in the form of alpha rhythm multimodality. This raises the question of possible perceptual alterations in such individuals. At the same time it has been found [12] that not the visual cortex can be the source of such heterogeneity, but rhythmic activity in the posterior areas of the cingulate cortex, the structure belonging to the retrosplenial cortex (RSC).

The study of the RSC is of interest due to its direct involvement in complex cognitive processes, such as spatial cognition, analysis and error correction for current sensory states with internal representations of the environment [13]. Occupying the posterior part of the cingulate cortex (Brodmann's areas 26, 29, 30, 23, 31) [14], this area is linked to the anterior thalamic nuclei, entorhinal and parietal cortex, subiculum and hippocampus [15, 16, 17], which determines its key role in the processes underlying spatiotemporal orientation (human self-determination and navigating in the surrounding space). Changes in the RSC activity may be the earliest signs of dementia [18], which has been confirmed by clinical trials [19–21]. Furthermore, the RSC is associated with memory and attention [22–24], as well as with knowledge of the world [24, 25]. The RSC is closely related to the visual stimuli encoding by the visual cortex [26] and to formation of personal orientation towards a specific goal [27–29]. This view is confirmed by the presence of structural links between the RSC and the prefrontal cortex, parahippocampal areas, hippocampus, anterior thalamic nuclei, and parietal cortex [30, 31]. The functional neuroimaging studies have shown that the RSC structures respond more strongly during virtual or imaginary navigating compared to other tasks [32–34]. Thus, according to current research, the RSC is a major area of the cerebral cortex that is associated with cognitive and mental functions. The RSC extensive study will make it possible to acquire new data on the features of the brain functional activity at the earliest stages of the disease development.

The study was aimed to demonstrate the possibility of assessing the RSC activity based on the analysis of the EEG alpha waves in order to determine the features associated with various relaxed wakefulness states.

METHODS

Study design

According to modern literature, the RSC is primarily an area responsible for spatial positional orientation (and possibly temporal orientation). That is why its EEG identification becomes possible during the periods when the RSC structures produce rhythmic activity in the conditions of afferent stimuli disconnected from the systems controlling body position in space, the main of which is proprioceptive system. Therefore, a matched study involving EEG recording of alpha waves became the main functional test. During the test the subject, who was in the relaxed wakefulness state, was seated in a chair (active proprioceptive system) or was lying in bed before falling asleep (a fragment of EEG recording with the same length as the first recording was extracted that showed strong occipital alpha activity before fragmentation), when his/her proprioceptive system was minimally involved. This functional test was selected based on the clinical phenomenon "falling sensation when falling asleep". Primary data were recorded with the digital electroencephalography system (Medical Computer Systems; Zelenograd, Russia). The analog-to-digital converter sampling rate was 500 Hz, and the signal filtering input parameters were 0.03–70 Hz. Electrodes were placed on the scalp according to the international 10–20 settlement system. The electrode positions were refined by performing linear measurements with subsequent adjustment of the electrode spatial arrangement standard tables. This electrode settlement system was selected due to the fact of the increasing number of the recording artifacts associated with exposure to physical and technological environmental factors in the multichannel system [35].

During the first phase of processing physical artifacts were minimized. For that the by-standing electrical devices that generated parasitic electromagnetic fields were switched off, and the interface impedance was controlled. The temperature in the room was also adjusted, and parasitic muscle movements were minimized whenever possible, which reduced the biological artifacts' intensity.

During the second phase the data pool obtained was through standardization of basic assembly to create a common electrode space, as well as to artifact removal via extraction of independent signal components. This made it possible to purify the native signal of various physiological artifacts that had not been eliminated by filtration.

During the third phase the EEG signal segmentation was performed to extract individual EEG microstates by using the procedure implemented in the sLORETA software package (v. 20210701 University of Zurich; Switzerland) involving allocating eight classes of individual microstates (conventional I–IV [36] and four extra ones (V and VIII) taking into account their variability). The final phase of the study involved solving the EEG inverse problem for each of the allocated EEG microstate classes using the EEG inverse problem solution algorithm implemented in the sLORETA software package. The results provided information about eight variants of sources of individual EEG microstates in accordance with the Brodmann area atlas (based on the atlas by the Montreal Neurological Institute (MNI)).

Patients

A total of 36 healthy volunteers of different ages, who submitted informed consent, were assessed. Among them 19 individuals were under the age of 30 years, while 17 were over the age of 30 years. The average age of the subjects was 29.1 years, (Mo — 10 years, Me — 26 years, 1st quartile —18 years, 1st quartile — 33 years). The average age of the subjects under the age of 30 years was 17.4 years (standard deviation — 1.7 years, Mo – 10 years, ME — 18 years, 1st quartile — 12.3 years, 3rd quartile — 23.3 years). The average age of thesubjects over the age of 30 years was 43.3 years (Mo — 31 years, Me — 34.5 years, 1st quartile — 31 years, 1st quartile — 55.8 years).

All the subjects were through EEG test involving assessing the background activity of the brain in the relaxed wakefulness state with the eyes closed performed when the subject was in a sitting position and the same test performed when the subject was lying down (the onset of physiological sleep was controlled), since in healthy people the RSC activity is represented by the development of the phenomenon "falling sensation when falling asleep" observed before falling asleep or when lying in bed with the eyes closed. It is associated with the sense of spatial disorientation described as flying and/or falling down before falling asleep [37]. This makes it possible to use this phenomenon as a physiological test for extraction of the RSC activity during the experiment.

Table 1. Pairwise comparison of the alpha activity frequency characteristics (Hz) in occipital and parietal areas in the relaxed wakefulness state in the sitting position (observation № 1) and in the relaxed wakefulness state when lying down before falling asleep (observation № 2) (Student's *t*-test, KS-test norm < 0.01)

Region	O1		O2		P1		P2	
Observation	1	2	1	2	1	2	1	2
M	10.3	10.3	10.3	10.3	10.3	10.1	10.3	10.1
σ	0.7	1	0.7	1	0.8	0.9	0.8	0.9
Mo	10	9.5	10	9	10	9.5	10	9.5
Me	10.2	10.4	10.2	10.3	10.2	9.8	10.2	9.8
p t-Student	1		0.8		0.2		0.1	

Inclusion criteria: no history of acute nervous system disorder; no exacerbation of chronic disorder; no history of severe traumatic brain injury, mental disorder, epilepsy.

Clinical assessment was performed in the La Salute Clinic in accordance with the cooperation agreement between the La Salute Clinic and the National Research Nuclear University MEPhI (№ 09-01/23 of 09 January 2023).

Statistical analysis

The results obtained were processed in accordance with the guidelines [38] using PSPP (GNU software ver. 1.6.2-g78a33a) for OC Linux Mate (v. 10.10, GNU-GPL licence). Calculation involved pairwise comparison of the EEG inverse problem solution results obtained for eight EEG microstates using the Kolmogorov-Smirnov test (KS-test) for normality; calculation of Student's *t*-test for samples with normal distribution and Wilcoxon signed-rank test for related samples with non-normal distribution. The same degree of freedom was used, the significance level was set as $\alpha < 0.05$.

RESULTS

The analysis of occipital and parietal alpha activity performed in the general group revealed the decrease in alpha activity frequency before falling asleep, but there were no significant differences in the values of the general group (Table 1) and individuals under the age of 30 years (Table 2). In contrast, in the group of subjects over the age of 30 years the decrease in alpha activity frequency observed before falling asleep was significant (Table 3).

When studying individual EEG microstates in the alpha range, heterogeneity of the alpha activity sources associated with the changes in the subject's state was revealed in the general group (Table 4). Thus, in the sitting position the rhythmic phenomena were generated mainly by Brodmann's areas 17, 18, and 19, which represented the expected alpha activity produced by the visual cortex structures functioning in the "idle" mode. Persistence of these indicators when lying down (without the emergence of significant differences) also suggested the visual cortex response to eye closing, however, when lying down, the recorded alpha activity source shifted to the Brodmann's areas 23, 29, 30, and 31 characterizing the RSC structures.

Assessment of the age-related features of this response showed that individuals under the age of 30 years demonstrated significant differences in alpha rhythm production, since when sitting in the relaxed wakefulness state, alpha activity was produced by the VC structures (Brodmann's areas 17, 18, and 19), while prior to falling asleep the RSC became the source of alpha activity (Brodmann's areas 23, 29, 30, and 31). A reliable RSC response was observed in individuals over the age of 30 years, while the VC structures showed no significant differences before falling asleep (Table 5).

DISCUSSION

The findings have shown that even the assessment of the brain rhythm frequency characteristics makes it possible to determine that alpha rhythm recorded during conventional EEG tests is not a stable parameter determining the "basic" characteristics of brain activity in humans. Alpha activity represents the group of rhythmic phenomena showing significant differences in individuals over the age of 30 years having fully developed brain structures.

However, the shift of alpha activity source between the visual cortex and retrosplenial cortex (clinically manifesting in the phenomenon "falling sensation when falling asleep") is clear in individuals under the age of 30 years that can be considered as involvement of the larger number of brain structures in implementation of higher nervous functions and the need for integration of their activity.

At the same time, after 30 years the neural centers are likely to acquire marked specialization, especially the brain's parietal and RSC structures. Specialization manifests itself in the changes of parietal alpha rhythm and the recording of rhythmic

Table 2. Pairwise comparison of the alpha activity frequency characteristics (Hz) in occipital and parietal areas in the relaxed wakefulness state in the sitting position (observation № 1) and in the relaxed wakefulness state when lying down before falling asleep (observation № 2) in individuals under the age of 30 years (Student's *t*-test, KS-test norm < 0.01)

Region	O1		O2		P1		P2	
Observation	1	2	1	2	1	2	1	2
M	10.3	10.7	10.3	10.6	10.2	10.3	10.2	10.3
σ	1	1.4	1	1.4	1.2	1.3	1.2	1.3
Mo	9.6	10.5	9.6	10.5	8.2	9.5	8.2	9.5
Me	10	10.6	10	10.6	10	10.5	10	10.5
p t-Student	0.357		0.525		0.789		0.857	

Table 3. Pairwise comparison of the alpha activity frequency characteristics (Hz) in occipital and parietal areas in the relaxed wakefulness state in the sitting position (observation № 1) and in the relaxed wakefulness state when lying down before falling asleep (observation № 2) in individuals over the age of 30 years (Student's *t*-test, KS-test norm < 0,01)

Region	O1		O2		P1		P2	
Observation	1	2	1	2	1	2	1	2
M	10.3	9.8	10.3	9.8	10.5	9.8	10.5	9.8
σ	0.8	0.9	0.8	0.9	0.8	0.9	0.8	0.9
Mo	10.2	9	10.2	9	10.5	9	10.2	9
Me	10.2	9.6	10.2	9.6	10.4	9.6	10.4	9.6
p t-Student	0.07		0.1		0.02		0.02	

Table 4. The data on the rate of EEG activity recording (%) over certain Brodmann fields acquired by solving the EEG inverse problem for the model of eight individual EEG microstates in the general group (Wilcoxon signed-rank test, KS-test norm > 0.5)

Subject's position	Brodmann areas 23, 29, 30, 31	Brodmann areas 17, 18, 19
Sitting	18.3%	34.2%
Lying down	41.7%	25.0%
p (*t*-Wilcoxon)	0.01	0.4

Table 5. Age-related features of the rate of EEG activity recording (%)over certain Brodmann fields acquired by solving the EEG inverse problem for the model of eight individual EEG microstates in various age groups (Wilcoxon signed-rank test, KS-test norm > 0.5)

RSC (Brodmann areas 23, 29, 30, 31)		
Age	1–30 years	> 30 years
Sitting	7.4%	12.5%
Lying down	28.7%	19.8%
p (*t*-Wilcoxon)	0	0.05
VC (Brodmann areas 17, 18,19)		
Sitting	20.1%	15.6%
Lying down	27.1%	23%
p (*t*-Wilcoxon)	0.03	0.5

activity produced by the RSC structures; according to our observations, these can be considered as related phenomena.

The use of advanced mathematical methods for EEG signal analysis enables clear differentiation of alpha activity and determining the sources in various brain structures [39]. Under the conditions of targeted functional load this makes it possible to link repetitive EEG recording fragments to the activity of certain neural networks of the brain [40, 41] involved in production of alpha activity not only by the cerebral visual cortex structures [42–49]. Such observations can be considered as formation of stable links and growing significance of visual cortex as the main source of information in individuals over the age of 30 years, including information about the position of the body in space, as previously reported for other cortical areas [50–52].

Thus, alpha activity identified when performing conventional EEG tests is not the common "basic" rhythm typical for brain structures, but the combination of several rhythms with similar frequency and amplitude characteristics. The above bioelectric activity is produced by various brain structures, particularly the RSC, which is confirmed by conclusions of several studies [5–9] suggesting the alpha rhythm cortical origin. This makes it possible to re-interpret the findings of the studies [53] showing heterogeneity of alpha rhythm spectra in individuals with various mental deviations, as well as the results of earlier studies [54], especially that focused on the multimodal alpha rhythm variants.

CONCLUSIONS

The use of the brain bioelectric activity frequency analysis within the framework of conventional technology is not an effective method for assessment of higher nervous functions. Modern EEG tests require using the combination of mathematical methods for extraction of individual EEG microstates and EEG inverse problem solution, thereby making it possible to obtain a simple and cost-effective tool for assessment of the brain structures' functional activity. The use of such technology will allow us to expand the scope of the research focused on assessing the brain functional activity in both research and clinical centers, thereby paving the way for understanding the features of the brain structures' activity in physiologically normal conditions and in individuals with mental disorders.

References

1. Delorme A, Makeig S. EEGLAB: an open source toolbox for analysis of single-trial EEG dynamics including independent component analysis. J Neurosci Methods. 2004; 134 (1): 9–21. Available from: https://doi.org/10.1016/j.jneumeth.2003.10.009.

PMID: 15102499.
2. Martínez-Cancino R, Delorme A, Truong D, Artoni F, Kreutz-Delgado K, Sivagnanam S, et al. The open EEGLAB portal Interface: High-Performance computing with EEGLAB. Neuroimage. 2021; 224: 116778. Available from: https://doi.org/10.1016/j.neuroimage.2020.116778. Epub 2020 Apr 11. PMID: 32289453; PMCID: PMC8341158.
3. Tadel F, Bock E, Niso G, Mosher JC, Cousineau M, Pantazis D, et al. MEG/EEG Group Analysis With Brainstorm. Front Neurosci. 2019; 13: 76. Available from: https://doi.org/10.3389/fnins.2019.00076. PMID: 30804744; PMCID: PMC6378958.
4. Jasper H, Penfield W. Electrocorticograms in man: effect of voluntary movement upon the electrical activity of the precentral gyrus. Archiv für Psychiatrie und Nervenkrankheiten. 1949; 183: 163–74.
5. Lopes Da Silva FH, Storm Van Leeuwen W. The cortical source of the alpha rhythm. Neurosci Lett. 1977; 6 (2-3): 237–41. Available from: https://www.doi.org/10.1016/0304-3940(77)90024-6.
6. Klimesch W. α-Band oscillations, attention, and controlled access to stored information. Trends Cogn Sci. 2012; 16 (12): 606–17. Available from: https://www.doi.org/10.1016/j.tics.2012.10.007.
7. Klimesch W. EEG alpha and theta oscillations reflect cognitive and memory performance: a review and analysis. Brain Res Brain Res Rev. 1999; 29 (2-3): 169–95. Available from: https://www.doi.org/10.1016/s0165-0173(98)00056-3.
8. Klimesch W, Sauseng P, Hanslmayr S. EEG alpha oscillations: the inhibition-timing hypothesis. Brain Res Rev. 2007; 53 (1): 63–88. Available from: https://www.doi.org/10.1016/j.brainresrev.2006.06.003.
9. Klimesch W, Doppelmayr M, Hanslmayr S. Upper alpha ERD and absolute power: their meaning for memory performance. Prog Brain Res. 2006; 159: 151–65. Available from: https://www.doi.org/10.1016/S0079-6123(06)59010-7.
10. Ivanov LB. Spektr moshhnosti ehlektroehncefalogrammy: oshibki i praktika primeneniya (lekciya pervaya). Medicinskij alfavit. 2021; (39): 45–52. Dostupno po ssylke: https://doi.org/10.33667/2078-5631-2021-39-45-52. Russian.
11. Lydon EA, Nguyen LT, Shende SA, Chiang HS, Spence JS, Mudar RA. EEG theta and alpha oscillations in early versus late mild cognitive impairment during a semantic Go/NoGo task. Behav Brain Res. 2022; 416: 113539. DOI: 10.1016/j.bbr.2021.113539. Epub 2021 Aug 17. PMID: 34416304.
12. Rusiniak M, Lewandowska M, Wolak T, Pluta A, Milner R, Skarżyński H. Mozliwości i problemy jednoczesnych rejestracji EEG-fMRI--badanie rytmu alfa [The possibilities and limitations of simultaneous EEG-fMRI registration--the alpha rhythm study]. Przegl Lek. 2015; 72 (11): 616–9. PMID: 27012118. Polish.
13. Alexander AS, Place R, Starrett MJ, Chrastil ER, Nitz DA. Rethinking retrosplenial cortex: Perspectives and predictions. Neuron. 2023; 111 (2): 150–75. Available from: https://doi.org/10.1016/j.neuron.2022.11.006. Epub 2022 Dec 1. PMID: 36460006.
14. Todd TP, Fournier DI, Bucci DJ. Retrosplenial cortex and its role in cue-specific learning and memory. Neurosci Biobehav Rev. 2019; 107: 713–28. Available from: https://doi.org/10.1016/j.neubiorev.2019.04.016. Epub 2019 May 2. PMID: 31055014; PMCID: PMC6906080.
15. Trask S, Fournier DI. Examining a role for the retrosplenial cortex in age-related memory impairment. Neurobiol Learn Mem. 2022; 189: 107601. DOI: 10.1016/j.nlm.2022.107601. Epub 2022 Feb 22. PMID: 35202816.
16. Olsen GM, Ohara S, Iijima T, Witter MP. Parahippocampal and retrosplenial connections of rat posterior parietal cortex. Hippocampus. 2017; 27 (4): 335–58. Available from: https://doi.org/10.1002/hipo.22701. Epub 2017 Jan 16. PMID: 28032674.
17. Sugar J, Witter MP, van Strien NM, Cappaert NL. The retrosplenial cortex: intrinsic connectivity and connections with the (para) hippocampal region in the rat. An interactive connectome. Front Neuroinform. 2011; 5: 7. Available from: https://doi.org/10.3389/fninf.2011.00007. PMID: 21847380; PMCID: PMC3147162.
18. Dillen KNH, Jacobs HIL, Kukolja J, von Reutern B, Richter N, Onur ÖA, Dronse J, Langen KJ, Fink GR. Aberrant functional connectivity differentiates retrosplenial cortex from posterior cingulate cortex in prodromal Alzheimer's disease. Neurobiol Aging. 2016; 44: 114–26. Available from: https://doi.org/10.1016/j.neurobiolaging.2016.04.010. Epub 2016 Apr 22. PMID: 27318139.
19. Squire LR, Genzel L, Wixted JT, Morris RG. Memory consolidation. Cold Spring Harb Perspect Biol. 2015; 7 (8): a021766. Available from: https://doi.org/10.1101/cshperspect.a021766. PMID: 26238360; PMCID: PMC4526749.
20. de Sousa AF, Cowansage KK, Zutshi I, Cardozo LM, Yoo EJ, Leutgeb S, Mayford M. Optogenetic reactivation of memory ensembles in the retrosplenial cortex induces systems consolidation. Proc Natl Acad Sci U S A. 2019; 116 (17): 8576–81. Available from: https://doi.org/10.1073/pnas.1818432116. Epub 2019 Mar 15. PMID: 30877252; PMCID: PMC6486739
21. Auger SD, Maguire EA. Retrosplenial Cortex Indexes Stability beyond the Spatial Domain. J Neurosci. 2018; 38 (6): 1472–81. Available from: https://doi.org/10.1523/JNEUROSCI.2602-17.2017. Epub 2018 Jan 8. PMID: 29311139; PMCID: PMC5815348.
22. Mitchell AS, Czajkowski R, Zhang N, Jeffery K, Nelson AJD. Retrosplenial cortex and its role in spatial cognition. Brain Neurosci Adv. 2018; 2: 2398212818757098. Available from: https://doi.org/10.1177/2398212818757098. PMID: 30221204; PMCID: PMC6095108.
23. Corcoran KA, Yamawaki N, Leaderbrand K, Radulovic J. Role of retrosplenial cortex in processing stress-related context memories. Behav Neurosci. 2018; 132 (5): 388–95. Available from: https://doi.org/10.1037/bne0000223. Epub 2018 Jun. 7. PMID: 29878804; PMCID: PMC6188831.
24. Milczarek MM, Vann SD. The retrosplenial cortex and long-term spatial memory: from the cell to the network. Curr Opin Behav Sci. 2020; 32: 50–56. Available from: https://doi.org/10.1016/j.cobeha.2020.01.014. PMID: 32715030; PMCID: PMC7374566.
25. Mitchell AS, Czajkowski R, Zhang N, Jeffery K, Nelson AJD. Retrosplenial cortex and its role in spatial cognition. Brain Neurosci Adv. 2018; 2: 2398212818757098. Available from: https://doi.org/10.1177/2398212818757098. PMID: 30221204; PMCID: PMC6095108.
26. Powell A, Connelly WM, Vasalauskaite A, Nelson AJD, Vann SD, Aggleton JP, et al. Stable Encoding of Visual Cues in the Mouse Retrosplenial Cortex. Cereb Cortex. 2020; 30 (8): 4424–37. Available from: https://doi.org/10.1093/cercor/bhaa030. PMID: 32147692; PMCID: PMC7438634.
27. Fischer LF, Mojica Soto-Albors R, Buck F, Harnett MT. Representation of visual landmarks in retrosplenial cortex. Elife. 2020; 9: e51458. Available from: https://doi.org/10.7554/eLife.51458. PMID: 32154781; PMCID: PMC7064342.
28. Fournier DI, Monasch RR, Bucci DJ, Todd TP. Retrosplenial cortex damage impairs unimodal sensory preconditioning. Behav Neurosci. 2020; 134 (3): 198–207. DOI: 10.1037/bne0000365. Epub 2020 Mar 9. PMID: 32150422; PMCID: PMC7244381.
29. Mao D, Molina LA, Bonin V, McNaughton BL. Vision and Locomotion Combine to Drive Path Integration Sequences in Mouse Retrosplenial Cortex. Curr Biol. 2020; 30 (9): 1680–8.e4. Available from: https://doi.org/10.1016/j.cub.2020.02.070. Epub 2020 Mar 19. PMID: 32197086.
30. Morris R, Pandya DN, Petrides M. Fiber system linking the mid-dorsolateral frontal cortex with the retrosplenial/presubicular region in the rhesus monkey. J Comp Neurol. 1999; 407 (2): 183–92. Available from: https://doi.org/10.1002/(sici)1096-9861(19990503)407:2<183::aid-cne3>3.0.co;2-n. PMID: 10213090.
31. Clark BJ, Simmons CM, Berkowitz LE, Wilber AA. The retrosplenial-parietal network and reference frame coordination for spatial navigation. Behav Neurosci. 2018; 132 (5): 416–29. Available from: https://doi.org/10.1037/bne0000260. Epub 2018 Aug 9. PMID: 30091619; PMCID: PMC6188841.
32. Aggleton JP, Yanakieva S, Sengpiel F, Nelson AJ. The separate and combined properties of the granular (area 29) and dysgranular (area 30) retrosplenial cortex. Neurobiol Learn Mem. 2021; 185: 107516. DOI: 10.1016/j.nlm.2021.107516. Epub 2021 Sep 3. PMID: 34481970.
33. Epstein RA, Parker WE, Feiler AM. Where am I now? Distinct roles for parahippocampal and retrosplenial cortices in place

recognition. J Neurosci. 2007; 27 (23): 6141–9. Available from: https://doi.org/10.1523/JNEUROSCI.0799-07.2007. PMID: 17553986; PMCID: PMC6672165.
34. Spiers HJ, Maguire EA. Thoughts, behavior, and brain dynamics during navigation in the real world. Neuroimage. 2006; 31 (4): 1826–40. Available from: https://doi.org/10.1016/j.neuroimage.2006.01.037. Epub 2006 Apr 11. PMID: 16584892.
35. Tamburro G, Fiedler P, Stone D, Haueisen J, Comani S. A new ICA-based fingerprint method for the automatic removal of physiological artifacts from EEG recordings. PeerJ. 2018; 6: e4380. DOI: 10.7717/peerj.4380. PMID: 29492336; PMCID: PMC5826009.
36. Lehmann D, Strik WK, Henggeler B, Koenig T, Koukkou M Brain electric microstates and momentary conscious mind states as building blocks of spontaneous thinking: I. Visual imagery and abstract thoughts. Int J Psychophysiol. 1998; 29 (1): 1–11. Available from: https://doi.org/10.1016/s0167-8760(97)00098-6.
37. Schacter DL, Crovitz HF. "Falling" while falling asleep: sex differences. Percept Mot Skills. 1977; 44 (2): 656. DOI: 10.2466/pms.1977.44.2.656. PMID: 866074.
38. Sarter M Fritschy JM Reporting statistical methods and statistical results in EJN. Eur J Neurosci. 2008; 28 (12): 2363–4. Available from: https://doi.org/10.1111/j.1460-9568.2008.06581.x.
39. Ivanov LB. Spektr moshhnosti po ehlektroehncefalogramme: oshibki i praktika primeneniya (lekciya vtoraya). Dispersionnyj analiz ehlektroehncefalogrammy po Rosmanu. Medicinskij alfavit. 2022; (9): 38–43. Available from: https://doi.org/10.33667/2078-5631-2022-9-38-43. Russian.
40. Croce P, Quercia A, Costa S, Zappasodi F. EEG microstates associated with intra- and inter-subject alpha variability. Sci Rep. 2020; 10 (1): 2469. Available from: https://doi.org/ 10.1038/s41598-020-58787-w.
41. Poskanzer C, Denis D, Herrick A, Stickgold R. Using EEG microstates to examine post-encoding quiet rest and subsequent word-pair memory. Neurobiol Learn Mem. 2021; 181: 107424. Available from: https://doi.org/ 10.1016/j.nlm.2021.107424.
42. Pascual-Marqui RD, Michel CM, Lehmann D. Segmentation of brain electrical activity into microstates: model estimation and validation. IEEE Trans Biomed Eng. 1995; 42 (7): 658–65. Available from: https://doi.org/10.1109/10.391164.
43. Milz P, Pascual-Marqui RD, Lehmann D, Faber PL. Modalities of Thinking: State and Trait Effects on Cross-Frequency Functional Independent Brain Networks. Brain Topogr. 2016; 29 (3): 477–90. Available from: https://doi.org/ 10.1007/s10548-016-0469-3.
44. Seitzman BA, Abell M, Bartley SC, Erickson MA, Bolbecker AR, Hetrick WP. Cognitive manipulation of brain electric microstates. Neuroimage. 2017; 146: 533–43. Available from: https://doi.org/10.1016/j.neuroimage.2016.10.002.
45. Mishra A, Englitz B, Cohen MX. EEG microstates as a continuous phenomenon. Neuroimage. 2020; 208: 116454. Available from: https://doi.org/ 10.1016/j.neuroimage.2019.116454. Epub 2019 Dec 10.
46. Milz P, Faber PL, Lehmann D, Koenig T, Kochi K, Pascual-Marqui RD. The functional significance of EEG microstates--Associations with modalities of thinking. Neuroimage. 2016; 125: 643–56. Available from: https://doi.org/ 10.1016/j.neuroimage.2015.08.023.
47. Pascual-Marqui RD, Esslen M, Kochi K, Lehmann D. Functional imaging with low-resolution brain electromagnetic tomography (LORETA): a review. Methods Find Exp Clin Pharmacol. 2002; 24 Suppl C: 91–5. PMID: 12575492.
48. Grech R, Cassar T, Muscat J, Camilleri KP, Fabri SG, Zervakis M, et al. Review on solving the inverse problem in EEG source analysis. J Neuroeng Rehabil. 2008; 5: 25. Available from: https://doi.org/ 10.1186/1743-0003-5-25.
49. Neuner I, Arrubla J, Werner CJ, Hitz K, Boers F, Kawohl W, et al. The default mode network and EEG regional spectral power: a simultaneous fMRI-EEG study. PLoS One. 2014; 9 (2): e88214. Available from: https://doi.org/ 10.1371/journal.pone.0088214
50. Vukovic N, Hansen B, Lund TE, Jespersen S, Shtyrov Y. Rapid microstructural plasticity in the cortical semantic network following a short language learning session. PLoS Biol. 2021; 19 (6): e3001290. Available from: https://doi.org/10.1371/journal.pbio.3001290. PMID: 34125828; PMCID: PMC8202930.
51. Hubert V, Beaunieux H, Chételat G, Platel H, Landeau B, Viader F, Desgranges B, Eustache F. Age-related changes in the cerebral substrates of cognitive procedural learning. Hum Brain Mapp. 2009; 30 (4): 1374–86. Available from: https://doi.org/10.1002/hbm.20605. PMID: 18537110; PMCID: PMC2935916.
52. Just MA, Keller TA. Converging measures of neural change at the microstructural, informational, and cortical network levels in the hippocampus during the learning of the structure of organic compounds. Brain Struct Funct. 2019; 224 (3): 1345–57. Available from: https://doi.org/10.1007/s00429-019-01838-4. Epub 2019 Feb 6. PMID: 30725233.
53. Nunez PL, Wingeier BM, Silberstein RB. Spatial-temporal structures of human alpha rhythms: theory, microcurrent sources, multiscale measurements, and global binding of local networks. Hum Brain Mapp. 2001; 13 (3): 125–64. Available from: https://doi.org/10.1002/hbm.1030. PMID: 11376500; PMCID: PMC6872048.
54. Rodriguez-Larios J, ElShafei A, Wiehe M, Haegens S. Visual working memory recruits two functionally distinct alpha rhythms in posterior cortex. eNeuro. 2022; 9 (5): ENEURO.0159-22.2022. DOI: 10.1523/ENEURO.0159-22.2022. Epub ahead of print. PMID: 36171059; PMCID: PMC9536853.

Литература

1. Delorme A, Makeig S. EEGLAB: an open source toolbox for analysis of single-trial EEG dynamics including independent component analysis. J Neurosci Methods. 2004; 134 (1): 9–21. Available from: https://doi.org/10.1016/j.jneumeth.2003.10.009. PMID: 15102499.
2. Martínez-Cancino R, Delorme A, Truong D, Artoni F, Kreutz-Delgado K, Sivagnanam S, et al. The open EEGLAB portal Interface: High-Performance computing with EEGLAB. Neuroimage. 2021; 224: 116778. Available from: https://doi.org/10.1016/j.neuroimage.2020.116778. Epub 2020 Apr 11. PMID: 32289453; PMCID: PMC8341158.
3. Tadel F, Bock E, Niso G, Mosher JC, Cousineau M, Pantazis D, et al. MEG/EEG Group Analysis With Brainstorm. Front Neurosci. 2019; 13: 76. Available from: https://doi.org/10.3389/fnins.2019.00076. PMID: 30804744; PMCID: PMC6378958.
4. Jasper H, Penfield W. Electrocorticograms in man: effect of voluntary movement upon the electrical activity of the precentral gyrus. Archiv für Psychiatrie und Nervenkrankheiten. 1949; 183: 163–74.
5. Lopes Da Silva FH, Storm Van Leeuwen W. The cortical source of the alpha rhythm. Neurosci Lett. 1977; 6 (2-3): 237–41. Available from: https://www.doi.org/10.1016/0304-3940(77)90024-6.
6. Klimesch W. α-Band oscillations, attention, and controlled access to stored information. Trends Cogn Sci. 2012; 16 (12): 606–17. Available from: https://www.doi.org/10.1016/j.tics.2012.10.007.
7. Klimesch W. EEG alpha and theta oscillations reflect cognitive and memory performance: a review and analysis. Brain Res Brain Res Rev. 1999; 29 (2-3): 169–95. Available from: https://www.doi.org/10.1016/s0165-0173(98)00056-3.
8. Klimesch W, Sauseng P, Hanslmayr S. EEG alpha oscillations: the inhibition-timing hypothesis. Brain Res Rev. 2007; 53 (1): 63–88. Available from: https://www.doi.org/10.1016/j.brainresrev.2006.06.003.
9. Klimesch W, Doppelmayr M, Hanslmayr S. Upper alpha ERD and absolute power: their meaning for memory performance. Prog Brain Res. 2006; 159: 151–65. Available from: https://www.doi.org/10.1016/S0079-6123(06)59010-7.
10. Иванов Л. Б. Спектр мощности электроэнцефалограммы: ошибки и практика применения (лекция первая). Медицинский алфавит. 2021; (39): 45–52. Доступно по ссылке: https://doi.org/10.33667/2078-5631-2021-39-45-52.
11. Lydon EA, Nguyen LT, Shende SA, Chiang HS, Spence JS, Mudar RA.

EEG theta and alpha oscillations in early versus late mild cognitive impairment during a semantic Go/NoGo task. Behav Brain Res. 2022; 416: 113539. DOI: 10.1016/j.bbr.2021.113539. Epub 2021 Aug 17. PMID: 34416304.
12. Rusiniak M, Lewandowska M, Wolak T, Pluta A, Milner R, Skarżyński H. Mozliwości i problemy jednoczesnych rejestracji EEG-fMRI--badanie rytmu alfa [The possibilities and limitations of simultaneous EEG-fMRI registration--the alpha rhythm study]. Przegl Lek. 2015; 72 (11): 616–9. PMID: 27012118. Polish.
13. Alexander AS, Place R, Starrett MJ, Chrastil ER, Nitz DA. Rethinking retrosplenial cortex: Perspectives and predictions. Neuron. 2023; 111 (2): 150–75. Available from: https://doi.org/10.1016/j.neuron.2022.11.006. Epub 2022 Dec 1. PMID: 36460006.
14. Todd TP, Fournier DI, Bucci DJ. Retrosplenial cortex and its role in cue-specific learning and memory. Neurosci Biobehav Rev. 2019; 107: 713–28. Available from: https://doi.org/10.1016/j.neubiorev.2019.04.016. Epub 2019 May 2. PMID: 31055014; PMCID: PMC6906080.
15. Trask S, Fournier DI. Examining a role for the retrosplenial cortex in age-related memory impairment. Neurobiol Learn Mem. 2022; 189: 107601. DOI: 10.1016/j.nlm.2022.107601. Epub 2022 Feb 22. PMID: 35202816.
16. Olsen GM, Ohara S, Iijima T, Witter MP. Parahippocampal and retrosplenial connections of rat posterior parietal cortex. Hippocampus. 2017; 27 (4): 335–58. Available from: https://doi.org/10.1002/hipo.22701. Epub 2017 Jan 16. PMID: 28032674.
17. Sugar J, Witter MP, van Strien NM, Cappaert NL. The retrosplenial cortex: intrinsic connectivity and connections with the (para) hippocampal region in the rat. An interactive connectome. Front Neuroinform. 2011; 5: 7. Available from: https://doi.org/10.3389/fninf.2011.00007. PMID: 21847380; PMCID: PMC3147162.
18. Dillen KNH, Jacobs HIL, Kukolja J, von Reutern B, Richter N, Onur ÖA, Dronse J, Langen KJ, Fink GR. Aberrant functional connectivity differentiates retrosplenial cortex from posterior cingulate cortex in prodromal Alzheimer's disease. Neurobiol Aging. 2016; 44: 114–26. Available from: https://doi.org/10.1016/j.neurobiolaging.2016.04.010. Epub 2016 Apr 22. PMID: 27318139.
19. Squire LR, Genzel L, Wixted JT, Morris RG. Memory consolidation. Cold Spring Harb Perspect Biol. 2015; 7 (8): a021766. Available from: https://doi.org/10.1101/cshperspect.a021766. PMID: 26238360; PMCID: PMC4526749.
20. de Sousa AF, Cowansage KK, Zutshi I, Cardozo LM, Yoo EJ, Leutgeb S, Mayford M. Optogenetic reactivation of memory ensembles in the retrosplenial cortex induces systems consolidation. Proc Natl Acad Sci U S A. 2019; 116 (17): 8576–81. Available from: https://doi.org/10.1073/pnas.1818432116. Epub 2019 Mar 15. PMID: 30877252; PMCID: PMC6486739
21. Auger SD, Maguire EA. Retrosplenial Cortex Indexes Stability beyond the Spatial Domain. J Neurosci. 2018; 38 (6): 1472–81. Available from: https://doi.org/10.1523/JNEUROSCI.2602-17.2017. Epub 2018 Jan 8. PMID: 29311139; PMCID: PMC5815348.
22. Mitchell AS, Czajkowski R, Zhang N, Jeffery K, Nelson AJD. Retrosplenial cortex and its role in spatial cognition. Brain Neurosci Adv. 2018; 2: 2398212818757098. Available from: https://doi.org/10.1177/2398212818757098. PMID: 30221204; PMCID: PMC6095108.
23. Corcoran KA, Yamawaki N, Leaderbrand K, Radulovic J. Role of retrosplenial cortex in processing stress-related context memories. Behav Neurosci. 2018; 132 (5): 388–95. Available from: https://doi.org/10.1037/bne0000223. Epub 2018 Jun. 7. PMID: 29878804; PMCID: PMC6188831.
24. Milczarek MM, Vann SD. The retrosplenial cortex and long-term spatial memory: from the cell to the network. Curr Opin Behav Sci. 2020; 32: 50–56. Available from: https://doi.org/10.1016/j.cobeha.2020.01.014. PMID: 32715030; PMCID: PMC7374566.
25. Mitchell AS, Czajkowski R, Zhang N, Jeffery K, Nelson AJD. Retrosplenial cortex and its role in spatial cognition. Brain Neurosci Adv. 2018; 2: 2398212818757098. Available from: https://doi.org/10.1177/2398212818757098. PMID: 30221204; PMCID: PMC6095108.
26. Powell A, Connelly WM, Vasalauskaite A, Nelson AJD, Vann SD, Aggleton JP, et al. Stable Encoding of Visual Cues in the Mouse Retrosplenial Cortex. Cereb Cortex. 2020; 30 (8): 4424–37. Available from: https://doi.org/10.1093/cercor/bhaa030. PMID: 32147692; PMCID: PMC7438634.
27. Fischer LF, Mojica Soto-Albors R, Buck F, Harnett MT. Representation of visual landmarks in retrosplenial cortex. Elife. 2020; 9: e51458. Available from: https://doi.org/10.7554/eLife.51458. PMID: 32154781; PMCID: PMC7064342.
28. Fournier DI, Monasch RR, Bucci DJ, Todd TP. Retrosplenial cortex damage impairs unimodal sensory preconditioning. Behav Neurosci. 2020; 134 (3): 198–207. DOI: 10.1037/bne0000365. Epub 2020 Mar 9. PMID: 32150422; PMCID: PMC7244381.
29. Mao D, Molina LA, Bonin V, McNaughton BL. Vision and Locomotion Combine to Drive Path Integration Sequences in Mouse Retrosplenial Cortex. Curr Biol. 2020; 30 (9): 1680–8.e4. Available from: https://doi.org/10.1016/j.cub.2020.02.070. Epub 2020 Mar 19. PMID: 32197086.
30. Morris R, Pandya DN, Petrides M. Fiber system linking the mid-dorsolateral frontal cortex with the retrosplenial/presubicular region in the rhesus monkey. J Comp Neurol. 1999; 407 (2): 183–92. Available from: https://doi.org/10.1002/(sici)1096-9861(19990503)407:2<183::aid-cne3>3.0.co;2-n. PMID: 10213090.
31. Clark BJ, Simmons CM, Berkowitz LE, Wilber AA. The retrosplenial-parietal network and reference frame coordination for spatial navigation. Behav Neurosci. 2018; 132 (5): 416–29. Available from: https://doi.org/10.1037/bne0000260. Epub 2018 Aug 9. PMID: 30091619; PMCID: PMC6188841.
32. Aggleton JP, Yanakieva S, Sengpiel F, Nelson AJ. The separate and combined properties of the granular (area 29) and dysgranular (area 30) retrosplenial cortex. Neurobiol Learn Mem. 2021; 185: 107516. DOI: 10.1016/j.nlm.2021.107516. Epub 2021 Sep 3. PMID: 34481970.
33. Epstein RA, Parker WE, Feiler AM. Where am I now? Distinct roles for parahippocampal and retrosplenial cortices in place recognition. J Neurosci. 2007; 27 (23): 6141–9. Available from: https://doi.org/10.1523/JNEUROSCI.0799-07.2007. PMID: 17553986; PMCID: PMC6672165.
34. Spiers HJ, Maguire EA. Thoughts, behavior, and brain dynamics during navigation in the real world. Neuroimage. 2006; 31 (4): 1826–40. Available from: https://doi.org/10.1016/j.neuroimage.2006.01.037. Epub 2006 Apr 11. PMID: 16584892.
35. Tamburro G, Fiedler P, Stone D, Haueisen J, Comani S. A new ICA-based fingerprint method for the automatic removal of physiological artifacts from EEG recordings. PeerJ. 2018; 6: e4380. DOI: 10.7717/peerj.4380. PMID: 29492336; PMCID: PMC5826009.
36. Lehmann D, Strik WK, Henggeler B, Koenig T, Koukkou M Brain electric microstates and momentary conscious mind states as building blocks of spontaneous thinking: I. Visual imagery and abstract thoughts. Int J Psychophysiol. 1998; 29 (1): 1–11. Available from: https://doi.org/10.1016/s0167-8760(97)00098-6.
37. Schacter DL, Crovitz HF. "Falling" while falling asleep: sex differences. Percept Mot Skills. 1977; 44 (2): 656. DOI: 10.2466/pms.1977.44.2.656. PMID: 866074.
38. Sarter M Fritschy JM Reporting statistical methods and statistical results in EJN. Eur J Neurosci. 2008; 28 (12): 2363–4. Available from: https://doi.org/10.1111/j.1460-9568.2008.06581.x.
39. Иванов Л. Б. Спектр мощности по электроэнцефалограмме: ошибки и практика применения (лекция вторая). Дисперсионный анализ электроэнцефалограммы по Росману. Медицинский алфавит. 2022; (9): 38–43. Available from: https://doi.org/10.33667/2078-5631-2022-9-38-43.
40. Croce P, Quercia A, Costa S, Zappasodi F. EEG microstates associated with intra- and inter-subject alpha variability. Sci Rep. 2020; 10 (1): 2469. Available from: https://doi.org/ 10.1038/s41598-020-58787-w.
41. Poskanzer C, Denis D, Herrick A, Stickgold R. Using EEG microstates to examine post-encoding quiet rest and subsequent word-pair memory. Neurobiol Learn Mem. 2021; 181: 107424. Available from: https://doi.org/ 10.1016/j.nlm.2021.107424.
42. Pascual-Marqui RD, Michel CM, Lehmann D. Segmentation of brain electrical activity into microstates: model estimation and validation. IEEE Trans Biomed Eng. 1995; 42 (7): 658–65.

Available from: https://doi.org/10.1109/10.391164.
43. Milz P, Pascual-Marqui RD, Lehmann D, Faber PL. Modalities of Thinking: State and Trait Effects on Cross-Frequency Functional Independent Brain Networks. Brain Topogr. 2016; 29 (3): 477–90. Available from: https://doi.org/ 10.1007/s10548-016-0469-3.
44. Seitzman BA, Abell M, Bartley SC, Erickson MA, Bolbecker AR, Hetrick WP. Cognitive manipulation of brain electric microstates. Neuroimage. 2017; 146: 533–43. Available from: https://doi.org/ 10.1016/j.neuroimage.2016.10.002.
45. Mishra A, Englitz B, Cohen MX. EEG microstates as a continuous phenomenon. Neuroimage. 2020; 208: 116454. Available from: https://doi.org/ 10.1016/j.neuroimage.2019.116454. Epub 2019 Dec 10.
46. Milz P, Faber PL, Lehmann D, Koenig T, Kochi K, Pascual-Marqui RD. The functional significance of EEG microstates--Associations with modalities of thinking. Neuroimage. 2016; 125: 643–56. Available from: https://doi.org/ 10.1016/j.neuroimage.2015.08.023.
47. Pascual-Marqui RD, Esslen M, Kochi K, Lehmann D. Functional imaging with low-resolution brain electromagnetic tomography (LORETA): a review. Methods Find Exp Clin Pharmacol. 2002; 24 Suppl C: 91–5. PMID: 12575492.
48. Grech R, Cassar T, Muscat J, Camilleri KP, Fabri SG, Zervakis M, et al. Review on solving the inverse problem in EEG source analysis. J Neuroeng Rehabil. 2008; 5: 25. Available from: https://doi.org/ 10.1186/1743-0003-5-25.
49. Neuner I, Arrubla J, Werner CJ, Hitz K, Boers F, Kawohl W, et al. The default mode network and EEG regional spectral power: a simultaneous fMRI-EEG study. PLoS One. 2014; 9 (2): e88214. Available from: https://doi.org/ 10.1371/journal.pone.0088214
50. Vukovic N, Hansen B, Lund TE, Jespersen S, Shtyrov Y. Rapid microstructural plasticity in the cortical semantic network following a short language learning session. PLoS Biol. 2021; 19 (6): e3001290. Available from: https://doi.org/10.1371/journal.pbio.3001290. PMID: 34125828; PMCID: PMC8202930.
51. Hubert V, Beaunieux H, Chételat G, Platel H, Landeau B, Viader F, Desgranges B, Eustache F. Age-related changes in the cerebral substrates of cognitive procedural learning. Hum Brain Mapp. 2009; 30 (4): 1374–86. Available from: https://doi.org/10.1002/hbm.20605. PMID: 18537110; PMCID: PMC2935916.
52. Just MA, Keller TA. Converging measures of neural change at the microstructural, informational, and cortical network levels in the hippocampus during the learning of the structure of organic compounds. Brain Struct Funct. 2019; 224 (3): 1345–57. Available from: https://doi.org/10.1007/s00429-019-01838-4. Epub 2019 Feb 6. PMID: 30725233.
53. Nunez PL, Wingeier BM, Silberstein RB. Spatial-temporal structures of human alpha rhythms: theory, microcurrent sources, multiscale measurements, and global binding of local networks. Hum Brain Mapp. 2001; 13 (3): 125–64. Available from: https://doi.org/10.1002/hbm.1030. PMID: 11376500; PMCID: PMC6872048.
54. Rodriguez-Larios J, ElShafei A, Wiehe M, Haegens S. Visual working memory recruits two functionally distinct alpha rhythms in posterior cortex. eNeuro. 2022; 9 (5): ENEURO.0159-22.2022. DOI: 10.1523/ENEURO.0159-22.2022. Epub ahead of print. PMID: 36171059; PMCID: PMC9536853.

CATAMNESIS OF CHILDREN WITH CONGENITAL CYTOMEGALOVIRUS INFECTION DEPENDING ON ETIOTROPIC THERAPY IN THE FIRST YEAR OF LIFE

Vasilyev VV[1,2] ✉, Rogozin NV[1], Markin IV[1], Ivanova RA[1,3], Grineva AA[4]

[1] Pediatric Research and Clinical Center of Infectious Diseases, Federal Medical Biological Agency, St. Petersburg, Russia

[2] North-Western State Medical University named after I.I. Mechnikov, Ministry of Health of Russia, St. Petersburg, Russia

[3] Pavlov First State Medical University of St. Petersburg, St. Petersburg, Russia

[4] Almazov National Medical Research Center, Ministry of Health of Russia, St. Petersburg, Russia

Cytomegalovirus infection (CMVI) continues to be a serious public health problem, being second to hypoxia and asphyxia in the list of reasons of morbidity and mortality of newborns. This study aimed to analyze therapeutic approaches to management of children with congenital cytomegalovirus with the regimens including an antiviral drug (direct action) and a specific anti-cytomegalovirus immunoglobulin (anti-CMV IG), depending on the clinical form of the disease. The total number of participants was 62, with the first group of children receiving the antiviral drug (n = 21), and the second group — an anti-CMV IG (n = 41). We analyzed the clinical, laboratory and instrumental research methods, and studied the catamnesis of children under 3 years of age. For statistical analysis, we used SPSS Statistics and StatTech v.3.1.6. In the first group, where the regimen included the direct action antiviral drug, the outcome was successful for 28.6% of the participants, and in the second group, which was treated with the anti-CMV immunoglobulin, this figure was 58.5%. Regardless of the regimen, by the age of 3, 50% of the children were practically healthy. Most of the participants tolerated the therapy satisfactorily. However, for 66% of the involved children, we had to shorten the direct action antiviral drug therapy to 14 days because of the problems with venous access, in 4.8% we registered thrombocytopenia, and in 9.5% — increased transaminase activity. Comparing the disease outcomes depending on the therapy initiation day, we established significant differences only for the specific antiviral therapy cases (p = 0.044).

Keywords: congenital cytomegalovirus infection, gancyclovir, anti-CMV immunoglobulin, outcomes

Funding: this study was performed under the research effort № 021-03 "Antenatal and early postnatal etiological diagnostics and etiotropic therapy of congenital infectious diseases of viral etiology" managed by the FMBA.

Author contribution: Vasilyev VV, Rogozina NV — study conceptualization and design; AA Grineva, Ivanova RA, Markin IV — collection and processing of the material, statistical data processing; Vasilyev VV, Rogozina NV — collection of literature data, article authoring, editing.

✉ **Correspondence should be addressed:** Valery V. Vasilyev
Mirgorodskaya, 3, korp. I, St. Petersburg, 191167, Russia; vcubed@ya.ru

Received: 12.08.2023 **Accepted:** 19.09.2023 **Published online:** 30.09.2023

DOI: 10.47183/mes.2023.041

КАТАМНЕЗ ДЕТЕЙ С ВРОЖДЕННОЙ ЦИТОМЕГАЛОВИРУСНОЙ ИНФЕКЦИЕЙ В ЗАВИСИМОСТИ ОТ ЭТИОТРОПНОЙ ТЕРАПИИ НА ПЕРВОМ ГОДУ ЖИЗНИ

В. В. Васильев[1,2] ✉, Н. В. Рогозина[1], И. В. Маркин[1], Р. А. Иванова[1,3], А. А. Гринева[4]

[1] Детский научно-клинический центр инфекционных болезней Федерального медико-биологического агентства, Санкт-Петербург, Россия

[2] Северо-западный государственный медицинский университет имени И. И. Мечникова Минздрава России, Санкт-Петербург, Россия

[3] Первый Санкт-Петербургский государственный медицинский университет имени И. П. Павлова, Санкт-Петербург, Россия

[4] Национальный медицинский исследовательский центр имени В. А. Алмазова Минздрава России, Санкт-Петербург, Россия

Цитомегаловирусная инфекция (ЦМВИ) продолжает оставаться серьезной проблемой общественного здравоохранения, занимая второе место после гипоксии и асфиксии в структуре заболеваемости и смертности новорожденных. Целью исследования было проанализировать лечебные подходы к ведению детей с врожденной цитомегаловирусной инфекцией с включением в терапию препарата прямого противовирусного действия и специфического антицитомегаловирусного иммуноглобулина (анти-ЦМВ ИГ) в зависимости от клинической формы заболевания. Пролечено 62 ребенка: в первой группе был назначен противовирусный препарат (n = 21), во второй — анти-ЦМВ ИГ (n = 41). Проведен анализ клинико-лабораторных и инструментальных методов исследований, изучен катамнез детей до 3 лет. Статистический анализ выполняли с использованием программы SPSS Statistics и StatTech v. 3.1.6. Благоприятный исход зарегистрирован у 28,6% детей, пролеченных препаратом прямого противовирусного действия, и у 58,5% детей, пролеченных анти-ЦМВ иммуноглобулином. Вне зависимости от терапии доля практически здоровых детей к 3 годам жизни составила 50%. Большинство детей, включенных в исследование, терапию переносили удовлетворительно. Однако у 66% детей курс терапии противовирусным средством прямого действия был сокращен до 14 дней из-за проблем с венозным доступом, у 4,8% обнаружена тромбоцитопения, у 9,5% повышение активности трансаминаз. При сопоставлении исходов заболевания в зависимости от дня начала терапии статистически значимые различия удалось установить только при применении специфической противовирусной терапии (p = 0,044).

Ключевые слова: врожденная цитомегаловирусная инфекция, ганцикловир, гипериммунный анти-ЦМВ иммуноглобулин, исходы

Финансирование: работа выполнена в соответствии с планом научно-исследовательской работы № 021-03 «Антенатальная и ранняя постнатальная этиологическая диагностика и этиотропная терапия врожденных инфекционных заболеваний вирусной этиологии» ФМБА.

Вклад авторов: В. В. Васильев, Н. В. Рогозина — концепция и дизайн исследования; А. А. Гринева, Р. А. Иванова, И. В. Маркин — сбор и обработка материала, статистическая обработка данных; В. В. Васильев, Н. В. Рогозина — сбор данных литературы, написание текста, редактирование.

✉ **Для корреспонденции:** Валерий Викторович Васильев
ул. Миргородская, д. 3, корп. И, г. Санкт-Петербург, 191167, Россия; vcubed@ya.ru

Статья получена: 12.08.2023 **Статья принята к печати:** 19.09.2023 **Опубликована онлайн:** 30.09.2023

DOI: 10.47183/mes.2023.041

Congenital infectious diseases (CID) are second to hypoxia and asphyxia in the list of causes of morbidity and mortality of newborns. In the developed countries, cytomegalovirus (CMV) is the main etiological factor of CIDs that can lead to disability [1]. Every third to sixth newborn out of 1000 live-born children receives CMV ante- or intranatally, and 20–25% of them exhibit symptoms at birth and/or long-term consequences [2]. This has a significant impact on public health.

The clinical picture of congenital cytomegalovirus infection (CMVI) varies widely from no signs thereof to a potentially life-threatening generalized form of the disease involving damage to the central nervous system (CNS), liver, bone marrow, gastrointestinal tract, and other organs [3]. The therapy tactics and monitoring depend on the additional tests and examinations that clarify the form of congenital CMVI and follow etiological verification of the diagnosis.

Today, ganciclovir and valganciclovir are the only direct-acting antivirals used to treat congenital CMVI. Numerous studies have confirmed the positive effect of these drugs on the clinical course of the disease, as well as reliable normalization of indicators learned with laboratory tests, improvement of the weight and height parameters, improvement of hearing, neurological status, and reduction of the CID-caused mortality [4, 5].

However, ganciclovir may cause adverse events, such as neutropenia, leukopenia, anemia, thrombocytopenia, increased creatinine levels, liver transaminase activity, etc. [4]. To children in their first years of life, this drug can be prescribed only off label, after a council that involves more than three specialized medical professionals once parents of the child in question have signed the informed consent form. Oral forms of valganciclovir (suspension, syrup) are not registered in the Russian Federation (RF).

Hyperimmune anticytomegalovirus immunoglobulin (anti-CMV IG) is another CMVI treatment option. It is a well-tolerated drug, however, to date, its high therapeutic efficacy has only been proven in subclinical and mild forms of congenital CMVI in children [6]. Anti-CMV IG as the sole drug is not indicated for children with clinically pronounced congenital CMVI that can cause severe consequences or death [7].

Today, there are no absolutely effective and safe antiviral therapy against congenital CMVI. This subject requires research efforts, including those designed to study long-term consequences of the disease against the background of antiviral therapy regimens.

The purpose of this work is to investigate the long-term consequences of congenital CMVI depending on the severity of the disease and the etiotropic therapy.

METHODS

This retrospective study examined the results of treatment of 62 children with congenital CMVI, based on their records from the Pediatric Research and Clinical Center of Infectious Diseases of the Federal Medical Biological Agency of Russia. The records covered the period from January 2017 to December 2022. Primary documentation (inpatient and outpatient medical records) provided data for the analysis of clinical manifestations, laboratory test results and long-term consequences in the observed children. The follow-up period ranged from 1 to 3 years. Most (69.4%) of the children were followed up for three years, 24.2% — for two years, and 6.5% for 1 year.

Criteria for inclusion in the study: confirmed congenital CMVI; no \perinatal HIV contact.

Criteria for exclusion from the study: HIV-positive mother; severe congenital disorders; chromosomal and/or genetic syndromes.

Congenital CMVI was diagnosed when the disease manifested clinically and the child's blood plasma sampled in the first three weeks of life carried DNA of CMV, as per clinical recommendations [3].

AmpliSense®CMV-FL reagents (Central Research Institute of Epidemiology of Rospotrebnadzor, Russia) and PCR tests (minimum sensitivity — 400 copies/ml) enabled detection of CMV's genetic material (DNA) in blood plasma, urine and saliva.

All patients underwent a history and physical examination, their complaints were analyzed. Examination involved registration of the following data: gender, gestation period at birth, course of pregnancy and childbirth, condition at birth and during the neonatal period, age at diagnosis, physical and psychomotor development, dynamics of the disease. Laboratory and instrumental tests were carried out in accordance with clinical recommendations [3].

All the children were examined by an ophthalmologist, a neurologist and a surdologist. The patients underwent neurosonography (NSG) and ultrasound examination of the heart, abdominal cavity and kidneys; Mindray M7 (Mindray; China) and Logiq E9 (GE Medical Systems Ultrasound and Primary Care Diagnostics; USA) systems were used for this purpose. Given appropriate indications, some patients were prescribed magnetic resonance imaging (MRI) or computed tomography (CT) of the brain and abdominal cavity, and those with hepatitis had liver fibroelastography performed with Fibroscan® (model 502, Touch Echosens; France) in accordance with the standard operating procedures. METAVIR score [8] enabled determination of the stage of fibrosis.

Depending on the etiotropic therapy regimen, all participating children were divided into two groups: group 1 — children who received a direct-acting antiviral drug (DAAD) (ganciclovir, 6 mg/kg, IV, every 12 hours, course duration — 14–21 days), $n = 21$; group 2 — children who were prescribed an anti-CMV IG as the initial drug (1 ml/kg, IV drip, 6 administrations every 48 hours), $n = 41$. The authors of this work did not participate in the choice of drugs because treatment of the children began before their cases were transferred for supervisory control to the Pediatric Research and Clinical Center of Infectious Diseases. The medical documentation contained no information about the use of valganciclovir.

The outcomes of the congenital CMVI with damage to the CNS were evaluated under the pediatric outcomes scale, which is a modification of the Rankin, Fisher and Glasgow scales [9]. The scale factored in presence/absence of the neuropsychiatric deficit (in comparison with the age norm); 0 points meant a fully healthy condition, 5 points — fatal outcome (Table 1). The sums from 3 through 5 points were considered adverse outcomes.

In the cases when cerebral palsy was part of the disease's outcome, we used the GMFCS Scale (Gross Motor Function Classification System, enables assessment of the gross motor skills in cerebral palsy cases), with motor skills at level I, II and III thereunder considered benign outcomes, and levels IV and V — adverse outcomes.

For statistical analysis, we used SPSS Statistics (version 23) and StatTech v.3.1.6 (StatTech; Russia). To assess conformity of the quantitative indicators to the normal distribution patterns, we used the Shapiro-Wilk test for samples smaller than 50 and the Kolmogorov-Smirnov test for samples larger than 50. The values that did follow the normal distribution patterns, they were described using arithmetic means (M) and standard deviations (SD) with CI at 95%. Comparison of the two groups by a quantitative indicator with normal distribution, given equality of the variances, was done using the Student's *t*-test. The data

Table 1. Pediatric scale of outcomes of purulent meningitis

Point	Characteristic
0	Healthy
1	No significant deviations from the age norm in motor functions and intellectual development; mild neurological deficit that can be fully remedied. Complete socialization
2	Mild motor or sensory deficits and/or delayed psychomotor and speech development, necessitating complex rehabilitation; symptomatic epilepsy controlled with antiepileptic drugs. For children over 3 years of age — preserved motor activity and self-care ability, despite the persistent neurological deficit. Good socialization in the family, group of children (with a little irregular help from adults).
3	Delayed psychomotor development that cannot be corrected in full by the complex methods of rehabilitation; epilepsy, poorly controlled with antiepileptic drugs; need for constant help from the others. Socialization in specialized groups/institutions
4	Severe neuropsychiatric deficit. Need for permanent care, specialized (neuropsychiatric) medical assistance. Socialization impossible
5	Death

by category were given in absolute values and percentages. To compare percentages in the fourfold contingency tables, we used Fisher's exact test (with the expected event values below 10), and for multifold contingency tables — Pearson's chi-squared test (with the expected event values above 10); the comparison of binary indicators characterizing two related aggregates was done with the help of McNemar's test. Assessment of the prognostic significance of quantitative signs in prediction of a certain outcome relied on the ROC curves analysis. The dividing value of the quantitative marker at the cut-off point was determined by the highest value of the Youden's index. The differences between the studied indicators were considered statistically significant at $p < 0.05$.

RESULTS

Patient characteristics

The study included 62 children: 27 (43.5%) aged from 1 to 3 months, 35 (56.5%) — from 4 to 6 months. Boys made up 53.2% of the participants, girls — 46.8%. For 88.7% of the participants, the course of the antenatal period included adverse events: threat of termination in 17 (27.4%) cases; intrauterine growth restriction (IGR) in 12 (19.4%) cases, with premature infants suffering the condition twice as often as full-term babies (9.7% and 4.8% of cases, respectively; $p = 0.001$); pregnant mother having ARVI of varying severity in 41.9% of cases. During pregnancy, the mothers were not tested for CMVI. The majority of the participating children were full-term (64.5%; 40 children). The average birth weight was from 650 to 1914 g. The age of patients at the initial visit to the Center was 3.8 ± 3.2 months.

The clinical manifestations were very diverse (Fig. 1). Central nervous system was damaged in more than 60% of children, the conditions including meningoencephalitis in three (4.8%) of them, encephalitis in one (1.6%), developing hypertensive hydrocephalus syndrome in six (9.7%). Eighteen (29%) infants had enlarged liver, 9 (14.5%) — a combination of hepatomegaly and splenomegaly, and the rest had hyperfermentemia (from 2 to 20 norms due to ALT). Hemorrhagic syndrome was registered in 3.2% of the observed children with hepatitis. In 9.7%, direct bilirubin disrupted pigment metabolism 9.7%. Eye damage was diagnosed in 19.4% of infants, sensorineural hearing loss — in two (3.2%), neutropenia — in 32.2% of children (neutrophil level did not

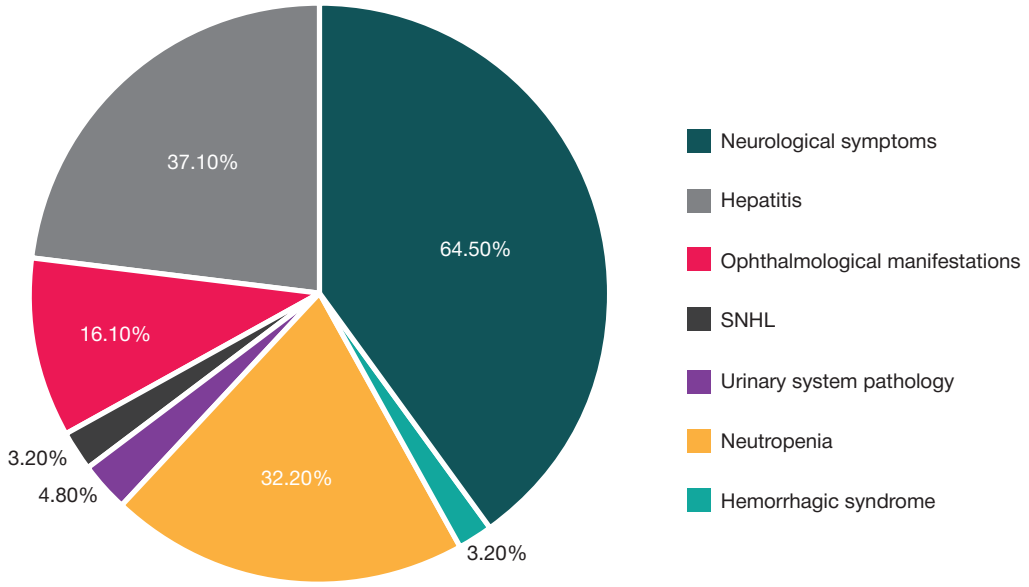

Fig. 1. Clinical manifestations in children with congenital cytomegalovirus infection

Table 2. Clinical manifestations in children with congenital cytomegalovirus infection, groups 1 and 2

Clinical manifestations	DAAD (n = 21)		Anti-CMV IG (n = 41)		Statistical differences between groups
	Abs.	%	Abs.	%	
Neurological symptoms	17	85.7	20	48.8	$p = 0.005$
Hepatitis	7	33.3	19	46.3	$p = 0.177$
Ophthalmological manifestations	3	14.3	5	12.2	$p = 1.000$
SNHL	1	4.8	1	2.4	$p = 1.000$
Urinary system pathology	0	0	3	7.3	$p = 0.545$
Neutropenia	5	23.8	15	36.6	$p = 0.156$
Hemorrhagic syndrome	2	9.5	0	0	$p = 0.111$

exceed 500/μl), and a combination of neutropenia and anemia was observed in 25.8% of the participants.

Children with congenital CMVI received the direct-acting antiviral drug if their CNS was severely damaged or there was combined damage to the CNS and other organs. Anti-CMV IG was used as a sole drug in mild cases with isolated manifestations (hepatitis, neutropenia) (Table 2); in that group, the dominating neurological symptom was hypoxic-ischemic perinatal encephalopathy.

The courses of the disease were identified based on the clinical recommendations [3]; in 58.1% and 12.9%, respectively, it took moderate and severe courses, in 17.7% and 11.3% of children — mild and subclinical.

Table 3 presents the results of examination of clinical manifestations of congenital CMVI depending on the course of the disease. Typically, severe course translated into damage to several organs, including CNS and liver. The prevailing disease associated with a mild course was hepatitis (91.7% of cases). In this study, only two children had sensorineural hearing loss; the infection course was moderate in them. As for neutropenia, it was registered in all mild course cases, 8.3% of moderate cases, and 62.5% of the severe course cases.

Therapy results

In our study, 21 children received DAAD (group 1), 41 children — anti-CMV IG (group 2).

Regardless of the type of therapy, the share of children that became healthy by the age of 3 was 50% of the entire sample. In group 1, 28.6% of the outcomes were benign, in group 2 — 58.5%. Mild neurological deficiency was observed in 17 children (27.4%), moderate deficit — in 6 (9.7%), gross organic deficit — in 8 (12.9%). Psychomotor retardation was diagnosed in 19 children (30.6%), and 6 (31.6%) children had cognitive impairments accompanied by various neurological syndromes (hypertensive hydrocephalus, convulsions, muscle tone disorder).

Six children (28.6%) from group 1 (DAAD) were diagnosed with cerebral palsy at the age of one year; it was the most severe form of motor disorders. By the GMFCS scale, 1 child out of these 6 had the motor functions of level III, 2 children — of level IV, and 4 children — of level V. Audiological examination revealed one child with 1st degree unilateral chronic sensorineural hearing loss.

In group 2 (anti-CMV IG), 31.7% of the participants (13 children) had psychomotor retardation, 12.2% (5 children) — convulsions, and one child (2.4%) was diagnosed with cerebral palsy, in this case the motor function disorders were of level II of the GMFCS scale, which is considered a benign outcome of the disease (Table 4).

Congenital CMVI can cause liver cirrhosis with subsequent fatal outcome. In our study, against the background of ongoing therapy, we observed normalization of the sizes of liver and spleen, as well as transaminase activity (Fig. 2), in all children ($p < 0.05$). Hepatitis was taking chronic course in four children, with one showing no signs of liver fibrosis, and three suffering this condition (stages 1–2).

According to the respective comparison, gestation period of newborns has no effect of the outcomes of congenital CMVI ($p = 1.000$). The chances of an adverse outcome of the congenital disease were equal in both groups (95% CI: 0.160–6.255).

Tolerability of DAAD amd anti-CMV IG therapy

There are known complications associated with use of DAAD, and yet, the children included in this study tolerated therapy

Table 3. Clinical manifestations of congenital cytomegalovirus infection depending on the course of the disease

Clinical manifestations	Mild		Moderate		Severe		Statistical differences between groups
	Abs.	%	Abs.	%	Abs.	%	
CNS	2	16.7	30	83.3	8	100	$p = 0.001$ (I + II)
Liver	11	91.7	10	27.8	3	37.5	$p = 0.285$
Organs of sight	1	8.3	7	19.4	2	25	$p < 0.001$ (II + III)
Hearing organs	0	0	2	5.6	0	0	
Kidneys	0	0	3	8.3	0	0	$p < 0.001$ (II + III)
Hematopoiestic organs	12	100	3	8.3	5	62.5	$p < 0.001$ (II + III)
Damage to more than two organs	2	16.7	18	50	8	100	$p < 0.001$ (II + III)
Total:	12	17.7	36	58.1	8	12.9	

Table 4. Neuropsychiatric deficit in children with congenital CMVI before and after DAAD therapy

Neuropsychiatric deficit against the age norm (according to the pediatric scale)	Before treatment		After treatment		Statistical differences between groups
	Abs.	%	Abs.	%	
Mild neurological deficit (1 point)	2	9.5	8	38.1	$p < 0.05$
Moderate neurological deficit (2 points)	0	0	2	9.5	$p < 0.05$
Gross neurological deficit (3-4 points)	16	76.2	8	38.1	$p < 0.05$

Table 5. Neuropsychiatric deficit in children with congenital CMVI before and after anti-CMV IG therapy

Neuropsychiatric deficit against the age norm (according to the pediatric scale)	Before treatment		After treatment		Statistical differences between groups
	Abs.	%	Abs.	%	
Mild neurological deficit (1 point)	0	0	14	34.1	$p < 0.05$
Moderate neurological deficit (2 points)	11	26.3	5	12.2	$p < 0.05$
Gross neurological deficit (3-4 points)	7	17.1	0	0	$p < 0.05$

satisfactorily. The main problem was hindered venous access, registered in 14 children (66%); their course of therapy was reduced to 14 days, but this did not prejudice the ultimate positive virological effect. Other side effects manifested in three children. One child (4.8%) with meningoencephalitis had thrombocytopenia, and his platelet level dropped below 50; one administration of DAAD was omitted from the course, then, when the platelet level returned to normal, it was resumed and completed. In two children (9.5%), transaminase activity was growing up (two-fold ALT maximum, 1.5 fold AAT maximum), but the situation did not require cancellation of the DAAD therapy. When the was over, transaminase activity normalized on its own.

Factors affecting the long-term results of DAAD anti-CMV IG therapy

A one-dimensional logistic regression model was used to analyze the factors associated with a benign or adverse outcome of congenital CMVI. The factors included in the univariate analysis were gestation period (full-term/premature), presence or absence of intrauterine growth retardation, adverse course of the antenatal period, course of the disease, specific therapy start date, damage to the organs (central nervous system, liver, organs of sight and hearing, hematopoietic organs), involvement of more than two organs in the infectious process.

Investigation of the effect of these factors revealed no associations with an adverse outcome of congenital CMVI (Table 6).

ROC analysis (Fig. 3) revealed that the probability of an adverse outcome is significantly lower when DAAD therapy starts in the first 3 months of the child's life. This pattern reaches statistical significance ($p = 0.044$; AUC = 0.759 ± 0.107 with 95% CI: 0.550–0.968; sensitivity — 80.0%, specificity — 72.7%).

The timing of initiation of the anti-CMV IG therapy (before or after the child turns 3-months-old) did not affect the overall frequency of pathological developments by the end of the follow-up period (up to 3 years of life) (Fig. 4; $p = 0.417$), but it significantly reduced the frequency of adverse neuropsychiatric outcomes (Table 5)

DISCUSSION

Clinical manifestations of congenital CMVI are diverse; the course may be severe, taking form of meningoencephalitis, cholestatic hepatitis, respiratory disorders and sensorineural hearing loss during the neonatal period, or mild, subclinical, with no such signs of conditions and accidental diagnosing later on [10–12]. Our study describes courses and outcomes of congenital CMVI in patients treated from January 2017 to December 2022 at the Pediatric Research and Clinical Center of Infectious Diseases of the Federal Medical Biological Agency of Russia; these patients received anti-CMV IG and DAAD. Most of the children (64%) were diagnosed with damage to the CNS. Majority of the studies addressing the subject conclude that such damage and neurosensory loss of hearing are currently the most common manifestations of congenital CMVI in children all over the world, including Russia.

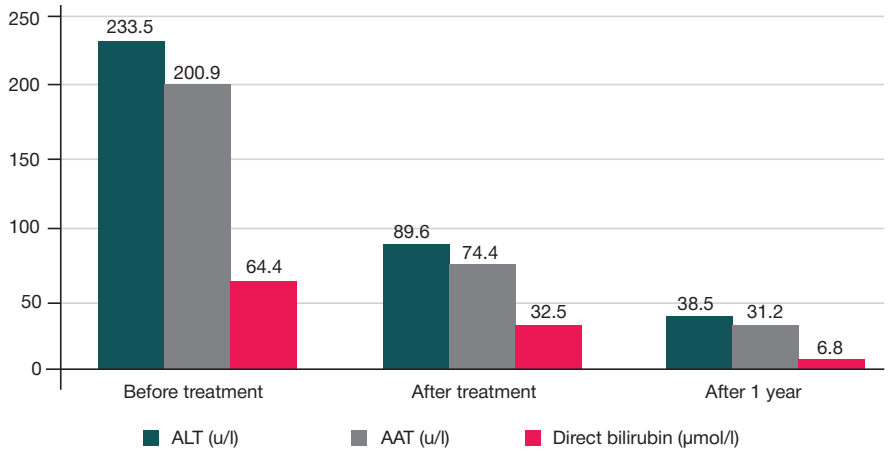

Fig. 2. Average values (μ) of ALT, AAT and direct bilirubin levels before therapy, after therapy and after 1 year

Table 6. Factors associated with an adverse outcome of congenital cytomegalovirus infection

№	Factor	*p*
1	Gestation period (full-term/premature)	0.312
2	Intrauterine growth retardation	0.438
3	Adverse antenatal course	0.834
4	Specific therapy start term	0.279
5	Course of the disease	0.52
6	CNS	0.187
7	Liver	0.297
8	Organs of sight and hearing	0.946
9	Involvement of more than 2 organs in the infectious process	0.266

In this study, meningoencephalitis was diagnosed in 4.8% of cases, encephalitis — in 1.6%, and other researchers put the incidence thereof at 3-32% of cases [13]; as for hypertensive hydrocephalus, it was registered in 9.7% of our patients, although other studies claim the incidence of this disorder to exceed 50% [14].

Hepatitis is a rather common disease for children with congenital CMVI, it is diagnosed in 17.4–26% of children [15, 16]; in 83% ALT exceeds 80 units/l, in 17% — 100 units/l [17]; there have been described cases of liver failure [18]. In this study, hepatitis was detected in 37.1% of the children, and a generally more severe course was notable; other characteristic features include the diagnosed combinations of hepatomegaly and splenomegaly (14.5% of cases), ALT and AAT values 2 to 20 times higher than normal, pigment metabolism disrupted by direct bilirubin (9.7% of cases), hemorrhagic syndrome (3.2% of cases).

Organs of sight were found damaged in 19.4% of the children, sensorineural hearing loss detected in two (3.2%), which is less frequent than in most other studies [19, 20]. Hematological pathology in the form of neutropenia was observed in 32.2% of children, a combination of neutropenia and anemia — in 25.8%.

Positively, this study disregarded many factors (e.g., gestation period in case of intrauterine infection) that affect prevalence and severity of the pathology in congenital CMVI cases, as well as the range of emerging long-term consequences and outcomes (Table 6).

Despite their toxicity, DAADs are used for etiotropic therapy against manifesting forms of the disease because of the high risk of death or subsequent disability it poses. Specific anti-CMV IG can be used as an additional etiotropic agent in severe congenital CMVI cases; if the course is mild or subclinical, anti-CMV IG can be the main drug of the regimen. The specifics of its use (doses, administration intervals, course duration), however, should be studied on a large sample of patients. In this study, we have shown that in mild cases, anti-CMV IG

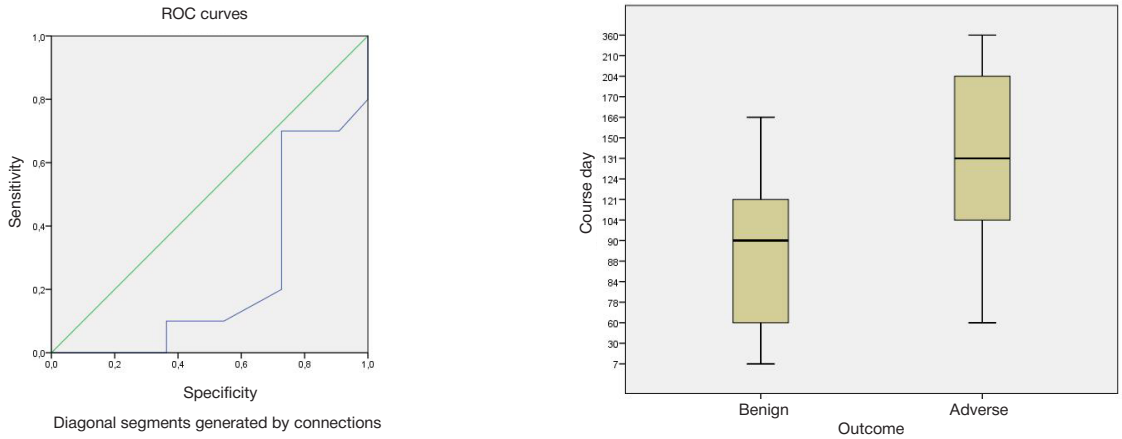

Fig. 3. ROC curve characterizing probability of an adverse outcome depending on the timing of DAAD therapy initiation

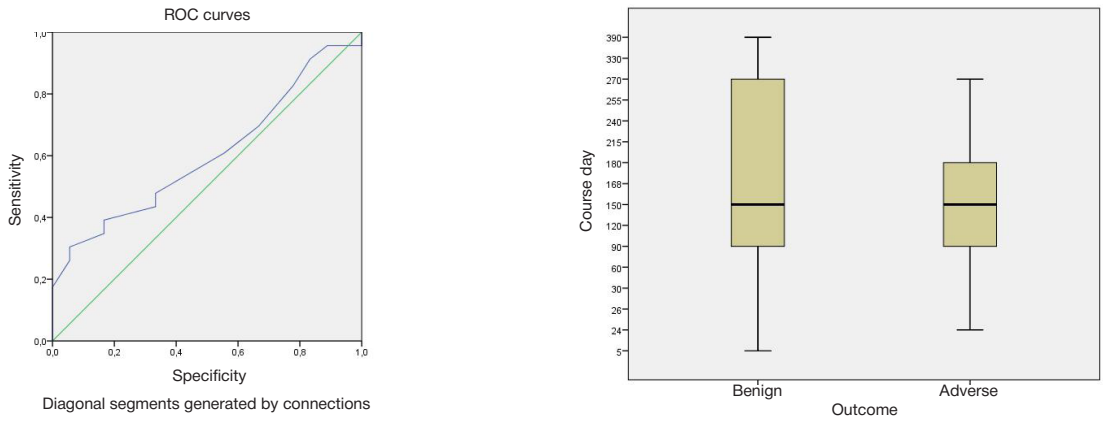

Fig. 4. ROC curve characterizing probability of an adverse outcome depending on the timing of anti-CMV IG therapy initiation

has a significant positive effect and relieves the symptoms of neuropsychiatric deficit; in particular, the drug completely eliminated gross neurological symptoms (Table 5). However, the data acquired should be tested on a larger number of observations in a randomized trial.

There is no doubt about value of early initiation of antiviral therapy in manifesting forms of CMVI [21]. However, the diagnosis is often made only 2–3 months after birth, and it is not always that doctor prescribe treatment in such cases. Unfortunately, most authors present isolated clinical cases describing the efficacy of DAAD and anti-CMV IG in children with congenital CMVI [22, 23]. This work shows that adverse outcomes in the form of cerebral palsy, psychomotor retardation, epilepsy, chronic sensorineural hearing loss, and disability since childhood were registered in 14.5% of children, which is much less than reported in observational studies where no antiviral drugs were used to treat congenital CMVI in children. We have not identified a single disability case caused by pulmonary fibrosis and liver cirrhosis as outcomes of congenital CMVI. A retrospective observational study of 2016 included 59 children with congenital CMVI who did not receive antiviral medicines; the authors of this study reported mental retardation in 94.4% of the patients, cerebral palsy in 38.9%, convulsive syndrome in 25.9% and hearing impairment in 66.7% [24]. There is a paper reporting the results of a three-month course of neocitotect given to 70 children with hypertensive hydrocephalus with congenital CMVI: the drug caused reduction of the size of ventricles in 28.5% of cases [25].

Tolerability of DAAD was a matter addressed specifically in the study. Apart from the hindered venous access, the drug was well tolerated. Only three children (14.2%) had side effects, thrombocytopenia and hyperfermentemia, that, however, did not lead to abortion of the course. In practice, limitations peculiar to the of DAAD are rooted not so much in their toxicity but in the need for frequent change of the infusion catheters [26].

CONCLUSIONS

Starting a DAAD therapy addressing severe and moderate congenital CMVI when the child is less then 3 months old significantly reduces the prevalence of all types of adverse outcomes, particularly, neuropsychiatric deficit; the effect is confirmed with a ROC analysis (by the end of the observation, gross deficit was twice as rare, and moderate manifestations of this type were completely eliminated). One of the possible reasons for persistence of adverse outcomes and long-term consequences - lack of prolonged valganciclovir course. There are mentions thereof in the medical documentation. In the context of this study, a course of anti-CMV IG prescribed to children with congenital CMVI manifesting mildly, regardless of the age of the child at its initiation (younger than 3 months, older than 3 months), was also significantly associated with alleviation of the neuropsychiatric deficit by the end of observation, and the gross neurological deficit was completely remedied. These data suggest that children with congenital CMVI can receive etiotropic therapy not only in the first weeks of life, but also later, if there are indications. Remembering that etiotropic therapy can be more successful when started early, it is necessary to conduct additional studies seeking to determine the critical period of a child's life within which initiation of such therapy is as effective as possible.

References

1. Leruez-Ville M, Foulon I, Pass R, Ville Y. Cytomegalovirus infection during pregnancy: state of the science. Am J Obstet Gynecol. 2020; 223 (3): 330–49. DOI: 10.1016/j.ajog.2020.02.018. Epub 2020 Feb 24. PMID: 32105678.
2. Pinninti S, Boppana S. Congenital cytomegalovirus infection diagnostics and management. Curr Opin Infect Dis. 2022; 35 (5): 436–41. DOI: 10.1097/QCO.0000000000000874. Epub 2022 Aug 19. PMID: 35984001.
3. Rossijskoe obshhestvo neonatologov, Rossijskaja associacija specialistov perinatal'noj mediciny. Klinicheskie rekomendacii «Vrozhdennaja citomegalovirusnaja infekcija». M., 2022; 62 s. Russian.
4. Chen SJ, Wang SC, Chen YC. Antiviral agents as therapeutic strategies against cytomegalovirus infections. Viruses. 2019; 12 (1): 21. DOI: 10.3390/v12010021.
5. Demin MV, Tihomirov DS, Tupoleva TA, Filatov FP. Ustojchivost' k protivovirusnym preparatam u virusov cheloveka iz podsemejstva Betaherpesvirinae. Voprosy virusologii. 2022; 67 (5): 385–94. DOI 10.36233/0507-4088-136. Russian.
6. Blázquez-Gamero D, Galindo Izquierdo A, Del Rosal T, Baquero-Artigao F, Izquierdo Méndez N, Soriano-Ramos M, et al. Prevention and treatment of fetal cytomegalovirus infection with cytomegalovirus hyperimmune globulin: a multicenter study in Madrid. J Matern Fetal Neonatal Med. 2019; 32 (4): 617–25. DOI: 10.1080/14767058.2017.1387890. Epub 2017 Oct 26.
7. Shahgildjan VI. Vrozhdennaja citomegalovirusnaja infekcija: aktual'nye voprosy, vozmozhnye otvety. Neonatologija: novosti, mnenija, obuchenie. 2020; 8 (4): 61–72.
8. Fu J, Wu B, Wu H, Lin F, Deng W. Accuracy of real-time shear wave elastography in staging hepatic fibrosis: a meta-analysis. BMC Med Imaging. 2020; 20 (1): 16. DOI: 10.1186/s12880-020-0414-5.
9. Vilnic AA, Skripchenko NV, Gorelik EYu, Egorova ES, Markova KV. Vozmozhnosti optimizacii patogeneticheskoj terapii gnojnyh meningitov u detej. Zhurnal nevrologii i psihiatrii im. S. S. Korsakova. 2019; 119 (12): 46–50. Dostupno po ssylke: https://doi.org/10.17116/ jnevro201911912146. Russian.
10. Xu H, Zhang L, Xuan XY, Zhu M, Tang J, Zhao XK. Intrauterine cytomegalovirus infection: a possible risk for cerebral palsy and related to its clinical features, neuroimaging findings: a retrospective study. BMC Pediatr. 2020; 20 (1): 555. DOI: 10.1186/s12887-020-02449-3.
11. Vasilev VV, Rogozina NV, Ivanova RA, i dr. Sravnitel'nyj analiz otechestvennyh i zarubezhnyh klinicheskih rekomendacij po aktual'nym vrozhdennym infekcionnym zabolevanijam. Pediatrija. Zhurnal im. G. N. Speranskogo. 2019; 98 (2): 141–6. DOI 10.24110/0031-403X-2019-98-2-141-146. Russian.
12. Njue A, Coyne C, Margulis AV, Wang D, Marks MA, et al. The Role of Congenital Cytomegalovirus Infection in Adverse Birth Outcomes: A Review of the Potential Mechanisms. Viruses. 2020; 13 (1): 20. DOI: 10.3390/v13010020.
13. Diogo MC, Glatter S, Binder J, Kiss H, Prayer D. The MRI spectrum of congenital cytomegalovirus infection. Prenat Diagn. 2020; 40 (1): 110–24. DOI: 10.1002/pd.5591. Epub 2020 Jan 6.
14. Krstanović F, Britt WJ, Jonjić S, Brizić I. Cytomegalovirus Infection and Inflammation in Developing Brain. Viruses. 2021; 13 (6): 1078. DOI: 10.3390/v13061078.
15. Zaplatnikov AL, i dr. Vozmozhno li predupredit' posledstvija vrozhdennoj citomegalovirusnoj infekcii? (Vzgljad akushera-ginekologa, infekcionista i neonatologa). Russkij medicinskij zhurnal. Medicinskoe obozrenie. 2018; 2 (10): 45–50. Russian.
16. Bilavsky E, Schwarz M, Bar-Sever Z, Pardo J, Amir J. Hepatic involvement in congenital cytomegalovirus infection — infrequent yet significant. J Viral Hepat. 2015; 22 (9): 763–8. DOI: 10.1111/jvh.12374.

17. Karpovich GS, Shestakov AE, Mihajlenko MA, Serova YuS. Citomegalovirusnyj gepatit u detej: sovremennoe sostojanie problemy. Lechashhij Vrach. 2022; 1 (25): 25–29. DOI: 10.51793/OS.2022.25.1.004. Russian.
18. Patterson J, Hussey HS, Silal S, Goddard L, Setshedi M, Spearman W, et al. Systematic review of the global epidemiology of viral-induced acute liver failure. BMJ Open. 2020; 10 (7): e037473. DOI: 10.1136/bmjopen-2020-037473.
19. Botti C, Palma S, Roversi MF, Monzani D, Berardi A, Genovese E. Different Audiologic Outcomes in Twins with Congenital Cytomegalovirus Infection. J Int Adv Otol. 2020; 16 (1): 130–3. DOI: 10.5152/iao.2020.6574.
20. Chatzakis C, Sotiriadis A, Dinas K, Ville Y. Neonatal and long-term outcomes of infants with congenital cytomegalovirus infection and negative amniocentesis: systematic review and meta-analysis. Ultrasound Obstet Gynecol. 2023; 61 (2):158–67. DOI: 10.1002/uog.26128.
21. Rogozina NV, Vasilev VV, Grineva AA, i dr. Ante i postnatal'naja diagnostika i kompleksnoe lechenie vrozhdennoj citomegalovirusnoj infekcii. Rossijskij vestnik perinatologii i pediatrii. 2019; 64 (6): 89–93. DOI 10.21508/1027-4065-2019-64-6-89-93.
22. Pata D, Buonsenso D, Turriziani-Colonna A, Salerno G, Scarlato L, Colussi L, et al. Role of Valganciclovir in children with congenital CMV infection: a review of the literature. Children (Basel). 2023; 10 (7): 1246. DOI: 10.3390/children10071246.
23. Petrova GV, Shahgil'djan VI, Chistozvonova EA, Pugacheva TA, Turkot NV, Egorova MV, i dr. Opyt primenenija protivovirusnoj terapii vrozhdennoj generalizovannoj citomegalovirusnoj infekcii. Detskie infekcii. 2016; 15 (2): 61–68.
24. Uematsu M, Haginoya K, Kikuchi A, et al. Asymptomatic congenital cytomegalovirus infection with neurological sequelae: A retrospective study using umbilical cord. Brain Dev. 2016; 38 (9): 819–26. DOI: 10.1016/j.braindev.2016.03.006.
25. Anciferova EV, Taranushenko TE, Geninova DG, Karpova LN, Filippova LA, Karaganova KI, et al. Vrozhdennaja citomegalovirusnaja infekcija: osobennosti klinicheskogo techenija i katamnez po dannym sobstvennogo nabljudenija. Zhurnal infektologii. 2022; 14 (4): 118–25. Russian.
26. Acosta E, Bowlin T, Brooks J, Chiang L, Hussein I, Kimberlin D, et al. Advances in the development of therapeutics for cytomegalovirus infections. J Infect Dis. 2020; 221: S32–S44. DOI: 10.1093/infdis/jiz493.

Литература

1. Leruez-Ville M, Foulon I, Pass R, Ville Y. Cytomegalovirus infection during pregnancy: state of the science. Am J Obstet Gynecol. 2020; 223 (3): 330–49. DOI: 10.1016/j.ajog.2020.02.018. Epub 2020 Feb 24. PMID: 32105678.
2. Pinninti S, Boppana S. Congenital cytomegalovirus infection diagnostics and management. Curr Opin Infect Dis. 2022; 35 (5): 436–41. DOI: 10.1097/QCO.0000000000000874. Epub 2022 Aug 19. PMID: 35984001.
3. Российское общество неонатологов, Российская ассоциация специалистов перинатальной медицины. Клинические рекомендации «Врожденная цитомегаловирусная инфекция». М., 2022; 62 с.
4. Chen SJ, Wang SC, Chen YC. Antiviral agents as therapeutic strategies against cytomegalovirus infections. Viruses. 2019; 12 (1): 21. DOI: 10.3390/v12010021.
5. Демин М. В., Тихомиров Д. С., Туполева Т. А., Филатов Ф. П. Устойчивость к противовирусным препаратам у вирусов человека из подсемейства Betaherpesvirinae. Вопросы вирусологии. 2022; 67 (5): 385–94. DOI 10.36233/0507-4088-136.
6. Blázquez-Gamero D, Galindo Izquierdo A, Del Rosal T, Baquero-Artigao F, Izquierdo Méndez N, Soriano-Ramos M, et al. Prevention and treatment of fetal cytomegalovirus infection with cytomegalovirus hyperimmune globulin: a multicenter study in Madrid. J Matern Fetal Neonatal Med. 2019; 32 (4): 617–25. DOI: 10.1080/14767058.2017.1387890. Epub 2017 Oct 26.
7. Шахгильдян В. И. Врожденная цитомегаловирусная инфекция: актуальные вопросы, возможные ответы. Неонатология: новости, мнения, обучение. 2020; 8 (4): 61–72
8. Fu J, Wu B, Wu H, Lin F, Deng W. Accuracy of real-time shear wave elastography in staging hepatic fibrosis: a meta-analysis. BMC Med Imaging. 2020; 20 (1): 16. DOI: 10.1186/s12880-020-0414-5.
9. Вильниц А. А., Скрипченко Н. В., Горелик Е. Ю., Егорова Е. С., Маркова К. В. Возможности оптимизации патогенетической терапии гнойных менингитов у детей. Журнал неврологии и психиатрии им. С. С. Корсакова. 2019; 119 (12): 46–50. Доступно по ссылке: https://doi.org/10.17116/jnevro201911912146.
10. Xu H, Zhang L, Xuan XY, Zhu M, Tang J, Zhao XK. Intrauterine cytomegalovirus infection: a possible risk for cerebral palsy and related to its clinical features, neuroimaging findings: a retrospective study. BMC Pediatr. 2020; 20 (1): 555. DOI: 10.1186/s12887-020-02449-3.
11. Васильев В. В., Рогозина Н. В., Иванова Р.А и др. Сравнительный анализ отечественных и зарубежных клинических рекомендаций по актуальным врожденным инфекционным заболеваниям. Педиатрия. Журнал им. Г. Н. Сперанского. 2019; 98 (2): 141–6. DOI 10.24110/0031-403X-2019-98-2-141-146.
12. Njue A, Coyne C, Margulis AV, Wang D, Marks MA, et al. The Role of Congenital Cytomegalovirus Infection in Adverse Birth Outcomes: A Review of the Potential Mechanisms. Viruses. 2020; 13 (1): 20. DOI: 10.3390/v13010020.
13. Diogo MC, Glatter S, Binder J, Kiss H, Prayer D. The MRI spectrum of congenital cytomegalovirus infection. Prenat Diagn. 2020; 40 (1): 110–24. DOI: 10.1002/pd.5591. Epub 2020 Jan 6.
14. Krstanović F, Britt WJ, Jonjić S, Brizić I. Cytomegalovirus Infection and Inflammation in Developing Brain. Viruses. 2021; 13 (6): 1078. DOI: 10.3390/v13061078.
15. Заплатников А. Л. и др. Возможно ли предупредить последствия врожденной цитомегаловирусной инфекции? (Взгляд акушера-гинеколога, инфекциониста и неонатолога). Русский медицинский журнал. Медицинское обозрение. 2018; 2 (10): 45–50.
16. Bilavsky E, Schwarz M, Bar-Sever Z, Pardo J, Amir J. Hepatic involvement in congenital cytomegalovirus infection — infrequent yet significant. J Viral Hepat. 2015; 22 (9): 763–8. DOI: 10.1111/jvh.12374.
17. Карпович Г. С., Шестаков А. Е., Михайленко М. А., Серова Ю. С. Цитомегаловирусный гепатит у детей: современное состояние проблемы. Лечащий Врач. 2022; 1 (25): 25–29. DOI: 10.51793/OS.2022.25.1.004.
18. Patterson J, Hussey HS, Silal S, Goddard L, Setshedi M, Spearman W, et al. Systematic review of the global epidemiology of viral-induced acute liver failure. BMJ Open. 2020; 10 (7): e037473. DOI: 10.1136/bmjopen-2020-037473.
19. Botti C, Palma S, Roversi MF, Monzani D, Berardi A, Genovese E. Different Audiologic Outcomes in Twins with Congenital Cytomegalovirus Infection. J Int Adv Otol. 2020; 16 (1): 130–3. DOI: 10.5152/iao.2020.6574.
20. Chatzakis C, Sotiriadis A, Dinas K, Ville Y. Neonatal and long-term outcomes of infants with congenital cytomegalovirus infection and negative amniocentesis: systematic review and meta-analysis. Ultrasound Obstet Gynecol. 2023; 61 (2):158–67. DOI: 10.1002/uog.26128.
21. Рогозина Н. В., Васильев В. В., Гринева А. А. и др. Анте и постнатальная диагностика и комплексное лечение врожденной цитомегаловирусной инфекции. Российский вестник перинатологии и педиатрии. 2019; 64 (6): 89–93. DOI 10.21508/1027-4065-2019-64-6-89-93.
22. Pata D, Buonsenso D, Turriziani-Colonna A, Salerno G, Scarlato L, Colussi L, et al. Role of Valganciclovir in children with congenital CMV infection: a review of the literature. Children (Basel). 2023; 10 (7): 1246. DOI: 10.3390/children10071246.

23. Петрова Г. В., Шахгильдян В. И., Чистозвонова Е. А., Пугачева Т. А., Туркот Н. В., Егорова М. В. и др. Опыт применения противовирусной терапии врожденной генерализованной цитомегаловирусной инфекции. Детские инфекции. 2016; 15 (2): 61–68.
24. Uematsu M, Haginoya K, Kikuchi A, et al. Asymptomatic congenital cytomegalovirus infection with neurological sequelae: A retrospective study using umbilical cord. Brain Dev. 2016; 38 (9): 819–26. DOI: 10.1016/j.braindev.2016.03.006.
25. Анциферова Е. В., Таранушенко Т. Е., Генинова Д. Г., Карпова Л. Н., Филиппова Л. А., Караганова К. И., et al. Врожденная цитомегаловирусная инфекция: особенности клинического течения и катамнез по данным собственного наблюдения. Журнал инфектологии. 2022; 14 (4): 118–25.
26. Acosta E, Bowlin T, Brooks J, Chiang L, Hussein I, Kimberlin D, et al. Advances in the development of therapeutics for cytomegalovirus infections. J Infect Dis. 2020; 221: S32–S44. DOI: 10.1093/infdis/jiz493.

PILOT SURVEY OF PHYSICIANS ON THE SYSTEM OF ASSIGNING PROFESSIONAL GRADES

Misharin VM[1], Kochubey AV[2] ✉

[1] Research Institute of Pulmonology of Federal Medical Biological Agency, Moscow, Russia

[2] Federal Scientific and Clinical Center of Specialized Medical Assistance and Medical Technologies of Federal Medical Biological Agency, Moscow, Russia

Stagnation of the institution of assigning professional grades (categorization) draws increasing attention to the study of the opinions of physicians aimed at understanding and addressing the issues of this system. The study was aimed to get an estimate of the categorization system, the need for and directions of its transformation from physicians. The study involved an absentee poll of 64 physicians. Among then 48.4% had professional grades, 42.2% had scientific degrees, 51.6% were members of professional communities, 45.3% were engaged in teaching, 48.4% published scientific research results, 26.6% presented the results of their work during scientific and practical events. The average work experience as a physician was 13.8 ± 6.13 years. The questionnaire consisting of 21 statements with 5-point Likert scales was divided into four items: assessment of current categorization system; refusal of categorization; need to transform the system; directions of transformation. As a result, it was found that the respondents having professional grades, scientific degrees, who were members of professional communities engaged in teaching and scientific research, rated the existing categorization system lower ($1.0 \le Me \le 1.8$ vs $2.6 \le Me \le 3.0$; $0.001 < p \le 0.034$), they more often agreed that there was a need to transform the system ($1.0 \le Me \le 1.33$ vs $2.7 \le Me \le 3.0$; $0.001 < p \le 0.013$), than the respondents with no listed above traits. A total of 71.9% respondents agreed that there was a need for change, 1.6% agreed with the refusal of categorization. No correlation between work experience and the scores of items was revealed ($0.144 \le p \le 0.627$). Thus, despite the fact that the categorization system was rated low, the majority of physicians don't want to abandon it seeing the need for transformation. The physicians' beliefs are affected by the levels of their professional development.

Keywords: categorization, professional grade, professional development

Author contribution: Misharin VM — research coordination, data analysis and interpretation, literature review; Kochubey AV — concept, design, statistical analysis, conclusions, manuscript writing.

✉ **Correspondence should be addressed:** Adelina V. Kochubey
Volokolamskoye shosse, 91, Moscow, 125371, Russia; kochoubeya@gmail.com

Received: 06.08.2023 **Accepted:** 20.09.2023 **Published online:** 29.09.2023

DOI: 10.47183/mes.2023.035

ПИЛОТНЫЙ ОПРОС ВРАЧЕЙ О СИСТЕМЕ ПРИСВОЕНИЯ КВАЛИФИКАЦИОННЫХ КАТЕГОРИЙ

В. М. Мишарин[1], А. В. Кочубей[2] ✉

[1] Научно-исследовательский институт пульмонологии Федерального медико-биологического агентства, Москва, Россия

[2] Федеральный научно-клинический центр специализированных видов медицинской помощи и медицинских технологий Федерального медико-биологического агентства, Москва, Россия

Стагнация института присвоения квалификационных категорий (аттестации) актуализирует изучение мнения врачей для понимания и решения проблем данной системы. Целью данной работы было получить оценку врачей системы их аттестации, необходимости и направлений ее преобразований. В рамках исследования проводили заочный опрос 64 врачей, 48,4% из которых имеют квалификационную категорию, 42,2% — ученую степень, 51,6% — состоят в профессиональном сообществе, 45,3% — преподают, 48,4% — публикуют результаты научной деятельности, 26,6% — представляют на научно-практических мероприятиях результаты своей работы. Средний стаж работы врачом — 13,8 ± 6,13 лет. Анкета из 21 утверждения с пятибалльной шкалой Лайкерта была разбита на 4 конструкта: оценка текущей системы аттестации; отказ от аттестации; необходимость преобразований системы; направления преобразований. В результате было выявлено, что у респондентов с категорией, ученой степенью, состоящих в профсообществах, ведущих преподавательскую и научную деятельность, оценка текущей системы аттестации ниже ($1{,}0 \le Me \le 1{,}8$ vs $2{,}6 \le Me \le 3{,}0$; $0{,}001 < p \le 0{,}034$), согласие с необходимостью преобразований системы более выражено ($1{,}0 \le Me \le 1{,}33$ vs $2{,}7 \le Me \le 3{,}0$; $0{,}001 < p \le 0{,}013$), чем у респондентов без названных выше черт. Согласие с потребностью в изменениях выразили 71,9% респондентов, с отказом от аттестации — 1,6%. Корреляции стажа с баллами по конструктам не обнаружено ($0{,}144 \le p \le 0{,}627$). Таким образом, при низкой оценке системы аттестации большинство врачей не хотят от нее отказываться, видя необходимость преобразований. На мнение врачей влияет уровень их профессионального развития.

Ключевые слова: аттестация, квалификационная категория, профессиональное развитие

Вклад авторов: В. М. Мишарин — координация исследования, анализ и интерпретация данных, работа с литературой; А. В. Кочубей — идея, дизайн, статистический анализ, формулирование выводов, подготовка рукописи.

✉ **Для корреспонденции:** Аделина Владимировна Кочубей
Волоколамское шоссе, д. 91, г. Москва, 125371, Россия; kochoubeya@gmail.com

Статья получена: 06.08.2023 **Статья принята к печати:** 20.09.2023 **Опубликована онлайн:** 29.09.2023

DOI: 10.47183/mes.2023.035

The importance of well-trained personnel for public healthcare is widely accepted and appreciated [1]. The fact that personnel is a group of specialists of various profiles makes a successful unified approach to their sustainable development impossible [2]. National healthcare systems face major challenges related to ensuring objective personnel competence estimation and effectiveness of incentives for continuous professional development of specialists [3].

In the Russian Federation, the institutions responsible for categorization, assigning professional grades (categorization), internal certification at the work place, independent qualification assessment, as well as the system of continuous medical education, are to ensure estimation of competence and incentives for the physicians' professional development [4–6].

Despite shortcomings in the work of evaluation committees, the categorization system systematically provided growth of physicians' qualification during the Soviet era [7], however, there was a talk about its problems resulting from outdated legislation and flawed methodology, as well as the lack of objective criteria for qualification assessment, since early 2000s [8–11].

Despite the updated legislation and methodology, the categorization systems are still a matter of debate [12–15]. The authors demonstrate stagnation and assume possible extinction of the categorization institution due to the lack of financial incentives, no occupational or professional motivation in specialists, indifference and resistance of employers, emergence of new qualification assessment institutions, gap between categorization and the system of continuous medical education, inadequacy of the professional grade differentiation estimates.

Pessimistic forecasts are not groundless: according to Rosstat, the number of physicians assigned the first and supreme grades reduced by 1.3 times in 2009–2021 in Russia [16].

The problems identified together with the lack of studies focused on assessing the physicians' opinions about the categorization system in the domestic database have defined the aim of the study: to estimate the current state of the system of assigning professional grades to physicians along with the need for and directions of its transformation.

METHODS

Developing a questionnaire for absentee poll

Data acquisition for the study was performed by the absentee poll of physicians involving the use of Google Forms (https://docs.google.com/forms/d/1_-xyoo1NF3Ch0sIT8qhhZ3jyfWriqraKA2YIH9Gw7jE/viewform?edit_requested=true). A request to complete a survey with the link to the questionnaire was sent to individuals previously trained in the Academy of Postgraduate Education, Federal Scientific and Clinical Center of Specialized Types of Medical Care of FMBA of Russia. Inclusion criteria: being a physician, work experience as a physician of at least five years. Exclusion criteria: citizenship of another country. The number of respondents was set as 500 based on the requirements for studies with improved accuracy to be conducted by the method by K. A. Otdelnova and the assumption of 20% refusals (500 = 400/(1–0.20)) [17]. The survey did not require the respondent's written consent, since participation was voluntary, and privacy was guaranteed by no information about surname, name and patronymic in the questionnaire.

The paper provides interim results that are based on the analysis of the questionnaires completed by the first 64 respondents, which is consistent with the sample size of the pilot study conducted using the method by Otdelnova.

The questionnaire used was developed by the authors based on the review of literature on the public healthcare human resource strategy and the issues of categorization system. The first version was tested in a focus group of 17 individuals to clarify the language of statements. The Cronbach's alpha coefficient ≥ 0.877 characterizes good internal consistency of the questionnaire items. The intraclass correlation coefficient (iCC) ≥ 0.91, but ICC ≤ 0.97 at $p \leq 0.001$ indicates the questionnaire test-retest reliability. The questionnaire consisted of two parts:

a) background information about the respondent: work experience as a physician, work experience in the specialty, being assigned professional grade or scientific degree, membership in professional communities (professional non-profit organizations created by medical, professionals and pharmacists, their associations and unions), being engaged in teaching or scientific research (with the results published) within a year before the survey, as well as experience of presentations at scientific and practical events for specialists. These parameters were selected as those affecting the physician's professional development;

b) opinions of physicians about the system of assigning professional grades (categorization). This part consisted of 21 statements with five-point Likert scales offering the following answer options: 1 — Strongly Disagree, 2 — Disagree, 3 — 50/50, 4 — Agree, 5 — Strongly Agree. All statements were divided into four items (K1, K2, K3, K4):

K1 — the existing categorization system was considered in terms of soundness of the professional level estimation, providing the same levels of objectivity, impartiality and completeness of testing, reports, interviews used for assessment or demonstration of the certified person's level of qualification, transparency and clarity of the categorization procedure, employer impact, difficulties when filling out paperwork, compliance of the categorization system with the today's requirements of public healthcare;

K2 — abandoning the categorization system was assessed based on the respondents' agreement with the statement about uselessness of the system of assigning professional grades to physicians for today's public healthcare;

K3 — the need to transform the categorization system was assessed relative to the respondents' attitude towards outdated approaches to building such system exclusively on providing incentives (rewards/punishments) to physicians to be assigned a grade, assessment of knowledge and skills only, key role of healthcare public administration;

K4 — the directions for the categorization system transformation included the principles of physician's professional development in modern public healthcare: development and management of working relationships with colleagues; physician's understanding of formal and informal social norms related to profession; planning professional career throughout the life; physician's contribution to the development of other specialists, profession and the body of medical knowledge; primacy of the motive to be assigned a grade as the greatest possible value; recognition of physician's achievements by professional community; key role of professional community.

Five points to items K1, K4 indicated the most positive assessment of the existing system and the directions of its transformation, to item K2 — agreement to abandon the categorization system, to item K3 — disagreement with the need to transform the system. By contrast, one point to items K1, K4 indicated the most negative assessment of the existing system and the directions of its transformation, to item K2 — disagreement to abandon the categorization system, to item K3 — agreement with the need to transform the system. The distribution of variables across statements and items was non-normal ($p \leq 0.001$).

Characteristics of respondents

Among 64 respondent physicians 31 (48.4%) had professional grades, 27 (42.2%) had scientific degrees, 33 (51.6%) were members of professional communities; 29 (45.3%) were engaged in teaching, 31 (48.4%) published original research results, 17 (26.6%) presented the results of their work in the specialty at scientific and practical events. The respondents' average work experience as a physician was 13.8 ± 6.13 years and their work experience in the specialty was 11.7 ± 5.83 years. The respondents' distribution by work experience was normal ($p = 0.200$; $p = 0.169$). There were significant differences in work experience between the respondents assigned and not assigned professional grades ($t = -2.31$, $p = 0.024$; $t = 2.25$, $p = 0.028$), being and not being members of

Table. Medians of items and asymptomatic significance of Mann–Whitney U test by groups of respondents

Groups	K1	K2	K3	K4
Grade	$p < 0.001$	$p = 0.023$	$p < 0.001$	$p < 0.001$
Yes	Me = 1.0	Me = 1.0	Me = 1.0	Me = 5.0
No	Me = 3.0	Me = 2.0	Me = 2.67	Me = 3.29
Scientific degree	$p = 0.034$	p = 0.227	$p = 0.013$	$p = 0.010$
Yes	Me = 1.0	Me = 1.0	Me = 1.0	Me = 5.0
No	Me = 2.60	Me = 2.0	Me = 2.67	Me = 3.57
Professional community	$p = 0.002$	p = 0.131	$p = 0.005$	$p = 0.002$
Member	Me = 1.8	Me = 1.0	Me = 1.33	Me = 4.57
Not a member	Me = 3.0	Me = 2.0	Me = 3.0	Me = 3.29
Teaching	$p < 0.001$	$p < 0.001$	$p < 0.001$	$p < 0.001$
Engaged	Me = 1.0	Me = 1.0	Me = 1.0	Me = 5.0
Not engaged	Me = 3.0	Me = 2.0	Me = 2.67	Me = 3.29
Published research results	$p < 0.001$	$p < 0.001$	$p < 0.001$	$p < 0.001$
Yes	Me =1.0	Me = 1.0	Me = 1.0	Me = 5.0
No	Me = 3.0	Me = 2.0	Me = 2.67	Me = 3.29
Presentations at scientific and practical events	$p < 0.001$	$p = 0.003$	$p < 0.001$	$p < 0.001$
Yes	Me = 1.0	Me =1.0	Me = 1.0	Me = 5.0
No	Me = 2.60	Me = 2.0	Me = 2.67	Me = 3.57

professional communities (t = –2.90, p = 0.005; t = –3.45, p = 0.01). There were no significant differences between the respondents having and not having scientific degrees (t = 1.17, p = 0.245; t = 0.83, p = 0.410), engaged and not engaged in teaching (t = –1.03, p = 0.305; t = 1.45, p = 0.153), having and not having scientific publications (t = 1.18, p = 0.244; t = 1.51, p = 0.137) and the experience of presentations at scientific and practical events (t = 0.41, p = 0.680; t = 0.94, p = 0.349).

Statistical processing was carried out using SPSS, ver. 23 (IBM Company; USA). The following was performed: calculation of mean values and standard deviations for the variables "work experience as a physician" and "work experience in the specialty", comparison of work experience by groups using Student's t-test, frequency analysis of scores by items, calculation of Spearman's rank correlation coefficient to assess the relationship between the work experience and the scores by items, calculation of the median for each item by groups, comparison of scores assigned to the items by groups using the Mann–Whitney U test.

RESULTS

The majority of respondents (41/64%) do not agree that the existing categorization system meets modern requirements of public healthcare, is complete in terms of assessing the professional development level, ensures equal levels of objectivity, that testing, reports, interviews are impartial and complete when used for assessment or demonstration of the physician's level of qualification, that the categorization procedure is transparent and clear, there are no difficulties when filling out paperwork and no employer impact. The majority of respondents (46/71.9%) do not agree with the outdated principles of the categorization system construction, however, they do not want to abandon the system (56/87.5%). More than a half of respondents (35/54.7%) agree with all new principles of the categorization system construction. A total of 42 respondents (65.6%) agree that there is a need for estimates of the development and management of working relationships with colleagues in the categorization system; 56 (87.5%) agree that there is a need for estimates of the physician's understanding of formal and informal social norms related to profession; 39 (60.9%) agree that there is a need for estimates of planning professional career throughout the life; 39 (60.9%) agree that there is a need for estimates of the physician's contribution to the development of other specialists, profession and the body of medical knowledge. A total of 38 respondents (59.4%) agree with primacy of the motive to be assigned a grade as the greatest possible value for the physician, 15 (23.4%) agree with primacy of incentives. A total of 56 respondents (87.5%) agree with the statement that the categorization system has to reflect recognition of physician's achievements by professional community. The majority of respondents (42/65.6%) acknowledge that professional community plays a key role in today's system of assigning professional grades to physicians, while 4 (6.3%) recognize that the key role is played by healthcare public administration.

The respondents, who were assigned grades, had scientific degrees, were members of professional communities, were engaged in teaching, had scientific publications and the experience of presenting at scientific and practical events, ranked the existing categorization system lower ($1.0 \leq Me \leq 1.8$ vs $2.6 \leq Me \leq 3.0$; $0.001 < p \leq 0.034$), to the greater extent agreed with the need to transform the system ($1.0 \leq Me \leq 1.33$ vs $2.7 \leq Me \leq 3.0$; $0.001 < p \leq 0.013$), ranked new principles of transformation higher ($4.6 \leq Me \leq 5.0$ vs $3.3 \leq Me \leq 3.6$; $0.001 < p \leq 0.010$), that the respondents with no listed above traits (Table). There were no differences in the extent of disagreement with the categorization system abandoning (K2) between the groups of respondents allocated based on the facts of having a scientific degree and membership in professional communities.

There were no strong significant correlations between the scores of items and the work experience as a physician (K1 rS = 0.26, p = 0.039; K2 rS = 0.06, p = 0.627; K3 rS = 0.17, p = 0.172; K4 rS = 0.19, p = 0.144) or work experience in the specialty (K1 rS = 0.28, p = 0.028; K2 rS = 0.08, p = 0.510; K3 rS = 0.19, p = 0.133; K4 rS = 0.21, p = 0.104).

DISCUSSION

The survey has shown that the majority of physicians see the shortcomings of the system of assigning professional grades, which is in line with the literature data on the issues of the existing categorization system [12–15]. Furthermore, discrepancies between the assumptions of a number of authors about the categorization institution uselessness and unwillingness of the vast majority of physicians (87.5%) to abandon this system have been revealed [11]. Many respondents are negative on the approaches of the existing categorization system and positive on new principles of professional development in modern public healthcare. In fact, the survey results indicate the desire of professional community to transform the categorization conceptual model. This conclusion is supported by the fact that almost 88% of respondent agree that categorization should reflect recognition of physician's achievements by professional community.

The fact, that almost 60% agree that the today's system should be based on the motive to be assigned a professional grade as the greatest possible value for the physician, is of special interest. Such an approach is fundamentally different from the most common proposal to use incentives to address the issue of disregard for professional grades [12, 15]. It should be noted that building the categorization system on the basis of incentives is supported by less than a quarter of respondents (23.4%). Moreover, primacy of the motive to be assigned a professional grade as the greatest possible value in almost 60% of respondents confirms the importance of respect, recognition, self-actualization via contribution to the development of other specialists and profession itself for physicians [18]. The identified lower significance of financial incentives for physicians needs to be confirmed by the survey with higher accuracy. If similar results are obtained, it would be rational to conduct a distinct study to reveal the reasons of the financial incentives' low significance.

Despite the fact that a half of respondents are not members of professional communities, almost 66% of respondents recognize that communities play a key role in today's categorization system, while only 6.3% believe that the key role is played by healthcare public administration. In our opinion, this confirms the growing importance of professional communities for realization of physicians' development [19].

We should also pay attention to the differences in estimation of all aspects of the categorization system and its transformation by the respondents with the higher level of professional development based on certain formal criteria. The differences revealed show that such respondents rank the existing categorization system lower ($0.001 < p \leq 0.034$), they to greater extent agree with the need to transform the system ($0.001 < p \leq 0.013$) and are more often positive on new principles ($0.001 < p \leq 0.010$). No association of estimates with the respondents' work experience can be explained by the fact that work experience is not always the criterion of physician's professional development [20, 21].

Study limitations

The study has a number of limitations. First, it is the small number of respondents compliant with the criteria of pilot survey, although, it allows us to draw interim conclusions on the feasibility of performing the study with improved accuracy. This constraint will be resolved during further research. Second, it is the respondents' bias towards the system of assigning professional grades that could affect the scores provided by the respondents and even become the reason for refusal of survey, thereby also distorting the overall picture. Third, the sample had a high share of individuals assigned professional grades, having scientific degrees, engaged in teaching and research activities relative to the general population. This limitation was partially removed by dividing the respondents into groups. This can be fixed completely by increasing the sample to the size appropriate for studies with improved accuracy.

CONCLUSIONS

Despite the low ratings of the existing categorization system, the vast majority of physicians do not want to abandon the system, however, they recognize the need for transformation in accordance with the principles of physician's professional development in modern public healthcare. The physicians' opinions about the categorization system are affected by the levels of their professional development.

References

1. Cioffi JP, Lichtveld MY, Thielen L, Miner K. Credentialing the public health workforce: an idea whose time has come. J Public Health Manag Pract. 2003; 9 (6): 451–8. DOI: 10.1097/00124784-200311000-00004. PMID: 14606183.
2. Gershuni O, Czabanowska K, Burazeri G, Cichowska Myrup A, Von Krauss MK. Is there a golden recipe? A scoping review of public health workforce development. Eur J Public Health. 2019; 29 (3): 401–8. DOI: 10.1093/eurpub/cky247. PMID: 30508074.
3. Ayivi-Vinz G, Bakwa Kanyinga F, Bergeron L, Décary S, Adisso ÉL, Zomahoun HTV, et al. Use of the CPD-REACTION Questionnaire to Evaluate Continuing Professional Development Activities for Health Professionals: Systematic Review. JMIR Med Educ. 2022; 8 (2): e36948. DOI: 10.2196/36948. PMID: 35318188; PMCID: PMC9112082.
4. Federal'nyj zakon ot 21.11.2011 #323-FZ «Ob osnovah ohrany zdorov'ya grazhdan Rossijskoj Federacii». Russian.
5. «Trudovoj kodeks Rossijskoj Federacii» ot 30.12.2001 #197-FZ. Russian.
6. Federal'nyj zakon ot 03.07.2016 238-FZ «O nezavisimoj ocenke kvalifikacii». Russian.
7. Prikaz Ministerstva zdravoohraneniya SSSR ot 14 iyulya 1970 g. N 472 «Ob attestacii vrachej-specialistov». Russian.
8. Filippov YuN, Abaeva OP, Razgulin SA. Sovremennye problemy realizacii prava specialistov zdravoohraneniya na prohozhdenie attestacii dlya polucheniya kvalifikacionnoj kategorii. Medicinskij al'manah. 2008; 2: 14–6. Russian.
9. Abakov SI, Vagner VD, Sorokin DV, Abakova DS. O neobhodimosti reorganizacii sistemy attestacii vrachej-stomatologov. Institut stomatologii. 2012; 54 (1): 18–21. Russian.
10. Ostrovskaya IV, Han NV. K voprosu o professional'noj ocenke kvalifikacii sestrinskogo personala. Medicinskaya sestra. 2012; 1: 31–5. Russian.
11. Batyukov NM, Kasumova MK, Shpilev DI, Yanchenko VM. Upravlenie kachestvom klinicheskoj raboty vrachej-stomatologov cherez vnutrifirmennuyu attestaciyu v ramkah korporativnoj sistemy standartizacii. 2015; 1 (66): 12–5. Russian.
12. Kolennikova OA, Toksanbaeva MS. Problemy sistemnosti institutov ocenki kvalifikacii medicinskih specialistov. Problemy social'noj gigieny, zdravoohraneniya i istorii mediciny. 2022; 30 (s1): 1027–32. DOI: 10.32687/0869-866X-2022-30-s1-. Russian.
13. Shishkin SV, Temnickij AL. Rol' attestacii medicinskih rabotnikov v povyshenii trudovoj motivacii. Voprosy gosudarstvennogo i

municipal'nogo upravleniya. 2019; 2: 141–67. Russian.
14. Bazetova AA. Problemy attestacii medicinskih rabotnikov i puti ih resheniya. Nauchnyj al'manah. 2022; 2–2 (88): 47–50. Russian.
15. Kolennikova OA, Toksanbaeva MS. Ocenka kvalifikacii medicinskix specialistov v aspekte razvitiya nepreryvnogo medicinskogo obrazovaniya. Problemy social'noj gigieny, zdravoohraneniya i istorii mediciny. 2021; 29 (specvypusk): 1318–23. DOI: 10.32687/0869-866X-2021-29-s2-1318-1323. Russian.
16. RosStat (Federal'naya sluzhba gosudarstvennoj statistiki). Chislennost' medicinskih kadrov, imeyushhih vysshuyu i pervuyu kvalifikacionnye kategorii (data obrashheniya 07.08.2023). Dostupno po ssylke: https://rosstat.gov.ru/folder/13721. Russian.
17. Otdelnova KA. Opredelenie neobhodimogo chisla nablyudenij v social'no-gigienicheskih issledovaniyah. Sb. trudov 2-go MMI. 1980; 150 (6): 18–22. Russian.
18. Maslow AH. Motivation and Personality. N. Y.: Harpaer and Row, 1954.
19. Polushin YuS, Shapovalov KG, Zaripova ZA. Rol' professional'nyh soobshhestv v podgotovke k procedure akkreditacii: pervye shagi. Virtual'nye tehnologii v medicine. 2017; 2 (18): 7. Russian.
20. Manturova NE, Kochubey VV, Kochubey AV. The competence of plastic surgeons. Bulletin of RSMU. 2018; 2: 63–7. DOI: 10.24075/brsmu.2018.023.
21. Dunivin Z, Zadunayski L, Baskota U, Siek K, Mankoff J. Gender, Soft Skills, and Patient Experience in Online Physician Reviews: A Large-Scale Text Analysis. J Med Internet Res. 2020; 22 (7): e14455. DOI: 10.2196/14455.

Литература

1. Cioffi JP, Lichtveld MY, Thielen L, Miner K. Credentialing the public health workforce: an idea whose time has come. J Public Health Manag Pract. 2003; 9 (6): 451–8. DOI: 10.1097/00124784-200311000-00004. PMID: 14606183.
2. Gershuni O, Czabanowska K, Burazeri G, Cichowska Myrup A, Von Krauss MK. Is there a golden recipe? A scoping review of public health workforce development. Eur J Public Health. 2019; 29 (3): 401–8. DOI: 10.1093/eurpub/cky247. PMID: 30508074.
3. Ayivi-Vinz G, Bakwa Kanyinga F, Bergeron L, Décary S, Adisso ÉL, Zomahoun HTV, et al. Use of the CPD-REACTION Questionnaire to Evaluate Continuing Professional Development Activities for Health Professionals: Systematic Review. JMIR Med Educ. 2022; 8 (2): e36948. DOI: 10.2196/36948. PMID: 35318188; PMCID: PMC9112082.
4. Федеральный закон от 21.11.2011 №323-ФЗ «Об основах охраны здоровья граждан Российской Федерации».
5. «Трудовой кодекс Российской Федерации» от 30.12.2001 №197-ФЗ.
6. Федеральный закон от 03.07.2016 238-ФЗ «О независимой оценке квалификации».
7. Приказ Министерства здравоохранения СССР от 14 июля 1970 г. N 472 «Об аттестации врачей-специалистов».
8. Филиппов Ю. Н., Абаева О. П., Разгулин С. А. Современные проблемы реализации права специалистов здравоохранения на прохождение аттестации для получения квалификационной категории. Медицинский альманах. 2008; 2: 14–6.
9. Абаков С. И., Вагнер В. Д., Сорокин Д. В., Абакова Д. С. О необходимости реорганизации системы аттестации врачей-стоматологов. Институт стоматологии. 2012; 54 (1): 18–21.
10. Островская И. В., Хан Н. В. К вопросу о профессиональной оценке квалификации сестринского персонала. Медицинская сестра. 2012; 1: 31–5.
11. Батюков Н. М., Касумова М. К., Шпилев Д. И., Янченко В. М. Управление качеством клинической работы врачей-стоматологов через внутрифирменную аттестацию в рамках корпоративной системы стандартизации. 2015; 1 (66): 12–5.
12. Коленникова О. А., Токсанбаева М. С. Проблемы системности институтов оценки квалификации медицинских специалистов. Проблемы социальной гигиены, здравоохранения и истории медицины. 2022; 30 (s1): 1027–32. DOI: 10.32687/0869-866X-2022-30-s1-.
13. Шишкин С. В., Темницкий А. Л. Роль аттестации медицинских работников в повышении трудовой мотивации. Вопросы государственного и муниципального управления. 2019; 2: 141–67.
14. Базетова А. А. Проблемы аттестации медицинских работников и пути их решения. Научный альманах. 2022; 2–2 (88): 47–50.
15. Коленникова О. А., Токсанбаева М. С. Оценка квалификации медицинских специалистов в аспекте развития непрерывного медицинского образования. Проблемы социальной гигиены, здравоохранения и истории медицины. 2021; 29 (спецвыпуск): 1318–23. DOI: 10.32687/0869-866X-2021-29-s2-1318-1323.
16. РосСтат (Федеральная служба государственной статистики). Численность медицинских кадров, имеющих высшую и первую квалификационные категории (дата обращения 07.08.2023). Доступно по ссылке: https://rosstat.gov.ru/folder/13721.
17. Отдельнова К. А. Определение необходимого числа наблюдений в социально-гигиенических исследованиях. Сб. трудов 2-го ММИ. 1980; 150 (6): 18–22.
18. Maslow AH. Motivation and Personality. N. Y.: Harpaer and Row, 1954.
19. Полушин Ю. С., Шаповалов К. Г., Зарипова З. А. Роль профессиональных сообществ в подготовке к процедуре аккредитации: первые шаги. Виртуальные технологии в медицине. 2017; 2 (18): 7.
20. Manturova NE, Kochubey VV, Kochubey AV. The competence of plastic surgeons. Bulletin of RSMU. 2018; 2: 63–7. DOI: 10.24075/brsmu.2018.023.
21. Dunivin Z, Zadunayski L, Baskota U, Siek K, Mankoff J. Gender, Soft Skills, and Patient Experience in Online Physician Reviews: A Large-Scale Text Analysis. J Med Internet Res. 2020; 22 (7): e14455. DOI: 10.2196/14455.